

The Principles of Naval Architecture Series



Strength of Ships and Ocean Structures

Alaa Mansour

University of California, Berkeley

Donald Liu

American Bureau of Shipping

J. Randolph Paulling, Editor

2008

Published by
The Society of Naval Architects and Marine Engineers
601 Pavonia Avenue
Jersey City, NJ

Copyright © 2008 by The Society of Naval Architects and Marine Engineers.

It is understood and agreed that nothing expressed herein is intended or shall be construed to give any person, firm, or corporation any right, remedy, or claim against SNAME or any of its officers or members.

Library of Congress Cataloging-in-Publication Data
A catalog record from the Library of Congress has been applied for
ISBN No. 0-939773-66-X
Printed in the United States of America
First Printing, 2008

A Word from the President

The Society of Naval Architects and Marine Engineers is experiencing remarkable changes in the Maritime Industry as we enter our 115th year of service. Our mission, however, has not changed over the years . . . “an internationally recognized . . . technical society . . . serving the maritime industry, dedicated to advancing the art, science and practice of naval architecture, shipbuilding, ocean engineering, and marine engineering . . . encouraging the exchange and recording of information, sponsoring applied research . . . supporting education and enhancing the professional status and integrity of its membership.”

In the spirit of being faithful to our mission, we have written and published significant treatises on the subject of naval architecture, marine engineering and shipbuilding. Our most well known publication is the “Principles of Naval Architecture”. First published in 1939, it has been revised and updated three times – in 1967, 1988 and now in 2008. During this time, remarkable changes in the industry have taken place, especially in technology, and these changes have accelerated. The result has had a dramatic impact on size, speed, capacity, safety, quality and environmental protection.

The professions of naval architecture and marine engineering have realized great technical advances. They include structural design, hydrodynamics, resistance and propulsion, vibrations, materials, strength analysis using finite element analysis, dynamic loading and fatigue analysis, computer-aided ship design, controllability, stability and the use of simulation, risk analysis and virtual reality.

However, with this in view, nothing remains more important than a comprehensive knowledge of “first principles”. Using this knowledge, the Naval Architect is able to intelligently utilize the exceptional technology available to its fullest extent in today’s global maritime industry. It is with this in mind that this entirely new 2008 treatise was developed – “The Principles of Naval Architecture : The Series”. Recognizing the challenge of remaining relevant and current as technology changes, each major topical area will be published as a separate volume. This will facilitate timely revisions as technology continues to change and provide for more practical use by those who teach, learn or utilize the tools of our profession.

It is noteworthy that it took a decade to prepare this monumental work of nine volumes by sixteen authors and by a distinguished steering committee that was brought together from several countries, universities, companies and laboratories. We are all especially indebted to the editor, Professor J. Randolph (Randy) Paulling for providing the leadership, knowledge, and organizational ability to manage this seminal work. His dedication to this arduous task embodies the very essence of our mission . . . “to serve the maritime industry”.

It is with this introduction that we recognize and honor all of our colleagues who contributed to this work.

Authors:

Dr. John S. Letcher

Dr. Colin S. Moore

Robert D. Tagg

Professor Alaa Mansour and Dr. Donald Liu

Dr. Lars Larson and Dr. Hoyte Raven

Professors Justin E. Kerwin and Jacques B. Hadler

Professor William S. Vorus

Prof. Robert S. Beck, Dr. John Dalzell (Deceased), Prof. Odd Faltinsen and

Dr. Arthur M. Reed

Professor W. C. Webster and Dr. Rod Barr

Hull Geometry

Intact Stability

Subdivision and Damaged Stability

Strength of Ships and Ocean Structures

Resistance

Propulsion

Vibration and Noise

Motions in Waves

Controllability

Control Committee Members are:

Professor Bruce Johnson, Robert G. Keane, Jr., Justin H. McCarthy, David M. Maurer, Dr. William B. Morgan, Professor J. Nicholas Newman and Dr. Owen H. Oakley, Jr.

I would also like to recognize the support staff and members who helped bring this project to fruition, especially Susan Evans Grove, Publications Director, Phil Kimball, Executive Director and Dr. Roger Compton, Past President.

In the new world’s global maritime industry, we must maintain leadership in our profession if we are to continue to be true to our mission. The “Principles of Naval Architecture: The Series”, is another example of the many ways our Society is meeting that challenge.

ADMIRAL ROBERT E. KRAMEK,
President

Foreword

Since it was first published 70 years ago, *Principles of Naval Architecture* (PNA) has served as a seminal text on naval architecture for both practicing professionals and students of naval architecture. This is a challenging task – to explain the fundamentals in terms understandable to the undergraduate student while providing sufficient rigor to satisfy the needs of the experienced engineer – but the initial publication and the ensuing revisions have stood the test of time. We believe that this third revision of PNA will carry on the tradition, and continue to serve as an invaluable reference to the marine community.

In the Foreword to the second revision of PNA, the Chairman of its Control Committee, John Nachtsheim, lamented the state of the maritime industry, noting that there were "...too many ships chasing too little cargo," and with the decline in shipping came a "...corresponding decrease in technological growth." John ended on a somewhat optimistic note: "Let's hope the current valley of worldwide maritime inactivity won't last for too long. Let's hope for better times, further technological growth, and the need once more, not too far away, for the next revision of *Principles of Naval Architecture*."

Fortunately, better times began soon after the second revision of PNA was released in 1988. Spurred by the expanding global economy and a trend toward specialization of production amongst nations around the world, seaborne trade has tripled in the last twenty years. Perhaps more than ever before, the economic and societal well being of nations worldwide is dependent upon efficient, safe, and environmentally friendly deep sea shipping. Continuous improvement in the efficiency of transportation has been achieved over the last several decades, facilitating this growth in the global economy by enabling lower cost movement of goods. These improvements extend over the entire supply train, with waterborne transportation providing the critical link between distant nations. The ship design and shipbuilding communities have played key roles, as some of the most important advancements have been in the design and construction of ships.

With the explosive growth in trade has come an unprecedented demand for tonnage extending over the full spectrum of ship types, including containerships, tankers, bulk carriers, and passenger vessels. Seeking increased throughput and efficiency, ship sizes and capacities have increased dramatically. Ships currently on order include 16,000 TEU containerships, 260,000 m³ LNG carriers, and 5,400 passenger cruise liners, dwarfing the prior generation of designs.

The drive toward more efficient ship designs has led to increased sophistication in both the designs themselves and in the techniques and tools required to develop the designs. Concepts introduced in Revision 2 of PNA such as finite element analysis, computational fluid dynamics, and probabilistic techniques for evaluating a ship's stability and structural reliability are now integral to the overall design process. The classification societies have released the common structural rules for tankers and bulk carriers, which rely heavily on first principles engineering, use of finite element analysis for strength and fatigue assessments, and more sophisticated approaches to analysis such as are used for ultimate strength assessment for the hull girder. The International Maritime Organization now relies on probabilistic approaches for evaluating intact and damage stability and oil outflow. Regulations are increasingly performance-based, allowing application of creative solutions and state-of-the-art tools. Risk assessment techniques have become essential tools of the practicing naval architect.

The cyclical nature of shipbuilding is well established and all of us who have weathered the ups and downs of the marine industry recognize the current boom will not last forever. However, there are reasons to believe that the need for technological advancement in the maritime industries will remain strong in the coming years. For example, naval architects and marine engineers will continue to focus on improving the efficiency of marine transportation systems, spurred by rising fuel oil prices and public expectations for reducing greenhouse gas emissions. As a consequence of climate change, the melting Arctic ice cap will create new opportunities for exploration and production of oil and other natural resources, and may lead to new global trading patterns.

SNAME has been challenged to provide technical updates to its texts on a timely basis, in part due to our reliance on volunteerism and in part due to the rapidly changing environment of the maritime industry. This revision of PNA emphasizes engineering fundamentals and first principles, recognizing that the methods and approaches for applying these fundamentals are subject to constant change. Under the leadership of President Bob Kramek, SNAME is reviewing all its publications and related processes. As the next SNAME President, one of my goals is to begin strategizing on the next revision of PNA just as this third revision comes off the presses. Comments and ideas you may have on how SNAME can improve its publications are encouraged and very much appreciated.

FOREWORD

PNA would not be possible without the contributions of SNAME members and other marine professionals worldwide, who have advanced the science and the art of naval architecture and then shared their experiences through technical papers and presentations. For these many contributions we are indebted to all of you. We are especially indebted to its editor, Dr. J. Randolph Paulling, the Control Committee, the authors, and the reviewers who have given so generously of their time and expertise.

R. KEITH MICHEL
President-elect

Acknowledgments

The authors wish to acknowledge their indebtedness to the author of Chapter 4, “Strength of Ships”, in the preceding edition of *Principles of Naval Architecture* from which they have freely extracted text and figures. They also acknowledge the advice and assistance of the Control Committee, members of which provided reviews of early versions of the manuscript.

The present volume, *Strength of Ships and Ocean Structures*, could not have been completed without the assistance of a number of associates, colleagues and former students who read and critiqued portions or all of the manuscript, helped with illustrations, tracked down references and provided other vital services. The authors wish especially to acknowledge the contributions of the following individuals:

Dr. Jianwei Bai, University of California, Berkeley
Dr. Hsao H. Chen (Ret), American Bureau of Shipping
Mr. Robert Curry (Ret), American Bureau of Shipping
Professor Jorgen J. Jensen, Technical University of Denmark
Mr. Gregory Pappianou, University of California, Berkeley
Professor Preben T. Pedersen, Technical University of Denmark
Mr. Martin Petricic, University of California, Berkeley
Dr. Yung S. Shin, American Bureau of Shipping
Dr. Ge Wang, American Bureau of Shipping
Mr. Omar El Zayat, University of California, Berkeley

Finally, the Editor extends his thanks to the authors for their time and monumental efforts in writing the volume, to the Control Committee, and to the individuals listed above as well as others whose advice and assistance was essential to the successful completion of the task. He is especially grateful to Susan Evans Grove, SNAME’s Publications Director, for her patience, ready advice and close attention to detail without all of which this work could not have been accomplished.

Biography of Alaa Mansour

CoAuthor “Strength of Ships and Ocean Structures”

Dr. Alaa Mansour is a Professor of Engineering in the Department of Mechanical Engineering of the University of California at Berkeley. He was the Chairman of the Naval Architecture and Offshore Engineering Department at the University of California, from 1985 to 1989, and Chaired the Executive Committee of the Ocean Engineering Graduate Program at Berkeley from 2002 to 2005. He received his Bachelor of Science degree in Mechanical Engineering from the University of Cairo and has M.S. and Ph.D. degrees in Naval Architecture and Offshore Engineering from the University of California, Berkeley. Between 1968 and 1975 he was Assistant then Associate Professor in the Department of Ocean Engineering at the Massachusetts Institute of Technology. He is a registered Professional Engineer in the Commonwealth of Massachusetts.

Dr. Mansour has been the North and South American Chief Editor of the Journal of Marine Structures since its inception and an editor of the Journal of Marine Science and Technology. In 2000–2003 he served as Chairman of the International Ship and Offshore Structures Congress and has authored or co-authored over 100 publications.

In 2001, the Technical University of Denmark conferred upon Dr. Mansour its highest honor, the Honorary Doctorate Degree, “Doctor Technices Honoris Causa”, in recognition of his “significant contributions to development of design criteria for ships and offshore structures.” He is the recipient of the Davidson Medal presented by the Society of Naval Architects and Marine Engineers for “Outstanding Scientific Accomplishment in Ship Research”, and is currently a Fellow of the Society.

Biography of Donald Liu

CoAuthor “Strength of Ships and Ocean Structures”

Dr. Donald Liu retired in 2004 from the American Bureau of Shipping as Executive Vice President and Chief Technology Officer after a 37-year career at ABS. He is a graduate of the U.S. Merchant Marine Academy, the Massachusetts Institute of Technology where he obtained both BS and MS degrees in Naval Architecture and Marine Engineering, and the University of Arizona where he received his Ph.D. in Mechanical Engineering. He has authored or co-authored more than forty papers, reports and book chapters dealing with Finite Element analysis, structural dynamics, ultimate strength, hull loading, structural stability, structural optimization and probabilistic aspects of ship loading and strength.

Dr. Liu has been an active participant in key national and international organizations that are concerned with ship structures research, development and design. He served as the ABS representative on the interagency Ship Structures Committee, and as a member of the Standing Committees of the International Ship and Offshore Structures congress (ISSC) and the conference on Practical Design of Ships and Mobile Units (PRADS)

In 1994 Dr. Liu received the Sea Trade “Safety at Sea” award in recognition of his role in developing the ABS SafeHull system. He is the recipient of the Rear Admiral Halert C. Shephard Award in 1998 from the Chamber of Shipping of America in recognition of his achievements in promoting merchant marine safety, and in 2002 was awarded the United States Coast Guard (USCG) Meritorious Public Service Award in recognition of his contributions to marine safety. In 2004 he was awarded the Society of Naval Architects and Marine Engineers David W. Taylor Medal for notable achievement in naval architecture and in 2006 he received the Gibbs Brothers Medal, awarded by the National Academy of Sciences for outstanding contributions in the field of naval architecture and marine engineering. Dr. Liu is a Fellow of the Society of Naval Architects and Marine Engineers.

Nomenclature

A	area, generally	M_{sw}	stillwater bending moment
AC	acceptance criteria	M_T	twisting moment
A_f	total flange cross-sectional area	M_u	ultimate bending moment
A_s	shear area	M_w	vertical wave induced bending moment
A_w	web cross-sectional area	N	shear flow
B	beam	NA	neutral axis
b	buoyancy	NE	non-encounter probability
c	crack length	p	probability, in general
C_b	block coefficient	p	pressure
CL	centerline; a vertical plane through the centerline	p.d.f, PDF	probability density function
C_w	water plane coefficient of ship	p_f	probability of failure
D	depth	q	load per unit length
T	Draft	R	auto-correlation function
D	diameter, generally	R	return period
d	distance, generally	r	radius
DLA	dynamic load approach	RAO	Response Amplitude Operator
DLP	dominant load parameter	s	contour coordinate
DWT	deadweight	SM	section modulus
E	mean value	$S_x(\omega)$	wave spectrum
E	Young's modulus of elasticity	$S_{xy}(\omega)$	cross spectrum
F	force generally	$S_y(\omega)$	response spectrum
FE	finite element	T	period, generally
FEA	finite element analysis	t	thickness, generally
FEM	finite element method	t	time, generally
F_H	horizontal shear forces	T	torsion moment
f_p	permissible bending stress	T_M	torsion moment amidships
FRP	fiber reinforced plastics	T_M	modal period
F_w	vertical wave shear force	T_m	twist moment
g	acceleration due to gravity	TMCP	Thermo-Mechanical Controlled Process
G	shear modulus of elasticity, $E/2(1 + \nu)$	V	Total vertical shearing force across a section
H	transfer function	V	velocity in general, speed of ship
H	wave height	w	deflection
h	head, generally	w	weight
HAZ	heat affected zone	x	distance from origin along X-axis
HSC	high-speed crafts	y	distance from origin along Y-axis
HSLA	high strength low alloy	z	distance from origin along Z-axis
J	torsional constant of a section	ε	strains generally
K	load combination factor	∇	volume of displacement
k	spring constant per unit length		
L	length, generally	α	Skewness
L	length of ship	α	ship heading angle
L	life in years	β	safety index
LBP, L_{pp}	length between perpendiculars	β	width parameter
LCF	load combination factor	β	wave heading angle
LCG	longitudinal position center of gravity	β	kurtosis
M	moment, generally	δ	non-linearity parameter
m	mass, generally	ε	bandwidth parameter
M	margin	Φ	standard normal cumulative distribution function
M_H	wave-induced horizontal bending moment	Γ	St. Venant torsional constant
m_n	spectral moment of order n	γ	shear strain, generally
MPEL	most probable extreme load	γ	safety factor
MPEV	most probable extreme value	η	torsion coefficient

λ	wave length	σ	standard deviation
μ	covariance	σ	Stress, generally
μ	wave spreading angle	ω	angular velocity
μ	heading	ω	circular frequency
ν	Poisson's ratio	ω	warping function
Θ	twist angle	ζ	wave amplitude
ρ	mass density; mass per unit volume	σ_T	ultimate tensile strength
ρ	effectiveness	σ_Y	yield strength
ρ	correlation coefficient	χ	curvature
ρ	virtual aspect ratio		

Abbreviations for References

AA	Aluminum Association	ISSC	International Ship and Offshore Structures Congress
ABS	American Bureau of Shipping	ITTC	International Towing Tank Conference
ANSI	American National Standards Institute	JIS	Japanese Industrial Standard
ASCE	American Society of Civil Engineers	KR	Korean Register
ASNE	American Society of Naval Engineers	LR	Lloyd's Register
ASTM	American Society for Testing and Materials	NF	Normes Francaises
BMT	British Maritime Technology	NK	Nippon Kaiji Kyokai
BS	British Standard	NSMB CRS	Netherlands Ship Model Basin Cooperative Research Ships
BV	Bureau Veritas	NSWCCD	Carderock Division of the Naval Surface Warfare Center
CCS	China Classification Society	RINA	Registro Italiano Navale
CFA	Composite Fabricators Association	RS	Russian Register of Shipping
CSA	Canadian Standards Association	SAMPE	Society for Advancement of Materials Processing and Engineering
DNV	Det Norske Veritas	SNAME	Society of Naval Architects and Marine Engineers
DTNSRDC	David Taylor Naval Ship Research and Development Center	SOLAS	Safety of Life at Sea
GL	Germanisher Lloyd	SSC	Ship Structure Committee
IACS	International Association of Classification Societies	UNI	Unificazione Nazionale Italiana
IMO	International Maritime Organization		
ISO	International Organization for Standardization		

Preface

During the twenty years that have elapsed since publication of the previous edition of this book, there have been remarkable advances in the art, science and practice of the design and construction of ships and other floating structures. In that edition, the increasing use of high speed computers was recognized and computational methods were incorporated or acknowledged in the individual chapters rather than being presented in a separate chapter. Today, the electronic computer is one of the most important tools in any engineering environment and the laptop computer has taken the place of the ubiquitous slide rule of an earlier generation of engineers.

Advanced concepts and methods that were only being developed or introduced then are a part of common engineering practice today. These include finite element analysis, computational fluid dynamics, random process methods, numerical modeling of the hull form and components, with some or all of these merged into integrated design and manufacturing systems. Collectively, these give the naval architect unprecedented power and flexibility to explore innovation in concept and design of marine systems. In order to fully utilize these tools, the modern naval architect must possess a sound knowledge of mathematics and the other fundamental sciences that form a basic part of a modern engineering education.

In 1997, planning for the new edition of Principles of Naval Architecture was initiated by the SNAME publications manager who convened a meeting of a number of interested individuals including the editors of PNA and the new edition of Ship Design and Construction. At this meeting it was agreed that PNA would present the basis for the modern practice of naval architecture and the focus would be *principles* in preference to *applications*. The book should contain appropriate reference material but it was not a handbook with extensive numerical tables and graphs. Neither was it to be an elementary or advanced textbook although it was expected to be used as regular reading material in advanced undergraduate and elementary graduate courses. It would contain the background and principles necessary to understand and to use intelligently the modern analytical, numerical, experimental and computational tools available to the naval architect and also the fundamentals needed for the development of new tools. In essence, it would contain the material necessary to develop the understanding, insight, intuition, experience and judgment needed for the successful practice of the profession. Following this initial meeting, a PNA Control Committee, consisting of individuals having the expertise deemed necessary to oversee and guide the writing of the new edition of PNA, was appointed. This committee, after participating in the selection of authors for the various chapters, has continued to contribute by critically reviewing the various component parts as they are written.

In an effort of this magnitude, involving contributions from numerous widely separated authors, progress has not been uniform and it became obvious before the halfway mark that some chapters would be completed before others. In order to make the material available to the profession in a timely manner it was decided to publish each major subdivision as a separate volume in the "Principles of Naval Architecture Series" rather than treating each as a separate chapter of a single book.

Although the United States committed in 1975 to adopt SI units as the primary system of measurement the transition is not yet complete. In shipbuilding as well as other fields, we still find usage of three systems of units: English or foot-pound-seconds, SI or meter-newton-seconds, and the meter-kilogram(force)-second system common in engineering work on the European continent and most of the non-English speaking world prior to the adoption of the SI system. In the present work, we have tried to adhere to SI units as the primary system but other units may be found particularly in illustrations taken from other, older publications. The symbols and notation follow, in general, the standards developed by the International Towing Tank Conference.

This new revised volume on Strength of Ships and Ocean Structures addresses several topics of ship strength in greater depth than in the previous edition of PNA, bringing much of the material up to date and introducing some new subjects. There is extensive coverage of the latest developments in dynamic sea load predictions, including nonlinear load effects, slamming and impact plus new sections on the mechanics of collisions and grounding. The incorporation of the various loadings in structural design and analysis is covered including long term extreme and cumulative fatigue effects. There is a more extensive treatment of strength analysis using finite element methods than was included in the previous edition. Ultimate strength evaluation of the hull girder and components is covered and there is a section on structural safety assessment applying reliability concepts including fatigue effects.

Particular attention is given to problems encountered in ships of special type and size that have been developed in recent years, many of which, by reason of size, configuration or lack of a history of design experience, require

PREFACE

a design approach based on first principles. Modern developments in classification society strength standards and modern rule developments are covered including Common Structural Rules for tankers and bulk carriers. The concluding sections discuss materials other than steel, including composites and aluminum, and vessels of unusual geometry and performance such as multihulls, hydrofoils, and SWATH craft.

J. RANDOLPH PAULLING
Editor

Table of Contents

	Page
A Word from the President	iv
Foreword	v
Preface	vii
Acknowledgements	ix
Authors Biography	x
Nomenclature	xi
1. Introduction	1
2. Ship Structural Loads	4
3. Analysis of Hull Girder Stress and Deflection	56
4. Load Carrying Capability and Structural Performance Criteria	134
5. Reliability and Structural Safety Assessment	154
6. Miscellaneous Topics	189
References	208
Index	225

Section 1

Introduction

1.1 Nature of Ship Structures. The size and principal characteristics of a new ship are determined primarily by its mission or intended service. In addition to basic functional considerations, there are requirements such as stability, low resistance, high propulsive efficiency, and navigational limitations on draft or beam, all of which influence the choice of dimensions and form. Within these and other basic constraints, the ship's structure must be designed to sustain all of the loads expected to arise in its seagoing environment. As a result, a ship's structure possesses certain distinctive features not found in other man-made structures.

Among the most important distinguishing characteristics of ship structures are the size, complexity, and multiplicity of function of structural components, the random or probabilistic nature of the loads imposed, and the uncertainties inherent in our ability to predict the response of the structure to those loads. In contrast to land-based structures, the ship does not rest on a fixed foundation but derives its entire support from buoyant pressures exerted by a dynamic and ever changing fluid environment.

The methods of analysis employed by the naval architect in designing and evaluating the structure of a ship must be selected with these characteristics in mind. During the past few decades, ship structural design and analysis have undergone far-reaching changes toward more rationally founded practices. In addition, the development of readily available computer-based analytical tools has relieved the naval architect of much of the routine computational effort formerly involved in the analysis of a ship's structural performance. Nevertheless, many aspects of ship structures are not completely amenable to purely analytical treatment, and consequently the design of the structure continues to involve a judicious and imaginative blend of theory and experience.

This section will deal in detail with the loads acting on a ship's hull, techniques for analyzing the response of its structure to these loads, and both current and evolving new methods of establishing criteria of acceptable structural design. A detailed description of ship structures and a discussion of the practical aspects of the structural design of ships as they are influenced by the combined experience and analysis embodied in classification society rules is given in Chapters 17 and 18 of Lamb (2003). This work should be treated as a complement to this chapter.

To aid in understanding the nature of the behavior of ship structures, further details of some of their most important distinguishing will be given in the following sections. In some cases, it is helpful to compare the ship and its structure with other man-made structures and systems.

1.2 Size and Complexity of Ships. Ships are the largest mobile structures built by man, and both their size and the requirement for mobility exert strong

influences on the structural arrangement and design. As an example, large oil tankers having fully loaded displacements exceeding 5978 MN (600,000 tons. Throughout this book tons indicate long ton-force, 1 ton = 2240 lbf) and dimensions of 400 m (1,312 ft) in length, 63 m (207 ft) in breadth, 35.9 m (118 ft) in depth, with a loaded draft of 28.5 m (94 ft), are currently in operation. Ships are among the most complex of structures and this is due in part to their mobility. Good resistance and propulsive characteristics dictate that the external surface of the hull or shell must be a complex three-dimensional curved surface, and because the shell plating is one of the major strength members the structural configuration may not always be chosen solely on the basis of optimum structural performance. Furthermore, the structural behavior of the many geometrically complex members that constitute a ship's hull is difficult to analyze, and the construction of the vessel may be complicated because there are few members having simple shapes.

1.3 Multipurpose Function of Ship Structural Components. In contrast to many land-based structures, the structural components of a ship are frequently designed to perform a multiplicity of functions in addition to that of providing the structural integrity of the ship. For instance, the shell plating serves not only as the principal strength member but also as a watertight envelope of the ship, having a shape that provides adequate stability against capsizing, low resistance to forward motion, acceptable controllability, and good propulsive characteristics.

Internally, many strength members serve dual functions. For example, bulkheads that contribute substantially to the strength of the hull may also serve as liquid-tight boundaries of internal compartments. Their locations are dictated by the required tank volume or subdivision requirements. The configuration of structural decks is usually governed by the arrangement of internal spaces, but they may be called upon to resist local distributed and concentrated loads, as well as contributing to longitudinal and transverse strength.

Whereas in many instances structural efficiency alone might call for beams, columns, or trusses, alternative functions will normally require plate or sheet-type members, arranged in combination with a system of stiffeners, to provide resistance to multiple load components, some in the plane of the plate and others normal to it. An important characteristic of a ship structure is its composition of numerous stiffened plate panels, some plane and some curved, which make up the side and bottom shell, the decks, and the bulkheads. Therefore, much of the effort expended in ship structural analysis is concerned with predicting the performance of individual stiffened panels and the interactions between adjoining panels.

1.4 Probabilistic Nature of Ship's Structural Loads.

The loads that the ship structure must be designed to withstand have many sources. There are static components, which consist principally of the weight and buoyancy of the ship in calm water. There are dynamic components caused by wave-induced motions of the water around the ship and the resulting motions of the ship itself. Other dynamic loads, usually of higher frequency than the simple wave-induced loads, are caused by slamming or springing in waves and by the propellers or propelling machinery. These sometimes cause vibrations in parts or in the entirety of the ship. Finally, there may be loads that originate due to a ship's specific function, such as ice breaking, or in the cargo it carries, as in the case of thermally induced loads associated with heated or refrigerated cargoes.

An important characteristic of these load components is their variability with time. Even the static weight and buoyancy vary from voyage to voyage and within a voyage, depending upon the amount and distribution of cargo and consumables carried. To design the structure of the ship for a useful life of 20 years or more, this time dependence of the loading must be taken into consideration.

Like the sea itself, the loads imposed by the sea are random in nature, and can therefore be expressed only in probabilistic terms. Consequently, it is generally impossible to determine with absolute certainty a single value for the maximum loading that the ship structure will be called upon to withstand. Instead, it is necessary to use a probabilistic representation in which a series of loads of ascending severity is described, each having a probability corresponding to the expected frequency of its occurrence during the ship's lifetime. When conventional design methods are used, a design load may then be chosen as the one having an acceptably low probability of occurrence within a stated period (Section 2.3). In more rigorous reliability methods (Section 5), the load data in probability format can be used directly.

1.5 Uncertainty Associated with Ship's Structural Response. As a consequence of the complexity of the structure and the limitations of our analysis capabilities, it is seldom possible to achieve absolute accuracy in predicting the response of the structure even if the loading were known exactly. In the case of the uncertainties present in the predictions of structural loading, it is necessary for the designer to consider the probable extent and consequences of uncertainties in the structural response prediction when making a judgment concerning the overall acceptability of the structure. One of the most important tasks facing the engineer is to properly balance the acceptable level of uncertainty in their structural response predictions and the time and effort that must be expended to achieve a higher level of accuracy. The existence of this uncertainty is then acknowledged and must be allowed throughout the design.

In ship structural performance prediction, there are at least three sources of uncertainty. First, the designer's

stress analysis is usually carried out on an idealization of the real structure. For example, beam theory may be used to predict the stress distribution in part or the whole of the hull girder, even though it is known that the ship geometry may not follow exactly the assumptions of beam theory.

Second, the actual properties of the materials of construction may not be exactly the same as those assumed by the designer. As delivered from the mill, steel plates and shapes do not agree precisely with the nominal dimensions assumed in the design. Similarly, the chemical and physical properties of the materials can vary within certain tolerance limits. The rules of classification societies specify both physical and chemical standards for various classes of shipbuilding materials, either in the form of minimum standards or in a range of acceptable values. The materials that are actually built into the ship should have properties that lie within these specified limits, but the exact values depend on quality control in the manufacturing process and are not known in advance to the designer. Furthermore, there will inevitably be some degradation of material physical properties, for example, caused by corrosion over the lifetime of the ship.

Third, the integrity of ship construction contains a significant element of skill and workmanship. When performing a stress analysis, the designer may assume perfect alignment and fit of load-carrying members and perfectly executed welds. This ideal may be approached by the use of a construction system involving highly skilled workmen and high standards of inspection and quality control. Nevertheless, an absolutely flawless welded joint or a plate formed precisely to the intended shape and fabricated with no weld-induced distortion or joint misalignment is a goal to strive for but one that is never attained in practice.

It will be obvious that the uncertainties involved in the determination of both the loads and the structural responses to these loads make it difficult to establish criteria for acceptable ship structures. In the past, allowable stress levels or safety factors used by the designer provided a means of allowing for these uncertainties, based upon past experience with similar structures. In recent years, reliability principles have been applied, using probability theory and statistics, to obtain a more rational basis for design criteria. In the reliability approach to design, structural response data as well as strength data can be expressed and used in probability format. These principles are discussed in Section 5.

1.6 Modes of Ship Strength and Structural Failure. Avoidance of structural failure is an overriding goal of all structural designers. To achieve this goal, it is necessary for the naval architect to be aware of the possible modes of failure and the methods of predicting their occurrence. The types of failure that can occur in ship structures are generally those that are characteristic of structures made of stiffened plate panels assembled through the use of welding to form monolithic

structures with great redundancy (i.e., having many alternative paths for lines of stress).

It should be noted that structural failure might occur in different degrees of severity. At the low end of the failure scale, there may be small cracks or deformations in minor structural members that do not jeopardize the basic ability of the structure to perform its function. Such minor failures may only have aesthetic consequences. At the other end of the scale is total catastrophic collapse of the structure, resulting in the loss of the ship. There are several different modes of failure between these extremes that may reduce the load-carrying ability of individual members or parts of the structure but, because of the highly redundant nature of the ship structure, do not lead to total collapse. Such failures are normally detected and repaired before their number and extent grow to the point of endangering the ship.

Four principal mechanisms are recognized to cause most of the cases of ship structural failure, aside from collision or grounding. These modes of failure are as follows:

- Buckling due to compressive or shear instability
- Excessive tensile or compressive yield
- Fatigue cracking
- Brittle fracture.

The first three modes of failure are discussed in more detail in Section 4. The last one, brittle fracture, was found to play a major role in the failure of many of the emergency cargo ships built during World War II. The causes of these failures ultimately were traced to a combination of factors associated with the relatively new techniques of welded construction employed in building the ships. The solution to the problem was obtained through the development of design details that avoided the occurrence of notches and other stress concentrations, together with the selection of steels having a high degree of resistance to the initiation and propagation of cracks, particularly at low temperatures. Features termed *crack arrestors* were incorporated to provide fail-safe designs by limiting the extent of propagation of any cracks that might actually have occurred.

Because the control of brittle fracture is accomplished principally through detailed design and material selection, it is only considered briefly in this chapter. Information on these topics may be found in Lamb (2003), Chapters 17 and 20.

1.7 Design Philosophy and Procedure. The development of completely rational structural design procedures is being pursued in several disciplines, including civil, aeronautical, and mechanical engineering, as well as in naval architecture. Using such procedures, a set of requirements or criteria to be met by the structure should first be formulated, then through the application of fundamental reasoning and mathematical analysis, augmented by the introduction of certain empirical information, it should be possible to arrive at a structural configuration and a set of scantlings that simultaneously

meet all the criteria. Although this ideal has not yet been attained, steady progress is being made in that direction.

The original set of requirements imposed upon the ship will include the functional requirements of the owner and, in addition, institutional requirements such as those established by government and other regulatory bodies concerned with safety, navigation, pollution prevention, tonnage admeasurement, and labor standards. The methods of selecting the overall dimensions and the arrangement of the ship to meet these requirements have been dealt with in Lamb (2003). Thus, when designing the principal members of the ship structure, it may be assumed that the overall dimensions of the ship and the subdivisions of its internal volume occupied by bulkheads, decks, and tank boundaries have already been determined to meet these various requirements. The problem of structural design then consists of the selection of material types, frame spacing, frame and stiffener sizes, and plate thickness that, when combined in this geometric configuration, will enable the ship to perform its function efficiently for its expected operational lifetime.

At this point, to select the criteria to be satisfied by the structural components of the ship, the designer must rely on either empirical criteria, including factors of safety and allowable stresses, or on the use of reliability principles discussed in Section 5. The term *synthesis*, which is defined as the putting together of parts or elements so as to form a whole, is often applied to the process of ship structural design.

However, an additional element is needed to complete the design synthesis: finding the optimal combination of the various elements. Due to the complexity of ship structures, as well as the probabilistic nature of available information needed for certain vital inputs to the design process, it is usually impossible to achieve an optimum solution in a single set of calculations. Instead, some sort of iterative procedure must be employed. The traditional method of ship structural design, involving the extrapolation of previous experience, can even be thought of as an iterative process in which the construction and operational experience of previous ships form essential steps. In each new design, the naval architect considers this past experience and modifies the new design intuitively to achieve an improved configuration. The successful designer is one whose insight, understanding, and memory, along with skill in methods of structural analysis, resulted in consistently improved previous designs in successive ships.

Even when the most advanced methods are used, much of structural design consists of a stepwise process in which the designer develops a structural configuration on the basis of experience, intuition, and imagination, then performs an analysis of that structure to evaluate its performance. If necessary, the scantlings are revised until the design criteria are met. The resulting configuration is then modified in some way that is expected to lead to an improvement in performance or cost, and the analysis is then repeated to re-ensure that the improved

configuration meets the design criteria. Thus, a key element in structural design is the process of analyzing the response of an assumed structure. The process of finding a structural configuration having the desired performance by synthesis is the inverse of analysis, and is not nearly so straightforward, especially in the case of complex structures. Consequently, it is only after completing several satisfactory design syntheses that the process of optimization can take place.

In summary, five key steps can be identified to characterize the structural design process, whether it be intuitive or mathematically rigorous:

- (a) Development of the initial configuration and scantlings.
- (b) Analysis of the performance of the assumed design.
- (c) Comparison with performance criteria.
- (d) Redesign the structure by changing both the configuration and scantlings in such a way as to effect an improvement.
- (e) Repeat the above as necessary to approach an optimum.

Formally, the final optimization step consists of a search for the best attainable (usually minimum) value of some quantity such as structural weight, construction cost, overall required freight rate for the ship in its intended service (see Lamb 2003), or the so-called *total expected cost* of the structure. The last of these quantities, as proposed by Freudenthal (1969), consists of the sum of the initial cost of the ship (or other structure), the anticipated total cost of complete structural failure multiplied by its probability, and a summation of lifetime costs of repair of minor structural damages (see also Lewis et al. 1973).

The search is performed in the presence of constraints that, in their most elementary form, consist of the requirement that each member of the structure does not fail under the expected loadings—Steps (b) and (c). Such an optimization procedure forms the basis for a sound economical design, whether it be carried out automatically, using one of the formal mathematical optimization schemes, or manually, with or without machine computational assistance for some parts of the process.

Section 2

Ship Structural Loads

2.1 Classification of Loads. It is convenient to divide the loads acting on the ship structure into four categories as follows, where the categories are based partly upon the nature of the load and partly upon the nature of the ship's response.

2.1.1 Static Loads. Static loads are loads that vary slowly with time and change when the total weight of the ship changes, as a result of loading or discharge of cargo, consumption of fuel, or modification to the ship itself. Static loads are influenced by:

- Weight of the ship and its contents
- Static buoyancy of the ship when at rest or moving
- Thermal loads resulting from nonlinear temperature gradients within the hull
 - Concentrated loads caused by dry-docking and grounding.

2.1.2 Low-Frequency Dynamic Loads. Low-frequency dynamic loads are loads that vary in time with periods ranging from a few seconds to several minutes, and therefore occur at frequencies that are sufficiently low, compared to the frequencies of vibratory response of the hull and its parts, that there is no appreciable resonant amplification of the stresses induced in the structure. The loads are called dynamic because they originate mainly in the action of the waves through which the ship moves, and therefore are always

changing with time. They may be broken down into the following components:

- Wave-induced hull pressure variations
- Hull pressure variations caused by oscillatory ship motions
 - Inertial reactions resulting from the acceleration of the mass of the ship and its contents.

2.1.3 High-Frequency Dynamic Loads. High-frequency dynamic loads are time-varying loads of sufficiently high frequency that they may induce a vibratory response in the ship structure. Some of the exciting loads may be quite small in magnitude but, as a result of resonant amplification, can give rise to large stresses and deflections. Examples of such dynamic loads are the following:

- Hydrodynamic loads induced by propulsive devices on the hull or appendages
 - Loads imparted to the hull by reciprocating or unbalanced rotating machinery
 - Hydroelastic loads resulting from the interaction of appendages with the flow past the ship
 - Wave-induced loads primarily due to short waves whose frequency of encounter overlaps the lower natural frequencies of hull vibration and which therefore may excite an appreciable resonant response, termed *springing*.

configuration meets the design criteria. Thus, a key element in structural design is the process of analyzing the response of an assumed structure. The process of finding a structural configuration having the desired performance by synthesis is the inverse of analysis, and is not nearly so straightforward, especially in the case of complex structures. Consequently, it is only after completing several satisfactory design syntheses that the process of optimization can take place.

In summary, five key steps can be identified to characterize the structural design process, whether it be intuitive or mathematically rigorous:

- (a) Development of the initial configuration and scantlings.
- (b) Analysis of the performance of the assumed design.
- (c) Comparison with performance criteria.
- (d) Redesign the structure by changing both the configuration and scantlings in such a way as to effect an improvement.
- (e) Repeat the above as necessary to approach an optimum.

Formally, the final optimization step consists of a search for the best attainable (usually minimum) value of some quantity such as structural weight, construction cost, overall required freight rate for the ship in its intended service (see Lamb 2003), or the so-called *total expected cost* of the structure. The last of these quantities, as proposed by Freudenthal (1969), consists of the sum of the initial cost of the ship (or other structure), the anticipated total cost of complete structural failure multiplied by its probability, and a summation of lifetime costs of repair of minor structural damages (see also Lewis et al. 1973).

The search is performed in the presence of constraints that, in their most elementary form, consist of the requirement that each member of the structure does not fail under the expected loadings—Steps (b) and (c). Such an optimization procedure forms the basis for a sound economical design, whether it be carried out automatically, using one of the formal mathematical optimization schemes, or manually, with or without machine computational assistance for some parts of the process.

Section 2

Ship Structural Loads

2.1 Classification of Loads. It is convenient to divide the loads acting on the ship structure into four categories as follows, where the categories are based partly upon the nature of the load and partly upon the nature of the ship's response.

2.1.1 Static Loads. Static loads are loads that vary slowly with time and change when the total weight of the ship changes, as a result of loading or discharge of cargo, consumption of fuel, or modification to the ship itself. Static loads are influenced by:

- Weight of the ship and its contents
- Static buoyancy of the ship when at rest or moving
- Thermal loads resulting from nonlinear temperature gradients within the hull
 - Concentrated loads caused by dry-docking and grounding.

2.1.2 Low-Frequency Dynamic Loads. Low-frequency dynamic loads are loads that vary in time with periods ranging from a few seconds to several minutes, and therefore occur at frequencies that are sufficiently low, compared to the frequencies of vibratory response of the hull and its parts, that there is no appreciable resonant amplification of the stresses induced in the structure. The loads are called dynamic because they originate mainly in the action of the waves through which the ship moves, and therefore are always

changing with time. They may be broken down into the following components:

- Wave-induced hull pressure variations
- Hull pressure variations caused by oscillatory ship motions
 - Inertial reactions resulting from the acceleration of the mass of the ship and its contents.

2.1.3 High-Frequency Dynamic Loads. High-frequency dynamic loads are time-varying loads of sufficiently high frequency that they may induce a vibratory response in the ship structure. Some of the exciting loads may be quite small in magnitude but, as a result of resonant amplification, can give rise to large stresses and deflections. Examples of such dynamic loads are the following:

- Hydrodynamic loads induced by propulsive devices on the hull or appendages
 - Loads imparted to the hull by reciprocating or unbalanced rotating machinery
 - Hydroelastic loads resulting from the interaction of appendages with the flow past the ship
 - Wave-induced loads primarily due to short waves whose frequency of encounter overlaps the lower natural frequencies of hull vibration and which therefore may excite an appreciable resonant response, termed *springing*.

2.1.4 Impact Loads. Impact loads are dynamic loads resulting from slamming or wave impact on the forefoot, bow flare, and other parts of the hull structure, including the effects of green water on deck. In a naval ship, weapon effects constitute a very important category of impact loads. Impact loads may induce transient hull vibrations, termed *whipping*.

The most important classes of loads are the static loads resulting from the ship's weight and buoyancy, the low-frequency dynamic loads, and slamming loads. In the following sections, attention will be devoted to the methods currently used to determine these loads, along with a brief discussion of impact loads and springing loads, which are usually found to be important only in very long flexible ships such as the U.S. and Canadian Great Lakes iron ore carriers, but recently also experienced in ocean-going bulk carriers (Vidic-Perunovic & Jensen 2005). A discussion of thermal loads can be found in Taggart (1980), Chapter 6.

In addition to the previously mentioned categories, there may be specialized operational loads that part or all of the structure may be called upon to withstand, and that may be the dominant loads for some ships. These loads may be either static or dynamic. Some examples are:

- Accidental loads caused by fire, collision, or grounding
- Sloshing and impact loads on internal structure caused by the movement of liquids in tanks
- Ice loads in vessels intended for icebreaking or arctic navigation
- Loads caused by impact with other vessels, piers, or other obstacles, as in the case of tugs and barges
- Impact of cargo-handling equipment, such as grabs or clamshells used in unloading certain bulk commodities
- Structural thermal loads imposed by special cargo carried at nonambient temperature or pressure
- Landing of aircraft or helicopters.

As may be seen from the brief descriptions given here, some of these loads may be of importance in all ships and other loads may be encountered only in specialized ships or circumstances.

2.2 Static Loading on a Ship Afloat in Still Water. The static loads acting on a ship afloat in still water consist of two parts: buoyancy forces and gravity forces, or weights. The *buoyancy force* is the resultant of the hydrostatic pressure distribution over the immersed external area of the ship. This pressure is a surface force per unit area whose direction is everywhere normal to the hull. However, the buoyant force is the resultant perpendicular to the water surface and directed upward. The weights are body forces distributed throughout the ship and its contents, and the direction of the weight forces is always vertically downward. These component force systems are illustrated schematically in Fig. 1.

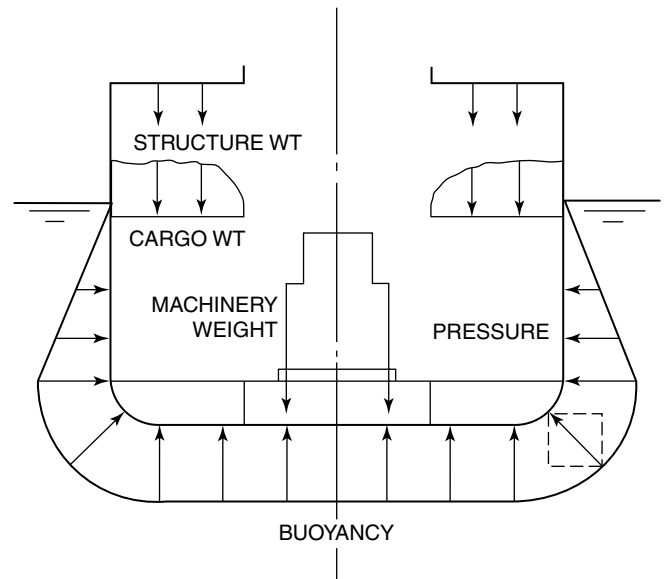


Fig. 1 Static load components on hull.

If we integrate the local buoyant pressures over a unit ship length around a cross section at a given longitudinal position, the resultant is a vertical buoyant force per unit length whose magnitude is given by $\rho g A$, where ρg is the weight density of water (ρ is the mass density, or mass per unit volume) and A is the immersed sectional area. Similarly, we may add all the weights contained in a unit length of the ship at this same section, resulting in a total weight per unit length. The net structural load per unit length is the algebraic sum of the unit buoyancy and the unit weight.

The individual loads can have both local and overall structural effects. A very heavy machinery item induces large local loads at its points of attachment to the ship, and its foundations must be designed to distribute these loads evenly into the hull structure. At the same time, the weight of this item contributes to the distribution of shear forces and bending moments acting at all locations along the length of the hull. If a part of the content of the ship is made up of liquids (e.g., fuel or liquid cargo), there will be hydrostatic pressure forces exerted by such liquids that are normal to the boundary surfaces of the tanks within which they are contained. These internal pressure loads can have important local structural effects and must be considered when designing the bulkheads and other tank boundary members.

The geometric arrangement and resulting stress or deflection response patterns of typical ship structures are such that it is usually convenient to divide the structure and the associated response into three components, which are labeled primary, secondary, and tertiary. These are illustrated in Fig. 2 and described as follows:

- *Primary response* is the response of the entire hull when bending and twisting as a beam, under the external

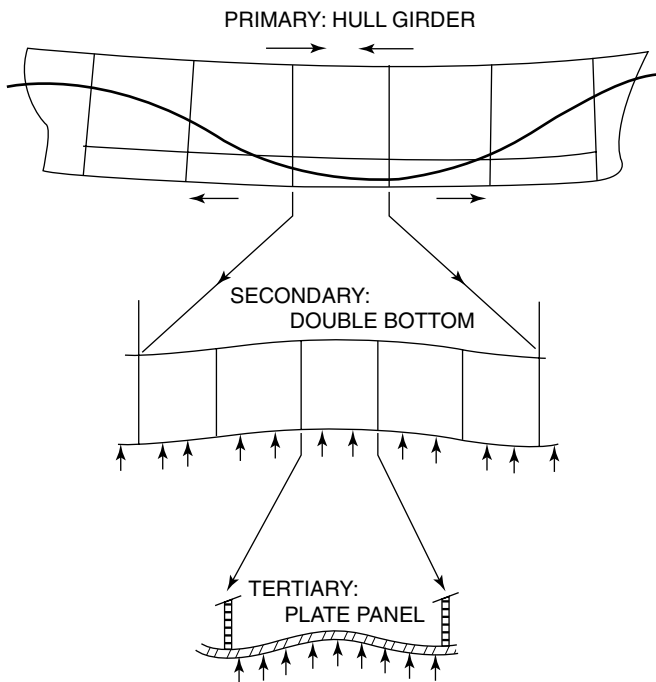


Fig. 2 Primary, secondary, and tertiary structure.

longitudinal distribution of vertical, lateral, and twisting loads.

- *Secondary response* comprises the stress and deflection of a single panel of stiffened plating (e.g., the panel of the bottom structure contained between two adjacent transverse bulkheads). The loading of the panel is normal to its plane, and the boundaries of the secondary panel are usually formed by other secondary panels (side shell and bulkheads). Boundary edge loads are also present due to primary bending of the hull.

- *Tertiary response* describes the out-of-plane deflection and associated stress of an individual panel of plating. The loading is normal to the panel, and its boundaries are formed by the stiffeners of the secondary panel of which it is a part. Boundary edge loads also exist as a result of primary bending of the hull.

Sometimes it is necessary to know the localized distribution of the loads and in other cases, depending upon the structural response being sought, to know the distribution of the resultants of the local loads—for example, the load per unit length for the entire hull. The primary response analysis is carried out by hypothesizing that the entire hull of a ship behaves like a beam whose loading is given by the longitudinal distribution of weights and buoyancy over the hull. As in any beam stress computation, it is necessary first to integrate the loads to obtain the longitudinal distribution of the total shear force, and then to integrate them again to obtain the bending moment. The still-water loads contribute an important part

of the total shear and bending moment in most ships, to which wave-induced effects must be added later.

Figure 3 illustrates a typical longitudinal distribution of weight and buoyancy for a ship afloat in calm water. A curve of buoyancy force per unit length is plotted in the lower part of this figure, which as noted previously is equal to the weight density, ρg , of water multiplied by the sectional area. The upper curve (2) in the figure shows the longitudinal distribution of the weight force plotted according to a commonly employed convention. In this procedure, the length of the ship is divided into a number of equal station spaces, for example, the 20 or so station subdivisions that were used to prepare the line drawing. The hull weights, equipment, and contents lying in the interval between station i and station $i + 1$ are added together and treated as a single uniformly distributed load over this station interval. This is essentially an accounting process in which every item in the ship—hull structure (plating, frames, weld material), outfit (piping, deck covering, cargo gear), propulsion machinery, cargo, and so on—is recorded and assigned to a station interval. The procedure must be performed with meticulous care and in great detail to assure accuracy. As is the case with most repetitive computations, it lends itself easily to use of computers.

The assumption of a uniform distribution of the sectional weights over the station intervals, which is implied in this step, is only an approximation of the actual weight distribution. Some weight items will occur as nearly concentrated weights in this longitudinal distribution. For example, the weight of a transverse bulkhead (in reality) will be distributed longitudinally over a very short portion of the ship length equal to the thickness of the bulkhead plating. The weights of certain items such as large machinery components (turbines, diesel engines) may be transmitted to the ship structure as point loads at the locations of the foundation bolt-down points. Similarly, cargo containers are usually supported on fittings located under their corners, and their total weight is transmitted to the hull structure as point loads at these locations. Therefore, the true weight distribution will be a much more irregular graph than that shown in Fig. 3, and will consist of some distributed items and some point weights. However, it may be shown that the integrations that are performed to obtain the shear and bending moment distributions from the loads tend to smooth out the effects of these local irregularities. Consequently, any reasonably accurate loading distribution that maintains the correct magnitude of the force over a local interval that is small compared to the total ship length will generally lead to the correct shear and bending moment distributions within acceptable error limits. However, localized structural effects caused by large point loads of especially heavy items may be analyzed separately, and their effects may be superimposed on the effects of the remaining loads.

Having determined the buoyancy and weight distributions, the net load curve (3) is the difference between the

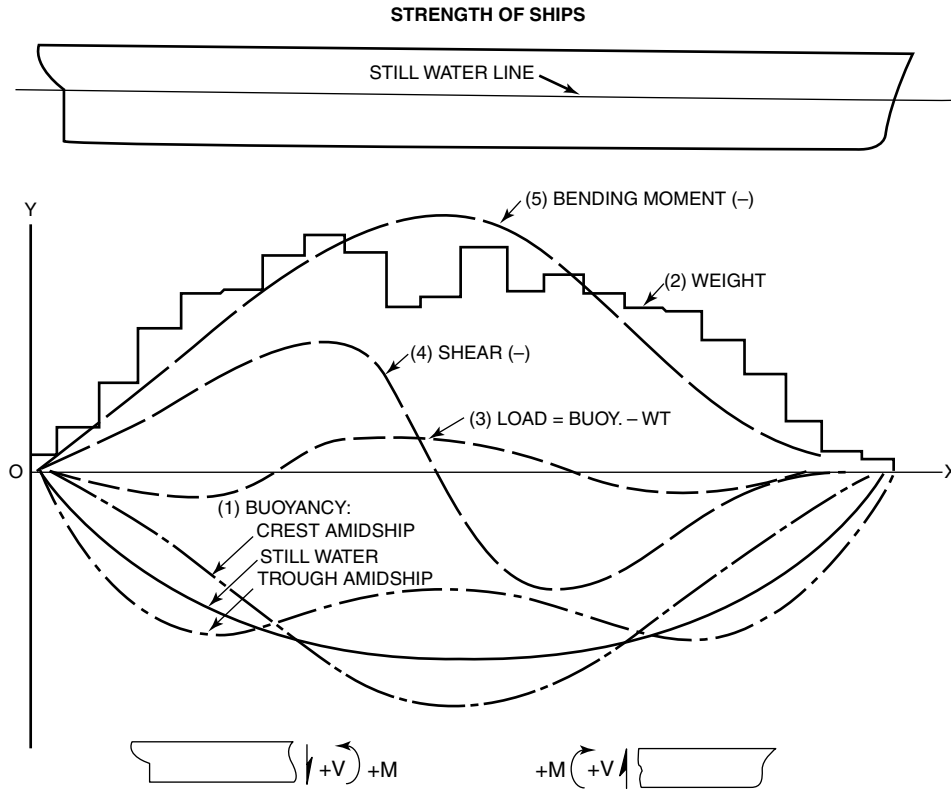


Fig. 3 Static loads, shear, and bending moment.

two. This is plotted as the third curve in Fig. 3, with positive buoyancy, upward. The conditions of static equilibrium require that the total weight and buoyancy be equal and that the center of buoyancy be on the same vertical line as the center of gravity. In terms of the load curve, this requires that the integral of the total load over the ship length and the integral of the longitudinal moment of the load curve each be equal to zero.

As in any beam calculation, the shear force at location x_1 , equal to $V(x_1)$, is obtained as the integral of the load curve, and plotted as the fourth curve of Fig. 3,

$$V(x_1) = \int_0^{x_1} [b(x) - w(x)] dx \quad (1)$$

where,

$$\begin{aligned} b(x) &= \text{buoyancy per unit length} \\ w(x) &= \text{weight per unit length.} \end{aligned}$$

The bending moment at location x_1 , $M(x_1)$, is the integral of the shear curve, and is plotted as the fifth curve in Fig. 3,

$$M(x_1) = \int_0^{x_1} V(x) dx \quad (2)$$

In the lower parts of Fig. 3, the significance of the shear and bending moment are shown, together with their sign conventions. If we consider a given longitudinal location, x , the shear force is the upward force that the left portion of the ship exerts on the portion to the right of this location. Similarly, the bending moment is the resultant moment exerted by the left portion on the portion to the right of location x . The conditions of static equilibrium require that the shear force and the bending moment be equal to zero at both ends of the ship.

In the practical execution of the still-water loading computation, a general ship hydrostatics computer program is almost invariably employed. Programs such as the U.S. Navy's SHCP and other commercially available computer programs, such as GHS, NAPA, TRIBON, and HECSALV, contain modules for performing computations of such quantities as hydrostatic properties, static stability, flooding, and static hull loading. A common database is normally employed containing the offsets or other descriptions of the hull geometry, which are required to compute the buoyancy distribution. Supplementary data, including the weight distribution, are then entered along with the specific computation of the load, shear, and bending moment. The principal task confronting the naval architect lies in preparing and checking the input data and in evaluating the results of the computation. The importance of complete and accurate

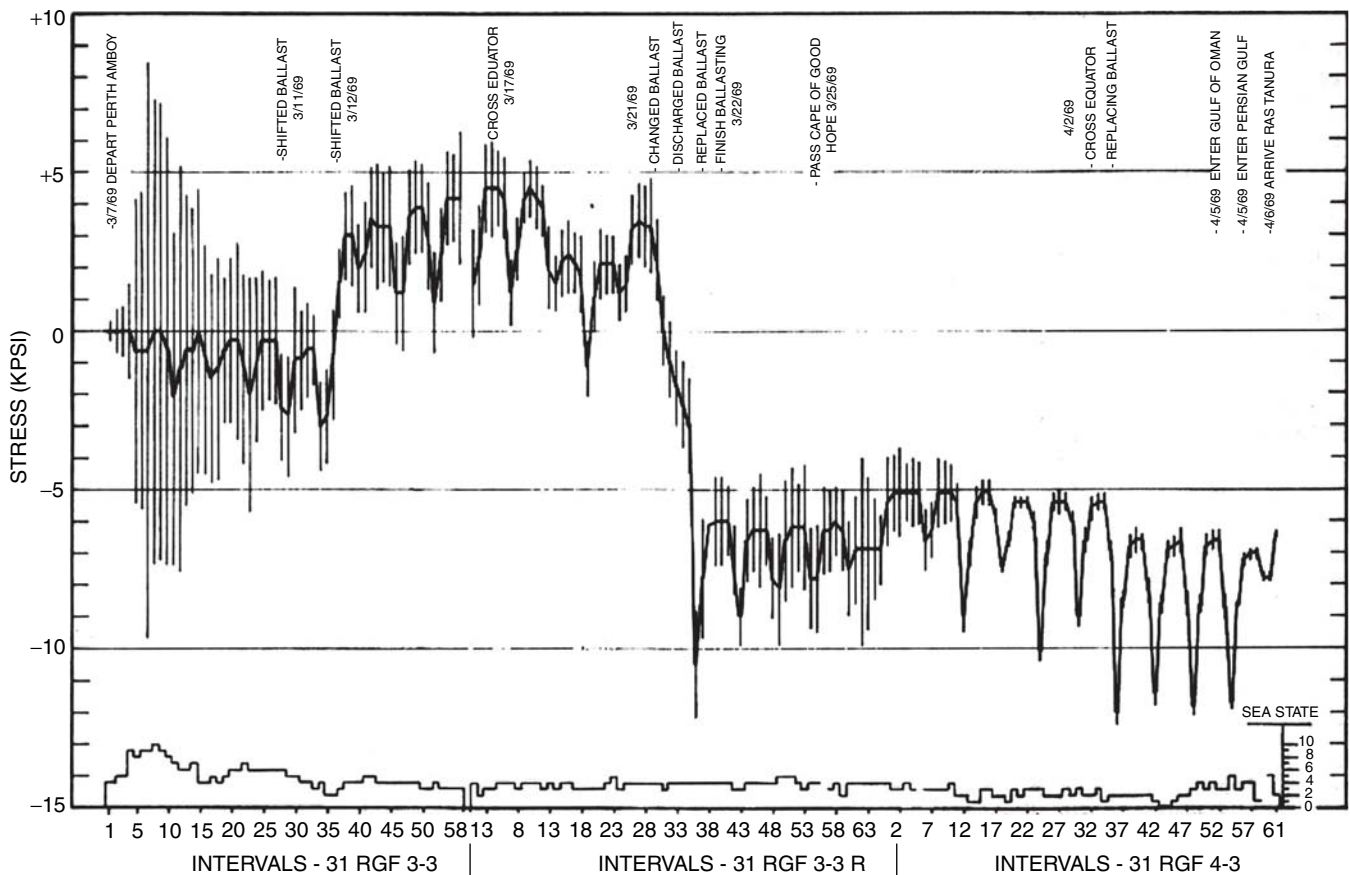


Fig. 4 Typical voyage variation in stresses, *R.G. Follis*, in ballast.

input cannot be overemphasized, and it may be readily perceived that the compilation of the complete weight data required for the computation of the shear and bending moment at the final design stage is not a trivial task. This data is often incorporated into a computer-based weight control and accounting system.

In conclusion, the static loading must be computed for several different distributions of cargo and other variable weights to obtain the extreme values of shear and bending moment. These extreme values will then be combined with other loads upon which the design of structural members will be based. Furthermore, it must be borne in mind that the static loading will change during the course of a single voyage as fuel is consumed, ballast is shifted, and cargo is loaded and discharged at the ports visited. A time history of the changes in static midship stress during the course of an outbound voyage of a large tanker can be seen in Fig. 4 (Little & Lewis 1971). Although it also shows stress variations due to waves, the large shifts in the heavy lines are primarily the results of changes in saltwater ballast amount and distribution. The recorded variations in still-water stress, excluding temperature and wave effects, range from about

27.6 MPa (4 kpsi) tension to 48.3 MPa (7 kpsi) compression.

2.3 Wave-Induced Loads. The principal wave-induced loads are those previously referred to as low-frequency dynamic loads or loads involving ship and wave motions that result in negligible dynamic stress amplification. Once these quasi-static loads are determined, the structural response in terms of stress or deflection can be computed by methods of static structural analysis. At least four procedures of varying degrees of sophistication may be used to estimate the wave-induced loads and their resultant bending moments and shear forces.

2.3.1 Approximate Methods. In the preliminary design process, it is often desirable to make an early estimate of the hull structural loading by some approximate method, perhaps even before detailed information concerning the weight distribution or hull lines have been developed. Approximate methods are available that include semi-empirical formulations and quasi-static computations.

Earlier texts on naval architecture contain descriptions of a procedure in which the ship is in a state of

static equilibrium on either the crest or trough of a wave whose length is equal to the ship's length between perpendiculars, L , and whose height is $L/20$. Using the longitudinal distribution of buoyancy up to such a wave profile and an assumed weight distribution, curves of the longitudinal distribution of shear force and bending moment may be computed, just as in the still water case. Experiments and more exact computational methods have shown that these highly simplified procedures overestimate the actual wave-induced bending moment for any given wave height by a substantial margin as a result of neglecting dynamic and hydrodynamic effects associated with wave pressures and ship motions. This procedure is of value chiefly when used in comparison with previous design data. Most hydrostatics computer programs, such as the previously mentioned SHCP, GHS, and HECSALV, include the static wave bending moment computation as an option.

Other standard wave heights have also been used. For example, $0.6(L)^{0.6}$ was used in certain investigations by the American Bureau of Shipping (ABS), and $1.1(L)^{0.5}$ is used by the U.S. Navy for longitudinal strength. Details of U.S. Navy standards for longitudinal strength are classified, but a general statement is given by Sikora, Dinsenbacher, and Beach (1983): "The primary hull girders of mild steel naval vessels are designed to a stress level of 129.2 MPa (8.5 t/in²) single amplitude by placing the ship on a trochoidal wave of $1.1(L)^{0.5}$ and length = LBP," and then by carrying out a conventional quasi-static calculation. However, in the design of unusual naval craft advanced reliability techniques have been applied, as discussed subsequently.

Over the past decades, the phenomenal growth in size of ships has developed an increasing magnitude of impact on the shipbuilding and shipping industries, in that ship design procedures can no longer be based solely on the static wave method using standard wave heights. This initiated the consideration of using the seaway as a basis and the probabilistic approach described in Sections 2.5, 2.6, and 2.7 to obtain the dynamic loads acting on the ships. In this respect, the International Association of Classification Societies (IACS) performed extensive detailed analyses of hull girder loads following the long-term extreme value approach based on the average sea condition of the North Atlantic as the standard environment condition for ocean-going vessels. The analyses were performed employing the computer codes of frequency domain linear strip ship motion theory available at the member societies. The study generated a large database that was used to develop a common standard or criteria of hull girder longitudinal strength prescribed in the IACS Unified Requirements S-11 (IACS 2001) on longitudinal strength (vertical bending moments and shear forces). The criteria formulated took into account the dynamic and hydrodynamic effects, and are therefore not subject to the limitations of the static wave computation. The underlining background of unified requirements S-11 is given in Nitta et al. (1992, 1992, 1995).

In addition to the vertical bending moment and shear force postulated in IACS UR S-11, major classification societies have also established criteria on the lateral bending moment and shear force, torsion moment, and local dynamic hydrodynamic pressure distribution for the purpose of structural strength evaluation. The wave loads criteria excerpted from IACS and ABS Rules for building and classing steel vessels are shown in the following sections.

2.3.1.1 Vertical Wave-Induced Hull Girder Loads.

Vertical wave bending moment amidships, M_w , and the maximum vertical wave shear forces, F_w , for ocean-going vessels are given in equations (3) and (4), adopted from IACS UR S-11. The vertical wave-induced bending moment, in conjunction with the still-water moment and the rule permissible stress, is used in determining the minimum required section modulus.

$$\begin{aligned} M_w &= -k_1 C_1 L^2 B (C_b + 0.7) \times 10^{-3}, \text{ for sagging moment} \\ &= +k_2 C_1 L^2 B C_b \times 10^{-3}, \text{ for hogging moment} \quad (3) \\ F_w &= +k F_1 C_1 L B (C_b + 0.7) \times 10^{-2}, \text{ for positive shear} \\ &= -k F_2 C_1 L B (C_b + 0.7) \times 10^{-2}, \text{ for negative shear} \quad (4) \end{aligned}$$

where k , k_1 , and k_2 are coefficients specified in the ABS Rules. The vertical wave-induced bending moment has a trapezoidal distribution along the ship length, with the value of M_w in the midship region between $0.4L$ and $0.65L$, and linearly tapers off to zero at the forward and after perpendiculars. F_1 and F_2 in equation (4) are shear force distribution factors along the ship length, which are defined in the Rules. L , B , and C_b are length, breadth, and block coefficient of the ships, respectively. C_1 is the wave coefficient specified in the Rules, and is graphically displayed in Fig. 5. As can be seen from the figure, C_1 shows a gradual upward trend with ship length, leveling off to a constant value at 305 m to 350 m (1000 ft to 1150 ft) and then following a slightly downward trend.

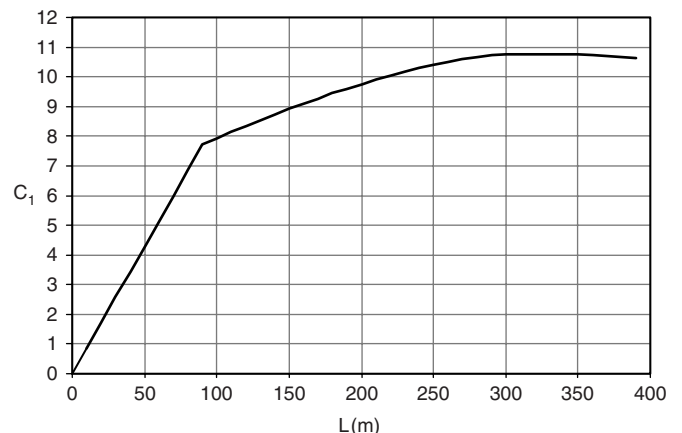


Fig. 5 Wave coefficient C_1 .

The constants in the previous equations are determined based upon extensive data obtained for a large number of ships by a combination of computation, model tests, and full-scale measurement, taking into consideration ship size and response as well as the severity of expected waves over the ship's lifetime. It has been shown (Liu et al. 1981a, 1981b) that the value predicted by the formula of the vertical moment is in fairly close agreement with analytic predictions using North Atlantic waves. It is also in agreement with other long-term estimates of the maximum wave bending moment for ships of average proportions and form having no unusual features of geometry or longitudinal weight distribution. Therefore, the formulas here are useful for preliminary design estimates, before the detailed weight distribution and hull geometry are finalized. In particular, when used with suitable allowable stresses specified in classification rules these formulas provide satisfactory empirically based longitudinal strength standards for conventional ships. Further discussions on their applications can be found in Lamb (2003).

2.3.1.2 Horizontal Wave-Induced Hull Girder Loads. The wave-induced horizontal bending moment, M_H , and horizontal shear force, F_H , given in equations (5) and (6) are derived in a similar manner as for the vertical hull girder loads.

$$M_H = \pm m_h k_3 C_1 L^2 D C_b \times 10^{-3} \quad (5)$$

$$F_H = \pm f_h k C_1 L D (C_b + 0.7) \times 10^{-2} \quad (6)$$

where k and k_3 are coefficients specified in ABS Rules. D is the depth of the ship, and C_1 , L , and C_b are defined in equations (3) and (4). m_h in equation (5) is the moment distribution factor, which is equal to unity in the midship region. The term f_h in equation (6) is the shear force distribution factor, which equals 1.0 at the quarter-length regions of the ship.

The equations here are applicable to vessels of large block coefficient. For small block coefficient and high-powered vessels, the criteria given in equations (5) and (6) are to be adjusted in accordance with ship speed and block coefficient to account for the higher dynamic responses of the ship (as given in the ABS Rules).

2.3.1.3 Wave-Induced Torsion Moment. For vessels with large hatch openings, criteria of torsion moment amidships, T_M , about the effective shear center is specified as follows:

$$T_M = k k_s L B^2 d [(C_w - 0.5)^2 + 0.1] [0.13 - (e/D)(C_0/d)^{1/2}] \quad (7)$$

where k_s , k , and C_0 are tabulated coefficients. e is the vertical distance of the effective shear center of the hull girder within the cargo space from the baseline of the vessel. L , B , D , d , and C_w are the length, beam, depth, draft, and water plane coefficient of the ship, respectively.

2.3.2 Strain and Pressure Measurements on Actual Ships. Full-scale measurements obviously cannot be

used to obtain specific data for new ship designs. Although the results apply only to the specific ships studied, they are of great value in testing probability-based prediction methods described in Sections 2.5, 2.6, and 2.7. Full-scale measurements suffer from a serious drawback in addition to the expense, which is the difficulty in accurately measuring the sea environment to obtain a correlation with the measured loads. Although numerous attempts have been made to develop inexpensive expendable wave buoys or ship-borne wave instruments, a completely satisfactory instrument has not yet been achieved. Therefore, the principal value of full-scale load response (stress or strain) measurements lies in the development of long-term statistical trends of seaway-induced hull loads from measurements carried out over a multiyear period. Because these trends can be related to general long-term climatologic wave data, the problem of wave sensing in the ship's immediate vicinity is of less importance.

Long-term continuous full-scale measurements on ships of various types and sizes have been conducted by several ship classification societies and research organizations, and descriptions of such work may be found in Little and Lewis (1971), Boentgen (1976), Nordenström (1973), and Stambaugh and Wood (1981). These long-term, full-scale measurements are used to verify theoretical predictions, and some of measured data—for example, those by Little and Lewis (1971)—are used as the basis for developing the long-term wave-induced hull girder load prediction being employed at ABS. Full-scale monitoring designed mainly as a decision support for ship maneuvering can also be used to monitor stresses in ships as predicted by numerical calculations. Works in this area can be found in Melitz et al. (1992), Witmer and Lewis (1995), Slaughter et al. (1997), and Brown (1999).

2.3.3 Laboratory Measurement of Loads on Models. In this procedure, a model geometrically and dynamically similar to the ship is equipped with instruments that measure vertical or horizontal shear and bending moment, or torsional moment, amidships and at other sections. This may be accomplished by recording the forces or deflections between several segments produced by transverse cuts through the model. Impact loads can also be determined by recording pressures at several points distributed over the model surface. The experiments are conducted in a towing tank that is equipped to produce either regular or random waves. The most versatile tanks are wide relative to their length, and the model may therefore be tested in oblique as well as head or following seas.

Although in principle, experiments of this type could evaluate the structural loads on a new ship design, this is seldom done because of the time and expense involved. Furthermore, a number of computer programs are now available, based upon procedures described in Section 2.3.4. These offer the possibility of studying a much broader range of sea and load conditions than would be possible in a model test program, and of

doing so at considerably less cost. Hence, the principal use for model testing is to provide verification for such computer techniques.

On the other hand, a number of early experiments were intended to shed light on the fundamental nature of the dynamic wave-induced loads. For example, a model test of a T-2 tanker (Numata 1960) was carried out to investigate the trend of wave-induced lateral (sometimes referred to as horizontal) hull girder bending moment. The measured results show that the lateral longitudinal bending moment amidships can approach or exceed the magnitude of the vertical longitudinal bending moment when running at an oblique heading in regular waves. However, it should be noted that the relatively greater lateral moment may not be an issue causing concern of the structural response to these loads because the horizontal section modulus and moment of inertia of a typical ship are generally larger than the corresponding vertical values.

The T-2 tanker model tests were run at 5.14 m/s (10 knots) vessel speed on courses oblique to waves having an effective length equal to the model length, the wave length being equal to the model length multiplied by the cosine of the wave-to-course angle. A wave height of 1/48 of the model length was used for all wavelengths to avoid excessive model wetness.

It was found that the lateral bending moments were quite sensitive to changes in wave direction and effective wavelength. The bending moment increased approximately linearly as the heading varied from 180° to 120°. The maximum lateral moments for zero and forward speeds are at a wave direction of approximately 135°. The phase lag between the lateral and vertical bending moments was in the region of one quarter-cycle.

The trend of lateral hull girder bending moments identified in the T-2 tanker model tests was also observed in the full-scale measurements of the *Ocean Vulcan* (Admiralty Ship Com. 1953), where lateral longitudinal bending moments of similar magnitude to the vertical moments were present in nearly all wave conditions. The maximum lateral moments occurred at a wave-to-course angle of 110° to 140°. The maximum range of moments was 243.29 MN-m (24,800 t-m, or 80,107 ft-ton) corresponding to a stress range of 38 MPa (2.5 t/in.²), and these moments were frequently in phase with the vertical bending moments.

Experiments have had the principal objective of providing more data with which to test or calibrate theoretical calculation procedures of the type referred to in Section 2.3.4. It is beyond the scope of this section to provide an exhaustive list, but examples of such experiments are given in Lewis (1954), Gerritsma and Beukelman (1964), Kim (1975), Kaplan et al. (1974), and the experiments of the container ship S175 coordinated by ITTC. More recent experiments refer to a series of systematic experiments of the S175 container ship carried out at the U.S. Naval Academy (O'Dea et al. 1992) for determining the nonlinearity in vertical motions and wave

loads. The review of measured wave loads of the S175 container ship and its comparison with analytically predicted results can also be found in ISSC Technical Committee I.2 Reports (2000).

2.3.4 Direct Computation of the Wave-Induced Fluid Load. In this procedure, appropriate hydrodynamic theories used to calculate ship motions in waves are applied to compute the pressure forces caused by the waves and ship motion in response to those waves. When determining the structural loads, the forces resulting from fluid viscosity can usually be neglected in comparison with the pressure forces, except for the case of rolling. The total structural loading at any instant is then the sum of the wave pressure forces, the ship motion-induced pressures, and the reaction loads due to the acceleration of the ship masses.

Note that a preliminary step in the computation of the motion-dependent part of the loads is the solution for the rigid-body motion response of the ship to the wave exciting forces. In this section, only a brief review of available tools of wave load computation is summarized. Detailed discussions on both the analyses of the hydrodynamic forces and the solution for the motion response are referred to Beck et al. (2009).

Presently available wave load computer codes of practical design application are developed with different levels of approximation, and are of one or several categories listed in the following—which are not related to their degree of sophistication:

- Frequency linear strip theory method based on two-dimensional potential flow theory
- Frequency linear three-dimensional theory based on potential flow boundary element method
- Frequency quadratic strip theory method, which consists of a perturbation method of potential flow theory expanded up to the second-order terms for the wave theory, the nonlinearity of restoring forces due to non-vertical ship sides, and the hydrodynamic forces
- Time domain strip theory method, where the hydrodynamic problem is handled according to linear theory but the hydrostatic and Froude-Krylov wave forces are included up to the incident wave surface
- Time domain three-dimensional potential flow boundary element method, where the hydrodynamic problem is handled according to linear theory but the hydrostatic and Froude-Krylov wave forces are accounted for either up to the mean water line (i.e., three-dimensional time-domain linear) or up to the incident wave surface (i.e., three-dimensional time-domain moderately nonlinear)
- Time domain three-dimensional nonlinear theory approach, which satisfies the body boundary condition exactly on the portion of the instantaneous body surface below the incident wave. It is assumed that both the radiation and diffraction are small compared to the incident wave so that the free surface boundary conditions can be linearized with respect to the incident wave surface,

whereas the hydrostatic and Froude-Krylov wave forces are included up to the incident wave surface. This approach solves a three-dimensional time-domain potential flow termed “body-nonlinear” problem.

The computer codes based on the different methods described previously are developed for specific purposes. However, those based on traditional frequency linear strip theory continue being widely used by the industry in computing linear transfer functions and short-term and long-term extreme values of ship responses, due to its simplicity and efficient computation. Wave loads obtained from linear strip theory are used to develop the “nominal” loads for structural design and strength evaluation. Linear strip theory programs are used for both routine design investigation and special studies of unusual loading situations that fall outside the range of the semi-empirical criteria of traditional classification rules. Examples of such programs are described in Raff (1972), Salvesen, Tuck, and Faltinsen (1970), and Meyers, Sheridan, and Salvesen (1975).

Although the methods employed in computing the hydrodynamic coefficients and wave excitation are not exactly the same among various codes, the results are comparable for specific wave environments. For example, Guedes Soares (1999) investigates the uncertainties of the long-term extreme value of vertical bending moments based on linear strip theory data of the S175 containership calculated by twelve organizations, consisting of seven classification societies, three research institutes, and two universities. His study indicates that the uncertainties due to the variations of computed response transfer functions and that due to various long-term extreme value prediction methods are comparable, which is 6 to 7 percent at the probability level of 10^{-8} . However, using different wave scatter diagrams such as IACS, Hogben and Lamb, Walden, DTNSRDC, and BMT global wave statistics, the uncertainty of the 10^{-8} characteristic value of vertical bending moment amidships could be as high as 14 percent. This indicates that the variation of wave data is far more sensitive than any other factors involved in computing wave loads by linear strip methods.

Computer programs based on three-dimensional frequency linear ship motion theory are also used by the industry to calculate wave pressure forces for input into finite element structural analysis, where the accurate distribution—particularly at the two ends of the hull—is of importance. The three-dimensional linear program models the hull form using a number of three-dimensional panels, and the hydrodynamic problem is solved employing a three-dimensional source or dipole distribution, satisfying the linearized free surface condition and the body boundary condition on the wetted surface below the mean water line. A number of three-dimensional frequency linear programs are available for practical application. One of such programs is the computer suite PRECAL, developed by an industry group, namely, the Netherlands Ship Model Basin Cooperative

Research Ships (NSMB CRS). This industry group consists of some 20 members, including classification societies, navies, ship operators, and research institutes, engaging in long-term research and development of ships.

The computer program PRECAL (“PREssure CALculation”) was developed for the purpose of computing the hydrodynamic pressure on the wetted surface of a ship moving in regular waves for input into a finite element structural model of mono-hull vessel (see Chen et al. 1988). This program handles the three-dimensional boundary value problems for radiation and diffraction using the three-dimensional forward speed Green’s function, and an approach similar to that of Inglis and Price (1982). This program also provides an approximate method where the zero speed Green’s function is evaluated and the motion of the vessel at forward speed is determined by incorporating the speed effect in the calculation of the velocity potential and hydrodynamic pressure. Correlation shows that pressure measurements of a fast cargo vessel are in reasonable agreement with calculated results from PRECAL and traditional frequency linear strip theory for points forward of midship section. At the aft end of the vessel, PRECAL seems to have values greater than linear strip theory, as exemplified in Fig. 6 (from Brook 1989), except at the irregular frequency, which has been eliminated in a later version of the program by incorporating the pressure relief scheme. Recent correlation of PRECAL with measured data of high-speed vessels can be found in Bruzzone et al. (2001).

Time domain nonlinear codes are used in determining loads for strength evaluation of special cases. Examples for methods of time domain strip theory can be found in Chen and Shen (1990), Watanabe et al. (1989), Fonseca and Guedes Soares (1998), and Xia et al. (1998). Time domain three-dimensional nonlinear theory methods can be found in the Large Amplitude Motions Program, LAMP (Lin et al. 1994; Lin & Yue 1993) and the Ship Wave Analysis, SWAN (Sclavounos 1996; Sclavounos et al. 1997). Most of the time domain codes are still in the research stage. These programs handle the vertical motions and wave loads quite well, but much work is still needed to properly handle motions and wave loads in the lateral plane of motion. As indicated by Shin (2000), one of the difficulties in the three-dimensional time domain approach is to obtain a convergent numerical solution for the case of oblique sea condition. Unlike the vertical plane of motion where strong restoring forces and moments exist from heave and pitch motions, the lack of restoring and constant drift motion in the lateral plane of motion cause numerical instability.

The direct numerical computation of hull girder and pressure loads for hull structure design and evaluation involves procedures for selecting loading conditions, determining the *dominant load parameter* (DLP), and establishing the structural analysis load cases for which the structural analyses are to be performed. First, a range of cargo loading conditions should be considered for the load cases, including the full load condition, the light

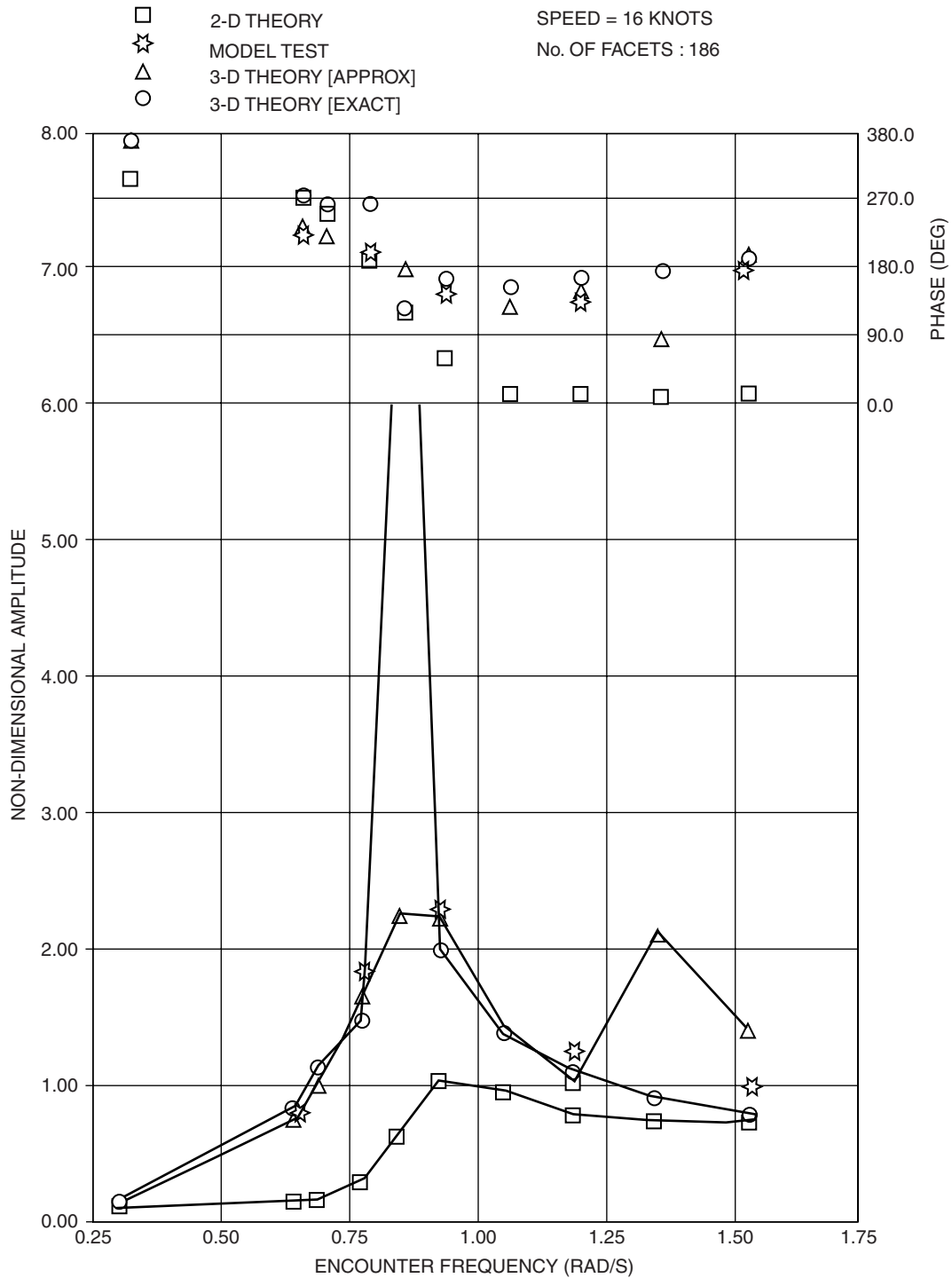


Fig. 6 Correlation for total pressure at a point on the aft end of a fast cargo ship with a speed of 8.23 m/s (16 knots) in head seas. (Brook, A. K. (1989), Hull Girder Loads Project – Summary Report, BMT Report 289088.R01, prepared for NSMB CRS)

draft ballast condition, and several partial cargo loading conditions in between these extremes. The loading conditions are to be so selected that they cover all the critical cases for the concerned structural components. The DLP

can be a global load effect, a global motion of the vessel, or a local dynamic response, such as vertical acceleration, lateral acceleration, rolling motion, or vertical hull girder bending moment. DLPs are determined based on

the responses of specific structural components critical to its strength evaluation. When used in structural analysis for the load cases described following, DLP is to be maximized up to its extreme value obtained from the short-term and long-term predictions discussed in Sections 2.6 and 2.7.

The structural analysis load case is an appropriate wave system that when the vessel is imposed in the system, the wave loads together with the corresponding inertial loads will result in a DLP maximized to its extreme value described previously. If both ship motions and waves are linear, the wave system considered in the load case is characterized by an equivalent regular wave amplitude, length, direction, and wave crest position. The application of such a system is considered in Section 3.16. For nonlinear motions and wave loads, analyses generally rely on time domain simulations, which are considered in Section 2.5. For all structural analysis load cases established, the global finite element hull structural analysis, followed by the local structural analysis, are performed for the evaluation of structural adequacy in both global as well as local levels. Effects of impact load on hull girder strength may be considered together with hull girder loads. However, strength of local structure subject to impact loads, such as bow flare impact and bottom slamming in container ships, is usually treated separately (see Shi et al. 2005).

2.4 Deterministic Evaluation of Wave-Induced Loading.

The calculation of the bending moment, shear force, and torsional loading on a ship hull in waves requires a knowledge of the time-varying distribution of fluid forces over the wetted surface of the hull together with the distribution of the inertial reaction loads. The fluid loads depend on the wave-induced motions of the water and the corresponding motions of the ship. The inertial loads are equal to the product of the local mass of the ship and the local absolute acceleration. The shear force and bending moment are then obtained at any instant by evaluating the first and second integrals of the longitudinally distributed net vertical or horizontal force per unit length. The expressions for these integrals are similar to those used in the calm water case, equations (1) and (2), with the buoyancy term replaced by the time-varying fluid force per unit length and the weight term replaced by the inertial reaction force per unit length. The results obtained are then added to the calm water values.

As previously noted, the computation of the inertial loads and a part of the fluid loads require that the wave-induced motions of the ship first be determined. The solution for these ship motions and the system of fluid loading is most frequently accomplished using a procedure based on the so-called strip theory. The details of strip theory, including the underlying assumptions and the limitations of the results, are developed in detail in Beck et al. (2009). This procedure has been implemented in several computer program examples, which are described by Raff (1972), Salvesen, Tuck, and Faltinsen (1970), and Meyers, Sherida, and Salvesen (1975).

Strip theory programs are now commonly used by design firms, classification societies, and government agencies for both routine design investigations of ship wave loading and for the investigation of unusual loading situations that fall outside the range of the simplified formulas and procedures.

The results predicted by strip theory appear to be in good agreement with experiments for the vertical motions of pitch and heave, but a somewhat lower degree of correlation is usually observed for the lateral motions of sway, roll, and yaw. Corresponding to these motion predictions, the vertical loads, shears, and bending moments are predicted somewhat more accurately than the horizontal and torsional loads, shears, and moments. It may be expected that ongoing research in ship hydrodynamics will result in continuing improvements in the capabilities of such programs.

The reader may refer to Beck et al. (2009) for details of the strip theory as applied to the more general aspects of ship motion computations. To summarize the principal features of the strip theory as it is applied to the prediction of the structural loading of a ship, it is meaningful to consider only the vertical load components that act on a ship proceeding into regular head seas, as illustrated in Fig. 7. As a result of symmetry about the longitudinal vertical plane of ship and waves, the motions and loads will have components only in this plane. At any instant of time, the motions of the ship will consist of the time-varying motions of pitch, heave, and surge superimposed on a mean ward velocity, U_o .

One of the important assumptions of linear theory is that both the wave and ship motion amplitudes are, in some sense, small. As a result, it is possible to consider the total instantaneous vertical force on a thin transverse strip or element of length, dx , to be composed of the sum of several terms that are computed independently of each other. Two of the elementary forces are the still water buoyancy and weight of the element of the ship length. These are the same forces that appear in equations (1) and (2) for the still water loads, shear, and bending moment, and it is not necessary to consider them here. The remaining time-varying forces result from inertial reactions and from the water pressures that are associated with the waves and the wave-induced motions of the ship. Viscous forces, which are found to be relatively unimportant (except for roll damping), are ignored when computing the vertical loads. Within this framework, the vertical fluid forces on the various elements can be subdivided into five categories as follows, all expressed in force units:

(a) A wave pressure force component computed as though the presence of the ship does not disturb either the incident waves or the dynamic pressure distribution in those waves. This is called the *Froude-Krylov force*.

(b) A wave pressure force component computed from the properties of the diffracted wave system. These waves result from the reflection and distortion of the

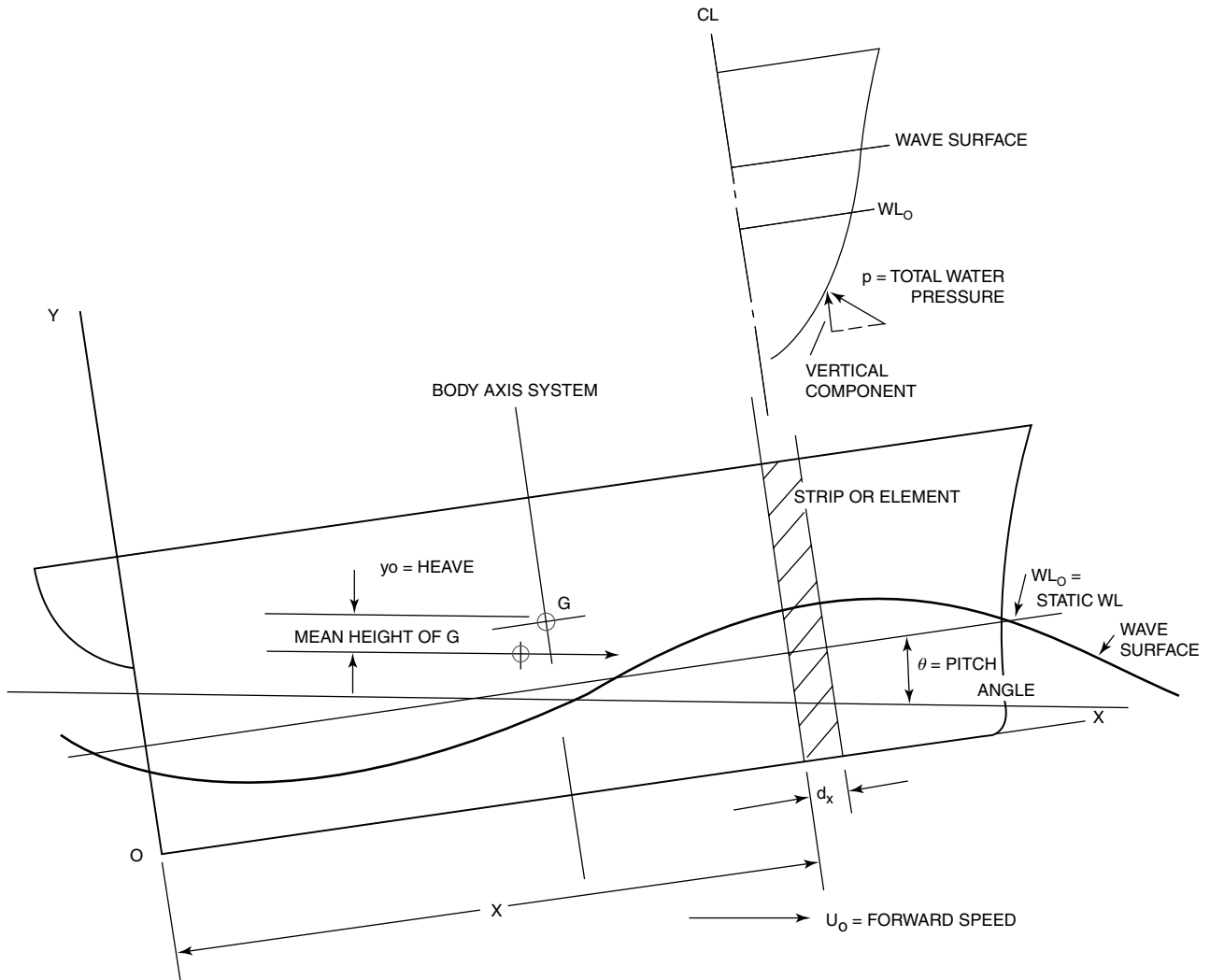


Fig. 7 Nomenclature for strip-wise force computations.

incident waves when they impinge upon the ship. This force represents a correction to the Froude-Krylov force for the disturbance introduced into the wave system by the presence of the ship.

(c) A term proportional to the instantaneous vertical displacement of the element of the ship from its mean position, as if in calm water. This is called the *hydrostatic restoring force* and is equal to the change in the mean static buoyancy of the element.

(d) A term proportional to the instantaneous vertical velocity of the element called a *damping force*.

(e) A term proportional to the instantaneous vertical acceleration of the element. This is called an *added mass force*.

When added together, the first two of these forces comprise the total wave-induced exciting force, computed as though the ship moves steadily forward through the waves but experiences no oscillatory motion re-

sponse to the wave forces. The last three forces are computed as though the ship is undergoing its oscillatory wave-induced motion while moving at steady forward speed through calm water.

In addition to forces (a) through (e), there must be added the inertial reaction force of that portion of the mass (weight/g) of the ship that is contained in the strip, dx . If the ship's mass per unit length is denoted by $m(x)$, this reaction force is given, according to D'Alembert's principle, by $-m(x)a_y dx$, where a_y is the component of the absolute acceleration of the section at x in the direction parallel to the ship y -axis. If we now denote the sum of the five component fluid forces acting on the strip, dx , as $f(x)dx$, then the total force at any instant is the sum of the fluid forces and the inertial reaction, denoted $q(x)dx$, given by

$$q(x)dx = [f(x) - m(x)a_y]dx \quad (8)$$

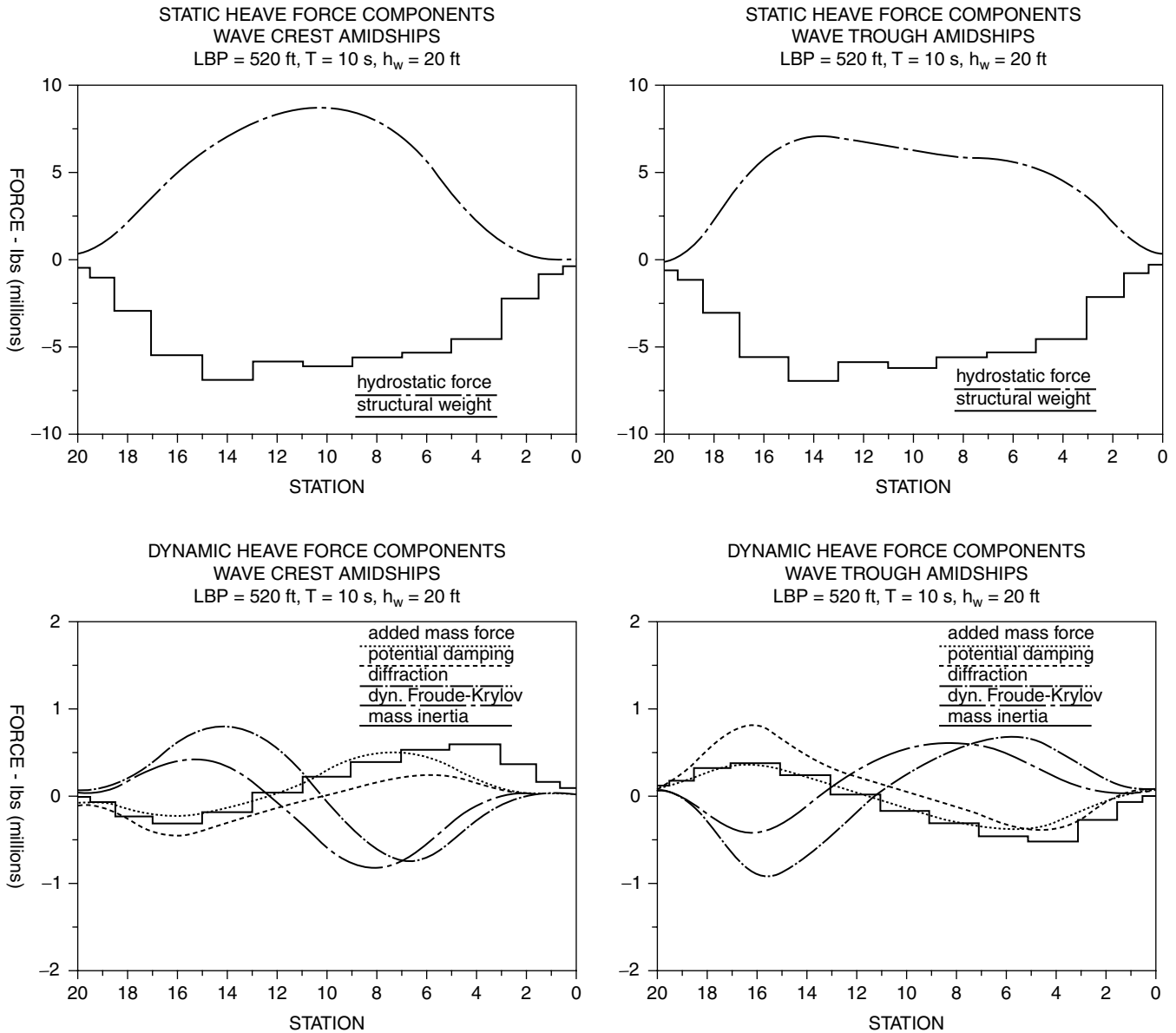


Fig. 8 Components of load distribution for unit wave amplitude.

At any instant of time, the shear force, $V(x_1)$, at a section whose x -coordinate is x_1 , is obtained by integrating $q(x)$ from the end of the ship, $x = 0$, up to the station where $x = x_1$. The bending moment at x_1 is obtained, in turn, by integrating the shear force, $V(x)$, from $x = 0$ to $x = x_1$:

$$V(x_1) = \int_0^{x_1} q(x) dx \quad (9)$$

$$M(x_1) = \int_0^{x_1} V(x) dx \quad (10)$$

Figure 8 illustrates the different components of the load distribution at a fixed time for a sample ship moving in a simple sinusoidal wave of unit amplitude. In this figure, the total loading consists of a number of terms of similar magnitude, which may differ in sign and phase. There may be cancellation or reinforcement among the different components, with the result that the total loading may be larger or smaller than any individual component. This cancellation or reinforcement varies along the ship length and with the frequency of wave encounters.

In the foregoing discussion of force applied on a ship section, a procedure is described in which the total force is subdivided into several components, each of which

can be computed independently of the others. Consequently, because of the assumed linearity underlying strip theory, it is possible to calculate shear and bending moments in regular waves of any desired amplitude and frequency. Most ship motion programs contain a module to perform this computation at oblique headings to the waves as well as the head sea case.

It is shown in Beck et al. (2009) that the component regular wave forces depend on the wave frequency, hull shape, ship speed, and heading. The hydrodynamic coefficients of damping and added mass depend upon the hull shape, the ship speed, and wave encounter frequencies. The wave forces act on the ship at a frequency equal to the encounter frequency and, as a consequence of the linear representation of the ship motion response, the motions and motion-related loads will occur at this same frequency. In general, each motion or load response variable can be divided into a component that is in phase with the encountered waves and a component out of phase with the waves. Therefore, the structural load components $q(x)$, $V(x)$, and $M(x)$ at a specific location, x , along the ship length are sinusoidal varying quantities whose frequency equals the frequency of wave encounter and whose amplitude and phase vary with frequency.

When considering a ship traveling through a realistic, irregular seaway, it is fortunate that linearity approximately applies in the description of the seaway. As shown in Beck et al. (2009) the seaway can be broken down into a theoretically infinite number of wave components of various amplitudes, frequencies (lengths), and directions. Because of the linearity assumption, the load responses of the ship to any regular wave component can be assumed directly proportional to the amplitude of that wave. The response of the ship to the random sea can be computed by linear superposition of the responses to the various seaway components present. As a result, the computations of the force, motion, and loading components are initially performed for a series of elementary regular wave components each of unit wave amplitude and having a frequency equal to one of the components of the random seaway. The resulting unit responses are then weighted by the actual component wave amplitudes and added together to obtain the corresponding response spectrum in the real random seaway. This process of linear superposition forms the basis of virtually all computations of ship responses to real random seaways, and the details may be found in Beck et al. (2009), including an example of bending moments. Results are in the form of root mean square (RMS) values of shear and bending moments, from which various short-term statistical properties of the response can be derived, as discussed in the next Sections 2.5 and 2.6. Extensions of the computation of the extreme loadings expected during the ship's lifetime are discussed in Section 2.7.

If during its lifetime the ship operates at several different conditions of load distribution and draft, there will be a different set of the functions $q(x)$, $V(x)$, and

$M(x)$ associated with each loading. For the naval architect to design for the most severe structural loading that the ship will experience during its operating lifetime, the strip theory computations must be carried out for the full range of frequencies, wave heights, and wave headings expected to be encountered. These computations must be repeated for all the combinations of speed and loading conditions in which the ship will operate. Many of the available computer programs contain the means to perform these multiple computations easily and efficiently. The more sophisticated calculations also contain provisions performing the superposition that yields the response to random seas together with the probabilistic analysis.

2.5 Probabilistic Analysis of Wave-Induced Loads in Random Seas. Prior to estimating the loads acting on ships or marine structures, a statistical representation of the environment is necessary. This includes waves, ice, wind, seismic events, and currents. The last three items are more important for fixed offshore structures than for floating vessels. Ice loads can be important for ships. About 30 percent of tankers have ice strengthening. The environmental information can then be used as input to determine the loads acting on the structure. Typically, an input/output spectral analysis procedure is used to determine the "short-term" loads in a specific sea condition (stationary condition). The required transfer function is determined either from strip theory and the equations of motion of the vessel or from a towing tank experiment. In the analysis of offshore structures, Morison's equation is usually used to determine the wave load transfer function.

Short-term prediction of the loads is not sufficient for a design. Extreme values and long-term prediction of the maximum loads and their statistics are more valuable. For this purpose, order statistics and statistics of extremes play a very important role throughout the design analysis. Gumbel's theory of asymptotic distributions is often used in this regard. In the long-term prediction, the fatigue loads (i.e., the cyclic repetitive loads that cause cumulative damage to the structure) must also be considered. Methods that combine loads such as static and dynamic, including high- and low-frequency loads, must be considered. In nature, many of these loads act simultaneously; therefore, their combination must be evaluated.

2.5.1 Probabilistic Representation of Random Seas. The sea surface is irregular and never repeats itself. An exact mathematical representation of it as a function of such variables as time, wind speed, wind direction and current is not possible. However, a representation using a probabilistic model is possible and more suitable. By means of the theory of random processes, one may represent the sea surface and determine certain statistical averages and extreme values, which may be suitable for design.

Such a probabilistic representation of a random phenomenon has been well developed in electrical engineering to analyze random noise (Rice 1944, 1954) and was

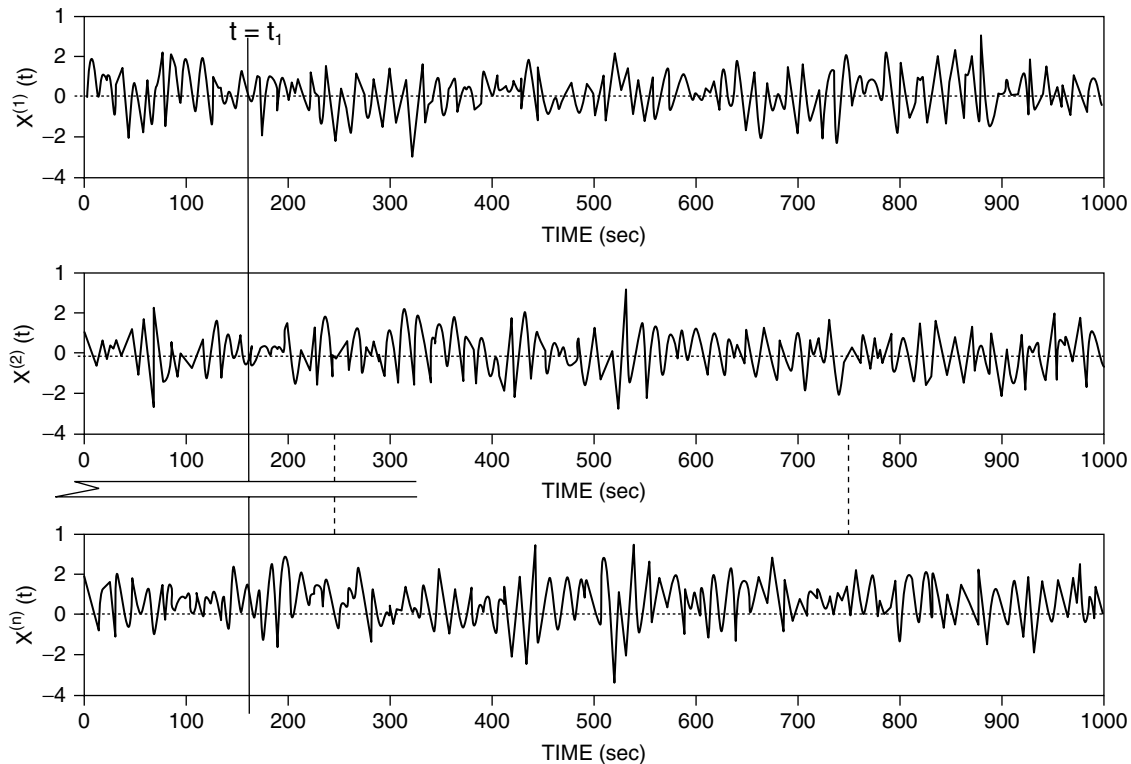


Fig. 9 Time history of wave record—ensemble of sample function.

used successfully in mechanical engineering to investigate random vibration (Crandall & Mark 1963). It has also been used in civil engineering for earthquake analysis. In the following paragraphs, a few definitions related to random processes and the associated probability distributions are discussed.

As an example of a random process, consider a test to determine the wave elevation as a function of time at a given location in the ocean. The top sample in Fig. 9, is a record of the wave elevation for a period of approximately 18 min. If the test is repeated several times under the same conditions as far as possible, the records obtained will not be identical (see Fig. 9). This randomness in the records is due to factors beyond one's control and ability to measure. The elevation of the water surface at any time is due to the entire history of the meteorological conditions in that area and surrounding areas. Therefore, under the given macroscopic parameters such as wind direction, speed and duration, one cannot exactly predict the wave elevation at the given point. The wave elevation records can be treated as records of a random process. Another example of a random process is an ensemble of time history records of a strain gage installed in a ferryboat operating between, say, San Francisco and San Rafael. If several records are obtained between these two neighboring cities under the same conditions, the resulting ensemble of records can be treated as records of a random process.

As discussed previously, the most important notion involved in the concept of a random process $X^{(i)}(t)$ is that not just one time history is described but the whole family of ensemble of possible time histories that might have been the outcome of the same test is described. Some of these samples are more probable than others and to describe the random process further, it is necessary to give probability information. Random samples can be characterized by some average amplitude (RMS) and decomposition in frequency (spectral density), as will be discussed later. This is similar to characterizing a sinusoid in a deterministic process by its amplitude and frequency (phase is not important in many cases).

If an ensemble of wave records such as the one shown in Fig. 9 is given, a designer may select the largest value in the ensemble and use it, with a factor of safety, for the new design. The designer will make no use of all the information given except for one specific value (i.e., the maximum value). Alternatively, the designer may try to obtain statistical information from all the records and use such information in the new design. In this case, a probability description of the random process is necessary. This is usually done through a probability density function (PDF), $f(x)$, that describes the probability of occurrence of different ranges of wave elevation at an instant of time, $t = t_1$ (see Fig. 9). A more accurate representation can be made by using a joint probability density function $f(x_1, x_2)$ (referred to as JPDP in later

sections) of the wave elevation at two instants of time t_1 and t_2 .

Ensemble averages of ocean waves are defined as follows. The expected value of a given function $g(x)$ is defined as

$$E[g(x)] = \text{expected value of } g(x) = \int_{-\infty}^{+\infty} g(x)f(x)dx$$

If $g(x) = x$, then

$$E[x] = \int_{-\infty}^{+\infty} xf(x)dx = \text{mean or ensemble average} \quad (11)$$

For ocean waves, the mean is usually close to zero. When $g(x) = x^2$, then

$$E[x^2] = \int_{-\infty}^{+\infty} x^2 f(x)dx = \text{mean square of the} \quad (12)$$

wave elevation

$$\text{Root mean square (RMS)} = \sqrt{E[x^2]}$$

Setting $g(x) = (x - E[x])^2$,

$$\begin{aligned} \sigma^2 &= E(x - E[x])^2 = \int_{-\infty}^{+\infty} (x - E[x])^2 f(x)dx \\ &= E[x^2] - (E[x])^2 = \text{variance of the wave elevation} \end{aligned} \quad (13)$$

$\sigma = \sqrt{\sigma^2}$ = standard deviation of the wave elevation

At two fixed values, t_1 and t_2 , let x_1 and x_2 denote $x(t_1)$ and $x(t_2)$, respectively; then the autocorrelation and covariance functions are defined, respectively, by

$$\begin{aligned} E[x_1, x_2] &= \int_{-\infty}^{+\infty} \int_{-\infty}^{+\infty} x_1 x_2 f(x_1, x_2) dx_1 dx_2 \quad (14) \\ \mu_{x_1 x_2} &= E\{(x_1 - E[x_1])[x_2 - E[x_2]]\} \\ &= \int_{-\infty}^{+\infty} \int_{-\infty}^{+\infty} [x_1 - E[x_1]][x_2 - E[x_2]] f(x_1, x_2) dx_1 dx_2 \\ &= E[x_1 x_2] - E[x_1]E[x_2] \end{aligned} \quad (15)$$

It should be noted that the covariance is equal to the autocorrelation minus the product of the means. Therefore, if one of the means is zero, the covariance is equal to the autocorrelation. The correlation coefficient $\rho_{x_1 x_2}$ can be defined as

$$\rho_{x_1 x_2} = \frac{\mu_{x_1 x_2}}{\sigma_{x_1} \sigma_{x_2}} \quad (16)$$

that is, a non-dimensional covariance.

The two random variables x_1 and x_2 are said to be independent if:

$$f(x_1, x_2) = f(x_1)f(x_2)$$

Therefore, from the definition of the autocorrelation function, it is easy to show in this case that

$$E[x_1, x_2] = E[x_1]E[x_2]$$

and thus, both the correlation coefficient $\rho_{x_1 x_2}$ and the covariance $\mu_{x_1 x_2}$ are zero. This means that independent random variables must necessarily be also uncorrelated (the converse is not necessarily true). Note that when $t_2 = t_1$, the covariance becomes equal to the variance and the autocorrelation becomes equal to the mean square.

Random ocean waves are usually considered a stationary random process over a short period (less than three hours). A random process is said to be stationary if its distributions are invariant under a shift of time scale, that is, independent of the origin. This implies that the first-order PDF $f(x)$ becomes a general distribution independent of time, and the mean (usually taken to be zero) and variance of the wave elevation are also constants independent of time. In addition, the second-order PDF does not change under translation of time scales; therefore, it must be a function of the lag between t_1 and t_2 and not of each individually. This implies that the autocorrelation function is also a function of $\tau = t_2 - t_1$ only:

$$E[x_1, x_2] = E[x(t)x(t + \tau)] = R(\tau) \quad (17)$$

$E[x_1, x_2]$ is the expected value of the product of the wave elevations at two instants of time, $x(t_1)$ and $x(t_2)$, and $R(\tau)$ denotes the autocorrelation function of a stationary random process. Note that $R(0) = E[x^2(t)]$ = mean square of the process.

$R(\tau)$ is an important function because it correlates the wave elevation at any instant of time with its past (or future). $R(\tau)$ has the following properties (see Fig. 10):

- (i) $R(0) = E[x^2]$ = mean square of the process
- (ii) $R(+\tau) = R(-\tau)$, i.e., an even function of τ
- (iii) $R(0) \geq |R(\tau)|$

If changes in the statistical properties of a random process occur slowly with time, then it is possible to

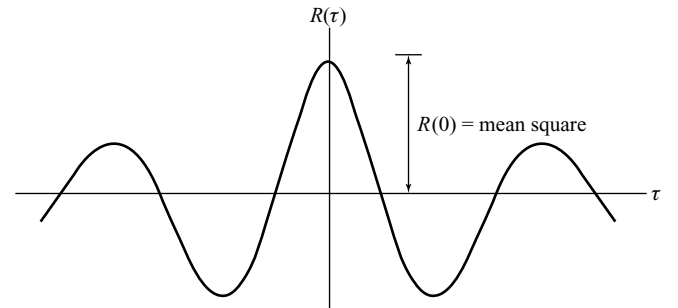


Fig. 10 Autocorrelation function.

subdivide the process into several processes of shorter duration, each of which may be considered stationary. It is usual to represent ocean waves as a stationary random process over a period of up to three hours.

The ergodic hypothesis states that a single sample function is typical of all other sample functions; therefore, one can estimate various statistics of interest by averaging over time instead of over the ensemble. If $f(t)$ represents such a sample function, then the following temporal averages can be determined. The temporal mean is

$$\langle f \rangle = \lim_{T \rightarrow \infty} \frac{1}{T} \int_{-T/2}^{+T/2} f(t) dt \quad (18)$$

The temporal autocorrelation function $\phi < \tau >$ is

$$\phi < \tau \rangle = \lim_{T \rightarrow \infty} \frac{1}{T} \int_{-T/2}^{+T/2} f(t) f(t + \tau) dt \quad (19)$$

The temporal mean square is

$$\langle f^2 \rangle = \lim_{T \rightarrow \infty} \frac{1}{T} \int_{-T/2}^{+T/2} f^2(t) dt \quad (20)$$

In equations (18) to (20), the period T over which the functions are averaged must be long (theoretically T should approach infinity). An ergodic process implies that $E[x] = \langle f \rangle$ and $R(\tau) = \phi < \tau \rangle$. An ergodic process is necessarily stationary because $\langle f \rangle$ is a constant whereas $E[x]$ is generally a function of the time $t = t_1$, at which the ensemble average is performed except in the case of a stationary process. However, a random process can be stationary without being ergodic. For ocean waves, it may be necessary to assume the ergodic hypothesis if there is only one sample function.

In many problems, it is customary to conduct a Fourier analysis of periodic functions. This simplifies the problem because linearity permits superposition of the Fourier component to obtain the total response. Similarly, a frequency decomposition of the autocorrelation function $R(\tau)$ of the ocean waves can be made:

$$R(\tau) = \int_{-\infty}^{+\infty} S_i(\omega) e^{i\omega\tau} d\omega \quad -\infty < \tau < \infty \quad (21)$$

where $S_i(\omega)$ is essentially the Fourier transform of $R(\tau)$ (except for the factor 2π) given by

$$S_i(\omega) = \frac{1}{2\pi} \int_{-\infty}^{+\infty} R(\tau) e^{-i\omega\tau} d\tau \quad -\infty < \omega < \infty \quad (22)$$

Relations (21) and (22) are known as Wiener-Khinchine relations. It can be shown that $S_i(\omega)$ is a non-negative even function of ω . A physical meaning can

be given to $S_i(\omega)$ by considering the limiting case when $\tau = 0$:

$$R(0) = \text{mean square} = E[x^2] = \int_{-\infty}^{+\infty} S_i(\omega) d\omega$$

that is, the mean square of the process equals the sum over all frequencies of $S_i(\omega) d\omega$, so that $S_i(\omega)$ can be interpreted as a mean square spectral density. The mean square (area under the spectral density curve) is the average of the square of the wave elevation, and the RMS is the square root of that value. Physically, the larger the mean square, the larger the wave elevation and the higher the sea state.

Because the spectral density is an important function in ocean waves, the following remarks are made:

- The units of ocean waves' spectral density are $\text{m}^2\text{-sec}$ or $\text{ft}^2\text{-sec}$ because

$$R(0) = E[x^2] = \int_{-\infty}^{+\infty} S_i(\omega) d\omega; [\text{m}^2 \text{ or } \text{ft}^2]; \text{ therefore} \quad (23)$$

$$S_i(\omega) = [L^2]/\text{unit of frequency}$$

- From the properties of a Fourier transform, it can be shown that $S_i(\omega)$ is a real and even function of ω .
- In practice, the negative frequency obviously has no significance. Because of the shape of $S_i(\omega)$, it is called a two-sided spectrum.
- In practice, a "one-sided spectrum" can be defined by simply folding the $S_i(\omega)$ curve about the $\omega = 0$ axis, that is,

$$\int_{-\infty}^{+\infty} S_i(\omega) d\omega = \int_0^{\infty} 2S_i(\omega) d\omega = \int_0^{\infty} S(\omega) d\omega$$

= mean square of the process

where

$$S(\omega) = \text{one-sided spectrum} = 2S_i(\omega) \text{ when } \omega \geq 0$$

$$= 0 \text{ when } \omega < 0$$

A sketch of $S(\omega)$ is shown in Fig. 11.

- It can be shown that the area under the ocean waves' spectral density—that is, the mean square—is proportional to the total energy per unit area of the waves' surface, which is given by

Total energy per unit area of the waves' surface is

$$\rho g \int_0^{\infty} S(\omega) d\omega$$

For this reason, $S(\omega)$ is sometimes called the energy spectrum. The energy in an increment $\delta\omega$ of wave frequencies at a central frequency ω_o is

$$\rho g S(\omega_o) \delta\omega \quad (24)$$

From simple gravity waves, the total energy (deep water), which is composed of half kinetic energy and half

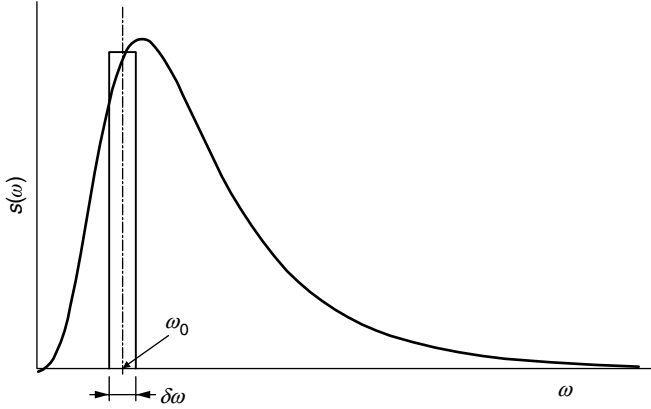


Fig. 11 Spectral density of a stationary random process.

potential energy, is

$$\text{Energy per unit area} = \frac{1}{2} \rho g \zeta_a^2,$$

where ζ_a is the wave amplitude.

It follows that the square of the amplitude of a wave having the same energy as all the wave components in the band of frequencies represented by $\delta\omega$ is

$$\frac{1}{2} \rho g \zeta_a^2 = \rho g \cdot S(\omega_0) \cdot \delta\omega$$

therefore,

$$\zeta_a^2 = 2S(\omega_0)\delta\omega \quad (25)$$

which is double the incremental area under the $S(\omega)$ curve. It should be noted that both the spectral density and the autocorrelation function are measurable quantities that can be determined from time history records of ocean waves.

Ocean waves are usually represented as a narrow band random process. A random process is said to be a narrow band process if $S(\omega)$ has significant values only in a band or range of frequencies whose width is small compared with the magnitude of the center frequency of the band ω_0 . This is to be distinguished from a wide band process, where $S(\omega)$ has significant values over a wide range of frequencies and the corresponding time history contains several local peaks between zero crossings.

The rate of wave amplitude crossing a certain level or a threshold is an important information in design. Similarly, the probability distribution of the wave peaks can be useful in estimating probabilities of exceedance of specified wave heights in a given sea state. Because of their importance, both of these statistics are discussed in the following paragraphs.

The problem of crossing a threshold was examined extensively by Rice (1944, 1954). Consider a random process $x^{(i)}(t)$ representing wave elevation. The process has a zero mean, that is, $E[x] = 0$. The mean rate of crossing

a given level, a , denoted by v_a^+ with positive slope (from below) was derived by Rice (1954) as

$$v_a^+(t) = \int_0^\infty \dot{x} f_{x,\dot{x}}(a, \dot{x}, t) d\dot{x} \quad (26)$$

where

$$\dot{x} = \frac{dx}{dt} \text{ and } f_{x,\dot{x}}(\cdot, \cdot, \cdot) \text{ is the JPDF of } x \text{ and } \dot{x}$$

Similarly, the mean rate of crossing (defined as the average number of crossings per unit time) with a negative slope (from above) is

$$v_a^-(t) = \int_{-\infty}^0 |\dot{x}| f_{x,\dot{x}}(a, \dot{x}, t) d\dot{x} \quad (27)$$

If the threshold level a is zero, the corresponding mean rate of crossing (from above and below) is

$$v_0(t) = \int_{-\infty}^\infty |\dot{x}| f_{x,\dot{x}}(0, \dot{x}, t) d\dot{x} \quad (28)$$

If the process is stationary and narrow band, then v_0^+ or v_0^- is the apparent (mean) frequency of the process and from the stationary property, they are constant (i.e., independent of time).

For a narrow band random process (e.g., ocean waves) every zero crossing from below is followed by a positive peak (crest), and every zero crossing from above is followed by a negative peak (trough). Therefore, the proportion of the positive zero crossings that also cross the level a with a positive slope represents the probability that the positive peak is larger than a , that is,

$$P[p > a] = 1 - P[p \leq a] = 1 - F_p(a) = \frac{v_a^+}{v_0^+} \quad (29)$$

where $F_p(a)$ is the cumulative distribution function (CDF) of the peak values. The corresponding PDF $f_p(a)$ is obtained as

$$f_p(a) = \frac{dF_p(a)}{da} = -\frac{1}{v_0^+} \frac{dv_a^+}{da} \quad (30)$$

As will be discussed later, ocean waves can be considered as a stationary narrow band Gaussian process with a zero mean. It can be shown that for such a process, the slope and magnitude are statistically independent (i.e., the slope is independent of the magnitude). Therefore, the JPDF is given by

$$f_{x,\dot{x}}(x, \dot{x}) = f_x(x) f_{\dot{x}}(\dot{x}) = \frac{1}{2\pi\sigma_x\sigma_{\dot{x}}} e^{-\frac{1}{2}\left(\frac{x^2}{\sigma_x^2} + \frac{\dot{x}^2}{\sigma_{\dot{x}}^2}\right)} \quad (31)$$

where the individual variances are given in terms of the wave spectral density $S(\omega)$ by

$$\sigma_x^2 = \int_0^{\infty} S(\omega) d\omega \quad (32)$$

$$\sigma_{\dot{x}}^2 = \int_0^{\infty} \omega^2 S(\omega) d\omega \quad (33)$$

Thus, from equations (26) and (31) the mean rate of positive crossing of an amplitude of level a is

$$v_a^+ = \frac{1}{2\pi} \frac{\sigma_{\dot{x}}}{\sigma_x} e^{-\frac{1}{2} \left(\frac{a}{\sigma_x} \right)^2} \quad (34)$$

Due to symmetry of the Gaussian process about zero,

$$v_a = \frac{1}{\pi} \frac{\sigma_{\dot{x}}}{\sigma_x} e^{-\frac{1}{2} \left(\frac{a}{\sigma_x} \right)^2} \quad (35)$$

and

$$v_o^+ = v_o^- = \frac{1}{2\pi} \frac{\sigma_{\dot{x}}}{\sigma_x} \quad (36)$$

Since a wave spectral density is a relatively narrow-banded spectrum, its apparent (mean) circular frequency ω_e is

$$\omega_e = 2\pi v_o^+ = \frac{\sigma_{\dot{x}}}{\sigma_x} = \left[\frac{\int_0^{\infty} \omega^2 S(\omega) d\omega}{\int_0^{\infty} S(\omega) d\omega} \right]^{1/2} \quad (37)$$

Furthermore, the PDF of the peaks from equations (30) and (34) is given by

$$f_p(a) = \frac{a}{\sigma_x^2} e^{-\frac{1}{2} \left(\frac{a}{\sigma_x} \right)^2} \quad (38)$$

which is the Rayleigh distribution with a parameter = σ_x .

Both equations (34) and (38) are important results for ocean waves. Equation (34) gives the average number per unit time (mean rate) of crossing a threshold of level a , and equation (38) gives the PDF of the peaks. Generally, the following result was obtained: The peaks of a stationary narrow-band Gaussian process (e.g., ocean waves) follow a Rayleigh distribution with parameter E_x , given by

$$E_x = \sigma_x^2 = \int_0^{\infty} S(\omega) d\omega \quad (39)$$

which equals the area under the energy (mean square) spectral density.

From wave data, oceanographers found that:

- Over a short period of time (less than 3 hours), the wave records can be assumed to be a stationary, relatively narrow-band random process.
- At any time t , the elevation of the wave surface from the mean follows a normal (i.e., Gaussian) distribution given by

$$f(x) = \frac{1}{\sigma_x \sqrt{2\pi}} e^{-\frac{1}{2} \left(\frac{x}{\sigma_x} \right)^2} \quad (40)$$

where σ_x is the standard deviation:

$$\sigma_x^2 = \int_{-\infty}^{+\infty} x^2 f(x) dx = E[x^2]$$

Notice that the variance is equal to the mean square because the mean of the wave elevation $E[x]$ is usually taken equal to zero.

• The peak amplitude is found to closely follow the Rayleigh distribution given by

$$f_p(a) = \frac{a}{E_x} \cdot e^{-\frac{a^2}{2E_x}} \quad a \geq 0 \quad (41)$$

where E_x is a parameter.

It has been shown in equation (38) that for a narrow-band normal process, with zero mean, the distribution of the peaks follows a Rayleigh distribution with a parameter equal to the mean square of the process, i.e., equation (41) is consistent with the theoretical result giving by equation (38).

The mean square of the process is equal to the area under the wave spectrum. This shows the importance of the wave spectrum.

Several wave statistics regarding wave amplitudes can be derived from the Rayleigh distribution. For example:

- Average wave amplitude = $1.25\sqrt{E_x}$
- Average wave height = $2.5\sqrt{E_x}$ (double amplitude)
- Average of 1/3 highest waves = $4.0\sqrt{E_x}$ (double amplitude)
- Average of 1/10 highest waves = $5.1\sqrt{E_x}$ (double amplitude)
- Average of 1/1000 highest waves = $7.7\sqrt{E_x}$ (double amplitude)

The average of the highest $1/m$ value is determined from the Rayleigh PDF as the center of the area under the curve, which lies beyond the $1/m$ value.

It is useful for design purposes to obtain representative spectra for different wind velocities or significant wave heights. A number of formulations are presented in Beck et al. (2009). An additional wave spectrum that is frequently used to determine structural loading is that adopted by the International Ship Structures Congress

(ISSC) in 1967. It is specified in terms of two parameters and is given by

$$S(\omega) = AB\omega^{-5}e^{-B\omega^{-4}} \quad (42)$$

where,

$$\begin{aligned} A &= 0.25 (H_{1/3})^2 \\ B &= (0.817 \times 2\pi/T)^4 \\ T &= \text{mean wave period} \\ H_{1/3} &= \text{significant wave height} \end{aligned}$$

This spectrum is intended to be used in conjunction with observed wave heights and periods.

In general, the shape of the wave spectrum depends on:

- Wind speed (most important parameter)
- Wind duration
- Fetch (distance over which the wind blows)
- Location of other storm areas from which swell may travel

It should be noted that waves might attain their fully developed state for winds up to 16.46 m/s (32 knots). Beyond that, it is unlikely for waves to attain their fully developed state. For example, according to Pierson a fully developed sea would result if a wind of 26.75 m/s (52 knots) blew for 80 hours over a fetch of 3333.6 km (1,800 nautical miles). Such conditions are not common.

So far, the so-called point spectrum has been discussed. This is obtained from records taken at a fixed point, with no indication of the direction of wave components, that is, no indication of how much each of the components of the wave in different directions contributes to the energy (spectrum). Such a representation is adequate for long-crested seas but a more complete representation is given by a directional spectrum $S(\omega, \mu)$, where μ is the angle between wave components' direction and prevailing wind direction. Directional spectra are discussed in Beck et al. (2009).

In a few cases of wave spectra (and vessel response), the narrow band assumption may not be adequate. Therefore, it is necessary to use the probability distribution of peaks of a stationary Gaussian (normal) random process with zero mean that is not necessarily narrow-banded. The following results were first obtained by Rice (1944, 1954) and later used by Cartwright and Longuet-Higgins (1956).

Instead of the Rayleigh distribution obtained earlier, the PDF for the peaks is given by:

$$\begin{aligned} f_p(a, \varepsilon) &= \frac{\varepsilon}{\sqrt{2\pi m_0}} e^{-\frac{a^2}{2\varepsilon^2 m_0}} + \sqrt{1 - \varepsilon^2} \frac{a}{m_0} e^{-\frac{a^2}{2m_0}} \\ &\times \Phi \left[\frac{\sqrt{1 - \varepsilon^2}}{\varepsilon} \frac{a}{\sqrt{m_0}} \right] \end{aligned} \quad (43)$$

and, by integrating, the corresponding cumulative distribution function (CDF) of the peaks is given by

$$\begin{aligned} F_p(a, \varepsilon) &= \Phi \left[\frac{a}{\varepsilon \sqrt{m_0}} \right] - \sqrt{1 - \varepsilon^2} e^{-\frac{a^2}{2m_0}} \\ &\times \Phi \left[\frac{\sqrt{1 - \varepsilon^2}}{\varepsilon} \frac{a}{\sqrt{m_0}} \right] \end{aligned} \quad (44)$$

where

$$\begin{aligned} \varepsilon^2 &= 1 - \frac{m_2^2}{m_0 m_4} \\ \Phi(u) &= \int_{-\infty}^u \frac{1}{\sqrt{2\pi}} e^{-\frac{z^2}{2}} dz \\ m_n &= \int_0^{\infty} \omega^n S(\omega) d\omega \end{aligned}$$

where ε^2 is the square of the bandwidth parameter, $\Phi(u)$ is the standard Gaussian CDF, and m_n is the n -th moment of the spectrum. It should be noted that m_0 is equal to the mean square or variance of the process.

As ε approaches zero, the process becomes narrow band, and both equations (43) and (44) reduce to the PDF and CDF of the Rayleigh probability law. On the other hand, as ε approaches one, the two equations reduce to the Gaussian (normal) probability law—that is, the peak distribution reduces to the distribution of the surface itself. It should be noted that both positive maxima and negative maxima are included in equations (43) and (44). Ochi developed a modified distribution that includes positive maxima only; this is discussed in Beck et al. (2009).

2.5.2 Dynamic Loads and Response of a Floating Vessel Considered as a Rigid Body. The objective now is to determine a floating vessel response to a given state of ocean waves (input) that are probabilistically described, as discussed in the previous section. To do this, some preliminary definitions are necessary.

A fixed parameter or time invariant system means that if a deterministic input $x(t)$ produces an output $y(t)$, then $x(t+\tau)$ produces $y(t+\tau)$, where τ is a time shift. A linear system means that if $x_i(t)$ produces $y_i(t)$, then $x(t) = a_1 x_1(t) + a_2 x_2(t)$ produces $y(t) = a_1 y_1(t) + a_2 y_2(t)$, where a_1 and a_2 are constants. Such a system is governed by a set of linear differential equations with constant coefficients. Some of the properties of such a linear system include:

If the input $x(t) = B e^{i\omega t}$, then $y(t) = A e^{i\omega t}$. Where A does not depend on time t , B is the input amplitude.

If the input has an amplitude $X(\omega)$ dependent on the frequency ω , then the output amplitude $Y(\omega)$ will also depend on ω , i.e., if $x(t) = X(\omega) e^{i\omega t}$, then $y(t) = Y(\omega) e^{i\omega t}$, where

$$\frac{Y(\omega)}{X(\omega)} \equiv H(\omega) \quad (45)$$

$H(\omega)$ is called the transfer function or frequency response function, or response amplitude operator (RAO).

The last term (RAO) usually refers to the modulus, $|H(\omega)|$. The transfer function is thus an output measure of unit input amplitude. In general, X , Y , and H are complex functions.

The next step is to determine the ship response (output) for a given state of ocean waves (input). Because the input $X(t)$ is random, it is expected the output $Y(t)$ also to be random. A floating vessel response (output) could be vessel motions such as pitch, heave and roll, the corresponding velocities and accelerations, bending moments (vertical and horizontal), torque, or shear forces. To determine the vessel response, the following assumption is made, introduced first by St. Denis and Pierson (1955). The ship is assumed to behave linearly so that the response can be described by the superposition of the response to all regular wave components that make up the irregular sea. It should be noted that in very severe seas, certain responses may not be linear, and nonlinear analysis must be conducted.

Using the linearity assumption, the following conclusions can be made:

1. If the excitation (wave input) is a stationary random process, the response (output) is also a stationary random process.
2. If the input is a normally distributed random process, the output is also a normally distributed random process.
3. If the mean of the input process is zero, the mean of the output process is also zero.
4. If the input is an ergodic process, the output is also an ergodic process.

Notice that if the input process is narrow band, the output is not necessarily a narrow band process. Over a short period, ocean waves can be assumed a stationary normal random process with zero mean. The process can be completely characterized by the spectral density, $S_x(\omega)$. The area under the spectrum is related to the mean square of the process, therefore certain averages such as average wave height, average of 1/3 highest waves, and so on, can be determined. (The subscript x in the wave spectrum $S_x(\omega)$ is used to distinguish it from the output (response) spectrum, $S_y(\omega)$).

Using conclusions (1), (2), and (3), it can be concluded that a floating vessel response is a normally distributed, stationary random process with zero mean over a short period of time. Again, just as in the input waves, if the spectral density of the vessel response is obtained, the mean square value, certain averages, and other statistics of the vessel response can be determined.

It is thus important now to find the relationship between the wave spectrum and the response spectrum. For linear systems, it can be shown that this relation is given in the form

$$S_y(\omega) = |H(\omega)|^2 S_x(\omega) \quad (46)$$

where $H(\omega)$ is the frequency response function or the transfer function, and its modulus $|H(\omega)|$ is the RAO—see also equation (45).

Equation (46) gives the input-output relation in a frequency domain, that is, between the spectra of the input (waves) and the output (vessel response). A similar relation can be obtained in the time domain between the response time history $y(t)$ and the wave time history $x(t)$. This relation as well as other relations in the time and frequency domains can be found in books on random processes. The important results are given here as follows.

The response of a vessel $y(t)$ (time domain) for any arbitrary known wave excitation $x(t)$ is given by

$$y(t) = \int_0^{\infty} x(t - \theta)h(\theta)d\theta \quad (47)$$

The mean of the response $E[y(t)]$ in terms of the mean of the stationary excitation $E[x(t)]$ (if different from zero) is

$$E[y(t)] = E[x(t)] \int_0^{\infty} h(\theta)d\theta \quad (48)$$

where $h(\theta)$ is called the impulse response function, which is the response of the vessel due to unit excitation. Notice that $E[y(t)]$ is actually independent of time because $E[x(t)]$ is independent of time if the process is stationary.

The relation (time domain) between the autocorrelation functions of the response $R_y(\tau)$ and the wave $R_x(\tau)$ is given by

$$R_y(\tau) = \int_{-\infty}^{+\infty} \int_{-\infty}^{+\infty} R_x(\tau + \theta_1 - \theta_2)h(\theta_1)h(\theta_2)d\theta_1d\theta_2 \quad (49)$$

The impulse response function $h(t)$ and the transfer function $H(\omega)$ are not independent. In fact, together they form a Fourier pair:

$$h(t) = \frac{1}{2\pi} \int_{-\infty}^{+\infty} H(\omega)e^{i\omega t} d\omega \quad (50)$$

and

$$H(\omega) = \int_{-\infty}^{+\infty} h(t)e^{-i\omega t} dt \quad (51)$$

Linear load and response determination for floating vessels is usually done in the frequency domain. Therefore, emphasis will be placed on frequency domain analysis, which is discussed in the following paragraphs.

The frequency response function $H(\omega)$, or the RAO, is a function that gives the vessel response to a regular wave of unit amplitude. For example, if the response under consideration is the bending moment amplitude, then

the bending moment can be calculated for the vessel in regular waves of different frequencies and for different vessel speeds and headings. Notice that in this case the ordinate of $|H(\omega)|^2$, it is the square of the bending moment per unit wave amplitude, ζ .

In general, the RAOs can be obtained either from calculations using the equations of motion of the ship or by towing tank experiment. Each of these will be discussed briefly in the following paragraphs. The general dynamic equations of motion of a vessel in regular waves can be obtained by applying Newton's law of motion for a rigid body. If the origin is taken at the center of gravity of the body, then

$$\bar{F} = \frac{d}{dt}(m \cdot \bar{V}) \quad (52)$$

$$\bar{M} = \frac{d}{dt}(I \cdot \bar{\omega}) \quad (53)$$

where

\bar{V} = velocity vector

\bar{F} = force vector

m = mass

\bar{M} = moment acting on the body

$\bar{\omega}$ = angular velocity vector

I = moment of Inertia about the coordinate axes

The first of these equations gives the three force equations in the x , y , and z directions (surge, sway, and heave equations). The second gives the three moment equations about the x -, y -, and z -axes (roll, pitch, and yaw equations).

These general six coupled differential equations for the six degrees of freedom are highly nonlinear and difficult to solve exactly. However, approximate solutions after decoupling some of the motions from each other and going through a linearization procedure are available, for example, see Salvesen, Tuck, and Faltinsen (1970). The decoupling of the equations is done by decoupling the motions in a vertical plane (surge, heave, and pitch) from the rest. The solution of these equations permits the calculation of the vessel motions and accelerations in regular waves of different frequencies. For further information on this subject, see Beck et al. (2009).

Once the vessel motions and accelerations are determined, the shear force and bending moment (or any other loads) can be computed. The values of these responses (including loads) due to waves of unit amplitude and different frequencies give the required RAOs. There are several computer programs available to perform these rather lengthy computations, for example, Raff (1972), Salvesen, Tuck, and Faltinsen (1970), and Meyers, Sheridan and Salvesen (1975).

The RAOs can also be determined by simply running a model in regular waves in a model tank at various speeds, headings, and wave frequencies. The model must be scaled properly to represent the ship mass distribution and hull geometry. The model motion, velocities,

accelerations, shear forces, bending moments, etc., are then measured and plotted versus the wave frequency. If the bending moment needs to be measured at the midship section only, then one may use a rigid wooden model jointed at the midship section with a dynamometer calibrated to read the bending moment acting on a bar connecting the two parts. If the bending moment is desired at more than one location, then a segmented model is usually used with a bar equipped with several strain gauges.

With the RAO determined, equation (42) can be applied to determine the spectrum of the response in long-crested seas. Equation (42) indicates that ordinates of the bending moment spectrum are obtained by multiplying the ordinates of the wave spectrum by the square of the ordinate of the response amplitude operator. Because over a short period the response is a stationary normal process, the response spectrum characterizes the process completely. If the resulting wave bending moment spectrum is narrow band, then the amplitudes of the wave bending moment follow the Rayleigh distribution, equation (34), with a parameter E_y related to the area under the bending moment spectrum:

$$E_y = \int_0^{\infty} S_x(\omega) |H(\omega)|^2 d\omega$$

Some statistics of the bending moment can be thus obtained from the Rayleigh PDF:

- Average amplitude of bending moment = $1.25\sqrt{E_y}$
- Average of $1/m$ highest bending moment amplitude is given by:

$$C_m \sqrt{E_y}$$

where C_m is equal to 2.0 for $m = 3$ and 2.55 for $m = 10$.

In general, if the response spectrum is not narrow band, then the peaks (including negative maxima) will follow Rice's distribution, given by equations (43) and (44) with the bandwidth parameter ε determined from the moments of the response spectrum. In this case, the multipliers C_m to be used to determine the average of the highest $1/m$ value must be determined from Rice's distribution and will be dependent on ε . It should be noted that the assumption of a narrow-band spectrum produces results that are more conservative and simplifies the analysis considerably.

The response spectrum discussed, $S_y(\omega)$, is not the spectrum that would be obtained from records taken of bending moment aboard a vessel. This is because when the vessel is moving, the waves are encountered at different frequencies to their absolute frequencies. A comprehensive discussion of frequency mapping and the encounter frequency is given in Beck et al. (2009).

In short-crested seas, when the directional wave spectrum $S(\omega, \mu)$ is used, the input-output relation becomes

$$S_y(\omega, \mu) = |H(\omega, \alpha - \mu)|^2 S_x(\omega, \mu) \quad (54)$$

where

μ = angle between wave component under consideration and the prevailing wind direction

$\alpha - \mu$ = angle between the vessel velocity vector and the wave component

The response of the vessel for all wave components can then be obtained by integration over μ :

$$S_y(\omega) = \int_{-\frac{\pi}{2}}^{\frac{\pi}{2}} S_y(\omega, \mu) d\mu \quad (55)$$

In the previous discussion, one of the major restrictions has been the assumption of stationarity, which limits the validity of the analysis to short periods. This leads to a Rayleigh distribution of the peaks for narrow-band spectra. However, it may be of interest to determine the distribution of the wave load peaks over long periods of time (years).

The distribution of the peaks over a long period of time can be determined by obtaining records of waves or wave loads and determining what probability distribution gives the best fit of the data. Several statistical methods can be used to estimate the parameters of the candidate distributions, and tests are available to examine the goodness-of-fit and to determine which distribution fits the data best.

Several investigators, such as Lewis (1967) and Fukuda (1970), examined long-term wave loads data with the aim of determining the long-term distribution of the peaks. It was found that the Weibull distribution is general enough and fits the long-term wave and bending moment data on ships. The PDF and CDF of the Weibull distribution are given by

$$f(x) = \left(\frac{l}{k}\right) \left(\frac{x}{k}\right)^{l-1} e^{-\left(\frac{x}{k}\right)^l} \quad x \geq 0 \quad (56)$$

and

$$F(x) = 1 - e^{-(x/k)^l} \quad x \geq 0 \quad (57)$$

where l and k are the shape and scale parameters, respectively, to be determined from the data.

The Weibull distribution is a generalized Rayleigh distribution, and if one inserts $l = 2$ and $k = \sqrt{2E}$ into equations (56) and (57), the Rayleigh distribution PDF and CDF are directly obtained—see equation (41).

When $l = 1$ and $k = \lambda$, the Weibull distribution reduces to the exponential distribution, given by

$$\begin{aligned} f(x) &= \frac{1}{\lambda} e^{-(x/\lambda)} & x \geq 0 \\ F(x) &= 1 - e^{-(x/\lambda)} & x \geq 0 \end{aligned} \quad (58)$$

where $\lambda = k$, which is the mean or expected value (also equal to the standard deviation).

In many regions of the ocean, a three-parameter Weibull distribution offers a better fit than the two-

parameter one given by equations (56) and (57)—see Mansour and Preston (1995). The cumulative and density distribution functions of the three-parameter Weibull distribution are given, respectively, by

$$F(x) = 1 - e^{-[(x-m)/k]^l}$$

and

$$f(x) = \frac{l}{k} \left(\frac{x-m}{k}\right)^{l-1} e^{-[(x-m)/k]^l} \quad (59)$$

where the new parameter, m , is the location parameter. All three parameters are to be determined from wave statistics in any ocean zone using, for example, regression analysis.

Another basic assumption in the preceding analysis of loads on ships is the linearity assumption. In high seas, this assumption is violated and the difference between sagging and hogging moments, which is not recognized by the linear theory, becomes important. Several semi-empirical, nonlinear strip theories are available in the literature (e.g., in a frequency domain), such as a quadratic theory that was first introduced by Jensen and Pedersen (1979, 1981).

Jensen and Pedersen's quadratic theory (1979) uses a perturbation procedure for determining the response of a ship. The linear terms in the response are identical to those of the classical linear strip theory. The quadratic terms arise due to the deviation of the ship sides from being vertical, the nonlinearity of the exciting waves, and the nonlinear hydrodynamic forces. The flexibility of the ship is taken into account by modeling the ship as a free-free Timoshenko beam with variable mass and stiffness distributions. The work represents a consistent second-order theory that can also be used to investigate springing response due to nonlinear wave forces. Since 1979, the theory has been further developed in a series of papers, e.g. Jensen and Dogliani (1996).

The inclusion of the quadratic transfer function makes it possible to estimate the difference between the sagging and hogging moments measured in ships with fine forms. This can be easier done in the frequency domain. However, the formulation becomes intractable if third or higher-order transfer functions need to be included, as in the case of wave loads in extreme seaways where deck immersion and slamming take place. At present, time domain solutions are required in such cases.

For nonlinear time-invariant problems, the relation between the excitation (waves) $x(t)$ and the response $y(t)$ is given by Volterra series expansion:

$$\begin{aligned} y(t) &= \int_{-\infty}^{+\infty} h_1(t-\tau)x(\tau)d\tau + \int_{-\infty}^{+\infty} \int_{-\infty}^{+\infty} h_2(t-\tau_1, t-\tau_2) \\ &\quad \times x(\tau_1)x(\tau_2)d\tau_1d\tau_2 + \dots \end{aligned} \quad (60)$$

where the impulse response functions h_1 and h_2 depend only on time differences. This is a generalization of the

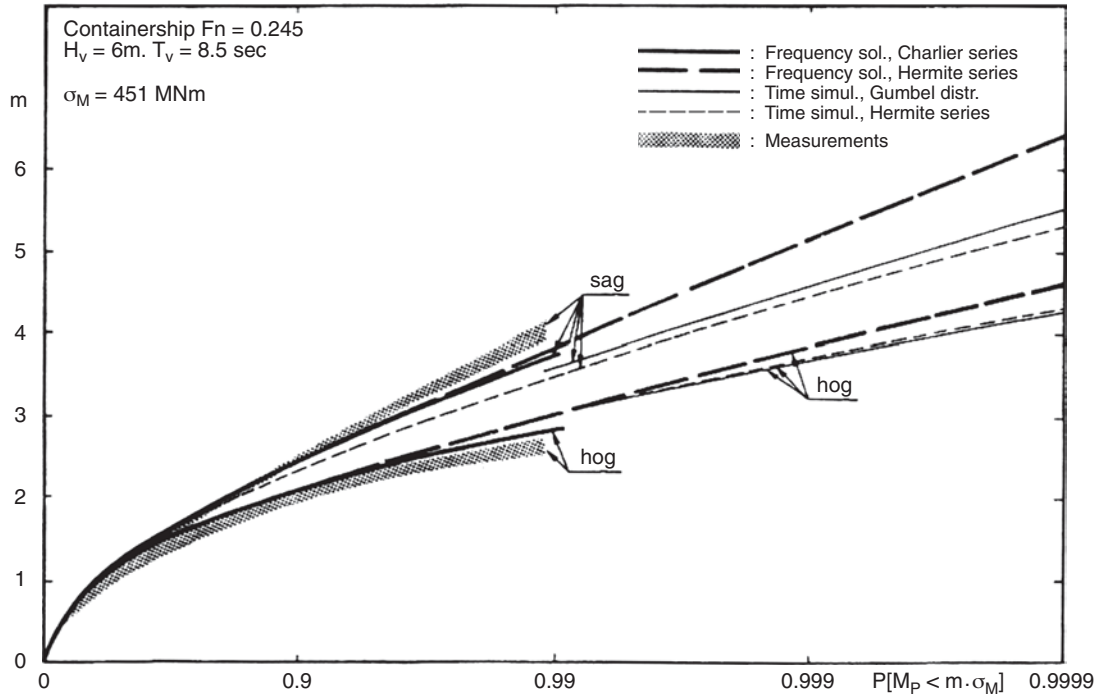


Fig. 12 A comparison between a quadratic frequency domain theory and time domain simulation (Jensen & Pedersen 1979).

linear case given by equation (47). For sufficiently small nonlinearities, the third and higher-order terms can be neglected in the expansion (60). The determination of the load $y(t)$ requires knowledge of h_1 and h_2 . This can be done conveniently in a frequency domain via the linear and quadratic frequency response functions by using the Fourier transforms—see equation (50):

$$H_1(\omega) = \int_{-\infty}^{+\infty} h_1(t) e^{-i\omega t} dt \quad (61)$$

$$H_2(\omega_1, \omega_2) = \int_{-\infty}^{+\infty} \int_{-\infty}^{+\infty} h_2(t_1, t_2) e^{-i(\omega_1 t_1 + \omega_2 t_2)} dt_1 dt_2 \quad (62)$$

The relations between the wave spectrum, $S_x(\omega)$, and the cross spectrum, $S_{xy}(\omega)$, is given by

$$S_{xy}(\omega) = H_1(\omega) S_x(|\omega|) \quad -\infty < \omega < \infty \quad (63)$$

and between the cross-bi-spectrum, $S_{xxy}(\omega_1, \omega_2)$, and the input wave spectrum is

$$S_{xxy}(\omega_1, \omega_2) = \frac{1}{2} S_x(|\omega_1|) S_x(|\omega_2|) \quad -\infty < \omega_1, \omega_2 < \infty \quad (64)$$

The transfer functions $H_1(\omega)$ and $H_2(\omega_1, \omega_2)$ for wave loads acting on a ship were determined by Jensen and Pedersen (1979), and further developed by Jensen et al. (1996). A comparison between results obtained by the

quadratic frequency domain theory and a time-domain simulation procedure using different statistical methods is shown in Fig. 12, adopted from Jensen and Pedersen (1979).

2.5.3 Time Domain Simulation. Within the framework of linear ship motion theory, all of the wave-induced components of the hull loading—including the pressure at a point on the hull surface, the hydrodynamic and inertial loads per unit length, the shear force, and the bending moment—are linearly related to the wave amplitude. When the principle of superposition is used in predicting the response to a random seaway, the methods described in Sections 2.6 and 2.7 may be applied in estimating the extreme values of responses. Such methods generally make use of an exact expression for the probability distribution of the individual peaks in combination with order statistics or Poisson upcrossings to arrive at a prediction of the extreme peak value within a given time period.

The validity of linear theory is well documented, and it is widely used for both ships and offshore structures. The linear theory is surprisingly accurate up to fairly large wave slopes. However, the difficulties arise in extreme seas where large-amplitude nonlinear waves prevail, when attempts are made to establish maximum lifetime loads of vessels of variable geometric hull forms as they move in and out of the water, as well as with slamming and wave breaking. For such cases, analysis must in general rely on time domain simulations using nonlinear ship motion theory.

Several time domain two-dimensional and three-dimensional nonlinear computer procedures of different levels of approximation are reviewed in Section 2.3. A summary of recent developments, correlation, and applications of available codes is also given in ISSC Special Task Committee VI.1 Report (2000).

Examples of time domain three-dimensional nonlinear codes are LAMP and SWAN. LAMP (see Lin et al. 1994; Lin & Yue 1993) is a multilevel motions and loads program suite that includes time domain linear three-dimensional theory, time domain moderate nonlinear, and time domain large amplitude body-nonlinear methods. The LAMP body-nonlinear program solves a general three-dimensional body floating on a free surface and undergoing arbitrary six degrees of freedom motion in the presence of incident waves. At each time step, the hydrodynamic, hydrostatic, and Froude-Krylov wave pressure forces are calculated on the instantaneous body wetted surface under the incident wave. The local incident free surface elevations are used to transform the body geometry into a computational domain with a deformed body and a flat free surface. By linearizing the free surface boundary conditions about this incident wave surface, the problem is solved in the computational domain using linearized free-surface transient Green's functions. SWAN (see Sclavounos 1996; Sclavounos et al. 1997) is also a multilevel motions and loads computer program suite. It solves the hydrodynamic problem similar to LAMP using the Rankine source.

Both SWAN and LAMP have been validated to some extent with model test data. Shin et al. (1997) further compares the measured frequency response functions (FRF) for heave, pitch, roll, and vertical and horizontal bending moments amidships of the S175 container ship, with two numerical calculations labeled by ABS-SM and LAMP-1, as shown in Fig. 13. Measured data shown in this figure are those of the vessel at 11.37 m/s (22.1 knots) in a 30° stern quartering sea, which is believed to be the most interesting and challenging heading condition. Results denoted by "ABS-SM" are data calculated by the ABS Ship Motion program, which is a frequency linear strip theory method similar to the one of Salvesen, Tuck, and Faltinsen (1970). Results labeled by LAMP-1 are the first-order harmonic components derived from the harmonic analyses of the response time histories simulated by LAMP in regular waves. For the oblique sea simulations, LAMP uses semi-empirical formulas similar to those in the U.S. Navy's SMP program (Meyers et al. 1981) to account for the roll damping and other associated viscous and lifting effects, and a proportional, integral, and a PID (Proportional, Integral, Derivative) control algorithm autopilot is employed for course keeping.

As shown in Fig. 13, the heave and pitch FRFs compare well. For roll motion, there seems to be a great deal of scatter in the experimental measurement. The roll predictions from the two linear results are very close in the high-frequency range but differ considerably in the medium-frequency range, indicating further investi-

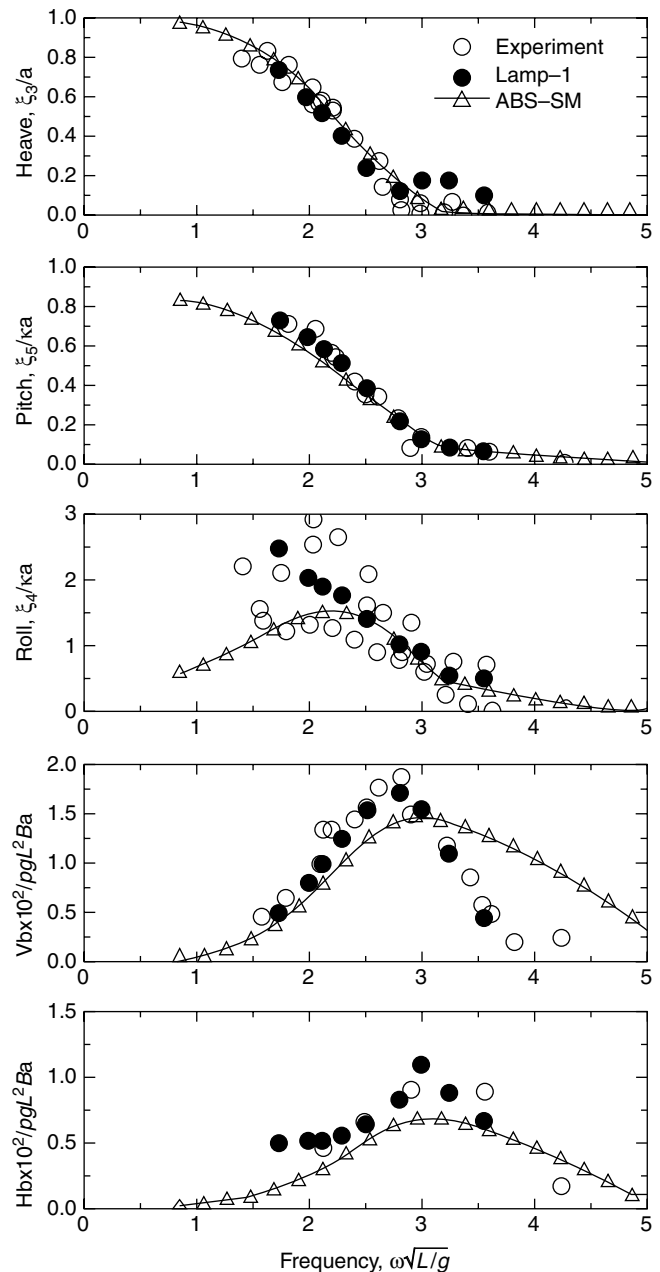


Fig. 13 Frequency response function for heave, pitch, roll, midship vertical bending (Vb) moment and midship horizontal bending (Hb) moment for S175 at 11.37 m/s (22.1 knots) 30° stern quartering sea. (Shin, et al., 1997)

gations are required to determine what effects need to be included to predict roll motion with improved accuracy. It is noted that the effect of rudder motion, which is included in LAMP but not in ABS-SM, could be another source causing discrepancies between the two analytic results. On the other hand, the vertical bending moment amidships calculated by LAMP-1 and ABS-SM agree very well with the experimental measurements

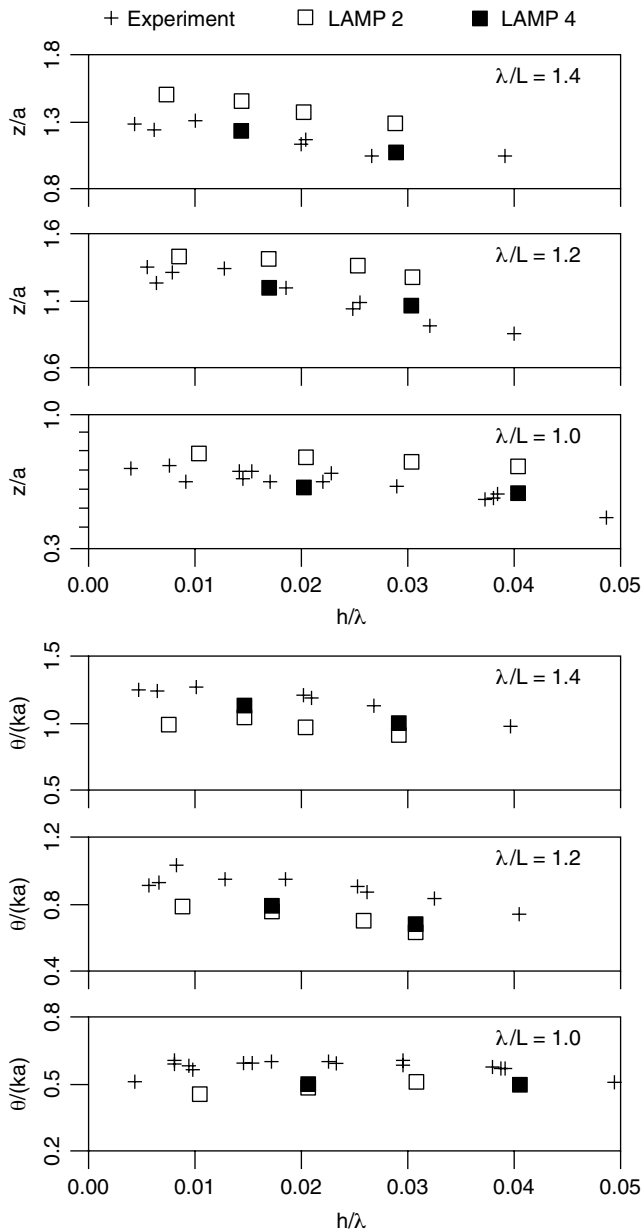


Fig. 14 Heave (upper half) and pitch (lower half) frequency response function as a function of wave height for S175 container ship at 11.37 m/s (22.1 knots) in three regular head wave conditions. (Shin et al., 1997)

in the medium-frequency range, and LAMP-1 prediction is better in the high-frequency range. The horizontal bending moment comparisons can only be assessed as reasonable.

Figure 14 (Shin et al. 1997) shows the comparisons of measured heave and pitch of the S175 container ship with two numerical results labeled by LAMP-2 and LAMP-4 for three wavelengths, $\lambda/L = 1.0, 1.2,$ and 1.4 . LAMP results labeled by LAMP-2 are obtained using a moderate nonlinear method where the hydrodynamic part of the pressure forces are computed using three-

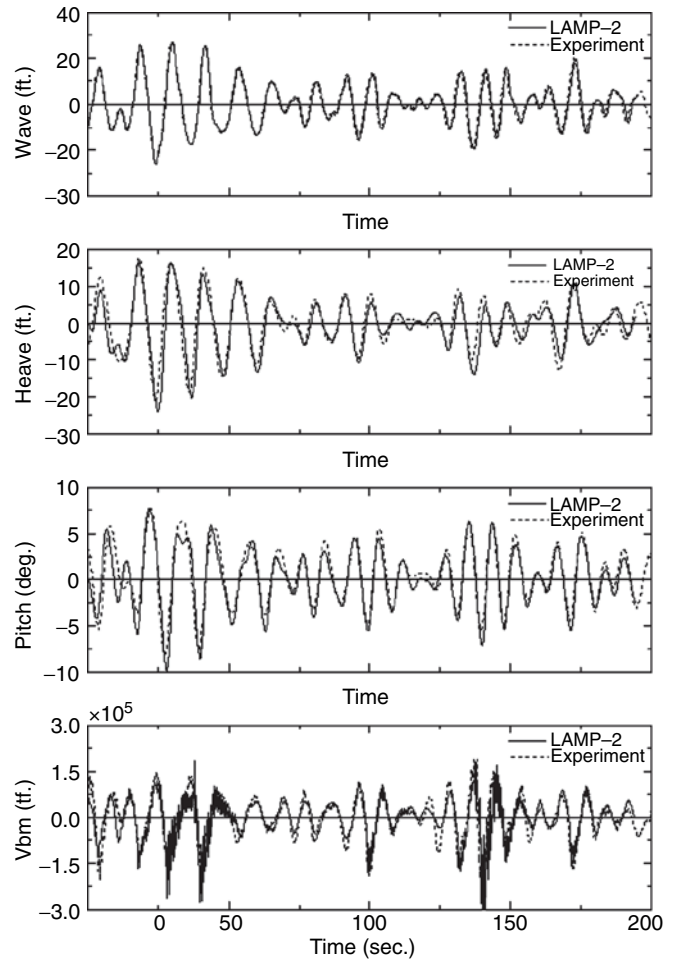


Fig. 15 Computed time history wave, heave, pitch, and vertical bending moment near midship compared with model test data for a naval ship. (Shin et al., 1997)

dimensional linear theory, whereas the hydrostatic and Froude-Krylov wave forces are calculated on the instantaneous body wetted surface under the incident wave. The LAMP-4 results are obtained using a body-nonlinear method described previously. It is encouraging to note that LAMP-4 results show very much the same nonlinear trend as the experiments. On the other hand, LAMP-2 results seem to capture the important nonlinear hydrostatic restoring and wave excitation contributions to a higher degree of accuracy while drastically reducing the need of computer resources and computing time (about 1/30th) as required by the LAMP-4.

Shown in Fig. 15 (Shin et al. 1997) are the measured time histories of wave elevation, heave, pitch, and vertical bending moment amidships from model tests of a fine form naval ship running at a speed of 5.14 m/s (10 knots) in a head storm-sea condition. Computed time histories by LAMP-2 are also shown for comparison. It can be seen that the predicted results agree very well with the corresponding measured time records. The vertical bending

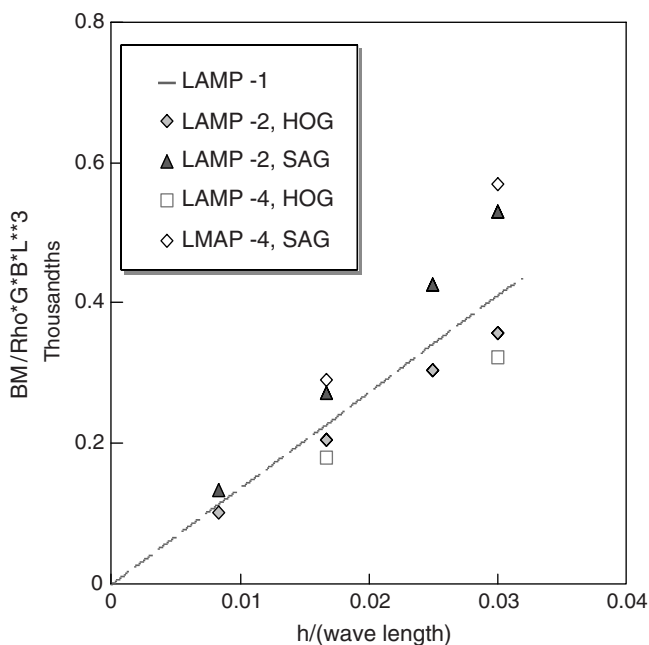


Fig. 16 Vertical midship bending moment (hog/sag) in regular head waves with $\lambda/L = 1.20$ as a function of wave height for a S175 container ship at 11.37 m/s (22.1 knots). (Shin, et al., 1997)

moment shown in this figure is the total combined bending moment including both the ordinary wave-frequency component as well as the wave-impact induced high-frequency whipping responses. It can be seen that the comparison between LAMP-2 results and the measurements is remarkable. Near the peak of the sagging moment, not only is the magnitude of the total moment comparable but also the frequency and amplitude of the calculated whipping response agreed well with the experimental results. Engle et al. (1997) also find that the linear theories typically under-predict the sagging bending moment amidships, and that the differences in peak sagging bending moments predicted by the linear and nonlinear theories are mainly caused by the nonlinear geometry, such as bow flare, above the water line.

Shin et al. (1997) further compares the wave-induced vertical bending moments amidships (hog/sag) from LAMP-1, LAMP-2, and LAMP-4 for the S175 container ship. Shown in Fig. 16 are the calculated results presented for different wave heights (h) of a wave-ship length ratio, $\lambda/L = 1.2$. The comparison reveals that a large amount of nonlinear effect occurs not only for sagging but also for hogging moments. For example, the nonlinear effects for the case of $h/\lambda = 0.03$ are substantial: 35 percent larger and 21 percent smaller for sagging and hogging, respectively, than those predicted by the linear procedure. Comparison also shows that the nonlinear effects shown in LAMP-2 results are comparable with those in LAMP-4. Together with the studies shown in Figs. 13 to 15, this may lead to a tentative conclu-

sion that the nonlinear effects in vertical hull girder loads mainly result from the nonlinear geometry above the still water line. In this sense, the moderate nonlinear procedure where the hydrodynamic pressure loads are determined by three-dimensional linear motion theory and the hydrostatic restoring and Foude-Krylov forces are calculated up to the wetted body surface under the incident waves can be a potential design tool for practicing engineering application.

The time domain simulation using three-dimensional nonlinear theory requires such a huge computational effort that only a short time period can be analyzed. In addition, a consistent analytic procedure is not yet available to take into account the nonlinearity in the hydrodynamic response together with the nonlinearity in the large ocean waves itself. Therefore, depending on the complexity of the hydrodynamic load analysis applied the nonlinear calculations are only performed in selected regular waves, conditional wave episodes, or short sequences of a random seaway. From these results, the variance of the responses in question can be predicted but extrapolation of the results to the extreme values that the vessel may encounter during its service lifetime is much more difficult. Because of this, it becomes important to identify the random incident wave sequences that yield extreme responses of the vessel. However, a priori such sequences are not known and cannot be determined from the wave environment itself because the required sequences also depend on the response type in question, that is, the DLP discussed in Section 2.3. They also vary with the characteristics of the vessel (i.e., size, loading conditions, geometric configuration), heading, and speed.

To overcome this problem, the most straightforward procedure is first to run a very long time-domain simulation in each relevant stationary condition using a linear transfer function for the response in question (DLP), and the wave sequence yielding the maximum linear response is then applied to the nonlinear analysis. To ensure that the correct extreme nonlinear response of interest can be captured, a fairly large number of critical wave episodes must be used (Torhaug et al. 1998). Because time domain analysis requires a significantly large amount of computing resources, a most-likely response method is suggested to reduce the number of wave sequences needed in the nonlinear calculations (Adeegest et al. 1998; Dietz et al. 2004). Alternatively, a semi-empirical method based on an ensemble of the pseudo transfer function obtained from nonlinear theory has been used in the industry. The semi-empirical method treats these pseudo transfer functions, which are valid only for the specific wave heights that characterize the seaway, as linear RAOs, and proceed in the standard way to obtain the extreme value as for the linear system. For all the aforementioned approaches, validation that the statistical predictions be compared with results from consistent statistical methods applied to the continuous time signal of the response is needed.

2.6 Short-Term Extreme Values in Stationary Seas. If wave loads acting on a marine structure can be represented as a stationary Gaussian process (short period), then at least four methods are available to predict the probability distribution of the maximum load in a given sea state. These methods were further developed for application to marine structures and generalized for any bandwidth spectrum (Mansour 1987). In the first method, the peaks are assumed to be statistically independent and identically distributed, and the extreme value distribution of the largest in N peaks is determined using classical order statistics. In the second, a discrete point process is assumed to determine the asymptotic type-I distribution based on Rice's distribution as an initial distribution. Cramer's procedure was used for determining the resulting asymptotic distribution. Conventional upcrossing analysis is used in the third method for determining the extreme value distribution. Finally, a two-stage description of the random process that leads to an extreme distribution derived by Vanmarcke (1975) is the basis for the fourth method. Each of these methods will be described briefly in the following sections.

2.6.1 Distribution of the Largest Peak in a Sequence of N Peaks using Order Statistics. The distributions of the largest peak in a sequence of N peaks can be determined using standard order statistics. Consider a sequence of random variables, Z_1, Z_2, \dots, Z_n , representing the peaks of a load on a marine structure. Assuming that these peaks are identically distributed and statistically independent, the cumulative distribution function (CDF) of the largest one using order statistics is given by (Gumbel 1958)

$$F_{Z_N}(z) = P(\max[z_1, z_2, \dots, z_N] \leq z) = [F_Z(z, \varepsilon)]^N \quad (65)$$

where $F_Z(z, \varepsilon)$ is the initial cumulative distribution function of the load peaks (maxima) and ε is the spectral width parameter, defined as

$$\varepsilon^2 = 1 - \frac{m_2^2}{m_0 m_4} \quad (66)$$

$$m_n = \int_{-\infty}^{+\infty} \omega^n S(\omega) d\omega, \quad n = 0, 2, 4$$

The PDF of the largest peak is determined by differentiating equation (65) with respect to z , thus

$$f_{Z_N}(z) = N[F_Z(z, \varepsilon)]^{N-1} \cdot f_Z(z, \varepsilon) \quad (67)$$

where $f_Z(z, \varepsilon)$ is the initial PDF of the load peaks. For any bandwidth load process, Rice's distribution can be used as the initial distribution.

Based on the analysis here, the expected value of the maximum load peak in a sequence of N peaks was deter-

mined by Cartwright and Longuet-Higgins (1956) and is approximated by

$$\frac{E[\max(z_1, z_2, \dots, z_n)]}{\sqrt{m_0}} \cong [2\ln(\sqrt{1 - \varepsilon^2}N)]^{1/2} + C[2\ln(\sqrt{1 - \varepsilon^2}N)]^{-1/2} \quad (68)$$

where $C = 0.5772$ (Euler's constant).

For a conservative estimate, ε may be taken equal to zero in equation (64) (Rayleigh peaks). In general, for any ε the extreme load peak with a probability of exceedence α is given by Siveria and Brillinger (1978):

$$Z_\alpha = [2m_0 \{ \ln(N) + \ln[\frac{1}{\ln(\frac{1}{1-\alpha})}] \}]^{1/2} \quad (69)$$

which is independent of ε (for small α).

2.6.2 Asymptotic Type I Distribution. It is known that as the number of peaks N increase without bound, a limiting or asymptotic form of the extreme value distribution—equations (65) and (67)—is reached. The asymptotic form of an extreme value distribution generally does not depend on the exact form of the initial distribution; it depends only on the tail behavior of the initial distribution. However, the parameters of the asymptotic distribution depend on the exact form of the initial distribution.

Mansour (1987) used a method developed by Cramer to derive the asymptotic distribution based on Rice's distribution as an initial distribution. The derived extreme value CDF is

$$F_{Z_N}(z, \varepsilon) = \exp \left\{ -N \left[\Phi \left(\frac{m_s - z}{\varepsilon \sqrt{m_0}} \right) + \sqrt{1 - \varepsilon^2} \left(e^{-\frac{1}{2} \left(\frac{z - m_s}{\sqrt{m_0}} \right)^2} \right) \cdot \Phi \left(\frac{\sqrt{1 - \varepsilon^2}}{\varepsilon} \cdot \frac{z - m_s}{\sqrt{m_0}} \right) \right] \right\} \quad (70)$$

that is, the asymptotic form is double exponential and the cumulative distribution itself depends on N . m_s is the mean value of the load if different from zero. Φ is the standard Gaussian CDF. Several years after the appearance of Cramer's book, Gumbel (1958) classified the asymptotic distribution of extremes in three types: type I, a double exponential form; type II, an exponential form; and type III, an exponential form with an upper bound. Convergence of an initial distribution to one of the three types depends largely on the tail behavior of the initial distribution. An initial distribution with an exponentially decaying tail in the direction of the extreme will converge to type I asymptotic distribution (i.e., the double exponential form).

Gumbel's analysis and classification provide another method for deriving an asymptotic distribution, and may be in a form easier to handle than that given by equation (70). The CDF of type I asymptotic form as given by Gumbel is

$$F_{Z_N}(z) = \exp[-e^{-\alpha N(z - u_N)}] \quad (71)$$

where u_N is the characteristic largest value of the initial variate Z and α_N is an inverse measure of the dispersion of Z_N . These parameters, α_N and u_N , must be determined and depend on the form of the initial distribution.

The corresponding PDF is given by

$$f_{Z_N}(z) = \alpha_N e^{-\alpha_N(z-u_N)} \cdot \exp[-e^{-\alpha_N(z-u_N)}] \quad (72)$$

The mean and standard deviation of the extreme value Z_N are given, respectively, by

$$\mu_{Z_N} = u_N + \frac{0.5772}{\alpha_N} \quad (73)$$

$$\sigma_{Z_N} = \frac{\pi}{\sqrt{6}\alpha_N} \quad (74)$$

The parameters α_N and u_N were determined (see Mansour 1987) for Rice's distribution as an initial distribution.

The results for α_N and u_N are

$$u_N = m_s \pm \left\{ 2m_o \ln \left[\frac{\sqrt{1-\varepsilon^2}\Phi(\beta)}{\frac{1}{N} - \Phi(-\alpha)} \right] \right\}^{1/2} \quad (75)$$

$$\alpha_N = \frac{N\varepsilon}{\sqrt{2\pi}m_o} e^{-\frac{\alpha^2}{2}} + \frac{N\varepsilon\beta}{\sqrt{m_o}} e^{-\frac{\alpha^2}{2}\varepsilon^2} \cdot \Phi(\beta) \quad (76)$$

where

$$\alpha = \frac{u_N - m_s}{\varepsilon\sqrt{m_o}} \quad \text{and} \quad \beta = \sqrt{1-\varepsilon^2} \cdot \alpha \quad (77)$$

The positive sign in equation (75) should be used if the mean value m_s is positive to obtain the larger characteristic value. It should be noted that both α and β contain u_N as defined in equation (77); therefore, an iterative procedure must be used to determine u_N . To start the iterative procedure, an initial value for u_N is necessary and may be taken as

$$u_N = m_s + \sqrt{2m_o \ln(N)}$$

The corresponding values of α , β , $\Phi(\alpha)$, and $\Phi(\beta)$ can then be determined. Equation (75) is then checked to see if the right side is equal to the left side, otherwise a new value of u_N equal to the right side of equation (75) should be used in the second step of the iterative procedure. Three or four steps are usually sufficient for convergence.

2.6.3 Extreme Value Distribution Based on Upcrossing Analysis. The distribution of the largest peak can be determined from upcrossing analysis of a time history of a stationary random process instead of the peak analysis presented previously. For example, the number of N peaks can be changed to a time interval, T , in the upcrossing analysis, and the problem of determining the characteristics of the largest peak in N peaks becomes that of evaluating characteristics of the maximum crest of a stationary Gaussian random process, $X(t)$, during a period T . The assumption of the statistical independence of the peaks is usually replaced by the assumption

that upcrossings of a level x by $X(t)$ are statistically independent. This leads to the Poisson's upcrossing process, which is valid only in the asymptotic sense.

From upcrossing analysis, it can be shown (see Rice 1954) that the probability of the largest value is less than a certain level x during a period T is given by

$$P[\max(X(t); 0 \leq t \leq T) \leq x] = e^{-v_x T} \quad (78)$$

where v_x is the rate of upcrossing level x , given by

$$v_x = v_o e^{-1/2\left(\frac{x-m_s}{\sqrt{m_o}}\right)^2} \quad (79)$$

and

$$v_o = \frac{1}{2\pi} \sqrt{\frac{m_2}{m_o}} \quad 1/\text{sec} \quad (80)$$

Therefore, the CDF of the largest X is

$$F_X(x) = \exp \left\{ -v_o T e^{-\frac{1}{2}\left(\frac{x-m_s}{\sqrt{m_o}}\right)^2} \right\} \quad (81)$$

that is, it has a double exponential form, although quite different from equation (71), with u_N and α_N given by equations (75) and (76), respectively.

2.6.4 Extreme Value Distribution Based on a Two-State Description of a Random Process. Vanmarcke (1975) estimated the probability distribution of the time to first passage across a specified barrier for a Gaussian stationary random process, considering the clustering effect of wave peaks. In his analysis, he considered a two-state description of the time history $X(t)$ relative to the specified barrier. Based on his results, the distribution of the extreme value can be determined from

$$F_X(x) = \exp \left[-v_o T \left(\frac{1 - e^{-\sqrt{2\pi}q\left(\frac{x-m_s}{\sqrt{m_o}}\right)}}{1 - e^{-\frac{1}{2}\left(\frac{x-m_s}{\sqrt{m_o}}\right)^2}} \right) \cdot e^{-\frac{1}{2}\left(\frac{x-m_s}{\sqrt{m_o}}\right)^2} \right] \quad (82)$$

where q is a bandwidth parameter, defined as

$$q = \sqrt{1 - \frac{m_1^2}{m_o m_2}} \quad 0 \leq q \leq 1 \quad (83)$$

The four extreme value distributions discussed here are valid for a load process represented by a stationary Gaussian process of any bandwidth. The corresponding equations for the special cases of a narrow-band process ($\varepsilon = 0$ or $q = 0$) and a wide-band process ($\varepsilon = 1$ or $q = 1$) can be found in Mansour (1987). The narrow-band process case ($\varepsilon = 0$) gives a conservative estimate of the extreme wave load distribution, and the resulting equations may be used for values of ε up to 0.60 because they are insensitive to ε in the range 0 to 0.60.

The extreme value distributions of the wave loads discussed here differ from each other in their basic derivation and underlying assumptions. The forms of their equations are drastically different, as can be seen by comparing equations (65), (70), (71), (81), and (82). It would be interesting to compare some typical results

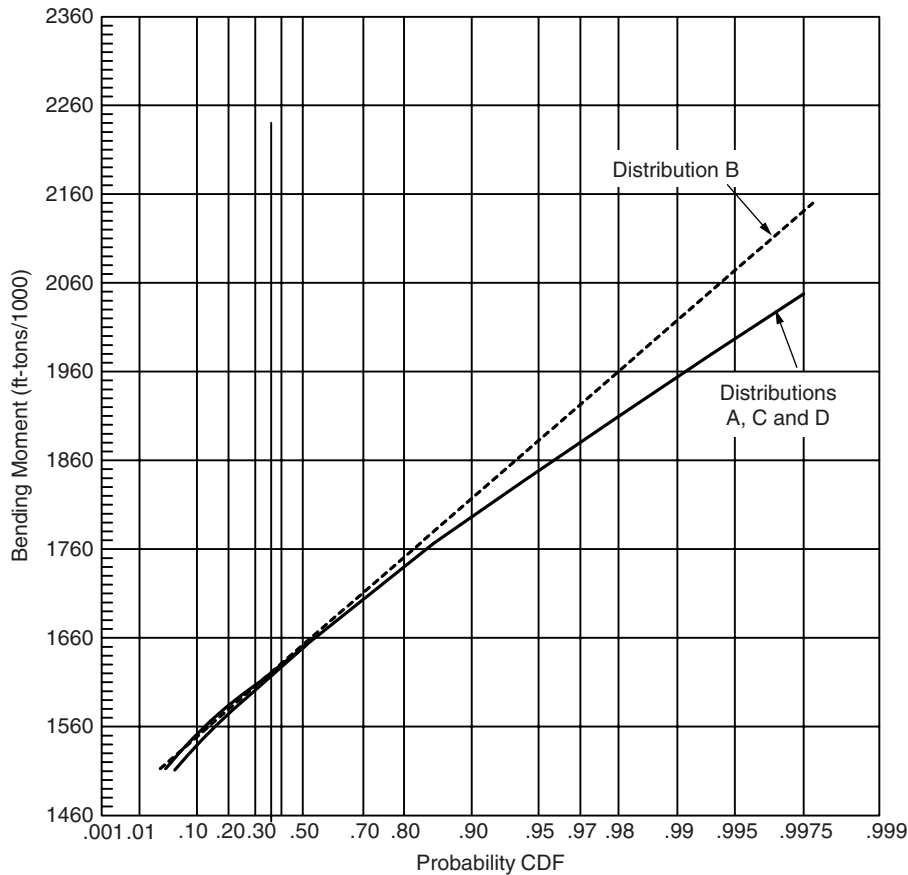


Fig. 17 Standard extreme variate—bending moment on a tanker (Mansour, 1987).

obtained from the different methods when applied to a marine structure. For this purpose, a tanker of length 232.6 m (763 ft), breadth 38.1 m (125 ft), and depth 16.6 m (54.5 ft) was considered by Mansour (1987). The results of the comparison are shown and plotted on a standard extreme probability paper in Fig. 17.

Based on these results, one surprising conclusion can be drawn. All extreme value distributions of the waveloads considered produce similar results, although their basic assumptions and derivations differ. In fact, if one inspects the equations representing the cumulative distribution functions, the equations are not similar in form and may conclude erroneously that they would produce very different results.

The extreme distribution based on the largest peak in N peaks equation (65) (i.e. distribution A), upcrossing analysis equation (81) (i.e. distribution C), and a two-state description equation (82) (i.e. distribution D) produce almost identical results as far as the probability of exceedance is concerned, as can be seen by inspecting Fig. 17. The asymptotic type I distribution (B) equation (71), results in slightly greater values of probability of exceedance. This is to be expected because the asymptotic distribution is an upper bound extreme distribution

and becomes more accurate as number of load peaks approach infinity. In the example shown for the tanker, the number of wave bending moment peaks, N , is approximately 277.

The difference between the bending moment obtained from the asymptotic distribution B and that obtained from the other three distributions is about 4.5 percent at an exceedance probability of 0.0025 (see Fig. 17). The extreme distribution based on upcrossing analysis given by equation (81) is the easiest to use and depends only on the number of peaks $\nu_o T$, the mean square m_o , and the mean m_s if different from zero.

The extreme value distributions described previously are valuable when conducting a reliability analysis where the important design variables are represented by their probability distributions. However, in deterministic and semi-probabilistic design analysis an extreme (characteristic) value of the load is sought instead of the probability distribution. This extreme or characteristic value is usually taken as the most probable extreme value (i.e., the mode of the extreme value PDF) or an extreme value with a specified probability of exceedance. In these cases, the following discussion and equations may be useful.

According to the linear theory and the associated extreme value statistics, the most probable extreme load (MPEL), as well as other characteristic loads in a stationary sea, depend only on the first two moments of the load probability distribution (i.e., the mean and the standard deviation). In many cases, the mean is either zero or can be taken as zero without loss of generality. The most probable extreme value (MPEV) thus depends only on the standard deviation and, for Rayleigh distributed peaks, is given in the form

$$MPEV = \sigma \sqrt{2 \ln v_o T} \quad (84)$$

where $v_o T = N$ is the number of peaks and σ is the standard deviation of the load. Note that a comparison between the modal value (MPEV), given by equation (84), and the mean value, given by equation (68) with $\varepsilon = 0$, shows that the two values will be nearly identical for N larger than 1,000.

However, the quadratic theory (Jensen & Pedersen 1979) gives (as will be shown later) an MPEV as well as other characteristic values that depend also on the higher-order statistical moments. Of special importance are the first four moments, namely, the mean, the standard deviation, the skewness (third moment), and the kurtosis (fourth moment). The skewness measures the deviation from symmetry of the PDF of the underlying load process, zero being a symmetrical density (e.g., Gaussian). The kurtosis measures the peakness of the density function. The Gaussian PDF has a kurtosis of three. These four moments characterize the MPEV rather accurately as well as other characteristic values for nonlinear wave loads (Jensen et al. 1996).

In both cases, linear and nonlinear, the extreme values will also depend on the frequency content of the underlying load processes. More specifically, for narrow-band processes the frequency content will influence the number of peaks N where $N = v_o T$ and v_o is the rate of zero upcrossing of the process. T is the period over which the extreme value is estimated.

For slightly nonlinear load processes, Mansour and Jensen (1995) introduced a nonlinearity parameter δ based on the quadratic theory results. The MPEV given by equation (84) now becomes

$$MPEV = \delta \sigma \sqrt{2 \ln v_o T} \quad (85)$$

where the non linearity parameter, δ , is defined by

$$\delta = k \left\{ 1 + \frac{\alpha(2 \ln v_o T - 1)}{(5.8 + 2\gamma)\sqrt{2 \ln v_o T}} + \frac{\gamma}{30} (2 \ln v_o T - 3) \right\} \quad (86)$$

and

$$\gamma = [1 + 1.5(\beta - 3)]^{1/2} - 1 \quad (87)$$

$$k = \left[1 + \frac{1}{2} \left(\frac{\alpha}{\gamma + 3} \right)^2 + \frac{\gamma^2}{54} \right]^{1/2} \quad (88)$$

For the linear case corresponding to a Gaussian distribution of loads, the skewness α and kurtosis β reduce to zero and three, respectively, and the nonlinearity parameter δ becomes one. In this case, equation (85) reduces to equation (84).

The difference between sagging and hogging moments manifests itself in the sign of the skewness, α (i.e., α is positive for sagging and has the same value but with a negative sign for hogging). We see from equations (85) and (86) that the result is a larger extreme sagging bending moment than hogging moment. This is consistent with observations and measurements recorded on ships at sea. Equations (85) and (86) tend to give larger values for the sagging moment than that obtained from the quadratic theory (i.e., a more conservative estimate).

Other characteristic values besides the most probable extreme value can also be approximately determined using an equation similar to equation (85). An extreme value of a load f_n associated with an exceedance probability, η , can be determined by replacing v_o by $v_{o\eta}$:

$$f_\eta = \delta \sigma \sqrt{2 \ln v_{o\eta} T} \quad (89)$$

where

$$v_{o\eta} \approx \frac{v_o}{\ln(1 - \eta)^{-1}} \quad (90)$$

The most probable extreme value is associated with an exceedance probability,

$$\eta \cong 1 - 1/e = 0.6321$$

In this special case, $v_{o\eta}$ given by equation (90) reduces to v_o and equation (89) reduces to equation (85). From equation (85), it is seen that estimation of the MPEV of a slightly nonlinear load can be made after evaluating the nonlinearity parameter δ , which depends on the skewness and kurtosis. These two parameters depend on the sea state (characterized by significant wave height and average wave period), ship speed, heading angle, and flare coefficient.

It should be noted that although the quadratic theory is a major improvement over linear strip theory, the excitation and response in very high sea states are highly nonlinear, and the quadratic theory results as well as equations (85) to (88) may no longer be accurate. The difficulty is inherent in the assumption of sectional breadth's linear variation with draft. A problem arises when the ship motion in very high seas exceeds the ship draft or free board (bow emergence or green water on deck). The previous equations apply to narrow-band and relatively narrow-band response spectra. An approximation for the wide-band case is possible for the MPEV if one uses equations (84) or (85) with (Cartwright & Longuet-Higgins 1956)

$$v_o T = \sqrt{1 - \varepsilon^2} N \quad (91)$$

where N is the number of peaks and ε is a spectrum broadness parameter.

2.6.5 Return Periods of Extreme Events and Encounter Probabilities. The concepts of return periods and encounter probability are used in design analysis. The probability that an extreme value of an event (say wave height, x , or wave load) will not be encountered during the life L of a marine structure is called non-encounter probability, $NE(x)$. Using order statistics, this is given by

$$\begin{aligned} NE(x) &= P[\text{no exceedence of } x \text{ occurs during life } L] \\ &= P[X_{\max} \leq x] = [F_X(x)]^L \end{aligned} \quad (92)$$

where

$$\begin{aligned} X_{\max} &= \text{maximum value during life } L \\ L &= \text{life in years} \\ F_X(x) &= \text{distribution function of annual} \\ &\quad \text{maximum} \end{aligned}$$

The waiting or return period, R , is the average length of time between exceedence. Thus, one may speak of a 100-year wave height or 50-year wind velocity.

The waiting period in years has a probability law given by

$$P[W = w] = F_X^{w-1}(x)[1 - F_X(x)]$$

and, therefore, the average waiting period (i.e., the return period, R) is

$$R = E[W] = [1 - F_X(x)]^{-1} \quad (93)$$

The relationship between the non-encounter probability, $NE(x)$, and the return period, R , can be determined by eliminating $F_X(x)$ from equations (92) and (93), thus,

$$NE(x) = P[X_{\max} \leq x] = [1 - R^{-1}]^L \quad (94)$$

If $R = L$, then $NE(x) \approx e^{-1}$ and the probability of exceedence in this case equals $1 - e^{-1} = 0.632$, that is, there is a high probability (0.632) of exceeding the event with a return period L during the life years, L , of the structure.

In selecting return periods, one must distinguish between an annual interruption of operation of the structure ($L = 1$ year) and an ultimate failure during a lifetime ($L = 20$ to 30 years). In the former case, a return period $R = 10$ years may be adequate. Using equation (94) with $L = 1$ and $R = 10$, one obtains a non-encounter probability of 90 percent. If R is increased to 100, the non-encounter probability becomes 99 percent. In the latter case, where a failure during life of, say, 20 years, is considered and the return period is 100 years, then the non-encounter probability from equation (94) is 81.8 percent. If the return period is increased to 1,000 years, the non-encounter probability becomes 98 percent.

For fixed offshore platforms, the useful life of the structure can be estimated and the corresponding encounter probability can be determined as outlined in the preceding paragraphs. However, for ships the estimate of the encounter probability is more complicated because of their mobility and because different zones in the ocean have different wave severities and wave statistics. A procedure that accounts for the operational profile of a ship

and the wave statistics along its route zones has been developed by Mansour and Preston (1995). The results showed that the ship's route has a large impact on the encounter probability.

Generally, encounter probabilities provide a more meaningful basis for establishing design criteria than return periods. The reason for this is that the encounter probabilities depend on the life of the structure as well as wave statistics in the region of operation, whereas return periods only reflect wave statistics.

2.6.6 Stochastic Combination of Loads. Undoubtedly, there are certain similarities between decomposing ship response records of full-scale measurements into their basic components and combining analytically calculated components to obtain the total response. Because decomposing full-scale measurements can be done with a certain degree of success, it is possible to invert the procedure to compute the combined response from the analytically determined components. In this section, a brief discussion is given of the decomposition of full-scale records into their basic components. This is followed by methods used to combine analytically determined response components. For more details, see Mansour (1995).

A typical measured stress time history of a bulk carrier is shown in Fig. 4 (from Little et al. 1971). Usually, such a record consists of a rapidly varying time history of random amplitude and frequency oscillating about a mean value. The mean value itself is a weakly time-dependent function and may shift from positive to negative (sagging to hogging). Two dominant factors that affect the mean value are:

- The still water loads, which can be accurately determined from the loading condition of the ship floating in still water
- The thermal loads, which arise due to variations in ambient temperatures and differences in water and air temperatures.

A closer look at the rapidly varying part shows that it also can be decomposed into components. Figures 18 and 19 illustrate records taken over shorter periods of time (larger scale). Two main central frequencies appear in these records. The smaller central frequency is associated with the loads resulting from the motion of the ship as a rigid body (primarily heave and pitch motions). This lower central frequency is therefore close in magnitude to the wave encounter frequency for wavelengths nearly equal to ship length.

The higher central frequency is associated with loads resulting mostly from the two-node mode response of the ship when it vibrates as a flexible body. This higher central frequency is thus close to the two-node mode natural frequency of the ship. The high frequency response itself can be due to springing of the flexible ship when excited by the energy present in the high-frequency wave components, as shown in Fig. 18. It can also be due to impact of the ship bow on the water as the ship moves

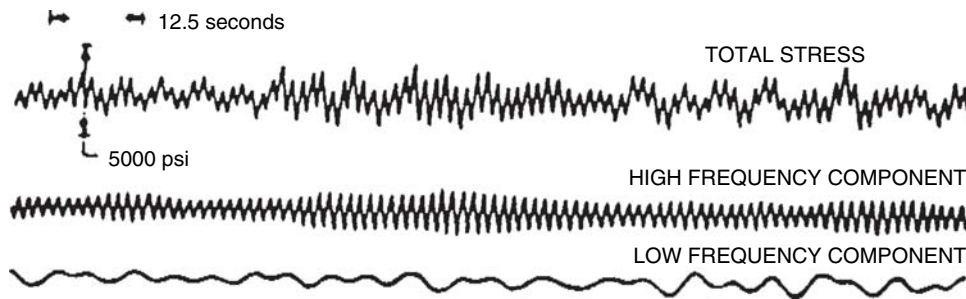


Fig. 18 Decomposition of a stress time history of a Great Lakes vessel into low- and high-frequency components.

into the waves (i.e., slamming; see Fig. 19). Although springing and slamming can occur simultaneously, it is unusual to see records that exhibit both clearly. These two responses can be distinguished from each other by inspecting the records' envelope. In general, a decaying envelope (see Fig. 19) indicates a slamming response, whereas a continuous envelope of varying amplitude, as shown in Fig. 18, indicates a springing response.

The rigid body and the high-frequency responses do not always occur simultaneously in the same record. Quite often, only the rigid body response appears in a record, particularly in records of smaller ships that have high two-node mode frequency. Occasionally, only the high-frequency springing response appears in a record when a ship is moving or resting in relatively calm water. This may occur in long flexible ships with low natural frequencies when operating in calm water or in a low sea state composed mainly of short waves. Figure 20 (from Critchfield 1973) shows a measured response spectrum of a large Great Lakes vessel. The response is purely in the two-node mode and higher frequencies, with no rigid

body response appearing in the spectrum (the two-node mode is labeled in the figure as the first mode). The figure shows that response at higher modes than the two-node mode can be measured, although small and relatively unimportant in most cases. On the other hand, slamming response never occurs separately without a rigid body response because, obviously, it is a result of the rigid body motion of the ship in waves.

2.6.7 Combining Analytically Determined Response Components. Two main steps can be used in the procedure for combining the primary responses of a vessel:

- *Step 1:* Combine the low frequency wave-induced responses (rigid body) with the high-frequency responses (springing or slamming).
- *Step 2:* Add the mean value to the response resulting from Step 1. The mean value consists of the still water and the thermal responses. The latter is usually neglected.

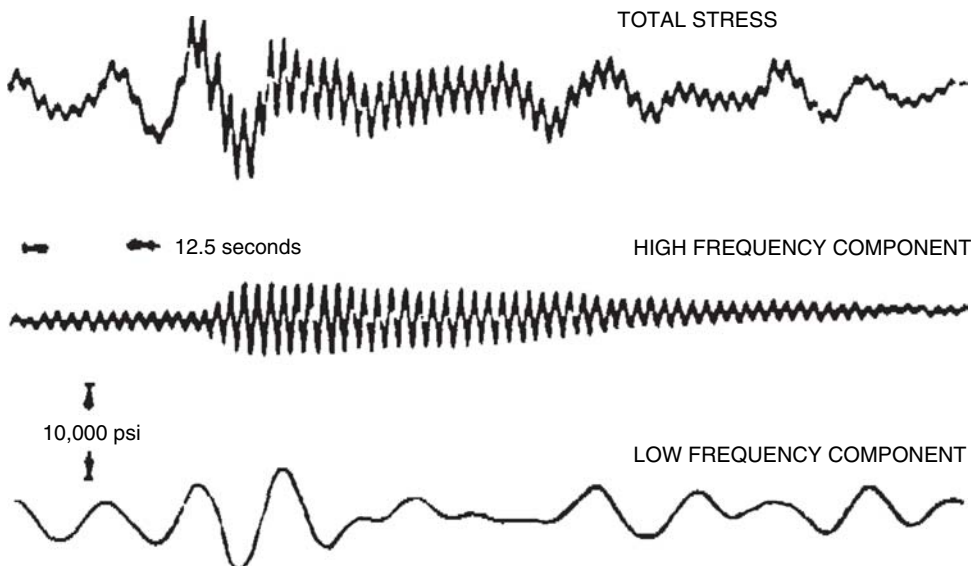


Fig. 19 Decomposition of a stress time history of an ocean-going bulk carrier.

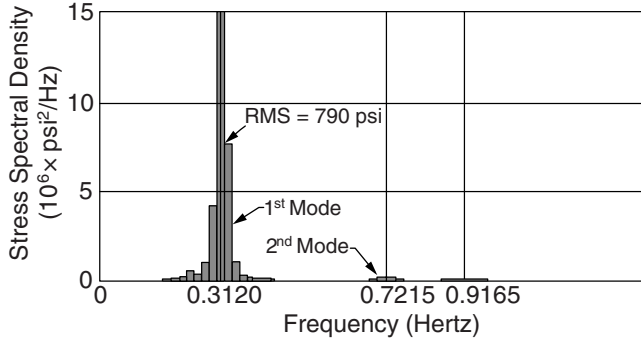


Fig. 20 Stress response spectrum of a large Great Lakes vessel (Critchfield 1973).

Each of these steps will be considered in the following paragraphs.

Step 1: A ship traveling in oblique irregular seas can be considered as a multiple linear system where the ocean waves represent a common input to the system. Over a short time period, the waves can be represented as a stationary random process. In general, the output of the system can be a time variation of any measurable quantity (e.g., motions, accelerations, velocities, loads, or stresses). The sum of the outputs of this multiple system represents the combined motion, acceleration, or stress. Therefore, the probabilistic definition of the sum is of interest in design.

The analysis presented next follows the development given by Mansour (1995). Figure 21 schematically describes the input/output procedure for n -linear systems. The analysis can be carried out in a frequency or time domain. For generality, the constants a_i are used to ensure uniformity of units and direction (e.g., to convert loads to stresses), all in the same direction. They can always be taken equal to one if not needed. The output is given by the convolution integral,

$$y(t) = \sum_{i=1}^n a_i \int_0^{\infty} h_i(\tau) x(t - \tau) d\tau \quad (95)$$

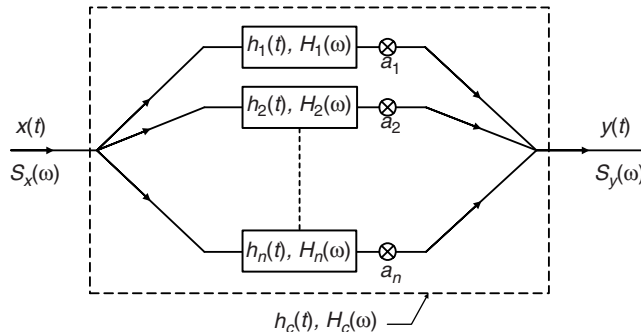


Fig. 21 Model for correlated wave loads acting on a marine structure.

where $h_i(\tau)$ are the impulse response functions of the individual components and x is the common input (i.e., a time history of wave surface elevation).

Because $x(t)$ is a common input to all terms of equation (95) and because the summation and integration signs can be interchanged in this case, a composite impulse response function, $h_c(t)$, can be defined as

$$h_c(t) = \sum_{i=1}^n a_i h_i(t) \quad (96)$$

Therefore, all the usual auto- and cross-correlation and spectral density relationships valid for a single linear system can be extended to the composite linear system using $h_c(t)$ as the system impulse response function.

In a frequency domain, the frequency response (transfer) function $H_i(\omega)$ for each component is obtained as the Fourier transform of $h_i(t)$,

$$H_i(\omega) = \int_0^{\infty} h_i(t) e^{-j\omega t} dt \quad (97)$$

Therefore, one can define a composite frequency response function $H_c(\omega)$ as

$$H_c(\omega) = \int_0^{\infty} h_c(t) e^{-j\omega t} dt \quad (98)$$

Substituting for $h_c(t)$ in equation (98) using equation (96) and noting equation (97), one can write

$$H_c(\omega) = \sum_{i=1}^n a_i H_i(\omega) \quad (99)$$

The relation between the input (sea) spectrum, $S_x(\omega)$, and the output (response) spectrum, $S_y(\omega)$, for a single component is given by the usual equation,

$$S_y(\omega) = H_i(\omega) H_i^*(\omega) S_x(\omega) = |H_i(\omega)|^2 S_x(\omega) \quad (100)$$

where $H_i^*(\omega)$ is the complex conjugate of $H_i(\omega)$. For the composite system, an equation similar to equation (100) can thus be written as

$$\begin{aligned} S_y(\omega) &= H_c(\omega) H_c^*(\omega) S_x(\omega) \\ &= S_x(\omega) \sum_{i=1}^n \sum_{j=1}^n a_i a_j H_i(\omega) H_j^*(\omega) \\ &= S_x(\omega) \sum_{i=1}^n a_i^2 |H_i(\omega)|^2 + S_x(\omega) \\ &\quad \times \sum_{i=1}^n \sum_{j=1}^n a_i a_j H_i(\omega) H_j^*(\omega) \\ &\quad \quad \quad i \neq j \end{aligned} \quad (101)$$

where $|H_i(\omega)|$ are the moduli of the individual frequency response functions and the double summation terms in

equation (101) represent the cross spectra terms. The first term in equation (101) is simply the sum of the individual response spectra, each modified by the factor a_i^2 . The second term, which can be either positive or negative, is a corrective term that reflects the correlation between load components.

If the frequency response functions $H_i(\omega)$ do not overlap on a frequency axis, that is, if $H_i(\omega)H_i^*(\omega) = 0$, then the second term in equation (101) drops out and the load components are uncorrelated. Furthermore, if the wave input is considered a normal process with zero mean, then the respective outputs of the n -components are jointly normal, and if uncorrelated it follows that they are also independent.

In general, the variance σ_c^2 of the combined output response is given as the zero moment m_0 of the output spectrum:

$$\begin{aligned}\sigma_c^2 = m_0 &= \int_0^\infty S_y(\omega) d\omega \\ &= \sum_{i=1}^n a_i^2 \int_0^\infty |H_i(\omega)|^2 S_x(\omega) d\omega \\ &\quad + \sum_{i=1}^n \sum_{j=1, j \neq i}^n a_i a_j \int_0^\infty H_i(\omega) H_j^*(\omega) S_x(\omega) d\omega \\ &\quad i \neq j\end{aligned}\quad (102)$$

Equation (102) can be written in a different form that makes it easier to define the correlation between the different response components:

$$\sigma_c^2 = \sum_{i=1}^n a_i^2 \sigma_i^2 + \sum_{i \neq j} a_i a_j \rho_{ij} \sigma_i \sigma_j \quad (103)$$

where σ_i^2 are variances of the individual load component,

$$\sigma_i^2 = \int_0^\infty |H_i(\omega)|^2 S_x(\omega) d\omega \quad (104)$$

and ρ_{ij} are correlation coefficients between individual load components,

$$\rho_{ij} = \frac{1}{\sigma_i \sigma_j} \int_0^\infty \text{Re}[H_i(\omega) H_j^*(\omega)] S_x(\omega) d\omega \quad (105)$$

The previous results can be generalized to the case of short-crested seas where the sea spectrum is defined in terms of frequency and wave spreading angle, μ . For a ship heading angle α , the combined response variance given by equation (103) is valid, but with equation (104) and (105) replaced by

$$\sigma_i^2 = \int_{-\pi/2}^{\pi/2} \int_0^\infty |H_i(\omega, \alpha - \mu)|^2 S_x(\omega, \mu) d\omega d\mu \quad (106)$$

and

$$\begin{aligned}\rho_{ij} &= \frac{1}{\sigma_i \sigma_j} \int_{-\pi/2}^{\pi/2} \int_0^\infty \text{Re}[H_i(\omega, \alpha - \mu) H_j^*(\omega, \alpha - \mu)] \\ &\quad \times S_x(\omega, \mu) d\omega d\mu\end{aligned}\quad (107)$$

“Re(·)” indicates the real part of the function, and H_j^* is the conjugate of the complex frequency response function.

Along with the definitions of equations (104) and (105) or (106) and (107), equation (103) forms the basis for combining the variances of a multiple system taking into consideration the correlation between the response components. If the response components are uncorrelated (i.e., if $\rho_{ij} = 0$), the second term in equation (103) drops out and the combined variance is simply the sum of the individual variances modified by the factors a_i^2 . On the other hand, if the individual components are perfectly correlated, ρ_{ij} will approach plus or minus one, and the effect of the second term in equation (103) on the combined variance can be substantial.

Considering a normal (Gaussian) seaway as a common input, the output of the multiple system is also normal. The PDF of the output peaks for a general normal random process with bandwidth parameter ε is given by equation (43) (Rice 1944) with m_0 given by equations (102) or (103). Extreme values of the peaks of the combined response can be estimated from equation (43) (and the corresponding CDF) using order statistics, outcrossing analysis, or Gumbel asymptotic distribution, as described previously.

Although the approach outlined here can be used to determine the extreme value of the combined response, equation (43) and the extreme value analysis are not suitable for direct use in design. A simplification of the described procedure is necessary. A simplified procedure has been developed by Mansour (1995) that reduces the outlined analysis to a simple formula. The combined response (stress) is

$$f_c = f_1 + K f_2 \quad f_1 > f_2 \quad (108)$$

where K is a probabilistic load combination factor and f_1 and f_2 are the individual extreme stresses (characteristic values) corresponding to two load components.

The characteristic design values f_1 and f_2 are usually determined from extreme value theory. For example, the expected extreme stress peak f_i in N_i peaks during a Gaussian design sea state is given by Cartwright and Longuet-Higgins (1956):

$$f_i = E[f_{i\max}] = \alpha_i \sigma_i \quad (109)$$

where σ_i^2 is the variance of the stress component i and α_i is a multiplier that depends on the number of peaks N_i and the bandwidth parameter ε_i ,

$$\alpha_i = [2\ell n(1 - \varepsilon_i^2)^{1/2} N_i]^{1/2} + 0.5772 [2\ell n(1 - \varepsilon_i^2)^{1/2} N_i]^{-1/2} \quad (110)$$

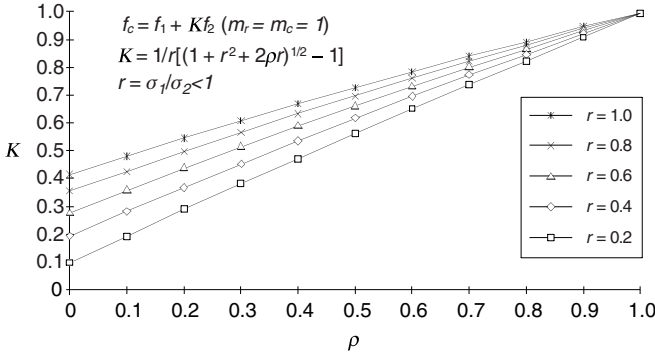


Fig. 22 Load combination factor for two correlated wave loads (Mansour 1995).

For two correlated responses, the load combination factor, K , was determined by Mansour (1995) to be

$$K = \frac{m_r}{r} [m_c(1 + r^2 + 2\rho r)^{1/2} - 1] \quad (111)$$

where

$$r = \frac{\sigma_2}{\sigma_1}, \quad m_r = \sqrt{\frac{\ln[(1 - \varepsilon_1^2)^{1/2} N_1]}{\ln[(1 - \varepsilon_2^2)^{1/2} N_2]}} \quad \text{and} \quad m_c = \sqrt{\frac{\ln[(1 - \varepsilon_c^2)^{1/2} N_c]}{\ln[(1 - \varepsilon_1^2)^{1/2} N_1]}} \quad (112)$$

The values σ_1 and σ_2 are the RMS values of the two load effects and ρ is the correlation coefficient between the two RMS stress components σ_1 and σ_2 , given by equation (105) for long-crested seas or equation (107) for short-crested seas. Typical values of ρ and the corresponding typical values of K for specific load combinations are given in Mansour (1995).

Figure 22 shows the trend of K as a function of the correlation coefficient and the ratio of the stresses for the special case when $m_r = m_c = 1$, as in the case when all processes are narrow band with approximately the same central frequency, which is approximately the case when combining stresses due to vertical and horizontal bending moments. In this figure, σ_1 was selected as the larger of the two stresses so that r always falls in the range zero to one. It is seen that for $\rho > 0.5$, K does not appreciably depend on r . From equation (111) or Fig. 22, the following extreme cases can be obtained:

- If $\rho = 1$ (i.e., the two stresses are fully correlated), $K = 1$ independent of the stress ratio, r .
- If $\rho = 0$ (i.e., the two stresses are uncorrelated), $K = 0.05$ for $r = 0.1$ and $K = 0.41$ for $r = 1$.

The second extreme case indicates that even though the two loads or stresses are uncorrelated, the fact that a second load exists will contribute somewhat to the combined stress (5 percent of f_2 for $r = 0.1$, or 41 percent of f_2 for $r = 1$).

2.6.8 Three Correlated Load Combinations. The simplified procedure for the three-load case is similar to that for the two-load case. The combined stress has the form

$$\begin{aligned} f_c &= f_1 + K_2 f_2 + K_3 f_3 \\ f_c &= f_2 + K_1 f_1 + K_3 f_3 \\ f_c &= f_3 + K_1 f_1 + K_2 f_2 \end{aligned} \quad (113)$$

where K_1 , K_2 , and K_3 are the load combination factors corresponding to the individual characteristic stresses f_1 , f_2 , and f_3 , respectively.

The characteristic stress (extreme) f_i in each instance is $\alpha_i(\text{RMS})_i$. The following load combination factors are restricted to the case when $\alpha_1 = \alpha_2 = \alpha_3 = \alpha_c$ (i.e., the case of narrow band processes with approximately the same central frequency). This case is adequate for combining stresses due to vertical and horizontal bending moments together with stress due to torsional moments or to local lateral pressure,

$$K_1 = \frac{1}{2} (\rho^* - r_2 - r_3 + 1) \quad (114)$$

$$K_2 = \frac{1}{2r_2} (\rho^* + r_2 - r_3 - 1) \quad (115)$$

$$K_3 = \frac{1}{2r_3} (\rho^* + r_3 - r_2 - 1) \quad (116)$$

where

$$r_2 = \frac{f_2}{f_1} \quad \text{and} \quad r_3 = \frac{f_3}{f_1} \quad (117)$$

and

$$\rho^* = [1 + r_2^2 + r_3^2 + 2\rho_{12}r_2 + 2\rho_{13}r_3 + 2\rho_{23}r_2r_3]^{1/2} \quad (118)$$

The correlation coefficients ρ_{12} , ρ_{13} , and ρ_{23} between the individual stress components f_1 , f_2 , and f_3 are to be determined from equation (105) for long-crested seas or equation (107) for short-crested seas. If available for these coefficients, experimental or simulation data may be used instead of equation (105) or (107). Because any of equations (113) will give identical results for the combined stress f_c , it is sufficient to use the first equation of (113) and equations (115) and (116) to determine K_2 and K_3 appearing in equation (113).

Equation (108) with K determined from equation (111) is applicable to many two-load combination cases in marine structures. For ships as an example, these two equations can be used to combine the effects of vertical and horizontal bending moments, vertical and torsional moments, vertical and springing moments, and horizontal and torsional moments. They can also be used to combine stresses due to primary vertical bending moment (or any of the other primary moments) with secondary stresses due to lateral pressure. In all cases, the characteristic stresses f_1 and f_2 may be taken as the most probable extreme values (or the expected values if preferred)

of the individual stress components, as given by equation (109) in the considered design state.

Note that the frequency response functions, $H_i(\omega)$, are readily computed in many ship-motion computer programs for individual loads or moments rather than stresses (e.g., primary vertical, horizontal, and torsional moments) as well as external hydrodynamic pressure. These individual load frequency response functions must be converted to stress frequency response functions by multiplying by an appropriate conversion factor (e.g., by one over a section modulus to convert a moment component to a stress component). These conversion factors are accounted for through the constants, a_i , appearing in equation (103). Therefore, in the case of a moment, a_i is equal to one over the section modulus. All stress components obtained from equation (109) must be at the same location and in the same direction. In case of a stress component due to external pressure, only the dynamic part of the pressure (i.e., excluding the still water pressure) is to be used in the calculation of the combined response. The still water stresses are to be added after obtaining the combined stress due to waves in the usual manner.

The presented model for load combination can also be used in conjunction with the finite element method. For example, in the case of vertical and horizontal moments, the K -factor determined from equation (111) provides the fraction of the horizontal bending moment to be applied simultaneously with the vertical bending moment on the hull. The load combination factor, K , depends on the correlation coefficient, ρ , which can be determined from equation (105) or (107), experimental data, or simulation. Some typical values of ρ are available for specific load combinations as follows:

- *Stresses due to primary vertical and horizontal moments.* For large tankers considered by Stiansen and Mansour (1975), the correlation coefficient was found to be dependent on the sea state and heading with values close to 0.45. In their 1973 session, the ISSC recommended $\rho = 0.32$. For $r = 0.67$, the first value of ρ results in $K = 0.65$ and the second value gives $K = 0.55$ ($m_r = m_c = 1$). That is to say, only about 60 percent of the stresses due to the horizontal moment should be added to those due to the vertical moment.

- *Stresses due to vertical moment and external hydrodynamic pressure.* For Mariner class ships, ρ was determined to be in the range 0.70 to 0.78 for panels near the midship section. If one assumes $\rho = 0.74$ and $r = 0.2$, equation (111) with $m_r = m_c = 1$ yields $K = 0.78$. Note the high correlation between the primary bending stress due to hull girder vertical moment and the secondary stress due to the hydrodynamic pressure near the midship section. Note also that ρ and the corresponding K -factor are associated with the time-dependent part of the individual stress components. The time-independent part of the stresses due to still water, for both hull girder

bending and hydrostatic pressure, should be added to the resulting combined wave stress in the usual manner.

Equation (113) for the three-load combination case can be also used in many applications to ships and marine structures. The K -factors appearing in the equation can be determined from equations (114) to (116). To get an appreciation of the factors K_2 and K_3 , consider the stress arising from vertical bending moment f_1 , horizontal bending moment f_2 , and local pressure f_3 near the midship section at a bottom plating. For $r_2 = 0.6$, $r_3 = 0.4$, $\rho_{12} = 0.4$, $\rho_{13} = 0.6$, and $\rho_{23} = 0.2$, equations (115) and (116) yield $K_2 = 0.67$ and $K_3 = 0.51$.

Note that for an extreme case when all three loads are fully correlated ($\rho_{12} = \rho_{13} = \rho_{23} = 1$), the values of the K -factors are always unity (i.e., $K_2 = K_3 = 1$), independent of the values of r_2 and r_3 . On the other hand, if all three loads are uncorrelated ($\rho_{12} = \rho_{13} = \rho_{23} = 0$), the K -factors will assume nonzero values and their magnitude will depend on r_2 and r_3 . The two-load combination case when $m_r = m_c = 1$ can be retrieved from the three-load combination equations by inserting zero for one of the load components.

Step 2: In this step, the still water and the thermal responses should be combined to form the mean value for the rigid body motion and higher frequency responses. The still water and thermal responses are weakly time-dependent variables so that in a given design extreme load condition, they can be considered as constants, say, over the duration of a design storm. Therefore, these two responses can be treated as static and can be combined for one or several postulated design conditions without difficulty. Alternatively, if statistical data are available for each of these responses the mean and variances of the combined response can be easily determined.

The still water response can be accurately determined for all loading conditions using many available computer programs. Several postulated extreme but realistic weight distributions can be assumed in the final stages of design, and the corresponding still water response can be computed. If a statistical description of the still water bending moment is adopted, data have shown that the general trend assumes a normal distribution for conventional types of ships. A mean value of the still water bending moment can be estimated for all voyages, or for a specific route such as inbound or outbound voyages. More detailed can be found in Soares and Moan (1998).

The still water response, the rigid body motion response, and higher-frequency responses are all functions of the ship weight and its distribution. For this reason, it is important that the combined response be calculated for a group of selected loading conditions and selected temperature profiles. Primary thermal response is usually induced by differences in water/air temperatures and by variations in ambient temperatures. Full-scale stress data measured on larger tankers indicate that the diurnal stress variations correlate well with the temperature differentials between air and sea.

Taking the North Atlantic route as an example, the average diurnal change of air temperature is about 5.6°C (10°F). The total diurnal change of deck plating temperatures may vary from -12.2°C (10°F) to 10.0°C (50°F), depending upon the cloud cover conditions and the color of the deck plating. For estimating the thermal loads on a ship hull, the sea temperature may be assumed as constant. Once the temperature differential along a ship hull is determined, the thermal stresses can be calculated using either a general-purpose finite element computer program or a simplified two-dimensional approach. The maximum thermal response can then be added to the still water response for certain postulated design conditions to form the mean value for the low- and high-frequency dynamic responses.

Although high thermal responses may not happen in high seas, a heavy swell can possibly occur under a clear sky. Therefore, several temperature conditions are to be considered when determining the combined design response. However, in many design analyses thermal stresses are ignored.

2.7 Long-Term Extreme Values in Non-Stationary Seas.

When concerned with predicting the most severe loading experienced by a ship or structure during the course of its useful lifetime, the sea conditions or the conditions of operation of the ship can no longer be assumed to remain constant. Sea states of varying severity from flat calm to the most severe storm may be encountered, and the occurrence and duration of sea conditions of various degrees of severity will depend on the geographic and seasonal operational profile of the ship or platform. The conditions of loading, speed, and heading will vary from one period to another, and the influence of all of these variables must be included in the computation of the long-term extreme loading. As in the short-term case, it is generally not possible to obtain a single precise value for the greatest load. Instead, the answer must be expressed in the form of long-term probabilities.

There are currently a half dozen methods used worldwide that obtain such long-term distributions, as summarized in Lewis and Zubaly (1981) and Stiansen and Chen (1982). The basic assumptions are the same in all these approaches. In addition to the assumed linearity of response, a fundamental assumption made in all methods is that in the short-term, the maxima of the response has a probability structure defined by the Rayleigh distribution ($\varepsilon = 0$). The short-term response is a zero-mean stationary Gaussian narrow-band process with a maxima defined by the single parameter, $m_0 = \sigma^2$. The short-term probabilities are conditional (i.e., to be specific they assume different values for each value of m_0) and the density can be written as

$$f(x | m_0) = [x/m_0] \exp[-x^2/2m_0] \quad (119)$$

where m_0 is the zero-th spectral moment (as treated in Section 2.6) representing the mean-square response of each short-term exposure. This single parameter, m_0 , defining a Rayleigh distribution is considered to be a

random variable depending on the sea condition and the speed, loading, and heading of the ship during each short-term interval. Because of the assumptions stated previously, the following development is believed to be conservative.

To obtain a long-term distribution, it is necessary to consider many different short-term intervals in which the response is defined by m_0 and can be calculated by the methods obtained from Section 2.7. This is the way by which the geometry and characteristics of the ship are injected into the analysis. The factors affecting the value of m_0 include speed, V , heading, μ , condition of loading, a measure of wave height, H , some measure of wave period, such as T_m , the modal period, and sometimes another measure of wave spectral form or shape.

To develop a long-term distribution in practice, some simplifications are needed. The speed, V , can be eliminated by recognizing that it is not an independent variable and specifying that for each time interval, the speed is appropriate for the prevailing sea condition, loading, and ship-to-wave heading on which it depends. (Note that the low frequency bending moment is not greatly affected by ship speed, in any case.) The heading variable, μ , cannot be eliminated but it is customary to assume that there is an equal probability of all headings, statistically independent of the other variables. This may not be true on any one voyage but it tends to average out over many round trips. Finally, loading can be handled by assuming that the number of conditions is limited (as out-bound loaded, ballast return), each with a different mean (still water) bending moment, and that completely independent calculations can then be carried out for each. Assuming that two parameters, H and T , suffice to describe the sea state, we are left with the parameters, μ , H , and T .

If the previous factors are assumed to be random variables, then the spectral moment, m_0 , is also, and its probability density is conditional. Recognizing the conditional relationships between the response, x , and m_0 , and the conditional relationship between m_0 and all the factors enumerated previously, a joint long-term probability density of all the variables may be assumed in the following form:

$$q(x, m_0, \mu, H, T) = f(x | m_0)q(m_0 | \mu, H, T)q(\mu, H, T) \quad (120)$$

where the first factor is the short-term conditional density of x , equation (119), and the second is the conditional density of m_0 , given the operational and environmental factors. Finally, the last factor is the joint probability density of the parameters influencing m_0 .

To obtain the long-term probability density of the response, x , equation (120) must be integrated with respect to m_0, μ, H , and T . However, the long-term probability of interest is that of the response peaks or maxima of x exceeding some level, x_1 . This is obtained by integrating the long-term probability density of x with

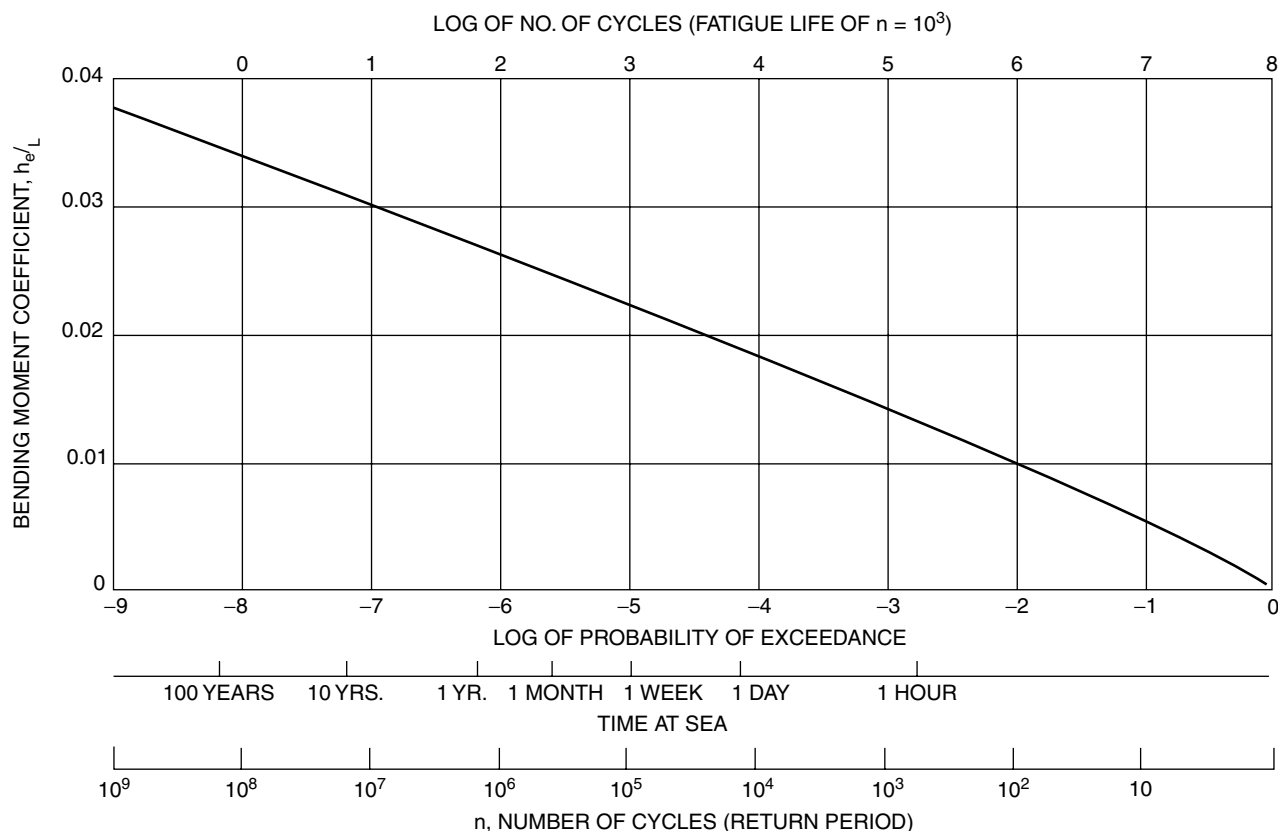


Fig. 23 Long-term probability distribution for wave-induced bending moment in *S.S. Wolverine State*, corrected to average North Atlantic weather (based on Band 1966).

respect to x over the interval x_1 to infinity. Under the Rayleigh assumption, equation (119), this last integration may be done formally, so that finally the long-term probability that a response exceeds x_1 can be written as

$$Q(x > x_1) = \int_{m_0} \int_{\mu} \int_H \int_T \exp[-x_1^2/2m_0] \cdot q(m_0 | \mu, H, T) \cdot q(\mu, H, T) dm_0 d\mu dH dT \quad (121)$$

After this point, the development of a useful engineering procedure requires the synthesis of the conditional and joint probabilities and their integration, and it is here that the divergence in several detailed approaches begins. We do not know the exact probability densities of any of the factors involved, much less the form of their joint density. The developers of the various methods have had to interpret historical wave data, devise means of using it in the required integrations, devise means of handling the speed, heading, and loading factors, and finally have had a choice of the order of integration. The result is that the various methods appear to differ. Details of several methods are given in Bennet et al. (1962), Band (1966), Nordenstrom (1973), Fukuda (1970), Soeding (1974), and Mansour (1972). However, Ochi (1978) adopts a some-

what different mathematical concept that leads to similar numerical results.

Whatever the method, the final result is a numerically defined initial distribution of the maxima in the great many short-term Rayleigh distributions, which in effect are superimposed in the synthesis. Some choose to plot the results on some form of probability paper. Figure 23 from Band (1966) is a somewhat common form of presentation. The ordinate is the level x_1 in the previous equation. The abscissa is a logarithmic scale of $Q(x > x_1)$ or its reciprocal, n , known as the return period (both are shown in the figure). The formulation results in the probability that the peak of a response excursion, chosen at random, will be greater than some level—in the example, the probability is about 10^{-8} that the bending moment coefficient will exceed about 0.035. Roughly, the formulation involves probability per cycle of response. This is the reason that the computations are carried out to such low probabilities. The auxiliary scale in the figure indicates that based on average encounter periods for the ship, the corresponding exposure time and probabilities less than 10^{-7} represent ship lives and multiples thereof.

To illustrate the considerations involved in the long-term prediction methods, a particular simplification of

equation (121) can be made. Suppose the ranges of all the variables μ , H , and T are systematically divided into discrete intervals of width such that the value of the variable at the center of the interval is representative of the variable anywhere in the interval. With this assumption, equation (121) may be approximated as a summation,

$$Q(x > x_1) \approx \sum_{\mu} \sum_H \sum_T \int_{m_o} \exp[-x_1^2/2m_o] \cdot q(m_o | \mu, H, T) \cdot p(\mu, H, T) dm_o \quad (122)$$

where it is understood that the discrete central values of the variables are intended. The function $p(\mu, H, T)$ denotes the probability that the variables μ , H , and T lie simultaneously in their respective intervals. The conditional probability of the spectral moment, m_o , accounts for statistical variation about the value that would be estimated by considering each of the fixed central values and applying the methods of Section 2.6.

For present purposes, a further simplifying assumption can be made. Suppose that the intervals into which the ranges of the variables μ , H , and T are divided are sufficiently small that the spectral moment is representative of the moment obtained so long as the variables were anywhere within the bounds of their respective intervals. The spectral moment can be estimated by considering the central values of the variables fixed. This amounts to saying that the spectral moment, m_o , is a deterministic function of ship heading and sea state. With this assumption, the conditional probability in equation (122) tends toward a delta function, and when the integration with respect to m_o is performed, the expression becomes

$$Q(x > x_1) \approx \sum_{\mu} \sum_H \sum_T \exp[-x_1^2/2m_o] p(\mu, H, T) \quad (123)$$

where the notation has been streamlined to facilitate further development. In particular, the summations are over all the discrete intervals previously defined, and the arguments of the joint probability symbolize the central values defined in conjunction with equation (122). Most importantly, the value of m_o in the exponential is taken as a deterministic function of the central values of the operational and environmental variables. In this form, the synthesis problem comes down to constructing a suitable discrete representation of the joint probability.

To illustrate how this joint probability might be constructed, we can argue as follows. We imagine the ship lifetime to be subdivided into a large number of short-term intervals—for example, four hours each—during which the conditions of loading, ship speed, heading, and sea state remain constant. Now assume that the values of all of the parameters μ , H , and T are known for each of these time intervals. In fact, this requires the ability to predict the operational profile of the ship in terms of its loadings, speeds, headings, and the weather conditions that it will encounter. The forecasting of the ship's cargo loading, speed, and routing is normally performed by the

ship owner or designer as a part of the preliminary design process. The forecasting of sea and weather conditions that the ship will encounter depends on the availability of a sea state database of suitable form and extent.

In equation (123), the sea state is represented by two parameters, measures of height, H , and of period, T . A discussion of the various means including standardized formulas currently used to represent spectral areas and shapes is given in Section 2.6 and in Beck et al. (2009). In some spectral formulas, only one parameter—for instance, significant wave height, $H_{1/3}$ —is used to characterize the sea state. In others, the additional parameter T_Z , the zero-crossing period, or T_M , the modal period, is employed, giving a somewhat more flexible means of representing a wide range of spectra of similar shape or form (i.e., “families”). Ideally, variations in the shape of the spectra should also be considered because actually measured ocean wave spectra show considerable variety—including double peaks resulting from superposition of waves from two or more storms. However, for simplicity it is often assumed that two parameters will be sufficient.

The long-term frequency of occurrence of sea states of different severity but of similar spectral form can then be expressed in terms of a joint probability density function for $H_{1/3}$ and T_M . This joint probability density of $H_{1/3}$ and T_M can be presented for a given ocean area in the form of a table, as in Hogben and Lumb (1967), or as a contour plot or scatter diagram, as shown in Fig. 24 and Table 1 in Section 3.15, respectively. The values in the tables, or contours of the plot, are equal to the probability (fraction of time) that the sea state is characterized by the simultaneous occurrence of values of H falling within the interval H_1 to H_2 , and T falling within the interval T_1 to T_2 . This diagram would assume a single form for the spectrum (e.g., Bretschneider or JONSWAP). If the ship operates in different geographic areas having different sea state characteristics, such diagrams would be required for each area of operation.

A composite sea state distribution can be constructed if we have such tables or diagrams for all parts of the ship's route of operation, together with information stating the fraction of time that the ship spends in each area. To illustrate this synthesis, consider a tanker trading between Europe and the Persian Gulf via the Cape of Good Hope. The tropical portions of the route would be characterized by a preponderance of low sea states, whereas the Cape region would have a greater portion of high sea states. A series of diagrams similar to Fig. 24, or a tabulation of the frequency of occurrence of pairs of values of $H_{1/3}$ and T_m similar to Table 1, would be necessary to represent these extremes as well as the gradations of sea climates typical of other portions of the route. Because each scatter diagram is, in fact, a bivariate probability density function representing the relative frequency of occurrence of sea states of all degrees of severity in the applicable ocean area, the integral of the diagram over all values of $H_{1/3}$ and T_m must equal unity. The ship will be

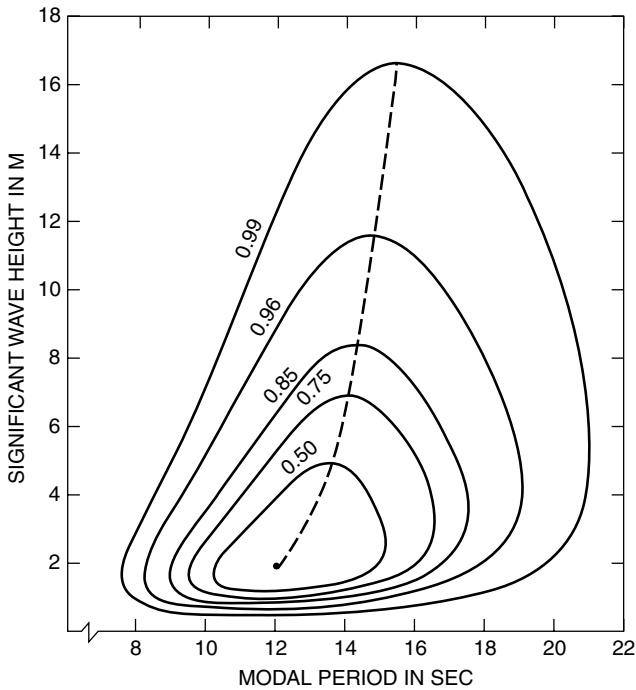


Fig. 24 Confidence domains of significant wave height and modal period for the (mean) North Atlantic (Ochi 1978).

exposed to different geographic areas for different periods during each fraction of its voyage. Therefore, the ordinates of the scatter diagram for each area along the route must be multiplied by the fraction expressing the proportion of time that the ship spends in that area. A composite diagram or tabulation for the entire voyage is then constructed by adding together such weighted ordinates of all the diagrams representing voyage segments. The IACS standard wave data given in Table 1 is an example of a composite wave scatter diagram for voyages in North Atlantic conditions.

For each set of values of the variables, μ , H , and T , the ship load response can now be determined and a value of the spectral moment, m_0 , of the loading computed. This computation would normally be performed using one of the standard ship motions and loads programs referred to previously. The summation in equation (123) is then approximated by

$$Q(x > x_1) \approx \sum_{\mu} \sum_{H_{1/3}} \sum_T \exp\left(\frac{-x_1^2}{2m_0}\right) p(\mu)p(H_{1/3})p(T_m) \quad (124)$$

The simple product form of equation (124) is based on the assumption that all of the remaining random variables are statistically independent. In effect, many Rayleigh distributions are superposed, and weighted by the expected frequency of occurrence of all the three variables' combinations. To use the results provided by equation (124) in selecting a design load value, a

load is chosen having an acceptably low probability of exceedance and, conceptually, one may proceed somewhat as follows. The average period of wave encounter at sea is about 10 seconds. In a 20- to 25-year lifetime, a ship will encounter approximately 10^8 waves; the exact value depends upon the operating profile and the portion of the time spent at sea. It is reasonable to design the structure so that the ship will withstand the greatest single peak excursion of the bending moment or other loading expected in that lifetime. Thus, the loading will have a probability of exceedance of once in 10^8 cycles, which would appear to be a reasonable target value. Equation (124) expresses the probability that any one oscillatory peak will exceed the value x_1 .

However, it should be noted that the load corresponding to this probability is subject to variation, just as in the short-term case. Thus, during one ship's lifetime there may be one peak value that exceeds the value corresponding to the 10^{-8} probability, and there may be none or there may be several. If the ship sails for another 20 years in the same service, or if a second identical ship is considered, this 10^{-8} value may be exceeded one or more times again. If it is exceeded again, the second exceedance may be by a margin much greater than that experienced the first time, or it may be less.

This random behavior of the expected greatest peak load may be taken into consideration by using a procedure suggested by Karst in an Appendix to Hoffman and Lewis (1969). He formulates a problem that can be restated as follows: To determine a bending moment (or stress), x_L , such that the probability that a ship will exceed it in its lifetime has a specified value $P(x_1 > x_L)$, where x_1 is the expected bending moment corresponding to a lifetime of n_L maxima (or cycles) at

$$Q(x > x_1)_L = 1/n_L$$

The specified probability $P(x_1 > x_L)$ is a risk factor or confidence level. Based on a Poisson model, the approximate result is that the design bending moment, x_L , can be read as

$$Q(x > x_1) = P(x_1 > x_L) \cdot Q(x > x_1)_L = P(x_1 > x_L)/n_L \quad (125)$$

The procedure is illustrated in Fig. 25, which shows a graph of the function $Q(x_1 > x_L) = 1/n$, plotted in the usual manner. At a probability level of 10^{-8} , the ordinate of the curve is the expected value of load (midship bending moment) having this probability of exceedance in any one cycle. Schematically, the small graph plotted along the vertical axis at this probability level is the probability density function for the lifetime 10^{-8} peak values. This density function expresses the random behavior of the greatest peaks occurring in many records containing n_L peaks each. The boundary of the shaded portion of this probability density function corresponds to the one-percent value (i.e., the shaded area is equal to one percent of the total area under the curve). Hence,

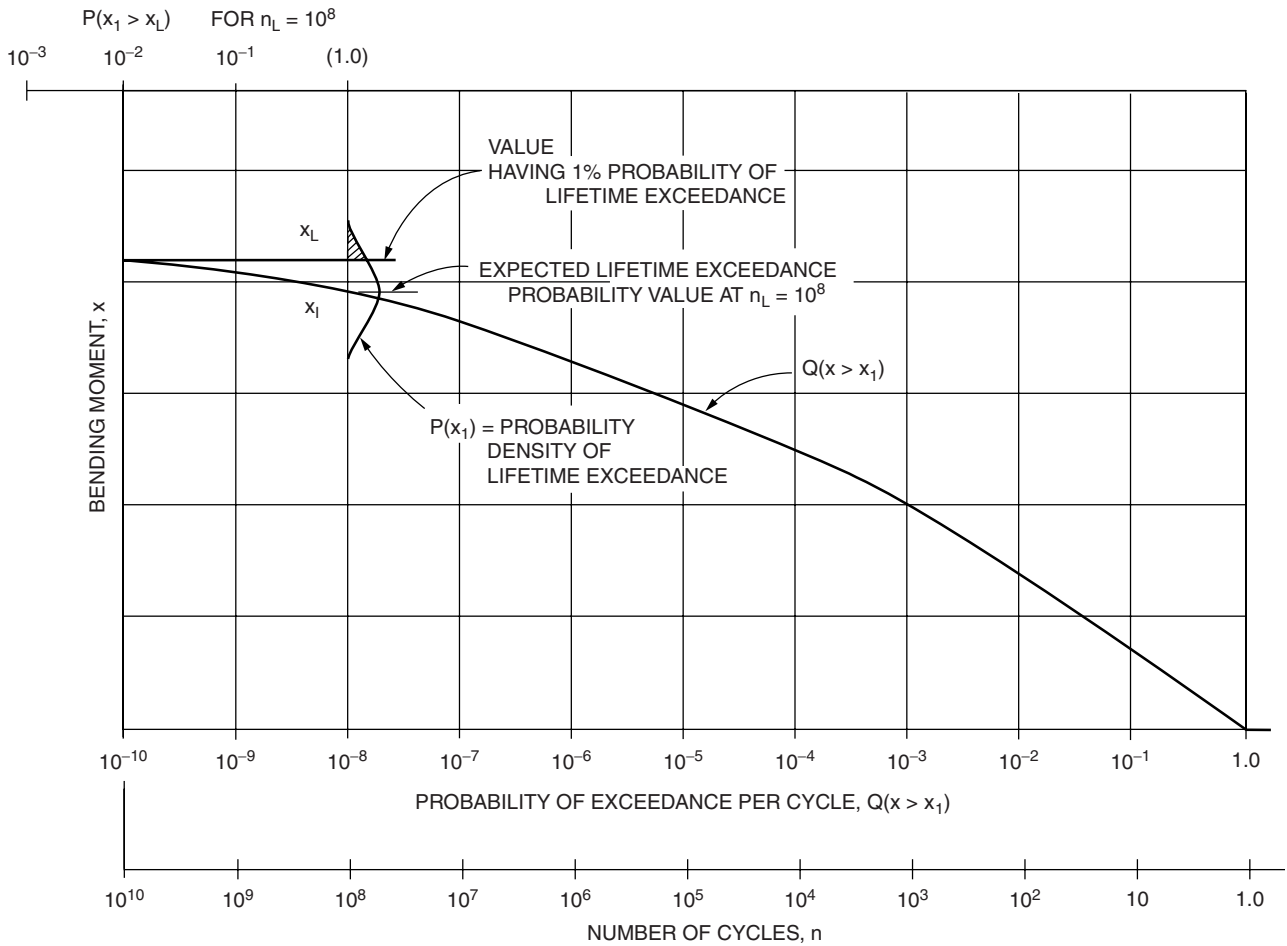


Fig. 25 Typical long-term exceedance probability of wave-induced bending moment.

$P(x_1 > x_L) = 0.01 = 10^{-2}$. If this one percent level is extrapolated horizontally to the left, it is found to intersect the $Q(x > x_1)$ curve very nearly at the probability of 10^{-10} , which is the value given by equation (125). This provides a convenient way of obtaining $Q(x > x_L)$ for a $P(x_1 > x_L) = 0.01$ by extrapolating the long-term curve to lower values of probability. The significance of the result is that it defines a design load that would be exceeded once in any one ship in a fleet of 100 similar vessels in the same service.

For example, if $P(x_1 > x_L)$ is set equal to 0.01 and n_L equal to 10^8 , it is found that to a close approximation, the design load x_L can be read at $Q(x > x_L) = 10^{-2}/10^8 = 10^{-10}$. Thus, it is seen that the one percent level of confidence is obtained by using a design load x_L corresponding to the probability of exceedance $Q(x > x_1)$ having a value equal to the product of the risk factor (or confidence level) and the expected probability of exceedance in a ship's lifetime of n_L cycles. Alternatively, the lifetime probability (risk factor) is

$$P(x_1 > x_L) = n_L \cdot Q(x > x_L) \quad (126)$$

However, note that equations (125) and (126) break down when $x_1 = x_L$ or $Q(x > x_L) = 1/n_L$. In this limiting case, $P(x_1 > x_L)$ is 0.667 instead of $P(x_1 > x_L) = n_L \times 1/n_L = 1.0$, as given by equation (126) (see Fig. 25). Equation (126) is useful in calculating probability of failure (Section 5.3) for the risk factor. $P(x_1 > x_L)$ can also be considered as the probability that any one ship in a fleet of many similar ships will exceed the design load, x_L , in its lifetime. Hence, it is sometimes referred to as the lifetime probability to distinguish it from the probability per cycle, $Q(x > x_1)$, or $1/n$. See further discussion in Faulkner and Sadden (1978). Note also that a curve of $P(x_1 > x_L)$ can be obtained for any value of n_L by adding a new scale to the plot of $Q(x > x_1)$. For example, a scale of $P(x_1 > x_L)$ has been added at the top of Fig. 25 for $n_L = 10^8$.

The foregoing analysis yields an estimate of the probable exceedance value to be expected during the long period of exposure in which the full range of variation of speeds, headings, and other variables is experienced. Equation (124) is based upon the Rayleigh distribution for the peak values of the random process

and, as pointed out by Ochi (1978), it does not explicitly contain the time of exposure. Instead, it should be thought of as applying to the large number of peak excursions roughly estimated for the ship's lifetime. The number of oscillatory peaks in the period can be accurately calculated as follows. During one of the short-term intervals in which the variables μ , $H_{1/3}$, V , and T_m remain constant, the mean number of zero crossings in unit time is given by

$$n_Z = \frac{1}{2\pi} \sqrt{\frac{m_2}{m_0}} \quad (127)$$

Here m_2 is the second moment of the spectrum of the response, as defined in Section 2.6. It is consistent with the Rayleigh assumption that each zero crossing corresponds to one peak of the random process, so that equation (127) will also give the number of peaks per unit time, n_2 . If T equals the long-term period in hours, the total time during which a specific set of the variables, μ_i , H_j , T_k , will prevail is given by

$$T_i = p(\mu)p(H)p(T)T \quad (128)$$

and the total number of oscillations during the time T is given by

$$N = T \sum n_Z p(\mu)p(H)p(T) \quad (129)$$

To incorporate this number into the calculation of the probability, Q , each term in equation (124) must now be multiplied by a weighting function that is the ratio of the number of oscillatory peaks corresponding to each of the intervals of summation to the total number of peaks given by equation (129),

$$n_Z^* = \frac{n_Z(\mu, H, T)}{\sum n_Z p(\mu)p(H)p(T)}$$

instead of 1.0, as assumed in equation (124). Hence the final result, modified to express the probability in terms of time, is

$$Q(x > x_1) = \sum_{\mu} \sum_H \sum_T n_Z^* \exp\left(\frac{-x_1^2}{2m_0}\right) p(\mu)p(H)p(T) \quad (130)$$

Lewis and Zubaly (1981) evaluated an example that indicates the result obtained by (124) and (130) are nearly the same for the container ship example. This is explained by noting that the greater bending moment values generally occur in head seas corresponding to the greater number of peaks, or greater mean frequencies of oscillation. The loadings in following seas are generally much lower and make very little contribution to the overall probabilities.

The foregoing procedure leads to an estimate of the long-term exceedance values that consider all the different sea conditions the ship may encounter during its life-

time. The weighted summation includes contributions from low sea states that occur frequently but individually have low probabilities of causing extreme events and from high sea states. Each has a high probability of causing an extreme event that occurs relatively infrequently. Because of the wide range of conditions to be included in a computation of this nature, it is seen that considerable computational resources will be required.

For the problem of determining cyclic loading for fatigue design, it is important to note that the long-term distribution discussed here can provide basic information. Figure 25 shows such a distribution, with a scale of probability and number of cycles at the bottom. If the life of the ship for fatigue studies is assumed to correspond to 10^8 cycles, a new reversed scale is constructed, as shown at the top, giving the number of cycles expected to reach any specified level of bending moment.

2.8 Short-Term Versus Long-Term Extreme Values and Design Considerations. Sections 2.6 and 2.7 describe procedures for determining extreme values in stationary short-term and non-stationary long-term seas, respectively. The former is restricted by the stationary condition to short periods (e.g., the peak three hours of a storm). The latter is based on "collection analyses" and estimates the lifetime extreme value from a projected mission profile of the ship (route, loading conditions, heading, and speed) and available wave statistics in the ocean zones along the ship route. Either method may be used to determine the design loads acting on a ship. Either may also be used to determine the probability distribution of the extreme (design) load, which is necessary to conduct reliability analysis.

If the short-term extreme value approach (Section 2.6) is adopted to determine the design load or load probability distribution, a design storm or several severe sea conditions should be postulated from which the extreme value or its probability distribution can be determined; see Mansour (1972) and Ochi (1978). The design storm can be derived from historical data of waves along the ship route and a prescribed encounter probability or return period; see Mansour and Preston (1995). The extreme value and its probability distribution can then be determined directly from the methods described in Section 2.6 (see also Ochi 1978). The main advantage of this procedure is its simplicity and consistency. It should be noted that the computed values from this procedure are conditioned values (i.e., conditioned on the ship encountering the specified storm or several severe sea states) for the specified length of time.

If the long-term extreme value approach (Section 2.7) is used to determine the design load or load probability distribution, the mission profile of the ship must be postulated including ship route, speed, heading, and loading conditions. The main advantage of this approach is that it provides additional information to conduct fatigue analysis, such as cyclic loading data. This elaborate procedure provides unconditional lifetime probabilities. Its

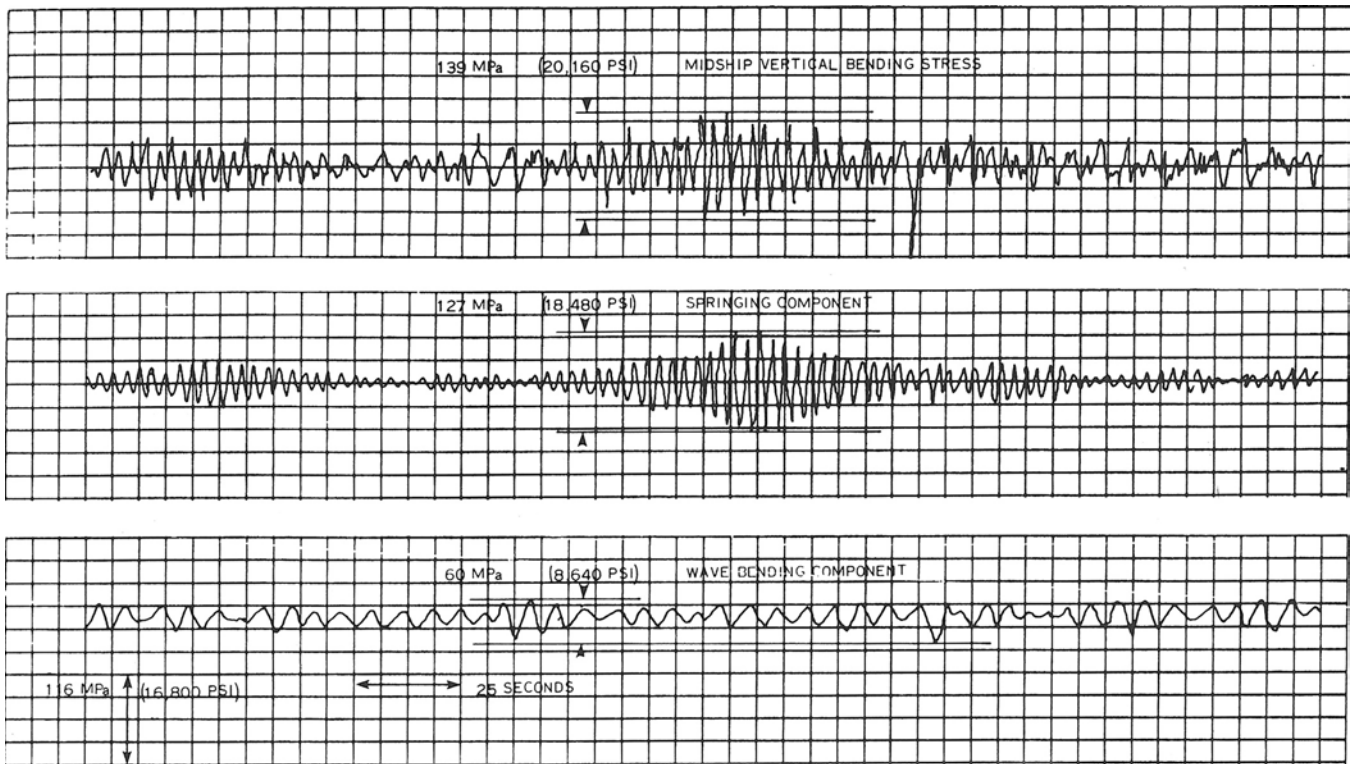


Fig. 26 Shipboard record of midship stresses—Great Lakes ore carrier, storm condition.

main disadvantage is its complexity relative to the short-term analysis.

2.9 Other Dynamic Loads. Some of the dynamic loads addressed in this section are strongly dependent of highly nonlinear characteristics of the fluid motion. For those areas—such as the bottom and flare slamming features, deck wetness, green water phenomenon, and cargo sloshing—pending the development of completely reliable theoretical methods, the value of direct experimental determination for a new design should be recognized.

2.9.1 Springing. An important effect of sea waves on some ships is the excitation of random hull vibration that may continue for extended periods of time. Known as *springing*, this phenomenon has been noticed particularly in Great Lakes bulk carriers (Matthews 1967), but it has also been reported on large ocean-going ships of full form by Goodman (1971), Little and Lewis (1971), and more recently by Melitz et al. (1992) and Witmer and Lewis (1995). The explanation of the occurrence of springing is that long ships of shallow draft and depth are comparatively flexible in longitudinal bending and consequently have an unusually long natural period of vertical hull vibration (two-noded periods of 2 sec or longer). Experimental and theoretical studies (Hoffman & van Hooff 1973, 1976) confirmed that when such a ship is running into comparatively short waves that give resonance with

the natural period of vibration, significant vibration is produced. A corresponding fluctuation in stress amidships due to springing is therefore superimposed on the quasi-static wave-induced bending stress. Shown in Fig. 26 is a typical stress record of the superposition of the two stress components as obtained from full-scale measurements of a Great Lakes ore carrier.

The well-developed strip theory of ship motions has been applied to springing in short waves (Goodman 1971). Although motions of a springing ship may be very small, the theory provides information on the exciting forces acting on the ship in the short waves that produce springing. Hence, when these forces are applied to the ship as a simple beam, the vibratory response can be predicted. Despite the fact that strip theory is not rigorously applicable to such short waves, results for one ocean-going ship were found to agree quite well with full-scale records. Further coordination between theory and experiment has been attempted for Great Lakes ships, including model tests where idealized wave conditions can be provided (Hoffman & van Hooff 1973, 1976; Stiansen et al. 1977; Troesch 1984a).

If the waves that excite springing were regular in character, the springing could be avoided by a small change in speed. But in a real seaway containing a wide range of frequencies, the springing varies in a random fashion and a speed change may have little effect. The

springing excitation and response can then be treated as stochastic processes that can be handled by the technique discussed in Section 2.6. However, it has been shown by Kumai (1974) and Troesch (1984b) that longer waves in the spectrum can also excite the hull vibration. This introduces nonlinear aspects that are important to consider.

2.9.2 Slamming Loads. When a ship operates at high speeds, especially in head seas, the bow may occasionally emerge from one wave and re-enter the next wave with a heavy impact of *slam* as the bottom forward comes in contact with the water. Related phenomena are associated with the impact of large waves on the bow topsides having pronounced flare and with green water on deck coming in contact with the front of a deckhouse or superstructure. In each case, the phenomenon involves the impact at high relative velocity between the free surface of the nearly incompressible water and a portion of the ship's structure.

Two noticeable effects can be caused by bottom slamming. There may be localized structural damage in the area of the bottom that experiences the greatest impact pressure. This may include set up plating and buckled internal frames, floors, and bulkheads. A second effect of bottom slamming is a transient vibration of the entire hull in which the principal contribution comes from the fundamental two-node vertical mode. This slam-induced vibration is termed *whipping*, and it may result in vibratory stress intensities that are equal in magnitude to the wave-induced low-frequency bending stresses (see Fig. 27).

Bottom slamming pressure prediction is considered in Beck et al. (2009). As indicated in that reference, approximate methods of calculating impact pressures are available, one by Ochi and Motter (1973) for merchant hull forms and the other by Stavovy and Chuang (1976) for high-speed vehicles. Recent progress of developing analytical methods for the latter case has been made. In contrast to slamming at bottom forward, aft slamming was recently noted on the ship stern of a large cruise vessel with a large flat after-body, propelled by azimuthing pod propulsion. Aft slamming may even take place in long waves of a low sea state in head seas in which the pitch-

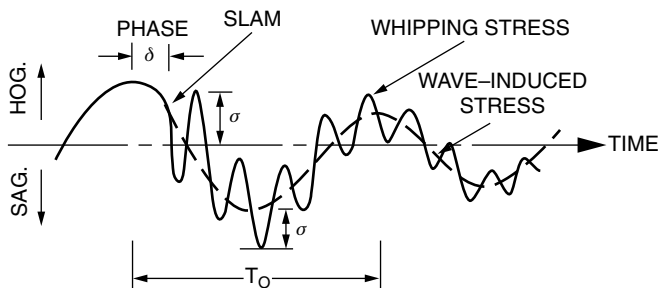


Fig. 27 Explanatory sketch of whipping stresses.

ing motion may cause the after body of the vessel to contact the waves, resulting in slam on a large area of the flat overhanging (Lepeix 2001).

With regard to slamming at bottom forward, Ochi (1964) has concluded that slamming is possible if two conditions are fulfilled simultaneously:

- The forefoot must emerge above the surface of the water, and
- At the time of re-entry, the relative velocity between the ship bottom and the water must exceed some threshold value. From model experiments, the threshold velocity was found to be 3.7 m/sec (12 ft/sec) for the Mariner class cargo ship.

The intensity of whipping depends on the magnitude of the force resulting from the impulsive pressure of the slam on its longitudinal location and on the duration of the force impulse. Much of the available information on the intensity of pressure, p , resulting from slamming has been obtained from model tests. These have been performed with two-dimensional models in calm water, and with full three-dimensional models moving through waves. Figure 28, from Ochi and Motter (1973), contains a compilation of such model test data. These results are usually fitted to a curve of the form given by $p = kv^2$,

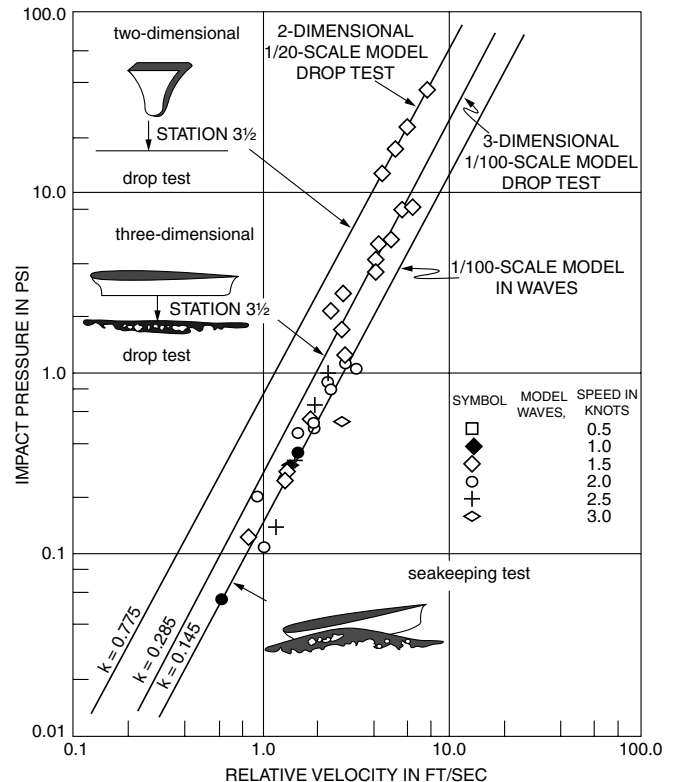


Fig. 28 Comparison of pressure-velocity relationship obtained in three different types of experiments.

where v is the relative vertical velocity. The coefficient k is shown for the three types of tests in the figure.

The impact pressure is distributed over an area of the ship bottom in the immediate vicinity of the point of re-entry, and is typically a maximum on the centerline at any instant of time. Greater pressures are found to occur where the bottom is nearly flat. The total force is then given by the integral of this pressure over the area of bottom on which it acts. As the ship forefoot re-enters the water, the point of maximum pressure tends to move toward the bow. At a given station along the length, the duration of the pressure pulse is typically a few tens of milliseconds, but as a result of the movement of the re-entry location the pressure pulse moves also, maintaining its peak intensity. The total duration of the force pulse that the ship experiences will therefore be several times as great as the pulse duration at a single station. This space-time behavior of the force is illustrated in Fig. 29, from Ochi and Motter (1973).

Slamming pressure rises and decays sharply with a very short duration for large ocean-going vessels. Consequently, unlike the wave loads—which can be treated as quasi-static loads—the slamming load is highly transient in nature, and is strongly affected by the dynamic characteristics of the structure on which it acts. Ng (1994) performed a parametric study to investigate the effect of the responses of bottom structures to the slamming loads if they were to be used in a static analysis for strength evaluation. He finds that to obtain compatible transient structural response from a static structural analysis, the slamming load commonly determined from a rigid ship model, either experimentally or analytically, must be modified by a factor called the dynamic load factor. In the parametric study, large bulk carriers of different sizes were considered. The forward part of the ship from the aft bulkhead of No. 2 hold to the fore peak is represented by a three-dimensional finite element model. The rest of the ship girder is modeled by 16 elastic beam elements of appropriate cross-sectional properties, and is connected to the finite element model of the fore end of the vessel by a rigid beam system. Linear static analysis is first carried out for the fore end bottom structures subjected to the load distribution determined following

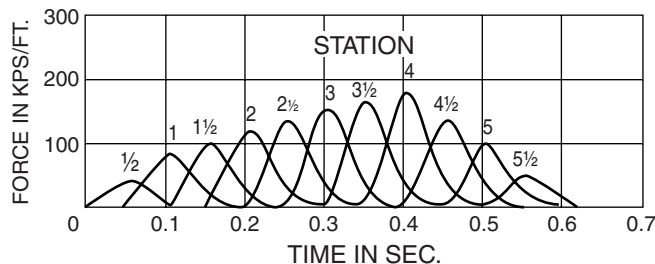


Fig. 29 Calculated force applied at various stations as a function of time—Mariner class, sea state 7, significant wave height 7.62 m (25 ft), ship speed 3.81 m/s (7.4 knots), light draft.

Ochi and Motter (1969, 1973). Linear dynamic analyses of the structural model of the entire hull girder are then performed, with the same magnitudes and spatial distributions as in the static case, except that the pressures are assumed to follow an isosceles triangle impulse to simulate the slam characteristics. These two analyses are then compared to identify the “reference” modal frequency for which the modal deflection of the fore end bottom structures follows the deflection of the static analysis. The dynamic load factor is obtained by dividing the maximum stress, obtained from the stress time history constructed using the harmonics of the “reference” and greater modal frequencies, by the static stress. Ng (1994) finds that the dynamic load factor varies with the impulse duration and depends on the type and scantling of bottom structures. Within the scope of the parametric study, the dynamic load factor is found to be around 0.25 to 0.55 for both longitudinal and transverse stresses.

2.9.3 Bow Flare Impact. Bow flare impact loads usually refer to the wave loads acting on the sides of the flared bow region, resulting from severe vertical relative motion. Early work by Kaplan and Sargent (1972) predicted forces due to flare entry in which the load is computed on the basis of the nonlinear variations in buoyancy and inertial forces, over and above those used in the linear ship motion analysis. Another approach is taken by Chen and Ng (1982), where a semi-empirical method is used to account for flare impact over and above the mean waterline in a time simulation by taking due consideration of the phase relation of relative motion obtained from linear strip theory. The semi-empirical formulation is derived based on pressure time histories measured from model tests of a fast cargo ship that suffered heavy buckling of deck plating in the forward region, presumably due to excessive flare impact in severe seaways. The model tests are intended to identify the impact loads on the flare causing the damage experienced by the vessel. A typical impact pressure time trace obtained from model tests is composed of a sharp rise of an impulsive type pressure followed by non-impulsive type pressure of duration directly proportional to bow submergence. Time traces of such form are also observed in recent tests subsequently described.

Significant progress has been achieved in the past decade in developing theoretical methods for predicting impact loads related to water entry and exit of ship sections. A large number of references on this subject are available, such as Arai and Matsunaga (1989) and Zhao et al. (1996). The former reference uses the volume of fluid (VOF) method to predict impact on arbitrary sections. The latter work uses the generalized Wagner method, which is numerically more robust and faster than the original two-dimensional boundary element method by Zhao and Faltinsen (1993).

To investigate the accuracy of presently available two-dimensional methods when applied to real ships, NSMB CRS carried out drop tests of a two-dimensional section and also model tests of a ship model in a towing

tank. Measured impact pressures and forces were then compared with numerical results from a computer code developed by NSMB CRS based on Zhao et al. (1996). The findings from this research project are highlighted in Krikke (2001). The two-dimensional section used in the drop tests was a section scaled down from the sectional shape at Station 18 (10% L from the forward perpendicular) of a container ship. In the two-dimensional drop tests, pressures, vertical velocity, and accelerations were measured. In the ship model tests, a three-dimensional segmented model of the same container ship was used that included a short segment at Station 18 to measure both impact forces and impact pressures, and a stem segment to measure the slamming forces on the front area of the vessel resulting from wave celerity. In addition, pressure taps were installed behind the stem segment to measure the impact pressures in the bow region of the vessel. The drop tests showed a similar form of pressure time trace as in Chen and Ng (1982), that is, first a sharp peak of duration of a few milliseconds having far less energy content and a very low repeatability, followed by a more gradual build-up of pressure peaking. Drop test results also showed a linear relationship of the pressure peaks with the vertical impact velocity squared, as shown on Fig. 30. On the other hand, the ship model tests also showed that the impact pressure exhibits a linear relation with the squared value of the velocity component normal to the transducer, derived from the vertical impact velocity, ship forward speed, and wave celerity. The trend of pressures from the ship model tests are shown in Fig. 31.

The numerical results from the two-dimensional boundary element method (BEM) computer code based on Zhao et al. (1996) compare well for peak pressures of the two-dimensional drop tests, as well as peak pressures and vertical forces at Station 18 of the ship model tests. For the impact pressures in the bow region behind the stem section, the calculated values from the two-dimensional BEM code do not compare well with the measured values, and the discrepancies between these two become larger with increasing forward speed of the vessel.

Impact forces on the stem segment were also computed using the two-dimensional BEM theory by summing up the calculated pressures on strips oriented normal to the bow stem profile, in a similar manner as in Kvaelsvold et al. (1997). However, compared with ship model test data, the vertical bow forces obtained from this approach were much larger. Together with the pressure correlation for locations forward of Station 18 as described previously, this result indicates that the forward speed and three-dimensional effects are significant, and must be considered for accurate theoretical prediction of impact loads on the forward region of the vessel.

2.9.4 Green Water Loading. The prediction of green water loading involves the probability of the relative wave motion exceeding the available bow freeboard,

with the bow submerging in the wave, and hence the shipping of water on deck. However, the latter is not a direct consequence of the former event as indicated by Hong et al. (1990), who found from experiments that not every deck exceedance leads to deck wetness. The observation of Hong et al. is in line with the observation that increased bow flare reduces the deck wetness (O'Dea & Walden 1984) but increases the relative motion, which apparently is caused by increased dynamic swell-up (Swaan & Vossers 1961; Takagi & Naito, 1993; Watanabe et al. 1989). Experiments carried out by Buchner (1995) further show that there is no direct relation between the orbit and phase velocities of the undisturbed waves and the flow of the water onto the deck. But when it happens, the flow onto the deck resembles the theoretical dam-breaking problem, and the water on deck behaves like a shallow water wave. Experiments also show that the forward part of the deck is generally more subjected to the dynamics of the flow than the aft part. This implies that in relating the static head of water on deck to green water loading, the dynamic amplification is more significant toward the bow. The same trend is obtained by Blok (1995) from model tests of a very large crude carrier (VLCC) in head seas where the flow in the aft part of the forward deck area behaves more in a static manner, and closer correlation is observed between pressure and water height. When deck wetness took place, dynamic amplification usually occurred, depending on wave length and ship speed.

Green water loading is usually used for local structural analysis. Effects of this loading on maximum hull girder bending moment are marginal (Wang et al. 1998) due to it being out of phase with the peak values of the bending moment. State-of-the-art calculations of the amount of green water on deck are often based on vertical relative motions of the bow calculated from ship motion theory, either linear strip or time domain nonlinear methods. The vertical relative motion is then based on estimating the water height at the deck boundary using an empirical formula derived from experimental data, whereas the three-dimensional shallow water flow over the deck is simulated by such as Glimm's theory (Zhou et al. 1999). However, the accuracy of such an approach requires further verification before it can be applied for design and evaluation purposes.

Because of the uncertainties involved in green water loading predictions, IACS uses an inverse process to define the nominal loads in terms of static water head for bulk carrier hatch cover strength evaluation. First, the short-term extreme values of bow relative motion are calculated using linear seakeeping analyses for a number of ships in the North Atlantic environment, assuming that the peak values of the relative motion follow a Rayleigh distribution. Ship speed reduction in high seas is considered in the analysis using a method suggested by Aertssen (1969). The nominal green water loading is then obtained by modifying the extreme

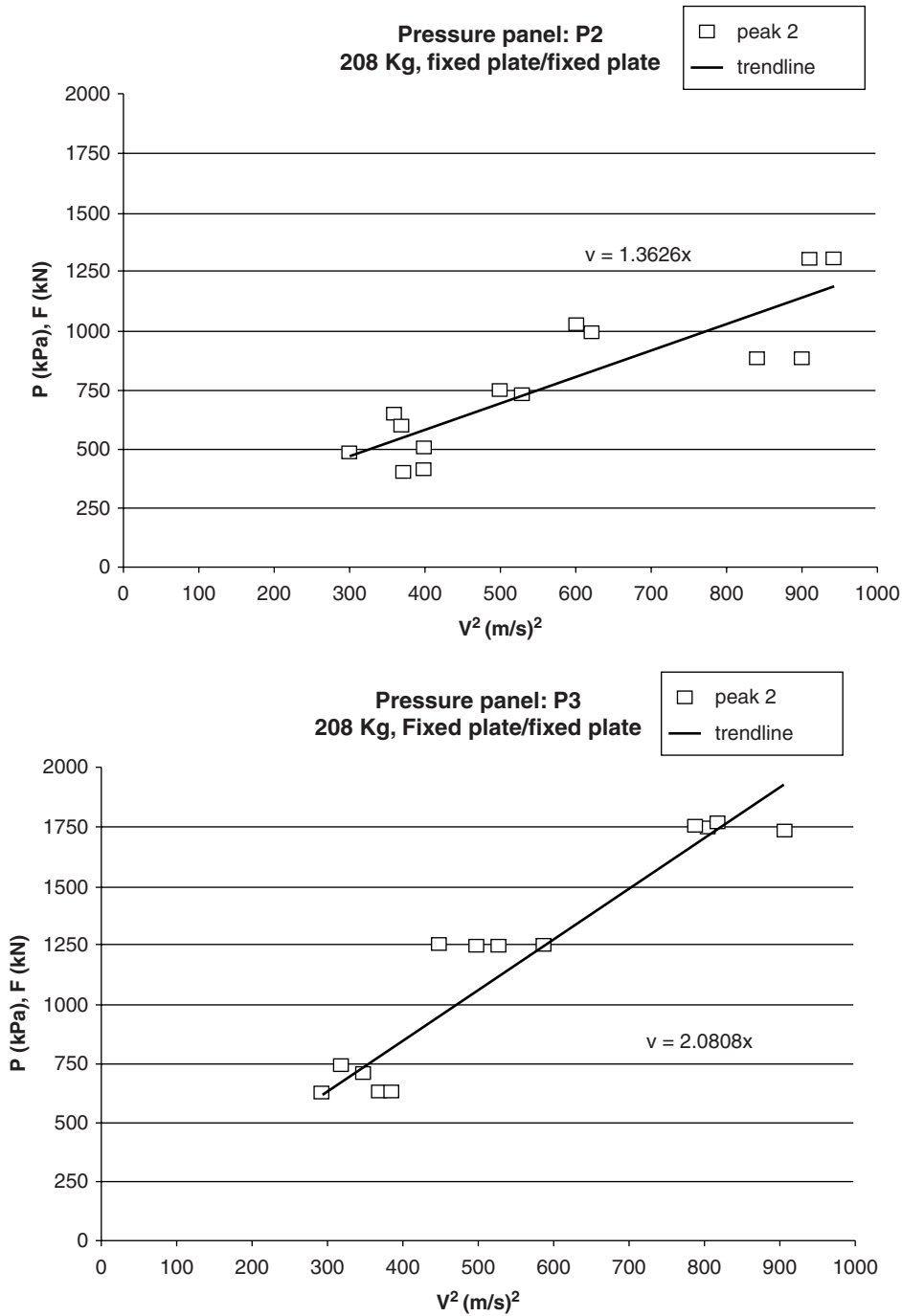


Fig. 30 Trend line of drop test results with two-dimensional section model.

relative motion used as static water head such that the resulting structural scantlings, as required from the analyses with the static load as input, are consistent with those of the existing successful designs and meet good engineering practice. The IACS green water loading criteria is presented in IACS UR S-21 (IACS 1997).

It should be emphasized that because the criteria are derived from an inverse approach, they must not be interpreted as a procedure independent of the process of the strength evaluation and failure assessment with specific acceptance criteria incorporated in classification rules.

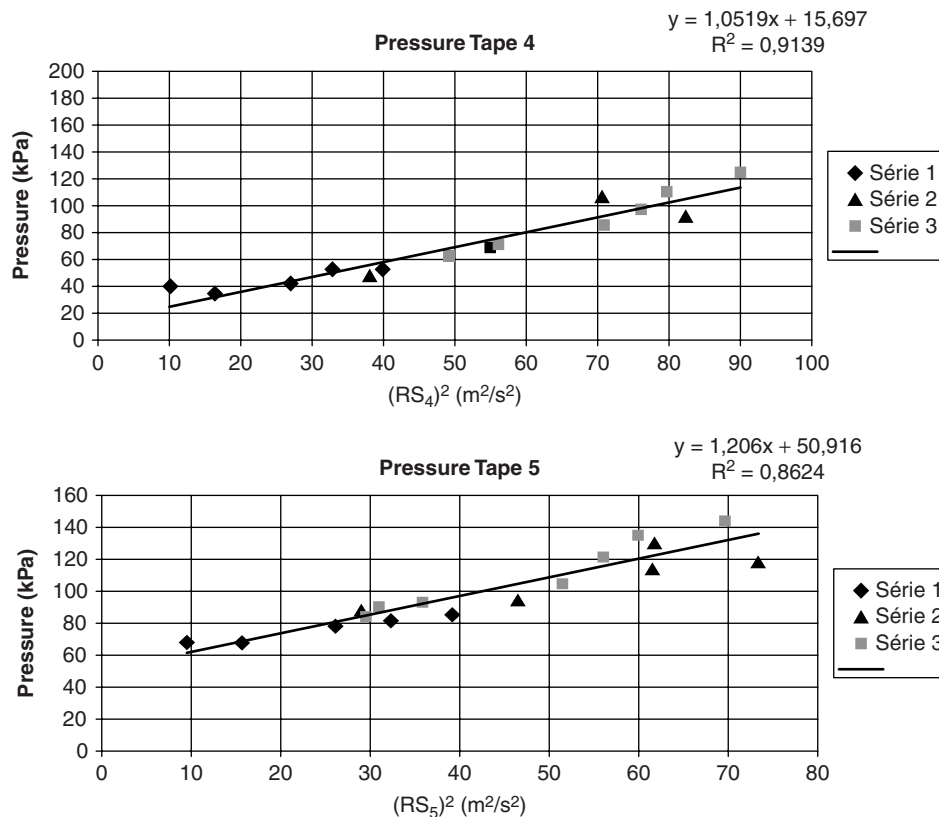


Fig. 31 Trend line of test results with segmented model.

2.9.5 Liquid Cargo Sloshing. Violent motion, and hence high sloshing pressures, of liquid cargo in partially filled tanks may take place when there is resonance between the ship motion and the natural mode of fluid motion in the tanks. As a result, the transportation of liquid cargo in slack tanks is usually prohibited for many of these vessels. However, a partially filled condition cannot be always avoided, due to chilled-down liquid required to maintain cold tanks on return trips for liquefied natural gas (LNG) carriers, partial unloading when multi-port stops are made, loading and unloading at sea, or other operational considerations.

Sloshing is generally affected by the depth of liquid in the tank, tank configuration, and motion of the vessel (hence, the tank). The liquid motion inside a tank has an infinite number of natural periods but the lowest mode is the most likely to be excited by the motion of the ship. The sloshing phenomena in cargo tanks that are basically rectangular in shape can usually be described by considering only two-dimension fluid flow except at the tank corners, where the three-dimensional effects are significant for the vessel operating in oblique seas.

The sloshing phenomenon in rectangular tanks can be divided into two classes: low and high liquid filling depths. The low filling depth case, where the liquid fill-

ing level is less than 20 percent of tank depth, is usually characterized by the formation of hydraulic jumps and traveling waves for excitation periods near resonance. At the high filling level, large standing waves are usually formed in the resonance frequency range. When hydraulic jumps of traveling waves are present in the case of low filling level, extremely high impact pressures can occur on tank walls. Figure 32 shows a typical pressure time trace from model tests in a sloshing condition (Bass et al. 1976). It is noted that the pressure pulses are neither harmonic nor periodic, even though the tests are with harmonic oscillation. Figure 33 is representative of a typical pressure time history that results when standing waves are present at higher filling levels or when non-resonant, small-amplitude sloshing occurs at any filling level. At higher filling levels, impact pressures typical of those shown in Fig. 32 can also occur on the tank ceiling in the resonance frequency range.

For spherical or cylindrical tanks, three-dimensional effects are to be considered, and the types of pressures exhibited in Figs. 32 and 33 can also occur. The most important loads on spherical or cylindrical tanks are the total forces or moments acting on the tank walls, which determine tank support structural requirements. As indicated by Bass et al. (1976), spherical or cylindrical tank

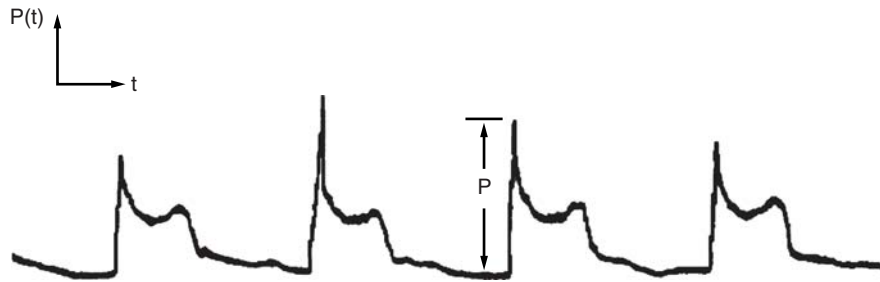


Fig. 32 Impact pressure time history for resonant sloshing with large amplitude hydraulic jumps of traveling waves.

walls are usually thick enough that local impact pressures do not present a problem. However, this is not the case for membrane tanks of LNG carriers. It is to be recognized that for either two- or three-dimensional resonant sloshing, the prediction of forces or pressures with large excitation amplitude is extremely difficult, and experimental data obtained with scale model tanks are usually needed to establish the loads for design or for verification of numerical analysis.

A comprehensive review on liquid cargo sloshing in slack tanks of ships can be found in Abramson et al. (1974) and Hamlin et al. (1986). Analytical prediction of sloshing loads usually relies on numerical time domain simulation. Work in this area includes those by Lou et al. (1980), Mikelis (1984), Arai et al. (1994), Lee et al. (1995), Wu, Ma, and Taylor (1998), FLOW3D (1999), Kim (2000), and Faltinsen et al. (2001). A comparative study on sloshing load numerical simulations was published by Cariou and Casella (1999).

For strength assessment of transverse and longitudinal bulkheads of tankers, the nominal sloshing load criteria specified in classification societies rule requirements are usually obtained from scaled model tests, analytical calculations, or both, and are to be used in conjunction with specific acceptance criteria on strength. In the ABS "Membrane Tank LNG Vessels Guide" (2002) and "Steel Vessel Rules" (2008), the sloshing load is expressed in terms of the equivalent static pressure head consisting of an average pressure distribution and additional pressures at the upper and lower portions of the bulkhead. The average sloshing pressure is obtained based on the

total sloshing force acting on the bulkhead of smooth tanks, calculated using the program NSLOSH. It is then modified by taking into consideration the blockage effects due to internal members and by incorporating the dynamic amplification factors to account for the structural dynamic characteristics of the impulsive load from sloshing. The general procedure and results of the initial study on this subject are given in Ng (1992). The NSLOSH program used in the study is a nonlinear procedure for computing the two-dimensional liquid sloshing in a moving rectangular container with no internal structural members. The numerical scheme used in this procedure is the VOF technique combined with the SOLA algorithm (Hirt et al. 1975). The SOLA-VOF technique (Lou et al. 1980) is a region-following scheme for the tracking of the complicated free surface. It works with a time cycle, or "movie frame," point of view. The calculation proceeds through a sequence of small time increments. The results of each cycle or time step act as an initial condition for the next cycle. Results from NSLOSH compare well with test data and the sloshing force formula given by Cox et al. (1980).

The blockage effects due to internal structural members such as deep transverses, swash bulkheads, deep ring-webs, and deep horizontal stringers incorporated in the ABS sloshing load criteria are based on measured data and observations published by the industry, such as those reported by Akita (1967) and IHI (1986). Effects of swash bulkheads and transverses on sloshing pressure reduction have also been investigated by Umemoto et al. (1997) using approximately a 1/50-scaled VLCC model.

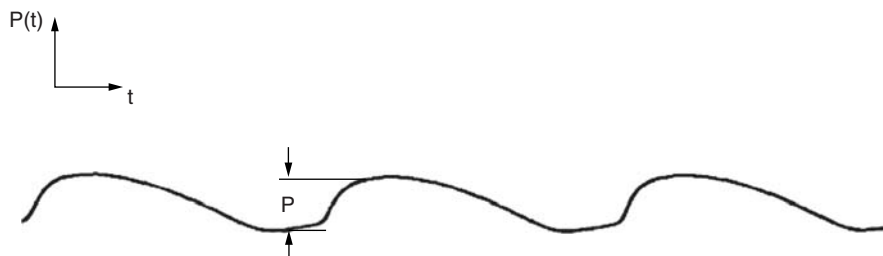


Fig. 33 Pressure time history for non-resonant low amplitude standing wave sloshing. (Bass, et al., 1976 – SSC-258)

To obtain an appropriate dynamic amplification factor, dynamic analyses of bulkhead structures subject to an isosceles triangular-shaped impulse with time duration of about 10 msec were performed for a large number of tanker designs with different tank dimensions. Analyses show that for typical tanker structures, the fundamental frequencies of transverse bulkheads are in the range of 55 to 75 Hz for the plate panels between two adjacent horizontal girders and bounded by two vertical boundaries of the transverse bulkhead, and its dynamic amplification factor is about 1.4. The fundamental frequencies of longitudinal bulkheads are in the range of 60 to 75 Hz for plate panels between two adjacent web frames and bounded by the deck and the bottom of the tank, and its dynamic amplification factor is about 1.25.

2.9.6 Bulk Cargo, Cargo Container, Liquids in Full Tanks, and Concentrated Loads. The bulk cargo, cargo container, liquids in full tanks, and concentrated loads are the inertial loads all produced by the accelerations resulting from the motions of a ship in a seaway. The magnitudes of these loads are often needed for the design of local structure, foundations, lashings, securing devices, for example. For such purposes, the estimated maximum values of the loads may usually be considered as static design loads because of the relatively long periods of ship motion amplitudes. Some comments related to the estimation of the inertial loads for strength evaluation are provided in the following sections.

2.9.6.1 Bulk Cargo Loads. The bulk cargo load for strength evaluation of bulk carrier structures consists of the static and dynamic forces corresponding to the weight of cargo and inertial forces of cargo due to acceleration. The vertical and transverse components of the static force on the cargo hold boundary surfaces can be determined by taking into account the instantaneous orientation of the surface in question. The accelerations in vertical, transverse, and longitudinal directions may be obtained based on its short-term or long-term extreme values from the linear ship motion analysis for a specific ship route in which the profile and the repose angle of the bulk cargo are usually assumed to remain unchanged. The vertical component of the inertial force on the hold surface can be determined in the same manner as the vertical component of static force. For the transverse and longitudinal components of the inertial force, in addition to the instantaneous orientation of the hold surface in question, a reduction factor to account for the cohesiveness of the dry bulk cargo material should be considered. A study carried out by Krivanec and Bea (1992) shows that the reduction factor of 0.33 may be adequate for general cargo.

2.9.6.2 Cargo Container Loads. In practical application, the cargo container loads are usually assumed to consist of three parts: static weight of cargo container in upright condition, added static load due to roll and pitch of the vessel, and inertial forces due to accelerations of the vessel. In computing the container loads, the containers are assumed stowed in stacks in the cargo hold

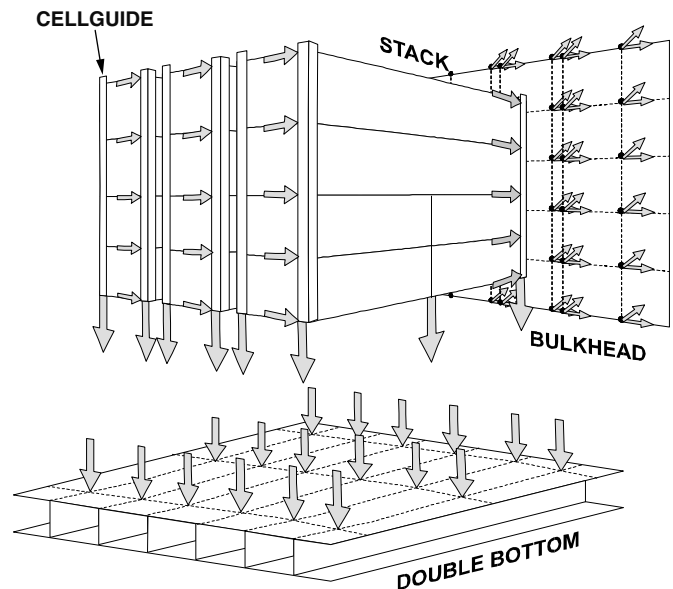


Fig. 34 Hold-stowed stack load distribution scheme.

and on deck, and the forces from each individual container are generally calculated at the volumetric center of the container. For the containers stowed in the hold, the containers are restrained by cell guides, which are a series of vertical steel angles suitably spaced according to the container length and width. The cell guides provide alignment and horizontal restraint for container stacks. The vertical container loads are transmitted to the bottom corners of each container stack. The transverse and longitudinal container forces acting on the cell guides are transmitted to supporting structural members (such as webs, girders and pillars) by statically distributing

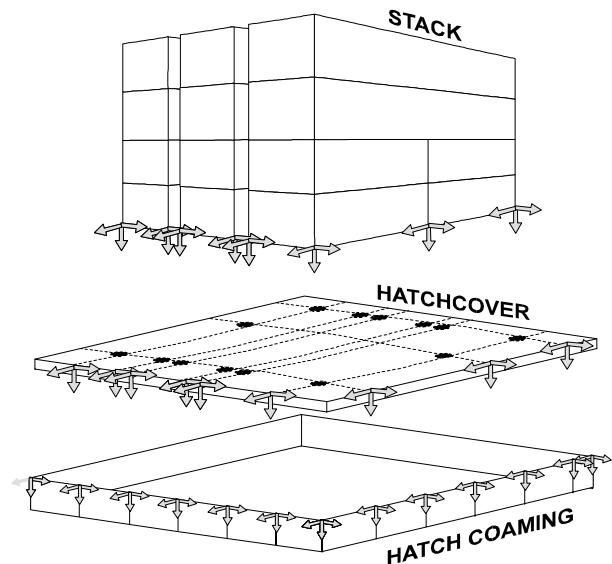


Fig. 35 Hatch-stowed stack load distribution scheme.

to adjacent support points along the cell guides. For containers stowed on deck on the hatch covers, the container loads are considered to be applied to hatch coamings, bulwark, or other supporting structures at the bottom of the container stack. For the purpose of structural strength evaluation, loads for containers stowed on hatch covers are calculated assuming that there is no support from the lashing gear. Figures 34 and 35 respectively show some available container load distribu-

tion schemes of stack loads stowed in hold and on hatch cover.

2.9.6.3 Liquids in Full Tanks. The loads acting on tank boundaries from liquid cargo and ballast water without free surface are composed of hydrostatic pressure, inertial force due to accelerations, and added pressure head due to the roll and pitch motion of the ship. For cargo tanks, consideration is also given to the pressure setting on pressure/vacuum relief valves.

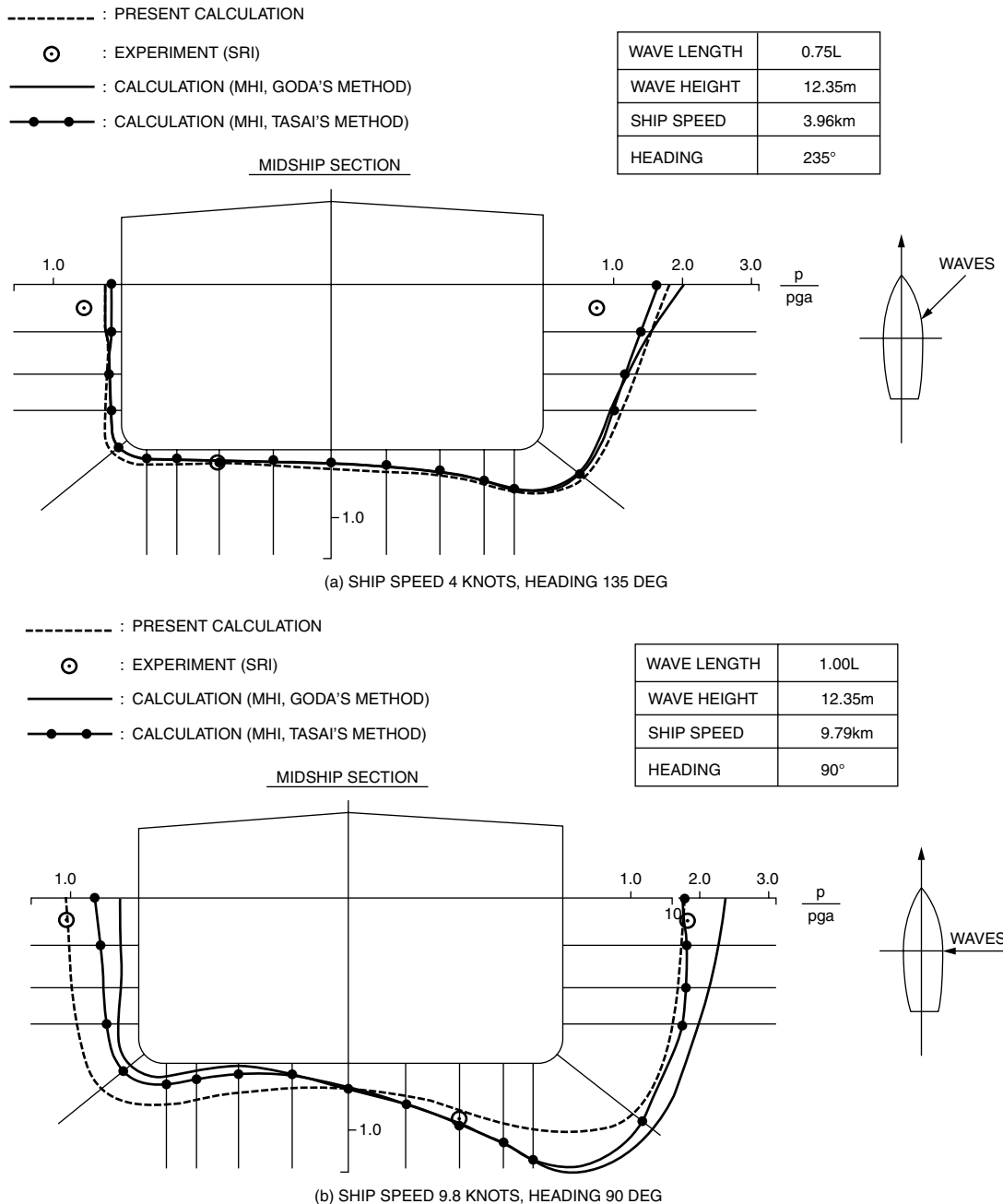


Fig. 36 Typical transverse wave load distribution—resultant hydrodynamic pressure amplitudes [Kim 1982].

The detailed procedure for computing the internal tank pressure load for structural evaluation can be found in classification rules.

2.10 Transverse Distribution of Wave Loads. To compute the secondary or tertiary response of structural components such as panels of stiffened or unstiffened plating, it is necessary to know the distribution of fluid pressures and acceleration loads acting on the surface of the panels. For the purpose of analyzing transverse strength, the distribution of loads transversely around the ship section is required.

To predict the dynamic loads for design and analysis, linear strip theory has been widely used as a practical analysis tool. Linear theory has proven to be robust, computationally fast, and provides reasonably acceptable results. However, it does not predict certain nonlinear loads, such as the nonlinear hull girder bending and torsional moments and the pressure loads acting on local structural members, particularly above the still water line, which are crucial in the structural design of vessels for the extreme design condition.

With the advances in free-surface hydrodynamic computational methods and improvements in computing speed in the past decade, nonlinear seakeeping computer codes dealing with the nonlinear extreme motions and loads have been developed and are available in the industry, as described in Section 2.5. These nonlinear codes show satisfactory predictions for the vertical plane of motion but require further improvements for the lateral plane of motion. As such, the prediction of pressure loads for design and evaluation of local structures continues to rely on the linear strip theory.

The wave and motion-induced distribution of pressure calculated from a linear strip theory is shown in Fig. 36 (Kim 1982). The two plots in this figure give the amplitude (but not the phase) of the dynamic pressure variation around the midship section, and this includes the effects of both ship and wave motions. It can be seen that the greatest dynamic pressure variation is found near the water line in all cases, and in beam or bow seas the amplitude is greatest on the side facing the incoming waves. The lowest amplitude of pressure variation is found in

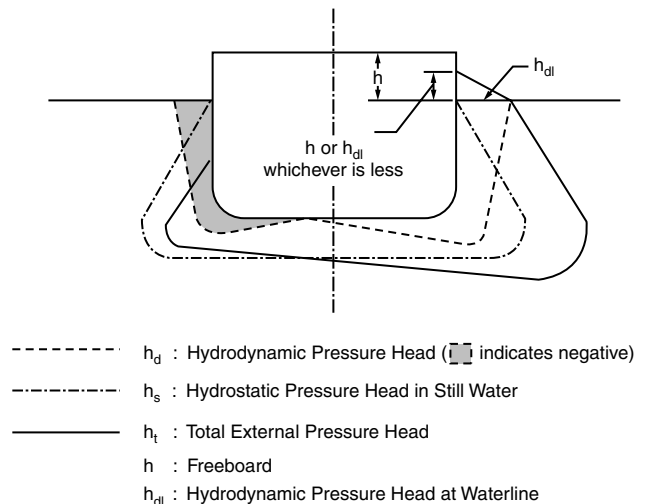


Fig. 37 Transverse distribution of total external pressure head.

the vicinity of the keel, which will experience the greatest static pressure. It is noted that the pressures in the wave above the still water line are not obtained because the linear hydrodynamic theory computes the fluid force on only the mean immersed portion of the ship. The pressure in this area must therefore be estimated separately.

In practical applications, the pressure distribution above the mean water line is generally approximated by a static head of the same value as the dynamic load at mean water line as shown in Fig. 37, where the distribution of total pressure (hydrodynamic and still water) of a vessel in a beam sea condition is presented. In this example, the hydrostatic pressure offsets the negative hydrodynamic pressure on the leeward side, whereas on the side exposed to the wave static pressure is added to the dynamic part. This represents a quasi-static pressure distribution of the vessel rolling into the wave where the racking stresses due to rolling reach a maximum in a beam sea each time the vessel completes an oscillation in one direction and is about to return.

Section 3

Analysis of Hull Girder Stress and Deflection

3.1 Nature of Ship Structural Response. The responses of structural components of the ship hull to external loads are usually measured by either stresses or deflections. Structural performance criteria and the associated analyses involving stresses are referred to under the general term of *strength*, whereas deflection-based considerations are referred to under the term *stiffness*. The ability of a structure to fulfill its purpose can be

measured by either or both strength and stiffness considerations. The strength of a structural component is inadequate and structural failure would be deemed to have occurred if the component's material experienced a loss of load-carrying ability through fracture, yield, buckling, or some other failure mechanism in response to the applied loading. On the other hand, excessive deflection may also limit the structural effectiveness of

The detailed procedure for computing the internal tank pressure load for structural evaluation can be found in classification rules.

2.10 Transverse Distribution of Wave Loads. To compute the secondary or tertiary response of structural components such as panels of stiffened or unstiffened plating, it is necessary to know the distribution of fluid pressures and acceleration loads acting on the surface of the panels. For the purpose of analyzing transverse strength, the distribution of loads transversely around the ship section is required.

To predict the dynamic loads for design and analysis, linear strip theory has been widely used as a practical analysis tool. Linear theory has proven to be robust, computationally fast, and provides reasonably acceptable results. However, it does not predict certain nonlinear loads, such as the nonlinear hull girder bending and torsional moments and the pressure loads acting on local structural members, particularly above the still water line, which are crucial in the structural design of vessels for the extreme design condition.

With the advances in free-surface hydrodynamic computational methods and improvements in computing speed in the past decade, nonlinear seakeeping computer codes dealing with the nonlinear extreme motions and loads have been developed and are available in the industry, as described in Section 2.5. These nonlinear codes show satisfactory predictions for the vertical plane of motion but require further improvements for the lateral plane of motion. As such, the prediction of pressure loads for design and evaluation of local structures continues to rely on the linear strip theory.

The wave and motion-induced distribution of pressure calculated from a linear strip theory is shown in Fig. 36 (Kim 1982). The two plots in this figure give the amplitude (but not the phase) of the dynamic pressure variation around the midship section, and this includes the effects of both ship and wave motions. It can be seen that the greatest dynamic pressure variation is found near the water line in all cases, and in beam or bow seas the amplitude is greatest on the side facing the incoming waves. The lowest amplitude of pressure variation is found in

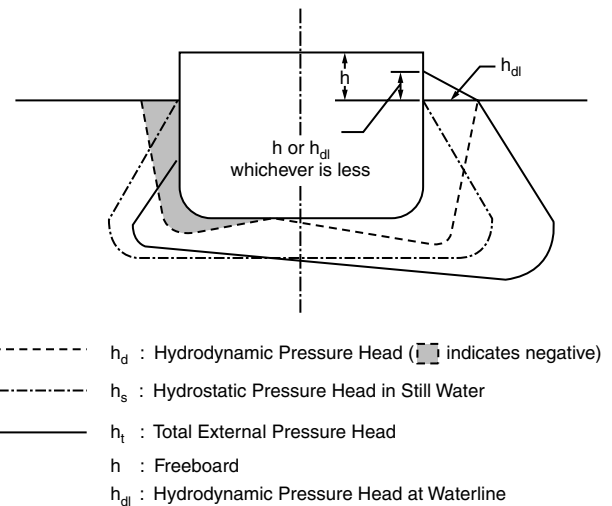


Fig. 37 Transverse distribution of total external pressure head.

the vicinity of the keel, which will experience the greatest static pressure. It is noted that the pressures in the wave above the still water line are not obtained because the linear hydrodynamic theory computes the fluid force on only the mean immersed portion of the ship. The pressure in this area must therefore be estimated separately.

In practical applications, the pressure distribution above the mean water line is generally approximated by a static head of the same value as the dynamic load at mean water line as shown in Fig. 37, where the distribution of total pressure (hydrodynamic and still water) of a vessel in a beam sea condition is presented. In this example, the hydrostatic pressure offsets the negative hydrodynamic pressure on the leeward side, whereas on the side exposed to the wave static pressure is added to the dynamic part. This represents a quasi-static pressure distribution of the vessel rolling into the wave where the racking stresses due to rolling reach a maximum in a beam sea each time the vessel completes an oscillation in one direction and is about to return.

Section 3

Analysis of Hull Girder Stress and Deflection

3.1 Nature of Ship Structural Response. The responses of structural components of the ship hull to external loads are usually measured by either stresses or deflections. Structural performance criteria and the associated analyses involving stresses are referred to under the general term of *strength*, whereas deflection-based considerations are referred to under the term *stiffness*. The ability of a structure to fulfill its purpose can be

measured by either or both strength and stiffness considerations. The strength of a structural component is inadequate and structural failure would be deemed to have occurred if the component's material experienced a loss of load-carrying ability through fracture, yield, buckling, or some other failure mechanism in response to the applied loading. On the other hand, excessive deflection may also limit the structural effectiveness of

a member even though material failure does not occur. If that deflection results in a misalignment or other geometric displacement of vital components of the ship's machinery, navigational equipment, or weapons systems, the system is rendered ineffective.

The present section is concerned with the determination of the response, in the form of stress or deflection, of structural members to the applied loads. Once these responses are known, it is necessary to determine whether the structure is adequate to withstand the demands placed upon it, and this requires consideration of the several possible failure modes, as discussed in detail in Section 4.

In analyzing the response of the ship structure, it is convenient to subdivide the structural response into categories logically related to the geometry of the structure, the nature of the loading, and the expected response. Appropriate methods are then chosen to analyze each category of structural component or response, and the results are then combined in an appropriate manner to obtain the total response of the structure.

As noted previously, one of the most important characteristics of the ship structure is its composition of an assemblage of plate-stiffener panels. The loading applied to any such panel may contain components in the plane of the plating and components normal to the plane of the plating. The normal components of load originate in the secondary loading resulting from fluid pressures of the water surrounding the ship or from internal liquids, and in the weights of supported material such as a distributed bulk cargo and the structural members themselves. The in-plane loading of the longitudinal members originates mainly in the primary external bending and twisting of the hull. The most obvious example of an in-plane load is the tensile or compressive stress induced in the deck or bottom by the bending of the hull girder in response to the distribution of weight and water pressure over the ship length.

The in-plane loads on transverse members such as bulkheads result from the edge loads transmitted to these members by the shell plate-stiffener panels and the weights transmitted to them by deck panels. In-plane loads also result from the local bending of stiffened panel components of structure. For example, a panel of stiffened bottom plating contained between two transverse bulkheads experiences a combined transverse and longitudinal bending in response to the fluid pressure acting upon the panel. In turn, this panel bending causes stresses in the plane of the plating and in the flanges of the stiffening members. Finally, the individual panels of plating contained between pairs of stiffeners undergo bending out of their initial undeformed plane in response to the normal fluid pressure loading. This results in bending stresses, and the magnitudes of these stresses vary through the plate thickness.

To perform an analysis of the behavior of a part of the ship structure, it is necessary to have available three

types of information concerning the structural component:

- The dimensions, arrangement, and material properties of the members making up the component
- The boundary conditions on the component (i.e., the degree of fixity of the connections of the component to adjacent parts of the structure)
- The applied loads.

In principle, it is possible using a computer-based method of analysis, such as the finite element method, to analyze the entire hull at one time without the necessity of such subdivision into simpler components. However, there are at least two reasons for retaining the subdivision into simpler components:

- By considering the structural behavior of individual components of structure and their interactions with each other, a greater understanding is developed on the part of the naval architect of their functions, and this leads to an improved design.
- Many of the problems facing the practicing naval architect involve the design or modification of only a limited part of a ship, and a full-scale analysis would be neither necessary nor justified.

A brief introduction to the finite element procedure is given in Section 3.16. It is a powerful tool that is widely and routinely used in most aspects of modern structural analysis, and standard computer programs are available from computer service bureaus and a number of other sources.

As noted in Section 2.2, it is convenient to subdivide the structural response into primary, secondary, and tertiary components, and we shall here examine these components in detail. Note that the primary and secondary stresses in plate members are membrane stresses, uniform (or nearly uniform) through the plate thickness. The tertiary stresses, which result from the bending of the plate member itself, vary through the thickness but may contain a membrane component if the out-of-plane deflections are large compared to the plate thickness.

From this, it is seen that the resultant stress at a given point in the ship structure is composed of several parts, each of which may arise from a different cause. In many instances, there is little or no interaction among the three (primary, secondary, tertiary) component stresses or deflections, and each component may be computed by methods and considerations entirely independent of the other two. In such cases, the resultant stress is obtained by a simple superposition of the three component stresses. An exception occurs if the plate (tertiary) deflections are large compared the thickness of the plate. In this case, the primary and secondary stresses will interact with this tertiary deflection and its corresponding

stress, so that simple superposition may no longer be employed to obtain the resultant stress.

Fortunately for the ship structural analyst, such cases rarely occur with the load magnitudes and member scantlings used in ships, and simple superposition of the three components can usually be performed to obtain the total stress. In performing this superposition, the relative phasing in time of the components must be kept in mind if the components represent responses to time-varying loads such as those caused by waves. Under such circumstances, for a particular location in the structure such as a point in the bottom plating, the maximum value of the primary stress may not necessarily occur at the same instant of time as the maximum of the secondary or tertiary stress at that same location (see sections 2.6.6 to 2.6.8 for more information on combining loads and stresses).

3.2 Primary Longitudinal Bending Stress. For the most part, the structural members involved in the computation of primary stresses are the longitudinally continuous members such as deck, side, bottom shell, longitudinal bulkheads, and continuous or fully effective longitudinal primary or secondary stiffening members.

However, the definition of primary stress also refers to the in-plane stress in transverse bulkheads due to the weights and shear loads transmitted into the bulkhead by the adjacent decks, bottom, and side shells.

Elementary Bernoulli-Euler beam theory is usually used in computing the component of primary stress or deflection due to vertical or lateral hull bending loads. In assessing the applicability of this beam theory to ship structures, it is useful to restate the underlying assumptions:

- The beam is prismatic (i.e., all cross sections are the same).
- Plane cross sections remain plane and merely rotate as the beam deflects.
- Transverse (Poisson) effects on strain are neglected.
- The material behaves elastically, with the moduli of elasticity in tension and compression being equal.
- Shear effects (stresses, strains) can be separated from, and do not influence, bending stresses or strains.

Many experiments have been conducted to investigate the bending behavior of ships or ship-like structures as noted—for example, in Vasta (1958). In many cases, the

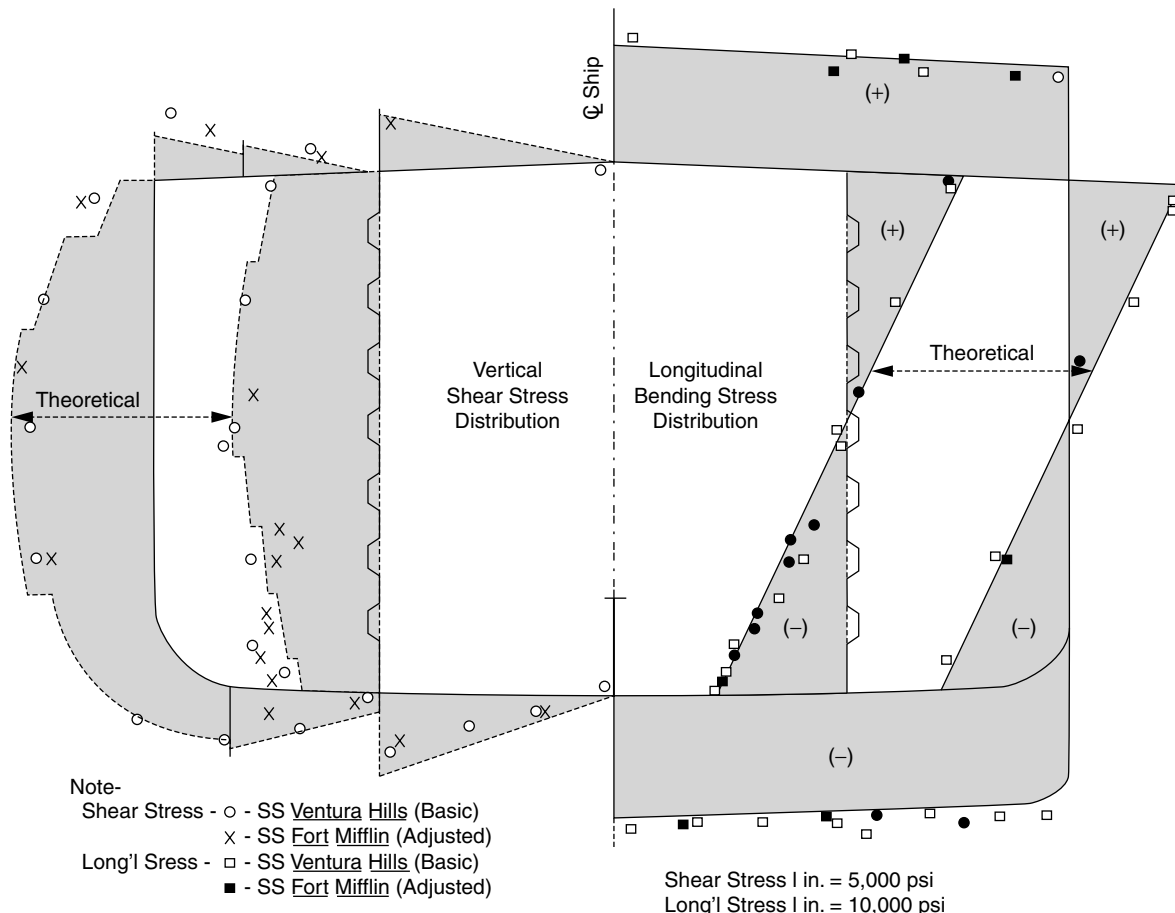


Fig. 38 Shear and bending moment study on tanker *Ventura Hills* (Vasta 1958).

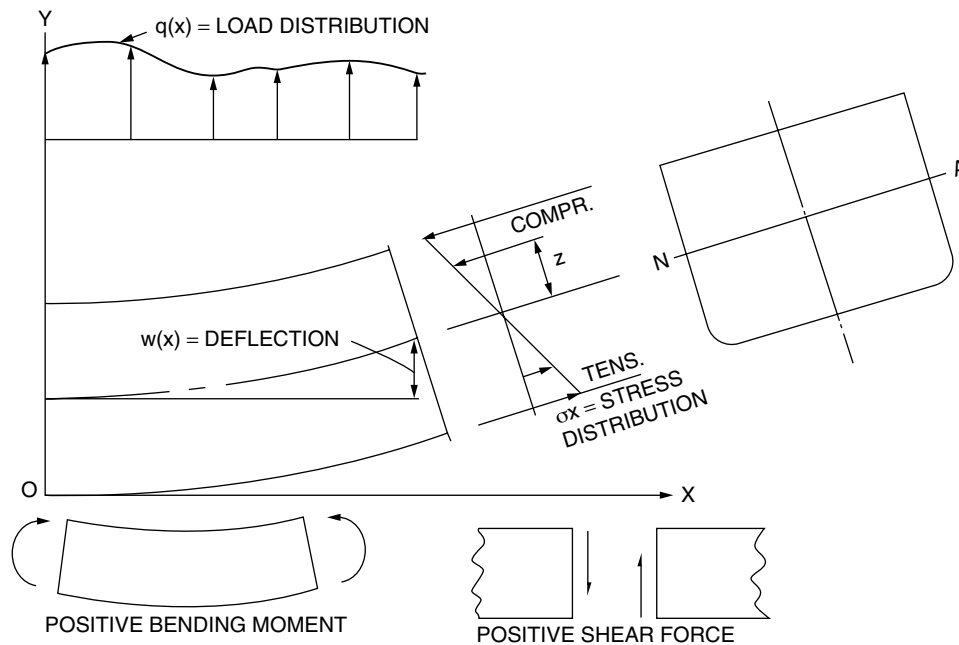


Fig. 39 Nomenclature for shear, deflection, and loading of elementary beam.

results agree quite well with the predictions of simple beam theory, as shown in Fig. 38, except in the vicinity of abrupt changes in cross section.

In way of deck openings, side ports, or other changes in the hull cross sectional structural arrangements, stress concentrations may occur that can be of determining importance in the design of the structural members. Proper design calls for, first, the avoidance where possible of abrupt changes in geometry and, second, the introduction of compensating structural reinforcements such as doubler plates where stress concentrations cannot be avoided. In most cases, serious stress raisers are associated with local features of the structure, and the design of such features is treated in detail in Chapter 17 of Lamb (2003). Because stress concentrations cannot be avoided entirely in a highly complex structure such as a ship, their effects must be included in any comprehensive stress analysis. Methods of dealing with stress concentrations are presented in Section 3.13.

The derivation of the equations for stress and deflection under the assumptions of elementary beam theory may be found in any textbook on strength of materials—for instance, Timoshenko (1956). The elastic curve equation for a beam is obtained by equating the resisting moment to the bending moment, M , at section x , all in consistent units:

$$EI \frac{d^2 w}{dx^2} = M(x) \quad (131)$$

where

w = deflection (Fig. 39)

E = modulus of elasticity of the material

I = moment of inertia of beam cross section about a horizontal axis through its centroid.

This may be written in terms of the load per unit length, $q(x)$, as:

$$EI \frac{d^4 w}{dx^4} = q(x) \quad (132)$$

The deflection of the ship's hull as a beam is obtained by the multiple integration of either of equations (131) or (132). It can be seen that the deflection—hence, the stiffness against bending—depends upon both geometry (moment of inertia, I) and elasticity (E). Thus, a reduction in hull depth or a change to a material such as aluminum (E approximately one third that of steel) will reduce the hull stiffness.

Because flexibility is seldom a problem for hulls of normal proportions constructed of mild steel, primary structures are usually designed on the basis of strength considerations rather than deflection. However, classification society rules deal indirectly with the problem by specifying a limit on the L/D ratio of 15 for ocean-going vessels and 21 for Great Lakes bulk carriers (which experience less severe wave-bending moments). Designs in which L/D exceeds these values must be “specially considered.” There is also a lower limit on hull girder moments of inertia, which likewise have the effect of

limiting deflection, especially if high-strength steels are used. A limit on the moment of inertia will also influence the vibrational response of the ship. An all-aluminum alloy hull would show considerably less stiffness than a steel hull having the same strength. Therefore, classification societies agree on the need for some limitation on deflection, although opinions differ as to how much.

Regarding strength considerations, the plane section assumption together with elastic material behavior results in a longitudinal stress, σ_x , in the beam that varies linearly over the depth of the cross section. The condition of static equilibrium of longitudinal forces on the beam cross section is satisfied if σ_x is zero at the height of the centroid of the area of the cross section. A transverse axis through the centroid is termed the *neutral axis* of the beam and is a location of zero stress and strain. Accordingly, the moment of inertia, I , in equations (131) and (132) is taken about the neutral axis.

The longitudinal stress in section x is related to the bending moment by the following relationship, as illustrated in Fig. 39:

$$\sigma_x = \frac{-M(x)}{I}z \quad (133)$$

It is clear that the extreme stresses are found at the top or bottom of the beam where z takes on the numerically largest values. The quantity $SM = I/z_0$, where z_0 is either of these extreme values, is the section modulus of the beam. The extreme stress, deck or bottom, is given by

$$\sigma_x = \frac{-M(x)}{SM} \quad (134)$$

The sign of the stress, either in tension or compression, is determined by the sign of z_0 . For a positive bending moment, the top of the beam is in compression and the bottom is in tension (sagging condition). The computation of the section modulus for a ship hull cross section, taking into consideration all of the longitudinally continuous, load-carrying members, is described later in this section.

Two variations on the previous beam equations may be of importance in ship structures. The first concerns beams composed of two or more materials of different moduli of elasticity, for example, steel and aluminum. In this case, the flexural rigidity, EI , is replaced by

$$\int_A E(z)z^2 dA = 0 \quad (135)$$

where

A = cross sectional area
 $E(z)$ = modulus of elasticity of an element of area dA located at distance z from the neutral axis.

A second related modification may be described by considering a longitudinal strength member composed of a thin plate with transverse framing. For example, this might represent a portion of the deck structure of a trans-

versely framed ship. Consider one module of a repeated system of deck plate plus transverse frame, as shown in Fig. 40, that is subject to a longitudinal stress, σ_x , from the primary bending of the hull girder. As a result of the longitudinal strain, ε_x , which is associated with σ_x , there will exist a transverse strain, ε_s . For the case of a plate that is free of constraint in the transverse direction, the two strains will be of opposite sign and the ratio of their absolute values, given by $|\varepsilon_s/\varepsilon_x| = \nu$, is a constant property of the material. The quantity ν is called *Poisson's ratio* and, for steel, has a value of approximately 0.3.

In the module of deck plating shown in Fig. 40, the transverse beams exert some restraint against this transverse strain, with the result that stresses of opposite sign are set up in both the beam and plate. Equilibrium of the transverse force resultants of these stresses for the module is expressed as

$$\bar{\sigma}\bar{A} + \sigma_s A_P = 0 \quad (136)$$

where

\bar{A} = cross sectional area of one stiffener

A_P = cross sectional area of one module of plating

$\bar{\sigma}$ and σ_s are defined in Fig. 40.

Hooke's Law, which expresses the relation between stress and strain in two dimensions, may be stated in terms of the plate strains:

$$\begin{aligned} \varepsilon_x &= \frac{1}{E}(\sigma_x - \nu\sigma_s) \\ \varepsilon_s &= \frac{1}{E}(\sigma_s - \nu\sigma_x) \end{aligned} \quad (137)$$

In the plate-stiffener field, there will be equality of strain at the joint of plate to stiffener. If the stiffeners are closely spaced, this is assumed to be applied (on average) to the entire plate field, and the procedure is sometimes referred to as a *smearing* of the effect of the stiffeners. The stiffeners themselves are assumed to behave as one-dimensional elastic members. Therefore, the previous equality of strain requires

$$\bar{\sigma} = \sigma_s - \nu\sigma_x \quad (138)$$

if the plate and bar are of the same material.

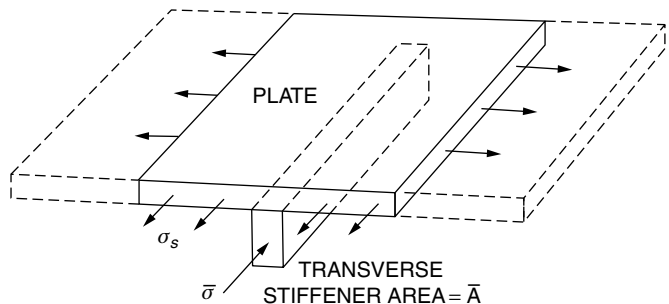


Fig. 40 Module of stiffened deck plate.

If $\bar{\sigma}$ and σ_s are eliminated from equations (136), (138), and the first of (137), the relation between longitudinal stress and strain in the plate may be written

$$\frac{\sigma_x}{\varepsilon_x} = E \frac{1+r}{1+r(1-\nu^2)} \quad (139)$$

Here $r = \bar{A}/A_p$ is the ratio of stiffener to plate area per module.

Thus, even though the entire cross section may be constructed of material having the same E , the section behaves as though it were a composite section if the stiffener size or spacing varies around the section. Note that the stress in the cross section is affected by the previous phenomenon through a change in the position of the neutral axis compared to the unstiffened plate. The stiffness against bending is affected by the geometry, through the moment of inertia, and the apparent modulus of elasticity. Although these effects are usually insignificant in the static analysis of ship structures, they may be of importance in vibration analysis.

3.2.1 Calculation of Section Modulus. An important step in routine ship design is the calculation of midship section modulus. As defined in connection with equation (134), it indicates the bending strength properties of the primary hull structure. The standard calculation is described in ABS (2008), Part 3, Chapter 2, Section 1: "The section modulus to the deck or bottom is obtained by dividing the moment of inertia by the distance from the neutral axis to the molded deck line at side or to the base line, respectively.

"In general, the following items may be included in the calculation of the hull girder section modulus, provided they are continuous or effectively developed:

- Deck plating (strength deck and other effective decks)
- Shell and inner-bottom plating
- Deck and bottom girders
- Plating and longitudinal stiffeners of longitudinal bulkheads
- All longitudinals of deck, sides, bottom, and inner bottom
- Continuous longitudinal hatch coamings."

The designation of which members should be considered as effective is subject to differences of opinion. The members of the hull girder of a ship in a seaway are stressed alternately in tension and compression. Some of them will take compression, although deficiency in the end connection makes them unable to take full tension. Other members, perhaps of light plating ineffectively stiffened, may be able to withstand tension stresses to the elastic limit but may buckle under a moderate compressive stress. In general, only members that are effective in both tension and compression are assumed to act as part of the hull girder.

The calculation of a section modulus is normally based on the following formula for moment of inertia of any

composite girder section:

$$I = 2 [I_n - Ad_g^2] = 2 \left[\sum (i_o + ad_n^2) - Ad_g^2 \right] \quad (140)$$

where

I = moment of inertia of the section about a line parallel to the base through the true neutral axis (center of gravity), expressed in $\text{cm}^2\text{-m}^2$ ($\text{in}^2\text{-ft}^2$)

I_n = moment of inertia of the half section about an assumed axis parallel to the true neutral axis

$$= \sum (i_o + ad_n^2)$$

A = total half-section area of effective longitudinal strength members, Σa , in cm^2 (in^2). See ABS (2008), Part 3, Chapter 2, Section 1, for effective areas included in the calculation.

d_g = distance from the assumed axis to the true axis, in m (ft)

i_o = vertical moment of inertia (about its own center of gravity) of each individual plate or shape effective for longitudinal strength

a = area of each such plate or shape, in cm^2 (in^2)

d_n = distance of the center of gravity of each such plate or shape from the assumed axis, in m (ft).

Owing to symmetry, it is necessary to include in the calculation only the structural parts on one side of the center line, the result of the calculation being multiplied by two as indicated in equation (140).

If the assumed axis is assigned an arbitrary location, the known or directly determinable values are i_o , a , and d_n ; hence I_n may be obtained. The value of A is also known and

$$d_g = \sum ad_n / \sum a = \sum ad_n / A$$

therefore, Ad_g^2 is determinable. The baseline may be used for the assumed axis. However, there is some advantage in using an assumed axis at about mid-depth in that lever arms are decreased. In that case, the assumed axis should be located at about 45 percent of the depth of the section above the baseline. The actual position of the neutral axis is normally at less than half depth because the bottom shell plating has a greater sectional area than the deck plating (except in such cases as tankers). This condition is accentuated when an inner bottom is fitted.

After I has been calculated, as outlined, the section modulus I/c can be obtained for both top and bottom extreme fibers. For the sake of convenience and uniformity, the following conventions are usually observed:

- Because the moments of inertia i_o of individual horizontal members are negligible, they are omitted from the calculations.

- The top c is taken from the neutral axis to the deck at side, the bottom c to the baseline.

3.3 Distribution of Primary Shear and Transverse Stress Components. The simple beam theory expressions given in the preceding section permits the evaluation of the longitudinal component of the primary stress, σ_x . As shown in Fig. 41, an element of shell or deck plating may generally be subject to two other components of stress, a direct stress in the transverse direction and a shearing stress. Figure 41 illustrates these as the *stress resultants*, defined as the stress multiplied by plate thickness. The stress resultants have dimensions of force per unit length and are given by the following expressions:

- $N_x = t\sigma_x, N_s = t\sigma_s$ = stress resultants
- $N = t\tau$ = shear stress resultant or shear flow
- σ_x, σ_s = stresses in the longitudinal and girth-wise directions
- τ = shear stress
- t = plate thickness

Here σ_s designates the transverse direct stress parallel to the vertical axis in the ship's side and parallel to the transverse axis in the deck and the bottom.

Through considerations of static equilibrium of a triangular element of plating, it can be shown that the plane stress pattern described by the three component stresses $\sigma_x, \sigma_s,$ and τ may be reduced to a pair of alternative direct stresses, σ_1 and σ_2 . The stresses σ_1 and σ_2 are called *principal stresses* and the directions of σ_1 and σ_2 are the principal stress directions. The principal stresses are related to $\sigma_x, \sigma_s,$ and τ by

$$\sigma_{1,2} = \frac{\sigma_x + \sigma_s}{2} \pm \sqrt{\left(\frac{\sigma_x - \sigma_s}{2}\right)^2 + \tau^2} \quad (141)$$

The two angles, θ , between the x -axis and the directions of σ_1 and σ_2 are

$$\tan 2\theta = \frac{2\tau}{\sigma_x - \sigma_s} \quad (142)$$

Detailed derivation of these expressions may be found in Timoshenko (1956).

In many parts of the ship, the longitudinal stress, σ_x , is the dominant component. However, there are locations in which the shear component becomes important, and under unusual circumstances the transverse component may likewise become important. A suitable procedure for estimating these other component stresses can be derived by considering the equations of static equilibrium of the element of plating illustrated in Fig. 41. In case the stiffeners associated with the plating support a part of the loading, this effect may also be included.

The static equilibrium conditions for the element of plate subjected to in-plane stresses (i.e., no bending of

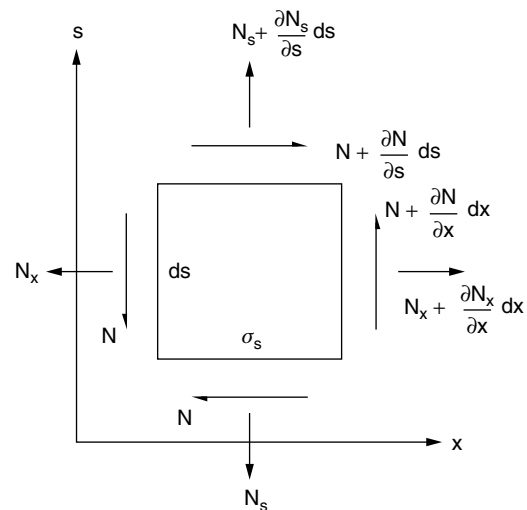
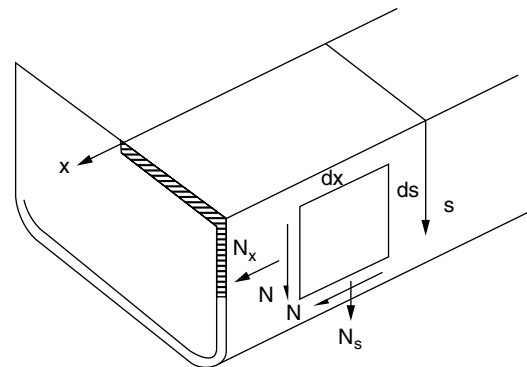
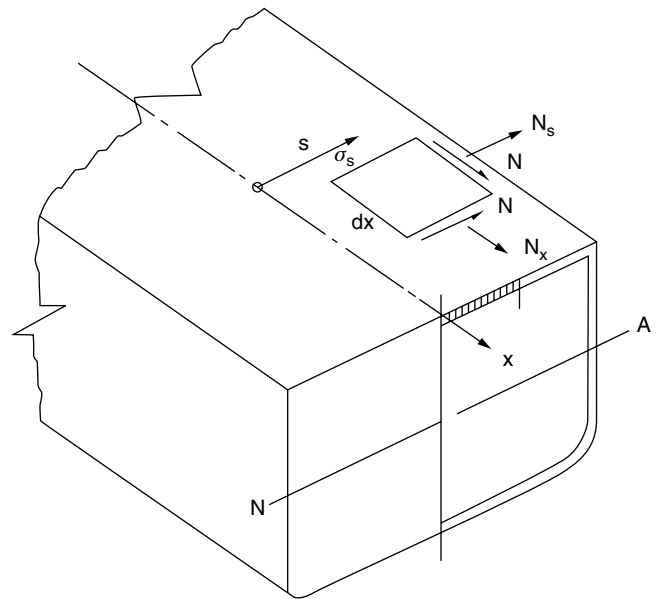


Fig. 41 Element of plate structure in deck or side shell, illustrating components of bending stress resultants.

the plate) are

$$\begin{aligned}\frac{\partial N_x}{\partial x} + \frac{\partial N}{\partial s} &= 0 \\ \frac{\partial N_s}{\partial s} + \frac{\partial N}{\partial x} &= 0\end{aligned}\quad (143)$$

In these expressions, s is the girthwise coordinate measured on the surface of the section from the x -axis as shown in Fig. 41.

The first of equation (143) may be integrated in the s -direction around the ship section to obtain the shear stress distribution. For this purpose, assume as a first approximation that the longitudinal stress σ_x is given by the beam theory expression (134). Then assume that the hull girder is prismatic (or that I changes slowly in the x -direction) so that only $M(x)$ varies with x , the derivative of N_x is given by differentiating equation (133),

$$\frac{\partial N_x}{\partial x} = -\frac{tz}{I} \frac{dM(x)}{dx} = -\frac{tz}{I} V(x) \quad (144)$$

where $V(x)$ is the shear force in the hull at x .

The shear flow distribution around a section is given by integrating the first of equation (143) in the s -direction:

$$N(s) - N_o = \int_0^s \frac{\partial N}{\partial s} ds = - \int_0^s \frac{\partial N_x}{\partial x} ds = \frac{V(x)}{I} \int_0^s t z ds \quad (145)$$

Here N_o , the constant of integration, is equal to the value of the shear flow at the origin of integration, $s = 0$. By proper choice of the origin, N_o can often be set equal to zero.

For example, in a section having transverse symmetry and subject to a bending moment in the vertical plane, the shear stress must be zero on the centerline, which therefore is a suitable choice for the origin of the girthwise integration. The shear flow distribution around a single-walled symmetrical section is then given by

$$N(s) = \frac{V(x)}{I} m(s) \quad (146)$$

with $N_o = 0$, in the case of such symmetry.

The quantity $m(s) = \int_0^s t z ds$ is the first moment about the neutral axis of the cross sectional area of the plating between the origin at the centerline and the variable location designated by s . This is the shaded area of the section shown in Fig. 41.

If a longitudinal stiffener or girder that carries longitudinal stress is attached to the plate, there will be a discontinuity in the shear flow, $N(s)$, at the stiffener corresponding to a jump in $m(s)$. Thus, in evaluating the moment, $m(s)$, in equation (146) a finite increment equal to \bar{m}_A is added, and there is a corresponding jump in $N(s)$ as the path of integration encounters a stiffener. \bar{m}_A is the moment of the section area of the stiffener about the ship's neutral axis.

The moment of the stiffener cross section can be written as

$$\bar{m}_A = \bar{A}_i \bar{z}_i \quad (147)$$

where

\bar{A}_i = sectional area of stiffener i

\bar{z}_i = distance from neutral axis to centroid of \bar{A}_i

Equation (146) then becomes

$$N(s) = \frac{V(x)}{I} \left[m(s) + \sum_i \bar{A}_i \bar{z}_i \right] + N_o \quad (148)$$

For a rectangular cross section having no stiffener, the shear flow distribution corresponding to equation (146) will have a linear variation in the deck and parabolic variation in the topsides as shown in Fig. 42.

The transverse stress, σ_s , or equivalently the stress resultant, N_s , can be found by integration of equation (149),

$$\frac{\partial N_s}{\partial s} = -\frac{\partial N}{\partial x} \quad (149)$$

Substituting equation (146) for N , we obtain

$$N_s(s) - N_{so} = - \int_0^s \frac{\partial}{\partial x} \left[\frac{V(x)}{I} m(s) \right] ds \quad (150)$$

Assuming a prismatic section so that only $V(x)$ depends on x , and noting that $\frac{\partial V}{\partial x} = q(x)$, the vertical load per unit length, is

$$N_s(s) - N_{so} = -\frac{q(x)}{I} \int_0^s m(s) ds \quad (151)$$

For a rectangular section, this expression gives a parabolic variation of N_s in the horizontal members and a cubic variation in the vertical members. The constant of integration, N_{so} , is adjusted so that N_s is equal to the resultant girthwise stress at some location where this stress can be determined. Examples of such locations are the edge of a deck, or a side or bottom panel.

In the side plating at the deck (upper) edge, the girthwise resultant, N_s , must be equal to the weight per unit length of deck cargo plus deck structure for one side of the ship. At the bottom (bilge), it would be one half of the total buoyancy per unit length less the downward forces such as those due to structural weight, internal cargo and liquids that are supported directly by the bottom plating. In the bottom plating, the girthwise resultant is in the transverse direction and will equal the resultant transverse hydrostatic force per unit length. Figure 42 illustrates the distribution of N_s for a rectangular ship section carrying deck cargo and subject to a hydrostatic load on sides and bottom. It is assumed that the transverse framing transmits all of the water pressure load from the bottom plate panel to the edge, where it is transmitted as in-plane stress into the side plating and similarly for the hydrostatic pressure on the sides and

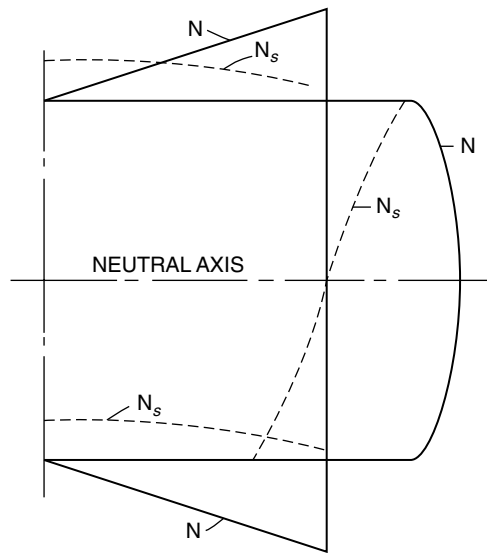


Fig. 42 Shear flow and girthwise stress around a rectangular ship cross section.

weight load on deck. With few exceptions—for example, a ship carrying a very large localized deck load—such vertical and horizontal in-plane stresses are usually negligibly small in comparison to the longitudinal and shear stresses.

3.4 Shear Flow in Multicell Sections Due to Primary Shear Forces. If the cross section of the ship shown in Fig. 41 is subdivided into two or more closed cells by longitudinal bulkheads, tank tops, or decks, the problem of finding the shear flow in the boundaries of these closed cells is statically indeterminate. To visualize this, refer to Fig. 43, showing a typical tanker midship section that is subdivided into three cells by the two longitudinal bulkheads. Equation (146) may be evaluated for the deck and bottom of the center tank space because the plane of symmetry at which the shear flow vanishes lies within this space and forms a convenient origin for the integration. At the deck-bulkhead intersection, the shear flow in the deck divides but the relative proportions of the part in the bulkhead and the part in the deck are indeterminate. The sum of the shear flows at two locations lying on a plane cutting the cell walls (e.g., at points A and B in Fig. 43a) will still be given by equation (146), with $m(s)$ equal to the moment of the shaded area. However, the distribution of this sum between the two components in bulkhead and side shell requires additional information for its determination.

This additional information may be obtained by considering the torsional equilibrium and deflection of the cellular section. To develop the necessary equations, first consider a closed, single-cell, thin-walled prismatic section subject only to a twisting moment, M_T , which is constant along the length, as shown in Fig. 44. The resulting shear stress may be assumed uniform through the plate

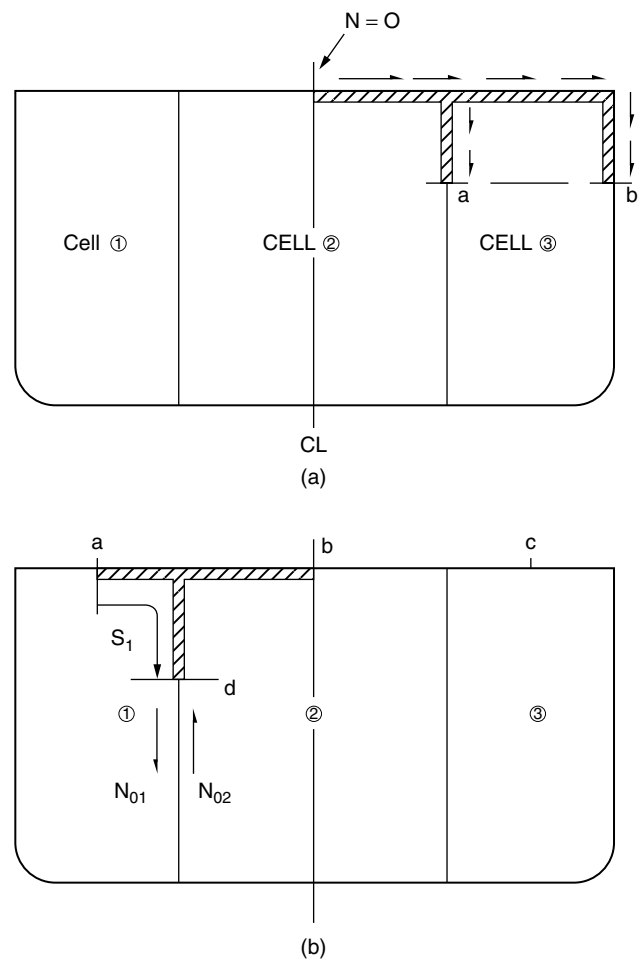


Fig. 43 Shear flow in a multiple bulkhead tanker section.

thickness and tangent to the mid-thickness of the material. Under these circumstances, the deflection of the tube will consist of a twisting of the section without distortion of its shape, and the rate of twist, $d\theta/dx$, will be constant along the length.

Now consider equilibrium of forces in the x -direction for the element $dxds$ of the tube wall as shown in Fig. 44b. Because there is no longitudinal load, there will be no longitudinal stress, and only the shear stresses at the top and bottom edges need be considered in the expression for static equilibrium, giving

$$-t_1 \tau_1 dx + t_2 \tau_2 dx = 0 \quad (152)$$

The shear flow, $N = t\tau$, is therefore seen to be constant around the section.

The magnitude of the moment, M_T , may be computed by integrating the moment of the elementary force arising from this shear flow about any convenient axis. If r is the distance from the axis, perpendicular to the resultant

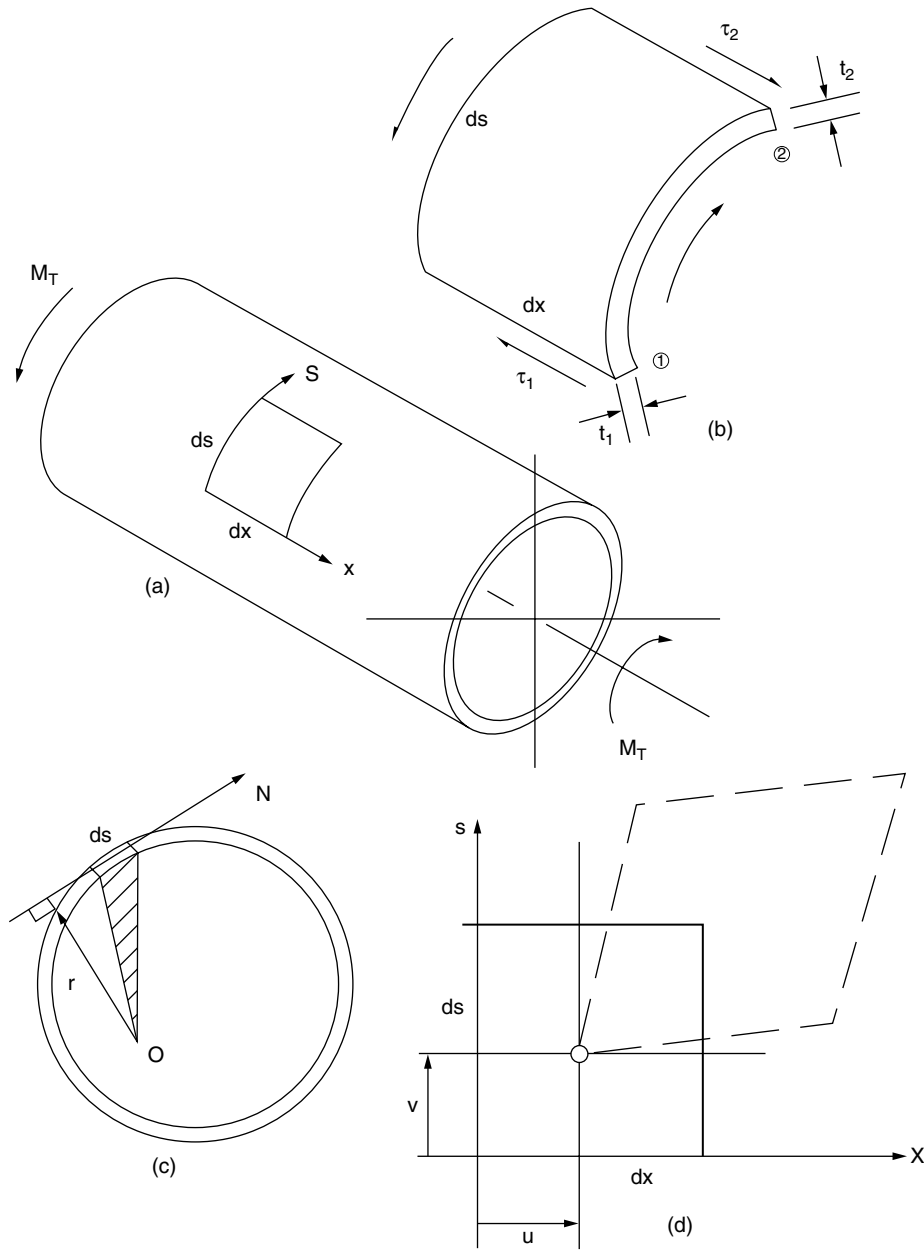


Fig. 44 Twisting of a closed prismatic tube.

shear flow at location s as shown in Fig. 44c, then

$$M_T = \oint rNds = N \oint rds = 2N\Omega \quad (153)$$

Here the symbol \oint indicates that the integral is taken entirely around the section and, therefore, Ω is the area enclosed by the mid-thickness line of the tubular cross section. The constant shear flow is then related to the applied twisting moment by

$$N = M_T/2\Omega \quad (154)$$

Consider the deformation of the element $dsdx$ that results from this shear. Let u and v be the displacements in the axial and tangential directions respectively of a point on the surface of the tube; this is shown in Fig. 44d. As a result of the constant twisting moment and prismatic geometry, u is seen to be a function of s only and v will be given by a rigid body rotation of the cross section,

$$\frac{\partial v}{\partial x} = r \frac{d\theta}{dx} \quad (155)$$

where r is defined as before.

From elementary elasticity, the shear strain, γ , is related to the displacements by

$$\gamma = \frac{\partial u}{\partial s} + \frac{\partial v}{\partial x} \quad (156)$$

Also, $\gamma = \tau/G$, where

$$G = \frac{E}{2(1+\nu)}$$

is the shear modulus of elasticity. Substituting equation (155) into equation (156) and rearranging, gives

$$\frac{\partial u}{\partial s} = \frac{\tau}{G} - r \frac{d\theta}{dx} \quad (157)$$

Because u depends only on s , this may be integrated to give

$$\begin{aligned} u(s) &= \int \frac{\tau}{G} ds - \int r \frac{d\theta}{dx} ds + u_o \\ &= \frac{1}{G} \int \frac{N}{t} ds - \frac{d\theta}{dx} \int r ds + u_o \end{aligned} \quad (158)$$

where u_o is a constant of integration.

The quantity, $u(s)$, termed the *warp*, is seen to be the longitudinal displacement of a point on the cell wall that results from the shear distortion of the material due to twist. If the section is circular, the rotation will take place without warping, but for most other shapes the warping will be nonzero and will vary around the perimeter of the section.

For a closed section, the differential warp must be zero if the integral in equation (158) is evaluated around the entire section—that is, two points on either side of a longitudinal line passing through the origin of the s -integration cannot be displaced longitudinally with respect to each other. This is expressed by

$$\frac{1}{G} \oint \frac{N}{t} ds - \frac{d\theta}{dx} \oint r ds = 0 \quad (159)$$

Noting that N is constant around the section and recalling that the second integral was previously represented by 2Ω , the relationship between shear flow and rate of twist is given by the Bredt formula,

$$\frac{d\theta}{dx} = \frac{N}{2\Omega G} \oint \frac{ds}{t} \quad (160)$$

Substituting equation (153) for the twisting moment gives

$$\frac{d\theta}{dx} = \frac{M_T}{4\Omega^2 G} \oint \frac{ds}{t} \quad (161)$$

Equation (158) for the warp, $u(s)$, applies to any thin walled prismatic tube if it can be assumed that the tube twists in such a way that cross sections rotate without distortion of their shape.

Now write the shear flow in the tanker section, equation (146), as the sum of two parts,

$$N(s) = N_1(s) + N_o$$

where N_o is an unknown constant shear flow. Under a pure vertical loading, the twist of the section, $d\theta/dx$, must be zero, and for this case, equation (159) becomes

$$0 = \frac{1}{G} \oint (N_1 + N_o) \frac{ds}{t} = \frac{1}{G} \oint N_1 \frac{ds}{t} + \frac{N_o}{G} \oint \frac{ds}{t} \quad (162)$$

This may be solved for the unknown constant,

$$N_o = \frac{\oint N_1 \frac{ds}{t}}{\oint \frac{ds}{t}} \quad (163)$$

Equation (163) provides the means of evaluating the constant of integration in equation (146) or equation (148) in the case of sections of general shape for which a location of zero shear flow cannot be determined by inspection.

A physical significance may be attached to the quantity N_o by the following reasoning. Assume that the closed tubular section subject to a vertical loading without twist is transformed into an open section by an imaginary longitudinal slit, and the edge of this slit is taken as the origin of the s -coordinate; this is shown in Fig. 45. Corresponding to the shearing strains, the two edges of the slit will displace longitudinally relative to each other. Comparing equations (161) and (162), it is seen that because $\frac{d\theta}{dx} = 0$ the two terms in equation (162) represent warping displacements of one edge of the slit relative to the other corresponding to N and N_o , respectively.

The first term is the warping displacement caused by the statically determinate shear flow, N_o , which is given by equation (148). The second term is the warp due to the constant shear flow, N_o . Equation (162) is the statement that N_o is of such magnitude that the net warp must be zero (i.e., it is of such magnitude that the slit is closed up).

Now apply a similar procedure to the multiple cell section shown in Fig. 43. Results will be given for the general case of several closed cells and later specialized for a case of symmetrical section as illustrated. First imagine each cell to be cut with longitudinal slits at points a , b , and c in Fig. 43b. Let $N_i(s)$ be the shear flow in cell i obtained by evaluating equation (148) with the origin of s located at the slit in that cell. Let N_{io} be the constant of integration for cell i . Note that when computing $m(s)$ in equation (148) for a location in the bulkhead, such as point d , the area of deck plating and frames up to the imaginary slit in the adjacent cell 2 must be included.

The relative warp at slit a due to $N_1(s)$ is given by

$$u_{1a} = \frac{1}{G} \oint_1 N_1(s) \frac{ds}{t} \quad (164)$$

where $N_i(s)$ is given by equation (148).

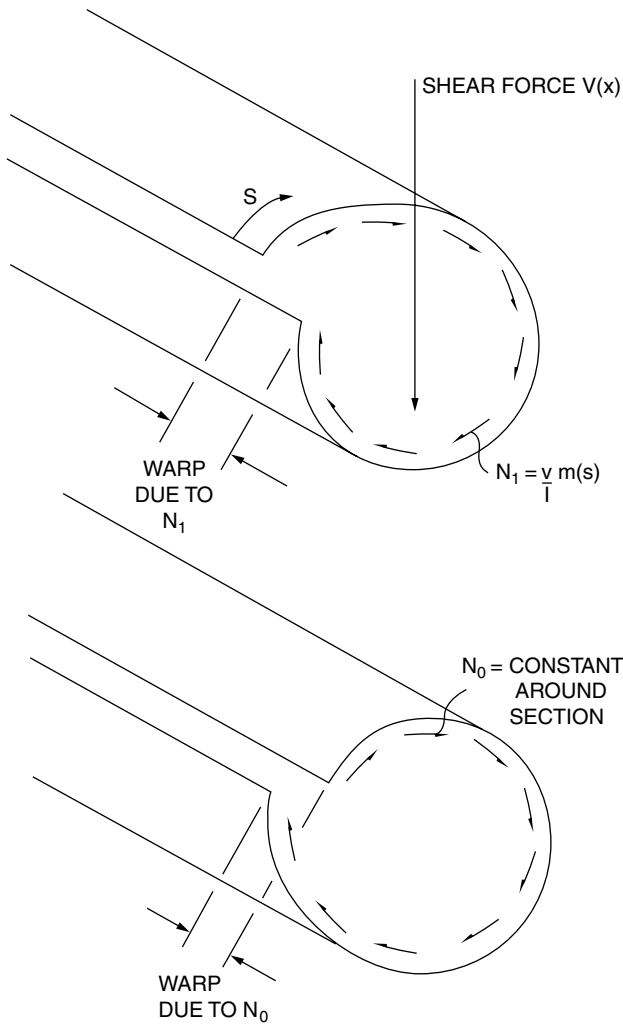


Fig. 45 Warp associated with N_1 and N_0 .

Equations similar to these may be written for each of the remaining cells. For each cell, there will be an additional constant shear flow corresponding to the constant of integration. The differential warp in the adjacent edges of one of the slits will include the effects of these constant shear flows for the present cell as well as the constant shear flows for adjacent cells acting along any interior walls that are common to the present and the adjacent cell. For cell 1, this additional warp at slit a , resulting from the constant shear flows acting on the boundaries of cell 1, is

$$u_{0a} = \frac{1}{G} N_{01} \oint_1 \frac{ds}{t} - \frac{1}{G} N_{02} \oint_{1-2} \frac{ds}{t} \quad (165)$$

The second integral in this expression is evaluated only over the bulkhead dividing cells 1 and 2, and is negative because the constant shear flows of the two cells oppose each other in the bulkhead.

Requiring that the total warp at slit a must vanish, is given by the condition

$$\oint_1 N_1(s) \frac{ds}{t} + N_{01} \oint_1 \frac{ds}{t} - N_{02} \oint_{1-2} \frac{ds}{t} = 0 \quad (166)$$

Similar equations may be written for the remaining cells. For the middle cell 2,

$$\oint_2 N_2(s) \frac{ds}{t} + N_{02} \oint_2 \frac{ds}{t} - N_{01} \oint_{2-1} \frac{ds}{t} - N_{03} \oint_{2-3} \frac{ds}{t} = 0 \quad (167)$$

and for cell 3,

$$\oint_3 N_3(s) \frac{ds}{t} + N_{03} \oint_3 \frac{ds}{t} - N_{02} \oint_{3-2} \frac{ds}{t} = 0 \quad (168)$$

Now observe that the first term in each of these equations can be evaluated and is, therefore, a known quantity. The three equations may therefore be solved simultaneously for the three constants of integration N_{01} , N_{02} , and N_{03} . Note also that the moment term, $m(s)$, in the expressions for N_1 , N_2 , and N_3 must include the moment of the area of longitudinal stiffeners as well as the plating, as shown in equation (148), whereas the integrals in equations (166), (167), and (168) include only the plating. The explanation for this is that the latter integrals evaluate the warping displacements, and these result from the shear deformation of the plating only.

In the case of a three-cell, twin-bulkhead tanker that is symmetrical about the centerline plane, slit b may be placed on the centerline, in which case N_{02} is zero. Equations (166) and (168) now contain only one unknown constant of integration each, and each may be solved explicitly. Furthermore, by symmetry it is necessary to solve for only one of the two constants of integration, and this is given by

$$N_{01} = -\frac{\oint_1 N_1(s) \frac{ds}{t}}{\oint_1 \frac{ds}{t}} \quad (169)$$

The resulting total shear flow in cell 1 (and cell 3 by symmetry considerations) will be given by

$$N(s) = \frac{V(x)}{I} \left[m(s) - \frac{\oint_1 m(s) \frac{ds}{t}}{\oint_1 \frac{ds}{t}} \right] \quad (170)$$

Of course, the shear flows in the deck and bottom of cell 2 are statically determinate and may be computed directly from equation (148) with the constant of integration set equal to zero. The resulting component and total shear flows in the tanker section are shown in Fig. 46.

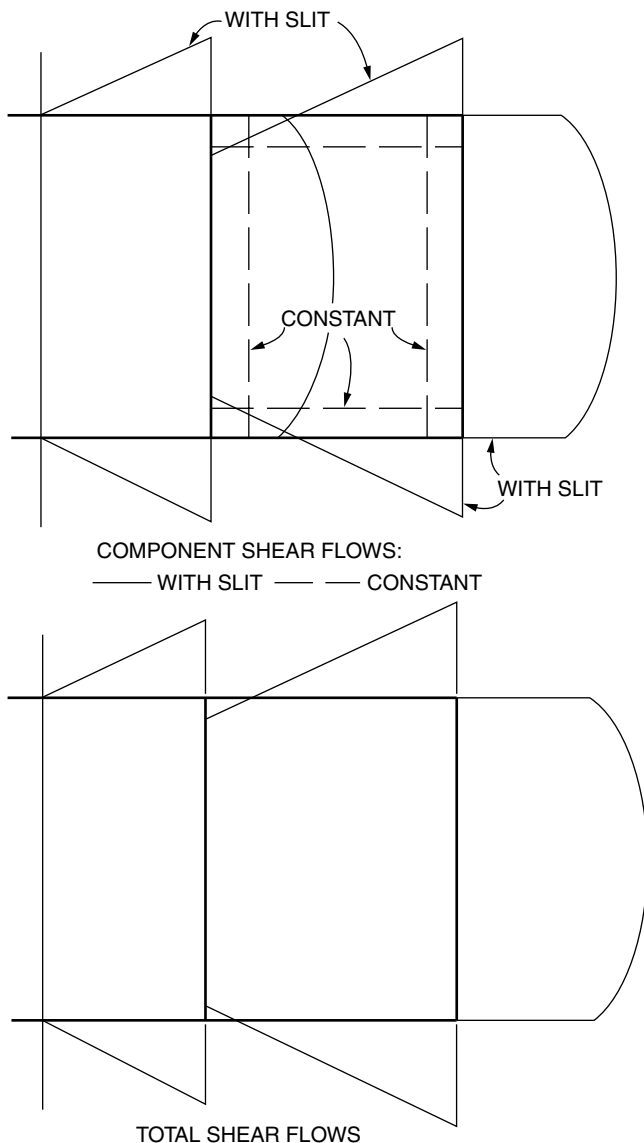


Fig. 46 Component and total shear flows in tanker midship section.

3.5 Shear Lag and Effective Breadth. In many ship structural components, the loading is resisted on a local level by web-type members before being transformed into a beam-bending load. A simple illustration of this, shown in Fig. 47, is a wide-flange girder supporting a concentrated weight. At the local level, the weight is first transmitted into the web of the girder, where it is resisted by vertical shears in the web. As a result of the concentrated load, the web tends to bend as shown, resulting in a compressive strain on the upper edge and tensile strain along the lower. The flanges are required to have a strain equal to the strain in the web at the joint between the web and the flange, and this results in a shear loading being applied to this edge of each flange member. Each of the four flange members may therefore be viewed as

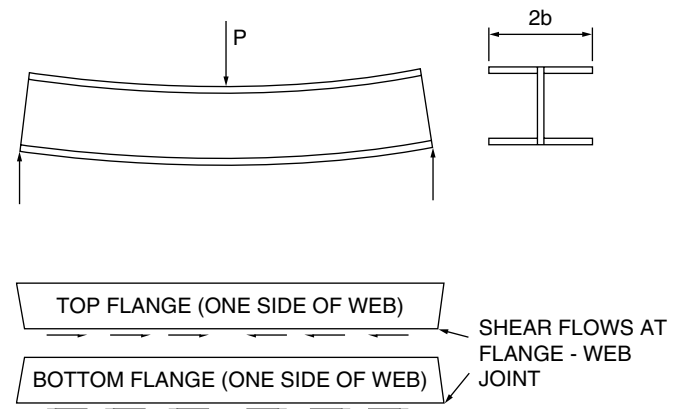
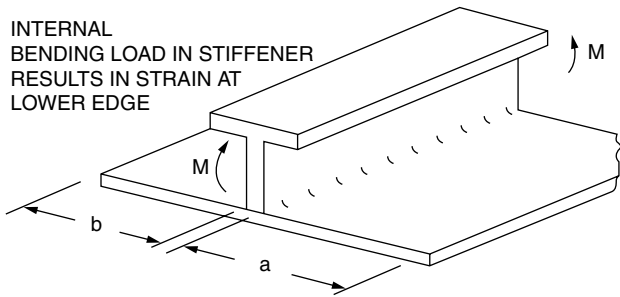


Fig. 47 Loading and resulting strain in flange of simple beam.

a rectangular strip of plating having a shearing load applied along one of the long edges. The resultant deformation is illustrated in Fig. 47.

The loading situation described here is not confined to isolated beams that support concentrated loads, but appears in many parts of the ship structure in association with distributed as well as concentrated loads. For example, consider the hull girder as a whole. Water pressure on the bottom is resisted locally by the plating that transmits the pressure load to the surrounding frames and floors. Longitudinal framing transmits the force system into the transverse bulkheads or web frames, which in turn transmit their loads into the longitudinal bulkheads or side shells. In the case of transverse frames, these resultant loads are transmitted directly into the side shell by each frame individually. Thus, the water pressure forces and, similarly, the weight forces are ultimately transmitted into the side shell or vertical web of the hull girder as concentrated shearing loads at each bulkhead or transverse frame. The bending tendency of the web (side shell) and the shear loading of the edges of the flange (deck plating) are directly analogous to the behavior of the simple girder illustrated in Fig. 47.

An important effect of this edge shear loading of a plate member is a resulting nonlinear variation of the longitudinal stress distribution. This is in contrast to the uniform stress distribution predicted in the beam flanges by the elementary beam equation (134). In many practical cases, the departure from the value predicted by equation (134) will be small, as shown in Fig. 38. However, in certain combinations of loading and structural geometry, the effect referred to by the term *shear lag* must be taken into consideration if an accurate estimate of the maximum stress in the member is to be made. This may be conveniently done by defining an *effective breadth* of the flange member. The nomenclature used in the definition of this quantity is illustrated in Fig. 48, where the effective breadth, ρb , is defined as the breadth of plate that, if stressed uniformly at the level



INTERNAL BENDING LOAD IN STIFFENER RESULTS IN STRAIN AT LOWER EDGE

STRAIN IN PLATE MUST EQUAL STRAIN IN STIFFENER AT THE JOINT AND THIS STRAIN IS INDUCED BY A SHEAR LOAD APPLIED TO THE PLATE BY THE STIFFENER AT THE JOINT

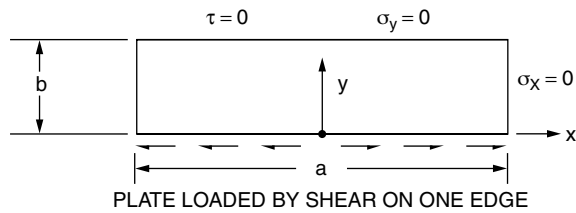
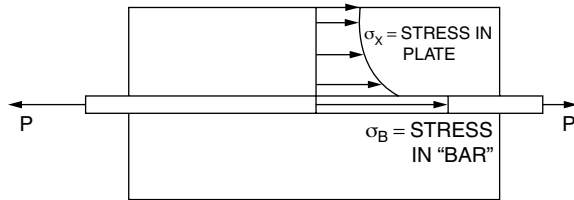


PLATE LOADED BY SHEAR ON ONE EDGE



ANALOG OF PLATE FLANGE: TWO PLATES WELDED TO BAR

Fig. 48 Nomenclature for shear lag analysis.

σ_B across its width, would sustain the same total load in the x -direction as the nonuniformly stressed plate. Hence,

$$\rho b = (1/\sigma_B) \int_0^b \sigma_x(y) dy \quad (171)$$

The quantity ρ is called the *plate effectiveness*.

The solution for ρ is seen to require the determination of the plane stress distribution in a plate field under the described edge shear loading. In addition to this edge shear loading, there are kinematic boundary conditions that must be satisfied, appropriate to the physical conditions that prevail on the other edges of the plate. Such conditions would include zero direct and shear stress on a free edge, and zero displacement in the direction normal to the edge if the plate-bar combination is part of a repeating arrangement.

A solution procedure for the stress distribution and the plate effectiveness may be developed making use of the *Airy stress function*, for which the fundamental considerations are given in Timoshenko and Goodier (1970). Define a function $\phi(x, y)$ such that the direct stresses, σ_x

and σ_y , are given by the following expressions:

$$\begin{aligned} \sigma_x &= \frac{\partial^2 \phi}{\partial y^2} \\ \sigma_y &= \frac{\partial^2 \phi}{\partial x^2} \end{aligned} \quad (172)$$

From the conditions of static equilibrium of a plane stress element, equation (143), the shear stress will be given by

$$\tau = -\frac{\partial^2 \phi}{\partial x \partial y} \quad (173)$$

If equations (172) and (173) are substituted into the stress-strain equation (137), the following relations are found:

$$\begin{aligned} \epsilon_x &= \frac{1}{E} \left(\frac{\partial^2 \phi}{\partial y^2} - \nu \frac{\partial^2 \phi}{\partial x^2} \right) \\ \epsilon_y &= \frac{1}{E} \left(\frac{\partial^2 \phi}{\partial x^2} - \nu \frac{\partial^2 \phi}{\partial y^2} \right) \\ \gamma &= -\frac{1}{G} \left(\frac{\partial^2 \phi}{\partial x \partial y} \right) \end{aligned} \quad (174)$$

A relationship between the direct strains and the shear strain is given by the condition of compatibility:

$$\frac{\partial^2 \gamma}{\partial x \partial y} = \frac{\partial^2 \epsilon_x}{\partial y^2} + \frac{\partial^2 \epsilon_y}{\partial x^2} \quad (175)$$

If equations (174) are now substituted into equation (175), the result is

$$\frac{\partial^4 \phi}{\partial x^4} + 2 \frac{\partial^4 \phi}{\partial x^2 \partial y^2} + \frac{\partial^4 \phi}{\partial y^4} = 0 \quad (176)$$

Equation (176) is recognized as the biharmonic equation, and is the field equation to be satisfied by the stress function, $\phi(x, y)$, at all points in the interior of the plate field. The complete solution of the stress distribution problem requires that we first obtain an expression for $\phi(x, y)$ by solving equation (176), subject to a set of appropriate boundary conditions on the edges of the plate field. Having this solution for $\phi(x, y)$, the stresses may be obtained by substitution in equation (172). The plate effective breadth is then found by evaluating the integral in equation (171). Examples of typical boundary conditions that may be encountered in ship structural configurations are shown in Fig. 49.

A solution to equation (176) was obtained by Schade (1951, 1953) using the method of separation of variables. In the Schade solution, the stress function is expanded in a Fourier series in the longitudinal coordinate,

$$\phi(x, y) = \sum_{n=1}^{\infty} f_n(y) \sin \frac{n\pi x}{L} \quad (177)$$

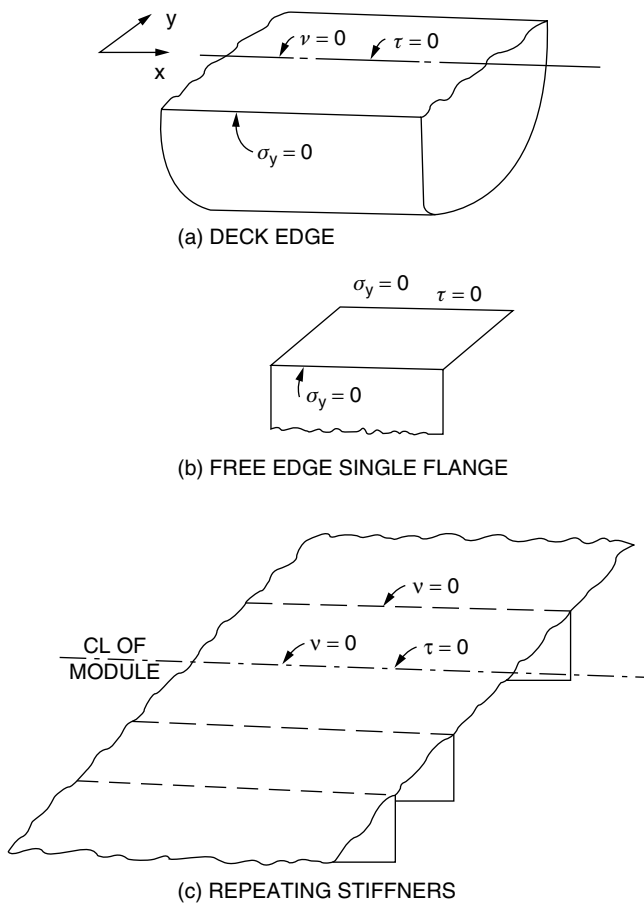


Fig. 49 Example of boundary conditions for shear lag problems in ship structures.

Here L is some characteristic length in the x -direction, and $f_n(y)$ is an unknown function of the transverse variable, y . Upon substituting this expression into the biharmonic equation (176), an ordinary differential equation is obtained for the unknown function $f_n(y)$. Details of the solution need not be repeated here but may be obtained by referring to the Schade papers.

The form of the solution is such that there is an insufficient number of constants of integration of equation (176) to allow the satisfaction of all of the necessary boundary conditions, and the solution must be considered as incomplete. However, by an appropriate choice of the partial boundary conditions, in combination with the application of *Saint-Venant's principle*, the solution may be considered accurate for most practical cases.

To illustrate this principle, consider the pair of plate panels loaded by the welded bar at the middle, which is illustrated in Fig. 48. The boundary conditions for one of the plate panels are shown in Fig. 49. Integration of the fourth-order differential equation (176) yields four constants of integration that are found by introducing boundary conditions on all of the plate edges, plus the condition of static equilibrium under the applied load

system. With the solution form that was assumed, three of these conditions plus the load equilibrium condition may be satisfied. In many practical cases, it is sufficient to satisfy the boundary conditions on the edges parallel to the x -axis, and to neglect the conditions at the ends of the plate panel. According to Saint-Venant's principle, the results will then be in error near the plate ends because the neglect of the boundary conditions is equivalent to the substitution of an equivalent but unspecified end loading. However, the error will be acceptably small in the interior of the panel if the length is large compared to the width. Many of the plate panels in ship structures are relatively slender—for example, the flanges of beams and girders—and the location of maximum stress is often at mid-length; thus this partial solution still provides results that are valid and useful in these cases. For built-in beams at the end having the maximum stress, the principle of reflection about the built-in end allows this location to be treated as though it were at the mid-length, thus allowing the present interior solution to apply to this important situation.

The Schade solutions have been expressed in the form of the effective breadth ratio, ρ , and this is generally a function of the geometry of the plate panel and the form of the applied load. The results are presented in a series of design charts, which are especially simple to use. An example of one of the charts is given in Fig. 50, and the remainder can be found in the Schade papers.

Examination of the chart reveals the following properties of the effective breadth:

- For long slender plate panels, the effective breadth is nearly 100 percent.
- For a given panel aspect ratio, the effective breadth is less for loads that are concentrated or vary abruptly than it is for loads that are evenly distributed over the length.

In Fig. 50, the factor R expresses the relative importance of the plate member (in which shear lag occurs) in comparison to the web or stiffener (assumed not to experience shear lag) in determining the section modulus of the composite. Figure 51 illustrates three typical combinations involving this symmetrical flange member:

- (a) H-section, having two identical flanges
- (b) T-section, or single flange
- (c) Plate flange with stiffener, consisting of a standard structural shape.

The corresponding expressions for R are as follows:

$$\begin{aligned} (a) \quad R &= 3A_f/A_w \\ (b) \quad R &= 4A_f/A_w \\ (c) \quad R &= A_f(r_s^2 + e_s^2)/I_s \end{aligned} \quad (178)$$

In all cases:

$$\begin{aligned} A_f &\text{ is the total flange cross-sectional area} \\ &= 4bt_f \text{ in (a)} \\ &= 2bt_f \text{ in (b) and (c)} \end{aligned}$$

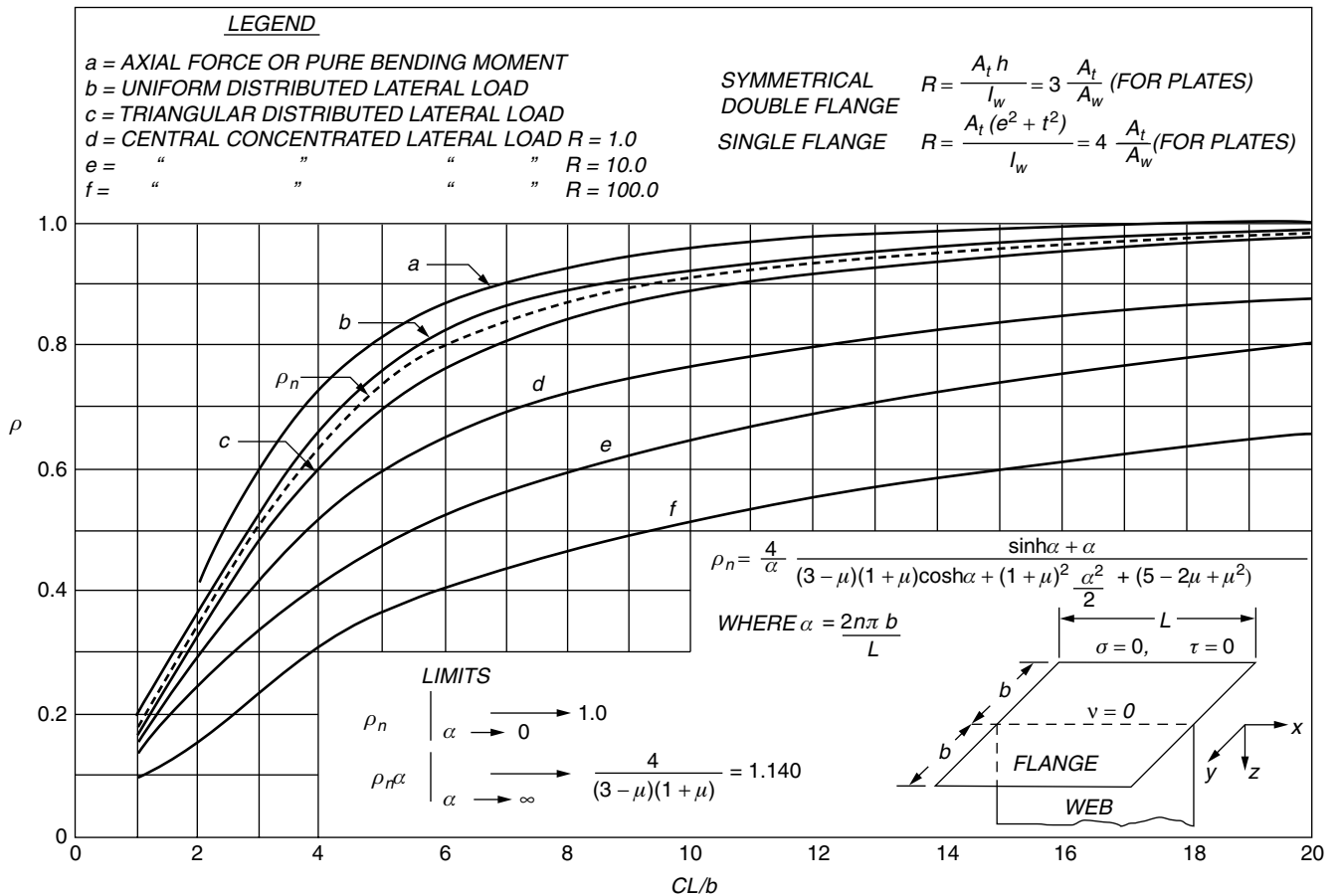


Fig. 50 Effectiveness ratio, ρ , at $x = L/2$.

A_w is the web cross sectional area

$$= 2ht_w \text{ in (a) and (b).}$$

In case (c), I_s is the stiffener moment of inertia about its own NA. r_s is the radius of gyration of the stiffener $\sqrt{I_s/A_s}$, where A_s is the stiffener cross sectional area. e_s is the distance from stiffener NA to the mid-thickness of the plate flange. The factor CL in Fig. 50 is the total span of the beam between locations of zero bending moment, and CL/b is the aspect ratio, AR . In the case of the constant bending moment or pure axial load, it is the physical length of the beam.

For example, consider a symmetrical section, case (a) having a flange area that is 3.33 times the web area; thus $R = 10$. Now assume that this is the cross section of a simply supported beam having a central, concentrated load, and assume the span of the beam to be 10 times the width, b , of one half the flange. From Fig. 50, curve e ($R = 10$) at an aspect ratio $CL/b = 10$, we see that the effective breadth of the flange is only 65 percent of the physical breadth. For cases other than the concentrated loads, the effective breadth is found to be relatively insensitive to R and, therefore, only a single curve corresponding to a composite value of R is shown in these load cases.

The effect of shear lag in a ship is to cause the stress distribution in the deck, for example, to depart from the constant value predicted by the elementary beam equation (134). A typical distribution of the longitudinal deck stress in a ship subject to a vertical sagging load is sketched in Fig. 52.

An extreme example of shear lag was observed in an experiment conducted by Glasfeld (1962). The experiment was conducted using a rectangular, thin-walled, steel box-girder model to represent the midship portion of a longitudinally framed ship. The vertical loading was applied to the model by means of a series of individual pneumatic pressure cells between the bottom of the model and the bed-plate of the supporting testing frame. Each cell applied a uniform pressure over a short portion of the length of the model, and the pressure in each cell could be adjusted individually. In the experiment in question, the pressure was adjusted in such a way that adjacent cells applied alternately positive and negative loads. The resulting bending moment was also found to show an alternating form, with relatively short spacing between zero points.

The longitudinal stress distribution measured at midships of the model is shown in Fig. 53, for a saddle shape

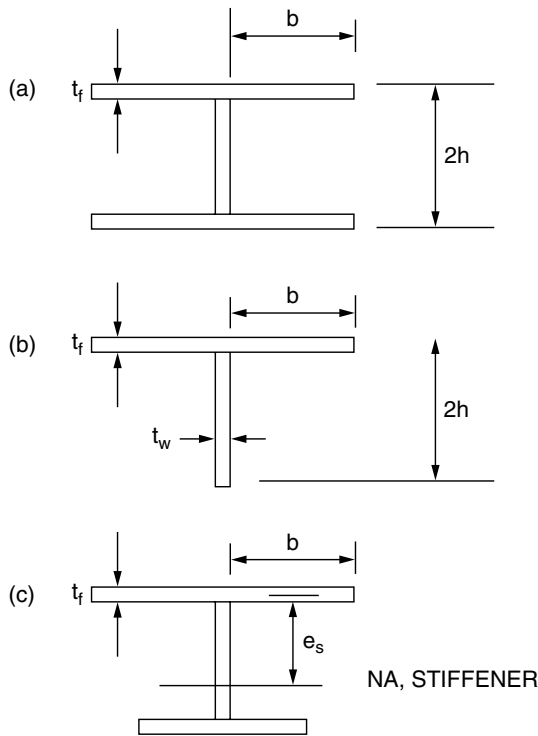


Fig. 51 Composite plate-stiffener beam section, to accompany Fig. 50.

bending moment, together with the corresponding stress computed by (a) the finite element method and (b) a stress function technique similar to that employed in deriving the effective breadth charts. It is remarkable to observe that the observed and computed stress distributions display such a pronounced shear lag effect that there is a complete reversal in the sign of the longitudinal stress between the centerline of the model and the edge of both the deck and bottom plating. This is obviously an extreme departure from simple beam theory, which predicts a constant longitudinal stress in these members. The longitudinal stress in the sides also shows

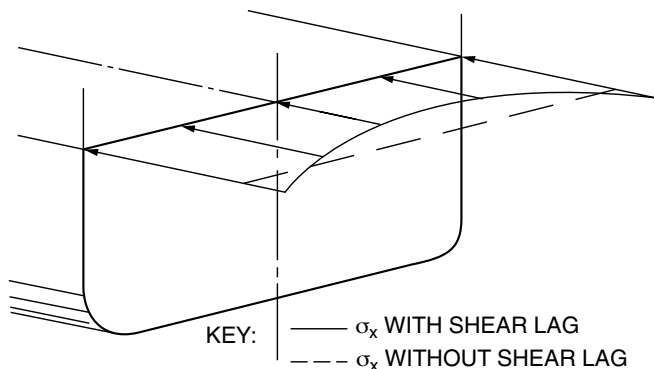


Fig. 52 Deck longitudinal stress, illustrating the effect of shear lag.

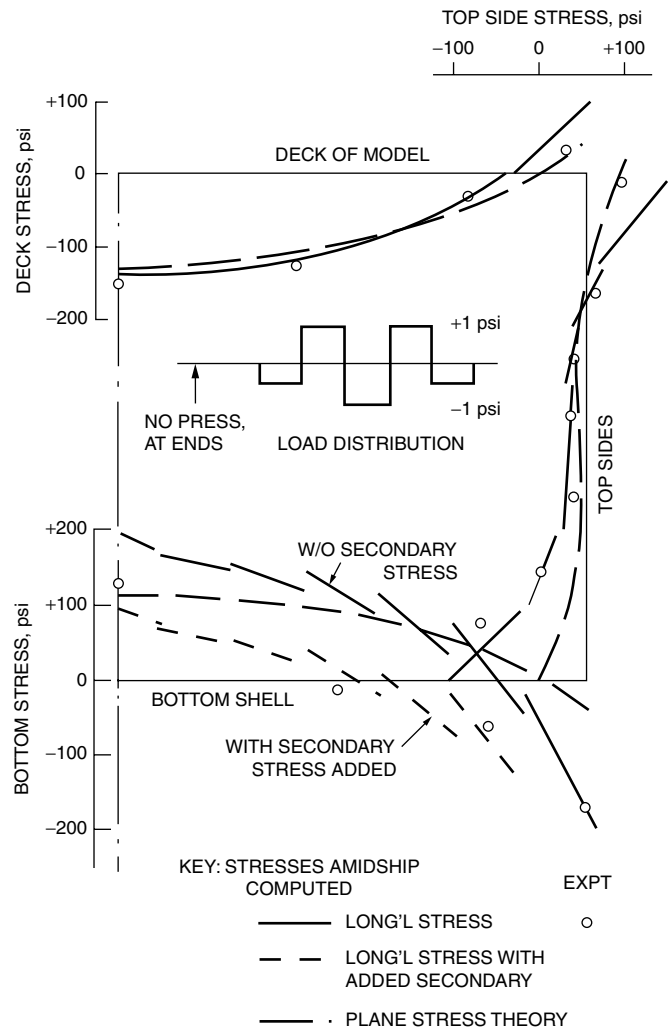


Fig. 53 Longitudinal stresses at midship section of box girder by experiment, theory, and finite element analysis (saddle bending moment).

a departure from beam theory in the S-shaped variation of this quantity from deck edge to bilge. This extreme departure from beam theory results is mainly due to the saddle shape of the bending moment.

A real situation in which an alternating load distribution may be encountered is a bulk carrier loaded with a dense ore cargo in alternate holds, the remainder being empty. An example computation of the effective breadth of bottom and deck plating for such a vessel is given in Chapter 6 of Taggart (1980).

3.6 Primary Lateral Bending and Torsional Stresses.

Up to this point, our attention has been focused principally on the vertical longitudinal bending response of the hull. As the ship moves through a seaway, encountering waves from directions other than directly ahead or astern, it will experience lateral bending loads and twisting moments in addition to the vertical loads (see Section 2.3). The former may be dealt with by methods that

are similar to those used for treating the vertical bending loads, noting that there will be no component of still-water bending moment or shear in the lateral direction. The twisting or torsional loads will require some special consideration. However, note that because of the subdivision of the loads and response into primary, secondary, and tertiary components, the response of the ship to the overall hull twisting loading should be considered a primary response.

The equations for the twist of a closed tube presented in Section 3.4, (154) and (160), are applicable to the computation of the torsional response of thin-walled sections. However, in ship structures it is found that torsional effects (stresses, deflections) are most often found to be of importance in ships that have large deck openings separated, perhaps, by narrow-transverse strips of structure and closed ends.

Such construction is typical of a modern container ship. Experience with the design of such partially opened deck ships has indicated that the torsional stresses alone have seldom been of a serious magnitude. However, when considered in conjunction with the primary bending stresses they can result in significant localized increases in the combined primary stresses. A more serious structural problem, requiring special attention in the design of such ships, is found at the transition from the torsionally weak open sections to the relatively stiff closed sections that are required to provide torsional rigidity to the hull. The abrupt change in structural properties may result in high stress concentrations in such areas, requiring special attention to the design of details (see Section 3.17.3). The principal design objective here is to select material and structural details that are appropriate for regions subject to stress concentrations.

The relative torsional stiffness of closed and open sections can be visualized by means of a very simple example. Consider two circular tubes, one of which has a longitudinal slit over its full length, as in Fig. 54. The closed tube will be able to resist a much greater torque per unit angular deflection than the open tube because of the inability of the latter to sustain a shear stress across the slot. The only resistance to torsion in the case of the open tube without longitudinal restraint is provided by the twisting resistance of the thin material of which the tube is composed. This is illustrated in the lower part of the figure. The resistance to twist of the entirely open section is given by the Saint-Venant torsion equation,

$$M_{T1} = GJ \frac{d\theta}{dx} \quad (179)$$

where

- $d\theta/dx$ = twist angle per unit length
- G = shear modulus of the material
- J = torsional constant of the section

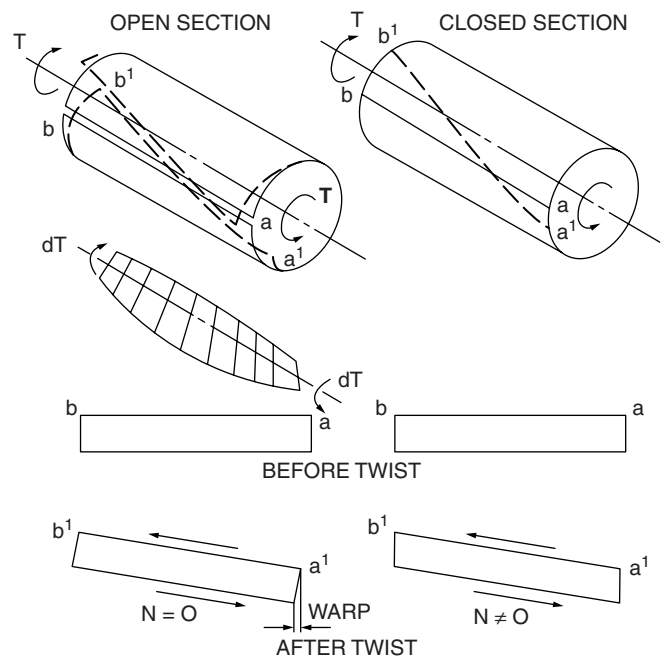


Fig. 54 Twisting of open and closed tubes.

For a thin-walled open section,

$$J = \frac{1}{3} \int_0^s t^3 ds$$

If warping resistance is present (i.e., if the longitudinal moment of the elemental strips shown in Fig. 54 is resisted), another component of torsional resistance is developed through the shear stresses that result from this warping restraint. This is added to the torque given by equation (179). In ship structures, warping resistance comes from four sources:

- The closed sections of the structure between hatch openings
- The closed ends of the ship
- Double wall transverse bulkheads and cross deck structure
- Closed, torsionally stiff parts of the cross section (longitudinal torsion tubes or boxes, including double bottom).

To understand the mechanism by which warping resistance leads to a component of torsional stiffness we refer to Fig. 55, which shows the open tube having a partially built-in condition at end b. The end condition may be visualized by imagining each of the elementary strips of which the tube is composed to be attached to a rigid wall through a set of springs. In this case, the tangential deflection of a point, a, on the right end of the tube is due primarily to the in-plane bending of the elementary

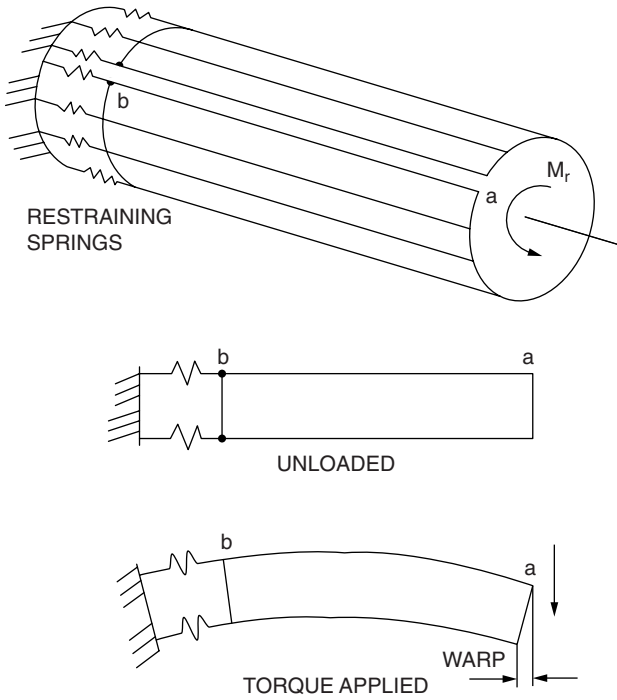


Fig. 55 Open tube with warping restraint.

strip, and this is shown in the lower part of the figure. Shear deformation of the strip is relatively unimportant in determining the resulting moment except in the case of a very short tube. The longitudinal displacement of a point on the surface of the tube, or warp, is then given by equation (158) with the shear deformation set equal to zero,

$$u(s) = -\frac{d\theta}{dx} \int_0^s r(s) ds = -2\omega(s) \frac{d\theta}{dx} + u_0 \quad (180)$$

The quantity $\omega(s) = \frac{1}{2} \int_0^s r(s) ds$ is called the *sectorial area*, and u_0 is the warping displacement at the origin of the coordinate s . If the origin of the s -integration is placed at the open edge of the section, point a in Fig. 55, then $u(s) - u_0$ is the warp of a point on the section measured with respect to the warp at this origin of s .

Compute the average warp, which is given by the integral of $u(s)$ around the entire section periphery, S , divided by S :

$$\begin{aligned} \bar{u} &= \frac{1}{S} \int_0^s u(s) ds \\ &= \frac{1}{S} \left[\int_0^s u_0 ds - \frac{d\theta}{dx} \int_0^s 2\omega(s) ds = u_0 - \frac{S_\omega}{S} \cdot \frac{d\theta}{dx} \right] \end{aligned} \quad (181)$$

The quantity $S_\omega = 2S\omega_0$ is called the first sectorial moment with respect to the origin of s . There will generally be one or more points on the contour that, if used as origins for the S -integration, will result in a zero value for S_ω or ω_0 . These points are referred to as sectorial centroids, and for a symmetrical section the intersection of the plane of symmetry and the contour is a sectorial centroid.

Now measure the warp, $u(s)$, from the plane of the mean warp,

$$u(s) = u - \bar{u} = \frac{d\theta}{dx} (2\omega_0 - 2\omega(s)) \quad (182)$$

If the origin of s were chosen as a sectorial centroid, the term containing ω_0 would vanish. The x -strain is

$$\varepsilon_x = \frac{\partial u}{\partial x} = 2 \frac{d^2\theta}{dx^2} (\omega_0 - \omega(s)) \quad (183)$$

Neglecting the transverse (Poisson) effect, the x -stress is

$$\sigma_x = E\varepsilon_x = 2E \frac{d^2\theta}{dx^2} (\omega_0 - \omega(s)) \quad (184)$$

From the condition of equilibrium of an element, the shear flow, N , is related to the x -stress resultant, N_x , by equation (143). After substituting equation (184) into the first of equation (143) and integrating, the shear flow is obtained as

$$N(s) = -2E \frac{d^3\theta}{dx^3} \int_0^s t(s) [\omega_0 - \omega(s)] ds \quad (185)$$

where the origin of the s -integration is now taken on a free edge of the contour for which the shear stress is zero. Note that by defining separate s -origins for the present and earlier s -integrations, the ω_0 term may be made to vanish from this expression. The twisting moment on the end of the section is obtained by integration of the moment of $N(s)$ around the entire contour,

$$T_2(x) = \int_0^s N(s) r(s) ds \quad (186)$$

where r is defined as in equation (180).

After substituting equation (185) into equation (186) and integrating by parts, the twisting moment due to restrained warping is obtained as

$$T_2(x) = -E \frac{d^3\theta}{dx^3} \int_0^s 4(\omega_0 - \omega(s))^2 t(s) ds = -E\Gamma \frac{d^3\theta}{dx^3} \quad (187)$$

where

$$\Gamma = 4 \int_0^s (\omega_0 - \omega(s))^2 t(s) ds$$

is called the warping constant of the section.

If $T(x) = T_1 + T_2$ is the total twisting moment at station x , the differential equation of twist—taking into consideration unrestrained warping, equation (179), and restrained warping effects, equation (187)—is

$$E\Gamma \frac{d^3\theta}{dx^3} - GJ \frac{d\theta}{dx} = -T(x) \quad (188)$$

In a ship made up of some closed and some open sections, the analysis leading to this equation is assumed to apply only to the open sections.

To solve equation (188), assume that the twisting moment at longitudinal position x may be expressed in the form of a Fourier series over the length of an open prismatic section of length L ,

$$T(x) = \sum_{n=1}^{\infty} (T_{nc} \cos p_n x + T_{ns} \sin p_n x) \quad (189)$$

The solution of the differential equation of the deflection is,

$$\theta(x) = A_0 + A_1 \sinh kx + A_2 \cosh kx + \sum (\alpha_n \cos p_n x + \beta_n \sin p_n x) \quad (190)$$

Here,

$$p_n = \frac{\pi n}{L}, \quad k^2 = \frac{GJ}{E\Gamma}$$

A_0 , A_1 , and A_2 are integration constants of the homogeneous solution, and are to be determined by boundary conditions at the ends of the segment of length L .

$$\alpha_n = \frac{T_{cn}}{GJ(p_n^3 + k^2 p_n)} \quad \beta_n = -\frac{T_{sn}}{GJ(p_n^3 + k^2 p_n)} \quad (191)$$

The Bredt formula, equation (160), is applicable to the torsional deflection of a closed prismatic tube, and is therefore applied to the decked-over sections of the ship between hatch openings. Because this is a first-order equation, there will be one constant of integration in its solution.

By subdividing the ship into a series of open or closed sections and applying the appropriate torsional deflection equations, the result is a system of algebraic equations containing three unknown constants of integration for each open section and one unknown constant for each closed section. These constants are found by imposing requirements of continuity of internal reactions and deflections across the junctions of the closed and open sections.

A model of a large container ship subdivided into a series of such prismatic segments is shown in Fig. 56a, taken from Westin (1981). The matching conditions at the junctions state that there is compatibility of twist, compatibility of warp, and continuity of the internal

loads across the junction between the two types of sections. Example analyses of this type that treat in detail the problem of matching closed and open sections can be found in Haslum and Tonnesen (1972), De Wilde (1967), and Westin (1981).

More recently, Pedersen (1982, 1985) developed a consistent beam model for the calculation of static and dynamic torsional response of ships with large hatch openings. The model considers the behavior of a beam with slowly varying properties, and takes into account warping and deflections due to shear and rotary inertia. Discontinuity conditions were introduced at the location where abrupt changes in the cross-sectional properties occur at the transitions between open and closed parts of the hull. The theory also takes into consideration the coupling between torsion and horizontal bending. Figure 57 shows the global and local deformations of a container ship due to warping (see Pedersen 1985). Pedersen (1991) also developed a consistent one-dimensional finite element procedure for analyzing a coupled torsional-bending response of thin-walled beam structures. The hull cross sections are assumed to have bulkheads and transverse stiffeners that restrain the deformation in the transverse plane. The paper examines the effect of the warping modes on the results and concludes that the higher-order warping modes are not important in the analysis of overall response of beam-like structures.

An inherent difficulty in establishing suitable matching conditions lies in determining the axis of rotation or center of twist of the two types of section. For a beam of uniform section, the center of twist coincides with the shear center of the cross section, which is also the center about which the moment of external loads is computed. For the nonuniform beam, the center of rotation is no longer at the shear center, which itself is at a different vertical location for the closed and open sections. For a closed ship section, the shear center will be near mid-depth, but for an open section it may be below the keel. Fig. 56b shows the height of the shear center for the structural idealization of the container ship of Fig. 56a.

In general, the torsion analysis described here, when applied to the computation of the actual stress distribution in a real ship under torsional loading, can be expected to give results somewhat less exact than were obtained when applying simple beam theory to the vertical bending of the ship structure. This is mainly the result of attempting to apply two separate theoretical procedures, each one of which is based on an assumption of uniformity of a cross section along a ship's length, to a problem in which the variation in the cross-sectional shape is itself of fundamental importance. The effect of the concentration of stiff and soft sections results in a distortion pattern in the ship deck that is somewhat as shown, to an exaggerated scale, in Fig. 58. The term *snaking* is sometimes used when referring to this behavior.

Fortunately, ship structures designed to withstand normal bending loads do not appear to experience large primary hull girder stresses as a result of the normal

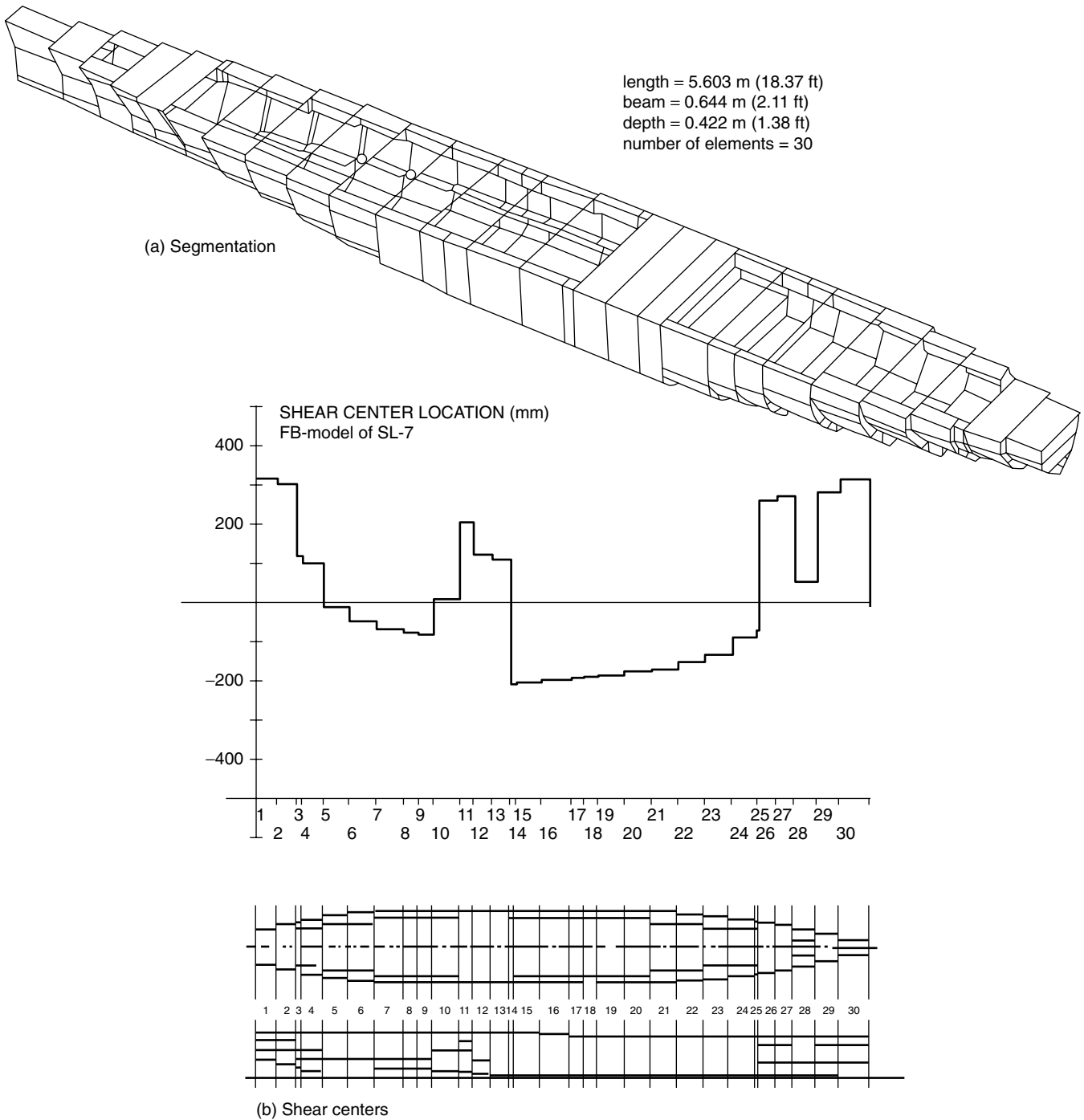


Fig. 56 SL-7 hull structure idealized with finite element method (Westin 1981).

torsional loads experienced in service. As previously noted, significant stresses may be induced at specific locations, such as hatch corners, as a result of stress concentrations due to discontinuities in the structure. The analysis of structures in which discontinuity plays an essential role is best handled by the finite element technique, which is described in Section 3.15 and many text-

books. Such an analysis of a large container ship and comparisons with model experiments are described by El Batouti, Jan, and Stiansen (1976).

3.7 Deckhouses and Superstructures. The terms *deckhouse* and *superstructure* refer to a structure usually of shorter length than the entire ship and erected above the strength deck of the ship. If its sides are

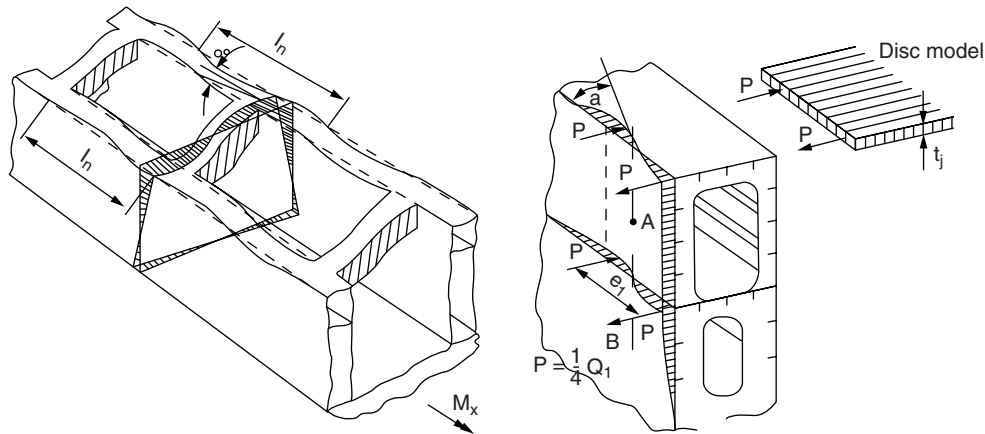


Fig. 57 Global and local deformations of a container ship due to warping (Pedersen 1985).

co-planar with the ship's sides, it is referred to as a superstructure. If its width is less than that of the ship, it is called a deckhouse. The latter will be used as an inclusive term to mean both types of structures because the superstructure may be considered as a special case of a deckhouse.

As the ship hull bends in response to the applied sea-way and other external loads, the deckhouse will bend also in response to the loads transmitted to it through its connection to the main hull. These loads will consist of distributed longitudinal shears and vertical loads acting at the lower edges of the sides of the deckhouse. Because there will be equal and opposite reactions applied to the hull, the presence or absence of the deckhouse is seen to affect the structural behavior of the hull. The combined stiffness may be appreciably greater than that of the hull alone if the deckhouse is of substantial length and the two are of the same material, effectively connected together.

In addition to the effects felt in the overall bending stiffness and the corresponding stress patterns, local stress concentrations can be expected at the ends of the deckhouse because here the structure is transformed abruptly from that of a beam consisting of the main hull

alone to that of hull plus deckhouse. Particular care is needed when designing the structural details and reinforcement in this region of both the main hull and the deckhouse to avoid localized structural problems.

The horizontal shears and vertical loads between hull and deckhouse will tend to produce opposing structural effects, as may be seen by considering two extreme cases. Consider the ship to be in a hogging bending condition, corresponding to a wave crest amidships. The deck of the ship will be in a state of positive or extensional strain. Assume that the condition of longitudinal strain compatibility is satisfied between the deck and the lower side of the deckhouse, and that there is no interference or vertical resistance force between the hull and the deckhouse (an extreme case). In this case, the deckhouse will tend to bend in a concave upward mode as a result of the extensional strain of its lower edge; thus, the deflection of the deckhouse will be opposite to the deflection of the hull.

As a second extreme case, assume that the condition of strain compatibility is not satisfied—that is, that the deckhouse longitudinal strain is independent of the strain in the hull at the connection between the two. However, let the deck of the hull in this case be very stiff so that the bending deflection of the deckhouse is forced to follow that of the hull. Because the bending deflection of the deckhouse is now concave downward, the lower edge of the deckhouse will be in compression, which is opposite to the tensile strain in the deck of the hull.

In the actual case, except for a small effect of shear lag, the longitudinal shear connection between the ship hull and deckhouse will be nearly completely effective and the condition of longitudinal strain compatibility will be satisfied. The vertical loads between hull and deckhouse will be associated with the relative vertical deflection between the two members, and this will depend upon the rigidity or foundation modulus of the deck structure upon which the deckhouse rests. Figure 59 illustrates three possible modes of hull-deckhouse interaction,

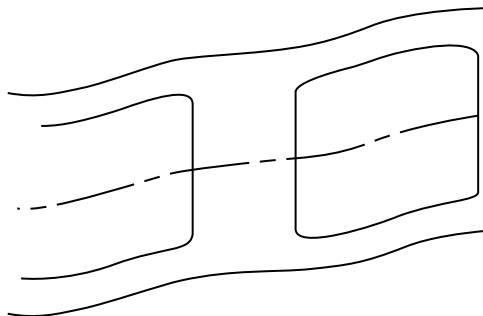


Fig. 58 Torsional distortion of a container ship deck.

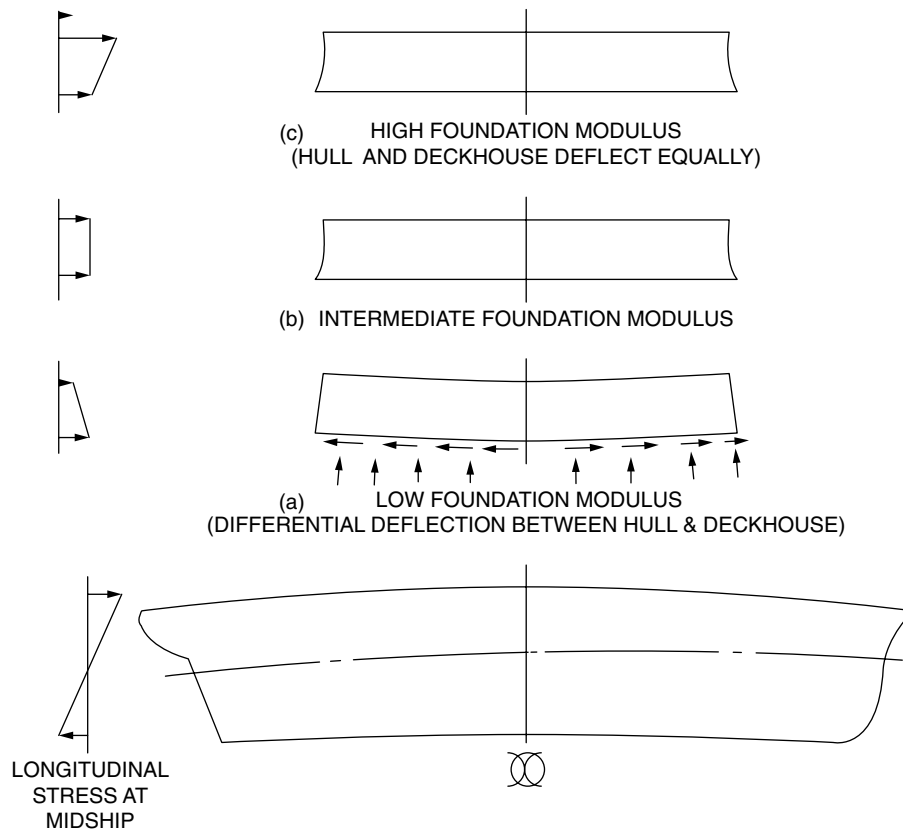


Fig. 59 Bending behavior of deckhouse and hull (Taggart 1980).

depending on the relative stiffness of the deck. In Fig. 59a, the deck structure is very flexible (low foundation modulus), allowing nearly unrestricted vertical deflection between hull and deckhouse. For the hogging condition illustrated, the lower edge of the deckhouse is in extensional strain as a result of strain equality at the hull joint. As a result of the flexible deck, this results in a differential deflection of the hull and deckhouse.

Figure 59c illustrates a case of very high foundation modulus, in which the deckhouse is constrained to deflect with nearly the same curvature as the hull. This is approximately the case of the superstructure where—if sufficiently long, so that end effects are confined to a short portion of the length—the middle part of the house acts merely as an extension of the structure of the main hull. The longitudinal stress distribution shown in the left part of the figure is co-linear with that in the hull if the two are constructed of the same material. The intermediate case of finite foundation modulus, in which there is some differential deflection between hull and deckhouse, is illustrated in Fig. 59b.

In the analysis of the hull-deckhouse interaction, assume that the hull and deckhouse each behave as a simple beam undergoing bending deflection. Under such simplifying assumptions, a complete analysis of the stress and deflection—particularly of the stress concen-

trations at the ends of the deckhouse—is not possible. However, it is possible to obtain meaningful results that describe the combined behavior of hull and deckhouse in the middle portion of the length of the house.

In Fig. 60, assume a vertical cut through the hull and deckhouse at location x , measured from the left end of the deckhouse. When each bend as separate beams, the hull and deckhouse will have individual neutral axes, NA_1 and NA_f , separated by the vertical distance e . The forces of interaction consist of a horizontal shear flow, N , and a vertical distributed loading, q_n , each having the dimensions of force per unit length. The vertical load is assumed proportional to the relative vertical deflection of the hull and deckhouse, and the proportionality constant, k , or foundation modulus has the dimensions of a spring constant per unit length (force per unit length/unit deflection). The separate bending moments in hull and deckhouse are M_1 and M_f , and the net longitudinal stresses in each are p_1 and p_f , respectively.

Now write equations of equilibrium of longitudinal forces and equilibrium of moments about the respective neutral axes for hull and deckhouse separately:

$$\begin{aligned} A_1 p_1 + A_f p_f &= 0 \\ M_1 + M_f - A_f e p_f &= M \end{aligned} \quad (192)$$

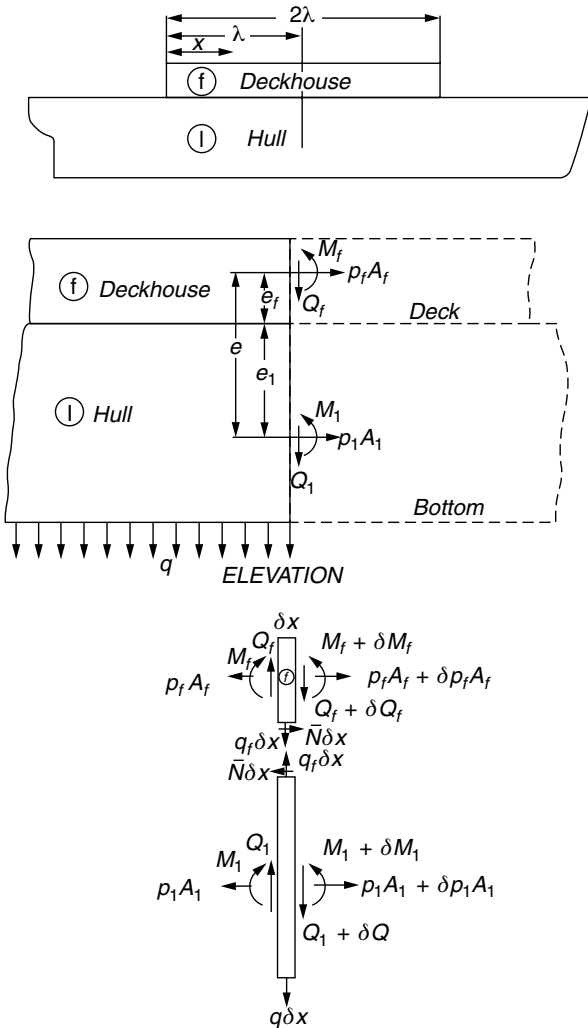


Fig. 60 Identification sketches for hull and deckhouse.

The longitudinal stresses at the joint of deckhouse and hull are given by the sum of the average stress due to p and the bending stress due to the moment,

$$p_1 - \frac{M_1}{Z_1} = \frac{1}{r} \left(p_f + \frac{M_f}{Z_f} \right) \quad (193)$$

where r is a factor included to allow for the effect of shear lag in the deck. Here A_1 and A_f are the cross-sectional areas of hull and deckhouse, respectively. Z_1 and Z_f are the sectional moduli, and the other parameters are shown in Fig. 60.

As noted previously, equality of longitudinal strain is required at the joint because the deckhouse is assumed attached to the hull continuously along its length. Neglecting transverse strain effects, as is the case in simple beam theory, this reduces to stress equality, or $\sigma_f = r\sigma_1$. Combining equations (192) and (193) and then solving

for M_f , gives

$$M_f = \frac{rZ_f}{rZ_f - Z_1} \left\{ p_f \left[A_f e + Z_1 \left(\frac{rA_f + A_1}{rA_1} \right) \right] + M \right\} \quad (194)$$

The foregoing considerations have given three equations in the four unknowns, p_1 , p_f , M_1 , and M_f . A fourth consideration involves the vertical interaction between hull and deckhouse, which is assumed proportional to the differential vertical deflection, $w_f - w_1$.

Noting that the deflection of each member must be related to the bending moment on that member by the equation of simple beam theory, equations (195) are obtained. Note that in this equation the total deflection, w_1 or w_f , has been corrected for the shear deflection in hull or deckhouse by deducting the shear deflection given by the second term in the parentheses on the right side:

$$\begin{aligned} M_1 &= -E_1 I_1 \left(\frac{d^2 w_1}{dx^2} + \frac{q_1}{a_1 G_1} \right) \\ M_f &= -E_f I_f \left(\frac{d^2 w_f}{dx^2} + \frac{q_f}{a_f G_f} \right) \end{aligned} \quad (195)$$

Here a_1 and a_f are the vertical shear-carrying areas of the hull and deckhouse, respectively, made up principally of the side plating and longitudinal bulkhead members. G_1 and G_f are the shear moduli of elasticity of hull and deckhouse, respectively.

From these considerations, a fourth-order differential equation can be obtained for the mean stress in the deckhouse, p_f . The solution has been condensed (Schade 1965), into a single design chart suitable for most practical ship structural applications and given in Fig. 61. In using this chart, it is necessary to compute the following three parameters:

- Section geometry parameter,

$$\Omega = \frac{(A_1 + A_f)(I_1 + I_f) + A_1 A_f (e_1 + e_f)^2}{(A_1 + A_f)(I_1 I_f) + A_1 A_f (I_1 e_f^2 + I_f e_1^2)} \quad (196)$$

- Foundation modulus parameter,

$$\omega^4 = \frac{k \Omega}{E_1 4} \quad (197)$$

- Shear stiffness parameter,

$$J^2 = \frac{1}{\frac{1}{a_1} + \frac{1}{a_f}} \frac{\Omega}{2(1 + \nu)} \quad (198)$$

It is assumed that Poisson's ratio, ν , is the same for the material in the hull and deckhouse. However, the shear carrying areas a_1 and a_f may be modified for any difference in the modulus of elasticity E , for example, as in the case of an aluminum deckhouse on a steel hull.

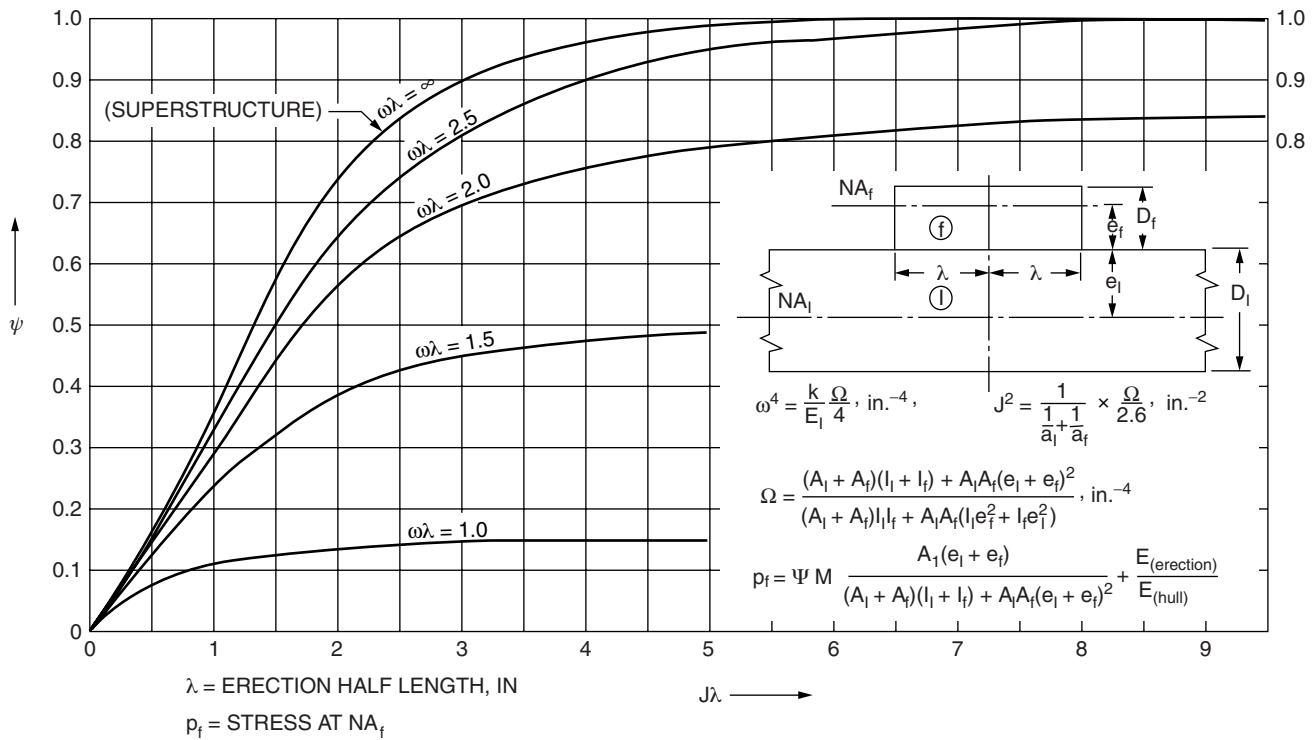


Fig. 61 Trends of erection efficiency ψ (Schade 1965).

If the deckhouse were fully effective, corresponding to Fig. 59c, the mean stress would be given by

$$\tilde{p}_f = \frac{MA_1(e_1 + e_f)}{(I_1 + I_f)(A_1 + A_f) + A_1 A_f (e_1 + e_f)^2} \quad (199)$$

Figure 61 expresses the efficiency of the deckhouse in terms of the ratio, Ψ , of the actual mean stress to this ideal value. Therefore, the actual stress is

$$p_f = \Psi \tilde{p}_f \quad (200)$$

Having p_f , the mean stress in the hull, p_1 , and the bending moments in the hull and deckhouse may be obtained from equations (192), (193), and (194). The stresses at top and bottom of hull and deckhouse can then be computed by equations (134) of elementary beam theory, using the respective bending moments, and added to the mean stresses, p_1 and p_f .

A somewhat similar analytic solution to that described here was developed by Bleich (1953), which however does not include the effect of shear deflection and shear lag. Both the Schade solution and the Bleich solution can be used to obtain the loads in the middle portions of the deckhouse, but such solutions do not apply near the ends where, as noted, large localized loads may occur. Such solutions are useful for assessing the extent to which the deckhouse contributes to the overall bending strength of the hull, or in deciding whether to design the deckhouse to participate in the hull bending strength or to design

it simply as an appendage having no contribution to the strength of the hull.

To design the structural details needed to withstand the concentrated loads near the ends of the deckhouse, an analysis method suitable for revealing the high stress concentrations in an area of abrupt changes in geometry is required. The most suitable means presently available for this purpose is the finite element method. Figure 62, taken from Paulling and Payer (1968), illustrates the computation of the high vertical and shear stresses in the vicinity of the corner of the deckhouse. Also shown on this graph are experimental values of the respective stresses, illustrating the extremely high stress gradients in the vicinity of the deckhouse corner. These experiments were conducted using the same experimental apparatus as Glasfeld (1962), on which the shear lag phenomenon illustrated in Fig. 53 was measured.

3.8 Secondary Stresses and Deflections. In the case of secondary structural response, the principal objective is to determine the distribution of both in-plane and normal loading, deflection, and stress over the length and width dimensions of a panel of stiffened plating. Recall that the primary response involves the determination of only the in-plane load, deflection, and stress as they vary over the length of the ship, considered as a beam or a box girder. Therefore, the secondary response is seen to be a two-dimensional problem, whereas the primary response is essentially one-dimensional in character.

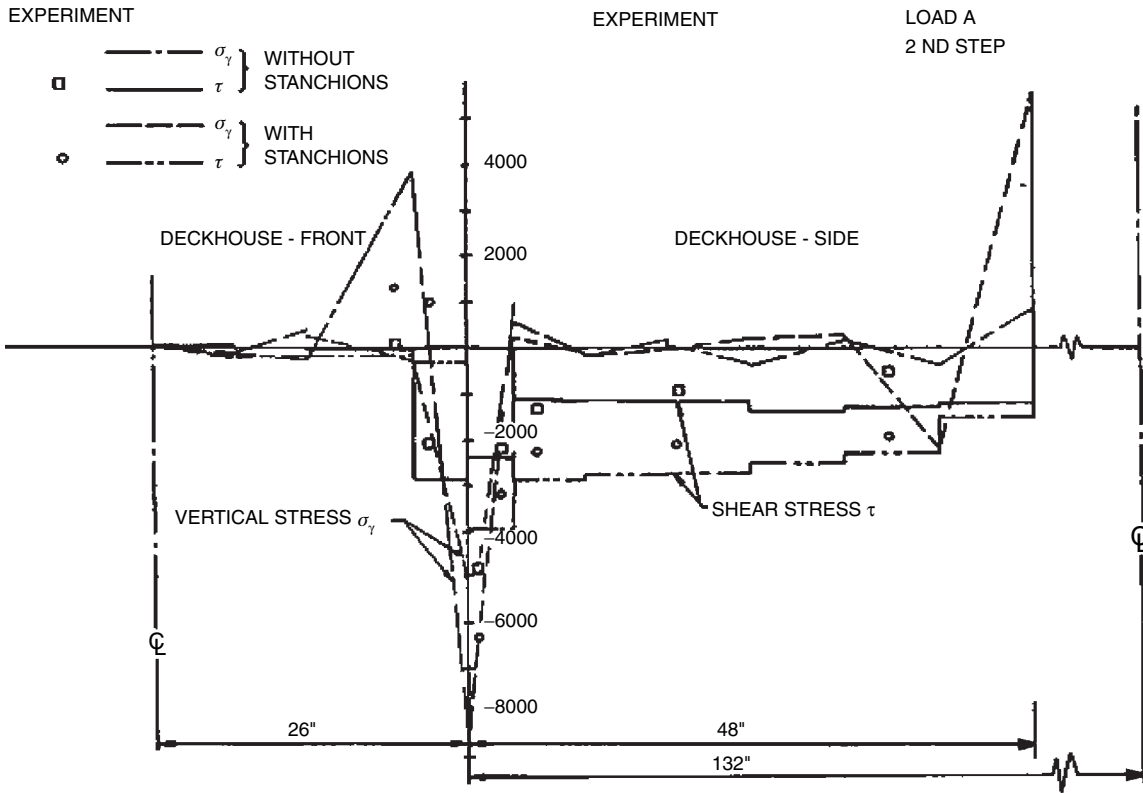


Fig. 62 Stresses in lowest members of the deckhouse—second step, showing the influence of foundation modulus (Paulling & Payer 1968).

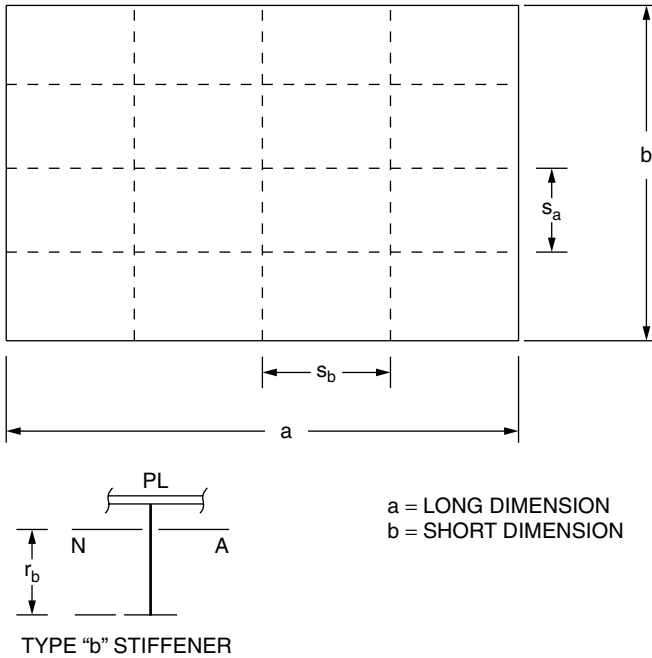


Fig. 63 Stiffened plate nomenclature.

As used in the present context, a panel of a structure usually consists of a flat or slightly curved section of plating with its attached stiffeners. There may be two sets of stiffeners arranged perpendicular to each other. Usually, the stiffeners comprising the set of parallel members in one direction will be of equal size and spacing, and the stiffeners in the other direction will also be of equal size and spacing but different from the first set. In some cases, the central stiffener in a rectangular stiffened panel is made somewhat larger than the remaining parallel stiffeners, as in the case of the center keel girder. In some cases, there may be stiffeners in one direction only. There may be a single panel of plating with stiffeners attached to one side, as in decks, side shells, and bulkheads; or there may be two parallel panels with the stiffeners between them, as in double bottom construction. The plating may be absent, in which case the module is a grid or grillage of beam members only rather than a stiffened plate panel.

In most cases, the boundaries of a panel are attached to other panels, either in the same plane or perpendicular to the original panel. As an example, consider a section of the double bottom structure of a typical dry cargo ship. The forward and after boundaries of this double bottom panel are formed by transverse bulkheads, which are perpendicular to the bottom panel, and by the

continuing bottom structure beyond the bulkheads, which is in the same plane as the present panel and of similar construction. The outboard edges of the double bottom panel are bounded by the plate and frame panels comprising the side structure of the ship. The bottom panel consists of two plate members, bottom shells, and inner bottom plating, with an orthogonal system of transverse floors and longitudinal girders between them. The center keel girder is typically somewhat heavier, thus stiffer than the other longitudinal girders. The transverse bulkheads and side shells are usually single plate panels with the stiffeners welded to one side. The loading on the bottom panel consists of the external fluid pressures, the distributed weights or pressures of liquids in the inner bottom space, and combinations of distributed and concentrated weights of cargo, machinery, and the structural material itself.

In principle, the solution for the deflection and stress in the secondary panel of the structure can be thought of as a solution for the response of a system of orthogonal intersecting beams. Interactions between the two-beam systems arise from the physical connections between the stiffeners, requiring equality of normal deflection of the two-beam systems at the points of intersection. A second type of interaction arises from the two-dimensional stress pattern in the plate, which may be thought of as forming a part of the flanges of the stiffeners. The plate contribution to the beam bending stiffness arises from the direct longitudinal stress in the plate adjacent to the stiffener, modified by the transverse stress effects, and from the shear stress in the plane of the plate. The maximum secondary stress can be found in the plate itself, but more frequently it is found in the free flanges of the stiffeners because these flanges are at a greater distance than the plate member from the neutral axis of the combined plate stiffener.

At least four different procedures have been employed for obtaining the structural behavior of stiffened plate panels under normal loading, each embodying certain simplifying assumptions:

- Orthotropic plate theory
- Beam on elastic foundation theory
- Grillage theory
- The finite element method.

Orthotropic plate theory refers to the theory of bending of plates having different flexural rigidities in the two orthogonal directions. In applying this theory to panels having discrete stiffeners, the structure is idealized by assuming that the structural properties of the stiffeners may be approximated by their average values, which are assumed to be distributed uniformly over the width or length of the plate. The deflections and stresses in the resulting continuum are then obtained from a solution of the orthotropic plate deflection equation,

$$a_1 \frac{\partial^4 w}{\partial x^4} + a_2 \frac{\partial^4 w}{\partial x^2 \partial y^2} + a_3 \frac{\partial^4 w}{\partial y^4} = p(x, y) \quad (201)$$

where

$$\begin{aligned} a_1, a_2, a_3 &= \text{express the average flexural rigidity} \\ &\quad \text{per unit length of the orthotropic} \\ &\quad \text{plate in the two directions} \\ w(x, y) &= \text{deflection of the plate in the normal} \\ &\quad \text{direction} \\ p(x, y) &= \text{distributed normal pressure load per} \\ &\quad \text{unit area} \end{aligned}$$

Note that the behavior of the isotropic plate (i.e., one having uniform flexural properties in all directions) is a special case of the orthotropic plate problem.

It is not appropriate to go into the detailed derivation of this equation or its solution, both of which have been presented in detail by Schade (1938, 1940, 1941). The results of Schade's solution have been presented in a series of easily used charts, and their use will be discussed later. The orthotropic plate method is best suited to a panel in which the stiffeners are uniform in size and spacing and closely spaced. The Schade design charts have been developed in such a way that a centerline stiffener that is heavier than the other stiffeners may be included.

The beam on elastic foundation solution is suitable for a panel in which the stiffeners are uniform and closely spaced in one direction and sparser in the other. One of the latter members may be thought of as an individual beam having an elastic support at its point of intersection with each of the closely spaced orthogonal beams. An average elastic modulus or spring constant per unit length can be determined by dividing the force per unit deflection of one of these closely spaced members by the spacing. Using this average spring constant per unit length, the effect of the closely spaced members is then represented as an elastic support that is distributed evenly along the length of the widely spaced members. Each of these members is then treated individually as a beam on an elastic foundation, for which the differential equation of deflection is

$$EI \frac{d^4 w}{dx^4} + kw = q(x) \quad (202)$$

where

$$\begin{aligned} w &= \text{deflection} \\ I &= \text{sectional moment of inertia of the} \\ &\quad \text{longitudinal stiffener, including} \\ &\quad \text{adjacent plating} \\ k &= \text{average spring constant per unit length} \\ &\quad \text{of the transverse stiffeners} \\ q(x) &= \text{load per unit length on the longitudinal} \\ &\quad \text{member} \end{aligned}$$

Michelsen and Nielsen (1965) have developed a solution method for this equation based upon use of the *Laplace transform*, which is particularly well-adapted to computers. Various realistic boundary conditions may be taken into account, and the solution can consider several intersecting panels of the structure. This procedure has been incorporated into a computer-based scheme for the

optimum structural design of the midship section as described by St. Denis (1970).

In the grillage method of Clarkson et al. (1959), each stiffener in the two orthogonal sets of members is represented as a simple beam. The external loading may be applied as a set of equivalent point forces at the intersections of the two beam systems. At the points of intersection, conditions of equilibrium of unknown reaction forces between the two beams—together with conditions of equal deflection—are required to be satisfied. The result is a system of algebraic equations to be solved for the deflections. From the solutions, the forces in each set of beams and the resulting stresses may be obtained.

The versatile finite element technique can model the structure in a number of different ways. For example, each segment of stiffener between intersection points can be represented by a short beam, and the plating can be represented as a membrane capable of supporting in-plane stress, as in the grillage technique. Conditions of equality of deflections and equilibrium of internal and external forces are then required to be satisfied at the points of intersection, leading to the formulation of a system of simultaneous algebraic equations relating external loads to deflections. Computer manipulation is necessary to formulate and solve the large number of equations that are necessary in a practical situation. This procedure is the most general of the four, being virtually unrestricted in the degree to which complex structural geometry, variable member sizes, boundary conditions, and load distributions can be represented (see Section 3.16.2).

In the first three of the methods described here, the shear lag behavior of the plating in a plated grillage is not automatically included but must be considered by the user when computing the bending stiffness of the orthotropic plate or grillage model. The finite element technique is inherently capable of including this effect, provided the proper choice is made for the plate element type and the mesh size in the representation.

For hand computations of secondary stresses, the Schade design charts based upon the orthotropic plate solution provide the most practical method of those described previously. However, Clarkson (1959) has presented a limited number of design charts based on the discrete grillage solution, which are useful in many cases.

Two of the charts from Schade (1941) are reproduced here as Fig. 65 and 66, after the following explanation of terminology and preliminary discussion. Referring to Fig. 63,

- p = uniform unit pressure loading
- $a(b)$ = length (width) of rectangular panel
- $s_a(s_b)$ = spacing of long (short) stiffeners
- $I_{na}(I_{nb})$ = moment of inertia, including effective breadth of plating, of long (short) repeating stiffener (as distinguished from central stiffener, which may be different)

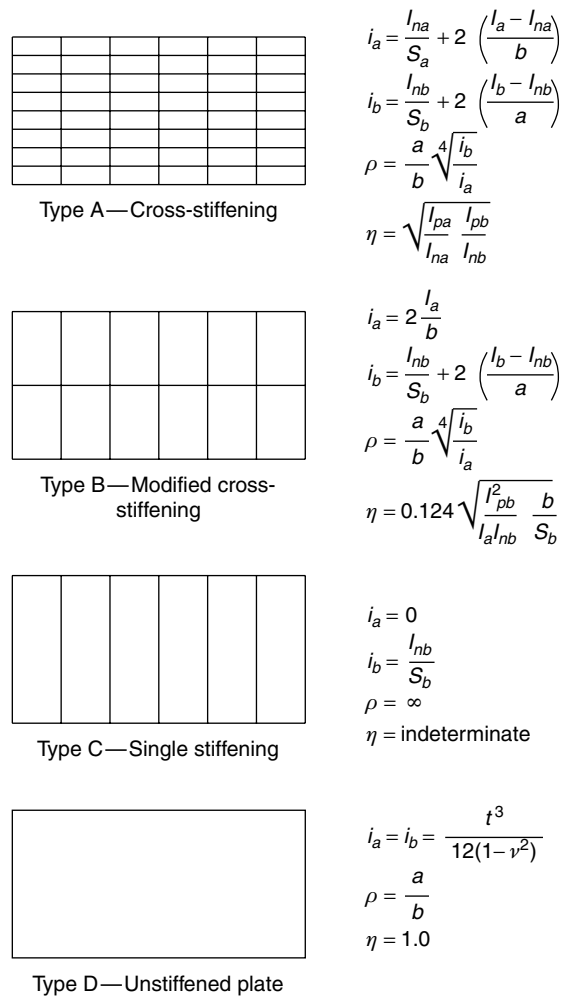


Fig. 64 Types of stiffening, with applicable formulas for parameters (Schade 1941).

$I_{pa}(I_{pb})$ = moment of inertia of effective breadth of plating working with long (short) repeating stiffeners

$I_a(I_b)$ = moment of inertia of central long (short) stiffener, including effective breadth of plating

$A_a(A_b)$ = web area of central long (short) stiffener

$r_a(r_b)$ = distance from its neutral axis to extreme fiber of central long (short) stiffener

The effective breadth of plating to be used in computing the moments of inertia can be estimated by use of the effective breadth charts given in Fig. 50. In many cases, the effective breadth is 100 percent of the stiffener spacing, in which case the moment of inertia should be computed by using a modified thickness obtained by multiplying the actual plate thickness by the factor $1/(1 - \nu^2)$.

Four types of stiffening are shown in Fig. 64, together with the definitions of certain additional parameters. The

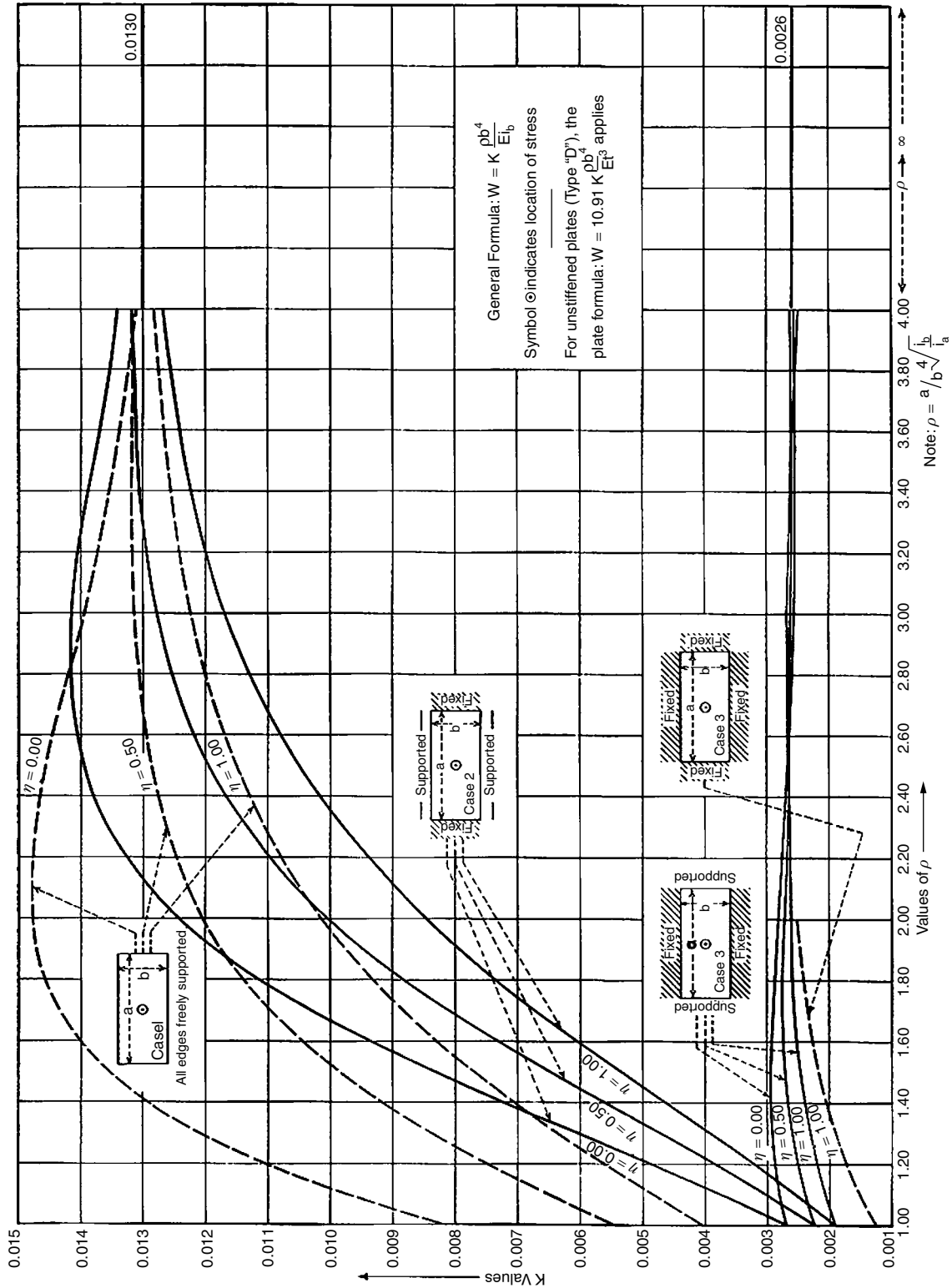


Fig. 65 Plate deflection at the center of a panel (Schade 1941).

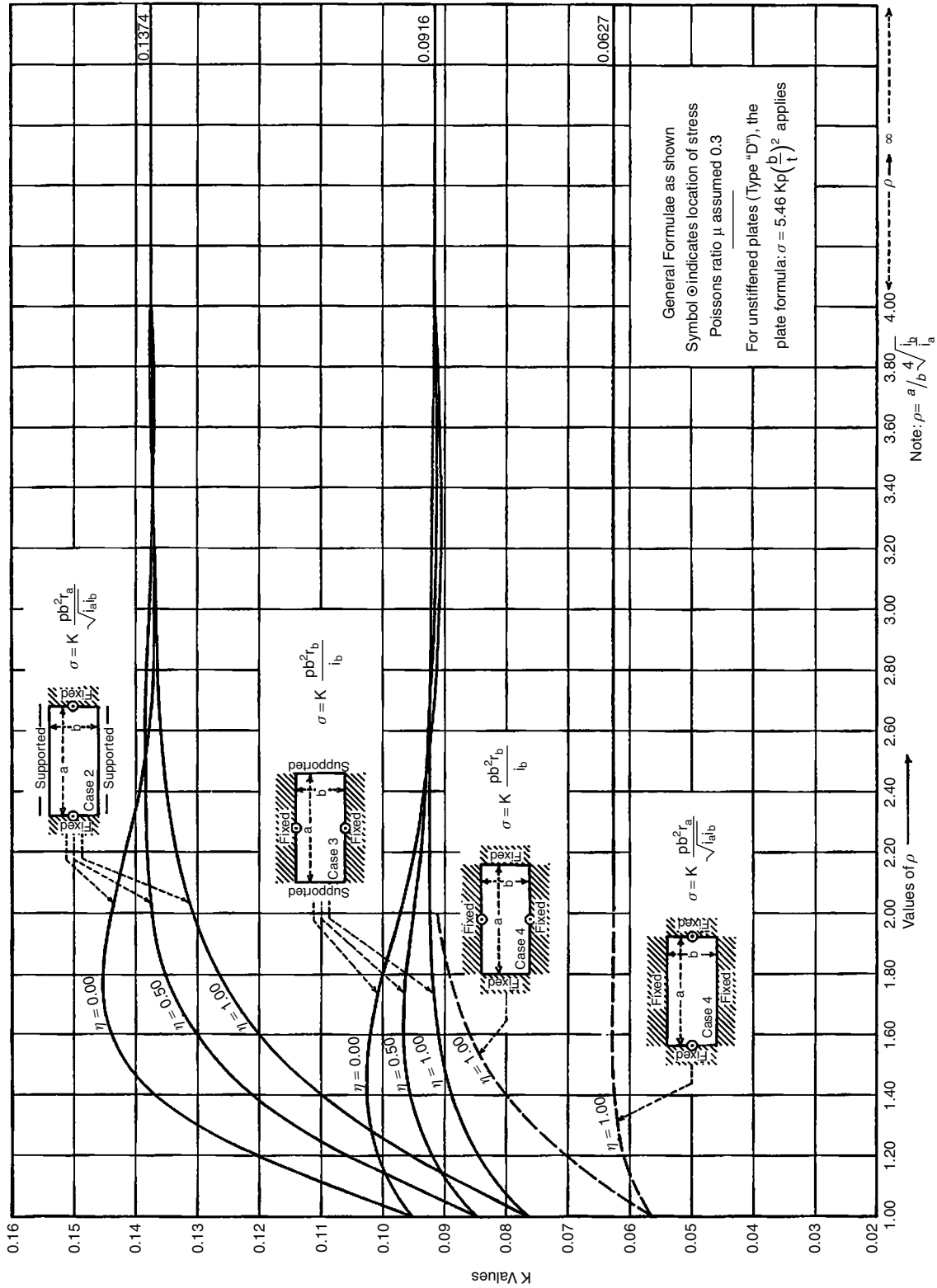


Fig. 66 Support bending stress in a plating panel (Schade 1941).

four types are as follows:

- Type A: Cross-stiffening. Two sets of intersecting stiffeners; the middle stiffener of either or both sets may be stiffer than the other stiffeners of the set.
- Type B: One set of repeating stiffeners and a single central stiffener in the other direction. The middle stiffener of the repeating set may be stiffer than the others, as in Type A.
- Type C: One set of repeating stiffeners only.
- Type D: Plating without stiffeners (isotropic plate).

For the first three types, there may be stiffeners without plating, there may be one panel of plating with stiffeners on one side, or there may be two courses of plating with stiffeners in between. The full range of possibilities for a rectangular panel stiffened in two directions is therefore covered. Type D, the case of plate alone without stiffeners, may be used in computing the tertiary stress.

There are many possible combinations of edge fixity and boundary support for the panels used in ship structures. The solution has been found and results are given for the following four combinations of built-in and simple support. These may usually be used as limiting cases of the actual—but usually indeterminate—boundary conditions that are found in actual ship structures.

- Case 1: All four edges simply supported (i.e., rigidly supported against normal deflection but without edge moment restraint).
- Case 2: Both short edges fixed (i.e., with both normal and rotational restraint, both long edges simply supported).
- Case 3: Both long edges fixed, and both short edges simply supported.
- Case 4: All four edges fixed (only partial results are given for this case).

In using the charts, several special parameters are required that are defined as follows:

- Unit stiffness,

$$i_a = \frac{I_{na}}{S_a} + 2 \left(\frac{I_a - I_{na}}{b} \right) \quad (203)$$

$$i_b = \frac{I_{nb}}{S_b} + 2 \left(\frac{I_b - I_{nb}}{a} \right) \quad (204)$$

- Torsion coefficient,

$$\eta = \sqrt{\frac{I_{pa}I_{pb}}{I_{na}I_{nb}}} \quad (205)$$

- Virtual aspect ratio,

$$\rho = \frac{a}{b} \sqrt[4]{\frac{i_b}{i_a}} \quad (206)$$

Expressions for these parameters are given for each stiffener configuration in Fig. 64.

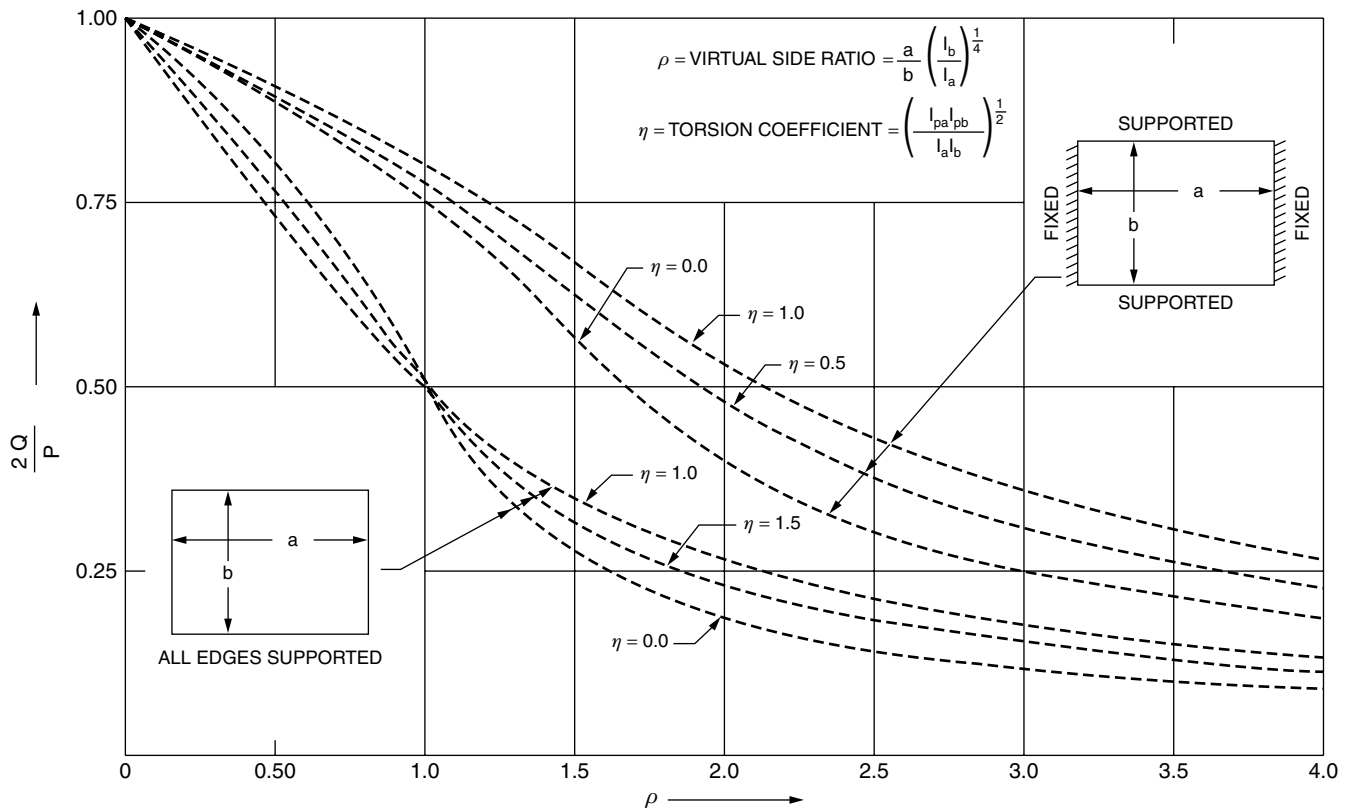
The charts from Schade (1941) contain the deflection at the center of the panel and the stress in the plating at the panel boundary. Charts containing other results—for example, the stress at the panel midpoint—can be found in the original reference. In general, the charts give a non-dimensional parameter, k , which may be substituted into a formula given on the chart for the corresponding stress or deflection.

The previous analysis and charts do not include the effect of the primary in-plane loads on the secondary deflection and stresses (i.e., what is referred to as the P - δ effect in beam columns). To take this into consideration, the differential equation (202) must be modified to include the in-plane loads resulting from primary bending of the hull as a whole. Solutions for deflections and stresses in this case have been obtained by Mansour (1976) and presented in a series of design charts. These charts provide the secondary deflection and stresses as functions of tensile or compressive primary in-plane loads acting on two opposite edges of the stiffened plate.

3.9 Diffusion of Vertical Loads into Structure. The description of the computation of vertical shear and bending moment by integration of the longitudinal load distribution implies that the external vertical load is resisted directly by the vertical shear-carrying members of the hull girder, such as the side shell or the longitudinal bulkheads. In the case of a ship framed by a closely spaced transverse framing system without the support of longitudinal girders, this condition is approached. In such a case, the fluid pressure loads on the bottom as well as the weight of cargo and other deck loads are largely transmitted to the side shell by the transverse frames. However, the double bottom structure has longitudinal as well as transverse supporting members, and the between deck beams are usually supported at their inboard ends by longitudinal girders. Therefore, such longitudinal structural members transmit part of the weight or pressure load to the transverse bulkheads, which in turn transfer the resultant loads into the side shell or longitudinal bulkheads in the form of localized shear forces.

In a longitudinally framed ship, such as a tanker, the bottom pressures are transferred principally to the widely spaced transverse web frames or the transverse bulkheads, where they are transferred to the longitudinal bulkheads or side shells, again as localized shear forces. Thus, in reality the loading, $q(x)$, applied to the side shell or the longitudinal bulkhead will consist of a distributed part due to the direct transfer of load into the member from the bottom or deck structure, plus a concentrated part at each bulkhead or web frame. This leads to a discontinuity in the shear curve at the bulkheads and webs. Figure 67 provides a simple means, based upon orthotropic plate theory, for estimating the proportion of the total load transmitted to each edge of a panel of such structure. In this figure, the symbols are defined as in the preceding Section 3.8.

In the derivation of the figure, it is assumed that the stiffening members are numerous and closely spaced in



NOTE:

- $I_a (I_b)$ = UNIT STIFFNESS IN LONGITUDINAL (TRANSVERSE) DIRECTION
- $I_{pa} (I_{pb})$ = MOMENT OF INERTIA OF PLATE ALONE, ASSOCIATED WITH A LONGITUDINAL (TRANSVERSE)
- $I_a (I_b)$ = MOMENT OF INERTIA OF A LONGITUDINAL (TRANSVERSE) EFFECTIVE WIDTH OF PLATING

Fig. 67 Proportion of total load, $2Q/P$, carried by transverse boundaries (uniform load, $P = \rho ab$) (D'Arcangelo 1969).

each direction so that the bending stiffness of the total panel is well represented by the average values of combined plates and stiffeners. Therefore, the curves may be reasonably applied, for example, to a double bottom structure in which there are closely spaced transverse floors and several longitudinal girders.

Figure 68 illustrates the components of the load that are transferred to the side structure and to the transverse bulkheads, which form the boundaries of the panel of the bottom structure. It is observed that the load transferred into the transverse bulkhead at its lower edge is resisted by vertical shearing forces in the bulkhead-side shell joint. These latter shearing forces have the effect of concentrated loads insofar as the primary hull girder is concerned. This effect of the concentrated bulkhead edge loads on the primary hull girder shear force is illustrated in the lower part of Fig. 68.

3.10 Tertiary Stress and Deflection. Tertiary response refers to the bending stresses and deflection in the individual panels of plating that are bounded by the stiffeners of a secondary panel. In most cases, the load that induces this response is a fluid pressure from either the

water outside the ship or liquid or dry bulk cargo within. Such a loading is normal to and distributed over the surface of the panel. In many cases, the proportions, orientation, and location of the panel are such that the pressure may be assumed constant over its area.

As previously noted, the deflection response of an isotropic plate panel is obtained as the solution of a special case of the earlier orthotropic plate equations, and is given by

$$\frac{\partial^4 w}{\partial x^4} + 2 \frac{\partial^4 w}{\partial x^2 \partial y^2} + \frac{\partial^4 w}{\partial y^4} = \frac{p(x, y)}{D} \quad (207)$$

where

$$\begin{aligned}
 D &= \text{plate flexural rigidity} \\
 &= \frac{Et^3}{12(1-\nu^2)} \\
 t &= \text{plate thickness (uniform)} \\
 p(x, y) &= \text{distributed unit pressure load}
 \end{aligned}$$

Appropriate boundary conditions are to be selected to represent the degree of fixity of the edges of the panel. The stresses and deflections obtained by solving this equation for rectangular plates under a uniform pressure

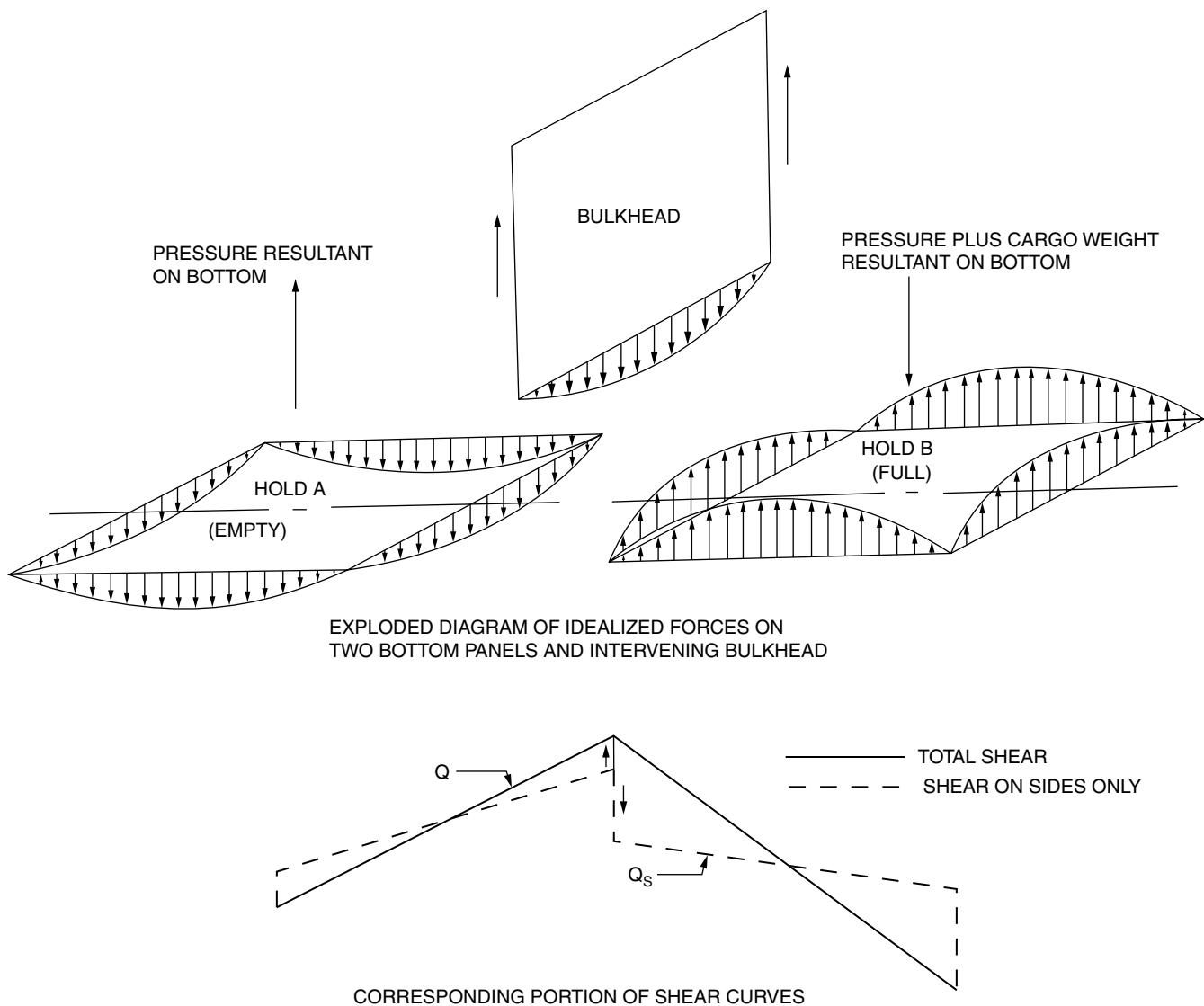


Fig. 68 Force systems on bottoms of two adjacent holds and on the intervening bulkhead, with corresponding shear curves.

distribution are contained in Figs. 65 and 66, and are labeled Type D in those figures (see also Fig. 64).

A special case of some importance, which is not covered in these charts, is that of a plate subject to a concentrated point load. Such loads occur when wheeled vehicles such as fork lift trucks are used for cargo handling. Information on plating subjected to such loads can be found in Hughes (1983) and in classification society rules.

In some cases where the deflection is large compared to the plate thickness ($w_{max} > 0.7t$), tertiary in-plane stresses may arise and the small deflection theory and equation (207) may not give accurate results for stresses and the deflection. In this case, results that are more accurate can be obtained by using von Karman's equa-

tions for large deflection of thin plates (see Timoshenko & Goodier 1970). The solution of these two fourth-order coupled differential equations enables the calculations of bending stresses, tertiary in-plane stresses, and deflections. Von Karman's equations have been modified to include orthotropic effects, and their solution has been presented in detail by Mansour (1976). The results have been presented in a series of charts that provide deflections and stresses that depend on the stiffness and material characteristics of the stiffened plate as well as the loading and boundary conditions. The results for isotropic plates are presented as a special case.

3.11 Superposition of Stresses. The calculated primary, secondary, and tertiary stress can be superimposed at the same location to obtain a maximum value

for the combined stress. In performing and interpreting such a linear superposition, several considerations affecting the accuracy and significance of the resulting stress values must be borne in mind. First, the loads and theoretical procedures used in computing the stress components may not be of the same accuracy or reliability. For example, the primary loading may be obtained using a theory that involves certain simplifications in the hydrodynamics of ship and wave motion, and the primary bending stress may be computed by simple beam theory, which gives a reasonably good estimate of the mean stress in deck or bottom but neglects certain localized effects such as shear lag or stress concentrations.

Second, the three stress components may not necessarily occur at the same instant in time as the ship moves through waves. The maximum bending moment amidships, which results in the maximum primary stress, does not necessarily occur in phase with the maximum local pressure on a midship panel of bottom structure (secondary stress) or panel of plating (tertiary stress).

Third, the maximum values of primary, secondary, and tertiary stresses are not necessarily in the same direction, or even in the same part of the structure. To visualize this, consider a panel of bottom structure with longitudinal framing. The forward and after boundaries of the panel will be at transverse bulkheads. The primary stress will act in the longitudinal direction, as given by equation (134). It will be nearly equal in the plating and the stiffeners, and will be approximately constant over the length of a midship panel. There will be a small transverse component in the plating, given by equation (151), and a shear stress, given by equation (148). The secondary stress will probably be greater in the free flanges of the stiffeners than in the plating because the combined neutral axis of the stiffener-plate combination is usually near the plate-stiffener joint.

Secondary stresses, which vary over the length of the panel, are usually subdivided into two parts in the case of normal tanker bottom structures. The first part, σ_2 , is associated with the bending of a panel of structure bounded by transverse bulkheads and either the side shell or the longitudinal bulkheads. The principal stiffeners in this case are the center, any side longitudinal girders, and the transverse web frames. The second part, σ_2^* , is the stress resulting from the bending of the smaller panel of plating plus longitudinal stiffeners that is bounded by the deep web frames. Because of the proportions of the panels of structure, the first of these components is usually larger in the transverse than in the longitudinal direction. The second is predominantly longitudinal. The maximum tertiary stress is in the plate but in the case of longitudinal stiffeners, the long dimension of the panel is fore and aft and, consequently, the maximum panel tertiary stress will act in the transverse direction (normal to the framing system) at the mid-length of a long side.

In certain cases, there will be an appreciable shear stress component present in the plate, and the proper interpretation and assessment of the stress level will require the resolution of the stress pattern into principal stress components. From all these considerations, it is evident that in many cases, the point in the structure having the greatest stress level will not always be immediately obvious but must be found by considering the combined stress effects at a number of different locations and times.

3.12 Transverse Stresses. Transverse strength refers to the ability of the ship structure to resist those loads that tend to cause distortion of the cross section. When distorted into a parallelogram shape, the effect is called *racking*. The primary bending and torsional strength analyses are based upon the assumption of no distortion of the cross section. Thus, there is an inherent relationship between transverse strength and both longitudinal and torsional strength. Certain structural members, including transverse bulkheads and deep web frames, must be incorporated into the ship structure to ensure adequate transverse strength. These members provide support to and interact with longitudinal members by transferring loads from one part of a structure to another. For example, a portion of the bottom pressure loading on the hull is transferred via the center girder and the longitudinal frames to the transverse bulkheads at the ends of the frames. In turn, the bulkheads transfer these loads as vertical shears into the side shell. Thus, some of the loads acting on the transverse strength members are also the loads of concern in longitudinal strength considerations.

The general subject of transverse strength includes elements taken from both the primary and secondary strength categories. The loads that cause effects requiring transverse strength analysis may be of several different types, depending upon the type of ship, its structural arrangement, mode of operation, and environmental effects.

Typical situations requiring attention to the transverse strength are:

- Ships out of water on building ways or on construction or repair dry dock
- Tankers having empty wing tanks and full centerline tanks, or vice versa
- Ore carriers having loaded centerline holds and large empty wing tanks
- All types of ships—torsional and racking effects caused by asymmetric motions of roll, sway, and yaw
- Ships with structural features having particular sensitivity to transverse effects—for instance, ships having largely open interior structure such as car carriers and RO-RO ships.

As previously noted, the transverse structural response involves pronounced interaction between transverse and

longitudinal structural members. The principal loading consists of the water pressure distribution around the ship, and the weights and inertia of the structure and hold contents.

In a conventional cargo ship having transverse bulkheads at spacing approximately equal to the ship's beam, the transverse response of the frame plus plating is strongly influenced by any significant longitudinal members of the structure to which it may be connected. In the two-dimensional frame computation, these effects can be and are normally taken into consideration by applying appropriate boundary restraint conditions at the intersection of the frame with such members. The most important of these members are the side and bottom shell, decks, tank top, and longitudinally continuous girders. These plate members are assumed to be completely rigid with respect to deflections in their own planes; thus, the appropriate boundary conditions in the direction of the plane of the deck or shell at the intersection with the frame would be a condition of complete fixity. However, rotational restraint of the joint is provided only by the flexural stiffness of the deck beams and side frames. As a result of their smaller cross-sectional dimensions, longitudinal girders are less stiff in resisting deflection, and their influence on the frame would be represented by elastic attachments having finite spring constants. The correct value of the spring constant would be determined by evaluating the load versus deflection characteristics of the girder, including the effective breadth of the deck or other plating to which it is attached, and assuming appropriate support conditions at the transverse bulkheads at its two ends.

The RO-RO ships present a particularly severe transverse strength problem because the demands of their mode of operation require a minimum of obstruction to longitudinal access within the ship. In some cases, transverse bulkheads are absent over the major portion of the middle length of the ship, and vertical support of the decks is accomplished by deep transverse web frames and vertical pillars. As a result of lateral shear deflection, the decks may no longer provide complete transverse fixity at their intersection with the frame ring and large racking stresses and deflections in the frame must be accounted. These result in large bending moments at the frame-deck beam intersections. An illustration of the midship section of such a vessel and the resulting moments, shears, and deflections are shown in Fig. 69 from ISSC (1979). It should be noted also that the principal load component in this case is associated with the rolling (heel) of the ship and includes important contributions from the transverse component of the gravity force as well as the inertia of the structure and contents. Both of these forces experience their maximum value at the same instant during the roll cycle when the angle of roll is at its maximum value, but they are in phase above the roll center and 180° out of phase below.

Oil tankers and bulk carriers present entirely different problems of transverse strength because of their struc-

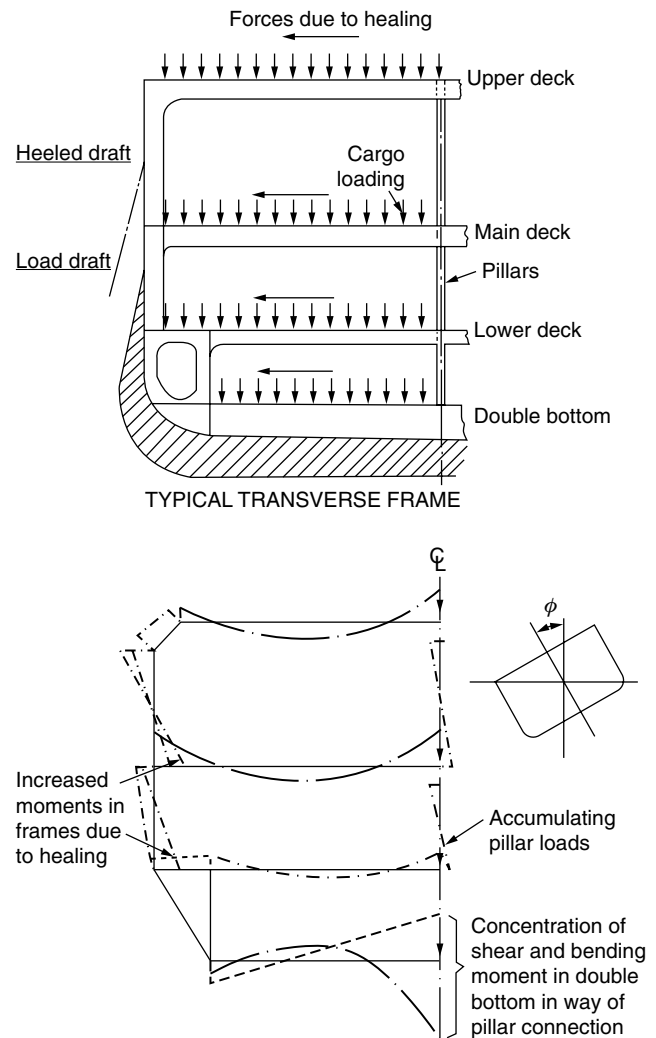


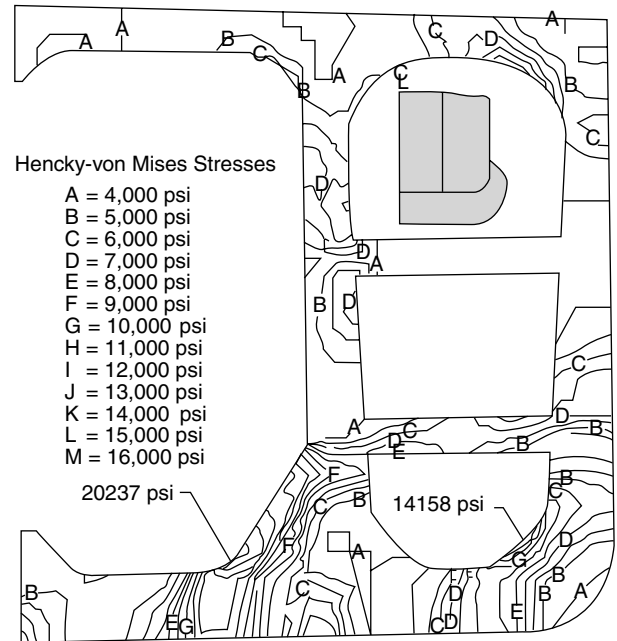
Fig. 69 Racking of a transverse frame.

tural arrangements and distribution of loading. In both types of ship, normal conditions of loading are characterized by pronounced discontinuities of the loads in the transverse plane. In single hull tankers, this comes about from the arrangement of cargo and ballast spaces in which it is customary to use a pair of wing tanks as clean ballast tanks, with the corresponding centerline tank used for cargo. In the loaded condition, the ballast tanks are empty; thus, there is an excess of buoyancy over weight in the wings and excess weight on the centerline. Forward and aft of such a ballast space, there will usually be fully loaded tanks across the entire width of the ship. In double hull tankers where the double hulls are used as ballast tanks, similar situations exist as in single hull tankers. Therefore, caution should be exercised in designing the connections of deck transverse with webs on longitudinal bulkheads and the connections of side transverses and bottom transverses of double hull designs, where pronounced deflections are

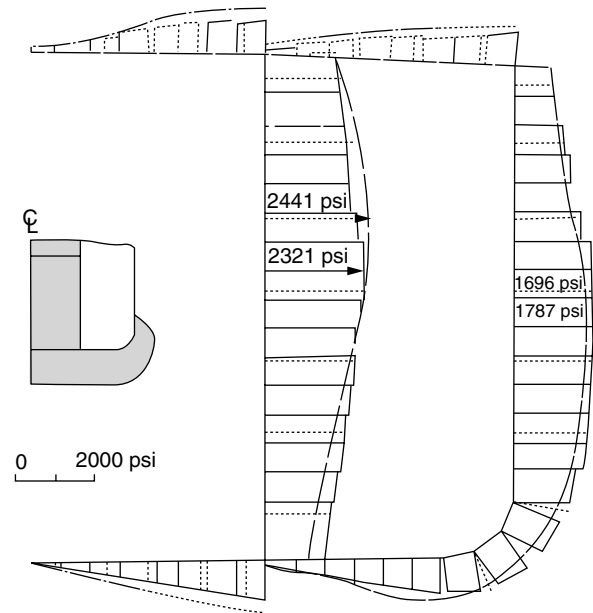
expected to occur. In some of the bulk carriers such as OBO carriers designed to carry dense cargoes, the compartment arrangement generally consists of a relatively narrow centerline cargo hold with large wing tanks and high inner bottom. This type of design, in contrast to the typical single-side skin bulkers designed with one cargo hold across the width of the vessel and lower and upper hopper tanks, will have an excess of weight in the centerline cargo hold in loaded condition when the wing tanks are empty. More detailed discussion of the arrangements of these ship types can be found in Lamb (2003).

Structurally, tankers and OBO carriers are invariably longitudinally framed with wide-spaced webs and may be thought of as consisting of several modules abutting each other. A module consists of several panels of stiffened plating including decks, bottom structure, longitudinal and transverse bulkheads, and side shells. Because the spacing of transverse bulkheads is usually of the same order of magnitude as the beam of the ship, a major module consisting of the section of the ship length contained between two transverse bulkheads will be approximately square when viewed from above. Within each module, there will be a secondary system of stiffening girders and webs oriented longitudinally and transversely, and these will be of about equal strength to each other. The principal transverse strength members are the bulkheads and transverse webs. However, because of the proportions of the hull module and the stiffness characteristics of the longitudinal and transverse members, there will be strong interactions between the transverse and longitudinal structure. A two-dimensional transverse strength analysis will seldom yield reliable results. For this reason, a three-dimensional analysis is usually performed to obtain results that are useful for more than comparative purposes. Because many of the important strength members in such an analysis consist of deep thin-plate structures with bracketed intersections, it is not possible to establish an accurate space-frame model. Consequently, finite element computations using plate and beam elements must be used to achieve an acceptable degree of accuracy in the modeling of the structural behavior.

Ideally, the entire ship hull should be included in such a finite element model as in the dynamic load approach (DLA) at ABS (see Section 3.16). Typical arrangement of the cargo and ballast spaces of a tanker, together with a suitable module for a three-dimensional finite element analysis, can be found in such as Liu et al. (1992). The results of such a three-dimensional analysis for a tanker are illustrated in Fig. 70 (Liu & Bakker 1981), which illustrates the degree of detail to be expected from such analysis. The three-dimensional finite element calculation of a structural arrangement similar to that in Fig. 70 has been compared with results from a three-dimensional space frame analysis. The members used in the latter were specially developed beam members having the capability of representing the neutral axis eccentricity and shear-carrying capacity of the deep webs. Comparison



(a) STRESS PLOT, FRAME 23



— Shear Stresses from the Classical Box Girder Analysis
 - - - Shear Stresses from the Finite Element Analysis

(b) COMPARISON OF SHEAR STRESS DISTRIBUTION, FRAME 31

Fig. 70 Results of finite element analysis of a tanker.

showed that the stresses in the middle portion of the web members was represented reasonably well, but the space-frame model did not contain the detailed description of stresses in the brackets and other members of varying geometry.

For vessels of conventional proportions, results of acceptable accuracy can usually be obtained by modeling a portion of the ship's length equal to about three tank lengths. If longitudinal symmetry of loading and structural arrangement prevails fore and aft of the space in question, the three-tank space can be reduced through symmetry considerations to one and one-half tank spaces. Of course, transverse symmetry can also be assumed in most cases, so the total finite element model would represent one and one-half tank spaces on one side of the centerline. Structural analysis using a model of partial length of the ship is routinely required by classification societies for the purpose of confirming the structural design of large ocean-going vessels (see Section 3.15).

The preparation and checking of input data for a finite element analysis of the extent described previously represents a major expenditure of time and effort. There are computer-based data generation procedures and graphics packages available for the presentation of results that can be used to keep the overall cost and labor of such an analysis at an acceptable level. A general review of recent progress of finite element model generation, modeling technique, as well as the systems developed by the classification societies is given by ISSC Technical Committee II.1—Quasi-static Response (2000).

3.13 Stress Concentration. Stresses such as those discussed previously are average stresses. In general, any discontinuity in a stressed structure results in a local increase in stress at the discontinuity. The ratio of the maximum stress at the discontinuity to the average stress that would prevail in the absence of the discontinuity is called a *stress-magnification factor*.

Discontinuities in ship structures range from the gross discontinuities formed by the ends of superstructures and by large hatches to the minute corners and notches that may occur in attachments to stressed structure. The most numerous classes of discontinuities are the many openings required for cargo handling access and engineering services. Every such opening causes stress concentrations. The importance of these stress concentrations is shown by the fact that the great majority of fractures in ship structures originate at the corners of openings.

At the ends of superstructures, the smoothest possible transfer of the stress in the superstructure into the structure below is required. Part (3) of Vasta (1949), reporting a full-scale investigation on the *President Wilson*, shows stress-concentration factors at various points near the ends of the superstructure varying from 2.4 to 4.6. Similar care is needed at the corners of large hatches. The great amount of study that has been devoted to the design of hatch corners is summarized in SSC (1952). Square corners in hatches in strength decks are an invitation to fractures.

Openings or cuts in structure present two problems: the reduction of the amount of material available to support the load (i.e., the strength of the member in which the hole is cut) and the stress concentrations adjacent to the opening. In many cases, the stress concentrations

will be more serious than the effect of removing material. In the classical case of a circular hole in an infinitely wide plate under tension, which will be illustrated subsequently, the change in stress due to lost area is infinitesimal but the stress at the edge of the opening is three times the nominal value. The stress-concentration factor increases with the width of the opening relative to the width of the member, and with the acuity of the corners of the opening.

If the size or location of an opening is such as to unduly impair the strength of a member, measures must be taken either to reduce the stress in way of the opening or to compensate for the loss of material, or both. This may be done by changing the location of the opening (e.g., in the case of a beam or girder under flexural loading, locating the opening at or near the neutral axis of the member), changing the shape of the opening, providing an insert or doubling plate at the area of the member circumscribing the opening, or by providing a reinforcing ring around the opening. The purpose of a reinforcing ring is to stabilize the edge of the cut member around the opening and to concentrate added material around the opening close enough to the plane of the loaded plate so that the ring will deform with the loaded plate, absorb energy, and reduce strains at the periphery of the opening.

Large openings in strength members may require the use of an insert plate abreast the opening, thicker than the material in which the hole is cut, or a doubling plate to compensate for the material lost at the opening, and possibly a reinforcing ring at the periphery of the opening. When insert or doubling plates are used as reinforcements, they must be tapered off in the direction of loading and well beyond the opening to minimize stress concentrations due to abrupt changes in thickness and to ensure that the cross-sectional area of the insert or doubler will become fully effective in way of the opening. Insert plates are preferable to doublers because they eliminate lamination and ensure effectiveness of the reinforcing material at the approaches to and in way of the opening. The design of compensation and reinforcement at openings is also discussed in sections of Chapter 17 of Lamb (2003).

3.13.1 Rectangular Openings. The stress-magnification factors at the corners of a rectangular opening in an axially loaded plate depend on the size of the opening and the radius of the corners. Figure 71 from Heller et al. (1959) is a family of curves that shows the maximum values of the boundary stress as a function of corner radius and aspect ratio of the openings in an infinite plate subjected to uniaxial stress. Theory shows that when the plate is at least approximately four times the width of the opening, the concentration factors for an infinite width of plate are sufficiently accurate.

For a sharp corner, the maximum stress occurs at the corner, and for finite radii the maximum stress is located between the midpoint of the fillet and the point of tangency. Figure 71 also gives the locus of minimum stress-concentration factors and the factors for an ovaloid when $r = l/2$. Figure 72 (from Brock 1957) gives

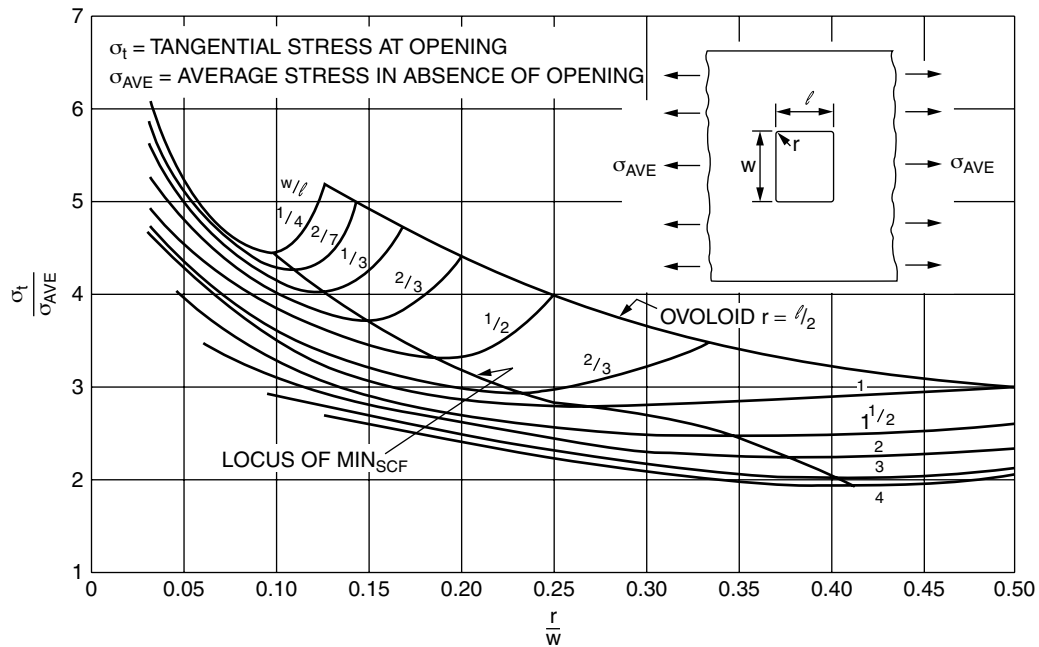


Fig. 71 Stress concentration factors for square hole tension parallel to side (Heller et al. 1959).

stress-concentration factors for a square hole with the applied load parallel to the diagonal of the hole. The maximum stresses are considerably greater under this condition of loading than when the applied load is parallel to the side of the opening, as in the case of Fig. 71.

Figure 73 (from D'Arcangelo 1969) gives the stress-concentration factor for rectangular openings in a finite plate. The nomenclature is the same as for Figs. 71 and 72, except the additions of W = width of plate, and σ'_{ave} =

average stress at minimum section. Increasing the length of the opening for a constant width reduces the stress-concentration factor. This is shown in Fig. 73, where the stress-concentration factor is halved as the w/l ratio is reduced from 3/1 to 1/2. Generally, the stress concentration is smaller when the long dimension of the opening is parallel to the load.

Figure 74 gives the maximum stress-concentration factors versus r/w ratio for a face-bar reinforced square

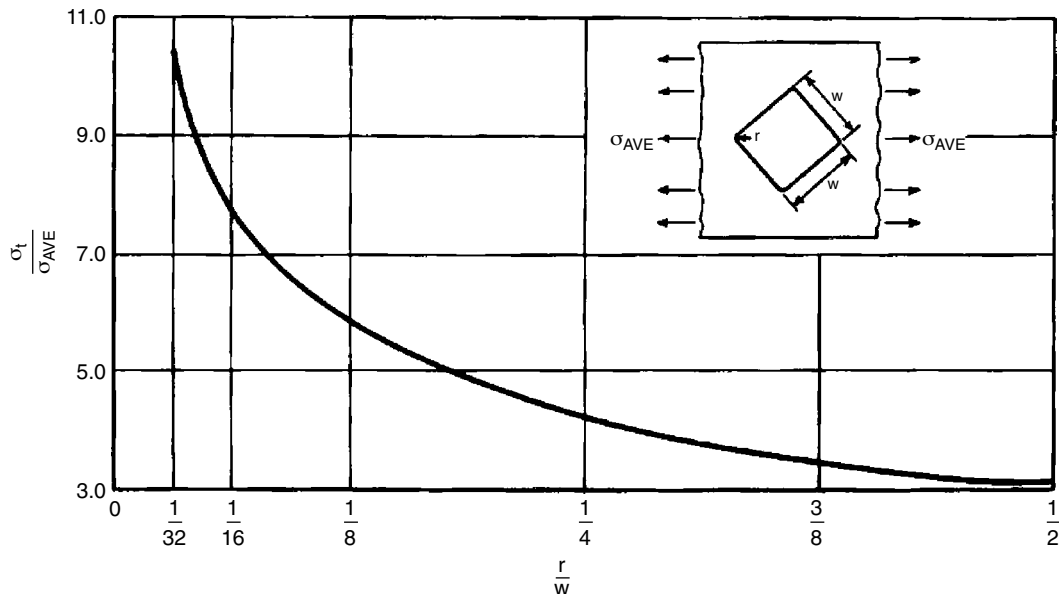


Fig. 72 Stress concentration factors for square hole tension parallel to diagonal (Brock 1957).

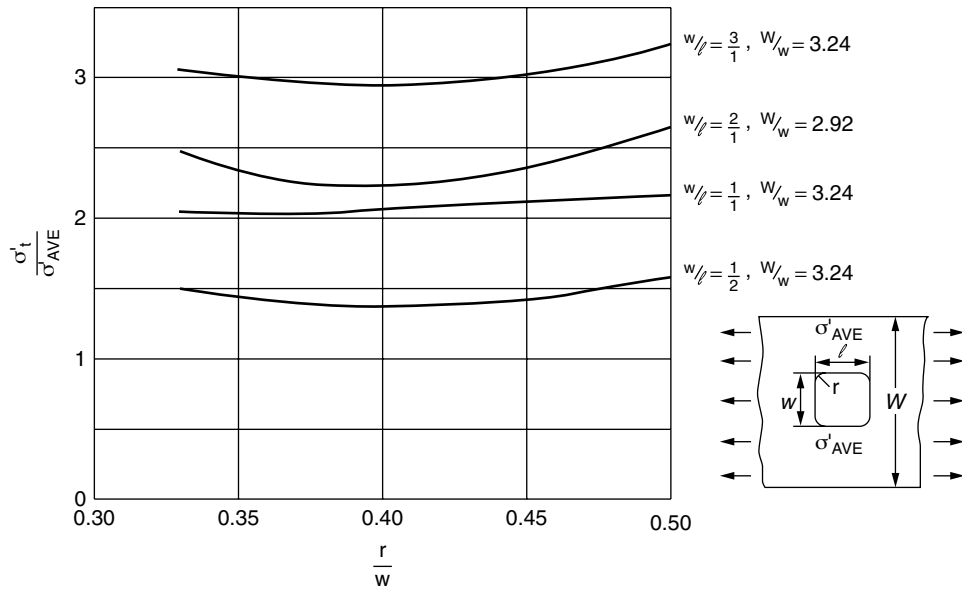


Fig. 73 Stress concentration factor in a finite plate with a square hole (D'Arcangelo 1969).

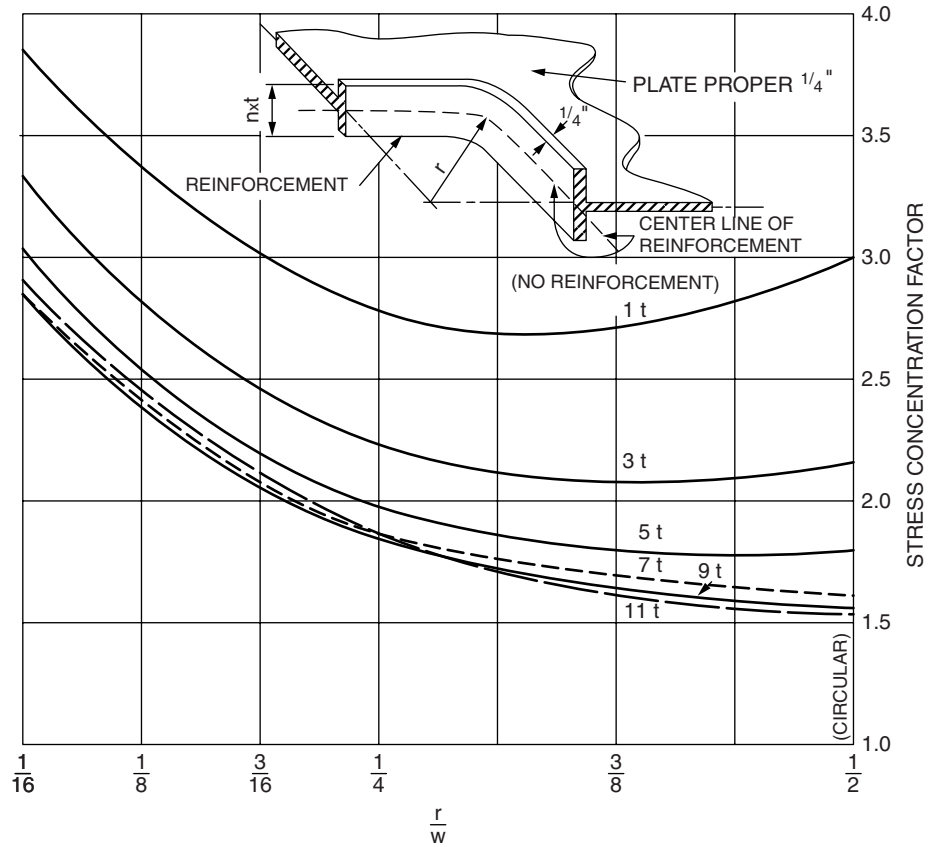


Fig. 74 Stress concentration factor for face-bar reinforced square openings with round corners (Kuntzman & Umberger 1959).

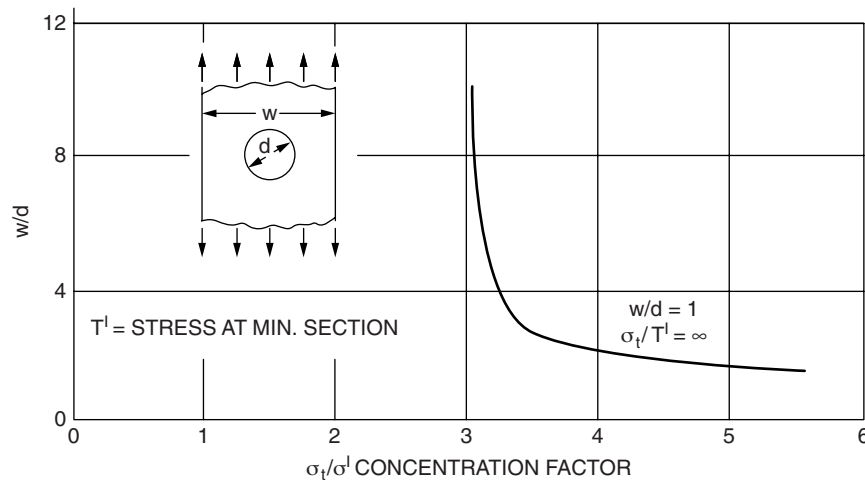


Fig. 75 Stress concentration factor in a finite plate with a circular hole.

opening of width w with rounded corners of radius r . Stress concentration factors for non-reinforced and reinforced circular openings in an infinite plate are obtained when r/w is equal to $1/2$; the minimum possible factor is 1.56. For reinforcement thickness equal to the plate thickness, the maximum effective reinforcement height (above which additional height has little effect) is seven times the plate thickness. The specimens from which the data were obtained were of sufficient size so that the loading arrangements and stress patterns were independent of the specimen boundaries.

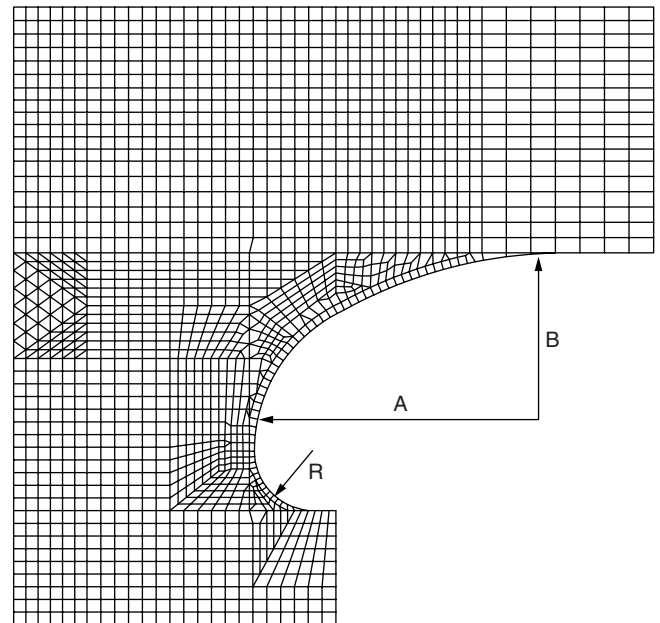
3.13.2 Circular Openings. Stress-concentration factors for non-reinforced and reinforced circular openings in an infinite plate are obtained from Fig. 74 when r/w is equal to $1/2$. Figure 75 (from Coker et al. 1919–1920) is a plot of photoelastic studies of tangential stress-concentration factors for openings, centrally located in the width of the plate, of various ratios of plate to opening width.

3.13.3 Hatch Corners. Hatch corner damages due to stress concentration on the deck of container vessels have been recognized by the industry. Early studies on stress and fatigue analyses and correlation with full-scale measurements can be found in a number of reports issued by the Ship Structure Committee for the SL-7 class container ships, such as Jan et al. (1979) and Chiou and Chen (1990).

Stresses in hatch corners at strength deck, top of continuous hatch side coaming, and lower deck generally arises from primary and secondary longitudinal hull girder loads, and bending of the cross deck structure in a longitudinal direction resulted from torsion-induced hull girder twist and dynamic container loads. Hatch corners are basically of circular, double curvature, or elliptical shape, or a combination of two of the basic configurations. Structural analyses show that a design of deck structure hatch corner with a cutout having a combined

configuration would have relatively less stress concentration than other arrangements. Illustrated in Fig. 76 is the finite element structural model of a commonly used configuration for a large container ship consisting of elliptical and radial contours with cutout.

3.14 Vibratory Response to Dynamic Loads. Two types of dynamic loading were discussed in Section 2.9. One is the slamming impact on bottom (bottom slamming) or flare forward (bow flare impact), followed by a transient vibratory response of the entire hull girder or whipping, and the other a more-or-less steady-state



A, B = Major and Minor Axes of Ellipse, respectively
R = Circular Radius

Fig. 76 Hatch corner configuration, a combination of elliptical and circular contours with cutout.

random vibration or springing excited by certain wave frequency components.

3.14.1 Impact Induced Response. Considering the response to bottom slamming first, the determination of the local structural response involving damage requires consideration of the inelastic behavior of the structure. The “dynamic load factor” discussed in Section 2.9 may be considered for quasi-static structural analysis.

The overall whipping response can cause large additional hull girder bending moments (see Dow et al. 1981). However, because of its transient nature slamming loads may be less effective in producing plastic collapse than more slowly varying hull bending loads due to buoyancy effects, and may be computed using a linear elastic model. Mansour (see Stiansen & Mansour 1975) assumes the probability density function of the hull girder bending moment due to a sequence of random bottom slamming of the vessel operating in a seaway follows a Poisson process. For a transient excitation of unit delta function, the impulse response function can be obtained using modal analysis, which can be written in a closed form in terms of generalized effective mass, generalized damping, natural frequency, and a step function. Further, using a truncated exponential law for the slam pressure and assuming that the pressure amplitudes are highly correlated spatially, the first and second moments of the slam random intensity are derived, which define completely the mean, the variance, and the RMS of the slam-induced bending moment. This approach has been programmed in the computer code, SLAM, where the form coefficient due to Ochi and Motter (1973) in computing the slamming and the short-term extreme value approach suggested by Ochi (1973) are employed.

The SLAM code was used in a parametric study analyzing the transient hull girder responses of a number of large block coefficient ocean-going vessels of 215 m to 280 m in length (ABS 1993). In this study, the H-family wave spectral data was used for computing the extreme value, where the ship speed reduction due to added resistance in waves was taken into account following Aertssen (1969). The study shows that the calculated extreme value of slamming induced a vertical bending moment along the length of the vessel is found to be maximum around the quarter length from the forward perpendicular, and the extreme slamming induced bending moment amidships can be 15 percent to 20 percent of the maximum wave-induced vertical bending moment.

Meanwhile, a number of cases of deck buckling have been reported on ships with large flare forward, which seem to be associated with slamming and whipping. The transient loading associated with flare immersion is characterized by a longer duration of impact than bottom slamming. Elementary beam theory shows that the dynamic load factor will therefore generally be greater. For example, consider the case of a 152.4 m (500 ft) cargo ship with a natural period of vibration, T , of 0.75 sec. Assume that the duration of a bottom slam impact, t_1 , is 0.1 sec and of a flare immersion impact is 0.5 sec. Then in

the first case, $t_1/T = 0.13$, and in the second, $t_1/T = 0.67$. Simple theory (Frankland 1942) assuming triangular or sinusoidal pulses gives a magnification factor of 0.3 in the first case and 1.5 in the second.

Bow flare slamming loads may be considered as quasi-static loads for local structural analysis. On the other hand, flare slamming induced whipping requires consideration together with the slowly varying wave load effects, which involves problems of phasing (see Lewis et al. 1973) and of duration of the high-frequency load peaks. Mansour and D'Oliveira (1975) compute the rigid body response combined with the elastic dynamic response of a ship in head seas using a free-free non-uniform Timoshenko beam. By neglecting the rotary inertia term, the dynamic response can be expressed in terms of a series of responses in normal modes. Further applying an orthogonality relationship, a linear second-order differential equation with constant coefficients for each mode can be obtained, and can be solved in a closed form.

The approach suggested by Mansour and D'Oliveira (1975) has been programmed in a time domain simulation code, BOWSLAM, where the bow flare impact pressure simulation is from Chen and Ng (1982). Calculated bow flare impact-induced hull girder dynamic bending moment results from program BOWSLAM have been shown to compare reasonably well with available model test and full-scale measurements of a fast cargo ship *Snow Drift* and model test results of other types of vessels, including a navy cruiser. Shown in Fig. 77 is the comparison of the full-scale measurements and the calculated results from BOWSLAM for the fast cargo ship *Snow Drift*, which experienced significant buckling in the forward deck. The comparison shown in the figure is made in terms of ratios of the total (wave plus

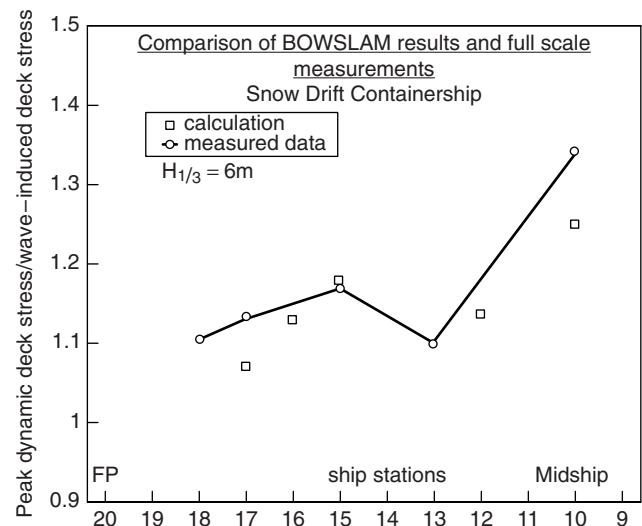


Fig. 77 Comparison of calculated total stresses by program BOWSLAM and full-scale measurements of fast cargo ship *Snow Drift*.

whipping-induced) stresses divided by the wave-induced stresses at ship stations where stress gauges were located. The sea condition in which full-scale measurements of deck stresses were recorded was about 6 m significant wave height, which corresponds to about Beaufort number 8. The calculated stress values are obtained by dividing the vertical bending moments by the actual section modulus at each station of the vessel. It can be seen that for this particular case, the whipping-induced stress is relatively large at about the quarter length of the vessel from forward perpendicular, and is about 35 percent of the wave-frequency bending stresses amidships. The larger whipping-induced response at midship section has also been shown in calculated results of Mansour and D'Oliveira (1975), as well as full-scale experimental data from Lewis et al. (1973) and McCallum (1975). The same trend is also observed by McTaggart et al. (1997) from measured whipping responses in regular waves on a hydroelastic model of a Canadian frigate, that whipping-induced vertical bending moment amidships could approach the wave-induced moment in magnitude at greater operating speeds and in steep waves. Flare impacts of high-speed craft, which present special problems, are treated in Section 6.2.

One difficulty in estimating the slamming response for design purposes is that the relative vertical velocity when a slam occurs depends on the ship speed and heading, as well as on the severity of the sea. Hence, it is to some extent under the control of the ship's captain. As shown by Maclean and Lewis (1970), the greatest slamming loads actually recorded on a typical cargo ship did not increase with sea severity after a certain level was reached because speed was gradually reduced voluntarily by the captain. This suggests the need for more data on actual slam loads permitted to be experienced by ships of various types.

3.14.2 Springing. Springing has been found to cause significant increases in wave bending moments and stresses in the case of long, flexible ships of full form, particularly Great Lakes bulk ore carriers and a few ocean-going bulk vessels and tankers (Melitz et al. 1992, Witmer & Lewis 1995). The solution to the problem of vibratory springing involves the assumption of an Euler or Timoshenko beam on an elastic foundation (buoyancy from the sea). The equations of motion in a vertical plane are set up—balancing the wave excitation against the elastic beam response of the hull, including effects of mass inertia and added mass—and both structural and hydrodynamic damping, as discussed in a general way in Beck et al. (2009). The solution for the simple two-noded case is of particular interest, and such solutions have been given by Goodman (1971) and Hoffman and van Hooff (1976); Stiansen et al. (1977) describe the ABS computer program SPRINGSEA II for carrying out routine calculations of linear springing response. As shown by model tests (Hoffman & van Hooff 1973) and confirmed by Troesch (1984a), the bending moment response operator (at constant speed in

head seas) shows an oscillatory character when plotted against wave length (encounter frequency). Peaks correspond to wave lengths such that hydrodynamic forces at bow and stern reinforce one another. (Forces along most of the ship length tend to cancel out.)

Bishop et al. (1978) presented a more general theoretical approach, which does not provide a solution to the important problem of damping. Stiansen (1984) notes that hydrodynamic damping is negligible and “the overall damping primarily consists of the speed correction, proportional to the derivative of added mass, and structural and cargo damping.” Analysis of full-scale data on the Great Lakes bulk carrier *Stewart J. Cort* gave results in good agreement with damping coefficients calculated by SPRINGSEA II.

Stiansen (1984) reviews research activities under ABS sponsorship on this and other aspects of dynamic behavior of large Great Lakes bulk carriers. Experiments in waves (Troesch 1984a) on a model joined amidships measured both wave excitation and springing response. The experiments showed that in addition to the response at ω_e , the encounter frequency, there was a measurable springing excitation at $2\omega_e$, and sometimes at $3\omega_e$. Should $2\omega_e$ or $3\omega_e$ equal ω_0 , the natural two-node frequency of the hull, there will be a large increase in the springing response. This nonlinear response is quadratic in wave amplitude; if wave amplitude doubles, response increases by a factor of four. The experiments also showed that responses in the natural frequency are excited when the sum of the encounter frequencies of two wave components equal the natural frequency.

Troesch (1984b) made use of exciting functions (first- and second-order inelastic bending moments) determined experimentally on a jointed model to calculate the two-noded springing response in typical Great Lakes wave spectra. Results showed that at certain speeds, the combined first- and second-order resonant response was significantly greater than the first-order alone. Work continues on developing a theoretical basis for calculating the nonlinear springing response, following the approach of Jensen and Pedersen (1981).

Jensen and Dogliani (1996) developed a theoretical basis for calculating wave-induced loads on flexible ships. The procedure is based on a nonlinear quadratic strip theory formulated in the frequency domain. Included in their analysis are the nonlinear effects due to changes in added mass and hydrodynamic damping and non-vertical hull sides. Because of these nonlinearities, the wave-induced and springing responses become non-Gaussian even if the input waves are Gaussian. The probabilistic aspects of the response have been determined by approximating the response probability density function using a Hermite series. The main result of the study is that springing is most pronounced in head or near head seas and in low sea-states where the zero crossing periods are small. This result is in agreement with the results cited by Stiansen, Mansour, and Chen (1977). Jensen and Dogliani (1996) also found that the nonlinear

contribution to springing response is at least as important as the linear contribution. However, the extreme peak of the springing was found to be relatively small compared with the extreme value of the wave-induced response. Therefore, for typical commercial ships the design bending moment may be determined without consideration of springing moment. However, the springing response can be important in the calculation of the fatigue life of ship details. Further studies of whipping and springing vibrations are given in Xia et al. (1998) and Jensen and Wang (1998).

3.15 Criteria Developed by Classification Societies, Including IACS. The way ships were built and designed until the early 1970s were essentially an evolutionary process without dramatic changes in configuration or size. Most importantly, mild steel was predominant in ship construction through that period. It was therefore relatively easy for classification societies to develop the strength criteria in their rules. These were based on practical experience gained over the years, and were typically presented in a semi-empirical type format. The strength of these rules was their simplicity in application and relative reliability in assessing the primary strength of the vessel structures. However, the very strength of the traditional rules, and the degree to which empirical data and service experience has been incorporated into their development, is also their primary weakness. Reliable application is dependent upon the similarity between the new design and the designs from which the rules were developed. Little guidance can be found in the traditional classification rules for dealing with the structural problems associated with sophisticated and complex designs for vessels that are larger, faster, or structurally different from any vessel that the naval architects have experienced.

The first major change to ocean-going vessel rules of major classification societies took place in the early 1970s when a significant change in ship design occurred, driven by the tanker market. The most noticeable change was the dramatic increase in the size of ships with the introduction of VLCC and ULCC size supertankers. Structural configurations changed. Also significant was the increasing use of greater strength steels that, with reduced scantlings facilitated by computer-aided design, had a noticeable impact on ship durability and structural problems in service. The change in classification rules entailed the introduction of criteria for the total bending moment and shear force, including both still water and wave-induced components, as the basis to determine the hull girder strength. This is in contrast to the traditional rules, which rely on the still water components only. The success of introducing the wave loads into the criteria is due to several developments available to the industry. One of these was the development of the long-term prediction scheme for hull girder loads. The others were the availability of the linear ship motion computer program for predicting ship responses in waves, and the development of a mathematical representation of the long-term

seaway of the North Atlantic Ocean correlated to the long-term hull girder responses recorded (see Stiansen & Chen 1982).

Despite the increasing use of advanced analytical methods, the development of initial designs continued to rely on the use of simplified methods, which primarily emphasizes the hull girder loads and overall hull girder strength. The dynamic load components imposed on local structures were not rationally accounted for in either the structural design or the design evaluation. In many cases, structural failures experienced in tankers and other types of large ocean-going vessels could be attributed to the lack of adequate consideration of local loads in design. Such problems were compounded due to the increasing use of higher strength steel in construction. Consequently, the classification rules have been changed to provide explicit requirements for local structural strength evaluation and failure assessment, as well as for the direct stress analysis as part of rule scantling determination or as a supplementary basis for scantlings.

In this regard, the so-called "Rule Restatement Project" was launched at the ABS in 1990 to "re-state" the prescriptive formulations of existing traditional classification rules prior to 1990 by applying first principles-based criteria. This project addressed large ocean-going vessels including tankers, bulk carriers, and container ships, and was intended to develop a complete, flexible, and user-oriented strength criteria for hull structures based on a first-principles approach to meet the immediate needs of the industry. This effort included the development of load criteria, strength criteria for minimum scantling requirements based on a net thickness concept, and strength assessment procedures using the finite element structural analysis to comply with specified failure criteria arising from material yielding, buckling/ultimate strength, and fatigue. Results of the re-statement project were incorporated in the ABS Rules for tankers, bulk carriers, containerships and LNG ships since 1993. To facilitate the application of the first principles-based criteria embodied in the rules, a computer program suite, the SafeHull System, was developed and made available to the industry. Efforts of the rule restatement are detailed in Conlon (1991, 1992), Chen et al. (1993, 1996), Liu et al. (1995), and Spencer et al. (1995, 1996).

In parallel to the criteria stipulated in classification rules, classification societies also provide procedures for ship structural analysis, which is offered as the "design by analysis" methodology, and is meant as an alternative to the explicitly stated local scantling requirements of the rules. The ABS "Dynamic Load Approach (DLA)" given in Liu et al. (1992) and ABS (2006) is one of such procedures offered by the classification societies. Further consideration of the design by analysis procedure is given in Section 3.16.

The procedures employed by the major classification societies for strength evaluation of hull girder and local structural components are similar but vary, except

for double hull tankers and bulk carriers included in the IACS common rules and those areas addressed by the IACS Unified Requirements. Beginning in 2001, in response to the demands of both the International Maritime Organization (IMO) and the industry for more robust structural requirements, the member classification societies of IACS undertook the joint development of common structural rules for tankers and bulk carriers. This effort resulted in the publication of two rule documents: “Common Structural Rules for Double Hull Tankers” (2006) and “Common Structural Rules for Single and Double Side Skin Bulk Carriers” (2006). The tanker rules were developed jointly by American Bureau of Shipping, Det Norske Veritas, and Lloyds Register, and are described by Horn (2005). The bulk carrier rules were developed jointly by Bureau Veritas, China Classification Society, Germanischer Lloyd, Korean Register, Nippon Kaiji Kyokai, Registro Italiano Navale, and Russian Register of Shipping. The development of the bulk carrier rules is described by Nieuwenhuijs et al. (2005). These common rules replace the various existing tanker and bulk carrier rules of the IACS classification societies. The philosophical concepts and key points of the common rules for tanker and bulk carriers are summarized in the following sections to provide some basic background information toward the understanding of strength evaluation procedures employed by classification societies.

3.15.1 Net Thickness Concept. The common rules are formulated using a net thickness approach. This approach assumes that various degrees of corrosion (or corrosion margin) will occur to the structural members during the life of the ship. The corrosion margins are defined as corrosion additions that are added to net scantlings to yield the gross scantlings for the ship. The strength of the ship structure is thus evaluated on a net scantling basis in which the gross scantlings are reduced by a corrosion margin representative of corrosion wastage over the life of the ship. This consists of applying a general average global hull girder and primary support member wastage such that the overall strength of these large structural members is maintained at an acceptable level. The strength of local structural members is assessed using the structural capacity in an increased wasted condition, or net thickness, applying the expected extreme loads. This will ensure that the ship will meet the minimum strength requirements even while in the defined extreme wasted condition. Because fatigue is a cumulative mode of failure that starts from the first day of service when the ship is delivered until the last days of service when the ship could be in a fully corroded state, the net thickness associated with hull girder and local thickness for fatigue is based on an averaged wastage or half of the full corrosion margin.

The net ship-based strength criteria has special value not only for design purposes but also in helping to formulate a maintenance strategy for the ship throughout its service life. The ship structure while in service is monitored for corrosion when thickness measurements or

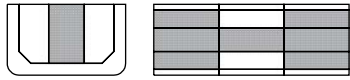
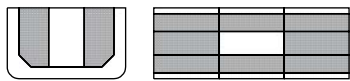
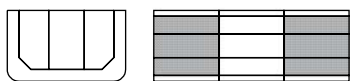
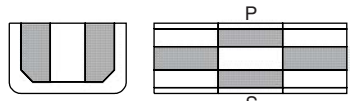
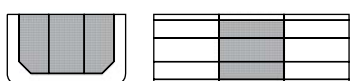
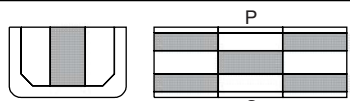
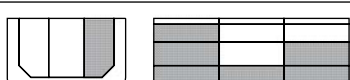
No.	Loading Pattern	Draft
1		0.9 T _{sc}
2		0.9 T _{sc}
3		0.55 T _{sc}
4		0.6 T _{sc}
5		0.8 T _{sc}
6		0.6 T _{sc}
7		T _{LC}
8		T _{balH}

Fig. 78 Tanker loading patterns (IACS CSR 2006).

gaugings are taken during periodic surveys. When the thickness measurements indicate that the amount of corrosion wastage results in the thickness being equal to the net thickness, then renewal of the plate or member is required.

3.15.2 Loads. The fundamental building block upon which the rules are based are the loads. The loads to be applied set up the two other fundamental building blocks, which consist of the engineering strength formulations and the acceptance criteria. The loads consist of two major categories comprising static and dynamic components. The static, or still water, components typically represent the loads associated with ship operation loading conditions such as lightship weight, cargo, ballast, and external buoyancy conditions. Figure 78 illustrates sample static load patterns used for a VLCC type of tank arrangements. The dynamic, or wave-induced, components represent the loads associated with ship motions and accelerations when operating in a seaway. The rules specify the loading conditions and tank loading patterns to use and the dynamic loads to be applied.

The dynamic loads are based on the fundamental ship parameters that are used to calculate characteristic ship

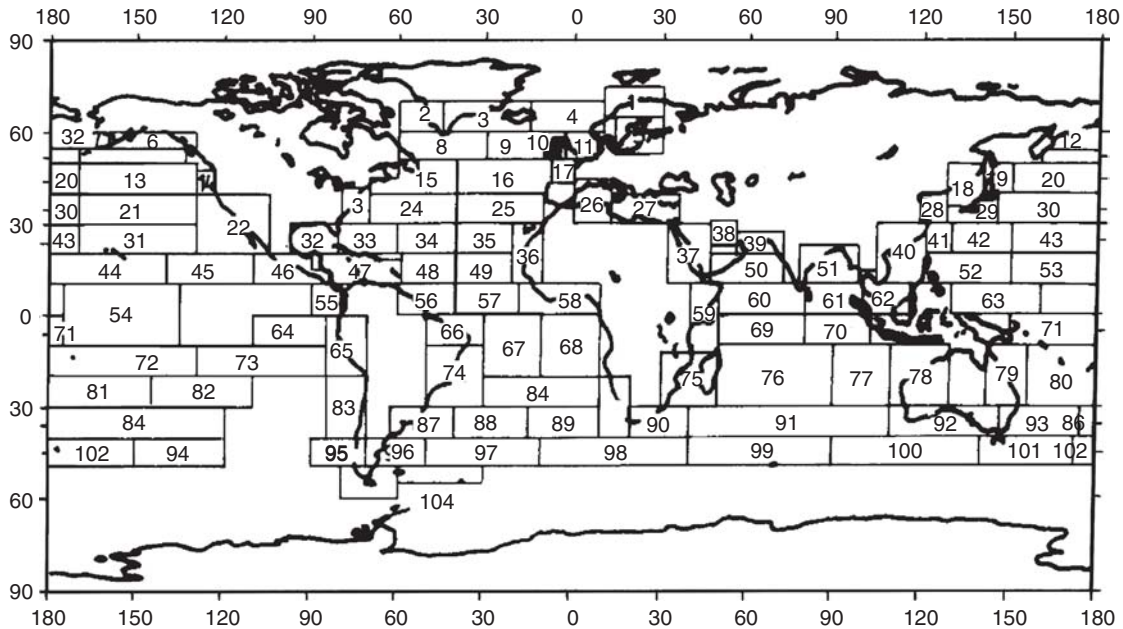


Fig. 79 Map of BMT Global Wave data.

motions, accelerations, and then the dynamic components of external pressure loads, hull girder bending and shear loads, and internal tank loads due to cargo and ballast carried. Dynamic loads associated with sloshing and local impact at the bottom forward, forward bow, and green water on deck are also specified. Many of these load components are based on existing IACS Unified Requirements.

The dynamic loads are further broken down into load scenarios that cover the range of operations associated with the rule requirements. For overall strength evaluations, the characteristic loads are imposed using extreme weather and waves a ship may encounter, which are based on a probability of exceedance of 10^{-8} . These loads represent the extreme loads based on exposure to the North Atlantic environment defined in IACS standard wave data over a 25-year design life. Although many vessels sail their entire life without ever transiting the North Atlantic, the North Atlantic was selected as the characteristic environment for design to not limit future operational flexibility.

Load combination factors (LCF) are used to combine the various load components. The loads are combined into sets that apply the specified maximum parameters along with the corresponding remaining components to set up equivalent wave approaches to represent realistic dynamic-based loads. The dynamic load parameters, such as hull girder bending, external pressure, or internal pressure, at a given location are each maximized in turn to impose corresponding static and dynamic loads on the various structural members. The principles of this approach are based on the Dominant Load Parameter procedure described in Sections 2.3.4 and 3.16. The ABS

Rules include specified load sets to be applied during the structural review process.

For fatigue evaluations, representative characteristic loads are used to represent the large number of modest fatigue-inducing fluctuating load ranges, which are based on a probability of exceedance of 10^{-4} . Because fatigue calculation results are very sensitive to load and corresponding stress range applications, the most representative characteristic loads are applied that strive to eliminate any large conservative assumptions. The following fatigue calculation methods impose safety margins later in the applied method and acceptance criteria itself, therefore imposing additional conservatism at the load determination stage is not necessary. Also as noted previously, the North Atlantic environment is used.

3.15.2.1 IACS Standard Wave Data. The IACS standard wave data describes the North Atlantic wave conditions in areas 8, 9, 15, and 16 of Fig. 79, defined in the BMT Global Wave Statistics (1986). The IACS standard waves are established based on BMT data with modifications according to Bitner-Gregersen, Guedes Soares, and Silvestre (1998). The standard wave scatter diagram is given in Table 1, and its spectral form follows the Bretschneider or two-parameter Pierson-Moskowitz spectrum:

$$S(\omega) = \frac{H_s^2}{4\pi} \left(\frac{2\pi}{T_z} \right)^4 \omega^{-5} \exp \left(-\frac{1}{\pi} \left(\frac{2\pi}{T_z} \right) \omega^{-4} \right) \quad (208)$$

where

H_s = the significant wave height (m)
 ω = angular wave frequency (rad/s)

Table 1—Probability of sea-states in the North Atlantic, described as occurrence per 100,000 observations, covering areas 8, 9, 15, and 16 in map of BMT Global Wave data.

Hs (m)	Tz (sec)																Sum
	3.5	4.5	5.5	6.5	7.5	8.5	9.5	10.5	11.5	12.5	13.5	14.5	15.5	16.5	17.5	18.5	
0.5	1.3	133.7	865.6	1186.0	634.2	186.3	36.9	5.6	0.7	0.1	0.0	0.0	0.0	0.0	0.0	0.0	3050
1.5	0.0	29.3	986.0	4976.0	7738.0	5569.7	2375.7	703.5	160.7	30.5	5.1	0.8	0.1	0.0	0.0	0.0	22575
2.5	0.0	2.2	197.5	2158.8	6230.0	7449.5	4860.4	2066.0	644.5	160.2	33.7	6.3	1.1	0.2	0.0	0.0	23810
3.5	0.0	0.2	34.9	695.5	3226.5	5675.0	5099.1	2838.0	1114.1	337.7	84.3	18.2	3.5	0.6	0.1	0.0	19128
4.5	0.0	0.0	6.0	196.1	1354.3	3288.5	3857.5	2685.5	1275.2	455.1	130.9	31.9	6.9	1.3	0.2	0.0	13289
5.5	0.0	0.0	1.0	51.0	498.4	1602.9	2372.7	2008.3	1126.0	463.6	150.9	41.0	9.7	2.1	0.4	0.1	8328
6.5	0.0	0.0	0.2	12.6	167.0	690.3	1257.9	1268.6	825.9	386.8	140.8	42.2	10.9	2.5	0.5	0.1	4806
7.5	0.0	0.0	0.0	3.0	52.1	270.1	594.4	703.2	524.9	276.7	111.7	36.7	10.2	2.5	0.6	0.1	2586
8.5	0.0	0.0	0.0	0.7	15.4	97.9	255.9	350.6	296.9	174.6	77.6	27.7	8.4	2.2	0.5	0.1	1309
9.5	0.0	0.0	0.0	0.2	4.3	33.2	101.9	159.9	152.2	99.2	48.3	18.7	6.1	1.7	0.4	0.1	626
10.5	0.0	0.0	0.0	0.0	1.2	10.7	37.9	67.5	71.7	51.5	27.3	11.4	4.0	1.2	0.3	0.1	285
11.5	0.0	0.0	0.0	0.0	0.3	3.3	13.3	26.6	31.4	24.7	14.2	6.4	2.4	0.7	0.2	0.1	124
12.5	0.0	0.0	0.0	0.0	0.1	1.0	4.4	9.9	12.8	11.0	6.8	3.3	1.3	0.4	0.1	0.0	51
13.5	0.0	0.0	0.0	0.0	0.0	0.3	1.4	3.5	5.0	4.6	3.1	1.6	0.7	0.2	0.1	0.0	21
14.5	0.0	0.0	0.0	0.0	0.0	0.1	0.4	1.2	1.8	1.8	1.3	0.7	0.3	0.1	0.0	0.0	8
15.5	0.0	0.0	0.0	0.0	0.0	0.0	0.1	0.4	0.6	0.7	0.5	0.3	0.1	0.1	0.0	0.0	3
16.5	0.0	0.0	0.0	0.0	0.0	0.0	0.0	0.1	0.2	0.2	0.2	0.1	0.1	0.0	0.0	0.0	1
Sum	1	165	2091	9280	19922	24879	20870	12898	6245	2479	837	247	66	16	3	1	100000

T_z = the average zero up-crossing wave period (s)

$$T_z = 2\pi \left(\frac{m_0}{m_2} \right)^{\frac{1}{2}}$$

The spectral moments of order n of the response process for a given heading is described as

$$m_n = \int_{\omega} \sum_{\theta_0-90^\circ}^{\theta_0+90^\circ} f_s(\theta) \omega^n \cdot S(\omega|H_s, T_z, \theta) d\omega \quad (209)$$

using a spreading function defined as

$$f_s(\theta) = k \cos^2(\theta)$$

where k is selected such that

$$\sum_{\theta_0-90^\circ}^{\theta_0+90^\circ} f_s(\theta) = 1$$

where θ_0 is the main wave heading, and θ is the relative spreading around the main wave heading.

3.15.2.2 Nominal Design Loads. The still water bending moments and shear forces at each section along the ship length are recommended to be calculated according to actual loading conditions specified in IACS Unified Requirement UR S-11 (2001). The nominal design values of wave-induced vertical bending moments and shear forces are also specified in IACS UR S-11, and are shown in Section 2.3.1.1. Bulk carriers have additional design loading condition requirements affecting hull girder strength. With regard to cargo carrying capabilities, bulk carriers are to comply with UR S-25 (2004), which specifies certain unified design loading conditions

if the bulk carrier is designed to carry dry bulk cargoes of cargo densities 1.0 ton/m³ and greater, or if it carries cargoes less than densities of 1.0 ton/m³. Also, conditions are specified for homogeneous cargo loaded condition, specified holds empty, and for normal and heavy ballast conditions. Bulk carriers are also to comply with IACS UR S-17 (2004) for the hold flooded condition.

For load components not covered by the IACS common rules for tanker and bulk carriers or IACS Unified Requirements, the nominal design values are generally determined from the long-term extreme value approach, as outlined in Sections 2.3 and 2.7.

3.15.2.3 Combined Load Cases for Strength Assessment. To assess the strength of the hull girder and individual structural members, finite element structural analysis of hull structures, as part of the design evaluation process, is performed. The analysis is performed for load cases selected for different ship types, and for possible variations of loading patterns such as those shown in Fig. 78 for a VLCC, environmental conditions, dynamic responses, hold or tank configurations, and phase relationship of various load components. Each of the load cases is associated with specified loading patterns of the cargo holds, draft of the vessel, and dynamic wave condition.

Each of the load cases defines a specific dynamic load component that is maximized. The magnitudes of the dominant load components are equal to their nominal design values, whereas the magnitudes of associated corresponding load components are calculated taking into consideration of their phase relations with the dominant component. The main consideration in selecting the load combination and load pattern of each of the load cases

Table 2—Dynamic load combination factors for tankers (IACS CSR 2006).

Wave direction			Head sea				Beam sea		Oblique sea	
			M_{wv} (Sag)	M_{wv} (Hog)	Q_{wv} (Sag)	Q_{wv} (Hog)	α_v		M_{wv-h} (Hogging)	
Dynamic Load Case			1	2	3	4	5a	5b	6a	6b
Global loads	M_{wv}	f_{mv}	-1.0	1.0	-1.0	1.0	0.0	0.0	0.4	0.4
	Q_{wv}	f_{qv}	1.0	-1.0	1.0	-1.0	0.0	0.0	0.0	0.0
	M_{wv-h}	f_{mh}	0.0	0.0	0.0	0.0	0.0	0.0	1.0	-1.0
Accelerations	a_v	f_v	0.5	-0.5	0.3	-0.3	1.0	1.0	-0.1	-0.1
	a_t	f_t	0.0	0.0	0.0	0.0	-0.6	0.6	0.0	0.0
	a_{ng}	f_{ng}	-0.6	0.6	-0.6	0.6	-0.5	-0.5	0.5	0.5
Dynamic wave pressure for port side	P_{WL}	f_{WL}	-0.3	0.3	0.1	-0.1	1.0	0.4	0.6	0.0
	P_{bilge}	f_{bilge}	-0.3	0.3	0.1	-0.1	1.0	0.4	0.4	0.0
	P_{ctr}	f_{ctr}	-0.7	0.7	0.3	-0.3	0.9	0.9	0.5	0.5
Dynamic wave pressure for starboard side	P_{WL}	f_{WL}	-0.3	0.3	0.1	-0.1	0.4	1.0	0.0	0.6
	P_{bilge}	f_{bilge}	-0.3	0.3	0.1	-0.1	0.4	1.0	0.0	0.4
	F_{ctr}	f_{ctr}	-0.7	0.7	0.3	-0.3	0.9	0.9	0.5	0.5

Where:

f dynamic load combination factors

is to maximize the local load effects for the design and assessment of selected critical structural members. A table of representative LCFs for tankers is given in Table 2. The LCFs are applied in combination with the static load patterns, as shown in Fig. 78.

The LCFs are used to combine the various load components. The loads are combined into sets, wherein each set or load case represents a scenario dominated by one selected load component at its maximum value. The rest of the load components are the possible corresponding values derived by applying the LCFs to each of the other associated load values. The dynamic load parameters, such as hull girder bending, external pressure, or internal pressure at a specific location, are each maximized in turn to impose corresponding static and dynamic loads on the various structural members. This approach provides the set of design loads that correspond to an equivalent design wave. The maximum dynamic load parameter value is based on the assumption that the maximum long-term value of the parameter is approximated by its maximum short-term value in the worst short-term conditions, and therefore an equivalent sinusoidal wave (in time and space) can also be defined that, when applied to the ship hydrodynamic model, will produce a sinusoidal load parameter having an amplitude equal to the long-term load parameter. Thus, each load set represents the ship poised (in time and space) in an equivalent wave with a specific load parameter being at its maximum or design value, and the other load parameters calculated also acting on the ship.

3.15.3 Structural Requirements. Hull girder and structural component strength requirements addressed in this section are established using the nominal design

loads described in the previous sections. Scantlings determined based on such criteria are considered as the initial minimum design values, and are required to be verified by the finite element stress analysis against the failure modes of yielding, buckling/ultimate strength, and fatigue to ensure structural integrity. The stress analyses provide not only an added degree of assurance on the vessel's safety but also useful insight that may help to monitor the condition of the as-built structure. Criteria for failure mode verification are summarized in Section 3.15.4, and the stress analysis procedure employing the finite element structural models is described in Section 3.16.

The structural requirements cover global hull girder strength, primary support members, and local structural members. The requirements employ easily understood transparent engineering principles along with the net thickness and load applications as previously summarized, with associated acceptance criteria. The acceptance criteria are defined in association with the load set applied and the failure mode being checked.

3.15.3.1 Hull Girder Bending and Shear Strength. All major classification societies are in compliance with IACS longitudinal hull girder strength standards (IACS UR S-11, 2001), where the longitudinal hull girder strength is specified in terms of section modulus of gross scantlings, SM , as

$$SM = (M_{sw} + M_w)/f_p, \text{ in cm}^2\text{-m} \quad (210)$$

where the still water bending moment, M_{sw} , and vertical wave induced bending moment, M_w , are defined in

Section 2.3.1.1, the permissible bending stress, f_p , is taken as 17.5 kN/cm² for ordinary hull structural steel, and the section modulus determined by equation (210) is in no case less than the minimum required gross scantling section modulus, SM_{min} , defined in UR S-7 (1989) as follows:

$$SM_{min} = 0.01C_1L^2B(C_b + 0.7), \text{ in cm}^2\text{-m} \quad (211)$$

where C_1 is the wave coefficient, defined in Section 2.3.1.2. L , B , and C_b are respectively the length, beam, and block coefficient of the vessel. IACS shearing strength requirements are determined based on vertical shearing forces, F_w , shown in Section 2.3, and the permissible shear stress of 11 kN/cm² for the structures in gross scantling.

Besides the vertical hull girder strength required by IACS, load effects such as horizontal bending, shearing, and torsion that are traditionally considered secondary in conventional rule formulations are also considered. Transverse bending moments and shear forces, and torsional moments described in Section 2.3, are those developed in the ABS Rules, and are given equal treatment as the primary vertical bending.

3.15.3.2 Primary Support Members. Prescriptive requirements are included for the double bottom and double side structure, longitudinal bulkhead vertical web frames, deck transverse web frames, cross ties, and bulkhead stringers. Loading tank patterns and load combinations for these members are specified so that the resulting loads are maximized to check relevant failure modes using load-based engineering formulations. General examples of the load-based requirements for tankers are shown in equations (212a) and (212b) for bending and shear, respectively. These requirements contain load, bending, or shear equations and allowable stress components. Representative web frame configurations are shown in Fig. 80, which illustrates some of the formula parameters. Additional minimum prescriptive depth, thickness, and stiffened panel ratio criteria are applied to control overall deflections and minimum robustness factors, and provide a first review of panel buckling and flange stability.

The primary support members are later checked using the required direct strength finite element analysis. The finite element analysis is better able to calculate the interaction of the structural members such as the hull girder, grillage effects and shear lag which cannot always be fully accounted for in the load-based prescriptive requirements. The load-based prescriptive requirements are typically more conservative than the finite element results so that in areas where finite element analysis is not performed, the prescriptive requirements satisfactorily provide necessary strength. However, in areas where finite element analysis is per-

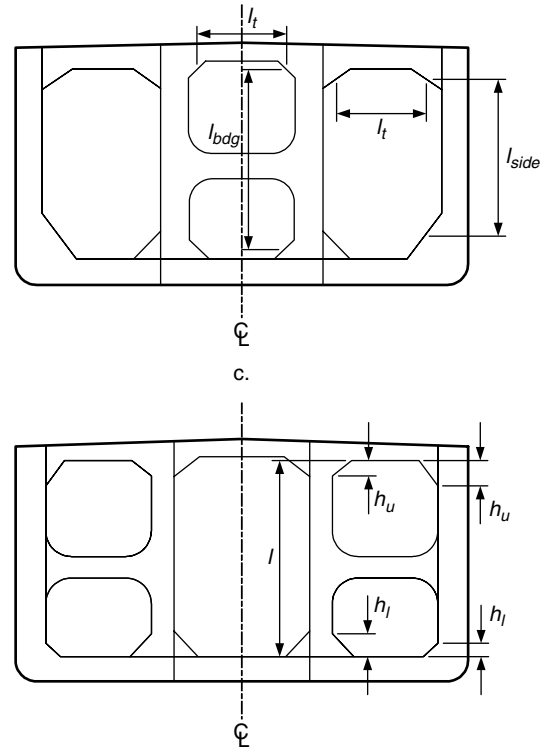


Fig. 80 Sample primary support member requirement.

formed in accordance with the common tanker rules, a 15-percent reduction below the load-based prescriptive requirements is permitted subject to acceptable associated results and analysis of the prescribed finite element analysis:

$$Z = \frac{1000M}{C_{s-pr}\sigma_{yd}} \text{cm}^3 \quad (212a)$$

where

- M = design bending moment, in kN-m
 $= cPSl_{bdg-vw}^2$
- P = design pressure for the Design Load Set being considered, in kN/m²
- l_{bdg-vw} = effective bending span, in m
- S = primary support member spacing of vertical web frames, in m
- C_{s-pr} = permissible bending stress coefficient
- σ_{yd} = specified minimum yield stress of the material, in N/mm²
- c = coefficient for structural configuration

$$A_{shr} = \frac{10Q}{C_{t-pr}\tau_{yd}} \text{cm}^2 \quad (212b)$$

where

- Q = design shear force, in kN
 $= S[c_u l_{vw}(P_u + P_l) - h_u P_u]$
 P_u = design pressure for the Design Load Set being considered, calculated at the mid-height of upper bracket of the vertical web frame, h_u , located at the mid-tank, in kN/m²
 P_l = design pressure for the Design Load Set being considered, calculated at the mid-height of lower bracket of the vertical web frame, h_l , located at the mid-tank, in kN/m²
 l_{vw} = length of the vertical web frame, in m
 S = primary support member spacing of vertical web frames, in m
 h_u = effective shear length of upper bracket of the vertical web frame, in m
 h_l = effective shear length of lower bracket of the vertical web frame, in m
 c_u = coefficient for structural configuration
 C_{t-pr} = permissible shear stress coefficient
 $\tau_{yd} = \frac{\sigma_{yd}}{\sqrt{3}}$, N/mm²
 σ_{yd} = specified minimum yield stress of the material, in N/mm²

3.15.3.3 Local Support Member. Prescriptive requirements are included for the hull envelope, inner hull, deck, and transverse and longitudinal bulkheads. The loads used for the evaluation of tank boundaries are based on the maximum possible loading assessed with a full tank on one side and an empty tank on the other side. The full and empty tanks are then reversed to reflect the opposite situation so that both load scenarios are considered. Similarly, the shell envelope is assessed for maximum external pressure at the deepest draft without internal counteracting loads, and then the opposite situation is evaluated so that the full tank is applied in association with the lightest draft. Relevant failure modes using load-based engineering formulations are applied to the plating and stiffening. The stiffener requirements also include detail checks of the end connection that take into account whether collar plates and web stiffeners are provided.

The local members are later checked for in-plane stress criteria using the required direct strength finite element analysis. The finite element analysis is better able to calculate the interaction of the structural members and their local influence on the local structural members such as the shell, inner hull, and transverse and bulkhead plating, which cannot always be fully accounted for in the load-based prescriptive requirements. This evaluation covers local yielding and buckling/ultimate strength considerations.

The local support members also include the requirements for evaluation of corrugated bulkhead stiffness and local plate, as well as the corrugated bulkhead stool structure. Additional minimum prescriptive thickness,

panel ratios, stiffener web and flange ratios, and other local minimum criteria are applied to control overall minimum robustness factors and provide a first review of panel buckling and stiffener stability.

3.15.3.4 Forward-Most and Aft-Most Tank Structural Members. These members are evaluated using the prescribed procedures for tapering the longitudinal strength members, as well as using the prescribed methods for local evaluation. A general procedure to apply the midship finite element analysis results to the tanks outside of the 0.4 length amidships is also included.

3.15.3.5 Forward, Machinery, and Aft Structural Members. These members are evaluated using the included detailed requirements. The forward structure is evaluated for bottom slamming and bow impact considerations, which take into account the various operating drafts and tank filling operations. In addition to the scantling requirements mentioned previously, general requirements such as welding, materials, closing appliances, superstructure, mooring and anchoring equipment are also included in the common tanker rules.

3.15.4 Strength Assessment. Strength assessment is an integral part of the design process. The assessment is performed using the stress results obtained from the structural analyses of the hull structure for the load cases described in Section 3.15.2, which are used to verify the suitability of the initial design established based on the strength assessment against the specified acceptance criteria. The probable failure modes of the hull structure relevant to the vessel type considered are yielding, buckling, fatigue, and ultimate hull girder strength. These identified failure modes encompass a wide spectrum of failure scenarios spanning global failure to local failures, and local failures that may develop into catastrophic global failure. Criteria for the flooded condition, which is a consideration of structural survivability for bulk carriers, are also assessed for hull girder strength.

3.15.4.1 Finite Element Analysis. Classification rules require an assessment of the hull structure using finite element analysis. As mentioned previously, the objective of the structural assessment is to verify that the stress levels, deflection, and buckling capability of the primary support members and hull structure are within acceptable limits associated with the applied static and dynamic loads. In addition, the fatigue strength of selected structural details also must be verified. A flow chart showing the general evaluation scheme of the finite element analysis for tankers is shown in Fig. 81. The analysis procedure for bulk carriers is similar.

The structural assessment is based on a three-dimensional finite element analysis in accordance with the detailed procedure included in the rules. The analysis procedure covers all aspects of the modeling details, loads, and boundary conditions to be applied, and acceptance criteria used to determine whether the structure arrangements and scantlings are within compliance. Also included in the rules is the procedure for local fine mesh and very fine mesh analysis to evaluate local high-stress

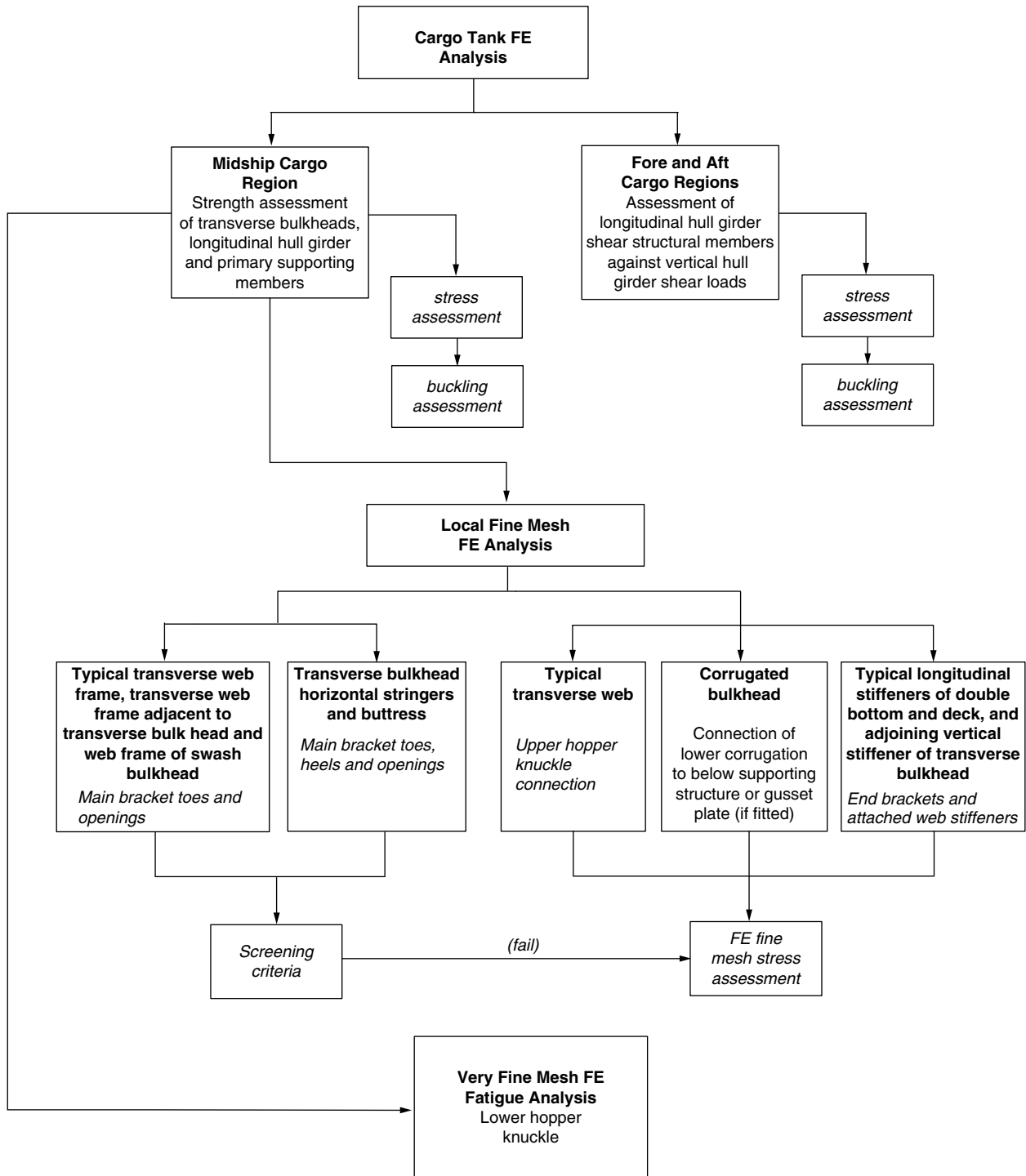


Fig. 81 Flow chart of finite element analysis procedure for oil tanker (IACS CSR 2006).

areas and details to ensure that the acceptance criteria is satisfied in these areas.

The rules specify the extent of the global finite element model, three tank or hold lengths, mesh density, and net thickness to use in the analysis. Figure 82 shows

examples of two global finite element models of a double hull tanker. The extent of fine mesh modeling and associated mesh density and net thicknesses are also included in the rules. Figure 83 shows an example of the fine mesh model with very fine mesh areas imbedded

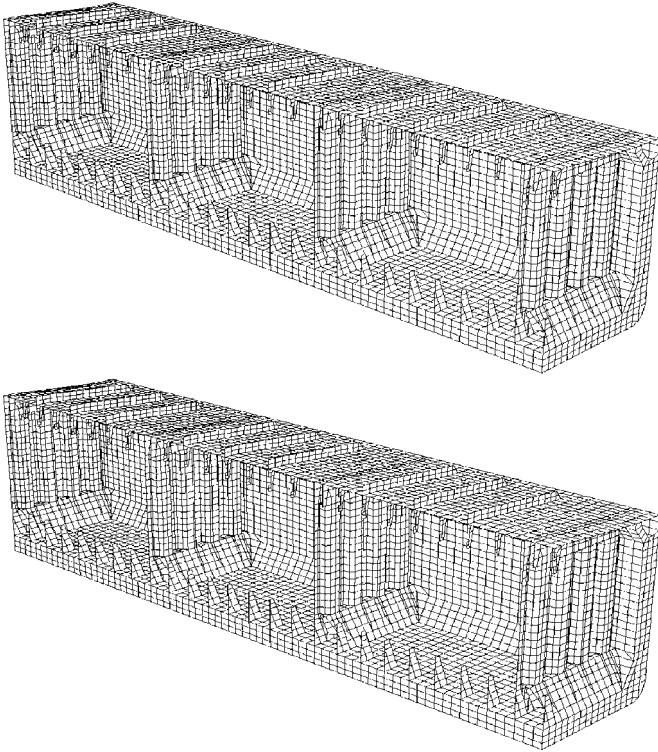


Fig. 82 Global finite element tanker models (IACS CSR 2006).

within the model. Figure 84 shows a global finite element model of three cargo holds of a single side bulk carrier. Figure 85 shows an example of very fine mesh areas imbedded within the model. The rules include full details of the acceptance criteria to apply to each structural member type, rule load condition, and analysis model employed.

For tankers, the acceptance criteria for rule requirements and finite element analysis are categorized into three sets shown in Tables 3 and 4. The acceptance criteria set AC1 is applied when the combined characteristic

loads are frequently occurring on a regular basis, typically for the static design load combinations, but also applied for the sloshing design loads. The acceptance criteria set AC2 is typically applied when the combined characteristic loads are extreme values (e.g., typically for the static plus dynamic design load combinations). The acceptance criteria set AC3 is typically applied for capacity formulations based on plastic collapse models such as those applied to bottom slamming and bow impact loads.

3.15.4.2 Hull Girder Ultimate Strength. The common structural rules include a hull girder ultimate strength criteria where the partial safety factor method is applied. The partial safety factor format is applied for this highly critical failure mode to better account for uncertainties related to static loads, dynamic loads, and capacity formulations. The criteria are applicable to ship conditions at net scantlings plus a 50 percent corrosion margin. For bulk carriers, the bending moments M_{sw} and M_w in sagging and hogging conditions for intact, flooded, and harbor conditions are considered in the ultimate strength check. Because the sagging condition is the limiting critical ultimate strength condition for double hull tankers, the tanker rules cover the sagging case for intact at sea conditions only. The vertical hull girder ultimate capacity is to satisfy the criteria in equation (213). The ultimate bending moment capacities of a hull girder transverse section, in hogging and sagging conditions, are defined as the maximum values of the curve of bending moment capacity M_U versus the curvature χ of the transverse section considered—for example, see Figs. 127 and 128. The curve M - χ can be obtained through an incremental-iterative procedure as described in the rules, or by advanced nonlinear finite element methods. Partial safety factors in equation (213) are given for two different design load combinations (a) and (b). Both design load combinations are to be satisfied for tankers, whereas only design load combination (a) is to be satisfied for bulk carriers. Note that the definition of M_{sw} is different for each combination.

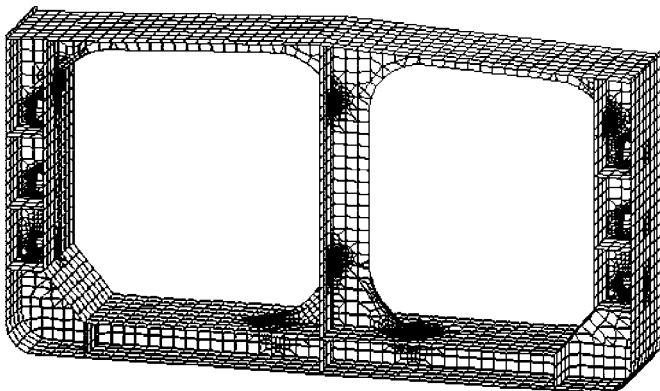


Fig. 83 Local fine mesh finite element tanker model.

$$\gamma_S M_{sw} + \gamma_W M_{ww} \leq \frac{M_U}{\gamma_R} \quad (213)$$

where

M_{sw} = still water bending moment at the hull transverse section considered, in kN-m

M_{ww} = vertical wave bending moment at the hull transverse section considered, in kN-m

M_U = vertical hull girder ultimate bending capacity at the hull transverse section considered, in kN-m

γ_S = partial safety factor for the still water bending moment

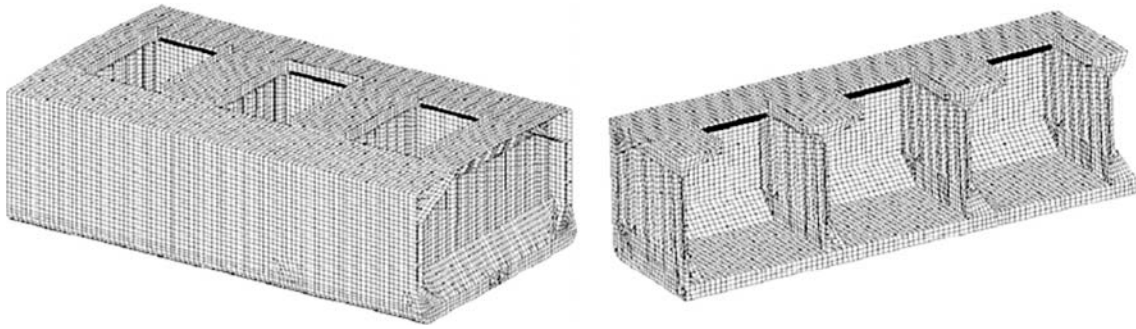
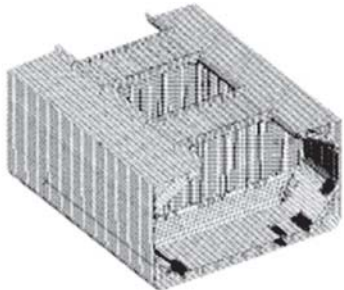


Fig. 84 Global finite element bulk carrier model (IACS CSR 2006).

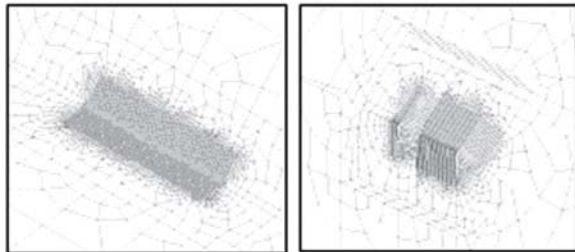
γ_W = partial safety factor for the vertical wave bending moment covering environmental and wave load prediction uncertainties
 γ_R = partial safety factor for the sagging vertical hull girder bending capacity covering material, geometric, and strength prediction uncertainties

Design Load Combination	Definition of Still Water Bending Moment, M_{sw}	Partial Safety Factors		
		γ_S	γ_W	γ_R
(a)	Permissible still water bending moment, $M_{sw-perm}$, in kN-m	1.0	1.2	1.1
(b)	Maximum sagging still water bending moment for operational seagoing homogenous full load condition, $M_{sw-full}$, in kNm*	1.0	1.3	1.1

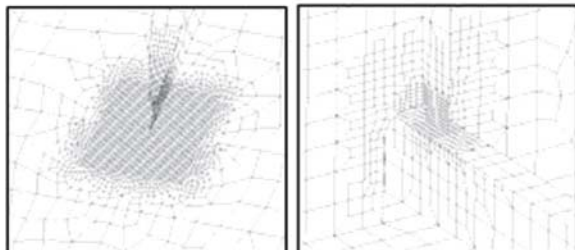
* The maximum sagging still water bending moment is to be taken from the departure condition with the ship homogeneously loaded at maximum draught and corresponding arrival and any mid-voyage conditions.



(a) Part of global cargo hold model with very fine mesh



(b) Edge bopper knuckle part



(c) End of hold frame

(d) Longitudinal

Fig. 85 Local fine mesh finite element bulk carrier models (IACS CSR 2006).

3.15.4.3 Fatigue Strength. The general aim of the fatigue control included in the rules is to ensure that the hull structure, subjected to fatigue (cyclic) loading, has an adequate fatigue life for the duration of the vessel design life. The procedure provides a designer-oriented approach to fatigue strength assessment that may be used for certain structural details in lieu of more elaborate methods, such as spectral fatigue analysis. The term “simplified approach” is used here to distinguish this approach from the more elaborate analysis.

The criteria in the rules were developed from various sources, such as the Palmgren-Miner linear damage model, S-N curve methodologies, and a long-term environment data of the North Atlantic Ocean (IACS Wave Data), and it assumes workmanship of commercial marine quality acceptable to the class surveyor. The capacity of structures to resist fatigue is given in terms of fatigue damage control to allow designers the maximum flexibility possible.

The procedure is specifically written to evaluate fatigue strength of tanker or bulk carrier structural details at welded connections based on a simplified fatigue assessment procedure. The assessment is applicable to the evaluation of longitudinal end connections using a beam theory-based nominal stress approach, and to other critical details, such as the bilge hopper corner, using a finite

Table 3—Rule requirement acceptance criteria.

Principal Acceptance Criteria—Rule Requirements

Set	<i>Plate Panels and Local Support Members</i>		<i>Primary Support Members</i>		<i>Hull girder Members</i>	
	<i>Yield</i>	<i>Buckling</i>	<i>Yield</i>	<i>Buckling</i>	<i>Yield</i>	<i>Buckling</i>
AC1	70–80% of yield stress	Control of stiffness and proportions; usage factor typically 0.8	70–75% of yield stress	Control of stiffness and proportions; pillar buckling	75% of yield stress	NA
AC2	90–100% of yield stress	Control of stiffness and proportions; usage factor typically 1.0	85% of yield stress	Control of stiffness and proportions; pillar buckling	90–100% of yield stress	Usage factor typically 0.9
AC3	Plastic criteria	Control of stiffness and proportions	Plastic criteria	Control of stiffness and proportions	NA	NA

element modeling-based hot spot stress or notch stress approach.

The main assumptions employed are listed here:

- A linear cumulative damage model (i.e., Palmgren-Miner's rule) has been used in connection with the S-N data.
- Cyclic stresses due to the loads have been used, and include the effects of mean stress.
- The minimum design life of the vessel is taken to be 25 years.
- The environmental data for the North Atlantic is used.
- The long-term stress ranges of a structural detail can be characterized using a modified Weibull probability distribution parameter (ξ). Weibull shape parameters are provided in the classification rules for various ship types and different structural details.
- Structural details are idealized and applied fatigue class is provided in the procedure.
- For longitudinal stiffener end connections, simple nominal stresses obtained by empirical formula and rule-based loads form the basis of nominal stress based fatigue assessment.

The structural detail classification in the rules is based on joint geometry under simplified loadings. Samples

of the fatigue joint types and associated fatigue class are included in Fig. 86. Where the loading or geometry is too complex for a simple classification, a finite element analysis of the detail is carried out to determine the fatigue stress of that detail. The tanker rules consider hot-spot stress range in assessing fatigue strength, whereas the bulk carrier rules use equivalent notch stress range. Guidance on the finite element analysis required to determine hot-spot stress and notch stress for weld toe locations that are typically found at longitudinal stiffener end connections are included in the procedure.

The rules also permit the optional use of more detailed spectral fatigue evaluation to assess fatigue; however, this more refined analysis may not be used to reduce the requirements of the prescriptive requirements.

3.15.4.3.1 Simplified Method for Fatigue Strength Assessment. The simplified fatigue assessment method is the first level of fatigue strength assessment for welded joints and details. It uses a linear, cumulative damage model in accordance with the Palmgren-Miner rule. It postulates the acceptable fatigue damage ratio, D , is less than 1. That is,

$$D = \sum_i \frac{n_i}{N_i} \quad (214)$$

Table 4—Finite element analysis acceptance criteria.

Principal Acceptance Criteria—Design Verification, Finite Element Analysis

Set	<i>Global Cargo Tank Analysis</i>		<i>Local Fine Mesh Analysis</i>
	<i>Yield</i>	<i>Buckling</i>	<i>Yield</i>
AC1	60–80% of yield stress	Control of stiffness and proportions; usage factor typically 0.8	Local mesh as 136% of yield stress; averaged stresses as global analysis
AC2	80–100% of yield stress	Control of stiffness and proportions; usage factor typically 1.0	Local mesh as 170% of yield stress; averaged stresses as global analysis

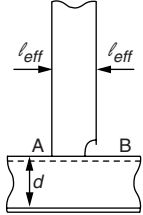
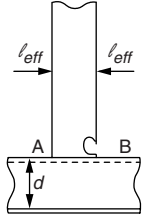
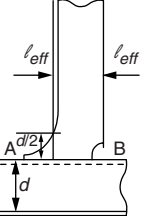
ID	Connection type	Critical Locations	
		A	B
1		F2	F2
2		F2	F2
3		F	F2

Fig. 86 Fatigue joint classification (IACS CSR 2006).

where n_i = the number of cycles of stress of level s_i during the period of exposure, N_i is the number of cycles of a sinusoidally varying stress of amplitude s_i required to cause failure, and the summation is taken over all levels of stress experienced during the period of time under consideration. Failure of the structure is then presumed to occur when the length of exposure is sufficient for this sum to equal to 1.

3.15.4.3.2 Closed-Form Expression of Cumulative Fatigue Damage. The closed-form expression of cumulative fatigue damage (see Chen & Mavrakis 1988) is derived based on Miner's cumulative damage law for associated specific class S-N data, with the assumption that the long-term fatigue load spectrum (i.e., long-term distribution of stress range) follows a two-parameter Weibull probability distribution. The closed form expression is

$$D = \frac{N_L}{K} \frac{S_R^m}{(\ln N_L)^{m/\xi}} \mu \Gamma \left(1 + \frac{m}{\xi} \right) \quad (215)$$

and

$$\mu = 1 - \left\{ \gamma \left(1 + \frac{m}{\xi}, v \right) - v^{-\Delta m/\xi} \gamma \left(1 + \frac{m + \Delta m}{\xi}, v \right) \right\} / \Gamma \left(1 + \frac{m}{\xi} \right) \quad (216)$$

where

- D = cumulative fatigue damage
- $N_L = fT$, total number of cycles in life time
- f = life time average of the response zero crossing frequency
- T = base time period (usually taken as the design life of the structures), sec
- S_R = long-term stress range as the most probable value in time T
- m, K = parameters of the upper leg of the S-N curve, given in equation (217)
- μ = endurance factor, to account for the Haibach effect of a piecewise linear S-N curve
- ξ = Weibull shape parameter of stress range
- $v = (S_q/S_R)^\xi \ln(N_L)$
- S_q = stress range at intersection of upper and lower legs in the S-N curve
- Δm = slope change of S-N curve at intersection point q
- $\gamma(a, x)$ = incomplete gamma function, Legendre form
- $\Gamma(a)$ = gamma function

Equation (215) indicates that cumulative fatigue damage, D , the Weibull shape parameter, ξ , and the long-term stress range, S_R , are inter-related for a specific S-N curve. For a given set of S_R , ξ , and S-N curve, the fatigue damage and thus the fatigue life (equal to T/D) can be readily computed using equation (215). Thus, for a given target design life the fatigue damage estimate using equations (214) rests on realistic representations of the expected maximum nominal stress ranges, the fatigue classification (S-N curve), and the Weibull shape parameter for the structural detail in question. For fatigue strength assessment of ocean-going ships for unrestricted service, the target design life is normally taken as 25 years, corresponding to a total number of stress cycles between 0.6×10^8 and 0.8×10^8 .

3.15.4.3.3 U.K. DEN Basic Design S-N Curves. The S-N data base used in conjunction with the simplified method is that published by the U.K. Department of Energy (1990). This S-N data base was chosen due to familiarity and confidence with it from use in offshore and ship classification work for over a long period of time. This data set also appears to be more consistent, offers better coverage of the high cycle (lower stress) regime of interest to ships and offshore structures, are more uniform and offer attractive mathematical convenience, and have broad acceptance worldwide.

U.K. DEN Basic Design S-N Curves shown in Fig. 87 consist of eight curves: B, C, D, E, F, F2, G, and W, and each of them represents a class of welded details, as shown in the ABS Rules (2008) and the IACS Common Structural Rules (2006). All eight curves are composed of two segments of different slopes, connected at N and equal to 10^7 cycles, with a linear relationship between

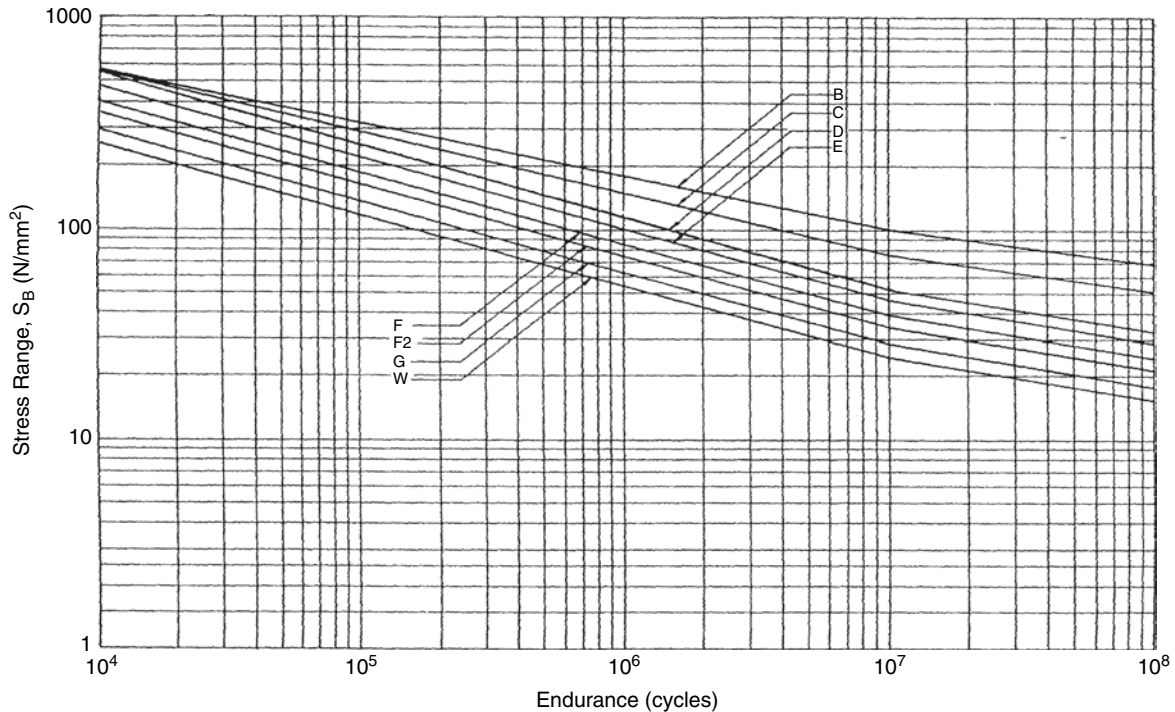


Fig. 87 U.K. DEN basic design S-N curves for non-nodal joints.

$\log(S)$ and $\log(N)$:

$$\log(N) = \log(K) - m \log(S) \quad (217)$$

or

$$N = K(S^{-m})$$

where

$$\log(K) = \log(K_1) - 2\sigma$$

S = stress range

N = number of cycles to failure under stress range S

K_1 = constant relating to the mean S-N curve

σ = standard deviation of $\log(N)$

m = inverse slope of S-N curve

3.15.4.3.4 Weibull Shape Parameter. The Weibull shape parameter, ξ , defines the shape of the long-term stress range distribution. The shape parameters need to be obtained by calibration with a spectral fatigue approach. In principle, any equivalent damage parameter so determined is a function of all of the factors that enter into a spectral fatigue approach. Analyses showed that by far the strongest effects appear to be the severity of the wave environment, the geometry and scantling of the structural detail itself, the location of the detail, and the type of vessel. Traditionally, when no other information is available, a Weibull shape parameter value of 1.0 has been conventionally used for ship structure evaluation. In this case, the distribution is an exponential function.

3.16 Finite Element Analysis of Ship Structures. Since its development in the 1960s, the successful application of the finite element method (FEM) in stress analysis is widely recognized as a significant contribution to structural engineering. In the marine industry, the use of finite element computer programs is commonplace for analyzing ship structures and offshore platforms. The FEM was first developed in the civil and aerospace industries to deal with simple linear structural problems. Beginning with an almost intuitive formulation, the FEM has evolved to where now its mathematical foundations are rigorously established. It has been proven that the FEM can be derived from variational methods, thereby providing a powerful tool for solving a broad range of problems in mathematical physics such as heat transfer, fluid flow, electromagnetic waves, and magneto-hydrodynamics. By analogy with discrete problems of structural analysis, a considerable degree of insight into finite element process to nonstructural applications can be made.

This section considers the application of the FEM for the structural analysis related to the design and strength evaluation of ship structures. The basic mathematical foundations of the FEM, which can be found in numerous textbooks such as Zienkiewicz (1971), Gallagher (1975), and Bathe and Wilson (1976), is not the subject of this section. Applications of FEM considered in this section are the “design by analysis” approach, which is a comprehensive integrated ship motions and finite element structural analysis approach to evaluating ship structures.

3.16.1 Design by Analysis. The “design by analysis” is an engineering analysis procedure where the combination of dynamic load components is used in investigating the structural responses of a particular vessel. The essential feature of this procedure, which is also true in the dynamic load approach (DLA), is that the initial design of the structure—which is subsequently proven by structural analysis—must fully meet the scantling requirements of the classification rules. Where the results of the structural analysis indicate a reduction below the rule-based values could be allowed, this will not be permitted under DLA. In this way, the results of DLA are intentionally biased to produce a stronger or more robust structure than indicated by analysis, and a minimum standard reflecting past successful experience is maintained.

DLA is built around a full ship finite element analysis integrated with ship motion analyses stemming from the well-established two- or three-dimensional linear ship motion theory and the linear elastic finite element analysis. The former aspect makes it possible to apply the spectral analysis to determine the extreme values through order statistics, eventually leading to the so-called equivalent wave system. As to the latter aspect, the use of linear elastic theory is justifiable, as the structural responses of hull structures are generally required within the linear elastic range. The underlining concepts and some of the key points of DLA procedure are described in the following sections, whereas the details can be found in Liu et al. (1992).

3.16.1.1 Loading for Structural Analysis. The most conceptually challenging and unique feature of DLA analysis is the subject of loads, which consist of the establishments of load cases, dynamic load parameters, equivalent wave system, and simultaneous load components for structural analysis.

The basic feature concerns the creation of each structural load case used in the analysis. A structural load case considered for analysis comprises combinations of a dominant load component and the other significant load components that are considered to be accompanying the dominant load component. Each structural load case contains the load components accompanying the dominant load component and a dominant load component that is characterized by a defining parameter, referred to as the *dominant load parameter* (DLP) which is also described in Section 2.3.

A load component consists of dynamic and static parts. For example, the load component, “external fluid pressure on the ship’s hull in the presence of waves,” has a hydrostatic component that combines with a dynamically considered pressure component. The determination of the static part of the load component is basic. The dynamically considered part reflects the wave-induced motion effects, which are the product of an inertial portion of the load and a portion representing the motion-induced displacement of the load relative to the structure’s axis system.

Examples of DLPs are “vertical hull girder sagging and hogging bending moments amidships,” “vertical and lateral accelerations at the vessel’s forepeak frame,” and “maximum roll angle.” For container ships, additional DLPs would include “horizontal bending moment” and “torsional moment.” The other significant load components accompanying the dominant load component in a structural load case include internal loads and external fluid pressures, and lightship weights including structural self-weight.

The combination of the load components composing a structural load case is done through a process where each dominant load is analyzed to establish its peak *frequency response function* (FRF) value or response amplitude operator. Using a combination of ship motion analysis involving ocean wave spectra and extreme value analysis of the DLP, an equivalent sinusoidal wave is derived. The wave (defined by wave amplitude, frequency, heading, and phase angle with respect to a selected reference location) is considered equivalent in the sense that when it is imposed on the structural model, it simulates the extreme value of the DLP.

From the FRFs of the dynamic portions of the other load components and the equivalent wave derived for the DLP, the magnitude and spatial distributions of the other load components accompanying the dominant load component are obtained.

3.16.1.2 Structural Load Cases. The ensemble of load cases for structural analysis is established considering a variety of “cargo loading conditions.” The full load, light draft ballast, and several partial cargo load conditions in between these extremes are usually considered. For example, five cargo loading conditions—including the homogeneous full load, normal ballast load, 33 percent partial load, 50 percent partial load, and 67 percent partial load conditions—are considered for the sample tanker by Liu et al. (1992).

The load cases used in the analysis also consider a DLP that is a global load effect, such as a global motion of the vessel, or a local dynamic response, such as an individual acceleration component of the fluid cargo at a representative tank boundary. Typical DLPs are the vertical and lateral bending moments and shear forces, torsional moments, vertical and lateral accelerations, and rolling motions. DLP is maximized to establish a critical structural load case to be employed in hull structural analysis, aiming to obtain the maximum responses of the structural components corresponding to the particular DLP in question. Because the relation between the maximized DLPs and the maximum structural responses are not obvious, a large number of structural load cases must be considered to obtain the maximum responses of various structural components, which are deemed to be critical. Considering again the sample tanker in Liu et al., (1992), DLPs addressed are the vertical bending moment (VBM), vertical acceleration (Vacc), lateral acceleration (Lacc), and roll. A total of 66 structural load cases shown in Table 5 are considered as being representative of the

Table 5—Representative Structural Load Case Matrix (Liu et al. 1992).

Structures	Cargo load condition	homogeneous full load design draft –A–	normal ballast load light draft –B–	partial load (33% full) –C–	partial load (50% full) –D–	partial load (67% full) –E–
Deck	plating, longit'l, girder	1a	–	–	–	1a
Botton	plating, longit'l, girder	1b, 2a, 2c, 4a	1b, 2a, 2c, 4a	2a	2c	1b, 2a, 2c
Bulkheads	longitudinal (midship)	1a, 1b	–	–	4a	1a, 1b
	transverse (midship)	4a, 4b	4a, 4b	–	–	4a, 4b
	stringer (midship)	2b, 2d	4a, 4b	4a	4b	2b, 2d
Side Shell	pltg, lngtl, fr (midship)	4a, 4b	4a, 4b	4b	–	4a, 4b
	pltg, lngtl, fr (fwd hold)	3a, 3b	3a	3b	–	3a, 3b
	pltg, lngtl, fr (aft hold)	3a, 3b	3a	–	3a, 3b	3a, 3b
Web Frames		4a, 4b, 2b, 2d	4a, db	–	4a, 4b	4a, 4b, 2b, 2d

Structural Load Case ID:

1a – VBM amidships (sagging at Tp and 180 or 0 deg)

1b – VBM amidships (hogging at Tp and 180 or 0 deg.

2a – Vacc (bow up, FP centerline) at Tp, 180 or 135 degs

2b – Vacc (bow up, FP off-centerline) at Tp, 150, 135, 105 or 75 degs.

2c – Vacc (bow down, FP centerline) at Tp and 180 or 135 deg.

2d – Vacc (bow down, FP off-centerline) at Tp and 150, 135, 105 or 75 degs.

3a – Lacc (fwd tank top corner, stdb down) at Tp and 105 or 90 degs.

3b – Lacc (fwd tank top corner, stdb up) at Tp and 105 or 90 degs.

4a – Roll (stdb down) at Tp and 90 or 75 degs.

4b – Roll (stdb up) at Tp and 90 or 75 degs.

Notes:

A) This table provided for illustrative purpose only.

B) Cargo Load Conditions A and B are required for consideration. The other conditions or additional ones may also be required depending on the specifics of a particular design.

C) One or more ship structure members can be examined with a structural load cases.

most severe cases that the ship's structure would have to withstand throughout its service life.

For each of the structural load cases such as those shown in Table 5, the global and local load component distributions are obtained using the so-called equivalent wave system (described in the following section), in such a manner that the instantaneous load distribution would result in the maximized DLP. The load components under consideration include the wave pressure, internal tank pressure, inertial forces, and hull girder loads. The maximized DLP is calculated based on its long-term extreme value, and the instantaneous global and local load components are calculated at the instant of time when the DLP reaches its maximum in the equivalent wave system based on its phase angles.

3.16.1.3 Long-Term Extreme Value for Maximized DLP. The long-term extreme value is chosen as the maximum value of the DLP in question. The extreme values of load components are generally obtained from the long-term extreme value approach, considering a return period of 20 to 25 years of service life with a 10^{-8} probability level, employing linear ship motion theory and the North Atlantic wave data.

Most of the linear ship motion theory procedures are based either on the two-dimensional strip method, similar to those by Raff (1972), Meyers et al. (1975), or

Salvesen et al. (1970), or the three-dimensional potential flow boundary element method such as the PRECAL computer program (CRS 1998). Long-term prediction schemes employed are based on the root mean square (RMS) values, such as Band (1966), Little and Lewis (1971), and Nordenstrom (1963), or based on the extreme values, such as Hoffman and Lewis (1969) and Ochi (1978). In computing the long-term extreme ship response, a reduced ship speed is generally considered. For example, IACS employs a zero forward speed in conjunction with the IACS standard waves. The heading angles are assumed to have an equal probability distribution from 0° to 360° . The linear ship motion theory and the long-term extreme value prediction are considered in greater detail in Section 2.7 of this book. In the standard DLA approach, a three-dimensional potential flow-based diffraction-radiation theory computer program such as PRECAL is used. This program is based on linear wave and motion amplitude assumptions and makes use of boundary element methods with constant-source panels over the entire wetted surface of the hull, on which the hydrodynamic pressures are computed. This requires that the wetted surface of the ship's hull be discretized into a large number of panels. PRECAL is used in combination with wave data representing the average sea condition of the North Atlantic to calculate the

short-term response. The long-term prediction based on the RMS value of the short-term statistics is used for calculating the extreme value (Lewis 1967). Calibrated with extensive measured hull girder strain database (Little & Lewis 1971), this procedure can be used as a yardstick to assess lifetime extreme value of responses.

The long-term prediction by Lewis (1967) is given by the following probability, denoted by $\Pr\{x_0\}$, of the response exceeding the quantity x_0 :

$$\Pr\{x_0\} = \Sigma \Sigma pr_i(\alpha_i) pr_j(W_j) \times \left\{ \int_j^\infty \exp(-x_0^2/E) g(\sqrt{E}|W_j) d\sqrt{E} \right\} \quad (218)$$

where

$pr_i(\alpha_i)$ = probability of the i -th heading angle α_i

$pr_j(W_j)$ = probability of encountering the j -th weather group of the H-family wave data

$E = 2m_0$, if the peak value is a single amplitude

$= 8m_0$, if the peak value is a double amplitude

$g(\sqrt{E}|W_j)$ = conditional probability density function of \sqrt{E} for a given weather group W_j

m_0 = mean square value of response

For short-crested seas, the response mean square value, m_0 , for a given heading, α_i , is described as

$$m_0 = \int_{\omega} \sum_{\alpha_i-90^\circ}^{\alpha_i+90^\circ} f_s(\theta) \times S(\omega|W_j, \alpha_i, \theta) d\omega$$

where the response spectral density function

$$S(\omega|W_j, \alpha_i, \theta) = S_\eta(\omega|W_j) |H(\omega|\alpha_i, \theta)|^2, \quad \text{where } S_\eta(\omega|W_j)$$

is the wave spectrum, and $H(\omega|\alpha_i, \theta)$ is the frequency response function. f_s is the spreading function, which is defined as

$$f_s(\theta) = \frac{2}{\pi} \cos^2(\theta)$$

such that

$$\sum_{\alpha_i-90^\circ}^{\alpha_i+90^\circ} f_s(\theta) = 1$$

where α_i is the main wave heading and θ is the relative spreading around the main wave heading.

The conditional probability density function $g(\sqrt{E}|W_j)$ in equation (218) is expressed by a trun-

cated normal distribution for each weather group,

$$g(\sqrt{E}|W_j) = \frac{1}{\sqrt{2\pi}\sigma_j^2} \exp\left(-\frac{1}{2\sigma_j^2}(\sqrt{E} - \mu_j)^2\right) \quad (219)$$

where μ_j is the mean value of \sqrt{E} in the j -th weather group and σ_j^2 is the variance of \sqrt{E} about μ_j in the j -th weather group.

The probability $\Pr\{x_0\}$ of equation (218) is related to the total number of cycles in which the response or load component is expected to exceed the value x_0 at least once during the vessel's service life. Denoted by $n(x_0)$, the total number of cycles, the relationship between the probability and $n(x_0)$ is:

$$\Pr\{x_0\} = 1/n(x_0) \quad (220)$$

The term $1/n(x_0)$ is often referred to as the probability level, or the total probability of exceeding x_0 . Therefore, using this relation when plotting equation (218), together with a knowledge of the number of cycles per unit time, enables the graph to represent a curve, such as the one shown in Fig. 88. This curve indicates the probable number of times that the random variable x exceeds a specified value x_0 at any time during a lengthy period of ship operation. If the number of cycles, n , of the random variable, x , which is the vertical bending moment in the example shown in the figure, is 10^8 in a 20-year ship service time, then the probability level is 10^{-8} . The vertical bending moment, x_0 , is expected to be exceeded once in a 20-year service time, which can be read from the response curve mentioned previously at the probability level of 10^{-8} . This value is referred to as the *long-term extreme value*. It is noted that the value of x_0 evaluated from equation (220) does not represent a value of x that will exceed exactly once in n cycles of wave encounter during a lengthy period of ship operation, nor does it represent the absolute maximum to be expected to occur. Instead, it represents a value of x that will exceed x_0 once as an average in n cycles.

3.16.1.4 Equivalent Wave Load Prediction. The equivalent wave load prediction procedure is to use an equivalent wave system to recast the result of spectral analysis to a deterministic format more suitable for finite element analysis, while the essence of all the probabilistic implications is retained. The equivalent wave system is a simple wave characterized by its amplitude, length, heading, and its crest position relative to the midship. When the vessel is imposed in such a wave, the resultant load distributions on the hull structure due to wave pressures and inertial loads would result in the DLP in question to reach its maximum value, determined from the long-term extreme value. The equivalent wave load predictions consist of the following three main steps:

- Step 1 Using linear ship motion theory, the FRFs of the DLP in question are calculated. The wave length, wave heading angle, and phase angle associated with the peak value FRF of the

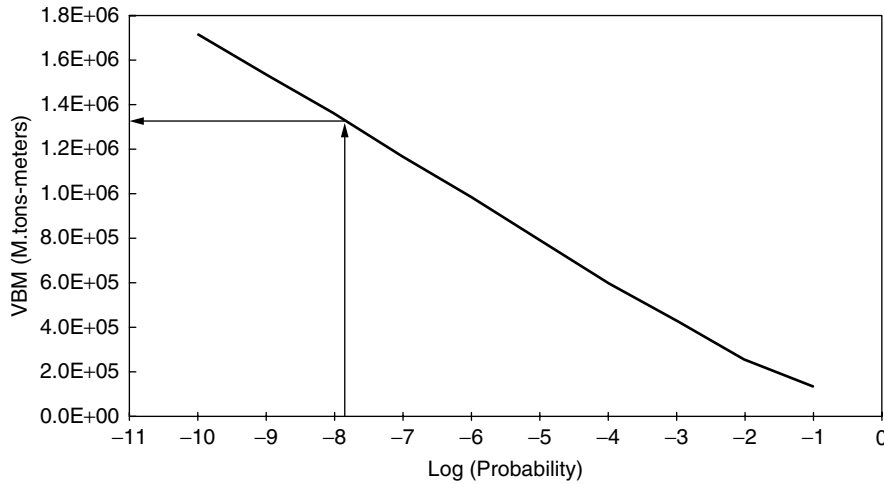


Fig. 88 Long-term extreme value and probability level.

DLP, together with the wave amplitude determined in Step 2, are the characteristics of the equivalent wave system.

- Step 2 The amplitude of the equivalent sinusoidal wave, a_w , is calculated by dividing the DLP long-term extreme value given by equations (218) to (220) by its peak value FRF as follows:

$$a_w = \frac{\text{Long Term Extreme Value}}{\text{Peak Frequency Response Function Value}} \quad (221)$$

- Step 3 With the wave length, wave amplitude, and direction determined from the previous steps, the wave crest position with respect to the longitudinal center of gravity of the vessel, x , for which the DLP reaches its maximum value is calculated by

$$x = \frac{\lambda \varepsilon}{-360 \cos \beta} \quad (222)$$

where

- λ = wave length
- ε = phase angle of the DLP in degrees
- β = wave heading angle

Then the longitudinal distribution of the dynamic load components (i.e., hydrodynamic pressures, internal tank pressure, acceleration induced inertial load, and the hull girder loads for the portion of the vessel being considered) can be calculated by taking into account the phase angle of each of the dynamic load components

$$M_i = A_i a_w \sin(\omega_e t_j + \varepsilon_i) \quad (223)$$

where

- M_i = instantaneous i -th load component in question
- A_i = amplitude of the i -th load component FRF
- a_w = equivalent wave amplitude
- ω_e = encounter frequency
- t_j = time instant when j -th DLP reaches maximum
- ε_i = phase angle of i -th load component FRF

With the equivalent wave system, nonlinear effects of wave loads resulting from bow flare impact and bottom slamming induced whipping bending moments can also be performed.

It is noted that the result from the linear superposition described here is more likely to be acceptable for vessels of large block coefficient, but is often on the conservative side for fine form ships. To avoid this problem, the time domain simulation using three-dimensional nonlinear theory may be performed in the equivalent wave system or in a critical wave episode. Alternatively, a semi-empirical method based on an ensemble of pseudo transfer functions from nonlinear theory can be used in lieu of the linear response function for the long-term prediction. As indicated in Section 2.5.3, the nonlinear theory approach requires further validation and improvement before it can be considered as a practical design tool. Because of this, the linear ship motion theory and the linear superposition approach are still relied upon by the industry, with the understanding that the load and strength requirements obtained based on a linear system be viewed as criteria that are "notional."

3.16.2 Finite Element Structural Modeling. The first step of the finite element modeling is to reduce a structure to a mathematical model by discretizing the physical continuum into an assemblage of finite elements

interconnected at discrete points. The formulation of such a model, termed *structural idealization* or *structural model*, permits the structure to be represented by a system of finite number of degrees of freedom, upon which matrix operations on the equilibrium equations of the element assemblage can be performed. For some types of structures such as truss or frame structures, this modeling leads to an exact representation of the actual structure system. However, for continuum structures this formulation only provides an approximate representation. In the case of ship structures, a finite element model generally involves approximation of both the geometric form and the elastic and inertia properties of the structure.

The finite element assessment procedure of the dynamic load approach employs two types of structural models developed according to the gross scantlings of the vessel. The first type of model is a three-dimensional global structural model of the entire ship structure. The global model is analyzed for the structural load cases previously described to determine the overall structural response of the hull girder structure and to determine critical areas where further refined analysis is required. The global model results provide boundary conditions for use in the refined finite element mesh analysis of sub-models of local structures. For some local structures—for example, hopper knuckle connections in double hull tankers and in bulk carriers, hatch corners, connections of longitudinal hatch girders to cross deck box beams, and intersections of transverse bulkheads with longitudinal wing box girders of container ships—stress concentrations will likely occur. In such cases, appropriate fine mesh models are needed. These local structural fine mesh models are loaded and analyzed, subject to the boundary conditions from the three-dimensional global analysis.

An alternative approach for structural strength evaluation is to use a one-step FE model instead of two steps described previously. The one-step approach employs a combined three-dimensional global model with

refined mesh models included in critical areas of the global model. One of the advantages of the one-step approach is that the number of separate refined mesh analyses can be reduced. A disadvantage of the one-step approach is that it can be much more time consuming for modeling and computing. Because of this, the one-step approach makes an iterative design procedure less feasible.

3.16.2.1 Three Dimensional Global Model. The specific procedures of structural modeling can be found in numerous published textbooks. Those related to the dynamic load approach are given in Liu et al. (1992), ABS (2006) and Shi et. al (2005). This section provides only a general description of the modeling used for the finite element analysis.

To determine the stress distributions in a hull structure, a three-dimensional global FEM of the entire length of the vessel is considered. The purpose of the global analysis is to determine the overall structural response of the hull girder structure, including the primary and the secondary bending moments under imposed loads. The stress results of the global response are the basis for assessing the hull girder structures of the deck, side shell, bottom, inner bottom, longitudinal bulkheads, transverse bulkheads, and other main supporting members. The global analysis is also used to obtain appropriate boundary conditions for refined mesh analysis of local structural areas.

Shown in Fig. 89 is the three-dimensional global model of a VLCC tanker. Both port and starboard sides of the structure are modeled.

3.16.2.1.1 General Considerations of Three-Dimensional Structural Modeling. The global model is constructed to include all primary load-carrying members, as well as those secondary structural members that may affect the overall load distribution. The model is constructed based on the stiffness and anticipated response of the structure, not totally on the geometry of the structure itself. All main longitudinal and transverse structural members are modeled. These

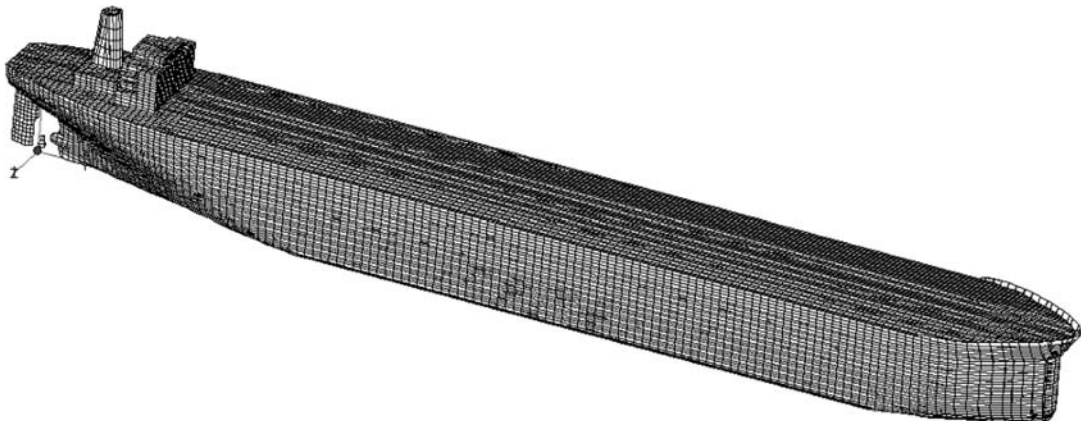


Fig. 89 Three-dimensional global model of a VLCC tanker.

include inner and outer shell, double bottom floor and girder system, transverse and vertical web frames, stringers, and transverse and longitudinal bulkhead structures.

Manholes on transverse and longitudinal structures, such as double bottom floors and longitudinal girders, are generally omitted in the global model. Leaving out plate elements or reducing plate thickness to account for such manholes in the global model are not advisable because this sometimes results in unrealistic shearing stresses for the thinned plates and adjacent elements. The actual behavior of a round or elliptical manhole with or without a flange is quite different from the modeled thin plate or element opening, which is usually rectangular in shape. To the same extent, the cell guide system of container ships need not be included in the global model.

The structural idealization must be verified to ensure that the structure is properly modeled and the loads are appropriately imposed for the structural analysis. The preliminary and important level of verification is to compare the stress results of the vertical bending moment with those obtained by beam theory because the vertical bending moment is the most dominant hull girder load effect and the vertical section modulus is also readily available. For a better correlation, the stresses at the deck at the side of the midsection in the mid-hold should be used. At this location, the effects of the local loads are minimized, and the stresses from the finite element analysis are mostly the primary direct stress. However, it should be noted that minor differences are anticipated between the finite element results and those from classical beam theory because the latter does not account for the load effects such as secondary bending and shear lag.

3.16.2.1.2 Mesh Size. Mesh size for global FEMs should follow the stiffening system as far as practicable. Desirable meshing arrangements are:

- One element between every longitudinal stiffener. Longitudinally, the element length should not be greater than two longitudinal spaces.
- One element between every vertical stiffener on transverse bulkheads.
- One element between every web stiffener on transverse and vertical web frames and stringers.
- At least three elements over the depth of double bottom girders and floors, transverse web frames in tankers, vertical web frames, and horizontal stringers on transverse bulkheads.
- Mesh on the hopper tank web frame of tankers and bulk carriers shall be fine enough to approximately represent the shape of the web ring opening.
- The mesh size of large brackets of primary support members should equal the stiffener spacing.
- The mesh size on the flange and web of corrugated bulkheads is in general to follow the stiffener spacing inside the bulkhead stool.

3.16.2.1.3 Structural Elements. The following four simple types of structural elements—which are

close to actual geometry, configuration, and stiffness of hull structures—are usually used in structural modeling. Although higher-order element types do exist, the simple types of element are considered sufficient for an adequate representation of the hull girder.

- Rod (or truss) elements, with axial stiffness only and constant cross-sectional area along the length of the member
- Beam elements, with axial, torsional, and bidirectional shear and bending stiffness, with constant properties along the length of the member
- Membrane (or plane-stress) elements with bi-axial and in-plane plate element stiffness with constant thickness
- Bending plate (or shell) elements, with in-plane stiffness and out-of-plane bending stiffness with constant thickness.

The use of triangular plate elements should be kept to a minimum. The aspect ratio of plate elements is generally not to exceed 3:1. Where possible, the aspect ratio of plate elements in areas where there are likely to be high stresses or a high stress gradient is to be kept close to 1:1.

A structural model consisting of membrane plate and rod elements will have a maximum of three degrees of freedom per node. In comparison, a model consisting of bending plate and beam elements will have five to six degrees of freedom per node. Bending plate elements, in association with beam elements, are used to represent stiffened panels in areas under lateral pressure. Plate-bending elements are used to represent unstiffened panels in areas under lateral pressure. Membrane and rod elements may be used to represent non-tight structures under no pressure loads.

All local stiffeners should be modeled. These stiffeners may be modeled using beams or rods positioned in the plane of the plating. Beam elements are to be used in areas under the action of lateral loads, whereas rod elements may be used to represent local stiffeners on internal structural members under no lateral loads. For beam elements, out-of-plane bending properties are to represent the inertia of the combined plating and stiffener. The width of the attached plate is taken as $1/2 + 1/2$ stiffener spacing on each side of the stiffener. The eccentricity of the neutral axis is not required. For beam and rod elements, other sectional properties are based on a cross-sectional area representing the stiffener, excluding the area of the attached plate.

Web stiffeners on primary support members—such as transverse webs, bottom transverses, deck transverses, and vertical webs—should be modeled. These stiffeners may be modeled using rod elements. Face plates of primary supporting members and brackets may be modeled using rod elements. Corrugated bulkheads and bulkhead stools are modeled using bending plate elements. Diaphragms in the stools and internal longitudinal and

vertical stiffeners on the stool plating are included in the model.

Regarding structural arrangement, bulk carriers are generally more complex than tankers and container ships. A typical bulk carrier usually has four different “frame” spacings in the cargo block. For a design with a floor spacing of 2,400 mm, the spacing can be 800 mm for hold frame, 4,800 mm for upper wing tank transverse, and 1,200 mm for pipe tunnel framing. Figure 96 shows a cut-out of a FEM of a bulk carrier showing the varying frame spacing in the cargo hold.

In bulk carriers and container ships, membrane plate elements are used to model the hatch coaming and coaming top plate, where the coaming brackets are modeled by membrane plates and by rod elements for the face plates. The hatch coaming is a critical component in determining the hatch opening distortion, especially for containerships. Accurate modeling is necessary, and consideration should be given to the subsequent fine mesh analysis of the hatch corner, which is required to determine the stress concentration.

Typical three-dimensional global mesh three hold structural models of a double hull tanker’s tanks and internal structure are shown in Figs. 90 and 91.

3.16.2.2 Fine Mesh Local Model. Fine mesh models are used to determine the stress distribution in main supporting structures, particularly at intersections of two or more major structural members where high stresses usually occur. The three-dimensional global model previously discussed provides a good structural representation of the hull girder to determine the primary and secondary stresses of the longitudinal plating

and longitudinal girders. However, for main supporting structures fine mesh models are required. This is because the mesh sizes of the global model are not fine enough to account for the responses of secondary structural members, the effects of which are sometimes significant to the responses of the main supporting members.

For tankers, fine mesh models are developed for upper and lower hopper knuckle connections, typical transverse web frame at mid-hold, web frame adjacent to the middle tank transverse bulkhead in way of the horizontal girders, bottom girders, transverse bulkhead horizontal girders (or vertical webs if the bulkhead is horizontally stiffened), and side stringers. Examples of fine mesh models of tanker structures are shown in Figs. 92, 93, and 94.

The fine mesh models of bulk carriers usually include a typical midship section and the section at the hatch end coaming. Because more than one frame spacing value exists in a bulk carrier, the typical midship section is selected to properly capture the responses of the structural component in question. When the floor framing is in line with the upper wing tank transverse, the midship section model should be at a location in the mid-hold where the frame consists of the pipe tunnel section, the floor, the lower wing tank transverse, the hold frame, and the upper wing tank transverse. When the floor framing is not aligned with the upper wing tank transverses, two midship sections should be considered. One section is selected to include the pipe tunnel section, the floor, the lower wing tank transverse, the hold frame, and the accompanying upper wing tank bracket. The second section consists of the upper

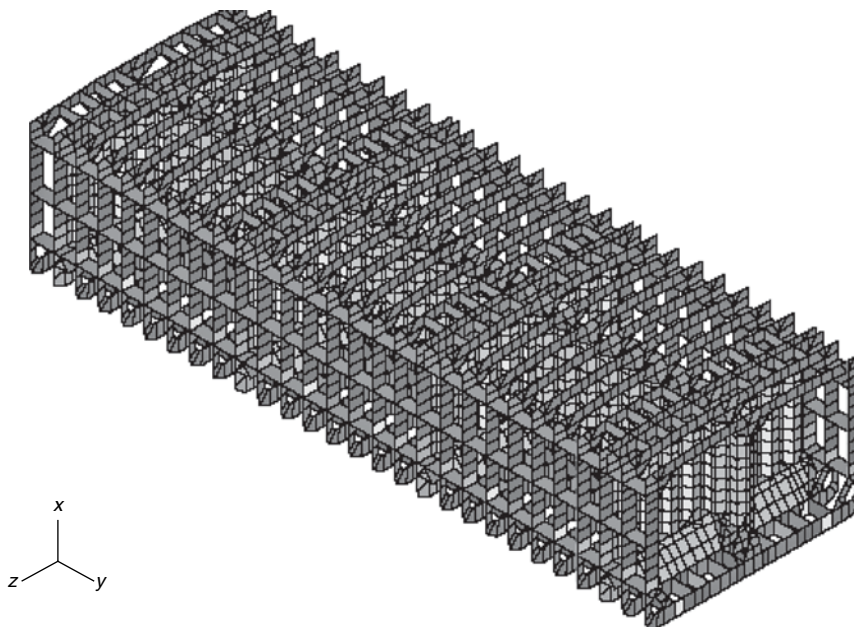


Fig. 90 Three-dimensional global FEM model—tank internals.

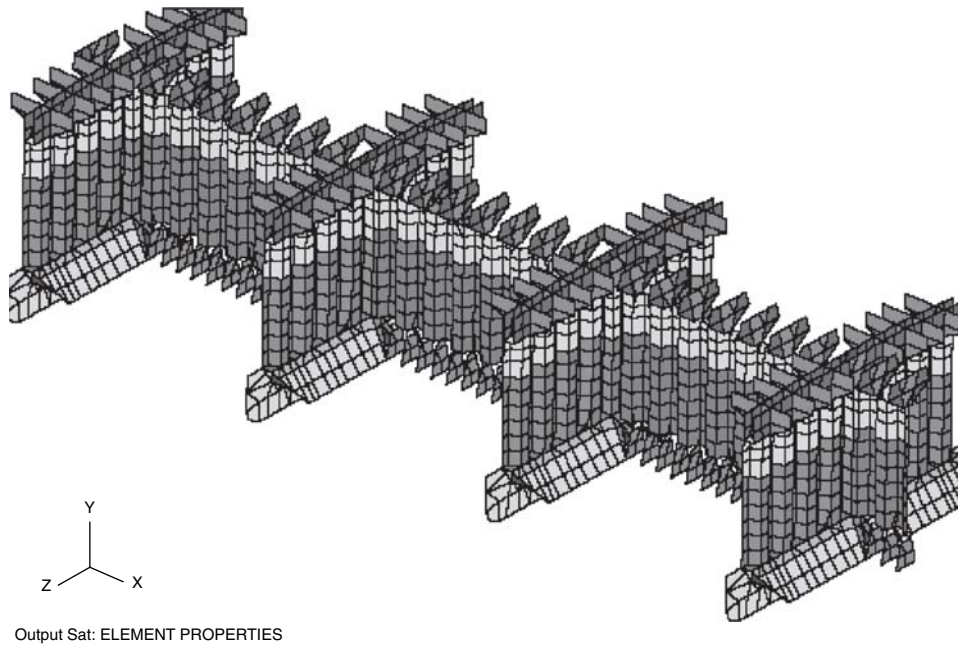


Fig. 91 Three-dimensional global FEM model—cargo tank bulkheads.

wing tank transverse, hold frame, and the accompanying lower wing tank bracket. Examples of fine mesh models of bulk carrier structures are shown in Figs. 95 and 96.

The fine mesh models of container ships required in structural analyses include a typical transverse frame, the centerline bottom longitudinal girder, a bottom longitudinal girder off centerline, the hatch-side longitudinal girder, a longitudinal side stringer, typical hatch corner of the midship cargo hold, forward hatch corners of forward cargo hold, hatch corners fore and aft of the deckhouse, and a typical hatch coaming top plate corner.

Examples of fine mesh models of container ship structures are shown in Figs. 97 and 98.

3.16.2.2.1 General Considerations for Fine Mesh Modeling. Fine mesh analysis can be carried out either by means of separate local FE models with fine mesh zones and with boundary conditions obtained from the larger global model, or with the fine mesh zones incorporated into the larger global model. The mesh size of fine mesh zones should not be greater than $50 \text{ mm} \times 50 \text{ mm}$. In general, the extent of the fine mesh zone should not be less than 10 elements in all directions from the area under investigation.

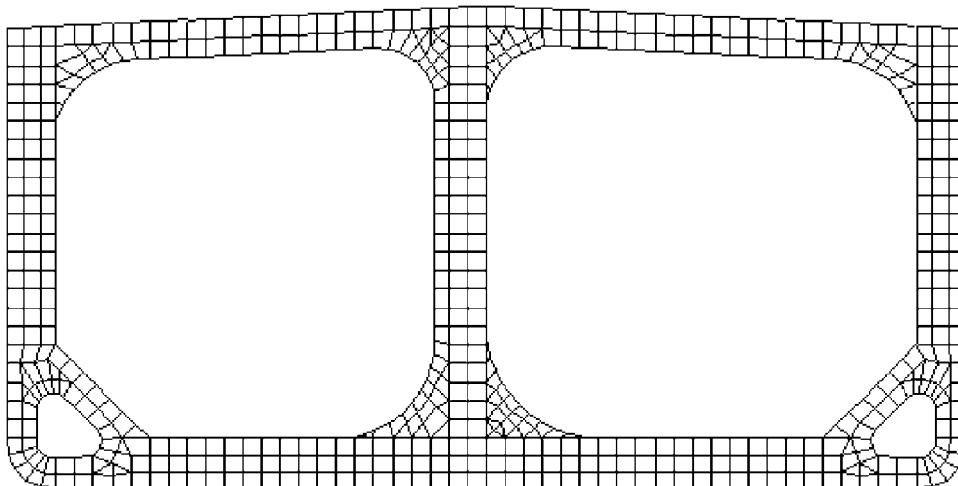


Fig. 92 Typical fine mesh of tanker web frame.

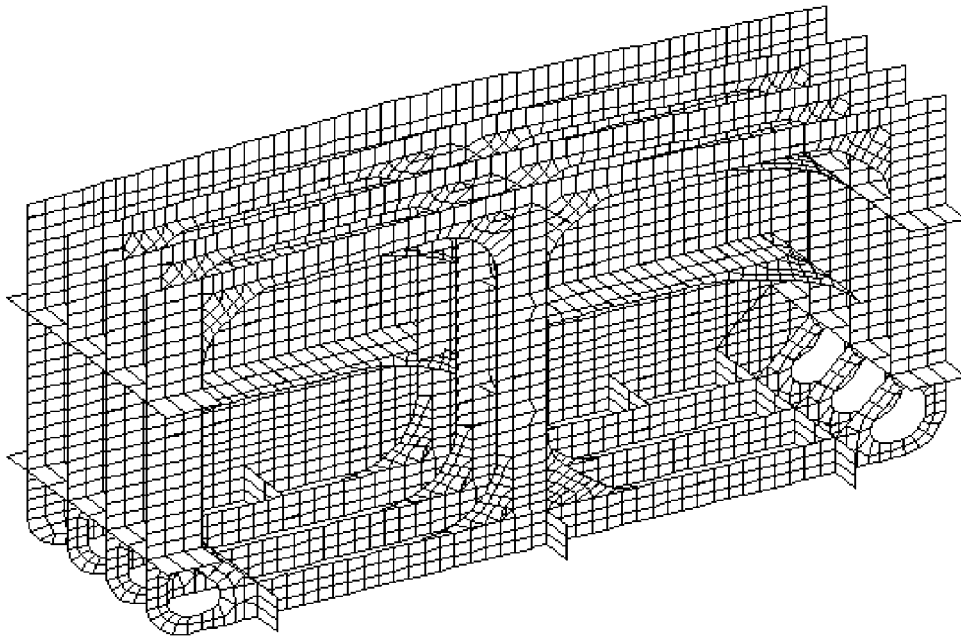


Fig. 93 Typical fine mesh of cargo tank structure.

Rectangular-shaped membrane elements of regular proportion should be used as much as possible. Shapes that are too irregular can often result in distorted stresses in the elements. As a general rule, it is preferable to keep the aspect ratios of plate elements as close to one as possible. Using elements with an aspect ratio higher than 3:1 is not advisable. Triangular elements should be avoided where possible.

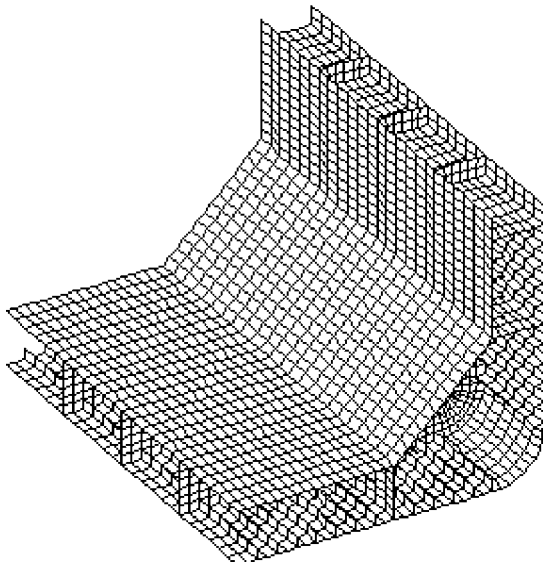


Fig. 94 Typical fine mesh of hopper knuckle.

3.16.2.3 Very Fine Mesh Local Model. Evaluation of hot-spot stresses for fatigue assessment requires the use of very fine finite element meshes in way of high stress concentration. This very fine mesh analysis is usually carried out by means of separate local FE models with very fine mesh zones in conjunction with boundary conditions obtained from a larger global model. The mesh size of very fine mesh zones should be $t \times t$, where t is the thickness of the plate element.

The guidelines on element aspect ratio for fine mesh models are applicable to very fine mesh models. Where stresses are evaluated on a free edge or corner welds, such as cut-outs for stiffener connections at web frames or butt welds on edges of plating and around hatch corners, a rod element of negligible cross section (e.g., 1 mm^2) is used to obtain the stress value. An example of a very fine mesh model to determine the hot-spot stress at the hopper knuckle connection is shown in Fig. 99.

3.16.3 Finite Element Structural Analysis. The structural adequacy of the hull is examined by the finite element method using a three-dimensional global model representing the hull structure and fine mesh models for local structures. Results of nodal displacements or forces obtained from the global analysis for the load distributions of the structural load cases are used as boundary conditions in the subsequent fine mesh analysis of local structures.

3.16.3.1 Three-Dimensional Global Structural Analysis. Three-dimensional global structural analyses are carried out for the structural load cases specified in Section 3.16.1.2 to obtain the overall structural responses. If there is a limitation of computer capacity

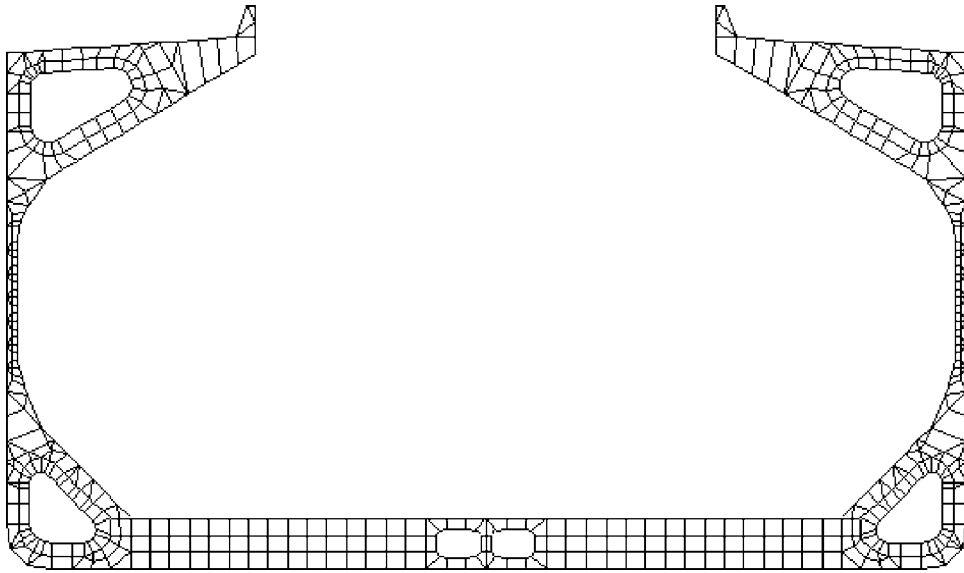


Fig. 95 Typical fine mesh of bulk carrier web frame.

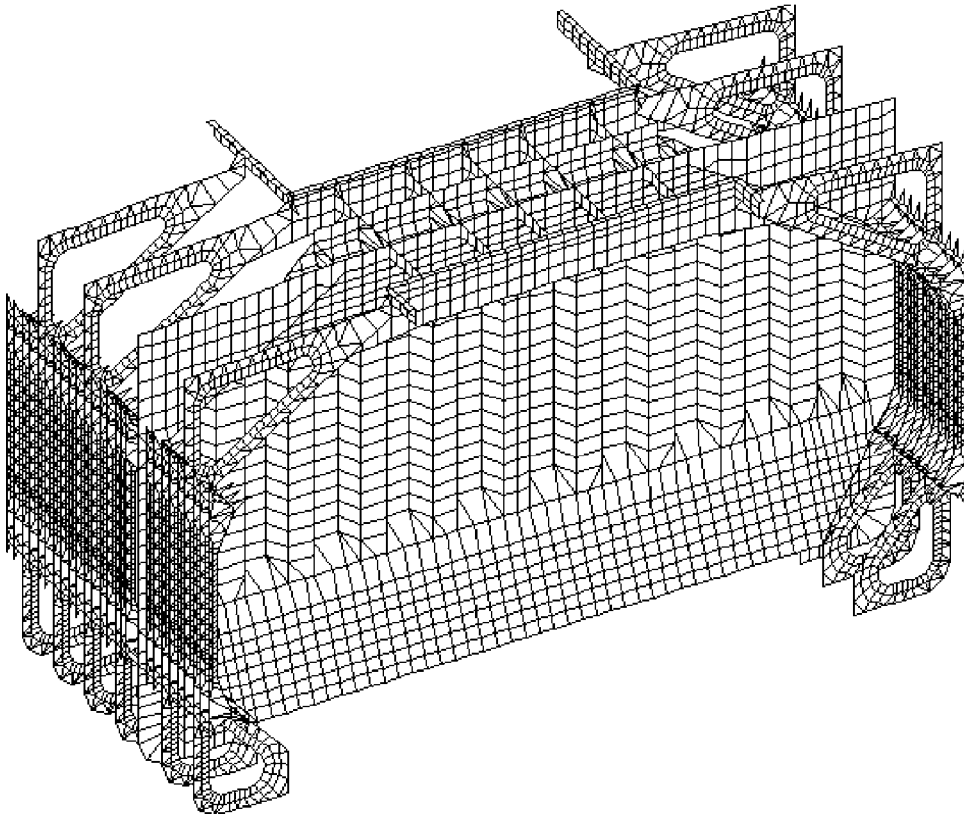


Fig. 96 Typical fine mesh of bulk carrier cargo hold structure.

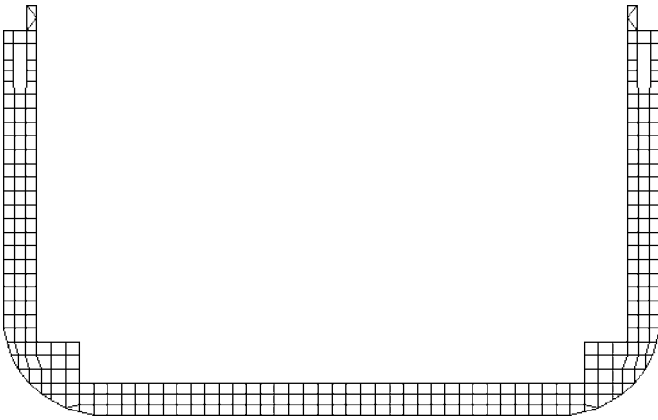


Fig. 97 Typical mesh of container ship midship section.

and the ship is symmetric about the centerline plane, the global structural model may be comprised of only one half (i.e., starboard or port side) of the hull. In such cases, the asymmetric loading associated with roll in beam or oblique seas may be decomposed into the symmetric and the anti-symmetric components, as shown in Fig. 100 for a typical asymmetric distribu-

tion of external hydrodynamic pressures at midship section.

In Fig. 100, P_{sym} stands for the symmetric load component, and $P_{anti-sym}$ stands for the anti-symmetric load component at a given node in either the x , y , or z direction, with the sign corresponding to the global coordinate system of the FE model, P_s and P_p are respectively nodal loads on the starboard and port sides of the vessel.

The symmetric and anti-symmetric load components are separately applied to the three-dimensional global models with corresponding symmetric and anti-symmetric boundary conditions. For each of the two boundary conditions, three specific degrees of freedom of all nodes on the centerline plane ($x - y$ plane) are suppressed, as shown in Fig. 101. The degrees of freedom are denoted by u_x , u_y , and u_z for translation, and by θ_x , θ_y , and θ_z for rotation in x , y , and z coordinates.

The asymmetric results of stresses and displacements for the port and starboard sides of the hull structure can then be obtained by superposition, adding or subtracting the symmetric and anti-symmetric components of results. That is,

$$\text{Starboard Side Results : } R_{stbd} = R_{sym} + R_{anti-sym}$$

$$\text{Port Side Results : } R_{port} = R_{sym} - R_{anti-sym} \quad (224)$$

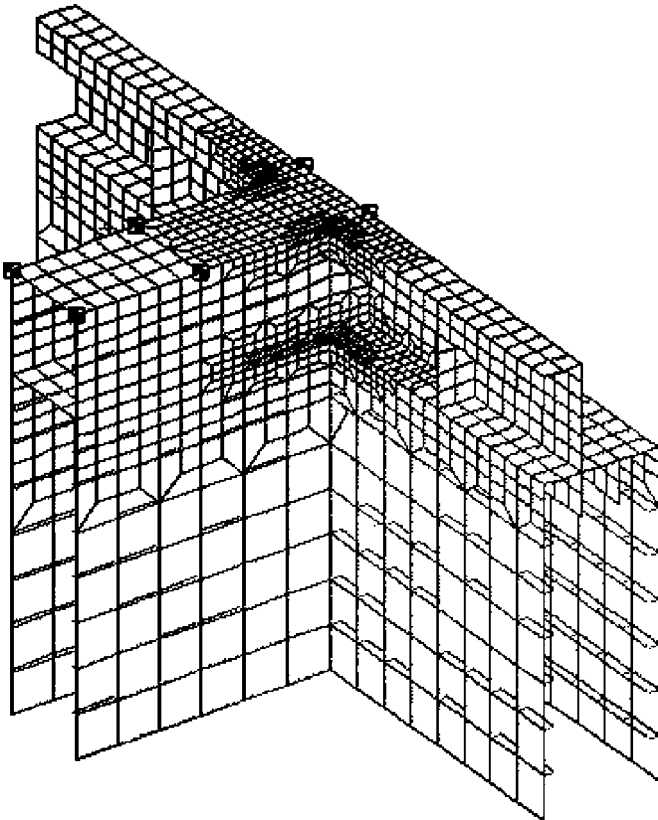


Fig. 98 Typical fine mesh of container ship hatch corners.

3.16.3.2 Fine Mesh Local Structural Analysis.

Fine and very fine mesh structural analyses are performed subject to the local loads acting on the members under consideration and the boundary conditions for all structural load cases considered in the global analyses. The boundary conditions required to support the fine mesh model are either the nodal forces or nodal displacements determined from the global finite element analysis. The boundary displacements, in lieu of the boundary forces, are more often used because the nodal displacements are readily obtained from the global analysis and can be applied in a systematic manner.

3.16.4 Strength Assessment and Acceptance Criteria. Stress results obtained from the global and fine mesh finite element analyses with the load distributions of corresponding structural load cases previously described are used to evaluate the adequacy of the hull structures against the failure modes of yielding and buckling, and the ultimate strength. Fatigue strength assessment is considered separately, using either spectral fatigue strength analysis or the simplified fatigue assessment procedures of the classification societies.

3.16.4.1 Yielding Strength. Yielding strength assessment of plating and stiffeners of structural members, such as deck structures, bottom structures, inner bottom, longitudinal bulkheads, side shell, and transverse bulkheads, are based on stress results of the three-dimensional global mesh finite element analysis. Results of the fine mesh analysis are used for yield strength evaluation of main supporting members. For edge stress or stresses in the extreme fiber of plate elements

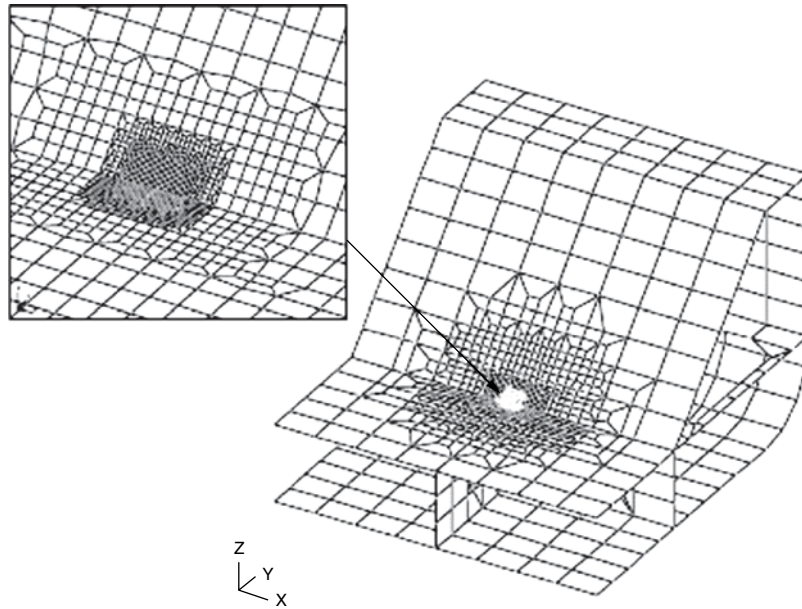


Fig. 99 Typical local finite element model of hopper knuckle connection $t \times t$, very fine mesh on inner bottom and hopper plate.

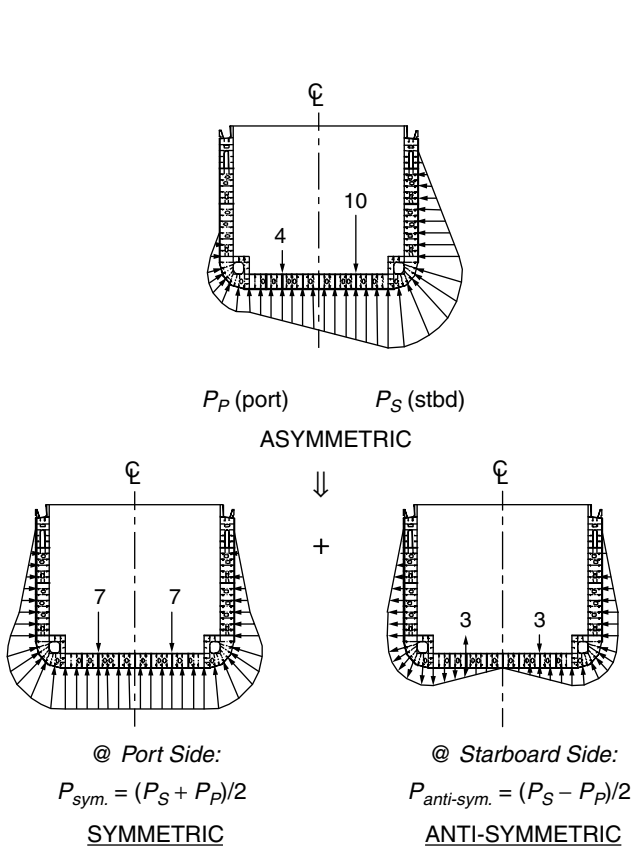


Fig. 100 Symmetric and anti-symmetric components of asymmetric loading.

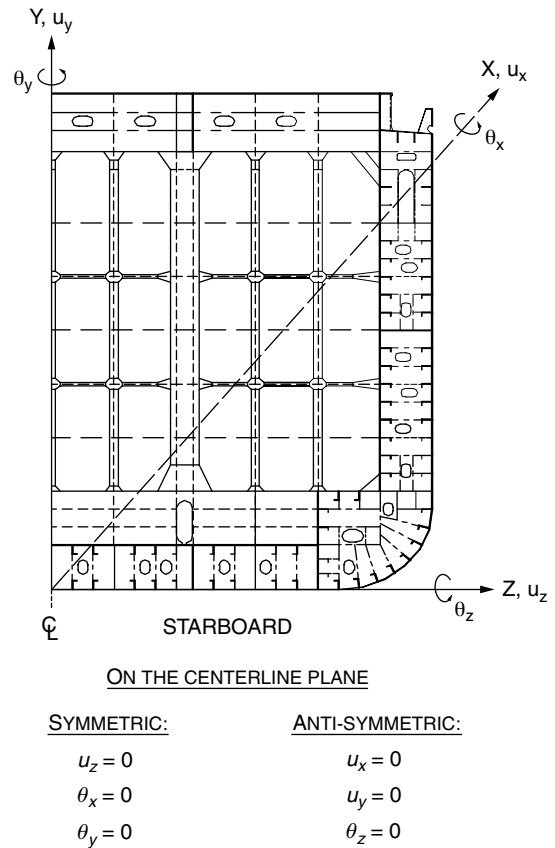


Fig. 101 Symmetric and anti-symmetric boundary conditions.

and axial stresses in rod elements, the yielding criteria of the structural members are to compare the normal stresses to the yielding stress of the material.

For the case of bi-axial stress in plate elements, a specific combination of stresses, rather than the maximum normal stress, constitutes the limiting condition. In this regard, the yielding criteria is that the Hencky-von Mises stress, σ , is not to exceed 95 percent of the yield stress of the material. That is,

$$\sigma = \sqrt{\sigma_x^2 + \sigma_y^2 - \sigma_x\sigma_y + 3\tau_{xy}^2} \leq 0.95 f_y \quad (225)$$

where σ_X and σ_Y are respectively the normal stresses in x - and y -directions, τ_{XY} is the shear stress, and f_y is the specified minimum yield point. The normal stresses σ_X and σ_Y in equation (225) comprise the primary and secondary bending stresses directly from three-dimensional finite element analyses.

3.16.4.2 Buckling Strength. Plate panels and primary supporting members are checked against buckling using stresses obtained from the FEM analyses. For this purpose, established analytical or empirical formulas suitable to the hull structure are used. The buckling limit state for plate panels between stiffeners, for example, is cast in terms of the notion of “unity check” that is familiar to most practitioners in the industry. The criteria are given in terms of ratios between the calculated nominal stress and the critical buckling stress for each independent stress component, with the sum of these stress ratios squared not to exceed unity. This together with buckling strength assessment for stiffeners and stiffened panels based on established analytical or empirical formulas suitable to the hull structure are used.

3.16.4.3 Fatigue Strength Assessment. In past decades, fatigue failures have increased in ship structures due to the greater use of high-tensile steel and the highly optimized structural design. With this increase of fatigue failures, extensive studies have been done on fatigue strength methods and their applications. According to the International Institute of Welding (IIW), fatigue strength may be assessed, aside from fracture mechanics, based on nominal stress, geometric (hot-spot) stress, and notch (peak) stress (see Fig. 102).

Nominal stress is the stress that can be determined elementarily from the sectional forces and moments and the sectional properties of the structure. This stress is widely used and serves as a basis for fatigue strength in the majority of existing strength codes because of its simplicity. When the nominal stress is applied, appropriate S-N curves will have to be specified for each weld detail.

Hot-spot stress includes all stress-raising effects due to structural discontinuities and the presence of attachments of a structural detail, excluding the stress concentration due to the weld profile itself. In contrast to the nominal stress application where a different S-N curve for each joint is needed, only one S-N curve is enough for fatigue assessment of welded structures in the hot-spot stress application.

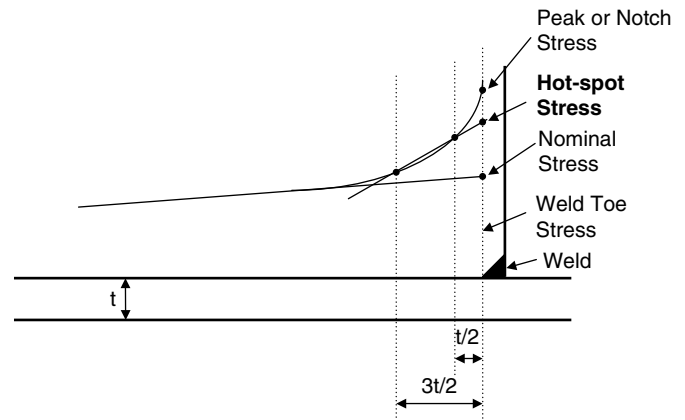


Fig. 102 Stress definitions at weld toe.

Notch stress is defined as the locally increased stress in a notch, including effects due to structural geometry and the presence of a weld. Nominal stress is estimated using an approximate method, and is used in the simplified fatigue strength assessment procedure for the first level of fatigue strength assessment of welded structural details in longitudinal strength members. The application of nominal stress in fatigue assessment is described in Section 3.15.4.3.

For locations of fillet weld toes where the effects of intersecting load-carrying members are significant, or at the contour of a cut-out away from welds, the stress ranges can no longer be adequately established by using a beam theory method to obtain nominal stresses. For such cases, hot-spot stress is used in lieu of nominal stress for all the combined load cases in conjunction with very fine mesh finite element analysis and fatigue strength evaluation described in Section 3.15.4.3, as follows.

3.16.4.3.1 Hot-Spot Stress. The hot-spot stress takes into account the influences of structural discontinuities due to the geometry of the connection but excludes the effects of the welds. Hot-spot stresses at the weld toes are determined by extrapolation of the finite element analysis results using fine mesh structural models. Structural details for which finite element analysis is needed are, for example, the brackets connecting transverse bulkhead vertical webs and double bottom or deck girders, end connections of transverse bulkhead horizontal girder to longitudinal of side shell or longitudinal bulkhead, and other similar structural connections.

The hot-spot stress approach of fatigue strength assessment has been widely applied for different types of welded joints, and much research has been performed to predict the more exact concentrated stress in the vicinity of the weld toe where potential cracks could occur. Analyses show that numerically calculated stress concentrations depend on the mesh size and element type of the

FE model, extrapolation method, and whether the weld bead is included or not.

Therefore, for the case where the stress needs to be obtained as a hot-spot stress at a weld toe using finite element analysis, one must define the element size of the structural model to be used, as this is an area of uncertainty because the calculated stress distribution can be unduly affected by both the mesh size used and the uniformity of the mesh adjacent to the weld toe. In addition, there is little test data available to confirm the approach. Because of these reasons, it is necessary to establish guidelines to be followed in producing the fine mesh model adjacent to the weld toe, and in establishing the stress at the location where the fatigue assessment is to be made.

As indicated in Fig. 102, the weld hot-spot stress is determined from linear extrapolation of the principal stresses at the centroid of the elements at $t/2$ and $3t/2$ from the toe, where t is the thickness of a plate or the flange of a longitudinal stiffener. This technique is used by many classification societies, and is considered an acceptable and reasonable approach that has been verified via successful experience for extracting and interpreting the “near weld toe” element stresses and to obtain an extrapolated stress at the weld toe. When stresses are obtained in this manner, the use of the E class U.K. DEN S-N data is considered acceptable. However, it should be understood that deviations from the specified finite element approach indicated in Fig. 102, such as a change of mesh size or locations where stresses are calculated, the hot-spot stress extrapolation procedure may require a change in the S-N curve to be applied.

3.16.4.3.2 Peak or Notch Stress. The *notch stress* is defined as the peak stress at the weld toe taking into account stress concentrations due to the effects of structural geometry as well as the presence of the welds. In the evaluation of fatigue strength, one approach used is to determine the equivalent peak stress range by multiplying the hot-spot stress range by an equivalent fatigue notch factor (see IACS Common Structural Rules for Bulk Carriers 2006). When stresses are obtained in this manner, the use of a modified B-class U.K. DEN S-N data is considered to be acceptable.

3.17 Specific Vessel Types. The size, principal characteristics, and arrangement of a new ship are determined primarily by its mission or intended service, the types of cargo to be transported, and by the method of handling and stowage. Depending on the type of ship, the structural responses could exhibit distinctive features due to the structural configurations that are arranged to suit the service and the cargo to be carried. Some of these features may warrant special consideration in design. Therefore, specific criteria addressing these features are needed, in addition to what was discussed in previous sections. To illustrate their potential importance, a brief discussion is presented about some of the special features of double hull tankers, bulk carriers, and container ships.

3.17.1 Double Hull Tankers. Tankers are normally designed to carry petroleum products ranging from crude oil to gasoline, with specific gravity in the range of 0.73 to 0.97. The cargo spaces are divided into tanks by longitudinal and transverse oil-tight bulkheads extending from deck to bottom shell, usually with one or more tanks across athwartship, in addition to the double bottom and double sides, port and starboard, for the case of double hull tankers. This division is dictated by practical considerations such as separate lots of cargo, structural requirements, restrictions of free surface of liquid, limitations of outflow in case of tank penetrations, and safety of ship in the event of collision. All tank boundaries must be oil tight with access by raised oil-tight hatches.

3.17.1.1 Areas of Concern. Due to the special features of its structural arrangement, the following general areas of double hull tankers need to be considered during the design.

3.17.1.1.1 Effects of Wide Cargo Tanks. For medium-size double hull tankers, some designs offer only a single cargo tank arrangement athwartship without longitudinal bulkheads except the inner hull. This type of arrangement results in a relatively large unsupported breadth of the deck and inner bottom panels, where shear lag would be more pronounced. A parametric study shows that the effectiveness of the deck plating of a medium-size double hull tanker without a centerline bulkhead is about 90 percent for a normal bending moment distribution, in comparison with approximately 100 percent effectiveness for a conventional single hull tanker. The 90 percent effectiveness of the deck plating can be interpreted as an increase of the longitudinal bending stress by 11 percent at the deck corners, which should not be ignored in the design process. The shear lag problem may be ameliorated by having a centerline longitudinal bulkhead, oil-tight or swash type. In addition, associated with an increasing width of cargo tank, the added liquid cargo pressure head due to roll and inertial force will increase. The increase due to ship motion is not generally accounted for in traditional rules, where only the static case is considered.

For a wide cargo tank, the occurrence of liquid sloshing in the transverse direction is more likely to take place than for a narrower design at a slack loading condition. Thus, strength of bulkheads to resist sloshing loads should be considered for not only the transverse but also the longitudinal bulkheads.

3.17.1.1.2 Stiffness of Transverse Supporting Structures. For double hull tanker designs, the stiffness of the side structures is generally improved in comparison with that of single hull designs. Besides the increased horizontal section modulus and stiffness of the hull girder, it also provides a relatively stiffer support to local longitudinal structures and other transverse supporting members. In spite of these advantages, caution should be exercised in designing the connections of deck transverses with webs on longitudinal bulkheads and the connections of side transverses and

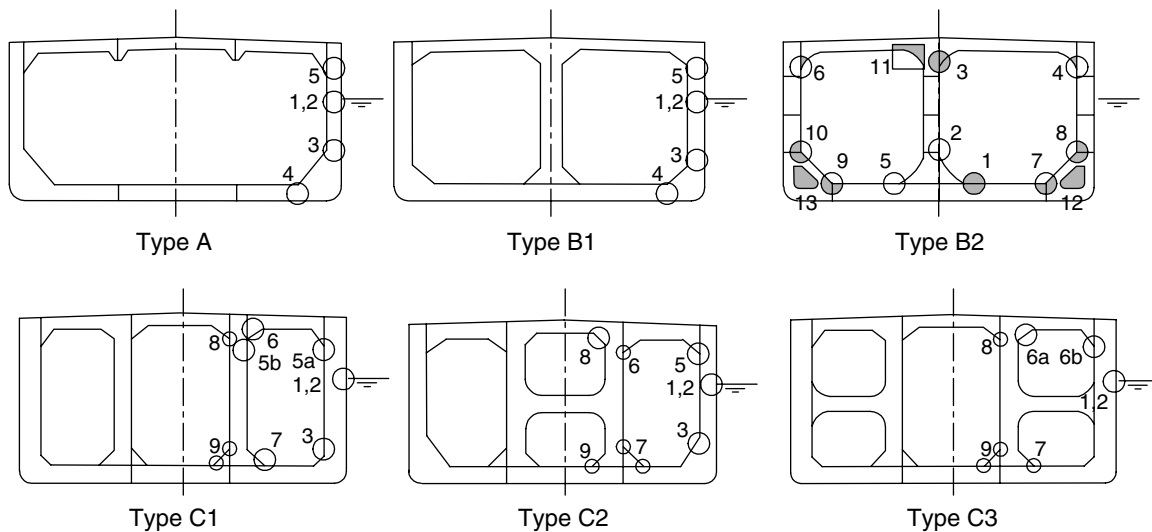


Fig. 103 Critical areas in tanker web frames.

bottom transverses of the double hull designs, where pronounced deflections are expected.

3.17.1.1.3 Compressive Stresses in Bottom and Inner Bottom Plating. One of the distinctive features of the double hull tanker structure is the relatively large magnitude of compressive transverse stresses in the inner bottom and bottom plating in the middle region of cargo tanks. For designs with lesser margins in the plate thickness, buckling with respect to bi-axial compression of plate panels between stiffeners could be a problem due to the limited buckling strength, as well as defined ultimate strength, of a wide plate.

In comparisons of double hull and single hull designs, it is apparent that the bottom and inner bottom plating of double hull tankers are subjected to greater local pressures for both the full load and ballast conditions. Also, the relocation of the neutral axis of the double bottom structure would result in secondary bending stresses in the bottom plating greater than those for a single bottom structure with equivalent section modulus and stiffness. As a result, the combined effects of the hull girder bending and structural panel bending between bulkheads could cause local buckling problems for the bottom and inner bottom plating. In this regard, a centerline swash longitudinal bulkhead can be considered to effectively reduce the bending stresses of the bottom structures.

3.17.1.2 Critical Areas. In addition to the areas described in the previous section, which require special considerations during design, locations of high stresses in tanker web frames as found from structural analyses are shown in Fig. 103 for three configurations: types A, B, and C of double hull tankers. They increase in size with two, three, and four longitudinal bulkheads, respectively.

Type A has a simple double hull form and is typical of small tankers. Type B tankers are usually Aframax and

Suezmax size with a centerline bulkhead. Type C tankers are common for VLCC size and have two additional longitudinal bulkheads with one or two struts in either the center or wing tanks.

Some specific areas (as marked) have been found to be subjected to high stress (against yielding and buckling failures) under various loading conditions, depending on the midship configurations. These high stress areas—except those in Locations 1 and 2 near the full load or ballast water line—are due primarily to high static loads. However, even in the cases with high static loads, significant portions of the stresses are motion-induced, and thus may also be susceptible to fatigue damage.

The aforementioned critical locations, which require more detailed modeling and evaluation by fine or very fine mesh finite element analysis, are summarized here:

- Location 1 is at the connections of the side longitudinal stiffeners near the water line to the transverse web frames. Location 2 is at similar connections at the transverse bulkheads. These connections are susceptible to fatigue damage primarily due to cyclic external pressure acting on the ship's side by waves, and partly to internal pressure fluctuation induced by ship motions. Similar problems occur at the same locations on the longitudinal bulkheads. This is true for all types A, B, and C vessels.

- Location 3 is at the lower part of the side transverse (or the double-side) for type A and type B vessels, as well as type C vessels without struts in the wing tanks. Under large angles of roll, these areas are subjected to high magnitude shearing stresses resulting from significantly higher internal loads induced by the ship's roll motions. Additional bending by the side transverse under the same loading further raises the stress level a

significant amount on the inboard side of the side transverse near the bottom.

- Location 4 is located at a fixed-end beam subjected to a uniformly distributed load. These “fixed ends” of the double bottom floors connecting to the longitudinal bulkheads usually experience a high magnitude of shearing stress. This is true for both type A and type B vessels, but is more severe for type A vessels. Furthermore, double bottom bending also causes significant additional stress in the floors near the connection of the inner bottom to the longitudinal bulkhead.

- Location 5 is similar to Location 3, but refers to the upper parts of the vertical webs. These locations at the side and longitudinal bulkhead also often experience high shearing stress. This is because the upper portion of the transverse web is usually designed with lighter scantlings, and under large angles of roll considerable pressure is added to the transverse web, resulting in high shear at both ends. Additional bending of the vertical webs and deck transverse webs also raises the stress level significantly in the area connecting to the deck transverse webs. This is true for type A and type B vessels, as well as for type C vessels without struts in the tanks.

- Locations 6 through 9 are in various bracket connections. In these bracket connections, high stresses are due primarily to the bending of the connecting members and, in some cases, due to shear.

Critical areas of horizontal stringers on transverse bulkheads are shown in Fig. 104.

- Locations 1 to 3 are bracket toes of the stringer, which are subject to high stresses due to bending of the connecting members.

- Locations 4 and 5 are the horizontal stringer connections to the longitudinal stiffeners. Because of the local bending of the stiffeners relative to the stringer at their connection, high stresses can develop in the faceplates of the connection bracket and at the bracket toes.

- Locations 6 and 7 are the connections of the inner skin and transverse bulkhead. These locations may need further analysis if the global analysis indicates high stress values.

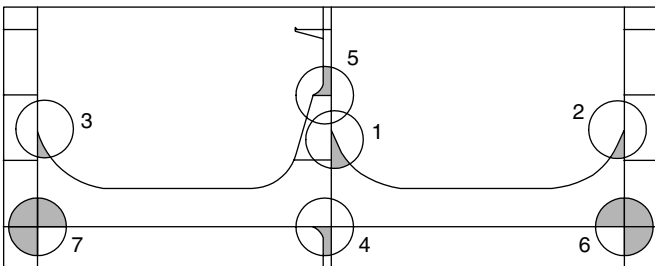


Fig. 104 Critical areas in tanker horizontal stringer sections.

Fitting of partial longitudinal girders is used to restrict the vertical displacements of the bottom floors adjacent to transverse bulkheads. The structural details of bottom and inner bottom longitudinal stiffeners, as well as bulkhead vertical stiffeners on the transverse bulkheads, are significantly affected by the behavior of partial girders.

Fitting buttress structures above the partial girders will transmit the lateral load acting on the transverse bulkhead to the double bottom structure through the partial girder and full girder. The top of the buttress structure is connected to the lower horizontal stringer. Critical areas of longitudinal girders and stiffeners in double bottoms intersecting vertical stiffeners on transverse bulkheads are shown in Fig. 105.

- Locations 1 to 3 are bracket toes of the lower vertical buttress structure, which are subject to high stresses due to bending of the connecting members.

- Locations 4 and 5 are the connections of vertical stiffeners to the upper deck longitudinals and buttress, respectively, which can be subject to high stresses due to bending of the bulkhead and vertical stiffeners.

- Locations 6 to 8 are stiffener end connections in the double bottom, which are subject to high stresses due to bending of the double bottom.

Other critical areas are:

- Inner bottom plating and inner side plating hopper knuckle connections
- Corrugation connections to stool shelf plating.

3.17.2 *Bulk Carriers.* *Bulk carriers* is the general connotation for those vessels intended to carry dry bulk

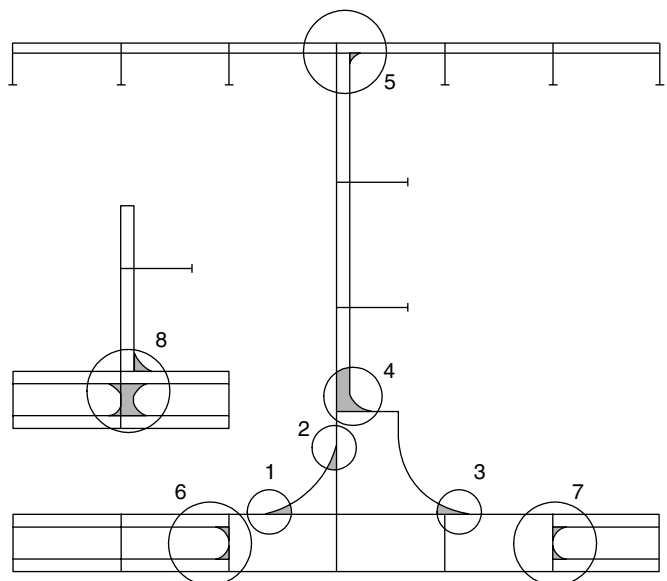


Fig. 105 Critical areas in tanker longitudinal girder sections in way of the transverse bulkhead.

cargoes, loaded into the vessel with no containment other than that of the ship's hold boundaries, as distinguished from the liquid bulk carrier or tanker. Dry bulk cargo may vary in nature and specific gravity, from iron ore to grain, and vessel proportions, internal arrangements, structure, and so on are strongly influenced by the specified cargo type, in addition to the usual logistic and economic constraints.

In this section, a "bulk carrier" means a ship constructed with a single deck, top side tanks and hopper side tanks in cargo spaces, and intended to primarily carry dry cargo in bulk. This type of bulk carrier, which is prevalent in today's worldwide trade, is designed with either a single or double side skin, cargo holds that are of octagonal-shaped cross section, extending to the hull sides or inner skins as a single transverse compartment, and with a shallow double bottom. The engine room and bridge are invariably aft. This configuration is in contrast to other bulk carrier types, such as those carrying dense cargoes and OBO carriers, where the cargo compartments are relatively small in section with large wing tanks and high inner bottom. The required narrow section and high inner bottom for bulk carriers carrying high-density cargoes are to prevent problems of cargo shifting, and to avoid violent motions that could result from excessive metacentric height.

The dry bulk carriers engaged in long international trade are most frequently intended to be combination carriers, with one principal commodity carried on the outbound leg of the voyage and a different one inbound. When the bulk carriers are designated to carry high-density cargo, arrangement of alternate holds appears most prudent for dense cargo to raise the center of gravity and to minimize hull girder bending stresses in this loading condition. However, such arrangement would inevitably result in very high vertical shear forces near the bulkheads, which may call for increased shell plate thickness and for the double bottom structures in the hold intended for carrying heavy cargoes to be augmented.

Bulk carriers are similar to tankers in hull form and proportions, powering, and so on for a given cargo deadweight, with perhaps a slightly larger block coefficient and a fraction less speed. The principal differences in configuration of bulk carriers as compared with those of tankers are the large hatch openings in the main deck leading into the dry cargo compartments, and in the shape and arrangement of the hold compartments themselves.

3.17.2.1 Areas of Concern. Typical bulk carrier structures represent a compromise between operational demands and structural requirements, such that the margins of safety among the structural components are not uniform. The nonuniformity and noncompatibility can be best exemplified by its side structures, consisting of a rigid double bottom and lower hopper structure connected to large upper wing tanks by slender side frames.

Another concern regarding the hull girder strength of bulk carriers is the lack of structural redundancy and inadequate support in the transverse direction. This is exemplified by the weak cross deck structures, which are intended to prevent excessive distortion of large hatch openings and to support the deflection of side structures and transverse bulkheads.

The vertically corrugated transverse bulkheads represent another unique feature of bulk carrier structures. These types of bulkhead have virtually no horizontal rigidity due to their vertical corrugated construction, and also exhibit a much lower ultimate strength than plane bulkheads due to the lack of membrane strength in overloaded conditions. Flattening and subsequent collapse of the corrugated bulkhead can occur when the cargo hold is flooded.

Of equal concern is the cargo handling practices during loading and unloading. The high-speed loading facilities in use at many loading terminals can induce overloading to the bottom structures. It is not unusual to find inner bottom structures, side shell, side frames, and transverse bulkheads damaged by discharging equipment such as pneumatic hammers, bulldozers, and grabs. Besides, some cargoes such as high sulfur content coal and even salt can cause more accelerated wastage in internal structures of the cargo holds than one would expect. All these factors, as well as improper maintenance, may have contributed to the reported large number of bulk carrier casualties and losses (see Curry 1995; NKK 1992).

3.17.2.1.1 Vertical Hold Frames. Vertical hold frames are considered to be one of the weakest links in a single side skin bulk carrier structure. These frames connect two highly rigid structures, namely, the double bottom and the upper wing tank, resulting in significant incompatibility in stiffness among the structural components in question. Hold frames in dry cargo holds exhibit maximum stresses when alternate holds are loaded with high-density ore cargo and the vessel is at a full draft condition. Due to the low cargo profile of the high-density cargo, hold frames in these loaded holds are flexed more readily because there is a lack of internal cargo pressures to counteract the large amount of the external wave pressure. The flexing is further magnified by the rotation of the rigid lower wing tank caused by the large downward force of the high-density ore cargo acting on the double bottom. All these effects contribute to greater fatigue damage in connecting brackets of the hold frame, and possibly lead to the detachment of the hold frame from the side shell. As a result, the fatigue damage could become one of the dominant failure modes in bulk carrier structures.

3.17.2.1.2 Cross Deck Structures. In evaluating longitudinal hull girder strength, emphasis is usually not given to the strength of the cross deck structures, which are the deck structures between the hatch openings. Because of this, buckling can often occur in these areas,

particularly in large and wide bulk carriers with large cargo holds.

The buckling of deck structures can result from several sources. The first source is related to block loading, a load condition in which two adjacent holds are loaded with heavy cargo. In this condition, large transverse sagging bending can occur in the transverse bulkhead, which in turn causes high compressive forces and stresses in the cross deck structures, in addition to those resulted from hydrostatic and hydrodynamic pressures acting on the side shell. The second source causing buckling in the cross deck is the torsion-induced longitudinal shear force in the cross deck in an oblique wave condition. The longitudinal shear force not only causes shear buckling of the cross deck plating but also produces lateral bending, often causing the hatch corners to buckle, and is in fact one of the governing factors in determining cross deck scantlings.

3.17.2.1.3 Corrugated Transverse Bulkheads. Vertically corrugated transverse bulkheads, especially those in dry cargo holds, are also considered critical in a bulk carrier structure. According to the International Load Line Convention and International Safety of Life at Sea (SOLAS), watertight transverse bulkheads are presumed able to prevent progressive flooding if the hold is accidentally flooded. However, nominal hydrostatic loads, which do not necessarily represent the actual dynamic load in a damaged condition, were used in traditional design practice. It is now believed that the collapse of vertically corrugated transverse watertight bulkheads after side structure failure, and subsequent progressive flooding, may be one of the primary causes for bulk carrier losses. Consequently, the design loads simulated in a flooded condition with an estimated equilibrium water line and the static and dynamic loads of the liquid, including sloshing, are currently used by the classification societies in determining the strength of the corrugated bulkheads. In this connection, the IACS has established the unified requirements of loading and corrugated bulkhead strength in a hold-flooded condition for bulk carrier new buildings (UR S-18, 2004) and for existing bulk carriers (UR S-19, 2004).

As shown by Vasilev et al. (1964), the corrugated bulkhead can be analyzed by considering it as constituted of separate beam-columns. Thus, the overall strength of the bulkhead can in principle be analyzed by considering each corrugation as a simple beam, elastically fixed at the upper and lower ends and subject to lateral pressure and the carryover bending moments. However, difficulties exist in solving the problem due to the fact that the exact boundary conditions and carryover moments are not readily obtained. In addition, the bulkhead quite often comprises several strakes of plating in different thickness. The nonuniformity of bulkhead plate thickness adds complexities to the issue. Because of this, the solution of the problem inevitably relies on finite element analysis.

3.17.2.2 Critical Areas. Figures 106a through 106e show the critical areas for typical configurations of single side skin bulk carriers. The critical areas for an OBO carrier and an oil/ore carrier are similar. The analyses of the transverse and longitudinal structures primarily consider the overall strength of the internal supporting structures. Therefore, attention is paid to obtaining the local stresses in these structures and the assessment of the yielding and buckling strength.

- Fig. 106a: Locations 1 are the hold frame upper and lower brackets. There are two types of hold frame brackets, lapped and inserted. The lapped bracket can fail where the bracket is lapped to the hold frame. The failure is likely to occur as fractures in the toe for the insert bracket.

- Fig. 106a to 106c: Location 2 is subject to buckling failures in the upper wing tank transverses. This is more likely to occur where collar plates are not fitted to the longitudinal stiffeners and skirt plates are not fitted to the corrugation.

- Fig. 106a: Location 3 is subject to fractures within the floor web of the lower wing tank. Excessive shear usually causes such failures.

- Fig. 106b and 106c: Location 4 is subject to buckling in the vertically corrugated bulkhead, primarily due to excessive wastage of the plating.

- Fig. 106c: Location 5 is subject to fractures of the corrugation connection at the upper wing tank, primarily due to excessive stress in the corrugation plate of the transverse bulkhead.

- Fig. 106d: Location 6 is subject to buckling of the coaming plate brackets for the hatch end frame in the upper wing tank. The buckling can be due to torsional hull girder loading.

- Fig. 106e: Location 7 is subject to high stresses in the contour of the hatch corner bracket. Although failure is typically associated with fatigue-induced fractures, a stress evaluation of the adjacent deck plating will indicate the severity of the problem. The hatch corner contour is typically an elliptical contour. The stress concentration factor for contour edge stress compared to that of the nominal stress in the adjacent deck plating is often 1.5 and higher.

Other critical areas are:

- Inner bottom plating connections to lower wing tank plating and stool plating
- Corrugation connections to stool shelf plating
- Transverse and longitudinal coaming bracket connections to the main deck.

3.17.3 Container Ships. The general cargo ship designed to be capable of carrying all of its cargo in unitized containers is designated as a *container ship*. Most of the ocean-going container ships are not self-sustaining, meaning they depend on shore facilities to load and unload them; others have lifting equipment aboard and,

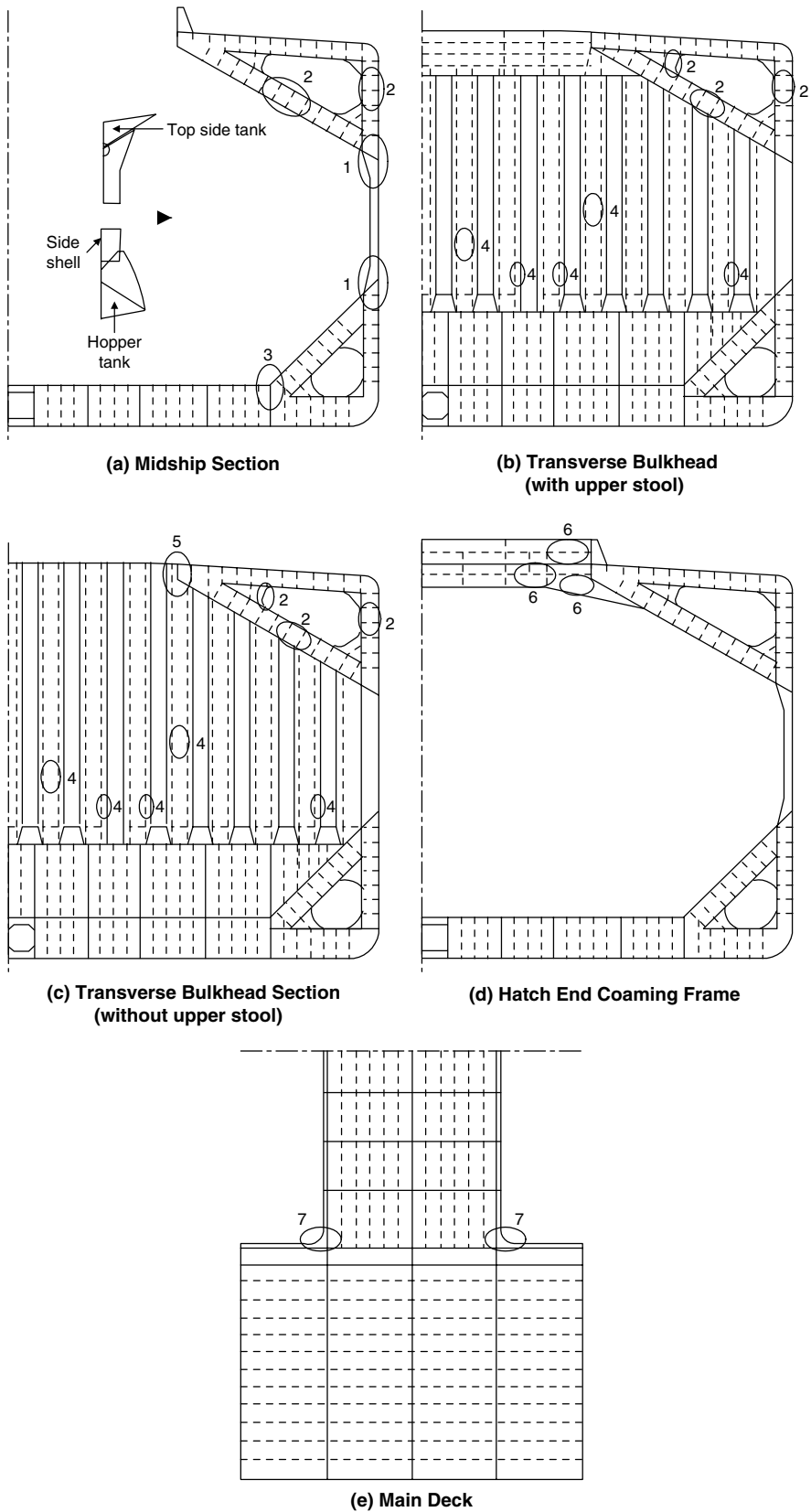


Fig. 106 Critical areas for bulk carriers.

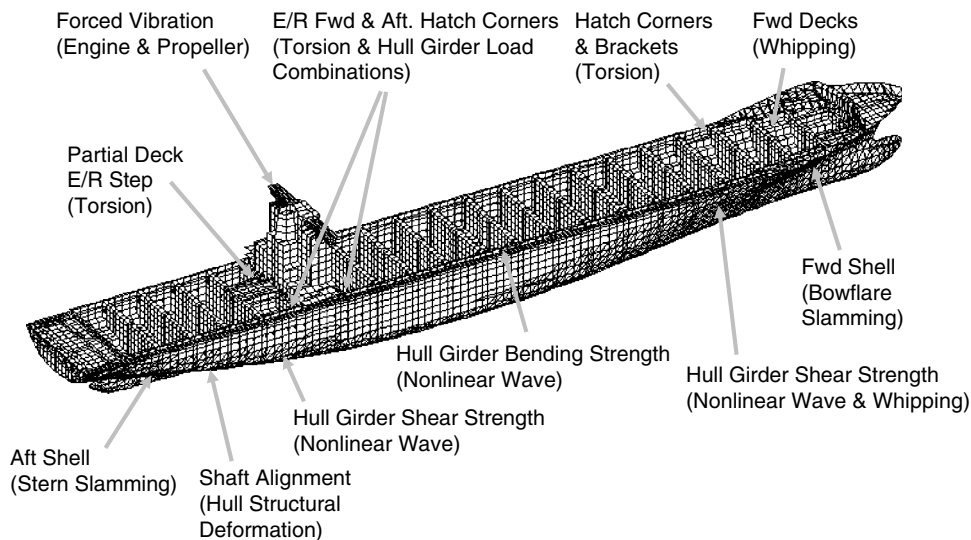


Fig. 107 Areas of concern in container ship structures (Shi et al., 2005).

with respect to loading and unloading containers, are self-sustaining. With regard to the ways that the containers are handled, container ships may be grouped into two types: the vertical cell type and the horizontal loading type. Other features such as the sizes, arrangements and methods of cargo handling of various types of container ship can be found in Chapter 36 of Lamb (2003). This section considers only those with vertical cells.

The container ship of vertical cell type embodies the concept of full cellular stowage within the holds, plumbing directly down through a multiple array of vertical cells in a guided arrangement necessary to secure the containers without damage against motions at sea. The vertical loads of the stacked containers in the hold are normally transmitted directly to the double bottom structure, with the vertical cell guide structure taking only the transverse forces due to ship motion, list, and trim. Additionally, container ships are designed to carry containers on deck, stacked four to five high and secured by systems of lashing, purposely to afford sufficient dead-weight carrying capacity for what is normally a high-cubic, low-weight cargo system. To protect this exposed cargo against the forces of sea, particularly with regard to green seas taken over the bow, an unusually high forecastle is provided, along with a well-flared bow shape.

Container ships demand high operational speeds, efficient stowage, and rapid handling of containers. Such a mission results in a long, fine form hull with a main deck devoted almost entirely to hatch openings throughout its length and breadth. A recent trend in container vessel design indicates that the length and width of the “open deck” section forward of the engine room have been stretched to more than 60 percent of the ship length and more than 90 percent of the ship breadth. For such types of configuration, considerations must be given to

longitudinal strength, transverse structure for racking and torsional strength, vertical structure to support deck loads, and tie-in structure to stabilize all major structural elements to keep them in working position and prevent buckling. Shown in Fig. 107 are some of the structural components where special considerations are required for design.

3.17.3.1 Areas of Concern. The structural configuration of a container ship with large open deck sections maximizes the load-carrying capacity and optimizes the loading and unloading operation, but at the same time results in a structural design that may be more critically affected by torsional loads in a seaway. In particular, the size of recent Super Post-Panamax or ultra large container ships exceed 9,000 TEU (twenty-foot equivalent units) capacity with lengths of about 350 m. For these ultra large container ships, the length overall is capped around 400 m, the length limit of some existing new building docks but considerably longer than that of the largest oil carrier in service. Ultra large container ships are designed with a breadth over 50 m to maximize on-deck container carrying capacity. With a typical double side width less than 3 m, the open deck structure of an ultra large container carrier is intrinsically more flexible than its smaller counterparts, resulting in greater hatch opening distortion. Reduced forebody deck area for the purpose of maximizing container capacity in forebody cargo holds can further aggravate this problem. Increased breadth for greater on-deck container capacity can lead to significant bow flare and an overhanging stern, which are the contributing factors for nonlinear motions and sea loads. Also with increased breadth, the double bottom structure becomes a greater load-bearing member, and the outboard portion of double bottom floors can be critically stressed.

The hull girder natural frequencies of Post-Panamax container carriers or larger, being inversely proportional to $L^{3/2}$, can fall within the frequency range of bow flare slamming forces. Therefore, whipping-induced hull girder loads should be explicitly considered for these vessels. Length overall can also influence the positioning of the deckhouse to meet the SOLAS visibility requirements. Ultra large container carriers can be either single or twin deck house designs. For the single deck house design, the deckhouse is more likely to be shifted towards the midship region. This shift has design implications on the most critical hatch corners fore and aft the deckhouse. In addition, a slender deckhouse sitting on a flexible hull structure is more likely to resonate under vibratory forces from the main engine that provides the necessary shaft power to maintain the vessel's service speed. Hence, forced vibration analysis should be an integral part of the design assessment.

The Post-Panamax and larger container ships can encounter significant torsion-induced displacement and longitudinal stresses along the strength deck and hatch coaming top. The torsion-induced stresses are maximized at the hatch corners and at the aft end of the hatch opening immediately forward of the engine room, where the stress has nearly the same order of magnitude as that induced by the vertical hull girder bending moments.

3.17.3.1.1 Hull Girder Torsional Stiffness. Of major concerns in hull structures of container ships is that the ship should have adequate torsional stiffness to prevent excessive hull girder distortion due to large torsion loads. There are several approaches for defining the stiffness requirements, and one of them is determined based on the distortion of hatch opening as described in the ABS SafeHull requirements for container ships.

Consider a hatch opening of l_0 in length, b_0 in width, and Δ_0 in diagonal length. Assume that the hull girder is distorted due to a torsion moment T , where the relative displacement of hatch opening is Δ_L in longitudinal direction and Δ_T in transverse direction. Denoting the diagonal length of hatch opening after distortion by Δ_1 , then the change of the diagonal length, denoted by Δ , is given by

$$\Delta = \Delta_1 - \Delta_0 = [(l_0 + \Delta_L)^2 + (b_0 + \Delta_T)^2]^{1/2} - (l_0^2 + b_0^2)^{1/2} \cong (\Delta_L l_0 + \Delta_T b_0)/(b_0^2 + l_0^2)^{1/2} \quad (226)$$

To find the relative displacements, Δ_L and Δ_T , assume that the torsion-induced longitudinal displacement u_i may have to be approximated assuming the thin-wall shell theory applicable to the open sections of the cargo block (see Chapter 4 in Lewis 1988). That is, the following differential equation is to be considered:

$$E\Gamma\Theta'''(x) - GJ\Theta'(x) = -T_m(x) \quad (227)$$

and

$$u(x, s) = 2\Theta'(x)\omega(s) \quad (228)$$

where

- Θ = twist angle
- Γ = Saint-Venant torsional constant
- E = modulus of elasticity
- G = shear modulus of the material
- J = torsional constant of the section
- T_m = total twist moment
- ω = warping function
- x = longitudinal coordinate along the vessel
- s = contour coordinate

Applying equation (228) leads to

$$\Delta_L = 2\omega d\Theta/dx \quad (229)$$

and

$$\Delta_T = h_e l_0 d\Theta/dx \quad (230)$$

where

- Θ = twist angle at mid-length of hatch opening
- h_e = distance between shear center and the strength deck
- ω = warping function

The rate of twist in equations (229) and (230) can be approximately expressed in a form (see Boytsov et al 1979):

$$d\Theta/dx = CTL_0^2/(E\alpha\Gamma) \quad (231)$$

where

- C = constant
- L_0 = length of cargo block of the vessel
- $\alpha = 1 + 0.04JL_0^2/\Gamma$

All the other parameters are defined in equations (228) and (229).

Substituting equations (229), (230), and (231) into (226), the ratio of the change in diagonal length in terms of original length can be written as

$$\Delta/\Delta_0 = C(2\omega + h_e b_0)l_0 T L_0^2/[E\alpha\Gamma(b_0^2 + l_0^2)] \quad (232)$$

from which the required hull girder torsional stiffness, $\alpha\Gamma$, can be obtained by specifying the acceptable distortion of Δ/Δ_0 . It is noted that the constant C in equation (232) varies with different arrangements of longitudinal deck girders and the rate of twist (slope of distortion) of the hull structure. The constant also depends on the torsional moment distribution along the length of the vessel, as well as the stiffness of the cross decks. Constant C is to be determined from adequate structural analyses.

3.17.3.1.2 Hatch Corners. High stresses may occur at hatch corners, particularly, adjacent to the engine housing and at the forward end of the open block due to an abrupt change in torsional rigidity. In the types of hatch openings found in traditional cargo ships, where

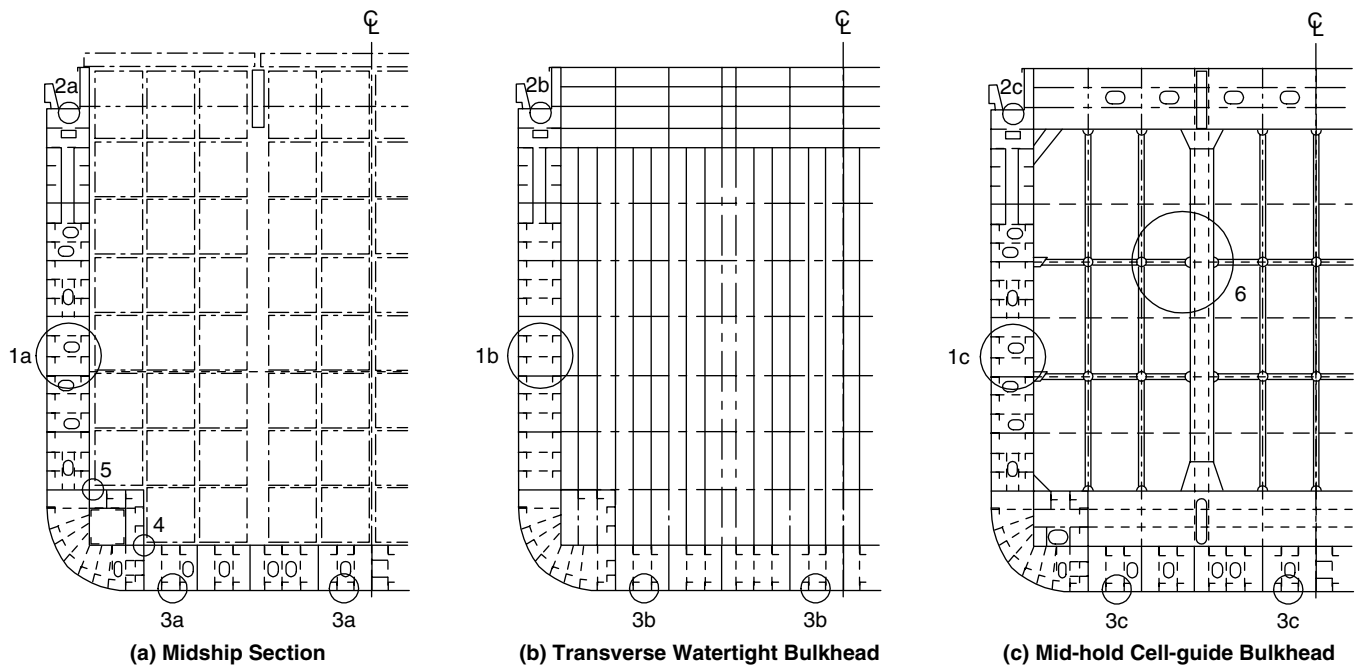


Fig. 108 Critical areas in container ships—transverse sections.

the hatch opening was less than half of the deck beam, the main deck structure where the torsional stresses were small was designed primarily to withstand longitudinal bending stresses and bending-induced local stresses in the vicinity of the hatch corner. When the size of hatch openings are increased, with deeper hatch coamings and heavier side deck stringers as found in large container ships, torsion effects must be included in evaluating deck structure strength and stress concentration at hatch corners.

The configurations of typical hatch corners can be of without or with cut-out, whereas the contour of the corner can be single circular, double curvature, elliptical, or a combination of any two of the basic configurations, as illustrated in Section 3.13. Estimation of stress concentrations at hatch corners usually relies on structural analysis. Numerical results of analyses indicate that for the case of hull structures under pure longitudinal bending, stress concentration factors at hatch corners with and without cut-out are similar, provided that the curvatures of the two are the same. When torsion effects such as longitudinal shear force or pure torsion in the cross deck beam are present, a hatch corner with cut-out would reduce the stress concentration more than one without the cut-out.

3.17.3.2 Critical Areas. Figures 108 and 109 show some critical areas in a typical container ship hull structure. These areas are found to be subject to high local stress under various loading conditions. The critical areas are often found in the following locations:

- Locations 1 to 3, (a) to (c), are possible areas of stress concentration susceptible to fatigue fractures.

- Location 4 is the intersection of the inner bottom to the inboard longitudinal bulkhead. High stresses can be expected in the floor web at the connection of the inner bottom to the inboard longitudinal bulkhead due to high shear and double bottom deformation.

- Location 5 is the intersection of the longitudinal bulkhead to the first stringer. High stresses are possible at the lower end of the longitudinal bulkhead and in the side web connecting to the first stringer above the inner bottom, mainly due to structural discontinuity at the connection.

- Location 6 is in the mid-hold transverse bulkheads. The mid-hold structure that supports cell guides is a load-carrying structure and an integral part of the ship hull. The structure should be included in the three-dimensional global model for analysis. High stresses are possible in the cell guide bulkhead due to cargo hold container loads and interaction with the hull girder structure.

- Location 7 are the main deck hatch corners, which are one of the most critical areas of the container ship hull structure, particularly the ones forward of the deckhouse. High stresses occur in hatch corner brackets or contour cut-outs due to additional stress caused by warping constraint under torsional loads. Hatch corner failures are usually associated with fatigue damage.

- Locations 8 are the corners of the hatch coaming top. The corners of the hatch side and hatch end

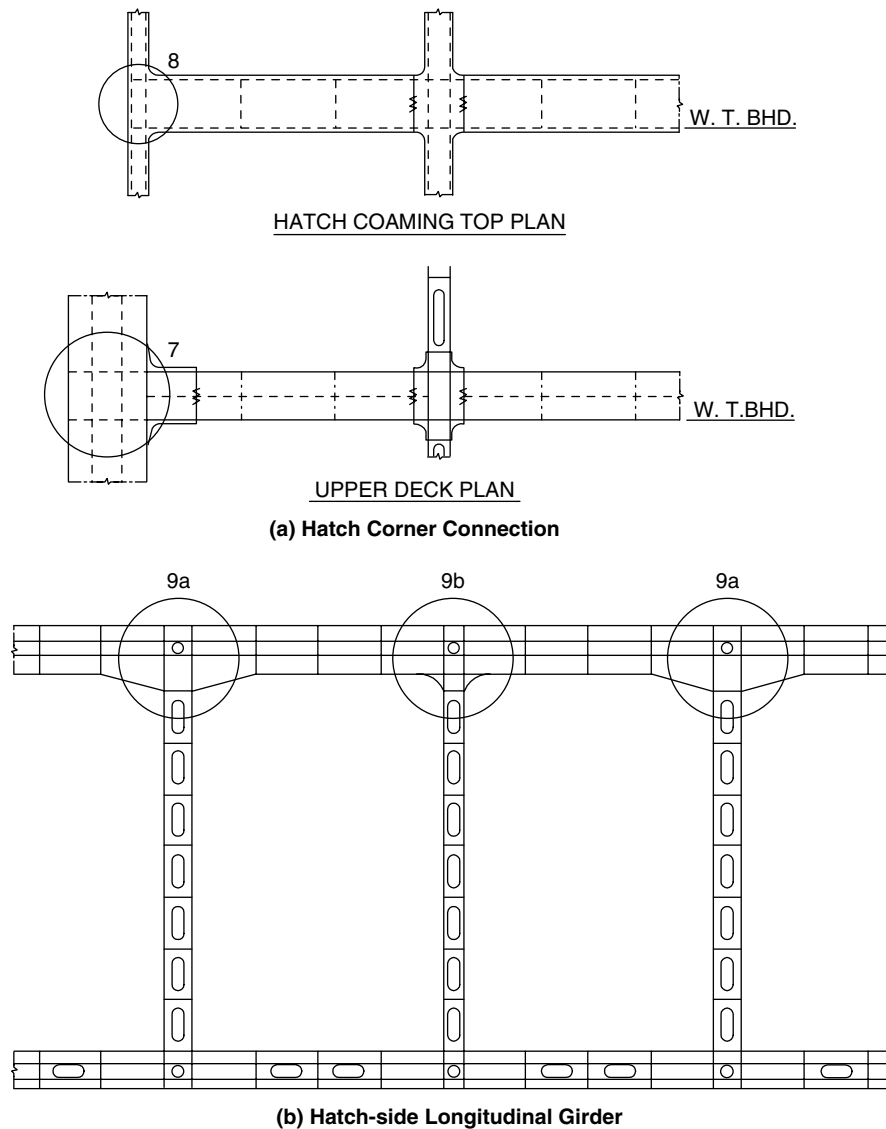


Fig. 109 Critical areas in container ships—deck and longitudinal sections.

coaming top plates have high stress concentration at midship and forward of the deckhouse, especially due to hull girder torsional loads.

- Locations 9 are the connections of the longitudinal hatch girder to the hatch end coaming. The hatch side girder is continuous over all cargo holds

and included in the three-dimensional global model (with consideration to its typically soft ending). High stresses are generally expected at the intersections of the hatch-side girder to the hatch end coaming, which is a result of the hull girder distortion under torsional loads.

Section 4

Load Carrying Capability and Structural Performance Criteria

4.1 The Nature of Structural Failure. As noted in the introduction, ship structural failure can occur as a result of a variety of causes, and the degree or severity of the failure may vary from a minor esthetic degradation to catastrophic failure resulting in the loss of the ship. In the report of the Committee on Design Procedures of the International Ship Structures Congress (ISSC 1973), four contributing failure mechanisms or modes were defined:

- Tensile or compressive yield of the material
- Compressive instability (buckling)
- Low-cycle fatigue
- Brittle fracture.

The finite mode of failure occurs when the stress in a structural member exceeds a level that results in a permanent plastic deformation of the material of which the member is constructed. This stress level is termed the material *yield stress*. At a somewhat higher stress, termed the *ultimate stress*, fracture of the material occurs. Although many structural design criteria are based upon the prevention of any yield whatsoever, it should be observed that localized yield in some portions of a structure is not necessarily serious and may, in case of non-reversing loads, result in a more favorable redistribution and equalization of stress throughout the structure.

Instability failure of a structural member loaded in compression can occur at a stress level that is substantially lower than the material yield stress. The load at which instability or buckling occurs is a function of member geometry and material modulus of elasticity rather than material strength. The most common example of an instability failure is the buckling of a simple column under a compressive load that equals or slightly exceeds the Euler critical load. A plate in compression will also have a critical buckling load whose value depends on the plate thickness, lateral dimensions, edge support conditions, and material modulus of elasticity. In contrast to the column, exceeding this load by a small margin will not necessarily result in the complete collapse of the plate but only in an elastic deflection of the central portion of the plate away from its initial plane. After removal of the load, the plate will return to its original undeformed configuration. The ultimate load that can be carried by a buckled plate is determined by the onset of yielding at some point in the plate material or in the stiffeners, in the case of a stiffened panel. Once begun, yield may propagate rapidly throughout the entire plate material near the edges with further increase in load.

Fatigue failure occurs as a result of a cumulative effect in a structural member that is exposed to a stress pattern alternating from tension to compression through many cycles. Conceptually, each cycle of stress causes some small but irreversible damage within the material and, af-

ter the accumulation of enough such damage, the ability of the member to withstand loading is reduced below the level of the applied load. Two categories of fatigue damage are generally recognized, and these are termed high-cycle and low-cycle fatigue. In *high-cycle fatigue*, failure is initiated in the form of small cracks that grow slowly and may often be detected and repaired before the structure is endangered. High-cycle fatigue involves several millions of cycles of relatively low stress (less than yield) and is typically encountered in machine parts rotating at high speeds or in structural components exposed to severe and prolonged vibration. *Low-cycle fatigue* involves greater stress levels, up to and beyond yield, that may result in cracks being initiated after several thousand cycles.

The loading environment that is typical of ships and ocean structures is of such a nature that the cyclic stresses may be of a relatively low level during the greater part of the time, with occasional periods of very high stress levels caused by storms. Exposure to such load conditions may result in the occurrence of low-cycle fatigue cracks after an interval of a few years. These cracks can grow to serious sizes if they are not detected and repaired.

In the fourth mode of failure, brittle fracture, a small crack suddenly begins to grow and travels almost explosively through a major portion of the structure. The originating crack is usually found to have started as a result of poor design or manufacturing practice, as in the case of a square hatch corner or an undetected weld flaw. Fatigue is often found to play an important role in the initiation and early growth of such originating cracks. The control of brittle fracture involves a combination of design and inspection standards aimed at the prevention of stress concentrations, and the selection of steels having a high degree of notch toughness or resistance to the growth of cracks, especially at low temperatures. Crack arrestors are often incorporated into the structure to limit the travel of a crack if it should occur (fail-safe design).

In designing the ship structure, the analysis phase is concerned with the prediction of the magnitude of the stresses and deflections that are developed in the structural members as a result of the action of the sea and other external and internal causes. Many of the failure mechanisms, particularly those that determine the ultimate strength and total collapse of the structure, involve nonlinear material and structural behavior that are beyond the range of applicability of the linear structural analysis procedures described elsewhere in this chapter, which are commonly used in design practice. It is one of the difficulties facing the structural designer who often use linear analysis tools in predicting the behavior of a structure in which the ultimate capability is governed

by nonlinear phenomena. This is one of the important sources of uncertainty referred to in the introduction.

After performing an analysis, the adequacy or inadequacy of the member or the entire ship structure must then be judged through comparison with some type of criterion of performance. The conventional criteria that today are commonly used in ship structural design are usually stated in terms of acceptable levels of stress in comparison to the yield or ultimate strength of the material, or as acceptable stress levels compared to the critical buckling strength of the structural member. Such criteria are intended specifically for the prevention of the first two of the four types of failure—tensile yield or compressive buckling.

Design criteria stated expressly in terms of cumulative fatigue criteria are used in ship and offshore structure design. Fatigue considerations are especially important in the design of details such as hatch corners, reinforcements for openings in structural members and at bracket toes. Because the ship loading environment, consisting in large part of alternating loads, is highly conducive to fatigue-type failures, fatigue resistance is an important design consideration.

As noted previously, the prevention of brittle fracture is largely a matter of material selection and proper attention to the design of structural details to avoid stress concentrations. Quality control during construction and in-service inspection form key elements in a program of fracture control.

4.2 Material Physical Properties and Yield Criteria.

The physical strength properties of shipbuilding materials are normally obtained from standardized testing procedures conducted under closely controlled conditions, as described in Chapter 20 of Lamb (2003). The yield strength of the material is defined as the measured stress at which appreciable nonlinear behavior accompanied by permanent plastic deformation of the material occurs. The ultimate strength is the highest level of stress achieved before the test specimen fractures. For most shipbuilding steels, the yield and tensile strengths in tension and compression are assumed equal.

The material properties described previously are expressed in the form of simple uniaxial stresses (i.e., the test from which they are obtained is conducted in such a way that the test specimen is subject to stress in the longitudinal direction only), and the transverse stresses are zero. Few ship structural members, chiefly the flanges of slender stiffeners or slender columns, experience pure uniaxial stress. However, in these cases the computed member stresses can be compared directly with the uniaxial test data to ascertain the adequacy of the member.

In the plate members of the hull structure, the stresses do not form a simple unidirectional pattern. The maximum values of the primary, secondary, and tertiary stresses may not coincide in direction or time, and therefore combined stresses should be calculated (as discussed in Section 3.11) at various locations and times. Furthermore, the stress at each point will not be a sim-

ple unidirectional tension or compression but, in most cases, will be found to form a bi-axial stress pattern.

The stress criterion that must be used in this situation is one in which it is possible to compare the actual multi-axial stress with the material strength expressed in terms of a single value for the yield or ultimate stress. For this purpose, there are several theories of material failure in use, of which the one usually considered the most suitable for ductile materials such as ship steel is referred to as the *distortion energy theory*. (This is also called the octahedral shear stress theory or Hueber-von Mises-Hencky theory.) To illustrate the application of this theory, consider a plane stress field in which the component stresses are σ_x , σ_y , and τ , and the corresponding principal stresses are σ_1 and σ_2 . The distortion energy theory states that failure through yielding will occur if the equivalent stress, σ_e , given by

$$\begin{aligned}\sigma_e &= (\sigma_x^2 + \sigma_y^2 - \sigma_x\sigma_y + 3\tau^2)^{1/2} \\ &= (\sigma_1^2 + \sigma_2^2 - \sigma_1\sigma_2)^{1/2}\end{aligned}\quad (233)$$

exceeds the equivalent stress corresponding to yielding of the material test specimen. However, the standard material test data are obtained from a uniaxial stress pattern for which $\sigma_x = \sigma_{yield}$, $\sigma_y = 0$, and $\tau = 0$. The material yield strength may therefore be expressed through an equivalent stress at failure, σ_0 , obtained by substituting the previous values into equation (233):

$$\sigma_0 = \sigma_{yield}\quad (234)$$

Therefore, the margin against yield failure of the structure is obtained by a comparison of the structure's σ_e against σ_0 , giving the result

$$\sigma_{0x}^2 = \sigma_1^2 + \sigma_2^2 - \sigma_1\sigma_2\quad (235)$$

Equation (235) is the equation for an ellipse in the $\sigma_1\sigma_2$ plane and is illustrated in Fig. 110. Pairs of values ($\sigma_1\sigma_2$)

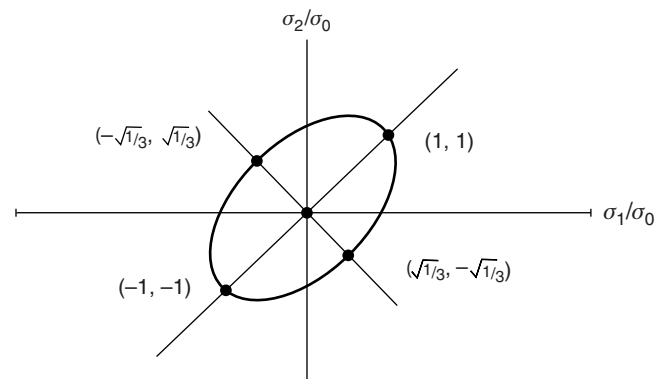


Fig. 110 Failure contour according to the distortion energy theory.

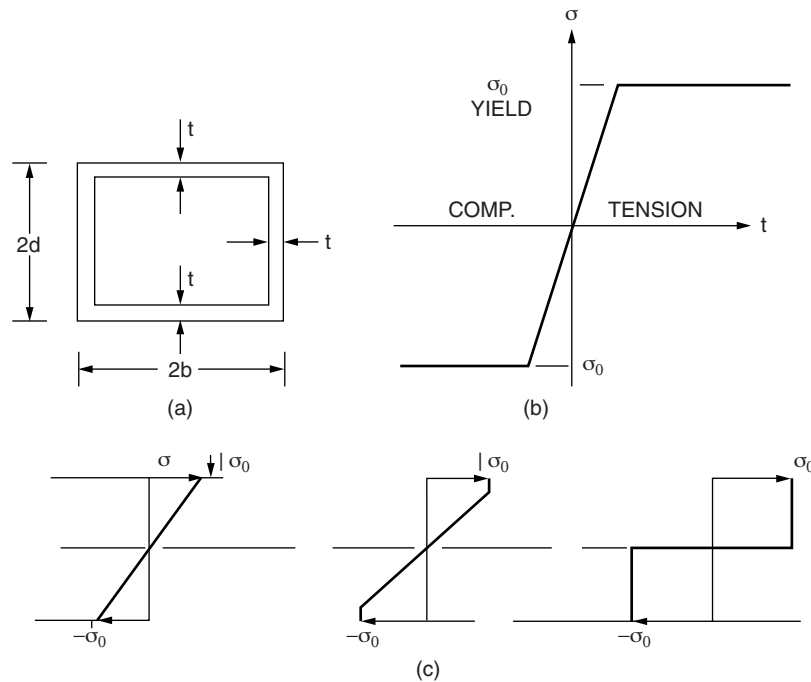


Fig. 111 Ultimate strength of simple box girder.

lying outside the ellipse correspond to failure by yielding according to this theory.

4.3 Ultimate Strength of Box Girder in Yield. As noted previously, the initial occurrence of local yielding does not necessarily signal the total collapse of the structure. Depending on the importance and function of the structural member in question, the appropriate design criterion may be severe, requiring the avoidance of any occurrence of yield, or it may be relaxed to require only the prevention of total collapse of the member. In the latter case, yield would be allowed to a limited extent under the maximum design load. For example, strength deck plating might be designed so as never to experience yield under any circumstances. Subdivision bulkhead stiffeners in a dry cargo hold could be designed to yield under conditions of flooding due to damage, so long as the bulkhead retains its watertight integrity, enabling the ship to remain afloat.

As an illustration of the differences in design that can be introduced by the use of an ultimate strength versus a yield criterion, consider the maximum bending moment sustainable by a simple box girder with the thin-walled rectangular cross section shown in Fig. 111a. Assume that the material stress-strain curve may be approximated, as shown in Fig. 111b, by two straight line segments. The initial, elastic part is given by a straight line having a slope equal to the modulus of elasticity. At a stress equal to yield, it is assumed that the strain increases indefinitely without further increase in stress. This is sometimes referred to as the elastic-perfect-plastic behavior of the material. The behavior in com-

pression is assumed to be similar to that in tension but with reversal of sign.

The next Fig. 111c shows the stress distribution in the side of the box girder for the cases:

- Stress is everywhere below yield stress, σ_0
- Stress has just reached yield at deck and bottom
- Stress equals yield everywhere across the section

In the first case, assuming the deck stress is just equal to yield, the moment supported by the section (resultant of the stress distribution) is

$$M_1 = \sigma_0 \left(4bdt + \frac{4d^2t}{3} \right) \quad (236)$$

In the third case, with the stress everywhere equal to yield,

$$M_3 = \sigma_0 \left(4bdt + \frac{4d^2t}{2} \right) \quad (237)$$

If the cross section is square, $b = d$, then the ratio of the ultimate moment to the moment at yield is

$$\frac{M_3}{M_1} = \frac{9}{8}$$

This result shows that the beam is capable of supporting a bending moment at total collapse that is 12.5 percent greater than the moment causing the initial occurrence of yield, if buckling is prevented.

In a complex structure such as a ship, the occurrence of progressive failure is seldom as simple as in this

example because some parts may experience failure by buckling and others by yield. The failure of one member in turn results in a redistribution of the load over the cross section and may drastically modify the load on other members. The analysis of the ultimate bending moment, including both yield and buckling, has been carried out by Caldwell (1965). The computation of the ultimate load capability of real ship structures by incremental finite element procedures is discussed in Section 4.9.

4.4 Instability Failure and Its Prediction. The fundamental characteristics of plate buckling are discussed in Section 4.1. The loads that may cause buckling are the primary hulls bending loads in the secondary panels of stiffened plating in deck and bottom, and the combined primary and secondary loads in the individual tertiary panels of plating between stiffeners. These in-plane stresses may alternate between tension and compression as the ship moves through waves. Tensile or compressive yield failure, which was discussed in the previous section, occurs if the combined stresses in a member exceed the load-carrying capability of the material of which the structure is fabricated. Buckling constitutes a different mode of failure that is possible as a result of instability of the members, and in some cases it may take place at a compressive load substantially less in magnitude than that necessary to cause material yielding. Instability failure depends on the material modulus of elasticity and member geometry. However, its initial occurrence does not depend on either the material yield or ultimate strength. Such an instability or buckling failure can occur in a single panel of plating between stiffeners in a transversely framed ship. The buckling may also be more extensive, involving the stiffeners as well as the plating to which they are attached, and this is the more probable mode in the case of longitudinal framing.

Two important modifications to the originally uniform, unidirectional stress pattern in a plate are found as a result of buckling. First, tensile membrane stresses in the transverse direction are set up near the middle of the plate that tend to resist the out-of-plane deformation. Second, the initially uniform longitudinal compressive stress distribution in the plate changes. The compressive stress in the central, deflected portion of the plate is reduced below the average stress, and the compressive stresses near the restrained edges become greater than the average compressive stress in the panel; this is illustrated in Fig. 112. If the total compressive load on the panel is increased sufficiently, the stress near the panel edges may reach the yield point of the material, resulting in permanent localized deformation. If the load is increased further, this will ultimately lead to total collapse of the panel as the yield zone continues to grow. On the other hand, if the load is relaxed before yield stress is attained at any location, the panel will return to its original undeformed shape. Stiffeners, which are nearly always present in ship structures, will modify the behavior of the plate as they participate in carrying a part of the load, as discussed subsequently.

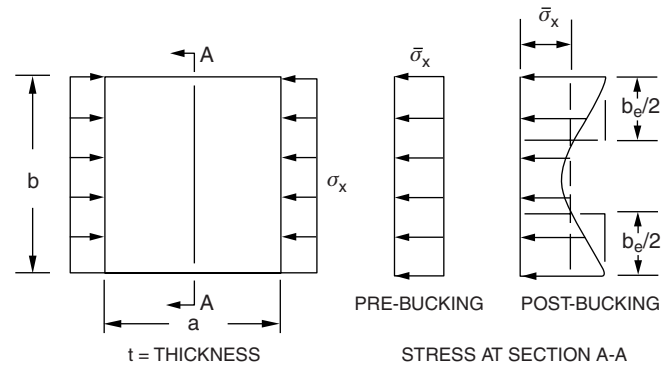


Fig. 112 Plate buckling nomenclature.

By the previous reasoning, it is clear that the maximum load carried by the panel at the time of collapse may be substantially greater than the critical load at the onset of buckling. The ratio of ultimate failure load to critical load is greater for thin plates (i.e., those whose thickness is small compared to their lateral dimensions) than it is for thick plates. In panels of plating having the proportions found in ship structures, this load ratio seldom exceeds 2:1. In the following sections, we shall consider first the elastic buckling of simple plate panels, and then proceed to a discussion of the post-buckling behavior and ultimate strength of stiffened panels.

4.5 Elastic Buckling of Rectangular Plates. The *critical stress* is defined as the highest value of compressive stress in the plane of the initially flat plate for which a nonzero out-of-plane deflection of the middle portion of the plate can exist. For values of stress lower than the critical stress, the plate may be compressed in length but no deflection out of the initial plane occurs. The theoretical solution for the critical buckling stress in the elastic range has been found for a number of cases of interest, and is given by the *Bryan formula*, equation (238). For a rectangular plate subject to a compressive in-plane stress in one direction,

$$\sigma_c = k_c \frac{\pi^2 E}{12(1 - \nu^2)} \left(\frac{t}{b} \right)^2 \quad (238)$$

where the plate nomenclature is shown in Fig. 112.

Here k_c is a function of the plate aspect ratio, $\alpha = a/b$, the boundary conditions on the plate edges and the type of loading. If the load is applied uniformly to a pair of opposite edges only, and if all four edges are simply supported, then k_c is given by

$$k_c = \left(\frac{n}{\alpha} + \frac{\alpha}{n} \right)^2 \quad (239)$$

where n is the number of half-waves of the deflected plate in the longitudinal direction.

Figure 113 presents, k versus a/b for rectangular plates with uniform compressive stress in one direction. Wah

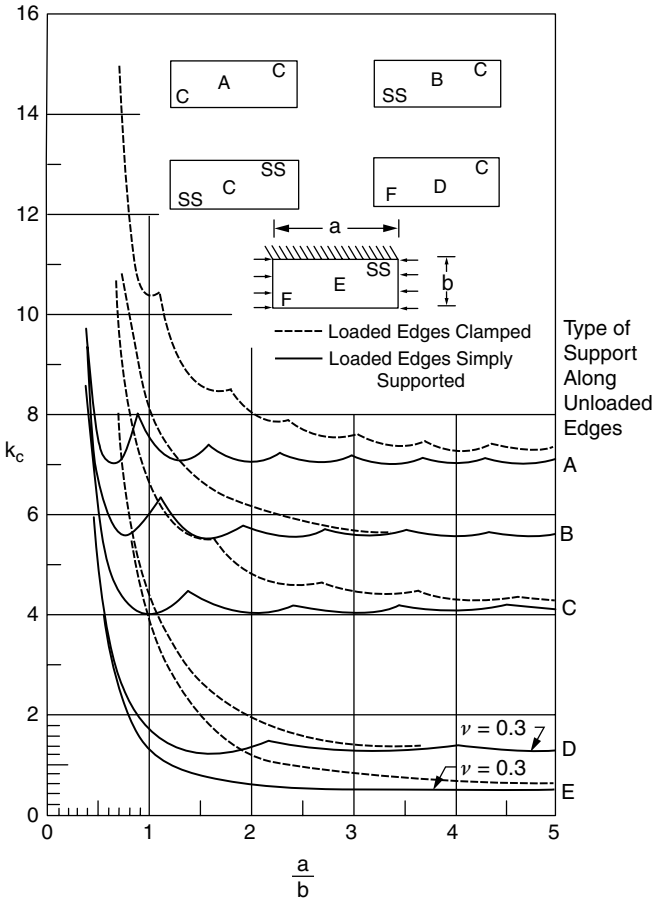


Fig. 113 Compressive buckling coefficients for plates.

(1960), in Chapter 5, presents graphs for a number of other cases including shear loads, linearly varying edge stress, and elastic restraint on the plate edges. If $\alpha < 1$ (wide plates), the critical stress for a simply supported plate at all edges will correspond to $n = 1$, and a more convenient expression for σ_c is given by

$$\sigma_c = \frac{\pi^2 E}{12(1 - \nu^2)} \left(\frac{t}{a}\right)^2 (1 + \alpha^2)^2 \quad (240)$$

where t is the plate thickness. For very wide plates, α approaches zero, this may be replaced by the limiting value,

$$\sigma_c = \frac{\pi^2 E}{12(1 - \nu^2)} \left(\frac{t}{a}\right)^2 \quad (241)$$

For narrow, simply-supported plates, $\alpha > 1$, the coefficient, k_c , of equation (238) is approximately 4 and the elastic critical stress is given by

$$\sigma_c = \frac{\pi^2 E}{3(1 - \nu^2)} \left(\frac{t}{b}\right)^2 \quad (242)$$

It should be emphasized that these formulations for critical stress do not describe the strength of the structural member in question, nor do they even give a stress at which the load-carrying ability of the structure can be expected to be impaired in any substantial way. Elastic material behavior is assumed even after buckling, and therefore upon removal of the load, the buckled member will return to its original undeflected shape. So long as the support of the unloaded edges of the plate remains intact, the only effect of buckling will be a visible deformation of the surface of the plate and an increase in the apparent rate of panel overall strain versus stress.

4.6 Postbuckling Behavior and Ultimate Strength of Simple Plates. In predicting the strength of a plate element, the objective is to determine the maximum average stress that the plate can sustain before the stress at some area reaches the yield strength of the material, at which point plastic deformation or panel collapse occurs. The plate strength data in most common use are based on the concept of an *effective width*, which follows directly from the typical plate stress distribution in the postbuckling regime, as shown in the right part of Fig. 112. The effective width, b_e , is defined as the reduced width of plate that would support the same total load as the buckled plate but at a uniform stress equal to the maximum stress, σ_c , at the plate edge:

$$b_e = (1/\sigma_c) \int_0^b \sigma_x(y) dy \quad (243)$$

where

$$\begin{aligned} \sigma_x(y) &= \text{stress in } x\text{-direction} \\ b &= \text{plate width} \end{aligned}$$

Note that the definition of effective *width*, equation (243), is equivalent to the definition of effective *breadth*, equation (195). Some authorities reserve the term effective *breadth* to refer to the shear lag phenomenon and effective *width* to refer to the postbuckling phenomenon. However, this distinction in terminology is not universal.

A comprehensive review of the numerous formulations proposed and in use for estimating b_e or related quantities for narrow unstiffened plates has been given by Faulkner (1975). Figure 114 adapted from this reference gives the effective breadth ratio, b_{em}/b , or equivalently, the ratio of maximum mean stress at failure to plate yield strength, σ_m/σ_0 . The width parameter, β , against which these curves are plotted is

$$\beta = (b/t) \sqrt{\sigma_0/E} \quad (244)$$

It is derived as follows. Consider a simply supported plate under uniaxial compression. If the aspect ratio, a/b , is greater than 1.0, the coefficient, k_c , of equation (238) is approximately 4 and the elastic critical stress is given, as in equation (242), by

$$\sigma_c = 4 \frac{\pi^2 E}{12(1 - \nu^2)} \left(\frac{t}{b}\right)^2 \quad (245)$$

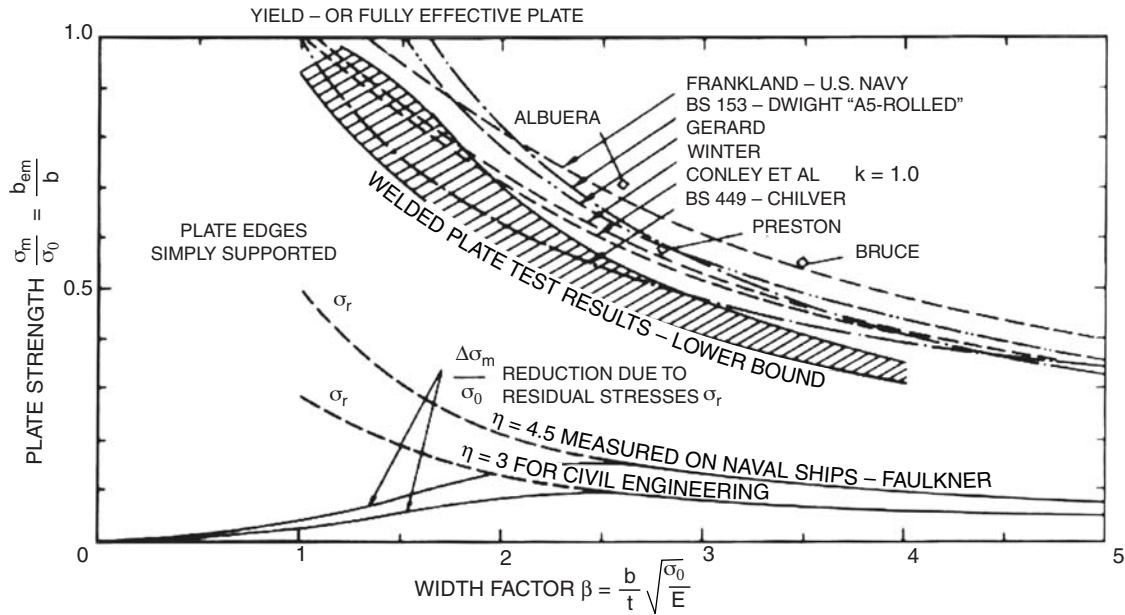


Fig. 114 Plate strength curves for simply supported edges (Faulkner 1975).

For steel, where ν is constant,

$$\sigma_c \propto E(t/b)^2$$

If the plate width, b_0 , is chosen in relation to the thickness, t , so that σ_c equals the yield stress, σ_0 , we obtain

$$b_0 = \pi t \sqrt{E/3(1 - \nu^2)\sigma_0} \propto t \sqrt{E/\sigma_0} \quad (246)$$

The factor β in Fig. 114 is proportional to the ratio of the actual width to this nominal width, given by

$$\beta = \frac{b}{t} \sqrt{\sigma_0/E} \quad (247)$$

This width parameter is often referred to as the plate slenderness ratio.

For steel, where the value of Poisson's ratio is $\nu = 0.3$, the actual value of b_0 in equation (246) becomes

$$b_0 = 1.9t \sqrt{E/\sigma_0} \quad (248)$$

For typical mild steel, the yield strength, σ_0 , is about 240 MPa (35,000 psi) and b_0 , from equation (248), is approximately 55 t. On the basis of experimental data, a somewhat lower value of 50 t is sometimes stated as an appropriate effective width of plating to be used in design.

A suitable design formula for expressing the effective width of simply supported rectangular plates without residual stress is suggested:

$$\frac{b_{em}}{b} = \frac{\sigma_m}{\sigma_0} = \frac{2}{\beta} - \frac{1}{\beta^2} \quad (249)$$

where

b_{em} = minimum effective width
 σ_m = maximum average plate stress

The effectiveness of plating in compression will also be modified by three factors, in addition to plate dimensions and material properties:

- Initial deformation, due principally to welding distortion
- Residual stresses, also resulting from welding
- Normal pressure.

It is suggested that if the maximum initial panel deflection is less than 0.3 t, buckling strength is not affected. On the other hand, Faulkner (1975) reports the results of numerous measurements of ships in drydock that indicate larger deformations may be expected in lightly plated naval vessels.

The effect of residual stress also is to reduce the maximum mean stress that the plate can sustain. For values of $\beta > 2$, it is suggested that σ_m be merely reduced by σ_r , where σ_r is the value of residual stress. For lower values of β , the reduction is dominated by inelastic effects and results can be found in Bleich (1952). These results are plotted, along with experimental data, in Fig. 114.

Cui and Mansour (1997) considered the simultaneous effect of initial deformation and residual stresses on the ultimate strength of plates. In their study, they included the impact of the shape of the initial deformation, as this may affect the ultimate strength even for the same magnitude of maximum initial deflection w_0 . Recently, Bai (2006) further verified this conclusion through finite element analysis. In Cui and Mansour's study, they also

suggested a semi-empirical equation for calculating the ultimate strength of imperfect plates (i.e., plates with initial deformation and residual stresses):

$$\frac{b_{em}}{b} = \frac{\sigma_m}{\sigma_0} = \phi_{up} R_d R_r \quad (250)$$

where

ϕ_{up} = ultimate strength ratio of a perfect plate (i.e., a plate without initial deflection or residual stresses)

$$= \frac{\sigma_{mp}}{\sigma_0}$$

$$\phi_{up} = 1.0 \quad \text{if } \beta < 1.9$$

$$= 0.08 + \frac{1.09}{\beta} + \frac{1.26}{\beta^2} \quad \text{if } \beta > 1.9$$

σ_{mp} = average stress in a perfect plate at failure

σ_m = average stress in an imperfect plate at failure

R_d = strength reduction factor due to plate unfairness

$$= 1 - 0.2433 f(\alpha) g(\beta) \left(\frac{\omega_0}{t} \right)^{0.911}$$

ω_0 = maximum initial deflection

$$f(\alpha) = 2.050 - 1.376\alpha + 0.366\alpha^2 - 0.0345\alpha^3$$

$$g(\beta) = 2.280 - 2.568\beta + 1.288\beta^2 \quad \text{for } 1.0 < \beta \leq 1.9$$

$$= 8.191 - 4.224\beta + 0.522\beta^2 \quad \text{for } 1.9 < \beta \leq 2.5$$

$$= 4.593 - 2.162\beta + 0.273\beta^2 \quad \text{for } 2.5 < \beta \leq 4.0$$

R_r = strength reduction factor due to residual stresses

$$= 1.00 - 0.46(\beta - 1.5)^{0.275} \eta^{0.725}$$

η = normalized residual stress

$$= \frac{\sigma_{rc}}{\sigma_0}$$

σ_{rc} = average compressive residual stress

As a default value, $\frac{\omega_0}{t}$ can be calculated from

$$\frac{\omega_0}{t} = 0.1\beta^2 \quad 1 \leq \beta \leq 2.5$$

$$= 0.25\beta \quad 2.5 \leq \beta \leq 4.0$$

The normalized residual stress η normally varies between 0.1 to 0.2.

For plate dimensions and pressures encountered in ship plating, the effect of normal pressure on plate strength is small and may be neglected. Theoretical and experimental studies reported by Okada et al. (1979) have shown that the effect of normal pressure on the ultimate strength of ship plating is usually negligible.

Recently, Bai (2006) examined the effect of fatigue cracks on the ultimate strength of simple plates using the finite element method. Some equations based on the numerical results for calculating the ultimate strength of

simple plates with fatigue cracks are proposed. Equations (251) and (252) give the nominal ultimate tensile strength of a plate with edge and center fatigue cracks, respectively, as a function of crack length to plate breadth ratio:

$$\phi_{eu} = \frac{\sigma_u}{\sigma_Y} = 1.2925 - 1.8514 \left(\frac{c}{b} \right) + 1.1291 \left(\frac{c}{b} \right)^2 - 0.5308 \left(\frac{c}{b} \right)^3 \quad (251)$$

$$\phi_{cu} = \frac{\sigma_u}{\sigma_Y} = 1.3367 - 2.3320 \left(\frac{c}{b} \right) + 3.4013 \left(\frac{c}{b} \right)^2 - 2.8880 \left(\frac{c}{b} \right)^3 \quad (252)$$

where

ϕ_{eu} = nominal ultimate tensile strength of the edge-cracked plate

ϕ_{cu} = nominal ultimate tensile strength of the center-cracked plate

σ_u = ultimate tensile strength of the cracked plate

σ_Y = yield strength of the cracked plate

c = crack length

b = plate breadth

It has been proposed in the literature to use the following simplified equations for ultimate strength:

- Simplified equation 1:

$$\sigma_u = \frac{A_c}{A_0} \sigma_Y$$

- Simplified equation 2:

$$\sigma_u = \frac{A_c}{A_0} \sigma_T$$

where

σ_T = ultimate tensile strength of an intact plate

A_c = remaining cross-sectional area of a cracked plate

A_0 = total cross-sectional area of an intact plate

Figure 115 shows a comparison between the proposed equation (251) and the simplified equations. It is obvious that the simplified equations provide lower and upper bounds of the ultimate strength for edge-cracked plates under axial tensile load, and the proposed equation can capture the ultimate strength behavior of the crack-damaged structure more accurately.

Based on the finite element results, equation (253) was derived by Bai (2006) using regression analysis to calculate the ultimate compressive strength of an edge-cracked plate. Equation (253a) was adopted from Paik et al. (2004):

$$\phi_u = \frac{\sigma_u}{\sigma_Y} = \phi_{uo} R_{ec} \quad (253)$$

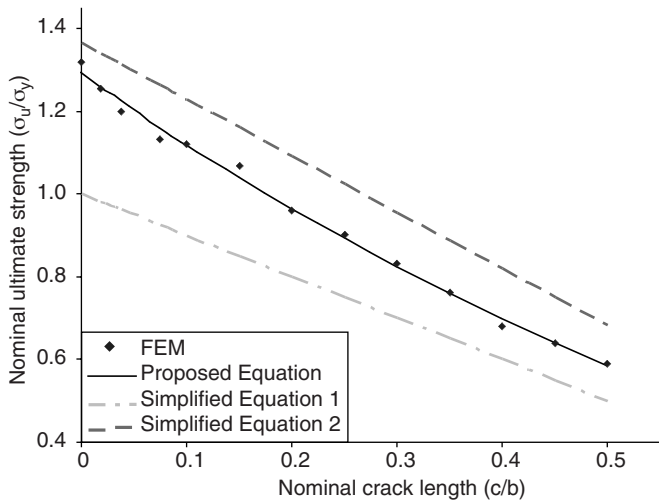


Fig. 115 Nominal ultimate tensile strength of edge-cracked plates obtained by FEM and simplified methods.

where

$$\phi_{uo} = \frac{\sigma_{uo}}{\sigma_Y} = \begin{cases} -0.032\beta^4 + 0.02\beta^2 + 1.0 & \text{for } \beta \leq 1.5 \\ 1.274/\beta & \text{for } 1.5 < \beta \leq 3.0 \\ 1.248/\beta^2 + 0.283 & \text{for } \beta > 3.0 \end{cases} \quad (253a)$$

$$R_{ec} = 1.0167 - 1.278 \left(\frac{c}{b}\right) + 0.3075 \left(\frac{c}{b}\right)^2 \quad (253b)$$

$$\beta = \frac{b}{t} \sqrt{\frac{\sigma_Y}{E}} \quad (253c)$$

c = crack length
 b = plate breadth
 t = plate thickness

Figure 116 shows a comparison of the equations proposed by Bai (2006) and Paik et al. (2005). From the experiments and finite element analysis, the edge crack has a relatively minor effect on the ultimate compressive

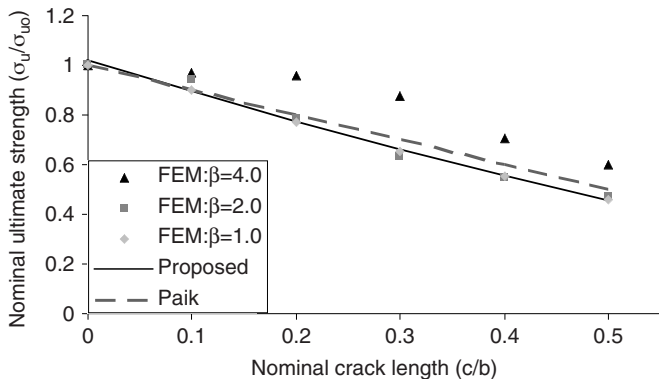


Fig. 116 Nominal ultimate compressive strength of cracked plates obtained by FEM, and comparison with simplified equations.

strength of a thin plate when the crack size is small. As the plate gets thicker, the effect of the crack becomes more and more crucial to the strength of the plate.

4.7 Elastic Buckling of Stiffened Panels. In the previous section, the stability and strength of individual simple plate panels was considered with various types of edge restraint. Stiffened plate panels are of greater practical interest, particularly when subject to in-plane loading resulting from the primary bending of the hull girder. This type of buckling behavior, as was the case with the bending behavior treated in Section 3.8, will involve the interaction of plates and stiffeners in response to the applied loading. In the case of longitudinally framed ships, the stiffened panel behavior plays a more important role than the individual plate panel in determining the ultimate strength of the ship's structure because, in this case, catastrophic buckling of the simple panel is unlikely without the involvement of its associated stiffeners. On the other hand, for transversely framed ships, individual panel buckling with the frames forming nodal lines is the most probable buckling mode. For a comprehensive review of the buckling behavior of stiffened plate panels, the reader is referred to Mansour (1977).

Four different modes of buckling are usually recognized in describing the behavior of a stiffened plate panel, and these are illustrated in Fig. 117. Mode 1 is the simple buckling of the plate panel between stiffeners, and was discussed in the previous section.

Mode 2 consists of flexural buckling of the individual stiffener together with its effective breadth of plating in a manner analogous to a simple column. For a panel with the edges simply supported, Mansour gives the following expression for the critical stress:

$$\sigma_{cr} = \frac{\pi^2 EI}{Al^2} \left[\frac{1}{1 + \frac{\pi^2 EI}{l^2 GA_s}} \right] \quad (254)$$

Here, I is the effective moment of inertia of the stiffener plus associated plating, where

A = total cross section area
 A_s = shear area
 l = length of the stiffener
 G = shear modulus

The effect of shear deformation is seen to be included in this expression. A treatment of panels subject to other boundary conditions is given in Bleich (1952).

Mode 3 is referred to as the lateral-torsional or tripping mode. In this mode, the stiffener is relatively weak in torsion, and failure is initiated by twisting of the stiffener in such a way that the joint between stiffener and plate does not move laterally. A portion of this adjacent plate may participate in the twisting, the flange of the stiffener may twist together with the web, or the two may twist differentially. The critical stress for the lateral-torsional Mode

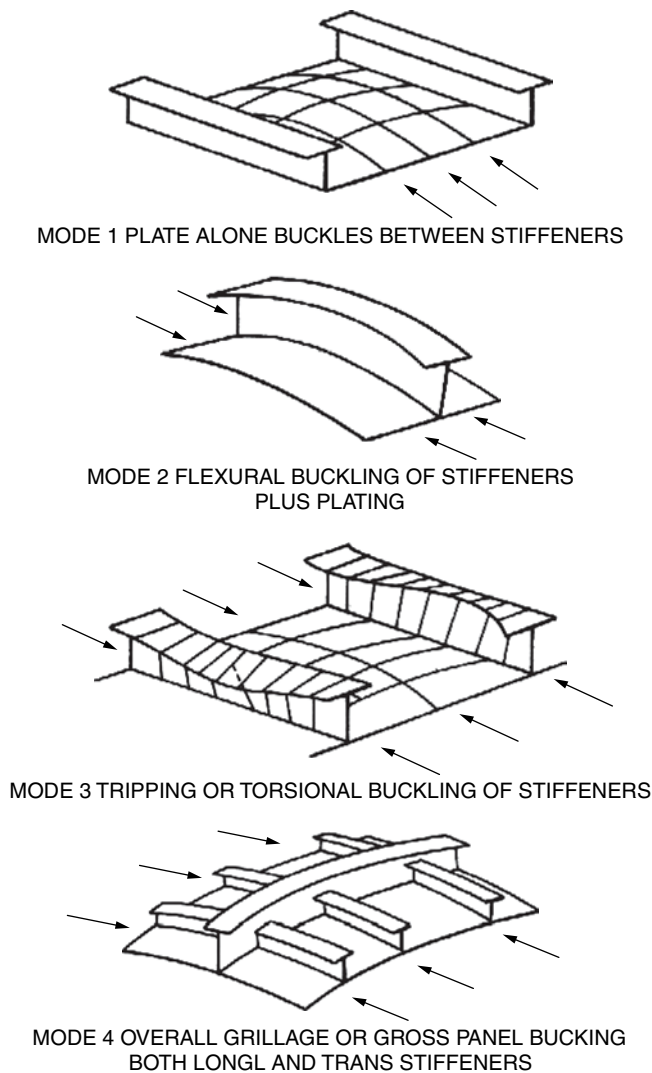


Fig. 117 Four modes of stiffened panel buckling.

3 is given by a formula from Bleich (1952):

$$\sigma_{cr} = \frac{\pi^2 E}{(l/r_c)^2} \quad (255)$$

Here,

l = stiffener length

r_c = effective radius of gyration of the cross section

Bleich gives expressions and charts from which to estimate the effective radius of gyration for a variety of stiffener cross sections. In general, the means of predicting the occurrence of this mode of buckling are somewhat less reliable than the other three modes. Fortunately, Mode 3 can usually be avoided by fitting tripping brackets to the web of the stiffener.

Mode 4, overall grillage buckling, has been treated by Mansour (1976, 1977) using orthotropic plate theory. The

following expressions taken from the latter reference may be used in this case if the number of stiffeners in each direction exceeds three. For gross panels under uniaxial compression, the critical buckling load is given by

$$\sigma_{xcr} = k \frac{\pi^2 \sqrt{D_x D_y}}{h_x B^2} \quad (256)$$

where

B = gross panel width

h_x = effective thickness

and k is given by different expressions, depending on the boundary conditions. For simply supported gross panels,

$$k = \frac{m^2}{\rho^2} + 2\eta + \frac{\rho^2}{m^2} \quad (257)$$

For gross panels with both loaded edges simply supported and both of the other edges fixed,

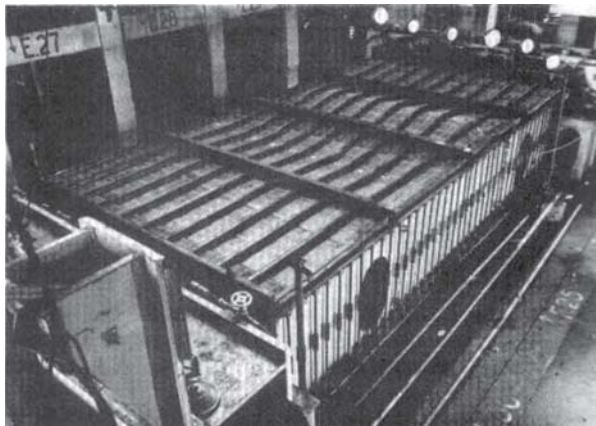
$$k = \frac{m^2}{\rho^2} + 2.5\eta + 5 \frac{\rho^2}{m^2} \quad (258)$$

where m is number of half-waves of buckled plate, and η and ρ are defined in equations (205) and (206).

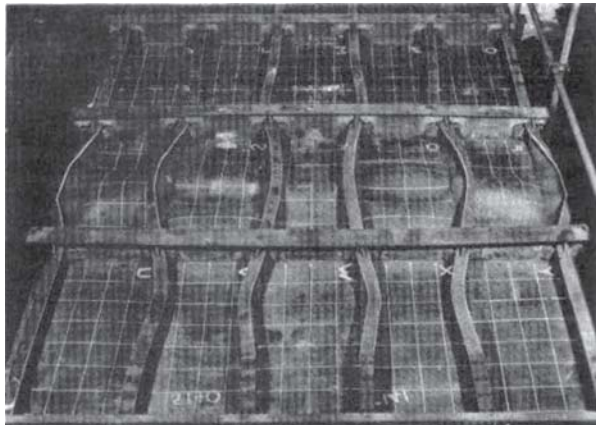
The Mansour (1976) reference contains an extensive treatment of the behavior of orthotropic plate panels in the buckling and elastic postbuckling range. Design charts are given that contain the mid-panel deflection, critical buckling stress, and bending moment at the mid-length of the edge. The loading conditions include normal pressure, direct in-plane stress in two directions, and edge shear stress.

4.8 Ultimate Strength of Stiffened Plate. The previous section dealt with stiffeners whose behavior remains in the elastic range. Ultimate strength involves deformations in which material behavior is no longer elastic, and combinations of analytic, numerical, and experimental methods have been employed to obtain understanding and design information. Failure is usually observed in one of the four modes defined in the previous section. The aforementioned reference by Mansour (1976) contains charts from which predictions can be made of the large-deflection behavior in Mode 4 up to the initiation of yield.

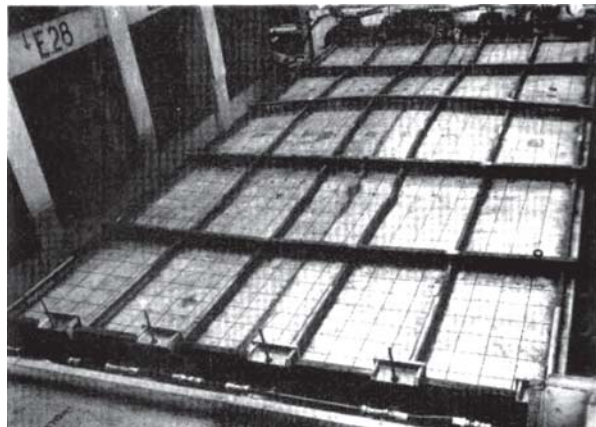
As noted by Smith (1975), despite a considerable body of research the understanding of collapse behavior of welded grillages is far from complete, and much reliance is still placed upon experiments. Fig. 118, reproduced from this last reference, shows test panels of stiffened plating in which examples of panel failures in each of the Modes 2 to 4 listed previously were observed. If the panel buckling occurs by one or more of the mechanisms shown in Fig. 117, the stress-strain curve for the corresponding part of the deck or bottom structure can no longer be represented by the ideal elastic-perfectly plastic curve.



(a) INTERFRAME FLEXURAL BUCKLING (MODE 2)



(b) INTERFRAME LATERAL-TORSIONAL BUCKLING (MODE 3)



(c) OVERALL GRILLAGE BUCKLING (MODE 4)

Fig. 118 Examples of test panel failure (Smith 1975).

Although the tension side of the curve will level off and remain at the constant stress level corresponding to yield, the compressive behavior is somewhat more complex, as may be seen by considering the behavior of a single stiffener and its associated plating under a

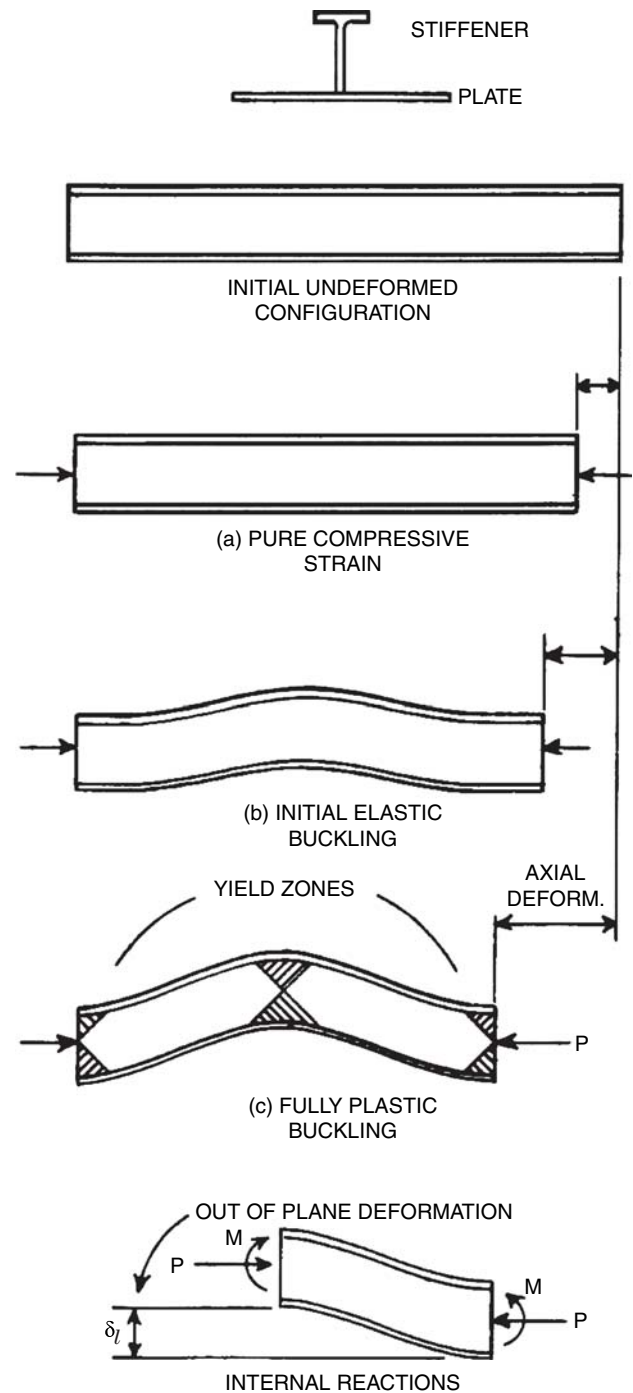


Fig. 119 Failure regimes in compression.

compressive load. This is illustrated in Fig. 119, showing the three distinct regimes in the behavior of the load versus deformation:

- (a) Simple elastic strain, or shortening before buckling occurs

(b) After initial buckling but before the development of extensive yield in the stiffener

(c) Development of yield over the full depth of the member to form one or more plastic hinges, normally at the ends and mid-span.

From considerations similar to those that underlie equation (237), the fully plastic resisting moment that may be developed in case (c) remains constant if there is further out-of-plane deflection of the stiffener. If the external compressive load, P , were to remain constant, the bending moment at the mid-span point would increase with an increase of out-of-plane deflection because the moment is equal to the product of the external load and deflection, δ_l . Increased out-of-plane deflection is accompanied by a shortening of the distance between the two ends of the stiffener (apparent strain). Therefore, to maintain moment equilibrium it is necessary for the external compressive load to decrease with an increase in apparent strain of the stiffener beyond the point of formation of the plastic hinges. This effect is termed *unloading* of the member.

An idealized graph of the load versus apparent strain is shown in Fig. 120. Here, the tension side is characterized by a nearly linear elastic zone followed by an idealized plastic zone in which the load remains constant with increasing strain. The compression side of the graph exhibits the three zones described previously. The first is the elastic compression without buckling. The second corresponds to either compressive plastic yield or elastic buckling, whichever occurs at the lower loading. The third is the unloading regime in which fully plastic hinges have developed in the stiffener.

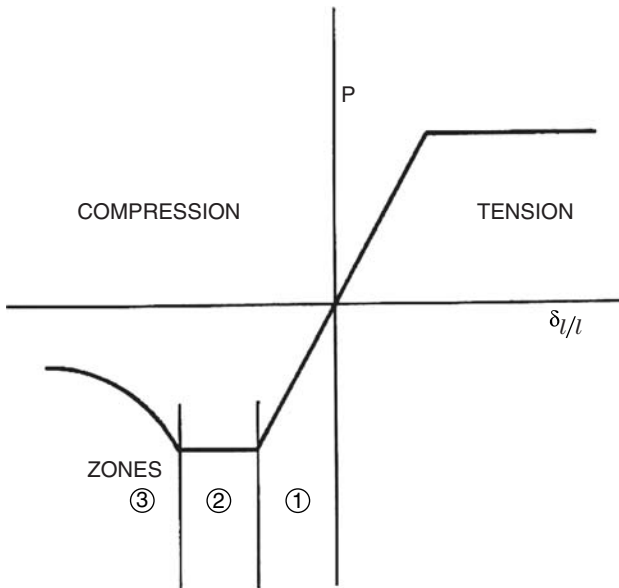


Fig. 120 Idealized load versus strain.

As mentioned previously, flexural buckling (Mode 2) is the most important failure mode for longitudinally stiffener ships because, in many cases, the lateral-torsional buckling mode (Mode 3) can be prevented by fitting tripping brackets to the stiffener. However, the flexural buckling mode is sensitive to initial deflection, particularly for a stiffener slenderness ratio, λ , close to one.

Recently, Masaoka and Mansour (2004) developed an approximate semi-empirical formulation for flexural buckling of longitudinally stiffened panels, including the effects of initial deflection and welding residual stresses. The formulation is based on modification of Perry-Robertson's equation and extensive nonlinear finite element ultimate strength analysis of several stiffened panels. Perry-Robertson's equation has been modified to include plate, flange, and hybrid modes of flexural failure and reduction factors that depend on the magnitude of imperfections. A summary of the results is given as follows.

Three flexural collapse modes of stiffened plates with initial deflection and residual stresses have been determined. In addition to the usual plate collapse mode and flange collapse mode, a hybrid mode was observed where initial failure starts in the flange of a stiffener but the stiffened panel can still support greater compression until it finally fails in a mode similar to the plate failure mode (see Fig. 121).

The ultimate strength, P_u , of the stiffened plate is determined by one of the equations (259), depending on the magnitude of the stiffener's slenderness ratio, λ , as follows (Masaoka & Mansour 2004):

$$\begin{aligned}
 P_u &= P_{pf} && \text{if } \lambda > 0.6 \text{ and } P_{pf} < P_{ff} && \text{Plate collapse mode} \\
 P_u &= P_{ff} && \text{if } \lambda > 0.6 \text{ and } P_{ff} < P_{pf} && \text{Flange collapse mode} \\
 P_u &= P_{pf} && \text{if } \lambda < 0.6 && \text{Hybrid collapse mode} \quad (259)
 \end{aligned}$$

where

$$\begin{aligned}
 P_u &= \text{governing ultimate strength} \\
 P_{pf} &= \text{ultimate strength in plate failure mode} \\
 P_{ff} &= \text{ultimate strength in a flange failure mode}
 \end{aligned}$$

The ultimate strength in a flange failure mode, P_{ff} , usually occurs when the plate is relatively thick or the cross-sectional area of the longitudinal stiffener is relatively small. The full breadth, b , of the plate should be used as an effective breadth, b_e , because the plate is initially under tension in this failure mode.

$$P_{ff} = P_Y ((\sigma_0 - \sigma_r)/\sigma_0) (B_r - (B_r^2 - 4\lambda_r^2)^{0.5}) / (2\lambda_r^2) \quad (259a)$$

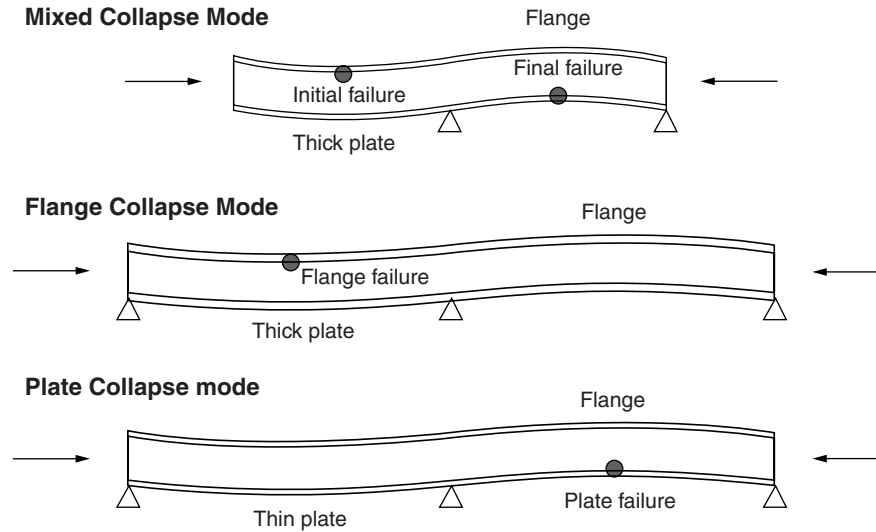


Fig. 121 Three collapse modes of stiffened plates subjected to compression (Masaaka and Mansour, 2004).

where

$$\begin{aligned}
 B_r &= 1 + \lambda_r^2 + \eta_e \\
 \lambda_r &= (a/(\pi r_e))((\sigma_0 - \sigma_r)/E)^{0.5} \\
 \eta_e &= A_e w_{0C} / Z_e \\
 Z_e &= I_e / y_f \\
 r_e &= (I_e / A_e)^{0.5} \\
 b_e &= b
 \end{aligned}$$

The ultimate strength in a plate failure mode usually occurs if the plate is relatively thin. P_{pf} is given by

$$P_{pf} = P_Y(A_e/A)(B_e - (B_e^2 - 4\lambda_e^2)^{0.5}) / (2\lambda_e^2) \quad (259b)$$

where

$$\begin{aligned}
 B_e &= 1 + \lambda_e^2 + \eta_e \\
 \lambda_e &= (a/(\pi r_e))(\sigma_0/E)^{0.5} \\
 \eta_e &= A_e w_{0C} / Z_e \\
 Z_e &= I_e / y_p \text{ (effective section modulus)} \\
 r_e &= (I_e / A_e)^{0.5} \\
 b_e &= b \phi_{up} R_d R_r
 \end{aligned}$$

Equations (259a) and (259b) should be used in conjunction with equation (259). Figure 122 explains the nomenclature used in these equations and shows the

- $\alpha = a/b = 3$ or 5
- $\beta = b/t_p$ (σ_0/E)^{1/2} = 1.56 or 3.12
- $\lambda = (\sigma_0/\sigma_E)^{1/2} = 0.197 \dots 1.188$
- $W_{0p}/t_p = 0.1$, $W_{0T}/a = 0.001$
- $W_{0C}/a = 0.001$ or 0.005
- $\sigma_r/\sigma_0 = 0.0$ or 0.1
- Stiffener type: tee-bar

Fig. 122 Range of parameters used to validate equations (259a) and (259b).

range of validity of the parameters. The subscript “e” refers to “effective” area, breadth, slenderness ratio, and so on. The effective breadth, b_e , can be determined from equation (259b), where the nomenclature used is the same as in equation (223), or it may be determined using other methods.

Figure 123 shows a stiffened steel panel with existing cracks. Bai (2006) proposed a model based on finite element analysis to calculate the ultimate tensile strength of a stiffened panel with fatigue cracks:

$$\sigma_u = \frac{\phi_{up}\sigma_{Yp}bt + \phi_{us}\sigma_{Ys}h_w t_w}{bt + h_w t_w} \quad (260)$$

where

- ϕ_{up} = nominal ultimate strength of plating; can be obtained using equation (252)
- ϕ_{us} = nominal ultimate strength of stiffener; can be obtained using equation (251)
- c_p = crack length in the plate
- c_s = crack length in the stiffener
- b = plate breadth
- t = plate thickness
- h_w = stiffener web height
- t_w = stiffener web thickness
- σ_u = ultimate tensile strength of the stiffened panel
- σ_{Yp} = yield strength of plate
- σ_{Ys} = yield strength of stiffener

Paik and Thayamballi (1997) developed an empirical formula for predicting the ultimate strength of a plate-stiffener combination under axial compression and with initial imperfections at an average level. Based on that equation, Bai (2006) made some modifications to predict the ultimate compressive strength of a stiffened panel with existing crack damage. Figure 124 shows an

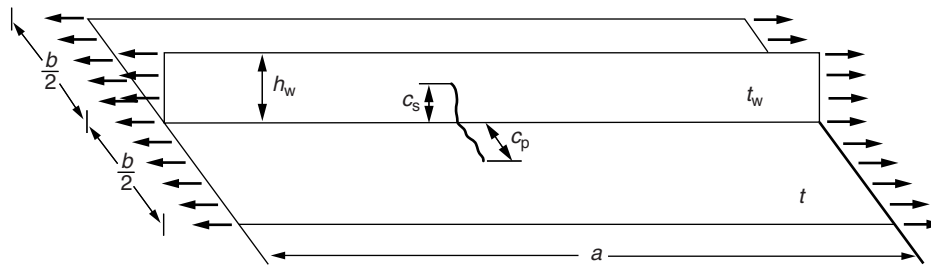


Fig. 123 A stiffened steel panel with existing cracks.

example of the effect of different crack sizes on the ultimate compressive strength of the stiffened panel.

4.9 Ultimate Strength of the Hull Girder. There are numerous plate-stiffener panel members in a ship structure. At any given instant, many of these members are subject to compressive loads, and the loads vary in intensity depending on the location of the member within the ship. Under conditions of extremely severe hull loading, it is apparent that the most highly loaded compression members may experience buckling and plastic yield, and enter the zone of unloading as described previously. A portion of the load that would otherwise be carried by such members is then shifted to nearby intact members. A further increase in the hull loading beyond this level will result in some of these members becoming so heavily loaded that they now experience yield. Further increase in the hull loading will eventually lead to total collapse of the structure as a complex sequence of interdependent panel collapses.

The ultimate strength of the hull is therefore a composite of the ultimate strength characteristic of all of these panels. The ultimate collapse behavior of the individual panel alone is a complex subject not amenable to a simple analytical description. Because each of the numerous panels making up the ship differs in geometry, loading, and boundary conditions, there is obviously considerable difficulty in developing a comprehensive analytic solution for the entire hull. Early investigations of hull ultimate strength have usually been experimental in nature. The most informative of these have been conducted on actual obsolete ships by applying static loads to the ship in drydock through ballast shifts and dewatering the dock. The reference by Vasta (1958) contains descriptions of several classic experiments of this type.

It is possible to perform an approximate numerical analysis of the ultimate strength of the ship hull by using nonlinear finite element methods. Two examples of such analyses are described by Smith (1977) and Dow et al.

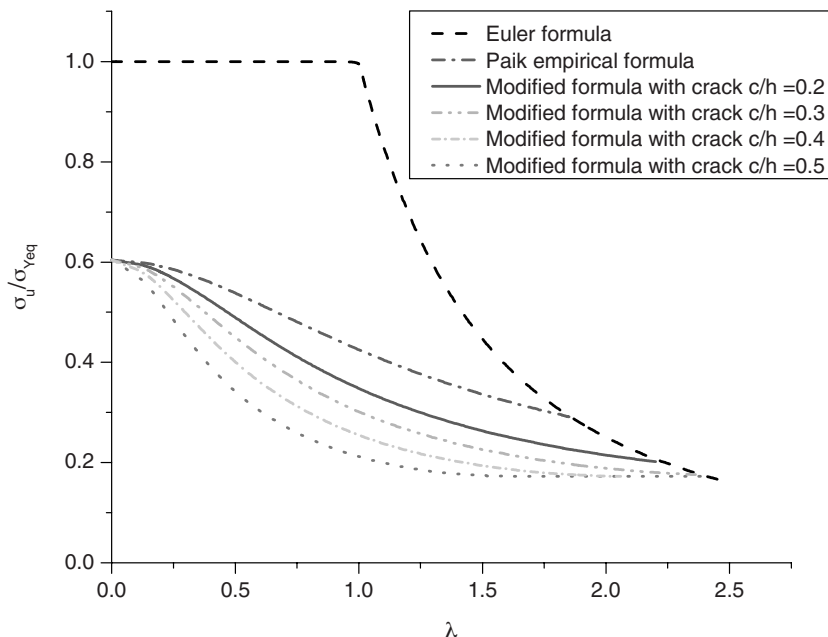


Fig. 124 Comparison of the ultimate strength for intact stiffened panel and panels with different crack sizes (Bai 2006).

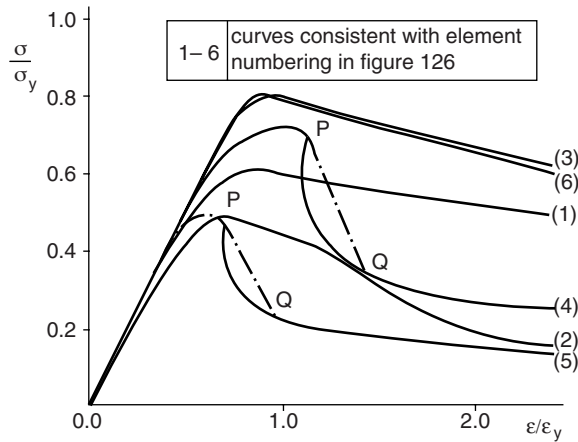


Fig. 125 Compressive stress-strain curves for stiffened panels (Dow et al. 1981).

(1981). (The latter includes a description of the computer program, ULTSTR, intended for design use.) In these procedures, the hull cross section is first subdivided into a number of panels consisting of plating and the associated stiffeners, and for each such panel the load-shortening curve of approximately the form of Fig. 120 is constructed. This can be accomplished by any number of methods. Experimental data could be used or, alternatively, one might perform a nonlinear finite element analysis of the individual panel itself. A third procedure would employ one or more analytic formulations suitable for describing the large amplitude deflection to be experienced by the member in the failure regime. Example stress-strain curves for plate-stiffener panels obtained by Dow et al. (1981) using a nonlinear finite element analysis are shown in Fig. 125. The unloading behavior in compression is clearly observed in this figure.

An appropriate collection of such elementary members is then assembled to represent the midship portion of the ship's hull. Some hard corner elements that exhibit exceptionally high buckling resistance will be included to represent portions of the structure at shell-deck or bulkhead-shell intersections, where buckling is not expected to be the primary failure mode. An example of such a discrete model is shown in Fig. 126.

The hull is then subjected to an incrementally increasing bending deflection pattern in which it is assumed that cross sections that are initially plane remain plane after deflection and experience only rotation about an assumed neutral axis. Recall that a similar assumption was made in developing the equations of elementary beam theory. After this rotation, the strain of each longitudinal member is determined to correspond with the assumed position of the neutral axis. By reference in the stress-strain curves of each member, the stress and thus the load on that member are determined. Next, the loads and their moments are summed over all members making up the cross section. The total load must be zero for longitudinal force equilibrium, and the total moment

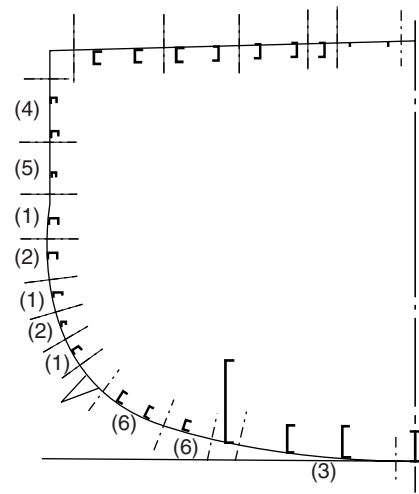


Fig. 126 Midship section of destroyer *Albuera*, showing elemental subdivision (Dow et al. 1981).

must be equal to the external hull bending moment at the cross section in question. As a result of the nonlinear stress-strain behavior of the members, the neutral axis will generally not be located at the geometric centroid of the cross section. Therefore, a trial-and-error procedure must be used at each increment of angular deflection to find the neutral axis location that results in equilibrium of longitudinal forces. Once this has been obtained, the moment of the longitudinal forces in the member can be computed. See also the papers by Billingsley (1980), Chen et al. (1983), Rutherford and Caldwell (1990), and IACS Common Structural Rules for Tankers and Bulk Carriers (2006).

Typical results for naval ships from Dow et al. (1961) and Smith (1977) are shown in Figs. 127 and 128, respectively. Several interesting characteristics are revealed by

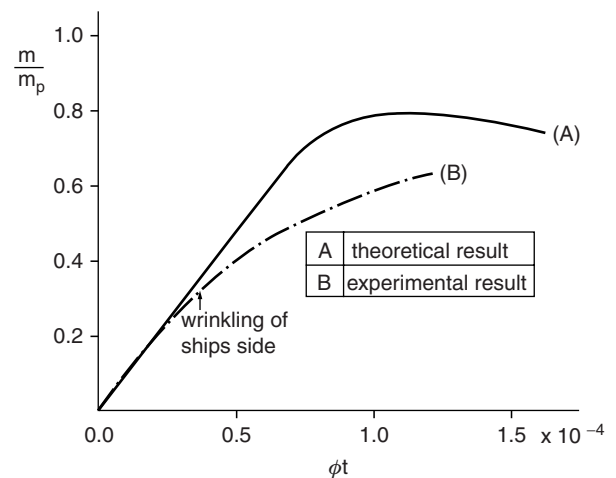
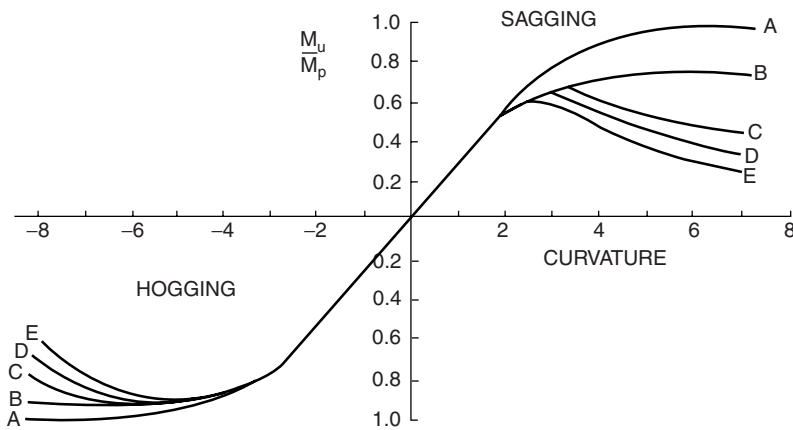
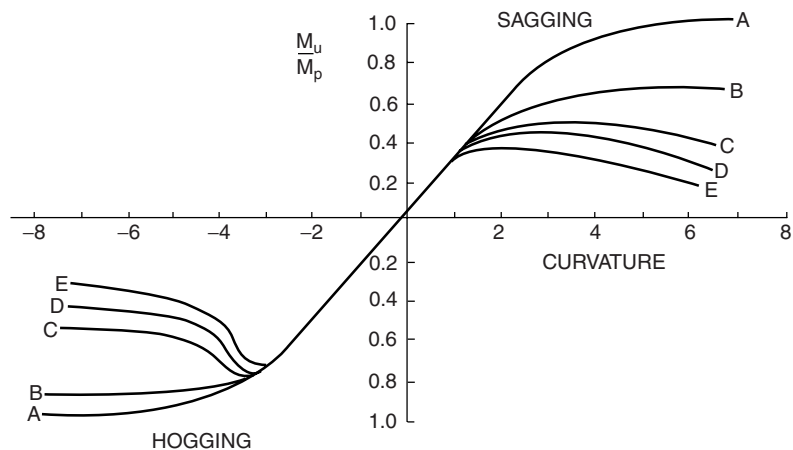


Fig. 127 Midship bending moment-curvature relationship, by theory and experiment (Adamchak 1982).



(a) FRAME SPACING = 100 h



(b) FRAME SPACING = 200 h

Fig. 128 Midship bending moment-curvature relationships for destroyer hull girder, under various assumptions (Smith 1977).

such computations. For example, it is quite apparent that for the lightly built type of ship investigated here, the ultimate strength of the midship section will be substantially less than the strength corresponding to yield failure alone, as depicted in Fig. 111. Furthermore, note an unloading effect in the overall hull strength that is similar to the unloading phenomenon in individual plate-stiffener members. If the strength curves corresponding to hogging are compared to those of sagging, an asymmetry is apparent that may be attributed to the difference in the buckling strength of deck and bottom structure.

As mentioned earlier, primary (also called global or hull) failure modes consist of the fully plastic moment mode, the initial yield moment mode, and the instability collapse moment mode. The last includes buckling and post-buckling strength of the hull, and is always the governing mode of failure. The fully plastic mode gives an upper bound on the ultimate moment. It is never attained in a hull of normal proportions. The initial yield mode

Case A: the entire cross-section is assumed to follow an elastic-perfectly plastic stress-strain curve, buckling effects being ignored.

Case B: element compressive stress-strain curves follow trends predicted by a detailed nonlinear F.E. analysis of stiffened panel behavior up to peak loads and thereafter remain horizontal, i.e., post-buckling reduction of load is ignored; "hard corners" are assumed to have conservative areas.

Case C: element compressive stress-strain curves are as in Case B except that post-buckling load reductions are included; "hard corners" have double the areas shown in Case B.

Case D: same as Case C except that "hard corners" have the same areas as Case B.

Case E: same as Case C except that "hard corners" are eliminated, the entire cross-section being assumed to follow the computed panel stress-strain curves.

assumes that buckling does not occur prior to yielding, and is considered here only because it is a function of the standard elastic section modulus of the ship and the yield strength of the material, both normally used in current design practice. This mode provides a point of reference relative to current practice. However, it should be noted that the initial yield moment is greater than the true instability collapse moment.

Ueda and Rashed (1975) developed an effective method for nonlinear and failure analyses of large size structures. The method is known as the *idealized structural unit method* (ISUM). In this method, the structure is modeled as a combination of various large size structural units (e.g., a stiffened panel), whose geometric and material nonlinear behavior are idealized. As a result, the total number of elements and nodal points in ISUM modeling is much smaller than in the FEM. Paik (1993) developed a computer program for the ultimate strength analysis of ships based on the ISUM. The computer

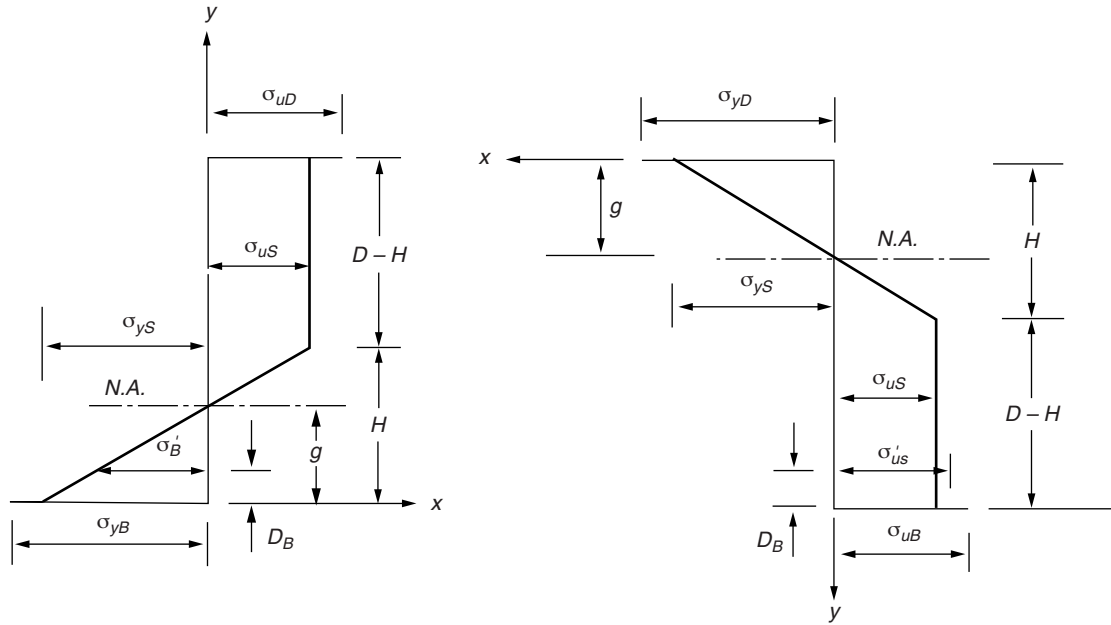


Fig. 129 Assumed distribution of longitudinal stresses in a hull cross section at the overall collapse state. Sagging condition is shown on the left, and hogging is shown on the right (Paik & Mansour 1995).

program ALPS/ISUM can be used to determine the ultimate strength the hull girder, stiffened plates, and unstiffened plates.

Paik and Mansour (1995) developed a semi-analytical expression for predicting the ultimate strength for single and double hull ships under vertical bending moment. A credible distribution of longitudinal stresses around the hull section at the instant of collapse was assumed. It was postulated that the ultimate limit state is reached when parts of the cross section under tension reach the yield strength of the material, and those under compression reach the buckling strength of the stiffened panels. It was further postulated that a linear stress distribution exists in parts of the side shell where stresses change from tension to compression. The neutral axis location as well as the depth at which the stress distribution starts to become linear (tension to compression) were determined from the conditions that the axial force must be zero and the stress distribution is linear in the vicinity of the neutral axis. The ultimate strength moment was then obtained by integrating the stress resultant moments with respect to the neutral axis.

Figure 129 shows the postulated distribution of longitudinal stresses of the hull cross section at the overall collapse state. The neutral axis has moved toward the tension flange from its initial position in the intact hull section. In the compressed parts of the section, the flange and a part of sides have reached their ultimate compressive limit state. The ultimate compressive strength of the flange may be different from that of the sides. In the parts of the section subjected to tension, the full yield strength in tension is assumed in the flange, but

the sides remain in the elastic state. The yield strength of the tension flange may be different from that of the sides. The stress distribution in the vicinity of the neutral axis is assumed to be linear.

The resulting sagging and hogging ultimate bending moments are given by

$$\begin{aligned}
 M_{us} = & -A_D(D-g)\sigma_{uD} \\
 & -\frac{A_S}{D}(D-H)(D+H-2g)\sigma_{uS} - A_B g \sigma_{yB} \\
 & +\frac{A_B}{H}(g-D_B)[D_B\sigma_{uS} - (H-D_B)\sigma_{yS}] \\
 & -\frac{A_S H}{3D}[(2H-3g)\sigma_{uS} - (H-3g)\sigma_{yS}] \quad (261)
 \end{aligned}$$

and

$$\begin{aligned}
 M_{uh} = & A_D g \sigma_{yD} + A_B(D-g)\sigma_{uB} \\
 & + A'_B(d-g-D_B)\sigma'_{uB} \\
 & +\frac{A_S}{D}(D-H)(D+H-2g)\sigma_{uS} \\
 & +\frac{A_S H}{3D}[(2H-3g)\sigma_{uS} - (H-3g)\sigma_{yS}] \quad (262)
 \end{aligned}$$

H and g in the equations here are defined by

$$H = D \frac{A_B \sigma_{uB} + A'_B \sigma'_{uB} + 2A_S \sigma_{uS} - A_D \sigma_{yD}}{A_S(\sigma_{uS} + \sigma_{yS})} \quad (263)$$

$$g = D \frac{A_B \sigma_{uB} \sigma_{yS} + A'_B \sigma'_{uB} \sigma_{yS} + 2A_S \sigma_{uS} \sigma_{yS} - A_D \sigma_{yD} \sigma_{yS}}{A_S(\sigma_{uS} + \sigma_{yS})^2} \quad (264)$$

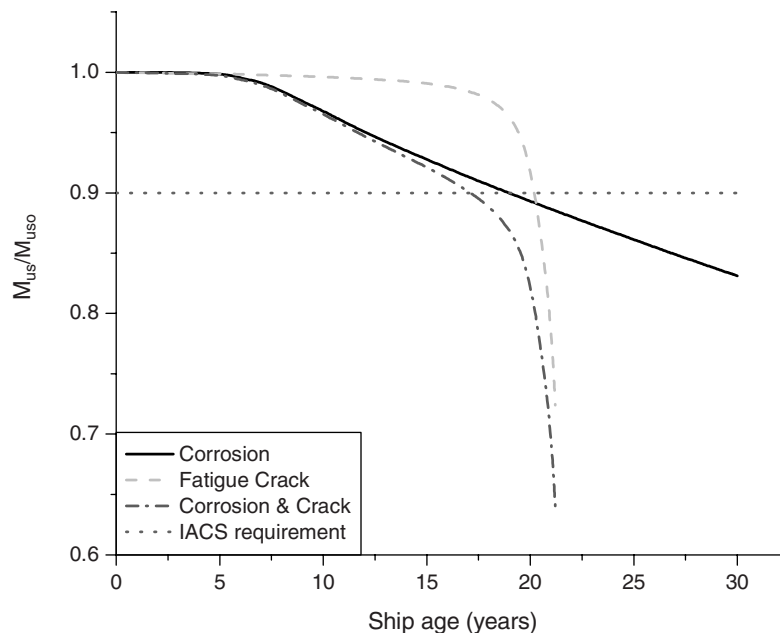


Fig. 130 Time-dependent ultimate hull girder strength considering fatigue and corrosion (Bai 2006).

In these equations, the following nomenclature has been used:

A_B = total sectional area of outer bottom

A'_B = total sectional area of inner bottom

A_D = total sectional area of deck

A_S = half sectional area of all sides (including longitudinal bulkheads and inner sides)

D = hull depth

D_B = height of double bottom

g = neutral axis position above the baseline in sagging condition or below the deck in hogging condition (see Fig. 129)

H = depth of hull section in linear elastic state (see Fig. 129)

M_{uS} , M_{uh} = ultimate bending moment in sagging or hogging condition, respectively

σ_y = yield strength of the material

σ_{yB} , σ'_{yB} = yield strength of outer bottom or inner bottom, respectively

σ_{yD} , σ_{yS} = yield strength of deck or side, respectively

σ_u = ultimate strength in compression

σ_{uB} , σ'_{uB} = ultimate buckling strength of outer bottom or inner bottom, respectively

σ_{uD} , σ_{uS} = ultimate buckling strength of deck or side shell, respectively

In these equations, the ultimate buckling strength σ_{uB} , σ'_{uB} , σ_{uD} , and σ_{uS} can be determined using the empirical equations developed by Paik and Thayamballi (1997).

The ultimate strength simplified formulation described previously has been tested for accuracy relative to experimental and numerical results (see Paik & Mansour 1995). The results showed less than 10 percent error for the nine models considered. However, the formulation should not be used for estimating the ultimate strength of multi-deck vessels such as naval or passenger ships.

The previous equations for ultimate strength were applied to a 307,000 DWT double hull tanker by Bai (2006). He modified the equations to include the impact of corrosion and cracks. Figure 130 shows the results. In his study, he also suggested an inspection and repair procedure based on IACS minimum requirement. The result is shown in Fig. 131.

4.10 Cumulative Fatigue Damage. Fatigue constitutes a major source of local damage in ships and other marine structures because the most important loading on the structure, the wave-induced loading, consists of large numbers of load cycles of alternating sign. The effects of fatigue are especially severe in locations of high stress concentration, and fatigue cracks have sometimes proven to be the triggering mechanism for brittle fracture. The prevention of fatigue failure in ship structures is strongly dependent on proper attention to the design and fabrication of structural details to reduce stress concentrations. This must be followed by thorough and regular inspection of the structure in service to detect and repair any fatigue cracks that do occur before they can grow to such size that the structure is endangered.

Much of the quantitative information on fatigue has been obtained by experiments in which an alternating

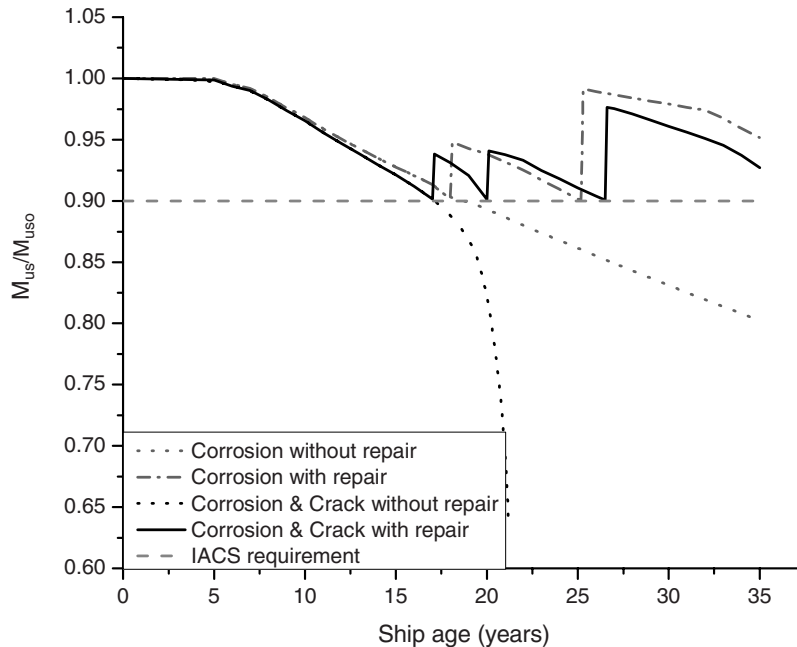


Fig. 131 Time-dependent ultimate hull girder strength considering repair and minimum IACS requirement (Bai 2006).

load is applied to a simple test specimen. In the most usual form of this experiment, the loading varies sinusoidally in time with constant amplitude and frequency. Under such a load, it is found that many engineering materials, including the steels commonly used in shipbuilding, will fracture after a sufficient number of cycles even though the alternating stress amplitude is less than the static yield stress of the material. The number of cycles that results in fracture of the specimen is found to depend on the amplitude of the alternating stress, and this number is less than the greater stress amplitude. For a sufficiently low stress level, some materials are found to be capable of withstanding an (apparently) indefinitely large number of cycles, and this threshold stress level is termed the *endurance limit*. A graph of stress amplitude versus the number of cycles to failure is termed the *S-N curve*, and an example is shown in Fig. 132, where σ is the fracture stress and σ_y is the yield stress. It is clear that the S-N curve is usually well-defined in the high-cycle range (as defined in Section 4.1) but more uncertain in the low-cycle range at stresses near the yield point.

The resistance of a material to fatigue failure depends on a number of factors including the material itself, the surface finish, corrosion extent, and the presence of stress concentrations. The simple sinusoidal loading that was described in the previous paragraph is approximated in the load experience of certain machinery parts that are subject to forces caused by rotational unbalance or vibration. Such parts are usually fabricated to close

tolerances and operate in a uniform environment, all of which contribute to a relatively predictable fatigue life. On the other hand, the ship hull structure is exposed to loads that vary randomly in time, the parts are fabricated by welding with much looser tolerances than machine parts, the surface finish is relatively rough, and the structure is exposed to a harsh and corrosive environment.

Therefore, the prediction of the fatigue life of the hull structure is much less certain than the corresponding prediction for many other types of members such as machinery components. Fortunately, fatigue cracks have been mostly of the nuisance variety, occurring in poorly designed brackets and other details and requiring repair at times of overhaul. Cracks in longitudinal strength members can be readily detected and repaired before the safety of the ship is threatened.

Fatigue damage criteria applied in the design of ship structures are based on classification rules as described in Section 3.15.4.3.

A major source of difficulty in predicting fatigue damage in ships and other marine structures lies in the form of the alternative loading, which is a random rather than simple periodic function. The stress at a given location in the ship varies in an irregular fashion, which may have an approximately constant mean value over a short term, but even this mean value changes with changes of sea state and ship loading. The estimation of the fatigue damage, or rather the probability of fatigue failure in the random loading case, is usually performed according to a procedure proposed by Miner (1945). By the Miner

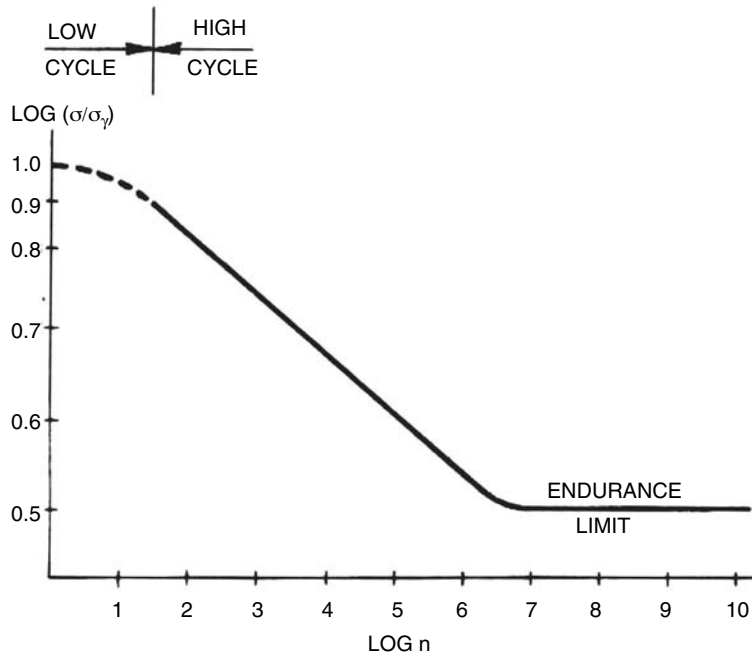


Fig. 132 Typical S-N curve for mild steel.

hypothesis, it is assumed that one cycle of the randomly varying stress, having an amplitude s_i , causes an amount of fatigue damage in the following proportion:

$$\delta D_i = \frac{1}{N_i} \tag{265}$$

Here N_i is the number of cycles of a sinusoidally varying stress of amplitude s_i required to cause failure.

The cumulative damage due to fatigue during exposure to the random stress environment will then be given by

$$D = \sum_i \frac{n_i}{N_i} \tag{266}$$

Here n_i is the number of cycles of stress of level s_i during the period of exposure, and the summation is taken over all levels of stress experienced during the period of time under consideration. Failure of the structure is then presumed to occur when the length of exposure is sufficient for this sum to equal unity.

For the spectral representation of the seaway and, thus the stress environment, the fatigue damage summation can be expressed in a more compact form in the high-cycle case. Let $p(s)$ be the probability density function for the stress. This is defined so that the quantity $p(s_i)ds$ equals the fraction of all of the oscillatory stress peaks whose values lie in the interval ds centered on the mean value, s_1 . Assume that the average frequency of the randomly varying stress is f and that the total time of exposure is T . The incremental damage caused by all of

the stress oscillations of amplitude s_1 occurring during the interval T is then given by

$$dD = Tf p(s_1)ds/N(s_1) \tag{267}$$

where $N(s_1)$ is the number of cycles to failure at stress s_1 as obtained from the S-N curve for the material or the structural component.

The expected value of the total damage during the time period T is then given by the integral of equation (267), or

$$E[D] = Tf \int_0^\infty \frac{p(s)ds}{N(s)} \tag{268}$$

The S-N curve in the high-cycle range is sometimes approximated by the following function, which is piecewise linear in log-log coordinates:

$$NS^b = C \tag{269}$$

The distribution function, $p(s)$, is often approximated by a Rayleigh distribution,

$$p(s) = \frac{s}{m_{os}} \exp\left(-\frac{s^2}{2m_{os}^2}\right) \tag{270}$$

In this case, the integral in equation (267) can be evaluated, giving

$$E[D] = \frac{Tf}{c} \sqrt{2} m_{os}^2 \Gamma(1 + b/2) \tag{271}$$

Here $\Gamma(x)$ is the Gamma function.

The prediction of fatigue life by the previous procedure involves uncertainties that depends upon three general categories or sources of error:

- Uncertainty in the estimated stress levels, including errors of stress analysis and errors in the loading prediction for the ship in the random sea environment
- Uncertainty in the basic fatigue life data for the structural detail in question, including scatter in the experimental data for the detail and effects of workmanship and fabrication in the real structure
- Uncertainty in the basic cumulative damage rule (Miner's hypothesis).

Predicting cycle loading (or stresses) from long-term distributions is discussed in Section 2.7. Of course, this procedure covers only primary bending loads, not local cyclic loads that may also be important for fatigue but are less well understood.

In welded structures such as ships, the fatigue strength is found to be closely related to the geometry and workmanship of the structure. For the steels commonly used in ship construction, fatigue strength is not strongly dependent on the material itself. Fatigue cracks in actual structures are usually found in details, of which examples are hatch corner reinforcements, beam-bracket connections, and stiffener-bulkhead intersections. In addition to attention to the design of such details, a high level of workmanship—including accurate fit-up and alignment of components—and good weld quality are of importance in achieving fatigue strength.

A very comprehensive treatment of the high-cycle fatigue characteristics of ship structural details is presented in a report by Munse (1983). Fatigue design criteria from other fields of engineering are examined with the objective of developing simple criteria for the design of ship structural details. An extensive catalog of structural details has been compiled, and fatigue data for these details are presented in tabular and graphical form. Methods of combining these data with information on ship loading are presented, and the errors and uncertainties in both the fatigue data and in the computations of fatigue life are examined. On the basis of an assumed lifetime cyclic loading pattern, it is possible to use these data to determine whether specific structural details can be expected to suffer high-cycle fatigue cracking during the ship's lifetime. If so, that particular detail can be redesigned.

Several difficulties in principle arise in applying the Miner hypothesis to ships and ocean structures. The infinite upper limit of the integral in equation (268), in conjunction with the use of an analytic expression for

the distribution function, implies the possibility of occurrence of infinite or very high-stress cycles, which would exceed the ultimate strength of the material. Cycles exceeding yield contribute to what was described in Section 4.1 as low-cycle fatigue damage. Presumably, one cycle exceeding the ultimate would cause fracture of the part under examination. Because of these and the other sources of uncertainty listed, the estimate of damage by the Miner hypothesis must be considered a probabilistic estimate to be characterized by its own level of uncertainty.

In the design criteria that are based upon the Miner hypothesis, it is customary to allow for the uncertainties by requiring the structure to have an extended value of the estimated fatigue life, or equivalently, a value less than unity for the damage parameter, $E(D)$, in equation (271). For ship structures the classification rules require the damage parameter value to be equal or less than unity for the design life of the ship. The ABS (1997) recommends that steel offshore structures be designed to have an estimated fatigue life of two to three times the design life of the structure. The factor of two is used in structures having a sufficient degree of redundancy that failure of the member under consideration will not result in catastrophic failure of the structure. If the degree of redundancy is less or if the redundancy would be significantly reduced by fatigue, the factor of three is used. Det Norske Veritas (1977) recommends values for $E(D)$ ranging from a low of 0.1 for major structural members that are inaccessible for regular inspection and repair to 1.0 for minor members that are readily accessible.

Low-cycle fatigue failure is less well understood than the high-cycle type discussed previously. However, because it is known to occur only when cyclic stresses reach the yield point, conservative design can be based on the avoidance of stresses exceeding that level at points of stress concentration, particularly in longitudinal strength members.

The prevention of fatigue failure is of paramount importance in submarine design, where the designer must deal with the fatigue life of highly stressed details in the 20,000-cycle range. This relatively low fatigue life is in the low-cycle range. Because any fatigue crack will destroy the watertight integrity of the pressure hull or of any other structures—such as tank bulkheads, which experience submergence pressure, and in some cases may impair the capacity of the structure to resist applied loadings—special attention must be given to the fatigue resistance of the many critically stressed structural members and details of submarines.

Section 5

Reliability and Structural Safety Assessment

5.1 Uncertainty Associated with the Design Variables.

As we have seen from the material in the preceding sections, there is a certain degree of randomness or uncertainty in our ability to predict both the loads imposed on the ship's structure (the demand) and the ability of the structure to withstand those loads (the capability). The sources of these uncertainties include phenomena that can be measured and quantified but cannot be perfectly controlled or predicted by the designer, and phenomena for which adequate knowledge is lacking. The term *objective* uncertainties is sometimes applied in describing the former, and the term *subjective* is used in describing the latter. In principle, the objective uncertainties can be expressed in statistical terms, using available data and theoretical procedures. The subjective uncertainties, which are known to exist but which cannot be fully quantified as a result of a lack of knowledge, must be dealt with through judgment and the application of factors of safety.

An example of an objective uncertainty is the variability in the strength properties of the steel used in constructing the ship. The magnitude of this variability is controlled to some extent through the practices of specifying minimum properties for the steel, and then testing the material as produced by the steel mill to ensure compliance with the specifications. Departures from the specified properties may exist for several reasons. For practical reasons, the sampling and testing cannot be applied to all of the material going into the ship, but only to a limited sampling of the material. As a result of slight variations in its manufacturing experience, some of the material may exhibit different properties from those of material manufactured by supposedly identical procedures. After arrival in the shipyard, the material properties may be altered by the operations such as cutting, forming, and welding, which are involved in building it into the ship. These variations in properties may be reduced by a more rigorous system of testing and quality control, all of which adds to the final cost of the ship. A compromise must therefore be reached between cost and the level of variation or uncertainty that is considered acceptable and that may be accommodated by the degree of conservatism in the design.

On the other hand, the subjective uncertainty cannot be quantified on the basis of direct observation or analytical reasoning but must be deduced by indirect means. The most common source of this uncertainty is a deficiency in the understanding of a fundamental physical phenomenon or incomplete development of the mathematical procedures needed for the purpose of predicting a certain aspect of the structural response. An example of incomplete theoretical knowledge is the small amplitude limitation inherent in the linear theory of wave loads and ship motions, as outlined in Section 2.6 of this

book. An analogous limitation exists in the application of linear elastic theory to the prediction of the structural response. Even though there have been important advances in theoretical and computational methods of nonlinear structural analysis, there is still a significant element of uncertainty in predictions of structural behavior in the vicinity of structural collapse. In this region, nonlinear material behavior as well as nonlinear geometric effects are present, and the overall response may involve the sequential interaction of several elementary response phenomena. Of course, it is the goal of ongoing research to change these subjective uncertainties into objective uncertainties.

Therefore, it is clear that the design of ship structures must take into account the uncertainties in the predictions of both demand and capability of strength. To arrive at the most efficient structure that will achieve an acceptable degree of reliability, it is necessary to attempt to quantify the uncertainties and allow for their possible magnitudes and consequences. Reliability assessment offers an excellent means for doing this.

A typical reliability assessment procedure for marine structures is described in Fig. 133. Starting with a configuration of the marine structure and using random ocean waves as input, the wave loads acting on the structure can be determined using spectral analysis, as discussed in Section 2.6 (refer to Fig. 133). Generally, for design analysis the most important loads are the large ones. Extrapolation procedures are usually used to determine the characteristics of these large loads. For example, in the case of ocean-going vessels this is done either through the determination of a long-term distribution of the wave loads or through the evaluation of an extreme load distribution that may occur in specified storm conditions (see Sections 2.6 and 2.7).

In general, wave loads acting on an ocean-going vessel include low-frequency loads due to the motion of the vessel in waves as a rigid body. They also include higher-frequency loads (and response) due to slamming and springing, which can be determined by considering the ship as a flexible body. In principle, these loads should be combined stochastically to determine the total wave load, as discussed in Section 2.6. Referring back to Fig. 133, other loads besides wave loads occur on a marine structure. These loads may be important in magnitude, though usually less random in nature (except possibly for wind loads on offshore structures). For example, in the case of ocean-going vessels, these loads consist mainly of still water loads and thermal loads.

Following Fig. 133, the response of the marine structure to the total combined loads is determined and compared with the resistance or capability of the structure. This comparison may be conducted through one of several reliability methods, which will be discussed later.

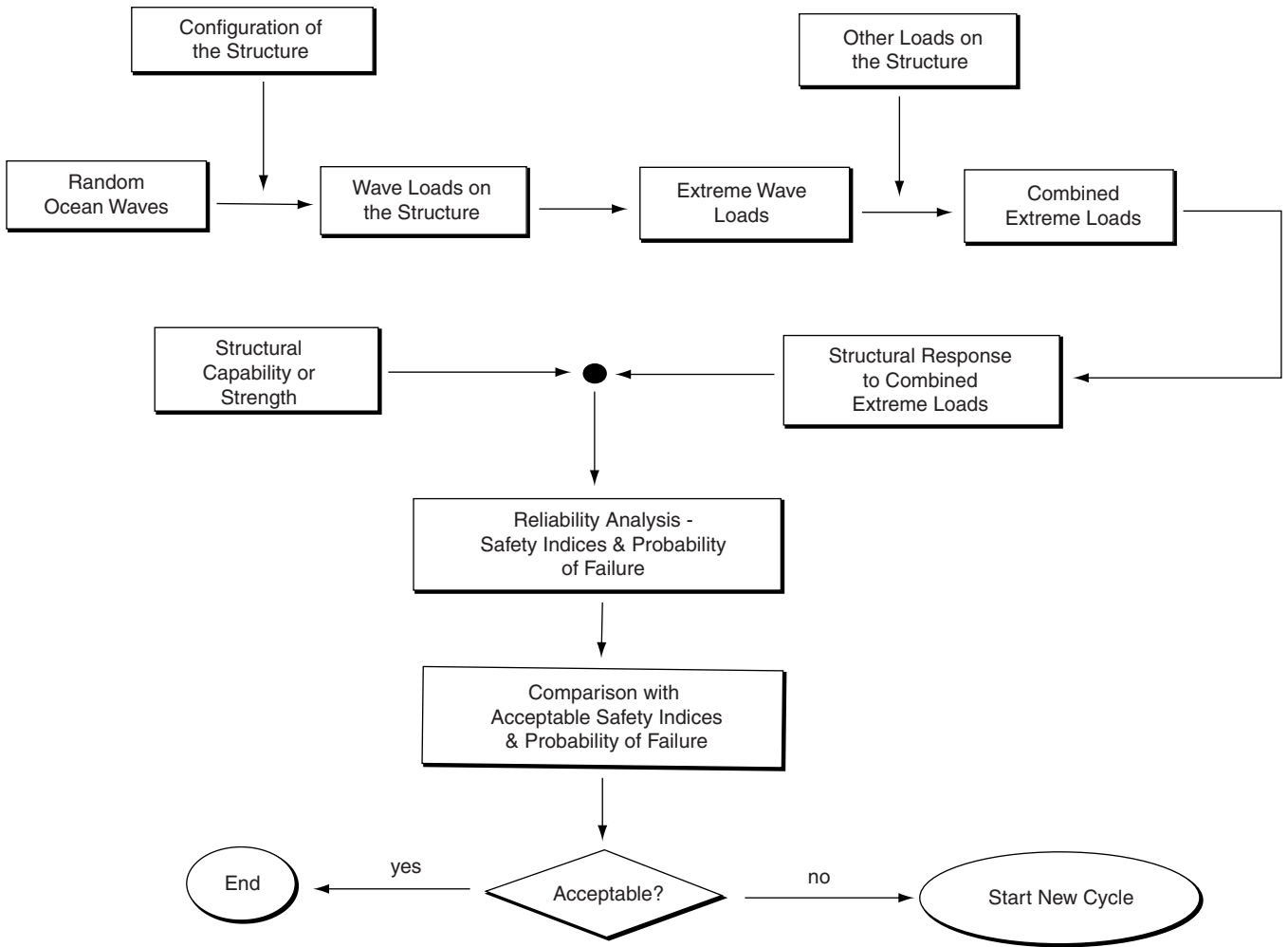


Fig. 133 Probabilistic analysis of marine structures.

Based on these methods, safety indices or probabilities of failure are estimated and compared with acceptable values. A new cycle may be necessary if the estimated indices are below the acceptable limits.

5.2 Basic Reliability Concept. To illustrate some aspects of the procedure described in Fig. 133 and to introduce the basic concept in the reliability analysis, the following example is given. Consider a simple beam subjected to a loading induced by the environment (e.g., wave load). Traditionally, in the design of such a beam designers have used fixed deterministic values for the load acting on the beam and for its strength. In reality, these values are not unique values but rather have probability distributions that reflect uncertainties in the load and the strength of the beam. Structural reliability theory deals mainly with the assessment of these uncertainties and the methods of quantifying and rationally including them in the design process. The load and the strength are thus modeled as random variables.

Figure 134 shows the probability density functions (PDF's) of the load and the strength of the beam in terms of applied bending moment and ultimate moment capacity of the beam, respectively. Both the load, Z , and the strength, S , are assumed in this example to follow the

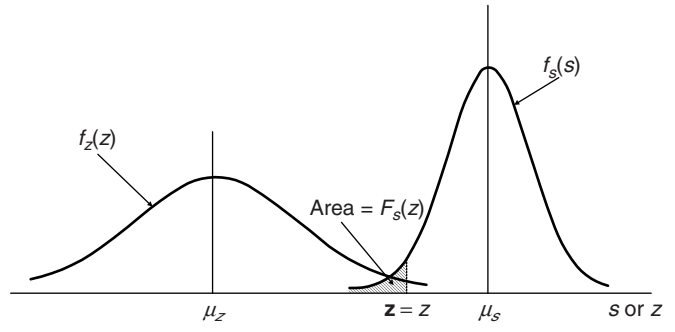


Fig. 134 Load and strength probability density functions.

normal (Gaussian) probability distribution with mean values of $\mu_Z = 60.74$ MN-m (20,000 ft-ton) and $\mu_S = 91.11$ MN-m (30,000 ft-ton), respectively, and standard deviations of $\sigma_Z = 7.59$ MN-m (2,500 ft-ton) and $\sigma_S = 9.11$ MN-m (3,000 ft-ton), respectively.

A simple function, $g(s, z)$, called the limit state function, can be constructed that describes the safety margin, M , between the strength of the beam and the load acting on it:

$$M = g(s, z) = S - Z \quad (272)$$

Both S and Z are random variables and may assume several values. Therefore, the following events or conditions describe the possible states of the beam:

(i) $M = g(s, z) < 0$ represents a failure state because this means that the load Z exceeds the strength S .

(ii) $M = g(s, z) > 0$ represents a safe state.

(iii) $M = g(s, z) = 0$ represents the limit state surface (line, in this case) or the border line between the safe and failure states.

The probability of failure implied in state (i) can be computed from

$$p_f = P[M = g(s, z) \leq 0] = \iint_{g(s, z) \leq 0} f_{(s, z)} ds dz \quad (273)$$

where $f_{S, Z}(s, z)$ is the JPDF of S and Z , and the domain of integration is over all values of s and z where the margin M is not positive (i.e., not in the safe state). If the applied load on the beam is statistically independent from the beam strength, the equation (273) can be simplified and interpreted easily as

$$p_f = \int_0^{\infty} F_S(z) f_Z(z) dz \quad (274)$$

where F_S and f_Z are the CDF of S and the PDF of Z , respectively, both of which in this example are Gaussian. Equation (274) is the convolution integral with respect to z and can be interpreted with reference to Fig. 93. If $Z = z$ (i.e., the random variable Z is equal to a specific value z), the conditional probability of failure would be $F_S(Z)$. But because $z < Z \leq z + dz$ is associated with probability $f_Z(z) dz$, integration of all values of z results in equation (274).

In our example, S and Z are both statistically independent and normally distributed. Equation (274) can be thus shown to reduce to

$$p_f = \Phi(-\beta) \quad (275)$$

where Φ is the standard normal cumulative distribution function (CDF) and β is called a safety index, defined as

$$\beta = \frac{\mu_S - \mu_Z}{\sqrt{\sigma_S^2 + \sigma_Z^2}} \quad (276)$$

—see plot of equation (275) in Fig. 135. Notice that as the safety index β increases, the probability of failure

p_f as given by equation (275) decreases. The safety of the beam as measured by the safety index β can be thus increased—see equation (276)—by increasing the difference between the means $\mu_S - \mu_Z$ or decreasing the standard deviations σ_S and σ_Z . Substituting into equation (276) the numerical values for μ_S , μ_Z , σ_S , and σ_Z given in our simple beam example results in a safety index $\beta = 2.56$. Equation (275) can be then used in conjunction with tables of standard normal CDF to yield a probability of failure $= 5.23 \times 10^{-3}$.

Typical reliability analysis of complex structures is more complicated than the simple example given here, for several reasons. The probability distributions of some or all the variables may not be normal, therefore equation (275) would be no longer valid. However, a transformation to normal variables is possible with various degrees of approximation. The limit state equations may contain more than two variables and may not have a linear form as given by equation (272). Finally, a complex structure will generally consist of several members and each member may fail in one of several modes of failure, thus requiring system reliability instead of the “member” reliability described in the previous example. A detailed discussion of these aspects can be found in Mansour (1989).

The reliability concept can be extended to several random variables, instead of only two, as given by equation (274). For the case of n random variables, the probability of failure (or generally, the probability of exceeding a specified limit state) can be determined from

$$p_f = \int \cdots \int f_{\underline{x}}(x_1, x_2 \dots x_n) dx_1 dx_2 \dots dx_n \quad (277)$$

where $f_{\underline{x}}$ is the JPDF of the design random variables $x_1 \dots x_n$. The domain of the multiple integration in equation (277) is over the unsafe region of a limit state associated with the structure. The limit state function $g(x_1 \dots x_n)$ is formulated such that the unsafe region, the integration domain of equation (277), is given by

$$g(x_1 \dots x_n) \leq 0$$

for which the limit state equation reduces to equation (272) for the simple two-variable case. From the computed probability of failure, the generalized safety index is defined by:

$$\beta = \Phi^{-1}(1 - p_f) \quad (278)$$

This level of reliability assessment (usually titled Level 3, or direct integration method) is limited in terms of applications to complex marine structures. However, it can still be applied to assess ship hull girder primary strength because in this case, the ship is usually considered as a beam. Examples of such applications can be found in Mansour (1972) and Mansour and Faulkner (1972).

The preceding discussion indicates that certain specific load and strength information are necessary for performing a reliability analysis of marine structures. It

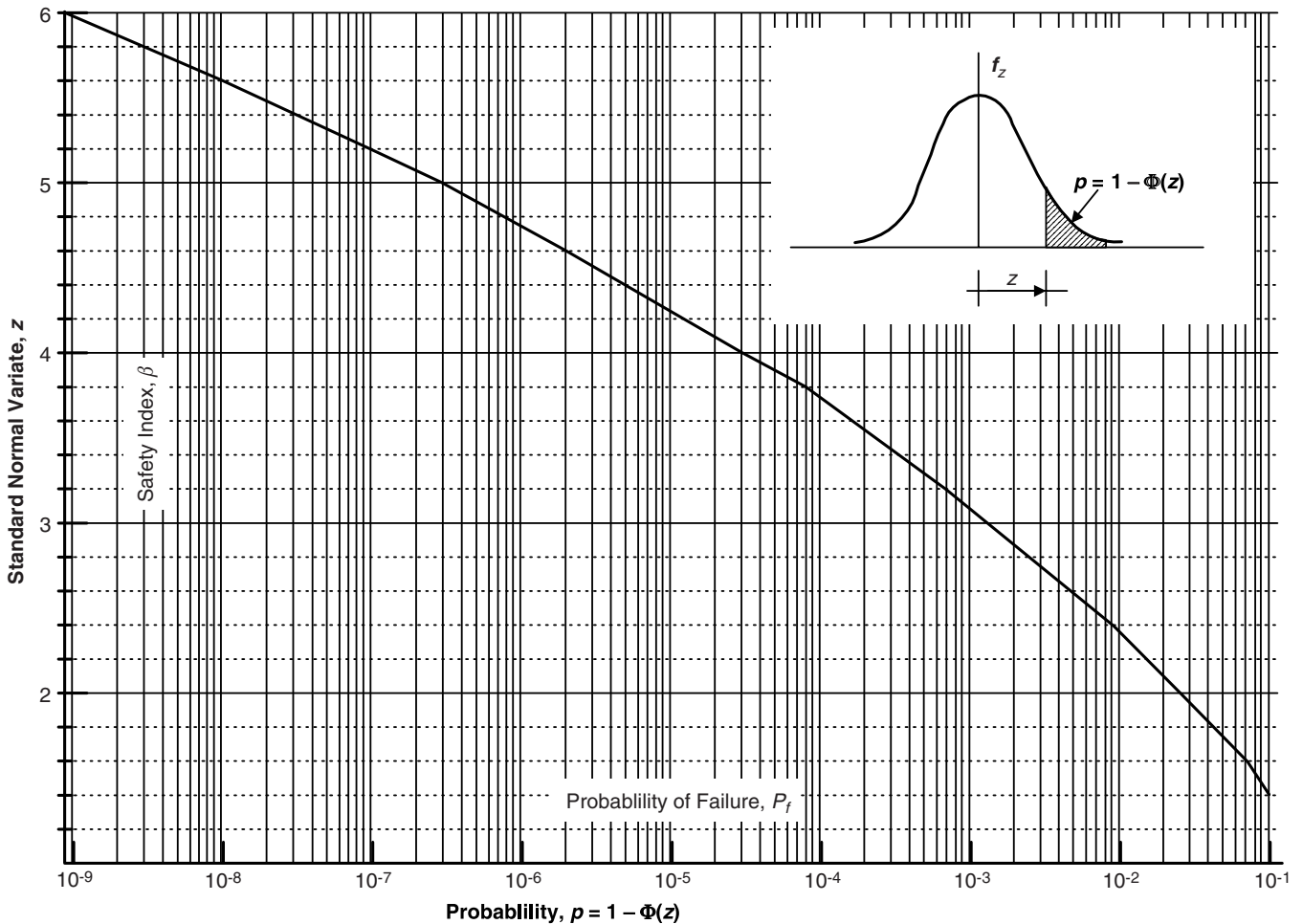


Fig. 135 Safety index versus probability of failure.

is mostly in this area that reliability analysis of marine structures differs from typical civil engineering structures. Prior to estimating the loads acting on ships or marine structures, a statistical representation of the environment is necessary. This includes waves, wind, ice, seismic activity, and current. (The last four items are more important for fixed offshore structures than for floating vessels.) The environmental information can then be used as input to determine the loads acting on the structure. Typically, an input/output spectral analysis procedure is used to determine the “short-term” loads in a specific sea condition (stationary condition)—see Section 2.6. The required transfer function is determined from strip theory using the equations of motion of the vessel or from a towing tank experiment. In offshore structures, Morrison’s equation is usually used to determine the wave-load transfer function.

Short-term prediction of the loads is not sufficient for the reliability analysis. Extreme values and long-term prediction of the maximum loads and their statistics are more valuable. For this purpose, order statistics and

statistics of extremes play a very important role. Gumbel’s theory of asymptotic distributions is often used in this regard. In the long-term prediction, the fatigue loads (i.e., the cyclic repetitive loads that cause cumulative damage to the structure) must also be considered. For a complete description of this aspect of reliability analysis, methods of combining the loads such as static and dynamic, including high- and low-frequency loads, must be considered. In nature, many of these loads act simultaneously, therefore their combination must be evaluated for a meaningful reliability analysis (see Section 2.6).

The second major component in the reliability analysis is the strength (or resistance) of the marine structure and the evaluation of its modes of failure. In this regard, several limit states may be defined such as the ultimate limit state, fatigue limit state, and serviceability limit state. The first relates to the maximum load-carrying capacity of the structure, the second to the damaging effect of repeated loading, and the third to criteria governing normal use and durability. Each of these limit states may include several modes—for example, the ultimate limit

state includes excessive yielding (plastic mechanisms) and instability (buckling failure).

5.3 Approximate Methods of Reliability Analysis. As discussed in the previous section, the direct integration method of reliability analysis (Level 3) can be difficult to apply in practice. The two main reasons for this are the lack of information to determine the joint probability density function (JPDF) of the design variables and the difficulty associated with the evaluation of the resulting multiple integral. For these reasons, approximate methods of reliability analysis were developed, most of these are classified as “Level 2” reliability analysis. These methods are:

- Mean value first order second moment method (MV-FOSM)
- First order reliability methods (FORM)
- Second order reliability methods (SORM)
- Advanced mean value method (AMV)
- Adaptive importance sampling (AIS)
- Monte Carlo simulation (MCS)

Some of these methods are discussed following.

5.3.1 Mean Value First Order Second Moment (MV-FOSM). If Z is a random variable representing the load and S is a random variable representing the strength, then the safety margin as defined previously is

$$M = S - Z \quad (279)$$

Failure occurs when the total applied load Z exceeds the ultimate capacity S , that is, when the margin M is negative. Therefore, the probability of failure (Ang and Tang, 1975), p_f , is

$$p_f = P[M \leq 0] = F_M(0) \quad (280)$$

where F_M is the cumulative distribution function of the margin M .

For statistically independent load Z and strength S , the mean μ_m and variance σ_m^2 of the margin are given by

$$\begin{aligned} \mu_m &= \mu_s - \mu_z \\ \sigma_m^2 &= \sigma_s^2 + \sigma_z^2 \end{aligned} \quad (281)$$

The standardized margin G , which has a zero mean and a unit standard deviation, can be written as

$$G = \frac{M - \mu_m}{\sigma_m} \quad (282)$$

Failure occurs (or a limit state is exceeded) when $M \leq 0$ so that equation (282) can be written as

$$p_f = F_M(0) = F_G\left(\frac{-\mu_m}{\sigma_m}\right) = F_G(-\beta) \quad (283)$$

where β is the safety index, which is the inverse of the coefficient of variation of the safety margin. Thus in the MVFOSM method, a safety index β is defined as

$$\beta = \frac{\mu_m}{\sigma_m} \quad (284)$$

If the distribution function F_G is known, then the exact probability of failure associated with the safety index can be determined. But even for unknown or unspecified distribution function F_G , there will be a corresponding though unspecified probability of failure for each value of β . Thus, β may be taken as a safety measure, as is the case in the MVFOSM method.

The foregoing results can be generalized as follows. Define a limit state (or performance) function g as

$$M = g(x_1, x_2 \dots x_n) \quad (285)$$

where x_i are the load and strength parameters considered as random variables, and the limit state function g is a function that relates these variables for the limit state of interest (serviceability or ultimate state). The limit state is exceeded (failure) when

$$M = g(x_1, x_2 \dots x_n) \leq 0 \quad (286)$$

Notice that equation (286) is the same as the integration domain in the Level 3 reliability—see equation (277). The limit state function can be expanded using Taylor’s series, and if only the first-order terms are retained, we get

$$g(x_1, x_2, \dots x_n) \cong g(x_1^*, x_2^* \dots x_n^*) + \sum_i (x_i - x_i^*) \left(\frac{\partial g}{\partial x_i} \right)_{x^*} \quad (287)$$

where x_i^* is the linearization point and the partial derivatives are evaluated at that point, see Ang and Tang, 1975. In the MVFOSM method, the linearization point is set at the mean values ($\bar{x}_1, \bar{x}_2, \dots \bar{x}_n$). The mean and variance of M are then approximated by

$$\mu_m \cong g(\bar{x}_1, \bar{x}_2, \dots \bar{x}_n) \quad (288)$$

$$\sigma_m^2 \cong \sum_i \sum_j \left(\frac{\partial g}{\partial x_i} \right)_{\bar{x}_i} \left(\frac{\partial g}{\partial x_j} \right)_{\bar{x}_j} \rho_{x_i x_j} \sigma_{x_i} \sigma_{x_j} \quad (289)$$

where $\rho_{x_i x_j}$ is the correlation coefficient and the subscripts \bar{x}_i and \bar{x}_j denote evaluation of the partial derivatives at the mean point. The accuracy of equations (288) and (289) depends on the effect of neglecting the higher-order terms in equation (287).

If the variables x_i are statistically uncorrelated, then equation (288) remains unchanged, but equation (289) becomes

$$\sigma_m^2 \cong \sum_i \left(\frac{\partial g}{\partial x_i} \right)_{\bar{x}_i}^2 \sigma_{x_i}^2 \quad (290)$$

As an example, if the margin M is represented by the variables S and Z only, that is,

$$M = g(x_1, x_2) = g(S, Z) = S - Z$$

then applying equations (288) and (290) for determining the mean and variance, one immediately obtains identical results as given by equation (281). This method is called the MVFOSM method because the linearization of

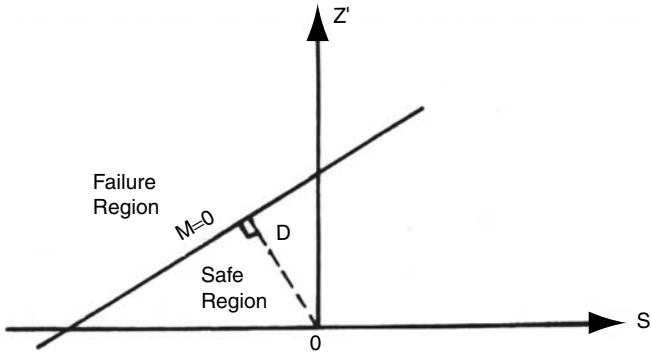


Fig. 136 Limit state function in the space of reduced variates.

the limit state function takes place at the *mean value* (MV); only the *first-order* (FO) terms are retained in Taylor's series expansion, and up to the *second moment* (SM) of the random variables (means and variances) are used in the reliability measure rather than their full probability distributions.

A geometric interpretation (see Ang and Tang, 1975) of the safety margin $M = S - Z$ will be particularly useful for the discussion of the first order reliability method (FORM), which will be presented later. First, we notice that $M > 0$ represents a safe state or region, $M < 0$ represents a failure state, and $M = 0$ represents a limit state or failure surface (or line, in the case of two variables). The standard or "reduced" variates of S and Z can be written as

$$S' = \frac{S - \mu_s}{\sigma_s}; \quad Z' = \frac{Z - \mu_z}{\sigma_z}$$

Therefore, the limit state function, $M = 0$, can be written in the space of reduced variates as

$$M = \sigma_s S' - \sigma_z Z' + \mu_s - \mu_z = 0$$

which is a straight line, shown in Fig. 136.

The region on one side of the straight line that contains the origin represents the safe state ($M > 0$), and the other region represents the failure state ($M < 0$). Thus, the distance from the origin to the line $M = 0$ can be used as a measure of reliability. In fact, from geometry the minimum distance, D , shown in Fig. 136, is given by (Ang and Tang, 1975):

$$D = \frac{\mu_s - \mu_z}{\sqrt{\sigma_s^2 + \sigma_z^2}}$$

Notice that D is equal to the safety index β for the case of the normal variates and linear limit state function discussed earlier, that is, for this case,

$$\beta = D = \frac{\mu_m}{\sigma_m} = \frac{\mu_s - \mu_z}{\sqrt{\sigma_s^2 + \sigma_z^2}}$$

and the probability of failure is thus

$$p_f = \Phi(-D)$$

5.3.2 First Order Reliability Method (FORM). The MVFOSM method described previously has three basic shortcomings. First, if g is nonlinear and the linearization takes place at the mean values of x_i , errors may be introduced at increasing distance from the linearization points by neglecting higher-order terms.

Second, the method fails to be invariant to different equivalent formulations of the same problem. In effect, this means that the safety index β depends on how the limit state equation is formulated. For example, if M is set to be a nonlinear function of S and Z , such as

$$M = S^2 - Z^2$$

then $p_f = F_M(0)$, still given as before by equation (283); however, when μ_m and σ_m are computed from equation (288) and (290) and substituted into

$$\beta = \frac{\mu_m}{\sigma_m} \quad (291)$$

the following β is obtained:

$$\beta = \frac{\mu_s^2 - \mu_z^2}{[4\mu_s^2\sigma_s^2 + 4\mu_z^2\sigma_z^2]^{0.5}} \quad (292)$$

which is different from the β obtained when M is taken as $M = S - Z$, even though the criterion of failure is still given by equation (278).

Third, in the MVFOSM method the safety index β can be related to a probability of failure in cases where the variables x_i are normally distributed (and when the function g is linear in x_i). It is known that many design variables may not be normally distributed. Thus, one of the improvements in the *first order reliability method* (FORM) is to include such distribution information.

The first two shortcomings discussed previously are avoided by using a procedure usually attributed to Hasofer and Lind (1974). Instead of expanding Taylor's series about the mean value point, which causes the invariance problem, the linearization point is taken at some point on the failure surface. On the failure surface, the limit state function g and its derivatives are independent of how the problem is formulated. The third shortcoming is avoided by transforming the non-normal variables to normal ones through appropriate transformation—for example, a Rosenblatt transformation (e.g., Mansour 1989).

In FORM, the load and resistance variables, x_i , are transformed to normal reduced (standard) variables with zero mean and unit variance given by

$$y_i = \frac{x_i - \bar{x}_i}{\sigma_{x_i}} \quad (293)$$

The FORM reliability index is defined as the shortest distance from the origin to the failure surface in the reduced space. This point is found by solving the following set of

equations:

$$G(y_1^*, y_2^*, \dots, y_n^*) = 0 \quad (294)$$

$$y_i^* = -\alpha_i^* \beta \quad (295)$$

$$\alpha_i^* = \frac{\left(\frac{\partial G}{\partial y_i}\right) y_i^*}{\sqrt{\sum_i \left(\frac{\partial G}{\partial y_i}\right)^2 y_i^*}} \quad (296)$$

G is the failure surface in the reduced space, and y_i^* are coordinates of the point closest to the origin in the reduced space (the design point). All partial derivatives are evaluated at the design point. All non-normal variables must be transformed to normally distributed ones (see Ang & Tang 1975) by requiring that the distribution functions of the basic variable and the standard normal variate be equal at the design point.

In the original space, the design point, or the most likely failure point, is obtained from

$$\begin{aligned} x_i^* &= \bar{x}_i + \sigma_{x_i} y_i^* \\ &= \bar{x}_i - \sigma_{x_i} \alpha_i^* \beta \end{aligned} \quad (297)$$

In general, for a linear limit state function and Normal variables, FORM will yield the same result for β as the MVFOSM method. For nonlinear limit state functions, FORM yields a safety index β that is invariant to the formulation of the limit state function and is more accurate than the MVFOSM safety index.

5.3.3 Second Order Reliability Method (SORM). It was found that FORM produces errors whose magnitudes are difficult to predict in advance. This observation led to the development of the *second order reliability method* (SORM). As mentioned previously, FORM involves approximating the higher-order failure surface by using hyperplanes that are tangent to the failure surface at the design point in a transformed standard normal space. SORM takes this idea one step further by fitting hyperparaboloids near the design point. This provides a more accurate approximation of the failure surface. The design point, or most likely failure point, is found by iterative method.

5.3.4 Monte Carlo Simulation. In general, simulation is a technique for conducting experiments in a laboratory or on a computer to model the behavior of a system. Usually, simulation models result in “simulated” data that must be treated statistically to predict the future behavior of the system. In this broad sense, simulation has been used as a predictive tool for economic systems, business environment, war games, and management games.

The name “Monte Carlo method” was introduced in 1944 by von Neumann and Ulam as a code name for their secret work on neutron diffusion problems at the Los Alamos Laboratory. The name was chosen apparently because of the association of the town Monte Carlo with

roulette, which is one of the simplest tools that can be used for generating random numbers.

Monte Carlo simulation is usually used for problems involving random variables of known or assumed probability distributions. Using statistical sampling techniques, a set of values of the random variables are generated in accordance with the corresponding probability distributions. These values are treated similarly to a sample of experimental observations and are used to obtain a “sample” solution. By repeating the process and generating several sets of sample data, many sample solutions can be determined. Statistical analysis of the sample solutions is then performed.

The Monte Carlo method thus consists of the three basic steps:

- (a) Simulation of the random variables and generation of several sample data sets using statistical sampling techniques
- (b) Solutions using the sampled data
- (c) Statistical analysis of the results

Because the results from the Monte Carlo technique depend on the number of samples used, they are not exact and are subject to sampling errors. Generally, the accuracy increases as the sample size increases.

Sampling from a particular probability distribution involves the use of random numbers. *Random numbers* are essentially random variables uniformly distributed over the unit interval [0,1]. Many codes are available for computers to generate a sequence of “pseudo” random digits, where each digit occurs with approximately equal probability. The generation of such random numbers plays a central role in the generation of a set of values (or realizations) of a random variable that has a probability distribution other than the uniform probability law. The Monte Carlo method is considered one of the most powerful techniques for analyzing complex problems due to the enormous computing power of computers.

As discussed previously, the reliability of a structure can be characterized by a limit state function $g(\underline{x}) = g(x_1, x_2, \dots, x_n)$, where x_i are random variables representing the basic design variables. The inequality $g(\underline{x}) \leq 0$ corresponds to failure, whereas $g(\underline{x}) > 0$ represents the safe region. In the Monte Carlo approach, a random sample of values x_i for the basic design variables is generated numerically according to their probability distributions using a random number generator. The generated sample values are then substituted in the limit state function, whose value is then computed to see if it is negative or positive (i.e., failure or no failure). Repeating this process many times, it is possible to simulate the probability distribution of $g(\underline{x})$. This will require a very large number of samples. The probability of failure can then be estimated from either of the following methods.

The probability of failure is given by

$$p_f = P[g(\underline{x}) \leq 0] = \lim_{n \rightarrow \infty} \frac{n}{N} \quad (298)$$

where N is the total number of trials or simulations and n is the number of trials in which $g(\underline{x}) \leq 0$. The ratio n/N is usually very small, and the estimated probability of failure is subjected to considerable uncertainty. In particular, the variance of n/N depends on the total number of trials, N , decreasing as N increases. That is, the uncertainty in estimating p_f decreases as N increases. Statistical rules can be used to establish the necessary number of trials that depend on the magnitude of p_f . Many variance reduction techniques have been developed to decrease the variance of n/N with a smaller number of trials than would have been necessary otherwise.

In the second method, the probability of failure is estimated by first fitting an appropriate probability distribution for $g(\underline{x})$ using the trial values described previously. The moment or any other established statistical method may be used in the fitting process. The probability of failure is then determined from

$$p_f = \int_{-\infty}^0 f_M(m) dm \quad (299)$$

where $M = g(\underline{x})$ is a random variable representing the margin and $f_M(m)$ is its PDF as estimated from the fitting process.

5.3.5 Ship Structural Reliability. Literature on the structural failure assessment of ships is extensive and dates back to the early 1970s (e.g., J. Ship Research 1972; Mansour, SNAME Tran. 1972; Mansour & Faulkner, RINA 1972). There have been a number of investigations that were built on this earlier work. Particular mention may be made to Stiansen et al. (RINA 1980), Faulkner and Sadden (RINA 1979), and White and Ayyub, who applied Monte Carlo simulation together with various efficient methods to reduce the number of cycles in estimating the failure probability (Naval Engineering Journal 1985). The Ship Structure Committee and the ABS have sponsored several projects related to this area, for example, Kaplan et al. (1983), Daidola and Baser (1983), and Mansour et al. (1990, 1995a, 1995b, 1997).

Specific research in the area of code development has also been carried out by the ABS and reported in Mansour et al. (1984). An in-depth evaluation of uncertainties in hull strength prediction was conducted by

Soares and Moan (1985), and application of first-order second moment method to ship hull was undertaken by Thayamballi et al. (1984, 1990). Moan (1994) and Wirsching and Chen (1988) applied reliability methods to offshore structures. A reliability study of oil production ships was conducted by Wang, Jiao, and Moan (1996). The study included a systematic analysis of the combination of still water and wave loads, ultimate strength of longitudinally stiffened panels, and reliability-based design. A more complete literature survey and summary of reliability methods for ship and offshore structures are included in Ship Structure Committee reports SSC-351 (Mansour 1989) and SSC-398 (Mansour et al. 1997).

In Mansour et al. (1997) a comprehensive methodology was developed for assessing the structural reliability of ships. Areas included cover extreme wave loads and load combinations, primary, secondary, and tertiary hull strength, the estimation of ship failure probabilities in the primary, secondary, and tertiary modes, fatigue reliability, and selection and recommendation of target reliabilities. In addition to incorporating the results of previous work, the report presents new developments and additional information in the various topic areas. In several cases, results have been presented in the form of design charts and equations with examples. Applications are made to four ships: two cruisers, a tanker, and an SL-7 container ship. For each of these ships, loads, strength, reliability, and sensitivity to design parameters have been estimated.

Table 6 from this study shows sample limit state equations for primary, secondary, and tertiary modes of failure. Figure 137 shows the computed safety indices using SORM for all modes of failure. The figure points out to the lack of consistency in the reliability level between the various ship types as well as the failure modes. Figure 138 shows the ratio of the ultimate strength safety index to the initial yield safety index for the primary failure modes. Because the bars are not of uniform (constant) height, it can be concluded that the primary initial yield moment is not a good predictor of the true strength and reliability of the ship, and cannot be used to rank the ships in terms of their safety. Designing a ship's structure based on yield strength criteria is unlikely to produce designs with a consistent level of reliability, given the nature of stiffened panel buckling.

Bai (2006) also applied reliability assessment to a double hull tanker to get the time-dependent reliability index

Table 6—Limit state equations (Mansour et al., SSC 398)

Failure Mode	Hogging	Sagging
Primary (initial yield)	$G = M_{IY} - [M_{sw} + k_w M_w]$	$G = M_{IY} - [-M_{sw} + k_w (M_w + k_d M_d)]$
Primary (ultimate strength)	$G = M_U - [M_{sw} + k_w M_w]$	$G = M_U - [-M_{sw} + k_w (M_w + k_d M_d)]$
Secondary	$G = S_{u,2} - \frac{[M_{sw} + k_w M_w]}{SM_b}$	$G = S_{u,2} - \frac{[-M_{sw} + k_w (M_w + k_d M_d)]}{SM_b}$
Tertiary	$G = S_{u,3} - \frac{[M_{sw} + k_w M_w]}{SM_d}$	$G = S_{u,3} - \frac{[-M_{sw} + k_w (M_w + k_d M_d)]}{SM_d}$

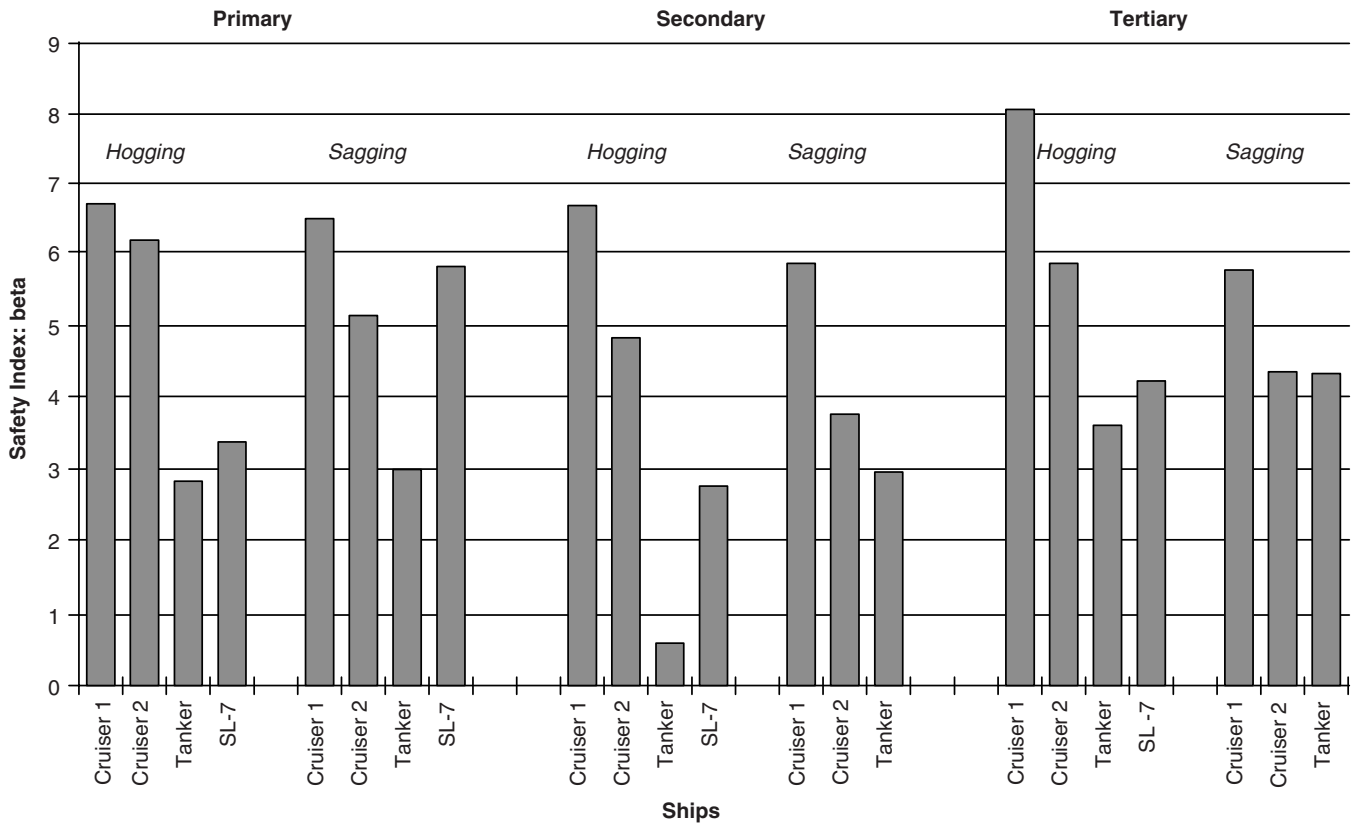


Fig. 137 Computed primary, secondary, and tertiary safety indices (Mansour et al., SSC 398).

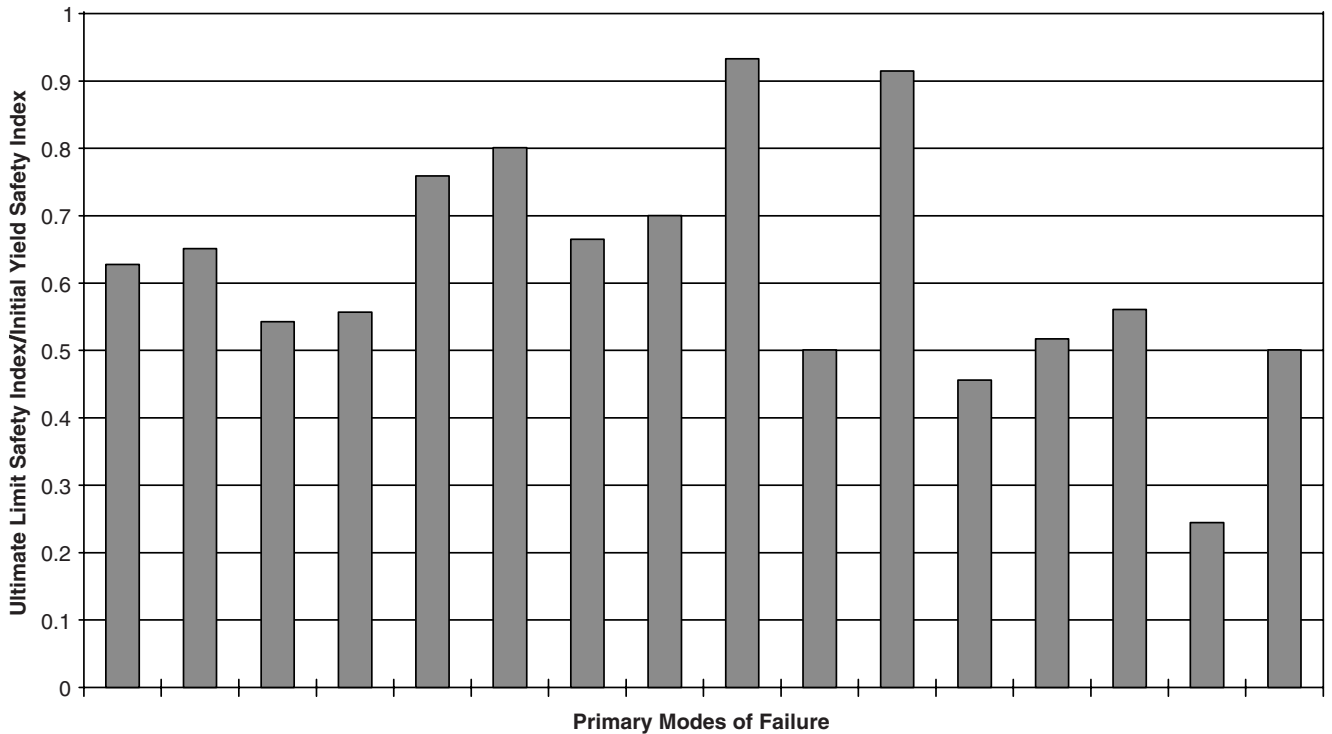


Fig. 138 Ratio of ultimate strength safety index to initial yield safety index (Mansour et al., SSC 398).

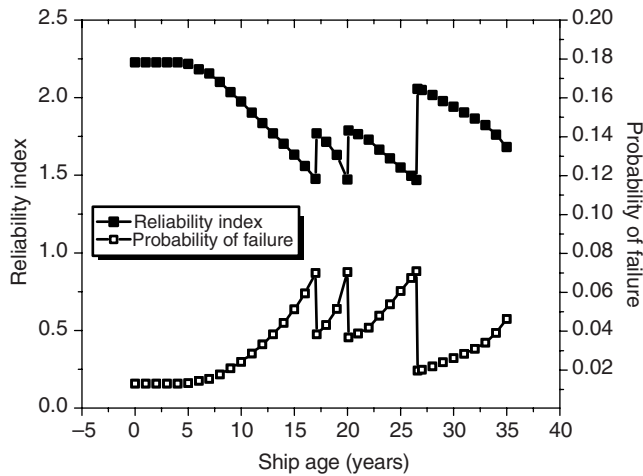


Fig. 139 Repair scheme and resulting time-dependent reliability index of the example vessel considering corrosion and fatigue cracks (Bai, 2006).

and probability of failure of the ship hull considering age-related degradations (i.e., corrosion and fatigue). The impact of the repair scheme was also studied. Figure 139 shows the results based on a minimum reliability index of 1.5.

5.4 Partial Safety Factors and Code Development

5.4.1 Partial Safety Factors The *partial safety factors*, or load and resistance factors, are factors that are multiplied by the design variables to ensure a specified reliability level β . They may be applied to the mean value of the design variable but, in many cases, they can be modified so that they can be applied to nominal or characteristic values. The partial safety factors, γ_i , associated with variable X_i are defined as

$$\gamma_i = \frac{X_i^*}{\mu_{X_i}} \quad (300)$$

where X_i^* is the value of the variable at the most likely failure point (the design point) and μ_{X_i} is its mean value.

It can be shown (see Ang & Tang 1975) that the partial safety factors γ_i can be expressed in terms of the reliability index β by

$$\gamma_i = 1 - \alpha_i^* \beta v_{X_i} \quad (301)$$

where v_{X_i} is the coefficient of variation of the variable X_i , and α_i^* is the direction cosine given by equation (296) and evaluated at the most likely failure point. For nonlinear limit state functions (including the product of two random variables), the determination of X_i^* and α_i^* requires an iterative solution. For a specified reliability level β , this can be done by first assuming a value for X_i^* , evaluating α_i^* , and calculating a new value for X_i^* . The new value of X_i^* is then used in the next step of iteration. When conversion is achieved, the partial safety factors γ_i are calculated from equation (301).

In the case of linear limit state functions of the form

$$g(x) = a_0 + \sum_{i=1}^n a_i X_i \quad (302)$$

the iterative procedure is not necessary, and an explicit form of the partial safety factors γ_i is given by

$$\gamma_i = 1 - \frac{a_i \sigma_{X_i}}{[\sum_i (a_i \sigma_{X_i})^2]^{1/2}} \beta v_{X_i} \quad (303)$$

Notice that the partial safety factors γ_i associated with variable X_i depend on the specified reliability level β , its own standard deviation, and to a lesser extent the standard deviations of all other variables. In the case of the simple limit state function,

$$g(s, z) = s - z$$

the partial safety factors reduce to

$$\gamma_s = 1 - \beta \frac{\sigma_s v_s}{(\sigma_s^2 + \sigma_z^2)^{1/2}} \quad (304)$$

$$\gamma_z = 1 + \beta \frac{\sigma_z v_z}{(\sigma_s^2 + \sigma_z^2)^{1/2}} \quad (305)$$

All the previous equations are valid for partial safety factors that apply to the mean values of the variables. If a nominal value is preferred (e.g., in the left or right tail of the variable distribution), the corresponding partial safety factors may be obtained by direct multiplication of γ_i by the ratio of the mean to the nominal values—see equation (300). Notice that equations (304) and (305) indicate that $\gamma_s < 1$ and $\gamma_z > 1$, as expected.

5.4.2 Code Development. The procedure described previously for the derivation of partial safety factors can be used to develop safety factors for use in codes. This necessitates a change in code format as well. Changing from a working stress design code to a reliability-based code is not an easy task. Complicating the procedure is the fact that there is no set method for introducing reliability into a code. The implementation of reliability theory in design codes changes from organization to organization. Even when two organizations use the same reliability-based design format, the details differ, as it must for different types of structures.

The organizations that adopted or developed reliability-based codes (often referred to as load resistance factor design, or LRFD) include the American Petroleum Institute (API LRFD-RP2A), the National Bureau of Standards (NBS A58), the American Bureau of Shipping (ABS), the American Institute of Steel Construction (AISC), the American Concrete Institute (ACI), and the National Building Code of Canada.

The fundamental differences between the reliability-based code format and the elementary safety factor procedure lie in the use of multiple (partial) safety factors expressing the variability in the load and strength variables—and possibly an additional factor expressing the economic, sociological, and other consequences of

failure of the structure—and that the multiple safety factors are calibrated to produce designs of uniform reliability. A typical expression is given in equation (306) for a structure of capacity C_j in which there may be several sources of loading that combine to form the total demand, D :

$$\gamma_c \sum_i \gamma_{fi} D_i \leq C_j \gamma_m \quad (306)$$

For each load component, D_i (still water load, wave load), there may be a different value of the load factor, γ_f , that reflects the variability of that load component and the uncertainty in our ability to predict it. Typical values of the load factors, γ_f , in a formula of the form of equation (306) will lie in the range of 1.0 to 1.5, whereas typical values of the material and fabrication factor, γ_m , will be in a range of 0.75 to 1.0.

The consequences of failure factor, γ_c , represents an attempt to quantify the broader effects of potential failure of the structure. This includes certain consequences that may be expressed in very specific quantitative terms, such as the value of the ship and cargo, the loss of earnings if the ship is out of service for repair or replacement, and the cost of restoration of the environment in the event of casualty-caused pollution. The potential consequences of loss of life, either of crew or passengers, would also be included in the value assigned to this factor. In the case of a passenger ship carrying a large number of persons untrained in seamanship and emergency procedures, a greater value would be assumed than in the case of a cargo ship having a small and highly trained crew.

The numerical values of the partial safety factors depend on the form of the equation in which they are combined and on the degree of structural reliability that is to be achieved; thus, a unique set of values cannot be stated for general use. For a specific application, the engineer should consult the relevant code to obtain the formula in which the partial safety factors are applied, and the relevant definitions and specific values of partial safety factors to be used. A discussion of the relationship of partial safety factor formulations and the rules and practices for ships and offshore structures can be found in Mansour et al. (1984).

The Ship Structure Committee sponsored a project (SSC-392) to demonstrate a reliability-based structural design code for ships. One reason for the development of such a code is to provide specifications that produce ship structure having a weight savings or improved reliability relative to structure designed by traditional methods. Another reason is that a calibrated code will provide uniform safety of ships within each type. Two ship types were considered in the report (Mansour, Wirsching, White, & Ayyub 1996), a cruiser and a tanker. For each ship type, the code requirements covered four failure modes: hull girder buckling, stiffened plate buckling, unstiffened plate yielding and buckling, and fatigue

of critical details. Both serviceability and ultimate limit state were considered. In all cases, examples of limit state equations and partial safety factors for the important design variables are provided.

5.5 System Reliability. The reliability analysis discussed in the previous sections has been mainly concerned with a single failure mode (or a limit state) defined by a single limit state equation. However, failure of marine structures may involve several modes of failure, that is, there is a possibility that a structure may fail in one or more of several possible failure scenarios. The subject of *system reliability* deals specifically with the methods of combining the probabilities of failure associated with these modes to determine the total reliability of the structure as a system.

Two main sources of “system effects” are identified (see Ang & Tang 1975). The first is due to possible multiplicity of failure modes of a component or a structural member. For example, a beam under bending and axial loads may fail in buckling, flexure, or shear. Each one of these modes can be defined by one limit state equation. Even though in this case we are dealing with a single member (beam), system reliability methods must be used to combine the possible failure modes and obtain an assessment of the total risk of failure of the beam. The probability of failure of one mode may be larger than the others, but the fact that there is a possibility that the others may occur indicates that they must be included and combined to obtain the total probability of failure of the beam.

Another example of multiplicity of failure modes is the primary behavior of a ship hull. In the primary behavior, one treats the ship as a single beam subjected to weight, buoyancy, and wave loads that induce sagging and hogging bending moments. The hull may fail (or exceed a limit state) in one of several possible modes (e.g., buckling of deck or bottom panels or grillages, yielding of deck or bottom plating). Here again, system reliability methods may be used to combine these different modes of failure and obtain a total probability of failure.

Multiple modes of failure of a member are usually modeled in system reliability analysis as a series system. A *series system* is one that is composed of links connected in series such that the failure of any one or more of these links constitute a failure of the system (i.e., “weakest link” system). For example, in the case of the primary behavior of a ship hull any one of the failure modes discussed previously will constitute failure of the hull (or a limit state to be prevented) and, therefore, can be considered as a series system. Series systems will be discussed in more detail in a later section.

The second source of “system effects” is due to redundancy in multicomponent structures. In such structures, the failure of one member or component does not constitute failure of the entire system. Usually, several members must fail to form a “failure path” before the entire structure fails. The failure of each member is defined by at least one limit state equation and a corresponding

probability of failure. These individual member probabilities of failure must be combined to get the probability of failure of the system for a particular failure path. Thus, system reliability methods must be used to determine the reliability of a redundant structure.

An example of a multicomponent redundant structure in which system effects are important is a fixed offshore platform. For such a platform to fail, several members must fail to form a failure path. The probability of failure of the system in this case is usually modeled as a parallel system in which all links along the failure path of the system must fail for the entire structure to fail. Moreover, there will be several possible paths of failure, any of which will constitute failure of the entire platform. Therefore, each failure path and the associated probability of failure can be considered as a link in a series system because failure of any link constitutes a failure of the system in the series model. The total offshore platform can be thus modeled as several parallel subsystems, each of which represents a failure path connected together in series because any of them constitutes failure of the platform. Parallel systems and general systems consisting of series and parallel subsystems will be discussed in later sections.

5.5.1 General Formulation. The exact system reliability problem taking into consideration possible time-dependent random variables is an outcrossing problem. If the time-dependent loads or response of the structure exceeds (outcrosses) one or more of several possible failure modes (surfaces), failure of the structure occurs. However, the problem formulated in terms of stochastic processes is difficult to solve.

The general problem is formulated as a time-independent problem, which is sufficient only for the evaluation of an instantaneous reliability. As such, the form of the equation to evaluate the system reliability is the same as that of component reliability equation (307) except that now, the multiple integration is carried out over all possible limit state functions corresponding to the potential modes of failure. For k modes of failure and n random variables, the system probability of failure can be written as

$$p_f = \int \cdots \int f_{\underline{X}}(x_1, x_2, \dots, x_n) dx_1 \dots dx_n \quad (307)$$

$$g_i(\underline{x}) \leq 0$$

$$i = 1, 2, \dots, k$$

where $f_{\underline{X}}(x_1, x_2, \dots, x_n)$ is the JPDF of the n random variables and $g_i(\underline{x})$ are the k limit state functions. The domain of integration in equation (307) is over the entire space where each of the k limit state functions is negative or zero.

The same difficulties encountered in the Level 3 computation (direct integration method) of component reliability will be encountered in determining system reliability from equation (307), namely, the determination of the joint density function and the evaluation of the mul-

tipole integration. In addition, the domain of integration over all possible modes of failure in equation (307) will present additional numerical difficulties. For these reasons, this general exact formulation is not used, and instead of determining the combined total probability of failure of the system as given by equation (307), only an upper and lower bound on that system probability are determined. These upper and lower bounds are usually determined by considering the structure to be a series system or a parallel system, or a combination of both (general system).

It should be noted that in principle, simulation methods and the Monte Carlo technique can be used to solve equation (302) in basically the same manner discussed in Section 5.3. In this case, numerical simulation of the random variables is performed according to their prescribed joint distribution, and all limit state equations are checked to see if failure occurs. The ratio of failure realizations to total number of simulations gives an estimate of the probability of system failure. Reduced variate techniques and other methods for improving convergence can be used here. Usually, for realistic structures the number of simulations required for a reliable estimate of the system probability of failure is still high but these methods have potential for application in system reliability.

5.5.2 Bounds on the Probability of Failure of a Series System. Schematically, a series system is represented as in Fig. 140. A typical example of a series system is a statically determinate structure where a failure of any member constitutes failure of the structure. Another example of a series system is a beam or an element that may fail in any of several possible modes of failure, each of which may depend on the loading condition of the beam. A ship hull girder in its "primary behavior" is such a system, with the additional complication that failure may occur in hogging or sagging condition. Each condition includes several modes of failure. A third example of a series system arises when combining the probabilities of failure of several possible failure paths in an offshore platform, any of which constitutes failure of the platform.

If F_i denotes the i -th event of failure, the event that $[g_i(\underline{x}) \leq 0]$, and S_i represents the corresponding safe event, that is, $[g_i(\underline{x}) > 0]$, then the combined system failure event F_S is determined as the union "U" of all individual failure events F_i as

$$F_S = \cup_i F_i, \quad i = 1, 2, \dots, k$$

The corresponding probability of system failure is

$$P(F_S) = P(\cup_i F_i) = 1 - P(\cap_i S_i) \quad (308)$$

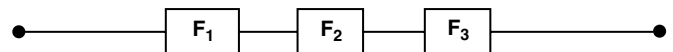


Fig. 140 Schematic representation of a series system.

where \cap represents the intersection or mutual occurrence of events.

The calculation of the probability of systems failure for a series system using equation (308) is generally difficult, and requires information on correlation of all failure events. Therefore, approximations are necessary, and upper and lower bounds on the system probability of failure are constructed instead of evaluating the exact value.

5.5.3 First Order Bounds. *First order bounds* are bounds on the probability of system failure that require no information on the correlation between the events of failure. If the events of failure of a series system are assumed to be perfectly correlated, the probability of system failure is simply the maximum of the individual probabilities of failure. For positively correlated failure events, this assumption leads to the lower nonconservative bound on the actual system probability,

$$\max_i P(F_i) \leq P(F_s) \quad (309)$$

On the other hand, if the events of failure are assumed to be statistically independent, an upper bound (conservative) can be determined. In this case, for independent failure events of a series system, the right side of equation (5.37) reduces to

$$1 - P(\cap_i S_i) = 1 - \prod_{i=1}^k P(S_i) = 1 - \prod_{i=1}^k [1 - P(F_i)] \quad (310)$$

where

$$\prod_{i=1}^k P(S_i)$$

represents the product of the probabilities of survival. The result given by equation (310) represents an upper bound on the true probability of system failure,

$$P(F_s) \leq 1 - \prod_{i=1}^k [1 - P(F_i)] \quad (311)$$

Combining equations (309) and (311), one obtains an upper and lower bound, that is, the bounds are given by

$$\max_i P(F_i) \leq P(F_s) \leq 1 - \prod_{i=1}^k [1 - P(F_i)] \quad (312)$$

The lower bound is based on the assumptions of perfectly correlated events of failure, whereas the upper bound is based on statistically independent failure events.

Although the upper bound in equation (312) is not difficult to evaluate, it can be further simplified and equation (312) can be written as

$$\max_i P(F_i) \leq P(F_s) \leq \sum_{i=1}^k P(F_i) \quad (313)$$

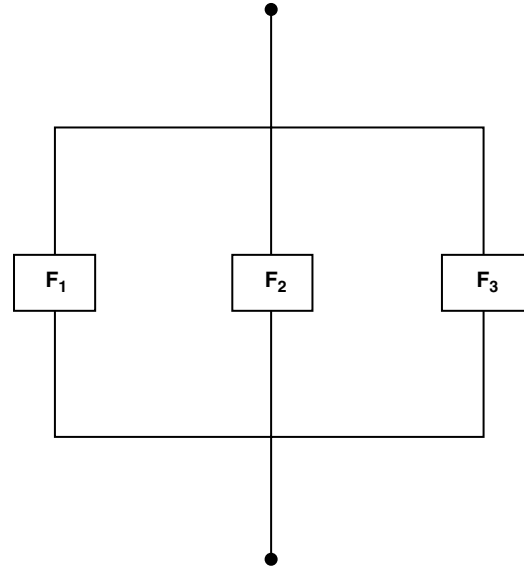


Fig. 141 Schematic representation of a parallel system.

Equation (313) states the obvious conclusion that the actual probability of series system failure lies between the maximum of the individual probabilities and the sum of all individual probabilities. These bounds are narrow if one mode of failure is dominant (i.e., if one of the individual probabilities of failure is much larger than the others). If not, these bounds may be too wide to be useful. In such cases, a more narrow set of bounds should be considered (second order bounds), which can be found in Ang and Tang (1975).

5.5.4 Bounds on the Probability of Failure of a Parallel System. A *parallel system* is one that fails only if all its components fail—failure of one component only will not necessarily constitute failure of the system. Schematically, such a system can be represented as shown in Fig. 141.

A typical example of a parallel system is a statically indeterminate structure where, because of redundancy, failure of several members along a “failure path” must take place for the entire structure to fail. The behavior of such a structure also depends on whether the members are brittle or ductile. Generally, brittle failure implies that the member completely loses its load-carrying capacity, whereas in ductile failure the member maintains a certain level of load-carrying capacity after failure.

If F_i denotes again the i -th event of failure and S_i the corresponding safe event, then the system failure event of a parallel system F_P of k components (i.e., failure events) is the intersection or mutual occurrence of all failure events,

$$F_P = \cap_i F_i \quad i = 1, 2, \dots, k \quad (314)$$

The corresponding probability of system failure is

$$P(F_P) = P(\cap_i F_i) = 1 - P(\cup_i S_i) \quad (315)$$

Equation (315) for failure of a parallel system should be compared with equation (308) for failure of a series system. It is clear that the failure of a series system is the union (any) of the component failures, whereas the failure of a parallel system is the intersection (all) of the component failures. Just as in a series system, the evaluation of equation (315) for determining the exact system failure of a parallel system is generally difficult, and approximation by constructing bounds is usually necessary.

Simple first order lower and upper bounds can be constructed using similar arguments as for the series system. However, now perfect correlation between all failure events ($\rho = 1.0$) corresponds to the upper bound, and no correlation between any pair corresponds to the lower bound. Thus, for positively correlated failure events these bounds are

$$\prod_{i=1}^k P(F_i) \leq P(F_p) \leq \min_i P(F_i) \quad (316)$$

Unfortunately, the bounds given by equation (316) on the probability of failure of a parallel system are wide and no second order bounds are available. However, in some special cases the "exact" system failure can be evaluated. For example, Thoft-Christensen and Baker (1982) evaluated the probability of parallel system failure under deterministic loading and other restrictive conditions.

5.5.5 General Systems. A *general system* is one that consists of a combination of series and parallel subsystems. An example of application for such a general system is an offshore platform where each failure path can be modeled as a parallel subsystem and all possible failure paths (parallel subsystems) are connected together in a series because any of them constitute failure of the platform. This representation is called "minimal cut set" because no component failure event in the parallel subsystem (a failure path) can be excluded without changing the state of the structure from failure to safe. A schematic representation of parallel subsystems connected together in a series is shown in Fig. 142. A general system may also consist of a series of subsystems connected together in parallel (minimal link set). However, such systems have less potential for application to structural reliability, and therefore will not be discussed further.

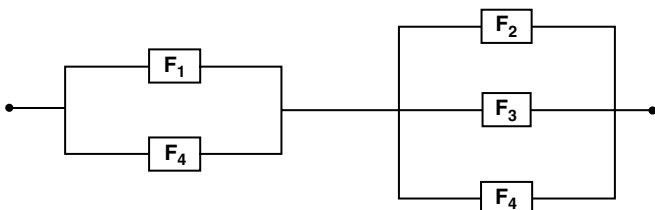


Fig. 142 Schematic representation of parallel subsystems connected in a series (minimal cut set).

The failure event, F_g , of a general system consisting of parallel subsystems connected together in a series (minimal cut set) is given by the union (series) of intersection (parallel) of individual failure events,

$$F_g = \cup_j \cap_i (F_{ij}) \quad (317)$$

where (F_{ij}) is the i -th component failure in the j -th failure path. The probability of failure of such a system is thus determined from

$$P(F_g) = P[\cup_j \cap_i (F_{ij})] \quad (318)$$

Exact evaluation of equation (318) is difficult and requires information of the joint dependence of failure events. Similarly, bounds on the probability of failure given by equation (318) are not available in general. However, if one is able to determine the probability of failure of each parallel subsystem (for example, under restrictive conditions), then bounds can be determined using equation (313) for the remaining series system.

5.5.6 Reliability Bounds for Ship Primary Strength. Reliability bounds for ship primary strength were developed in 1972 (see Mansour 1972). In the primary behavior, the ship hull is considered as a free-free nonuniform beam supported by water pressure. Wave loads (bending moment) are calculated using the equations of motion of the ship if dynamic effects are to be included, otherwise by balancing the vessel on a wave configuration. The loads on the vessel alternate from hogging, which produce compression in the bottom plating, to sagging, which induces compression in the deck. This hog/sag variation must be considered in the hull reliability analysis.

In each hog/sag condition, there will be several possible modes of failure (e.g., plate and panel buckling, tensile yield). If F^h and F^s represent hogging and sagging events of failure, respectively, then the combined event of failure F^c is given by the union of the two events,

$$(F^c) = (F^h) \cup (F^s) \quad (319)$$

Because hogging and sagging are mutually exclusive events (i.e., the vessel can be either in hogging or in sagging condition but not both at the same time), then the union of the two events given in equation (319) is simply their sum. The probability of combined event of failure is thus

$$P(F^c) = P(F^h) + P(F^s) \quad (320)$$

As mentioned previously, each of the hogging and sagging conditions will have several possible modes of failure (or limit states). In each case, these modes can be modeled as a series system because any of them constitute a failure of the hull (or a limit state to be prevented). Thus, bounds on the probability of failure in hogging condition $P(F^h)$ and in sagging condition $P(F^s)$ can be constructed using equation (313). The bounds on the combined probability $P(F^c)$ are simply the sum of the bounds on each condition as implied by equation (320).

Experience indicates that in many cases, either the hogging or sagging condition is the dominant governing condition in the reliability analysis, depending on whether the still water bending moment is hogging or sagging (in much the same manner as in the usual deterministic analysis). However, in some cases both conditions must be included; otherwise, the estimated reliability will be nonconservative.

5.6 Collision and Grounding. The potential for environmental pollution has grown in recent years. This is mainly due to increasing ship sizes and the amount of hazardous goods, including crude oil, being transported by sea. Tanker groundings and other tanker accidents that cause oil outflow created public concern over the need for improved environmental protection, with renewed discussions on ways of preventing accidental oil spills. Because about 85 percent of the accidents are caused by human error, it is essential to reduce human errors by education and by introducing advanced navigation systems. It is equally important that the design of hull structures be considered from the point of view of minimizing the oil outflow after an accident.

In 1990, the United States Congress passed the Oil Pollution Act (OPA90). It mandates that all tankers entering U.S. waters must be double hull, as an effective means of protecting the ocean environment from accidental oil outflow in case of grounding or collision. OPA90 was later followed by similar international regulations issued by the IMO.

The state-of-the-art research on collision and grounding has been reviewed in Wang, Spencer, and Chen (2001) and ISSC (1994, 1997, 2000, 2006). Research and development in the 1990s was characterized by the following: several national and international large model testing projects and pilot simulation studies using nonlinear analysis tools, theoretical development of the structural crashworthiness concept and methodology, and development of environmentally friendly tank arrangements and structural designs. More recently, the focus has been the integration of key research achievements into risk-based methodology, improved application of advanced simulation tools (such as FEM), concepts to develop relevant rules and regulations, and continued development of innovative crashworthy structures.

5.6.1 Probabilities of Collision and Grounding. One of the important issues for a design standard is to define a set of events, or accident scenarios, that are considered in evaluating a design. A clear definition of such events includes typical accident scenarios and a probability of occurrence for each accident scenario. Accident scenarios and the probability of occurrence can be determined through statistical investigations of historical data, consulting and gathering expert opinions, or performing risk analyses.

Marine casualties have always been the driving forces for developing new regulations. Statistics of previous accidents are regarded as a very reliable source for predicting what will happen in the future, and have been

the basis for new requirements of classification societies and international regulatory agencies. For example, the IMO requirements for the double hull designs were established based on accident statistics of survey records of four major classification societies in the period of 1980 to 1990.

Some investigations of casualties were reported by Card (1975), Kite-Powell et al. (1999), Bjerneboe et al. (1999), and Randrup-Thomsen et al. (2001). However, many in-depth statistical studies are not available in the public domain for reasons of confidentiality, or because of litigation. As a result, the available casualty statistics are too scarce to be used effectively in predicting accidents in sensitive geographic areas.

In addition, some characteristics of statistics should be kept in mind so that the chances of misinterpretation of historical data can be minimized. Statistics are based on past experience and may not reflect present situations. Statistics from damage cases can even penalize designs, although the designs may be able to resist such damage. In view of these concerns, combining limited historical data with risk analysis techniques and experts' opinions provides a better basis to determine realistic and critical accident scenarios (Friis-Hansen et al. 2004; ISSC 2006; Wang et al. 2003).

The early studies of probability of ship accident occurrence were carried out by Fujii (1974) and his coworkers in Japan. A model for stranding accidents has been established on the basis of observations of ship routes in four straits in Japan. In Europe, Macduff (1974) developed a different model for ship collisions based on statistics of accidents in the Straits of Dover. Pedersen et al. (1993) extended Fujii's model to collisions and applied it to ship traffic in the Great Belt Bridge area in Denmark. There is more recent work done by Gluver and Olsen (1998), Urban et al. (1999), and Otto et al. (2001).

The main principle behind the commonly used risk models is the determination of the number of possible ship accidents (i.e., the number of grounding or collision if no evasive maneuvers are made). This number is then multiplied by a causation probability to estimate the "actual" accident frequency. Therefore, the causation probability is a fraction of the accident candidates that result in an accident. It can be estimated on the basis of available accident data collected at various locations and then transformed to the area of interest. Another approach is to analyze the cause of human inaction or external failures and set up a fault tree procedure. Pedersen (1995) provides simplified expressions to calculate the expected number of collisions or grounding per year for two categories: ships following ordinary, direct routes at normal speed, and ships that fail to change course at a given turning point near an obstacle.

5.6.2 Behavior of Ship Plates Subjected to Large Impact Loads. Most engineering structures are designed to use their capacity in the elastic deformation range. When considering this type of approach, the structure has exceeded its design capacity when it reaches a

failure due to buckling, yielding, fatigue, or cracking. When a very large impact load occurs such as in an accident, the deformations of the ship's plates are often far beyond the elastic deformation range. In severe situations, the plates of a ship's hull may be heavily dished, torn open, or even peeled away from supporting members.

The plastic response of structures plays an essential role in assessing the potential consequences that might result from accidental damage of a marine structure. The theory dealing with plastic behavior of structures was introduced in ship structural analysis in the 1960s. Since then, the plastic method of analysis has been employed in a wide range of applications. This theory has been widely accepted, and often predicts adequate estimates suitable for design purposes. Jones (1997) summarized the plastic deformation theory and its applications to many topics related to marine structures.

The 1990s saw remarkable advances of knowledge in behaviors of plates subjected to large impact loads as a result of the achievements in research on ship collision and grounding. Many new patterns of plastic behavior of steel plates have been identified. Many involve mechanisms of membrane stretching, local plastic bending, complex object geometry, rupture, cracking, and friction. These mechanics interact in differing ways, resulting in varying behaviors of ship plates.

Structural crashworthiness concepts and methodologies provide powerful tools to investigate these behaviors. To confront the difficulties in analysis, many new theoretical models have been added to the body of analytical models of the plastic behavior of structures, broadening the understanding of plastic deformation of plate structures. Some recent studies on the plastic behavior of steel plates relevant to collision and grounding are introduced following. Further details and many other behaviors can be found in Simonsen (1999) and Wang (2002).

5.6.2.1 Structural Crashworthiness Methodology. In the simplest sense, *structural crashworthiness* refers to the load-carrying capacity or energy absorption capacity of a structure during an impact. The structural crashworthiness methodology provides a means for developing analytical formulae that are physically realistic in describing the physics of the phenomenon. It generally captures major mechanisms using idealized models that are very straightforward. It is therefore possible to derive formulae that are simple in mathematical expression.

The basic theory is best presented by equation (321), which describes the equilibrium of a loaded plate (Wierzbicki & Thomas, 1993):

$$F_p V = \dot{E}_b + \dot{E}_m \quad (321)$$

where F_p is the plastic resistance force, V is the velocity of the load, \dot{E}_b is the rate of plastic bending work, and \dot{E}_m is the rate of membrane work. The work rates \dot{E}_b and

\dot{E}_m are defined by

$$\dot{E}_b = \int_S M_{\alpha\beta} \dot{\chi}_{\alpha\beta} dS + \sum M_0^i \dot{\phi}^i l^i \quad (322)$$

$$\dot{E}_m = \int_S N_{\alpha\beta} \dot{\epsilon}_{\alpha\beta} dS \quad (323)$$

where $\dot{\chi}_{\alpha\beta}$ and $\dot{\epsilon}_{\alpha\beta}$ are the curvature rate and the strain rate tensors, respectively; M_0 is the fully plastic bending moment for a unit width of plate; $M_{\alpha\beta}$ and $N_{\alpha\beta}$ are the corresponding bending moment and membrane force tensors, respectively; and S is the plastic deformation region.

The first term of equation (322) is the contribution from bending in the continuous plastic deformation field integrated over S . The second term of equation (322) is the contribution of the discontinuous field summed over a finite number of straight or curved line segments with length l^i , each of which is the so-called plastic hinge. If the plastic hinge is stationary, $\dot{\phi}$ is its rotation rate, but if it is a moving hinge, $\dot{\phi}$ is the discontinuity of the rotation rate.

For rigid-perfectly plastic material, equation (321) gives an approximate expression for the instantaneous force, F_p , if a velocity field can be constructed that is compatible with the kinematic boundary conditions and the strain rate field. The problem consists of choosing a suitable kinematic flow field that describes the major mechanisms in a damage process. If necessary, a minimization process should be performed with respect to some free parameters to arrive at the lowest resistance force. Other effects such as friction can be added into the final expression.

5.6.2.2 Tearing of Plate. Plate tearing is regarded as highly relevant to a bottom raking process, where a ship's bottom is torn open for as long as tens or even hundreds of meters in length. Similarly, the deck in a collision can be cut and torn by the striking bow. Plate tearing has recently been extensively investigated. Figure 143 is a photograph of a tested specimen from Paik (2001).

Plate tearing refers to a plate cut by a rigid wedge. As the wedge pushes into the plate, the plate buckles and bends out of plane. After reaching the plate's ultimate strength, the load decreases and there is no separation of material. Eventually, as the wedge pushes further material separates and the load picks up again. This marks the commencement of a tearing process. The plate is torn apart in front of the wedge tip in the transverse direction. Near the wedge tip, the plate develops a global deformation pattern, where the plate deforms out of the plane and separates at or close to the proximity of the wedge tip. The separated material then bends over, forming two curls or flaps. The wedge keeps pushing the curved plate flaps, which roll up in the wake of the wedge. The load keeps building up as the tearing proceeds. Under some circumstances, the plate may bend in the opposite direction and the curls reverse.



Fig. 143 Plate tearing of a tested specimen.

The tests demonstrated that there are three distinct mechanisms in plate tearing: membrane stretching in the region near the wedge tip, plastic bending of the separated material in the wake of the wedge, and friction between the wedge sides and the plate. Energy dissipation due to plastic bending and friction is straightforward to compute. On the other hand, the calculation of plastic membrane work near the crack tip can be based on either a fracture mechanics approach or a classical rigid-plastic approach.

Applying fracture mechanics to explain material separation, Wierzbicki and Thomas (1993) derived equation (324) for the tearing load:

$$F = \frac{1.67\sigma_o(\delta_t)^{0.2}t^{1.6}l^{0.4}}{(\cos\theta)^{0.8}} \left[(\tan\theta)^{0.4} + \frac{\mu}{(\tan\theta)^{0.6}} \right] \quad (324)$$

where F is the tearing load, σ_o is the flow stress, t is the plate thickness, l is the tearing length, δ_t is a crack opening displacement parameter, 2θ is the spreading angle of the wedge, and μ is the friction coefficient.

Applying the rigid-plastic approach is to assume the absence of fracture. This assumption matches the observation in many tests where there is no crack extending ahead of the wedge tip. Rupture occurs due to ductile failure. The formula based on this approach is (Ohtsubo & Wang 1995)

$$F = 1.51\sigma_o t^{1.5} l^{0.5} (\sin\theta)^{0.5} \left(1 + \frac{\mu}{\tan\theta} \right) \quad (325)$$

where F , σ_o , t , l , 2θ , and μ are defined in equation (324).

The local stretching area near the crack tip is not independent from the “far-field” deformation where there are two flaps. Geometrically, these two areas are related, and there is not a distinct separating line. In the two analytical models, the local membrane stretching zone

and the bending zone of the two flaps are linked through the instantaneous radius of the plastic hinges. Equations (324) and (325) were obtained by minimizing the tearing load with regard to this instantaneous radius, a technique commonly used. This leads to the conclusion that the membrane stretching and the plastic bending interact with each other to determine the behavior of the plate structure. Other analytical formulae are Zheng and Wierzbicki (1995), Simonsen (1999), and Zhang (2002). The research on plate tearing represents many advances in fundamental structural mechanics, which has established the basis for applying the structural crashworthiness methodology in marine impact problems.

Some empirical formulations derived from mechanical tests are also available. Generally, an empirical formula has the following form:

$$\frac{F}{\sigma_o t^2} = C \left(\frac{1}{t} \right)^n \quad (326)$$

where F , σ_o , l , and t are defined in equation (324), C and n are related to the actual tearing or crushing configuration, and the exponent n is in the range of 0.3 to 0.5. Examples are Lu and Calladine (1990) and Paik (1994). These empirical formulations are similar in mathematical expression to the analytical solutions (324) and (325).

Shown in Fig. 144 is a comparison of a tearing test (Simonsen 1999) with the analytical results from equations (324) and (325), as well as the empirical results of Lu and Calladine (1990) and Paik (1994). Though these formulae are derived using different methodologies, they compare very well with the test results. The research of plate tearing mechanisms represents advances in structural crashworthiness and has been the most investigated mechanisms since the early 1990s. Comparison studies are also found in Pedersen et al. (1993), Simonsen (1999), ISSC (1997, 2003), and Yamada (2006).

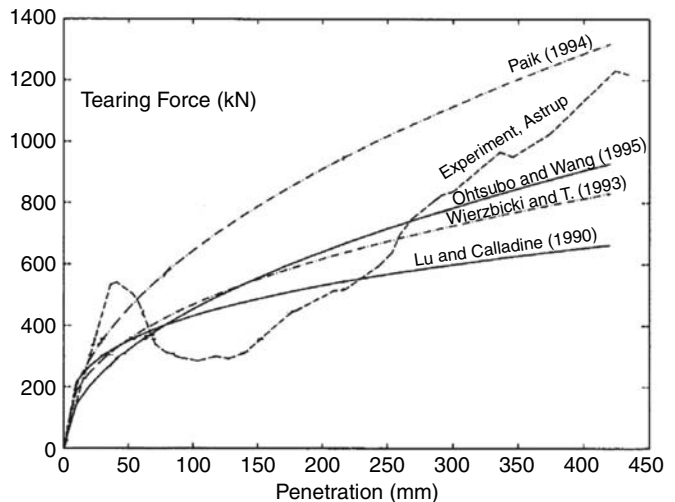


Fig. 144 Comparison of a tearing test with analytical and empirical formulations.

5.6.2.3 Concertina Tearing of Plate. When a stiffened plate panel is cut with a wedge, cracking of the plate may take place at the connection to stiffening members. Two cracking lines (instead of one) advance with the wedge, and there is no crack directly in front of the wedge tip. This process is termed *concertina tearing*. Concertina tearing damage has been found in the bottom of grounded ships.

The concertina tearing is similar to a crushing of plate in that structures are folded. Thus, applying the structural crashworthiness concept, the formula for the mean load of concertina tearing can be derived as shown in equation (327) (Wierzbicki 1995):

$$F_m = \frac{1}{\lambda}(3.25\sigma_o b^{0.33} t^{1.67} + 2Rt) \quad (327)$$

where F_m is the mean tearing load, σ_o is the flow stress, t is the plate thickness, b is the width of the folded plate, λ is the factor for effective crushing length, and R is the fracture parameter.

5.6.2.4 Local Denting of Plate. When decks and side stringers collide with a striking bow, compression takes place mostly in the plane of these structural members. It is likely the load does not spread much and is limited over a certain length, a situation very similar to the so-called patch loading on web girders. The compressed decks or side stringers develop some local mechanisms to accommodate the large deformation. In a bottom raking accident, the bottom shell behind a transverse structure behaves in a similar manner.

Figure 145 (Wang 2002) shows a crushing test on a web and flange combination. The web is used to simulate the behavior of a deck or side stringer in a collision, and the flange, the side shell. Evidently, the structure bends and forms some local folds. A plate subjected to patch load-

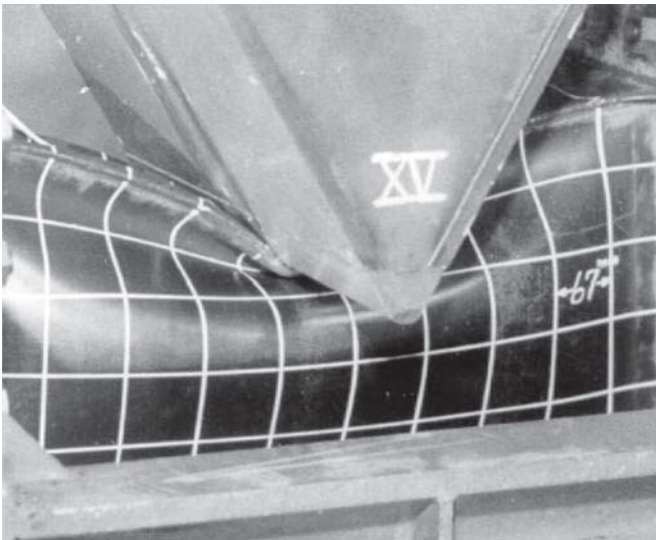


Fig. 145 Crushing a web flange combination (formation of local folds).

ing has been studied as one of the design issues for web girders. Attention has been given to the buckling or ultimate strength of web girders where the local deformation is similar in magnitude to the plate thickness.

Where the impact energy is very large, the web's buckling capacity can be exceeded. Out-of-plane deformation increases as compression proceeds, and loads also increase. This bulge will eventually evolve into structural folding. If the energy is still not spent, a new bulge will occur directly behind the fold, and it will develop in a process similar to that of the first fold. In many cases, two folds are formed prior to rupture and termination of the denting process.

The mean load for the first fold is of interest. In an analytical model, heavily deformed plate portions are separated from less or nondeformed portions by some plastic hinges. Areas bounded by plastic hinges are in a membrane stretching state. The plastic bending is assumed to be concentrated in the plastic hinges. The stretching and bending interact to determine the behavior of the plate. A formula that gives the mean load (Wang & Ohtsubo 1997) for this local denting mechanism is

$$F_m = \frac{2.32}{\lambda}\sigma_o b^{0.33} t^{1.67} \quad (328)$$

where F_m is the mean load of plate denting, b is the width of the deformed plate, t is the plate thickness, and λ is the factor for the effective crushing length, which is usually in the range of 2/3 to almost 1.0.

Simonsen and Ocakli (1999) developed a somewhat different model that is valid for the deformation up to the full compression of the first fold. The solution is derived for the general case when the compression can be at any point of the span.

5.6.2.5 Plate Punching. When impacted by a striking bow in a ship-to-ship collision, side plate tends to stretch in all possible directions to resist impact loads and, generally, attains very large permanent deformations after the accident. *Plate punching* is relevant to this behavior, which generally refers to a piece of plate that is acted upon by concentrated lateral loads. The bottom shell in a stranding is also loaded laterally and behaves in a very much similar way to the side shell in a collision.

When a plate starts to deform under the action of a lateral load, bending plays a major role for small deformations, generally the order of the plate thickness. With an increase in transverse deformation, the importance of bending and shearing diminishes and the membrane force quickly develops. At sufficiently large deformations, the membrane force dominates the behavior. This is known as a string response. Whether the plate is clamped or simply supported is not critical because the contribution from plastic bending is negligibly small when the deformation is large.

Plate punching has been intensively investigated. In classical structural mechanics, there are two basic load types: concentrated and distributed loads. Loads on a structure are generally modeled as either or a

combination of both. The plate considered is circular, square, or rectangular, and is simply supported or fixed at its boundaries. The loads may be concentrated at specific locations or distributed across the entire plate surface, or over part of the plate surface. Earlier work can be found in Onat and Haythornthwaite (1956), Zaid (1958), Reid and Reddy (1978), Christodoulides and Oliveira (1982), Jones (1989), Jones and Walters (1971), McKenny (1991), and Ohtsubo et al. (1995), to mention a few.

A ship's bow form has a surface that is very complicated and cannot be easily described by mathematical functions. Recent laboratory tests have demonstrated that the geometry of a striking ship has an influential effect on the impact behavior of the struck ship. Permanent deformations on the struck ship depend greatly on the size of the striking ship, or more precisely, the size and geometry of the striking bow.

The recent formulations for a plate punching problem take into account the geometry of the objects involved in the impact (Simonsen & Lauridsen 2000; Wang et al. 1998; Yu 1996). Shown in Fig. 146 (Wang 2002) are the load-deformations measured from the test of a circular plate of radius R punched by rigid spheres of radius r . Predictions using the recently developed analytical formulae are also included. The punching forces are normalized by the flow stress of material, plate thickness, and the radius of plate, R . Punching displacements are normalized by the radius of plate, R .

5.6.2.6 Ruptured Plates. The side shell in a collision and the bottom shell in a grounding can be pene-

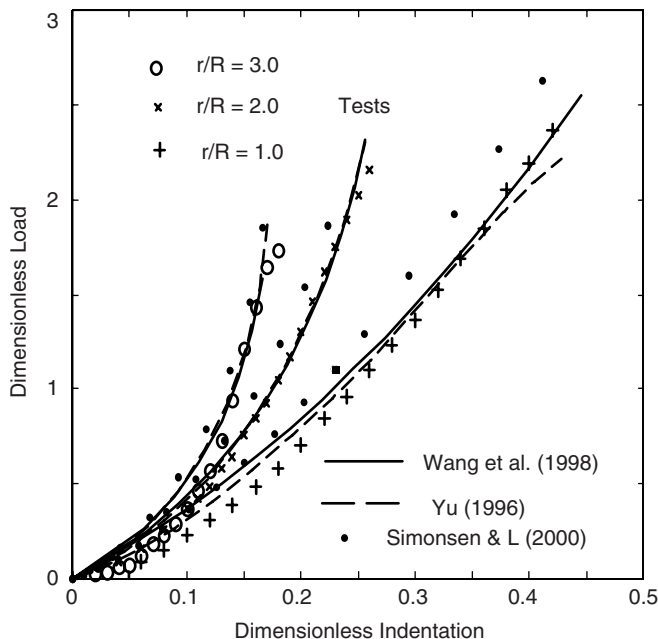


Fig. 146 Comparisons of analytical and measured load-deformation results for a circular plate punched by three rigid spheres.

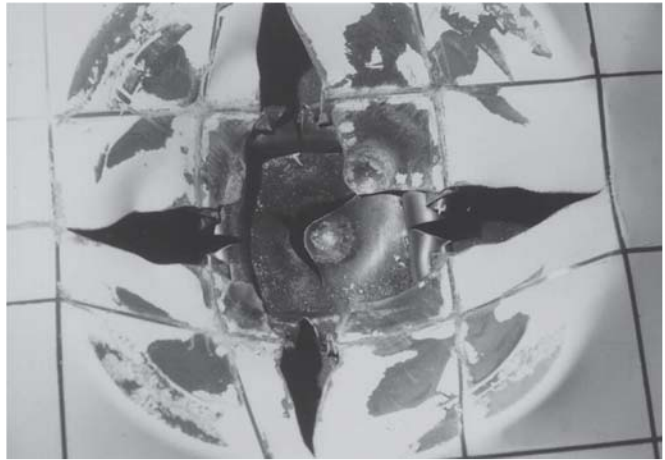


Fig. 147 A punctured plate—four cracks in a radial direction resulting from penetration by a cone with a spherical nose (Wang et al. 1992).

trated, ruptured, or separated from supporting structural members. Plate punching is only relevant before the occurrence of the rupture of the material. The plate will break, or *rupture*, when the strains in the plate arrive at a state beyond which the material separates, releasing the energy stored in the plate. A plate can no longer absorb impact loads beyond the strength of the material limits, or its ultimate load-carrying capacity. Once this happens, the plate behaves in a different way.

Traditionally, a ruptured plate has been treated as losing all capacity to carry a load. However, recent tests such as Kaminishi et al. (1992) and others show no instance when the load drops to zero, though a structure was penetrated and rupture took place. Figure 147 is a photo (Wang et al. 2000) of a tested plate specimen ruptured by a punching cone with a spherical nose. The punching cone first produced a circumferential neck in the plate, which then cracked. This crack did not propagate all the way around to detach a “cap” of material. Instead, the “cap” was left hinged to one side as the penetration proceeded. At a certain point, radial necking occurred, then it evolved into some radial cracks, which were then followed by subsequent fractures along the necked region. The strips that formed between cracks bent into curls, or petals. When the striking cone penetrated further, the petals were pushed sideways and bent to a larger extent. At the same time, the cracks advanced as the penetration proceeded.

Figure 148 is the measured load-displacement curves of a test on penetrating a circular, a square, and a rectangular plate using a cone with a spherical nose of 10-mm radius (Simonsen & Lauridsen 2000). Prediction using an analytical formula is also included (Wang 2002). Rupture took place at a displacement of about 0.03 m, as evidenced by a sharp decline in these curves. Following that, four cracks emerged and evolved with further penetration. The plate still carried the load at an almost constant level, which was about 40 percent of the

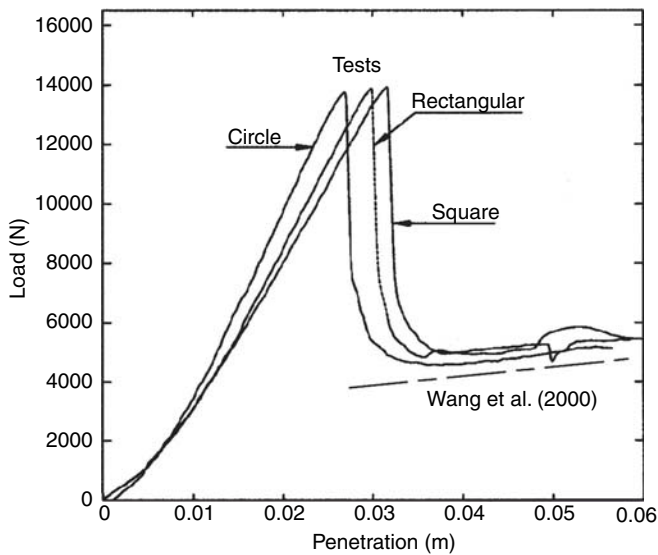


Fig. 148 Measured load-penetration curves for a circular, rectangular, and square plate penetrated by a cone with a spherical nose.

maximum load-carrying capacity of the plate. This indicates that in some cases, the load-carrying capacity of a punctured plate is comparable to its intact condition before rupture, and still maintains a significant portion of the load-carrying capacity after the plate is punctured. This is in contrast to the traditional assumption that the plate would not have strength once rupture takes place.

5.6.2.7 Axial Crushing of Thin-Walled Structure. Axial crushing of bow structures plays a major role in energy absorption during a bow impact. The basic crushing behavior of a bow structure can be exemplified by a thin-walled structure under predominantly axial compressive loads. Figure 148 (Jones 1997) represents a typical history of the resulting load versus displacement curve. As the compressive load increases, the structure eventually reaches the ultimate strength, which is the first peak in Fig. 148. If the displacement continues to increase, the internal load decreases rapidly. During the unloading process, some parts of the structure may be bent or stretched. A lobe emerges, and folding of walls starts. As the deformation continues, walls come in contact with each other, which ends the first fold and initiates a new fold. The internal load increases until the adjacent walls buckle. The structure starts to fold in a similar manner to the previous one. This process repeats itself until the entire structure is completely crushed. The complete folded structure then behaves as a rigid body. Each pair of peaks and troughs in Fig. 149 is associated with formation of one structural fold.

Figure 150 (Paik 2001) is a photo showing a crushed tube after cutting off half of the structure. It is apparent that many folds are formed during the crushing process. Forming of these folds results in large axial compressive displacements. Usually, the folds develop sequen-

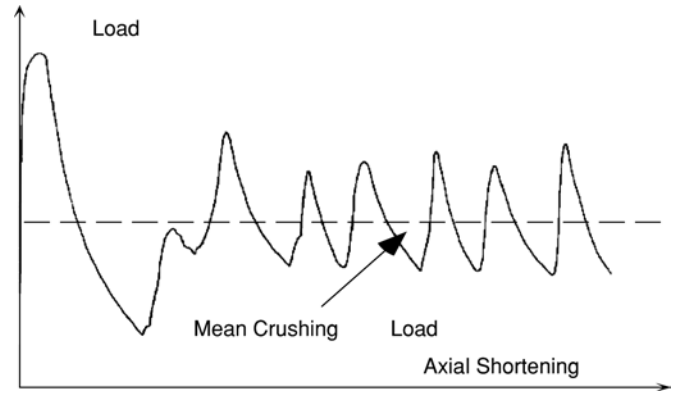


Fig. 149 Crushing response of a thin-walled structure under predominantly compressive loads.

tially from one end of the tube so that the phenomenon is known as progressive crushing. The concept of structural crushing is the basis for a ship's bow to be designed crushable to achieve high energy absorption capacity in a collision accident.

In a usual loading condition where the deformation is relatively small, the primary concern is the ultimate strength of the structure, or the initial peak load in Fig. 148. However, in an accidental loading condition the energy absorption capability is the more likely concern. The peak load of the structure is not always of primary interest, and the analysis of the detailed crushing behavior is not an easy task.

A convenient measure of the energy absorption is the "mean crushing load," which is the mean value of fluctuating loads as shown in Fig. 148. With this mean crushing load and the crushing displacement known, the absorbed energy can be calculated by multiplying these two values, which approximately equal the area below the corresponding load-displacement curve.



Fig. 150 A crushed tub under axial compressive load (forming of many folds) (Paik 2001).

The analytical approach to calculate the crushing strength is typically based on introducing rigid-plastic collapse mechanisms into the basic structural unit. In most of the research, an intersecting unit modeling technique is employed (Amdahl 1983; Ohtsubo & Suzuki 1994; Pedersen et al. 1993; Wierzbicki 1983; Wierzbicki & Abramowicz 1983; Yang & Caldwell 1988). This technique models a structure as an assembly of typical intersecting units. The intersecting unit method allows for a number of possible crushing mechanisms. The structure assumes the mode that gives the lowest crushing strength. Some researchers treat a bulbous bow of a ship as a cylindrical shell (Lehmann & Yu 1995), or model a bow section as a collection of individual plate units (Paik & Pedersen 1995).

The mean crushing load is generally expressed as shown in equation (329):

$$F_m = \alpha_m \sigma_o A \quad (329)$$

where F_m is the mean crushing load, σ_o is the flow stress, A is the cross-sectional area of the structure, and α_m is the energy absorption factor. In the interaction unit method, the energy absorption factor depends on the intersection of plates in which the crushing mode gives the lowest energy absorption. The flow stress σ_o is often defined as the average of the yield stress and the ultimate tensile stress of the material. For the cases when the dynamic effects are prominent, the increased yield stress can be taken into account using the concept of Cowper and Symonds (1957) and test data such as Paik et al. (1999).

5.6.3 Progressive Structural Damage in Collision and Grounding. Ship structures are inherently redundant. In the event of an accident such as collision or grounding, a ship's structure is damaged in a progressive manner. It does not fall apart once impacted, which avoids accelerated disintegration of hull and loss of the entire ship. Damage to a ship's hull is usually concentrated in localized areas. Even in the event of bottom raking, when gashes in the bottom may run more than half the ship's length, permanently deformed structures do not spread widely; they are often in the proximity of the gashes and are localized near the protruding seabed rock.

Ship collisions are normally classified into side collisions and head-on collisions. A *side collision* refers to a situation in which a ship's side is collided by the bow of another ship. A side collision may also refer to the case when a ship collides sideways into a quay in a harbor. The initial kinetic energy is partly or entirely consumed by damage to the side structure of the struck ship and the bow structure of the striking ship. A *head-on collision* typically refers to a situation in which the bow of a vessel collides with rigid stationary obstacles such as a bridge pier or gravity-based offshore platform. Most of the initial kinetic energy is absorbed by damage to the bow structure of the colliding vessel.

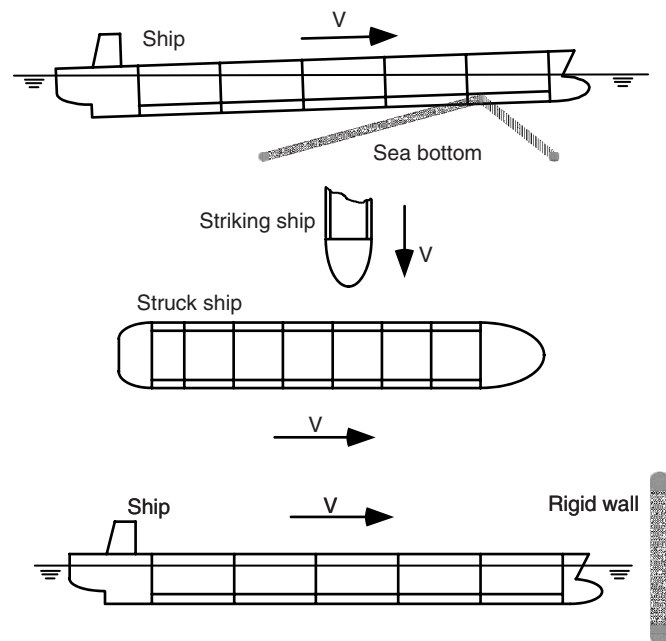


Fig. 151 Collision and grounding of ships.

Ship grounding refers to the cases when a ship runs onto protruding rocks for a distance before it is stopped (raking), or slides on the sea floor (grounding on a sloping sea floor), or rests upon a seabed (stranding). In a raking, the ship's bottom is penetrated, scratched, torn, or crushed. When a ship grounds on a sloping sea floor, the bottom shell may not be penetrated but the hull girder loads increase because of the direct contact with the sea floor and loss of buoyancy. A stranded ship suffers from the substantial vertical loads from the sea floor, which can become worse in a receding tide. In shallow water, a ship can squat, resulting in damage to the bottom shell. Figure 151 shows schematically the various accident scenarios under consideration.

5.6.3.1 Side Collision. The behavior of a ship side in a collision is similar to that of a bottom in a stranding condition. The progressive damage process of the side structures follows the possible sequences of failure of major structural members, including shell plating and main supporting members. Longitudinals and stiffeners likely deform with the plates to which they are attached.

As a demonstration of the progressive damage process in a side collision, the test W-50 results of Wang et al. (2000) are presented in Fig. 152, where the measured and the predicted load-indentation curves are shown. In the tests, a rigid cone with spherical nose of 50-mm radius was used to penetrate a double hull. Initially, the indenter was pointed at the location of a web girder. The load increased rapidly until buckling occurred—point (a)—in the compressed web plate. The increase in loads slightly decreased, and then quickly increased again because of the substantial buildup of the membrane stress in the

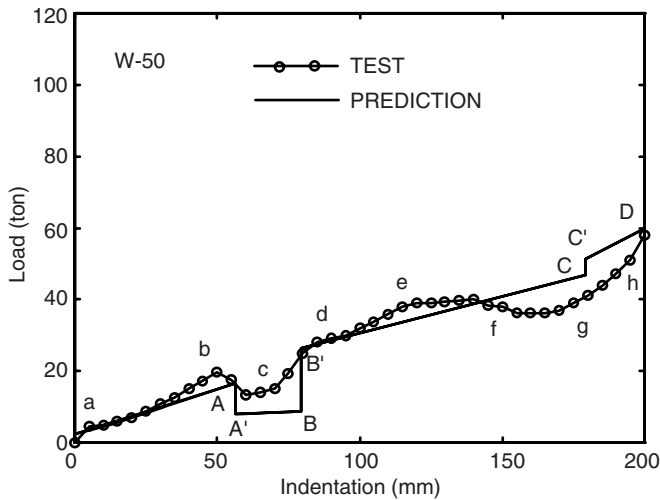


Fig. 152 Progressive damage sequences of a test on a double hull in a side collision.

outer skin. At point (b), rupture occurred in the outer skin. Energy accumulated in the outer skin released, and the load started to decrease. Rupture initiated in the circumferential direction, then evolved in a radial direction. The outer skin lost a portion but not all of its load-carrying capacity. When the cone contacted the first set of intersections of web girders, the load increased again. At point (b), buckling occurred in the first set of intersections of web girders, followed by continuous crushing of these intersections of plates. With the deformation zone of the outer skin extended, the cracks in the outer skin advanced with the compression. The load first increased slowly then decreased slightly, though the main trend was load increase. When the second set of intersections of web girders was contacted, the load started to increase again, and the deformation zone of the outer skin extended further.

The progressive damage process varies if the penetration location changes or the structure designs are different. As evidenced in the test shown in Fig. 151, many factors such as geometry and rupture play a role, and the combined effects determine the behavior of the ship structures.

5.6.3.2 Head-On Collision. Extensive experimental studies and many accident data show that the bow structures are heavily crushed and deform in a manner very close to the axial crushing mode of thin-walled structures. A bow normally deforms from the fore end. Many folds form between the transverse frames, and this formation progressively moves aft with increasing intensity of the collision. Related studies are Amdahl (1983), Yang and Caldwell (1988), Pedersen et al. (1993), Ohtsubo and Suzuki (1994), Paik and Pedersen (1995), and Wang and Ohtsubo (1999).

5.6.3.3 Bottom Raking. The resistance from the bottom structure during bottom raking is exemplified in Fig. 153 (from Wang et al. 1997). When a rock on the

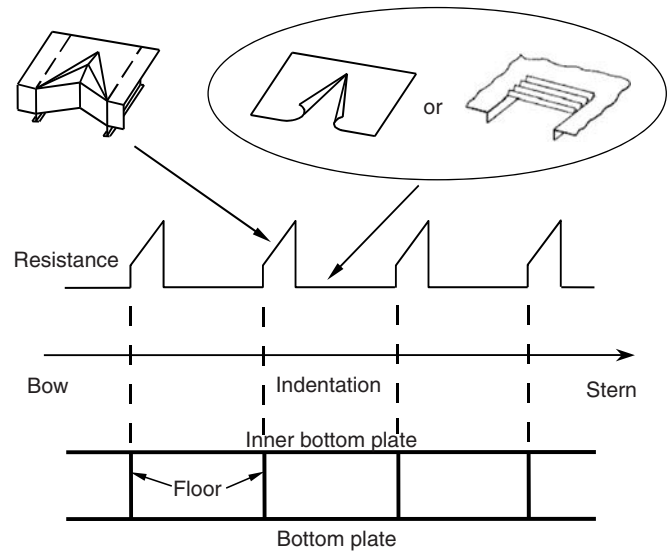


Fig. 153 A progressive bottom damage in a raking accident (Wang et al. 1997).

seabed makes contact with a transverse structure such as floors, that structure and the bottom plating immediately behind it interact and can show a very complicated deformation pattern. The transverse frame in such a case fails mainly by in-plane stretching. The bottom plate behind the transverse structure bulges and folds in front of the intruding rock. Usually, many folds are found in that part of the bottom plate. During this damage stage, the internal resistance force of the bottom increases as the rock penetration increases.

Eventually, as ductile rupture occurs in the overstretched plates, the resistance force reaches its ultimate value and then begins to decrease. This state of damage can then give way to a different damage process in which the contribution from the transverse structure becomes negligible. Only bottom plate and inner bottom plate may then provide resistance against the intruding rock. Usually, the resistance force drops to a low level. The bottom plate and the inner bottom plate may be torn open by the rock, and steel material within it separates at the part of the plate near the front of the rock. In the wake of the rock, the plate is subjected to loads mainly in the lateral direction. It then deflects out of its original plane to avert compression, forming two flaps.

A second possible type of damage is the wavy deformation pattern. The bottom plate in this case is peeled at its connection lines with the bottom longitudinal stiffeners or support members. The detached plate then folds in front of the rock. Now if the ship does not stop because it still has unspent kinetic energy, the next transverse structure will become involved in the raking process as well. This marks the end of one so-called structural resistance period and the beginning of a new period.

Works on structural damage in grounding also can be found in Little et al. (1996), Simonsen (1999), Tikka et al.

(2001), and Zhang (2002). The analysis methods of the progressive structural damage process can be categorized into four groups: simple empirical formulae, simplified analytical approach, simplified FEM, and nonlinear FEM simulation. Their advantages and disadvantages are summarized in ISSC (2007).

5.6.3.4 Empirical Approach. Empirical approaches generally calculate the energy absorption of a ship in an accident, and provide an easy and quick estimation of the global structural performance of ships. The most well-known empirical approach to collision analysis is the one developed by Minorsky (1959) based on 26 ship collision accidents, mainly between collided single hull vessel side structure and the colliding vessel's bow. Minorsky's method has been widely used for the design of ship structures against collision due to its simplicity, and is a very important approach for design analysis, as discussed by Chang et al. (1980). Minorsky's original formula is:

$$E = 414.5 \times R_T + 121,900 \quad (330)$$

which relates the absorbed energy, E , in tons-knots², to the destroyed material volume, R_T , in ft²-in. Assuming the damaged structural members are proportional to the member thickness, R_T can then be expressed in terms of certain parameters relating to the amount of damage sustained, and the member thickness involved. That is,

$$R_T = \sum_{N=1} P_N \times L_N \times t_N + \sum_{n=1} P_n \times L_n \times t_n \quad (331)$$

where P_N , L_N , and t_N are respectively the depth, length, and thickness of damage of the N -th member of the colliding vessel; P_n , L_n , and t_n are respectively the depth, length, and thickness of the n -th member of the collided vessel.

Minorsky's formula in equation (330) can be rewritten by changing the dimensional units for the parameters as

$$E = 47.2 \times R_T + 32.7 \quad (332)$$

where E is in MJ and R_T is in m³. Minorsky's formula has been modified by a number of investigators, for example, Woisin (1979), Reardon and Sprung (1996), Suzuki et al. (1999), Paik et al. (1999), Wang and Ohtsubo (1999), Pedersen and Zhang (2000), and Zhang (2002). New additions of simple formulae have incorporated the latest accomplishments from analytical and FEM simulation results, and are more suitable to be applied to modern designs of commercial ships.

5.6.3.5 Simplified Analytical Approach. A number of investigators have analyzed ship collisions or groundings by employing simplified analytical approaches, where closed-form solutions of resistance of the individual structural members (such as those in Section 5.6.2) are used. These closed-form solutions and the related theoretical models capture the main features of the damaged patterns of structural components that are observed from actual damages or small-scale experiments.

Reflecting more closely the behavior of ship structures in accidents, analyses using simplified analytical methods provide insights at both global and local levels. The progressive damage process can be modeled properly, and the load-deformation relationship can be derived. The extent of structural damage is determined by coupling the model of internal mechanics to the global dynamics (external mechanics) of the ships. Using a simplified analytical method, a design can be evaluated very quickly while still having reliable conclusions. Some methods only require hand calculations, an advantage when evaluating a number of design options.

Simplified analytical approaches have been applied to a wide range of accident situations, including ship-to-ship collisions, head-on collisions, raking of ship bottom structures, and stranding. Research in these areas can be found in Wierzbicki (1983), Amdahl (1983), Wierzbicki et al. (1993), Wang et al. (1997, 2000), Zhang (1999), Pedersen and Zhang (1998), Wang and Ohtsubo (1999), Simonsen (1999), Suzuki et al. (1999, 2000), Tikka (2001), Brown (2001), Urban et al. (1999), and Simonsen et al. (2004).

5.6.3.6 Simplified Finite Element Approach. The basic idea of a simplified finite element approach is to use a coarse mesh to model a complex structure. The simplified finite element approach relies on some special structural damage models for the behavior of plates in the large plastic deformation range, such as those in Section 5.6.2, and combines with the algorithm of conventional finite element approach. This group of approaches is between nonlinear finite element analyses and the simplified analytical methods in terms of the modeling effort and calculation time needed. The simplified FEM programs are not as complicated as nonlinear FEM simulations, and the costs of analyses are reasonable. Works in this area may be referred to Ito et al. (1992), Bockenhauer and Egge (1995), and Paik et al. (1999).

5.6.3.7 Nonlinear Finite Element Method. Application of nonlinear FEM simulation has been the main theme of recent studies. This trend was clearly demonstrated in the Second and Third International Conference on Collision and Grounding of Ships. There will be more FEM simulation applications due to the rapid advances in computer technology and software capacity. Several nonlinear FEM computer programs are available for analyzing collision and grounding. These include DYNA3D, DYTRAN, and PAM. These programs account for large deformation, contact, nonlinearity in material properties, and rupture. Some programs can analyze the coupled mechanics of both ship motion and structural responses. Nonlinear FEM simulations have been mostly used as a research tool, or as an effective alternative to large-scale tests that are prohibitively expensive.

In general, two FEM simulation methodologies are available: implicit and explicit algorithms. The implicit methodology uses the common approach to structural engineering problems (static or dynamic) where the actions are well-defined in space and time. The explicit

methodology requires solving a system of equations. Usually, the explicit methodology is more suitable for analyzing collisions and groundings. The required calculation efforts are less than the commonly used implicit methods. Convergence of calculations is also much easier to realize.

Because structures behave in very complex patterns, many special modeling techniques are needed. Challenges involved in this highly nonlinear problem include criteria for material's rupture, crack propagation, and proper mesh sizes, among others. Simulations of an accident are still not fully "transparent" to the industry at large.

Compared to application of FEM analysis for design purposes, simulations of an accident use very fine mesh. An FEM model for accident simulation of a tanker may have 720,000 elements, whereas the FEM model for the same tanker may have only 20,000 elements in a linear elastic analysis. Simulation of a one-second time period of an accident requires much greater computer time than a linear analysis for design purposes.

How fine the FEM mesh should be can be an issue. Too fine of a mesh will only increase the calculation time, whereas if not fine enough, some failure modes may not be captured and the calculated loads may differ from reality. Analytical formulations as those introduced in Section 5.6.3 can be used to guide the decision for mesh size.

Simulations using the nonlinear FEM can be found in Lenselink and Thung (1992), Amdahl et al. (1995), Kitamura (1996, 1998, 2001), Kuroiwa (1995, 1996), Glykas et al. (2001), and Lehmann et al. (2001), Wu et al. (2004), Endo et al. (2004), Jiang and Gu (2004), Tornqvist (2003), Kajaste-Rudnitski et al. (2005), Lehmann and Biehl (2004), Klanac et al. (2005), Ozguc et al. (2005), Alsos and Amdahl (2005), and Yamada et al. (2005).

5.6.3.8 Grounding onto Sloping Sea Floor. The reaction loads from the sea floor lift the ship but may not penetrate the bottom shell. Consequently, the ship loses buoyancy gradually, and the hull girder bending moments and shear loads increase. Under certain circumstances, the increase of hull girder loads are substantial, and may cause progressive collapse of the hull girder.

5.6.4 Mechanics and Analysis Methods. A collision or grounding accident is characterized by a kinetic energy, governed by the mass of the ships, the added mass effects of the surrounding water, and the speed of the ships at the instant of the accident. Immediately after the occurrence of an accident, a part of the kinetic energy may remain as kinetic energy after the accident, with the remaining energy being dissipated as strain energy in the damaged structures. Damage can be large structural deformations and penetration of hulls.

Ship collision and grounding can be described by the principle of energy conservation: the total loss in the kinetic energy at the end of the accident equals the total strain energy dissipated by the damaged structures. An analysis of a collision or grounding accident can be cat-

egorized into external and internal mechanics. The former deals with the rigid body motion of the ships with account for the added mass effect of the surrounding water. The latter deals with analyzing the structural responses and the resulting damages to the ships involved in an accident. These two mechanics are in most cases treated independently.

5.6.4.1 External Mechanics. The external accident mechanics of a ship-to-ship collision or head-on collision deals with the movements of the ships involved before and after collision. In this part, an estimate is made of the lost kinetic energy, which will have to be absorbed by plastic damage to the structures of the ships involved.

The external forces acting on the ships during collision are the results of propeller, rudder, wave, current, and hydrodynamics in addition to the collision forces arising from the deformation of the material. The hydrodynamic and collision forces usually dominate all others. In the case of ship grounding, the analysis of external accident mechanics involves the motion of the ship and the ground reaction forces. The hydrodynamic forces acting on the ship during grounding varies with the water depth and the change in draft. The ground reactions are difficult to determine, and depend on the combined action of soil deformation in the case of grounding on a sloping sea floor and the local structural crushing of the ship. The deformation of the soil of a sand or clay bottom depends on pore water pressure as well as the rupture of the soil skeleton. Works on the external accident mechanics may be referred to in Petersen and Pedersen (1981), Rawson et al. (1998), Pedersen and Zhang (1998), Paik et al. (1999), and Brown et al. (2000).

5.6.4.2 Internal Mechanics. The internal accident mechanics deals with the energy dissipation in damaged ship structures. This is usually governed by buckling, yielding, tearing, and rupture. Estimation of the energy dissipation can be obtained from well-designed tests, empirical formulae based on statistical investigations of previous accidents, or from analyses using calculation methods of varying complexities. Analytical and numerical approaches have been more often used as powerful tools for predicting the load-deformation relationships, based on which the energy dissipation can be calculated. Work in this area can be found in Wierzbicki et al. (1993), Little et al. (1996), Simonsen (1999), Paik et al. (1999), and Wang et al. (2000). Section 5.6.3 introduced representative publications of internal mechanics research. Surveys of available tools for analyzing internal mechanics can be found in Pedersen (1995), Daidola (1995), Ohtsubo et al. (1997), Wang et al. (2001), and ISSC (1994, 1997, 2003, 2006).

5.6.4.3 Experiments. A number of experiments related to ship collisions and grounding have been carried out. Most of the tests were performed for structural components, such as those cited in Section 5.6.2. Full-scale collision tests and large-scale grounding tests have also been carried out. These tests were to better correlate test results with real cases of accident by minimizing the

scaling effects. In 1991 and 1997, two series of full-scale ship collision experiments were carried out at Hollands Diep near Rotterdam (Kitamura 1998; Vredeveldt & Wevers 1992) using two inland waterway tankers of approximately 80 m in length. In 1994, a series of four large-scale grounding experiments were performed using a scrap-bound waterway tanker and a submersible pontoon. The tested section of about 7 m × 5 m × 0.8 m was fitted in the tanker's bow, which ran into an artificial rock fitted in a rock support structure on the submerged pontoon (Vredeveldt & Wevers 1995).

The Carderock Division of the Naval Surface Warfare Center (NSWCCD) also carried out grounding tests using one-fifth scaled models of a conventionally framed and several variants of the advanced (unidirectional) double hull tanker designs (Rodd 1996). Mounted on twin railroad flatcars, the test sections ran down an inclined set of rails and hit an instrumented rounded steel cone that served as a grounding rock. The focus of the NSWCCD tests is to determine the structural failure mechanisms that lead to the rupture of the inner hull, and to compare the energy dissipation characteristics of several designs.

Being able to predict the grounding on sloping sea floor, the Great Belt Link company conducted a series of large-scale tests in 1993 in Denmark (Sterndorff & Pedersen 1996). A condemned fishing vessel was sailed to run aground on selected beaches at selected impact velocity. Measurements were taken for surge, heave, and pitch accelerations, deformations of the beach and the ship bow, and forces arising from the interaction between the ship bow and the soil.

5.6.4.4 Rupture Criteria. It is most challenging to model rupture and tearing when applying the structural crashworthiness concept or performing nonlinear FEM simulation (ISSC 2006). The structural crashworthiness concept also forms crucial background for the important criteria of crashworthy ships. Advanced FEM packages enable reliable automated simulation of the structural failure process up to when fracture occurs, beyond which software aids such as a user-defined subroutine are needed for tracing the initiation and propagation of cracks.

Traditionally, it is assumed that rupture occurs when the equivalent plastic strain in an analyzed structure reaches a critical value. This critical value, sometimes referred to as *rupture strain*, is related to the strain-stress curves obtained from mechanical tests of uni-axially stretched metal coupons. In the simplified analytical approaches, the rupture strain varies from 1 percent to 20 percent, and the determination is normally based on calibration or judgment. One research focus was defining rupture strain for FEM analyses (Alsos & Amdahl 2005; ISSC 2003; Karr et al. 2007; Kitamura et al. 1998; Lehmann & Biehl 2004; Törnqvist 2003; Yamada et al. 2005). This critical value is found to be dependent on mesh size.

There are also studies of developing more refined models. Urban (2003) and Törnqvist (2003) reported estimations of critical equivalent plastic strain as a function of

the stress tri-axiality using model tests and FEM analyses. Several simple failure criteria and damage models were implemented in the explicit finite element code LS-DYNA. Törnqvist and Simonsen (2004) have shown that the so-called combined Rice-Tracey and Cockcroft-Latham (RTCL) criteria that account for the tri-axial nature of the fracture provide a good comparison to test results for different materials and various stress/strain states. They tested varying stress and strain states for validating these fracture criteria and damage models.

5.6.5 Predictions of Collision Damage. For the purposes of evaluating collision or grounding, a designer needs to have information on possible accident scenarios, the movement of the ships, the global energy absorption capability, the behavior of local structural members, and acceptance criteria. Analyses of the behavior of a ship once a scenario is given are summarized following.

5.6.5.1 Procedure. A potential design procedure for residual strength of collision and grounding is proposed by Amdahl et al. (1995), as shown in Fig. 154. The starting point is identifying the structural designs, tank arrangements, loading condition (draft, trim, total mass, and so on) and ship speed. For the striking ship, the geometry and structural design of the striking bow are very important. For the struck ship, the collision angle and location should be defined properly. The rigid body motion is primarily governed by motion in the horizontal plane. Other motions can generally be neglected. Procedures for detailed motion analysis or closed-form solutions can be developed. Penetration of hull of struck ship and progressive crushing of striking bow can be calculated using many approaches introduced previously. The design can be evaluated judging the structural performance in a collision, oil outflow performance following an accident, and hull girder integrity of the damaged hull.

5.6.5.2 External Mechanics Analysis. To illustrate the analysis procedure of external collision mechanics, we consider a simple classical case of the colliding ship with a speed of V_1 and the collided ship with a speed of V_2 . The relative motion between the vessels in the sailing direction of the struck vessel is assumed to be zero. At the end of the collision, the common velocity of the two vessels is V in the direction perpendicular to the sailing direction of the struck vessel. The collision angle between the two ships is assumed unchanged during the collision (i.e., the collided vessel does not rotate). This assumption is strictly correct only in a nearly central right-angle collision situation. For such a situation, the total loss of kinetic energy during collision of the two vessels in a free-floating condition can be obtained from momentum equilibrium as follows:

$$\Delta E = \frac{1}{2} \frac{(1 + C_{a1})(1 + C_{a2})m_1m_2}{(1 + C_{a1})m_1 + (1 + C_{a2})m_2} (V_r)^2 \quad (333)$$

where m_1 and m_2 are respectively the masses, and C_{a1} and C_{a2} are respectively the added masses of the colliding and collided vessels. V_r is the relative velocity

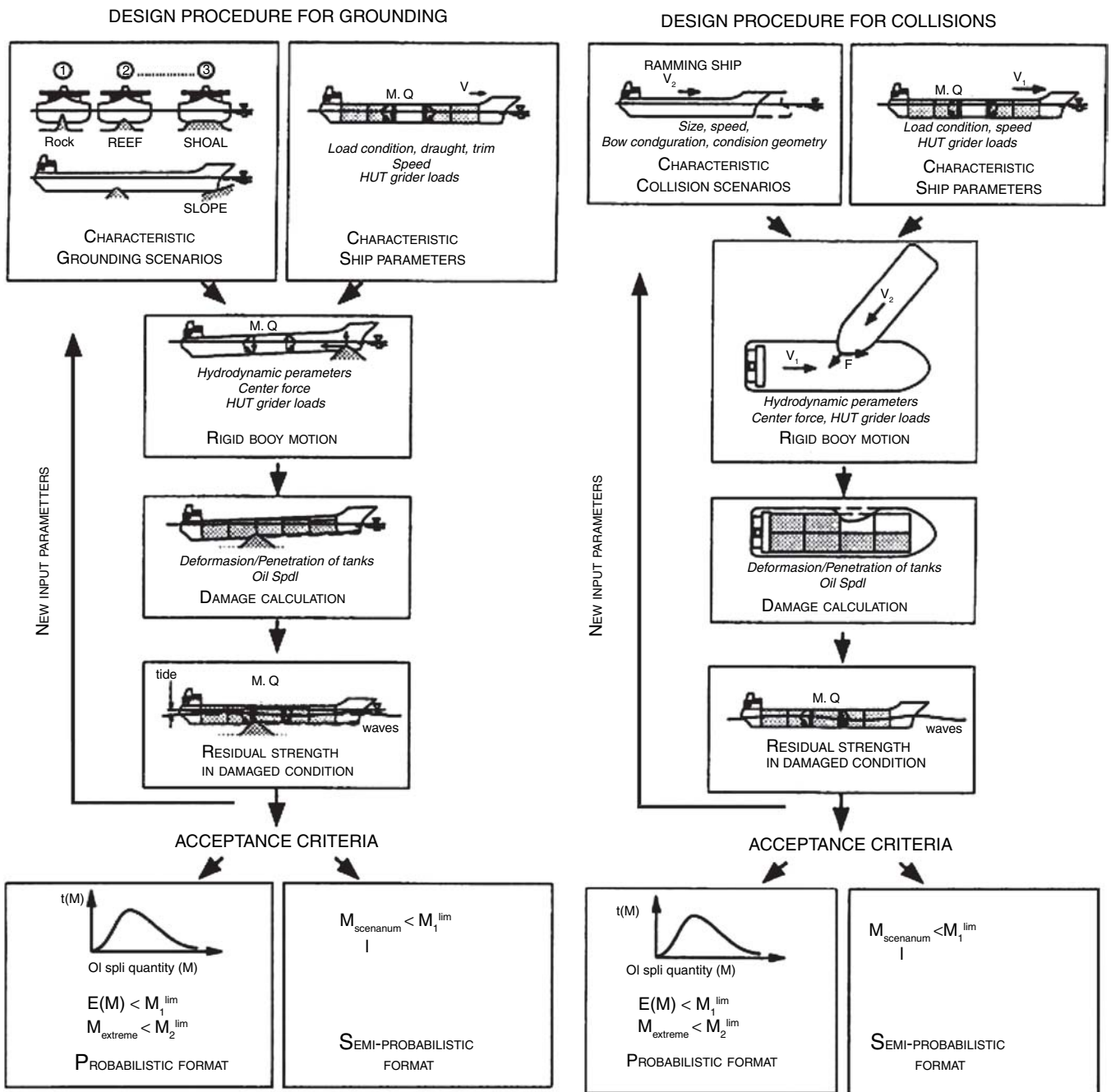


Fig. 154 Procedures for designing against collision and grounding (Amdahl et al. 1995).

between these two ships. Equation (333) illustrates that taking into account effects such as the energy absorbed by the deformation of fenders, can be computed by

taking into account effects such as the energy absorbed by the deformation of fenders, can be computed by

$$\Delta E = \frac{1}{2}(1 + C_{a1})m_1(V_1)^2 \tag{334}$$

When the collided vessel is at standstill (i.e., $V_2 = 0$ and $V_r = V_1$)—for example, at a pier—the mass of the collided vessel can be assumed to be infinite (i.e., $m_2 \rightarrow \infty$). In such a case, the loss of kinetic energy, without

where V_1 is the impact speed of the colliding vessel. For arbitrary ship-ship collisions, general equations governing the motions of the two ships have been

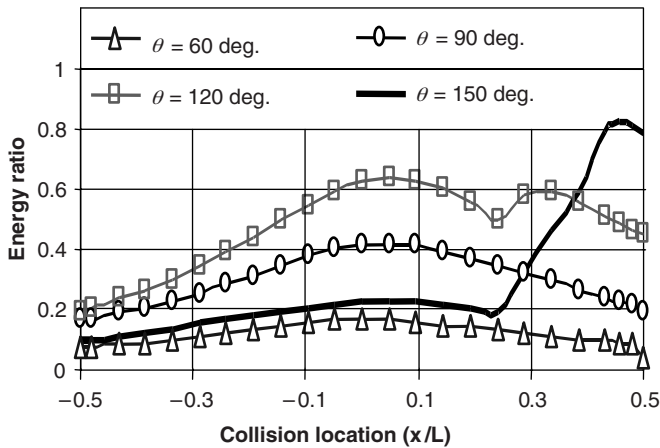


Fig. 155 Energy loss in a collision involving two identical ships, varying the collision angle θ and collision location (Pedersen and Zhang, 1998).

developed (Pedersen & Zhang 1998). The ships are assumed to have surge and sway motions, and the subsequent sliding and rebounding in the plane of the water surface are analyzed. The energy loss due to dissipation by structural deformations is expressed in closed-form expressions. The procedure is also based on rigid-body mechanics, where it is assumed that the contact region is local and small.

Figure 155 is one sample from Pedersen and Zhang (1998): the collision of two identical offshore supply vessels traveling at the same speed. The kinetic energy loss is normalized by the total initial kinetic energy at the instant of collision. The collision angle θ and the collision location are varied to investigate their effects. A 180° angle corresponds to a head-on collision. This figure reveals that the energy loss is large if the collision occurs at the fore part of the struck vessel. The collision angle has a strong effect on the kinetic energy loss. This figure also reveals that depending on the collision location, the energy loss in an accident would be different, which is maximized when the ship is hit near midship.

5.6.5.3 Internal Mechanics Analysis. The kinetic energy lost in the collision is dissipated as strain energy in the damaged structures. Both ships contribute to the energy dissipation, though under certain circumstances one ship's share is very small. The shared energy concept is schematically shown in Fig. 156 (Elinas & Valsgard 1985; Paik et al. 1999). In this figure, F_S and u_S are the reaction force and indentation of the collided side structure, respectively, and F_B and u_B are the reaction force and indentation of the colliding bow structure, respectively.

During the collision, reaction force between the struck and striking vessels must be in equilibrium, and equal to the collision force. Thus, the relation between u_S and u_B can be obtained from Fig. 156 by equating F_S to F_B , and the amount of structural damages can be calculated

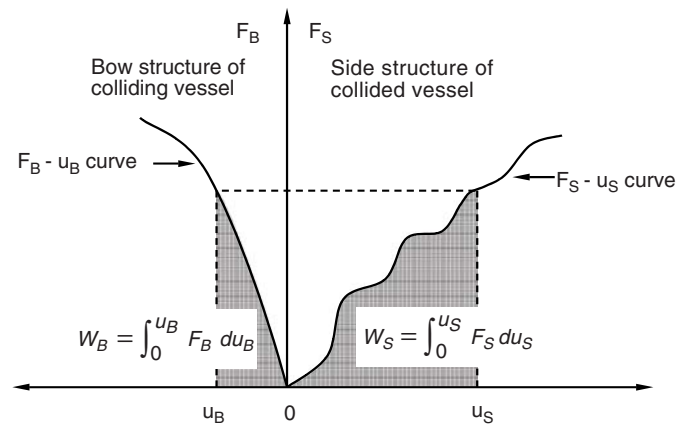


Fig. 156 Energy components absorbed by the colliding and collided vessel structures.

in such a way that the energy conservation is satisfied. That is,

$$\Delta E = W_S + W_B \quad (335)$$

where ΔE is the total kinetic energy loss, given in equation (333) for the simple example under consideration. W_S and W_B are respectively the strain energy dissipated by damage of the struck and striking vessel structures, calculated by integration of the areas below the corresponding reaction force versus indentation curves, as in the following equations:

$$W_S = \int_0^{u_S} F_S \cdot du \quad (336)$$

and

$$W_B = \int_0^{u_B} F_B \cdot du \quad (337)$$

Solving simultaneously both equations of (336) and (337) is very difficult and time-consuming. As a practical alternative, the internal mechanics problems for the striking and struck ships are handled separately (Paik et al. 1999). The strain energy dissipated in the struck ship is computed by assuming a rigid striking bow penetrating the struck ship, and the strain energy dissipated in the crushed bow is obtained by analyzing the problem of the bow striking a rigid vertical wall.

Because the damages of the struck side structure and the striking bow structure are interrelated, the force-indentation relationships of both the struck and the striking structures are better solved as parts of the solution of the collision process as a whole. When the force-indentation curves can be established in this manner, equations (336) and (337) are valid for the general cases. Numerical simulations using nonlinear FEM, such as Kuroiwa (1996), can be carried out for a collision or grounding accident using the explicit finite element computer program DYNA3D, together with a ship motion program. The contact force was first calculated by the

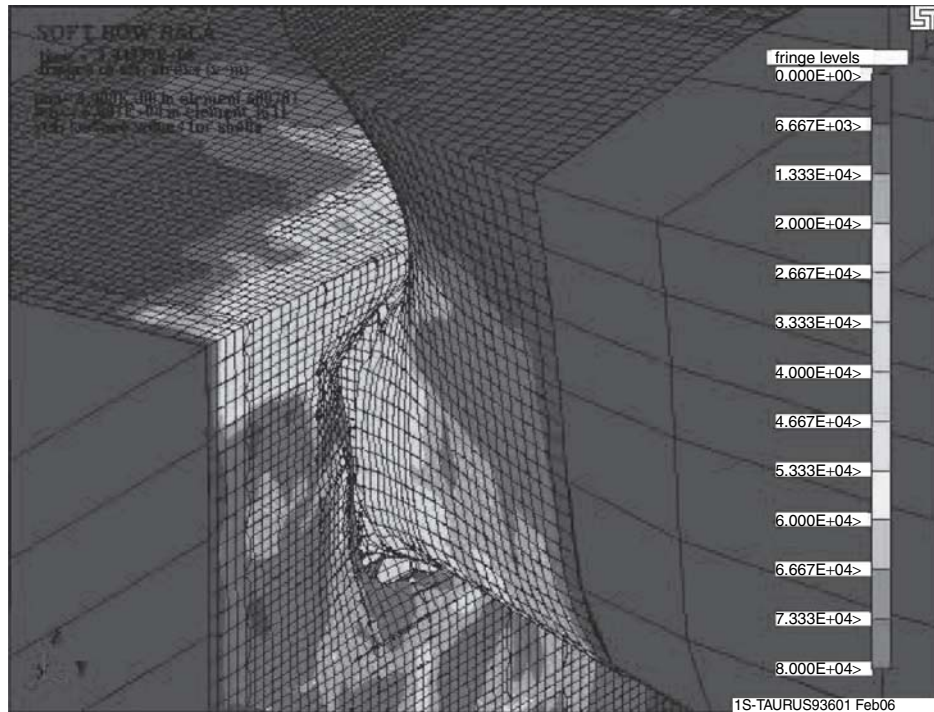


Fig. 157 Nonlinear finite element simulation of a collision between a VLCC and a Suezmax tanker (Kitamura et al. 1998).

finite element program for structural failure and passed to the ship motion program for determining the contact force induced ship motions (positions, velocities, and so on), which are in turn passed to the finite element program for structural failure. Then, deformation of structure and collision force in the new time step is calculated, and the routine continues. The damaged side structure of the struck vessel and the damaged bow structure of the striking vessel were modeled with finite elements, which can deform elastically and plastically and can simulate rupture of plate and failure of weld.

Figure 157 shows a simulation of a collision accident between a VLCC and a Suezmax tanker (Kitamura et al. 1998). Very fine meshes are used in the simulation, and the stress and strain distributions around the impact area are obtained to a very detailed level.

5.6.6 Predictions of Grounding Damage. Ship grounding has several patterns that need different approaches to analyze. Damage predictions of three ship grounding scenarios, namely, grounding on hard rock, or raking, and grounding on sloping sea floor, are briefly described following.

5.6.6.1 Procedure. A design procedure for the residual strength of ship grounding is illustrated in Fig. 154. The ship is first characterized by hull scantlings, tank arrangement, loading condition, and ship speed. The sea floor conditions at the site are the most important. The sea floor can be clay or sand bottom, or hard protruding rocks. At present, very little is known about the sea floor conditions for different waters. The ground-

ing scenarios have been based on experts' opinions to a large extent.

There is a tendency to focus on the worst-case scenarios, for example, a sea floor of very sharp rocks. In reality, this may be a small likelihood. A more common case is grounding on relatively flat seabed or blunt rocks. Recent experimental (Sterndorff & Pedersen 1996; Wang et al. 2000) and numerical (Amdahl et al. 1995; Pedersen 1996) studies have demonstrated that the shape of the sea floor has a significant influence on the behavior of a grounding ship. It is essential to have a set of accident scenarios covering both sharp rocks and shoals extending over the entire ship breadth (Wang et al. 2001).

For each grounding scenario, the ship's rigid body motion is analyzed. Normally, it is sufficient to consider motions in the vertical plane only (i.e., surge, heave, and pitch). The rigid body motion depends upon the ship's mass and hydrodynamic properties, generally influenced by shallow water effects. The resistance of the ship's bottom against the grounding is provided by the deformation of the ship's bottom, friction, potential tearing of bottom shell, and crushing of supporting members.

5.6.6.2 Grounding on Hard Rock (Raking). When a ship with a forward speed V runs on a rock pinnacle, the initial kinetic energy may be approximately estimated by

$$\Delta E = \frac{1}{2}(1 + C_a) \cdot m \cdot V^2 \quad (338)$$

where m is the mass of the grounded ship and C_a is the added mass coefficient accounting for the surrounding water effect. A relationship has been established between the vertical grounding reaction and the heave, surge, and pitch of the ship (Simonsen 1997). The motion of a grounding ship is based on the static equilibrium for the cases when the vertical inertia forces can be neglected.

The basic idea in dealing with the problem of ship grounding is to consider the process as a time series of events, where the ship is incremented forward. At each increment, the rock penetration, the ground reaction, and the heave, pitch, and surge motion corresponding to the static equilibrium of the ship are determined. As the ship is incremented forward, the work of the horizontal forces is tracked all long. When the work of the ground reaction plus the potential energy of the ship equals the initial kinetic energy, the ship has been brought to a stop. The structural resistance in grounding can be derived using various approaches discussed previously, assuming that the contact area between the hull and the rock is a point on the ship's bottom. However, there is more than one possible equilibrium path due to the fact that the structural resistance is not a continuous function of rock penetration, and thus complicates the analysis that is a coupled external and internal mechanics problems.

The Joint MIT-Industry Program on Tanker Safety (Little et al. 1996; Simonsen 1999) developed simplified models for analyzing a raking accident. The results from the studies were used to develop a computer program with a user-friendly interface. Many closed-form solutions have been included for analyzing the structural resistance. Heave, roll, and pitch motions of the ship are expressed based on static equilibrium. Surge motion is calculated based on energy balance. Sway and yaw motions are neglected. This program provides a tool for comparative studies that involve a large amount of calculations.

McGee et al. (1999) developed a damage prediction model for high-speed craft in association with the investigations for IMO HSC Code development. This model incorporates four grounding mechanisms in a manner similar to Wang et al. (1997), taking into account material properties, structural layout, grounding object geometry, and ship speed. Failure of transverse members was discussed, and the difference of aluminum and steel was demonstrated in McGee et al. (1999).

As in ship collision, structural damage of ship bottom raking can be analyzed using nonlinear FEM simulation, such as in Kuroiwa (1996), and simplified analytical and empirical approaches, such as in Wang et al. (1997), Simonsen (1999), and Pedersen and Zhang (2000). When approximation is made, the grounding bottom structure can be considered as an assembly of individual structure elements. The relationship of the grounding force versus damage is then obtained by appropriately summing up the grounding force versus raking length relationships of individual elements. The energy absorption capability of

individual elements can be calculated by integrating the area below each grounding force versus raking length curve, and the total strain energy of the damaged bottom structure is the summation of the energy absorption capabilities of all individual members. During the raking process, the raking damage will continue until the initial kinetic energy is consumed by the total strain energy.

5.6.6.3 Grounding on Sloping Sea Floor. Pedersen (1994) analyzed in detail the mechanics of grounds on relatively plane slopes, where the external dynamics—including the motion of the ship and the ground reaction forces—are described. As indicated, the hydrodynamic forces acting on the ship during grounding are affected by the water depth and the change in draft. The ground reactions are difficult to determine and depend on the combined action of soil deformation and the local structural crushing of the ship. In the case of sand or clay bottom, the deformation of the soil is governed by pore water pressure and rupture of the soil skeleton.

The event of grounding on sloping sea floor can be divided into two phases. The first, Phase I, is the initial impact against the slope. It involves an instant transfer of the kinetic energy into heave and pitch motions, as well as energy dissipation either due to plastic deformation of the bow or penetration of the bow into the seabed. The initial impulse is assumed to be completely inelastic, and leads to a rapid change of the ship's speed. In the second, Phase II, the ship bow will slide with decreasing velocity along a trajectory assumed parallel with the sloping bottom. In this phase, it is important to determine the ground reaction force as the ship moves up the slope. To find how far the ship bow will be lifted, the energy dissipation during the motion must be determined. When energy dissipation in Phases I and II are equal to the initial kinetic energy, the ship will stop.

Grounding forces in terms of sectional forces and longitudinal moments are determined and are compared to the ultimate strength of the hull girder. It is revealed that the longitudinal strength of ship hulls may not be adequate to withstand a severe grounding. The strength margin depends on ship size, loading state, the shape of the sloping sea floor, and friction.

Fig. 158 from Pedersen (1994) shows the computed kinetic energy after initial impact as a function of the ground slope for a 4,000 DWT general cargo vessel. It is seen from this figure that for slope angles less than about 0.10 rad, the loss of kinetic energy during the initial impact phase can be neglected, but for slope of about $\pi/4$, nearly all the kinetic energy is transferred in this phase.

How far the ship will proceed along the surface of the ground can be determined using an energy balance method. Assuming the ship structure is not severely damaged, this distance can be determined by balancing the kinetic energy of the ship before it strikes the ground with the energy lost in the initial impact, and the work performed by friction between the ship bottom and the ground plus the increase in potential energy from the initial free-floating position to the end of the grounding.

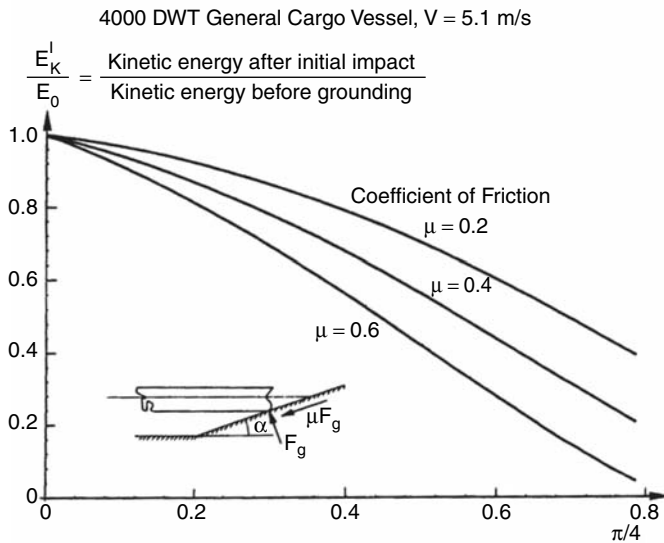


Fig. 158 Energy after initial impact as a function of a slope α for a 4,000 DWT general cargo vessel (Pedersen, 1994).

Figures 159 and 160 from this reference show the final resting position and the resulting longitudinal bending moment aground for a 4,000 DWT cargo vessel.

5.6.7 Residual Strength of Ships after Collision and Grounding. Collision and grounding accidents can very often lead to shell ruptures. Various aspects should be examined such as fatalities, cargo spills, damage stability, residual strength capability, increased load demands on the hull girder, and economic and social impacts. Indirect costs can be much higher than those strictly connected with the accident.

A ship may collapse after a collision or grounding because of inadequate longitudinal strength. It is important

to keep the residual strength of damaged structures at a certain level to avoid additional catastrophic consequences. It is also important to assess the damage stability before transferring cargo or towing the damaged vessels. Damage stability calculations do not present problems because of existing modern software. Many of the existing procedures for ultimate strength analysis of ships can also be modified to give estimates of the residual strength after the accident. Damage caused by collision and grounding can be in the form of structural parts that have been torn away, reduced material yield strength due to fire following the collision, and strength members with changed distribution of residual stresses and geometric imperfections.

Paik et al. (1996) and Wang et al. (2002) developed analytical procedures for the assessment of residual strength of damaged ships after collision and grounding. Both of these two studies evaluate the residual strength based on the ultimate bending strength and the section modulus. Paik et al. (1996) considered the collision and grounding levels specified in the ABS hull girder residual strength guides for tankers and bulk carriers (ABS 1995), and the residual strength was presented in terms of a residual strength index. The *residual strength index* is the ratio of the ultimate bending strength of the damaged ship divided by the extreme bending moment, or the residual section modulus divided by the required minimum section modulus. Wang et al. (2002) defined a vertical extent in a ship's side for a collision damage and a width in the bottom for a grounding damage. The residual strength was evaluated in terms of the ratios of section modulus and ultimate bending strength divided by the corresponding values at intact condition. It is noted that the ship length has little influence on the relations between the residual strength with damage extent, whereas different ship types show somewhat different correlation.

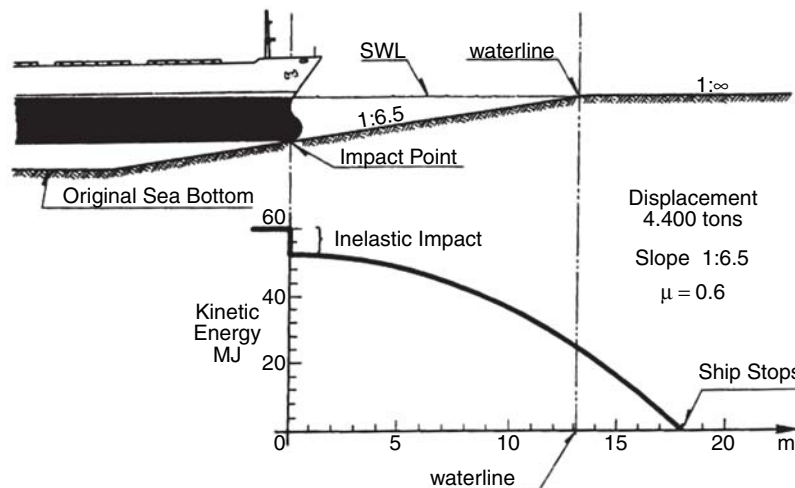


Fig. 159 Final resting position for a 4,000 DWT general cargo vessel (Pedersen, 1994).

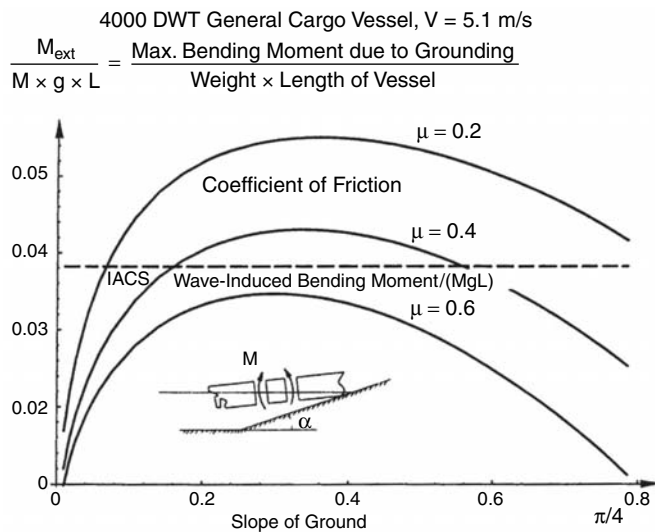


Fig. 160 Resulting longitudinal bending moment in grounding for a 4,000 DWT general cargo vessel (Pedersen, 1994).

Because the extent of damage is one of the critical parameters in determining the residual strength in designing ships, the key points of the ABS guide (1995) for assessing hull girder residual strength of tanker structures are summarized in the following. For bulk carriers, the corresponding guide is to be referenced.

The ABS guide considers tanker accidents due to grounding on a rocky sea floor with considerable rupture of the double bottom structures, and collision when another ship strikes the ship on one side, which results in extensive rupture of the side structure. The location and extent of the hypothetical damage are assumed to be the most unfavorable with regard to the residual strength of the damaged hull girder. Therefore, its location along the hull is assumed to be within the area of the maximum bending moment or maximum shear force. The length of the damage zone is assumed to be long enough to exclude all damaged structural members from participating in general hull girder bending.

The hypothetical transverse dimensions of the damaged zone are specified with due consideration of the MARPOL 73/78 regulations (IMO 2006) and available reports on vessel collisions and grounding. The depth of the damage zone, required by MARPOL for double bottom and double side structures of tankers, has been specified in accord with an acceptable probability-based risk of “non-failure” of the inner hull due to collision and grounding. Here “non-failure” is understood as the absence of extensive disintegration of the inner bottom or inner hull plating. Therefore, it is assumed in the ABS guide that the inner hull plating, even if damaged, is still fully capable of withstanding the hull girder bending, whereas the side shell plating is totally destroyed within the damaged zone and is to be excluded from the hull girder. Consequently, all longitudinal stiffeners attached

to the inner hull are assumed to be intact, whereas those attached to the destroyed shell plating are assumed to be destroyed as well, and thus excluded from the hull girder. The longitudinal girders (stringers) of the double bottom and double side structures are assumed to be damaged only partly, depending on their location within the damaged zone. The longitudinal stiffeners attached to the destroyed web plates of the longitudinal girders are also assumed destroyed.

The vertical extent of the damaged zone of a double side is assumed in the ABS guide to be $D/4$ (D is the depth of the vessel) or 4 m, whichever is greater. This is different from the MARPOL 73/78 (Regulations 22 and 23) where an unlimited vertical extent of damage is assumed for assessing hypothetical outflow and damaged zone stability. The horizontal width of the damaged zone of a double bottom is assumed in the ABS guide to be the same as that in MARPOL for tankers with the molded breadth ranging from 24 to 60 m. For smaller tankers with breadth less than 24 m, the damaged bottom width in the ABS guide is assumed to be 4 m versus the MARPOL regulation of $B/6$, where B is the breadth of the ship.

The ship grounding load criteria for assessing the residual strength are developed taking into account that all the grounding accidents occur only in shallow and often in restricted waters. For those cases, the wave-induced bending moment and shear forces experienced by the grounded vessel are significantly lower than those in open seas. The still water bending moment and shear force can also change due mainly to the flooding of the empty double bottom tanks after damage, and the supporting reactions of the ground. The combined effect to the still water bending moment can be approximately 10 percent decrease for sagging and 10 percent increase for hogging.

The hypothetical collision scenarios are much more variable than grounding in terms of locations and extent of the damage zone and the sea states. However, the available data on actual collision accidents reveal that relatively calm sea or moderate waves are more typical for collisions than storm conditions. As such, wave-induced bending moment less than that in open seas is considered for assessing the residual strength of damaged vessels. On the other hand, the effect of a collision on the still water bending moment and shear force can vary much more than that due to grounding. A number of factors ranging from details of collision scenarios to arrangement of tanks and loading conditions of the tanker in question can affect the changes in the still water bending moment and shear force. Detailed analysis of the still water loading for an actual accident is needed for a reasonably accurate estimation. Without calculations in detail, the ABS guide considers the still water loading the same as that in the intact condition.

5.6.8 Principles and Methodology of Collision and Grounding Design Standards. There are no generally accepted collision and grounding design standards. Although principles may be based on design objectives

(i.e., oil outflow standards or survivability standards), none are universally accepted (ISSC 2006; Wang & Pedersen 2007).

Essentially, the principles of collision and grounding design standards would be composed of the following elements:

- How and why accidents occur: navigation, accident scenarios, probability of occurrence of certain types of accidents
- What happens structurally when a collision, grounding, stranding, or allision occurs: structural mechanics in collisions and groundings
- What are the consequences of structural damage: property damages, environmental damages, and loss of life
- How can each of these points addressed: accident prevention, minimization of structural damage, mitigation of damage consequence, response to damage and loss of life.

The risks of collisions and groundings exist with ships. Traditionally, these risks are addressed in damage stability and compartment requirements. These rules and regulations are mostly prescriptive in nature, and often address individual events separately. Over the past decades, the structural engineering design community has increasingly applied limit state and risk assessment methodology.

In ship designs, four limit states are often considered: serviceability, ultimate, fatigue, and accidental limit states. The accidental limit state represents excessive structural damage due to accidents that affect the safety of a human being, the integrity of structures, and the environment.

The accident limit state designs may be based on safety (including security for some situations) and environmental objectives. There could be many combinations of these objectives, such as loss of life prevention, injury or loss prevention, property damage prevention or mitigation, and environmental pollution prevention or mitigation. Structural design criteria have been based on meeting these defined objectives. There may be many different methodologies for defining accident limit states, depending on the nature of the range of accident types, which create different loading scenarios. Accident types can range from explosive scenarios like fires, explosions, or blasts, to relatively lower loading rates such as low-speed groundings and collisions.

Traditionally, ship collisions and groundings have been regarded as most relevant to damage stability or cargo spill from damaged hulls. Recently, more attention has been given to a vessel's structural resistance to an accident. Similarly, there is more focus on the impact that structural designs have on the extent of resulting damage and the consequential loss of stability, oil outflow, and residual strength.

5.7 Cost Optimization and Economic Value Analysis. Making decisions between many competing objectives

subject to some degree of uncertainty requires special skill and the use of a decision-making model. Several decision-making models are available; the challenge is to choose one that best describes the problem at hand. Almost all decision models rely on two basic elements:

- Identification and quantification of the possible consequences associated with each alternative
- Assignment of preferences for each of the consequences.

The first element is usually investigated through probabilistic and reliability methods, which have been discussed previously.

The assignment of preferences for the various consequences of failure is not an easy task, and can depend on many variables. In many cases, the amount of information, experience, and data availability are limited. In addition, the assignment of preferences is often subjective and depends on time and place. For example, recent accidents may lower the tolerance to risk. Personal biases also play an important role in the assignment of preferences and may include societal and organizational biases.

From an economic point of view, the most practical decision model would minimize costs and maximize reliability (economic value analysis). The expected total life-cycle cost of the system, $E(C_i)$, is the sum of the initial costs, C_i , and the future costs. The future costs, C_f , are those costs associated with a failure in the system multiplied by the probability of that failure occurring, p_f , and an additional factor to account for the value of money over time, PVF :

$$E(C_i) = C_i + (C_f)(p_f)(PVF) \quad (339)$$

where

$$PVF = \frac{1 - [1 + (r - i)]^{-L}}{(r - i)}$$

PVF = present valuing function

r = net rate of return on investment (%)

i = inflation rate (%)

L = compounding period

= life of structure

The objective of cost analysis is to find the minimum expected total life cycle cost, $E(C_i)$. Figure 161 shows an example of a typical cost versus quality or risk curve. Note that not all curves will show a characteristic "hol-low" or minimum point within a range of practically attainable probabilities of failure. In such cases, the optimum cost is that associated with the lowest practical probability of failure, or the highest quality.

Use of a method based solely upon monetary costs can be quite problematic. Some consequences of failure, such as loss of human life, cannot be easily assigned a socially accepted dollar value. Other obvious

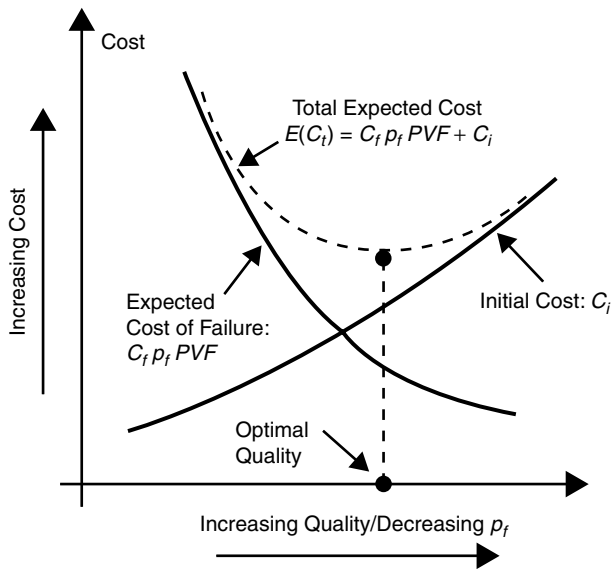


Fig. 161 Typical cost versus risk curve.

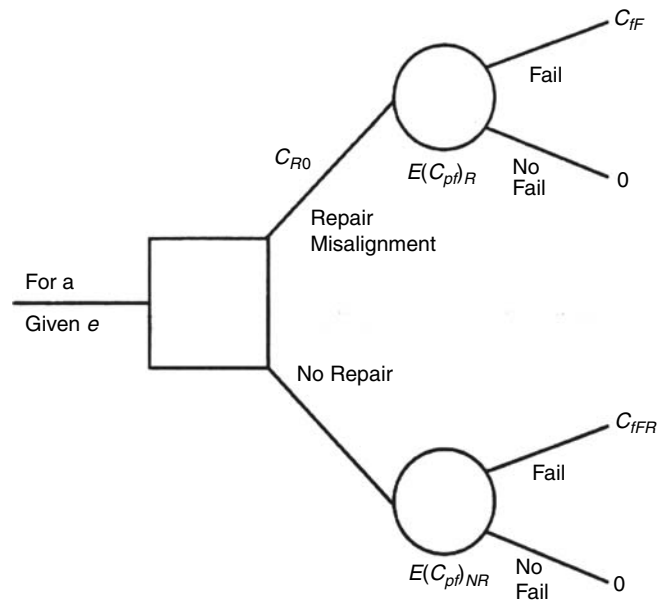


Fig. 162 Decision tree for repair/no repair decision to fix misalignment during construction.

consequences of failure that are difficult to quantify economically are damage to the environment and public reaction to an accident. One way to include intangible costs in the analysis without assigning a dollar value to them is through the use of utility theory.

Utility theory allows the engineer to assign preferences for consequences based on the input of impacted organizations and available data. Several steps are usually taken in the analysis using utility theory. First, the risk consequences are identified. This will require first identifying the decision makers within an organization, including those responsible for design decisions. These decision makers should have the foresight to predict what the future consequences of failure may be. Decision trees and analysis of previous accident data can be helpful in this regard. Some consequences of failure in a ship's system (the ship as a whole) include:

- Loss of ship through sinking, foundering, and so on
- Loss of human lives
- Loss of time available for service
- Damage to environment (e.g., oil spills)
- Damage to ship's structure and repairs of the structure
- Fires and adverse public reaction.

Formal reliability analysis and statistical data analysis can be used for estimating the probability of occurrence of any of these consequences.

Next, a utility function is constructed describing the organization's and society's tolerance to risk. The risk tolerance function can be one of three types: risk adverse, risk neutral, or risk tolerant. A percentage weight may be assigned to each of the consequence utility functions to reflect the decision maker's preference among

the failure consequences. Finally, evaluation of the alternatives is carried out to determine the best one. From a utility standpoint, the best alternative is the one that has the maximum expected utility.

Decision models can be also used to derive tolerances and misalignment requirements for ships. For example, when a misalignment is observed during construction, a repair/no repair decision must be made. The obvious tradeoff is that it will cost money to correct the misalignment versus a possible cost later when a failure is observed. The situation is illustrated in the decision tree of Fig. 162. As an example for an observed misalignment due to eccentricity, e , between abutting plates, two decisions are available:

Repair Misalignment. The total expected present cost for a structure that is repaired during construction is

$$E(C_P)_R = C_{R0} + E(C_{pf})_R \tag{340}$$

where C_{R0} is the present cost of repairing the misalignment during construction of the ship, and $E(C_{pf})_R$ is the expected cost of a failure during the life of the ship.

Do Not Repair the Misalignment. The total expected present cost for a structure that is not repaired during construction is

$$E(C_P)_{NR} = E(C_{pf})_{NR} \tag{341}$$

where $E(C_{pf})_{NR}$ is the expected present cost of failure associated with the eccentricity, e . Clearly, the higher value of e , the larger will be the expected cost of failure.

The maximum allowable tolerance is determined as follows. $E(C_P)_{NR}$ will increase as e increases. At some

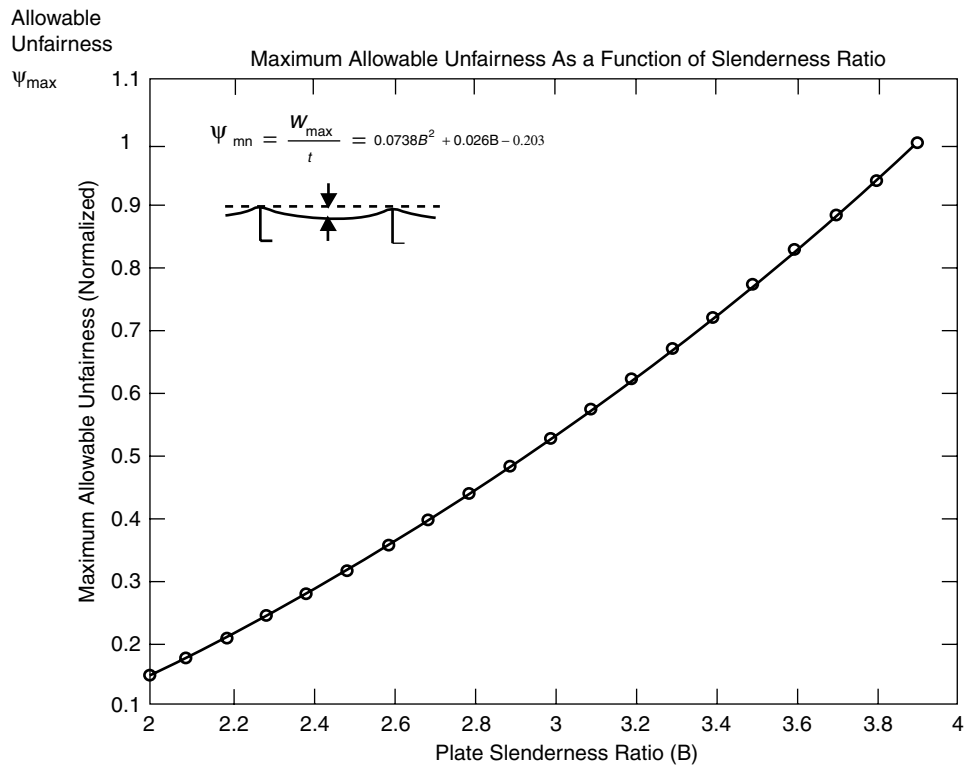


Fig. 163 Maximum allowable unfairness as a function of plate slenderness (Mansour et al. 1998).

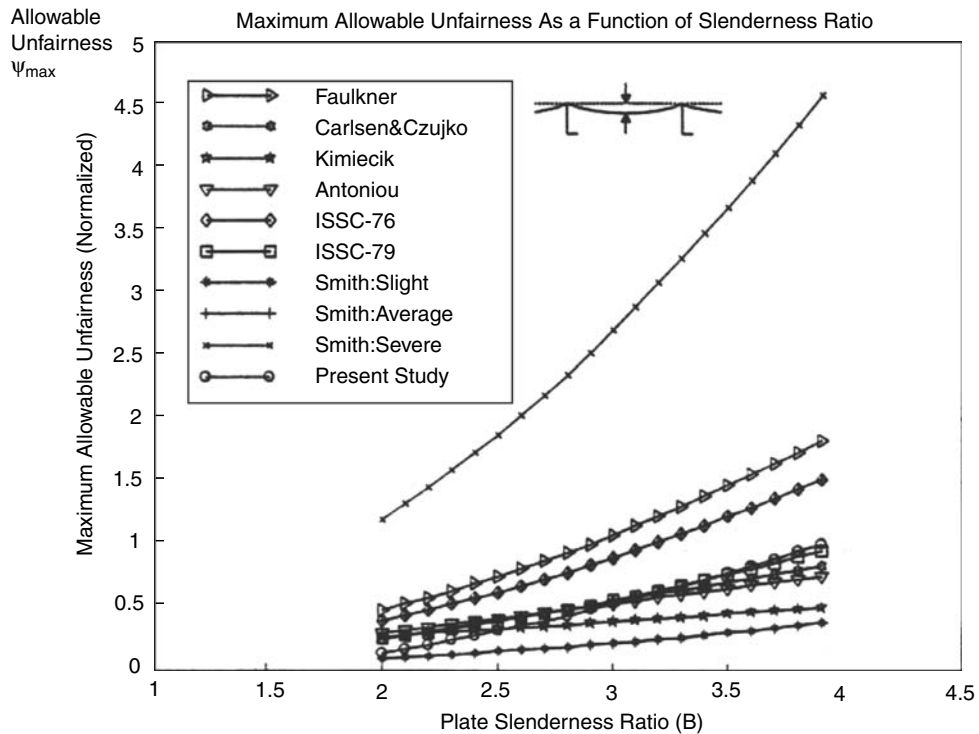


Fig. 164 Comparison between current development and existing formulas in the literature (Mansour et al. 1998).

value of e , say, \hat{e} , $E(C_P)_{NR} = E(C_P)_R$. For larger e , $E(C_P)_{NR} > E(C_P)_R$, and the best economic strategy would be to repair the misalignment. Thus, the maximum allowable misalignment tolerance can be identified.

5.8 Influence of Fabrication Imperfections on Strength and Reliability. Excessive fabrication and construction tolerances, together with welding distortions, may cause general degradation in structural strength, difficulties in assembly work of components and substructures, and poor hydrodynamic performance. On the other hand, stringent requirements for tolerances will lead to more costly ships. In many cases, it is not clear what the limit is on tolerances that satisfy both minimum cost and minimum acceptable reliability. Design guidelines are available that restrict the degree of distortion and inelastic deformations permitted in new construction. Most of these guidelines are based on tradition and have not been tested analytically or experimentally.

Aside from costs associated with failure of a component due to excessive tolerance and distortion, assembly costs during ship production can be prohibitive. Currently, effective ship construction practice is accomplished by building blocks and units that can be extensively outfitted with equipment in the safe environment of the fabrication shops before final erection of the ship-building berth. However, these advanced construction techniques have placed a new emphasis on dimensional accuracy of individual components and assemblies because rework is undesirable and extremely expensive in the block erection stage.

Selecting an optimal tolerance level is a problem of optimization under uncertainty. It is desired to minimize construction and life cycle costs of the ship. These are conflicting requirements. Lower construction costs dictate greater tolerance levels by reducing rejection margins. Higher performance during the service life of the ship mandates tighter tolerances. Hence, a balance between these two requirements must be attained. This balance is the basis of the economic value analysis and decision tree optimization procedures described in Section 5.7.

In a study supported by NAVSEA, Mansour et al. (1998) developed a procedure for determining the maximum allowable tolerances based on reliability principles, economic value analysis, and decision tree optimization (see Section 5.7). Several tolerances have been analyzed in the study including plate unfairness, stiffener unfairness, misalignment, plate thickness, material strength, and welded joints.

Based on the reliability and cost analysis conducted in the study, the recommended maximum tolerance limit on unstiffened plate unfairness is

$$\frac{W_{0\max}}{t} = 0.973B^2 + 0.026B - 0.203 \quad \text{for } 2.0 \leq B \leq 4.0 \quad (342)$$

where

$W_{0\max}$ = maximum unfairness (i.e., allowable tolerance)

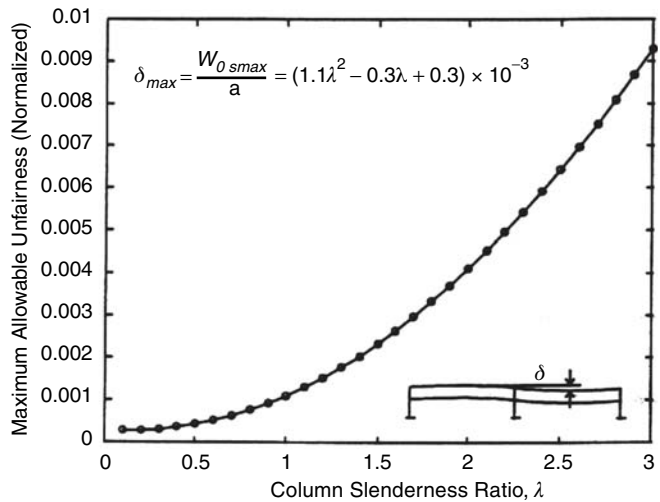


Fig. 165 Maximum allowable stiffener unfairness (Mansour et al. 1998).

- t = plate thickness
- B = plate slenderness ratio
- $= \frac{b}{t} \sqrt{\frac{\sigma_0}{E}}$
- b = plate width
- σ_0 = yield strength of the material
- E = modulus of elasticity

Figures 163 and 164 from Mansour et al. (1998) show, respectively, the recommended maximum plate unfairness versus plate slenderness ratio, and a comparison between the developed expression—equation (343)—and existing formulas in the literature.

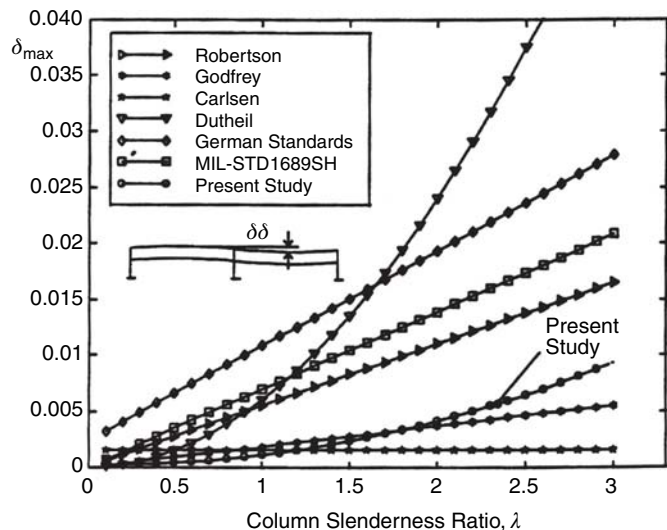


Fig. 166 Comparison between the developed expression and other formulas in the literature for stiffener unfairness (Mansour et al. 1998).

The recommended formula for the maximum allowable stiffener unfairness from the same study is

$$\frac{W_{0s \max}}{a} = (1.1\lambda^2 - 0.3\lambda + 0.3) \times 10^{-3} \quad (343)$$

where

$w_{0s \max}$ = maximum allowable stiffener unfairness
(i.e., stiffener tolerance)

a = stiffener length

λ = stiffener slenderness ratio

$$= \frac{a}{\pi r_e} \sqrt{\frac{\sigma_0}{E}}$$

r_e = radius of gyration of effective section

$$= \sqrt{\frac{I_e}{A_e}}$$

I_e = moment of inertial of stiffener, including effective plate

A_e = area of stiffener with effective plate

σ_0 = yield strength of the material

E = Young's modulus of elasticity

Figures 165 and 166 from the same study show, respectively, the recommended maximum stiffener unfairness

versus column slenderness ratio and a comparison of equation (343) with other existing formulations.

With regard to misalignments in butt-welded joints, the main conclusions of the study are:

- For general structural ship steel (yield strength less than 413.7 MPa, or 60 ksi), the maximum misalignment tolerance is $e/t = 0.26$. This requirement is slightly less conservative but compatible with other specifications currently in force.
- For steels having yield strength in excess of approximately 448.2 MPa (65 ksi), the misalignment tolerance should be defined by the fatigue failure mode. The tolerance level would depend on the factor of safety used in an ultimate strength safety check. For example, the analysis suggests that a maximum $e/t = 0.10$ requirement for 551.6 MPa (80 ksi) steel would be reasonable.
- The computed misalignment tolerances are not strongly influenced by the discount rate.
- The computed misalignment tolerances are not strongly influenced by the cost ratio (cost of in-service repair/cost of repair during construction).
- To a first approximation, the computed misalignment tolerances do not appear to be sensitive to the choices of statistical distributions of the stress and strength, or to the level of uncertainty of stress and strength.

Section 6

Miscellaneous Topics

6.1 Materials—Steel, Aluminum, and Composites. A major change in ship construction occurred over 100 years ago when steel was introduced to replace iron and wood as a hull material. Subsequent important developments in material and ship construction were the all-welded ship and the application of concepts of notch toughness to prevent the brittle hull fractures experienced with the all-welded steel ships of the 1940s.

Over the past half-century, many new designs such as container ships, liquid gas carriers, high-speed surface-effect-ships, and so on have been introduced. To meet requirements for such designs, high strength-to-weight ratio alloys and alloys intended for low-temperature service have been introduced into shipbuilding. The increasing size of ships such as the VLCC tankers and the concern of economy stimulated the automation of fabrication processes. The relatively simple concept of material toughness developed to answer the brittle fracture problems in ordinary strength steel hulls required refinement and extensive development before it could be applied to the newer materials and structures. In addition to the properties associated with static strength, fatigue

strength, and toughness, other factors must be considered when materials are to be selected for construction. These include electrical and thermal conductivity, magnetic permeability (for handling during fabrication, for example), susceptibility to various types of corrosion and environmental effects, fabrication (weldability, machinability, formability, repairability), paintability, cost (both material and fabrication), availability, and maintenance. Commercial ships may be fabricated of mild- or high-strength steel for reasons of affordability and availability. Cargo containment systems carrying liquid nitrogen gas or chemicals may be fabricated of stainless steel. Minesweepers would tend to use nonmagnetic material such as wood and glass-reinforced composites or even stainless steel. Icebreakers would need high-strength and high-toughness steels to sustain the high local impact of ice loads. Other applications warranted the use of aluminum, titanium, or composites to reduce top-side or hull weight. For example, higher-strength steels, aluminum alloys, and composite materials are used depending on the vessel size in high-speed craft constructions to reduce weight. Titanium has a proven record as

The recommended formula for the maximum allowable stiffener unfairness from the same study is

$$\frac{W_{0s \max}}{a} = (1.1\lambda^2 - 0.3\lambda + 0.3) \times 10^{-3} \quad (343)$$

where

$w_{0s \max}$ = maximum allowable stiffener unfairness
(i.e., stiffener tolerance)

a = stiffener length

λ = stiffener slenderness ratio

$$= \frac{a}{\pi r_e} \sqrt{\frac{\sigma_0}{E}}$$

r_e = radius of gyration of effective section

$$= \sqrt{\frac{I_e}{A_e}}$$

I_e = moment of inertial of stiffener, including effective plate

A_e = area of stiffener with effective plate

σ_0 = yield strength of the material

E = Young's modulus of elasticity

Figures 165 and 166 from the same study show, respectively, the recommended maximum stiffener unfairness

versus column slenderness ratio and a comparison of equation (343) with other existing formulations.

With regard to misalignments in butt-welded joints, the main conclusions of the study are:

- For general structural ship steel (yield strength less than 413.7 MPa, or 60 ksi), the maximum misalignment tolerance is $e/t = 0.26$. This requirement is slightly less conservative but compatible with other specifications currently in force.
- For steels having yield strength in excess of approximately 448.2 MPa (65 ksi), the misalignment tolerance should be defined by the fatigue failure mode. The tolerance level would depend on the factor of safety used in an ultimate strength safety check. For example, the analysis suggests that a maximum $e/t = 0.10$ requirement for 551.6 MPa (80 ksi) steel would be reasonable.
- The computed misalignment tolerances are not strongly influenced by the discount rate.
- The computed misalignment tolerances are not strongly influenced by the cost ratio (cost of in-service repair/cost of repair during construction).
- To a first approximation, the computed misalignment tolerances do not appear to be sensitive to the choices of statistical distributions of the stress and strength, or to the level of uncertainty of stress and strength.

Section 6

Miscellaneous Topics

6.1 Materials—Steel, Aluminum, and Composites. A major change in ship construction occurred over 100 years ago when steel was introduced to replace iron and wood as a hull material. Subsequent important developments in material and ship construction were the all-welded ship and the application of concepts of notch toughness to prevent the brittle hull fractures experienced with the all-welded steel ships of the 1940s.

Over the past half-century, many new designs such as container ships, liquid gas carriers, high-speed surface-effect-ships, and so on have been introduced. To meet requirements for such designs, high strength-to-weight ratio alloys and alloys intended for low-temperature service have been introduced into shipbuilding. The increasing size of ships such as the VLCC tankers and the concern of economy stimulated the automation of fabrication processes. The relatively simple concept of material toughness developed to answer the brittle fracture problems in ordinary strength steel hulls required refinement and extensive development before it could be applied to the newer materials and structures. In addition to the properties associated with static strength, fatigue

strength, and toughness, other factors must be considered when materials are to be selected for construction. These include electrical and thermal conductivity, magnetic permeability (for handling during fabrication, for example), susceptibility to various types of corrosion and environmental effects, fabrication (weldability, machinability, formability, repairability), paintability, cost (both material and fabrication), availability, and maintenance. Commercial ships may be fabricated of mild- or high-strength steel for reasons of affordability and availability. Cargo containment systems carrying liquid nitrogen gas or chemicals may be fabricated of stainless steel. Minesweepers would tend to use nonmagnetic material such as wood and glass-reinforced composites or even stainless steel. Icebreakers would need high-strength and high-toughness steels to sustain the high local impact of ice loads. Other applications warranted the use of aluminum, titanium, or composites to reduce top-side or hull weight. For example, higher-strength steels, aluminum alloys, and composite materials are used depending on the vessel size in high-speed craft constructions to reduce weight. Titanium has a proven record as

hull material used for all-welded submarine hulls, as well as riser applications in the offshore industry.

Comparisons of strength and construction cost have been made for various materials. A recent study by Farinetti (1998) presented comparisons for high-tensile steels versus aluminum alloys together with an analysis on workmanship standards and experimental fatigue tests of aluminum alloy. Goubalt and Mayers (1996) compared composite materials with steel and aluminum using the primary structure of a patrol boat as an example, and Jastrzebski (1999) compared the strengths of steel and aluminum alloys versus titanium alloys.

An overview of marine structural material properties and applications can be found in the work of Chalmers (1988), and in a more recent study by Fach and Rothe (1999) for especially lightweight construction in high-speed marine craft. The required chemical properties, mechanical properties associated with static strength, fatigue and toughness, as well as testing procedure guidelines for materials to be considered for viable use as a shipbuilding material are specified in classification society rules, such as the ABS Rules (ABS 1975, 1978, 2001, 2008). A brief comparison of some known basic strength characteristics of commonly used materials are shown in Table 7 (excerpted from Specialist Committee V.6 Report, ISSC 2000).

6.1.1 Hull Structural Steel. Steel still remains the principal structural material in ship construction. How-

ever, the requirements related to its main properties are changing, and they become more and more demanding with innovative ship concepts like ultra large container ships or super RO-RO ships. The development of new concepts and the introduction of innovative joining processes such as lasers was only possible with corresponding developments on the materials side. To reduce weight and because of fabrication issues like the increase of plate thickness in highly stressed areas, high-strength steels are increasingly being used.

6.1.1.1 Microstructure and Steel-Making of Hull Structural Steel. The microstructure of shipbuilding steels consists of iron-carbide (cementite) dispersed in a matrix of ferrite (the metallographic name for one form of iron in steel). As the temperature of a steel increases to a transformation temperature, the iron that is in the ferrite phase transforms to another form of iron (austenite), in which the cementite is highly soluble. Upon cooling below the transformation temperature, the austenite with dissolved cementite reverts back to ferrite and precipitated cementite. A laminated microstructure of cementite and ferrite, referred to as pearlite, is a major constituent of the common ship steels. In general, the carbon content and rate of cooling influence the microstructure, which in turn determines the strength and hardness of the resulting steel. Most hull structural steels are cooled in air after hot rolling or heat treatment. Some high-strength hull steels above 350 MPa yield strength are water quenched from above their transformation temperature and then tempered by heating to a temperature well below the transformation temperature. The quenching and tempering treatment produces a microstructure called tempered martensite, which is characterized by high strength and high toughness.

In low-carbon steels, in the absence of deoxidizers the reaction of carbon with oxygen produces carbon monoxide during ingot solidification. The resulting ingot has an outer rim free of voids, and an inner zone containing voids derived from shrinkage and occluded gases. Such steels, which are identified as rimmed steels, are generally not used as hull steel over 13 mm because of their relative unsoundness. *Semi-killed steels* are derived from ingots that are partially deoxidized, and are sounder than rimmed steels and commonly used as hull structural steels. ABS Grades A and B are examples of semi-killed steels. *Killed steels* are completely freed of the gassing reaction by additions of strong deoxidizing agents such as silicon or aluminum, and are the soundest of the three steel types. *Fine grain practice* is the addition of elements such as aluminum, niobium, or vanadium to limit grain size during the period of grain formation. Steel quality may be further enhanced by a normalizing heat treatment, which homogenizes and refines the grain structure. Normalizing involves reheating steel to a temperature above its transformation range and cooling in air. Fine grain practice, fully killing, and normalizing enhance steel quality.

Table 7—Basic Characteristics of Materials for Ship Structures

Material	Grade	Density (g/cm ³)	$R_e, R_{0.2}^a$ (MPa)	R_m^b (MPa)	E^c (1,000 MPa)
Aluminum alloy, plates	5083	2.70	125	275	69
Aluminum alloy, profiles	6082T6	2.70	260	310	69
Mild steel	A, B, D, E	7.80	235	400	205
HT steel	A, D, E36	7.80	355	490	205
QT steel	D, E, F46	7.80	460	570	207
GRP laminate (φ 0.35)	500 g/m ²	1.65		260	14
Carbon epoxy (φ 0.62)		1.6	N/A	1500	140
Titanium, plates	Grade II	4.50	310	420	127
Titanium alloy, plates	Ti-6Al-4V	4.40	930	985	110

^a Specified minimum yield stress. If stress-strain curve does not show a defined yield stress, the 0.2% proof stress applies.

^b Specified minimum tensile strength.

^c Modulus of elasticity.

Table 8—Chemical properties of ordinary strength hull structural steel, 100 mm (4.0 in.) and less (chemical composition, ladle analysis, is in % maximum; see ABS Rules for details)

Grade	A	B	D	E
<i>Deoxidation</i>	<i>Killed or Semi-Killed (t ≤ 50 mm); Killed (t > 50 mm)</i>		<i>Killed (t ≤ 25 mm); Killed or Fine Grain (t > 25 mm)</i>	<i>Killed and Fine Grain</i>
C	0.21	0.21	0.21	0.18
Mn (min)	2.5 × C	0.80	0.60	0.70
Si	0.50	0.35	0.10–0.35	0.10–0.35
P	0.035	0.035	0.035	0.035
S	0.035	0.035	0.035	0.035
Ni	See notes	See notes	See notes	See notes
Cr	See notes	See notes	See notes	See notes
Mo	See notes	See notes	See notes	See notes
Cu	See notes	See notes	See notes	See notes
C+ mn/6	0.40	0.40	0.40	0.40

Note: As specified in ABS Rules.

6.1.1.2 Ordinary Strength Hull Structural Steel. Ordinary strength hull steels such as ABS Grades A, B, D, and E are the most extensively used group of shipbuilding steels. The properties of these plain carbon steels depend on their chemical content and microstructure. In addition to carbon, these steels contain manganese, silicon, phosphorus, and sulfur; minor amounts of other elements are also present. Ordinary strength hull structural steels have a minimum specified yield strength of 235 MPa, and a tensile strength of 400 to 520 MPa (for the Grade A section, the upper limit of tensile strength may be 550 MPa). Chemical properties and tensile properties of the ordinary strength steels are shown in Tables 8 and 9. These information are excerpted from ABS Rules (2008), where requirements for other properties associated with elongation, impact, and other factors are also specified.

Specifications of ABS grade hull structural steels (ordinary strength as well as high-strength) are essentially the same as those of the major classification societies worldwide. Certain American Society for Testing and Materials (ASTM) grades of steels have been used as substitutes for ABS steels, and to meet requirements for strength levels above those provided by the classification society steels. The military specifications also cover the steels analogous to those of ABS and ASTM grades. In addition, there exists in most industrial nations a series of standards corresponding to ASTM standards. These include the International Organization for Standardization (ISO), British Standard (BS), Canadian Standards Association

(CSA), Japanese Industrial Standard (JIS), Normes Francaises (NF), Unificazione Nazionale Italiana (UNI), and others. Some compilations relating ASTM and other industrial standards are given in Ross (1972). Examples of ASTM grades and military specifications for steels used in marine structures can be found in Stern (1980).

6.1.1.3 High Strength Hull Structural Steel. High-strength hull structural steels may be considered as four groups: normalized steels, fine grained TMCP steels, quenched and tempered steels, and low alloy steels.

The high-strength hull structural steels as specified by the classification societies have been available in three yield strength classes— 315, 355, and 390 MPa. The higher-strength steels were alloyed with combinations of vanadium, niobium, carbon, and aluminum, and were heat-treated by normalizing to provide the required combination of strength, toughness, and weldability. With more sophisticated thermomechanical processes developed by steel makers, the normalizing operation can be dispensed with. The most advanced of those processes is referred to as the *thermomechanical controlled process* (TMCP), which produces a finer ferrite grain size than is typically obtained through normalizing, resulting in an elevation in yield strength and toughness with lower carbon and alloy contents. The lowering of total alloy content as compared with conventional processes produces steels with enhanced weldability (freedom from hydrogen-induced cracking) and better heat-affected zone toughness, leading to a lowering of overall fabrication costs compared to other higher-strength steels.

Table 9—Tensile properties of ordinary strength hull structural steel, 100 mm (4.0 in.) and less (see ABS Rules for details)

Grade	Tensile Strength N/mm ² (kgf/mm ² , ksi)	Yield Point (minimum) N/mm ² (kgf/mm ² , ksi)	Elongation (minimum) %
A, B, D, E	400–520 (41–53, 58–75)	235 (24, 34)	22

For structural steels, weldability is often a limiting consideration, which will be determined by carbon content and alloying elements. To achieve high yield strength with good toughness and weldability, these steels have often been produced through quenching and tempering. Theoretically, structural steels with yield strengths of about 960 MPa can be produced, but the normal upper economic limit for quenched and tempered steels has been about 690 MPa. The quenched and tempered higher-strength steels have been used fairly extensively in naval ship construction, and to a more limited extent in the offshore industry. The so-called HY-80 and HY-100—yield 0.55 MPa (80 psi) and 0.69 MPa (100 psi)—steels have been popular but have required special considerations for welding. Further improvement of strength is obtained with the high-strength low-alloy (HSLA) steels (350 to 700 MPa yield strength) to replace quenched and tempered steels with better weldability (see Anderson et al. 1987; Czyryca et al. 1990; Primon et al. 1989; Susuki et al. 1989). The use of HSLA steels in shipyard building conventional vessels is limited, mainly for military vessels (Chalmer 1993; Christein & Warren 1995) and most recently to major high-speed vessels.

The concept of making the ferritic grain size smaller to increase the yield strength and making the grain size finer to increase the fracture toughness is used in TMCP structural steel. TMCP steel plate is referred to as *surface ultra fine* (SUF) steel and is shown to exhibit fracture properties superior to those of typical carbon-manganese structural steel (Ishikawa et al. 1997a, 1997b). TMCP steel plate has surface layers of 1 to 3 mm thick consisting of ultra-fine grains that are resistant to brittle fracture. Even if a brittle crack were to propagate in the plate, the surface layers would tend to fracture in a ductile manner, absorbing crack propagation energy and promoting crack arrest. However, the superior crack growth performance of SUF steel has not yet been conclusively demonstrated, but results are encouraging. In addition, fatigue strength of weldments of SUF steels must be compared to that of other shipbuilding steels. The cost of SUF steel could be high in comparison with ordinary TMCP steels, but no exact information is yet available.

The most widely used higher-strength steels for commercial ship construction are those with yield strength up to 390 MPa, such as ABS grades AH, DH, EH, and FH. Chemical and tensile properties of such steels are respectively shown in Tables 10 and 11 (excerpted from ABS 2008). In these specifications, the grade is a letter designation followed by a numerical designation indicating yield strength in kgf/mm² and ksi.

6.1.1.4 Special Steels. The common structural steels are intended for the service normally encountered by most ships and marine structures. Special steels with enhanced properties are available where service conditions involve exposure to unusual temperatures, corrosion, or loading conditions. In some cases, the use

Table 10—Chemical properties of high-strength hull structural steel (see ABS Rules for details)

Grades	AH/DH/EH 32, AH/DH/EH 36, and AH/DH/EH 40	FH 32/36/40
	<i>Killed, Fine Grain Practice</i>	<i>Killed, Fine Grain Practice</i>
<i>Deoxidation</i>		
C	0.18	0.16
Mn	0.90–1.60	0.90–1.60
Si	0.10–0.50	0.10–0.50
P	0.035	0.025
S	0.035	0.025
Al (acid soluble) min.	0.015	0.015
Nb	0.02–0.05	0.02–0.05
V	0.05–0.10	0.05–0.10
Ti	0.02	0.02
Cu	0.35	0.35
Cr	0.20	0.20
Ni	0.40	0.80
Mo	0.08	0.08
N	—	0.009 (0.012 if Al present)

of special steel may be mandated by requirements of a regulatory agency, or in other cases it may be a design selection for the purpose of achieving improved serviceability. Special steels commonly used in commercial shipbuilding are the steels for low temperature, corrosion-resistant steels, and abrasion-resistant steels.

6.1.1.4.1 Steels for Low-Temperature Applications. In general, steels equivalent to the ABS grades when used in applications appropriate for each grade may be used for all applications where the lower limit of service temperature is primarily related to the lowest possible sea temperature. Where extraordinary cooling effects exist, consideration should be given to the use of steels with

Table 11—Tensile properties of high-strength hull structural steels (see ABS Rules for details)

Grade	Tensile Strength	Yield Point (minimum)	Elongation (minimum) %
	N/mm ² (kgf/mm ² , ksi)	N/mm ² (kgf/mm ² , ksi)	
AH 32	440–590	315	22
DH 32	(45–60, 64–85)	(32, 46)	
EH 32 FH 32			
AH 36	490–620	355	21
DH 36	(50–63, 71–90)	(36, 51)	
EH 36 FH 36			
AH 40	510–650	390	20
DH 40	(52–66, 74–94)	(40, 57)	
EH 40			
FH 40			

Table 12—Steel grade applications in low-temperature conditions

Minimum Design Temperature of Hull Structure (°C)	Maximum Thickness for Steel Grades (mm)						
	A	B	D	E	AH	DH	EH
0 and above	Normal practice						
Down to -5	15	25	30	50	25	45	50
Down to -10	NA	20	25	50	20	40	50
Down to -20	NA	NA	20	50	NA	30	50
Down to -30	NA	NA	NA	40	NA	20	40

fracture transition temperatures and toughness characteristics appropriate to the service temperature involved. Such special requirements for low-temperature service may be derived from the cooling effects of cargo, such as refrigeration ships and liquefied gas carriers. They may also be derived from service where steel temperatures are not moderated by ocean temperatures, as in the case of upper structures of mobile offshore drilling units.

The commonly used ABS grade hull structural steels are applicable in certain design conditions of low temperature, such as steel forming and adjacent to the refrigerated areas of refrigeration ships, or structures of temperatures below -5°C due to the effect of the low cargo temperature. However, the application is limited according to plate thickness, and its guidelines are shown in Table 12 (from ABS Rules Part 5C 2008). ABS AB/V-OXX (minimum yield strength of 235 MPa) and AB/VH-OXX (minimum yield strength of 355 MPa) steels are useful for service temperatures below 0°C and down to -55°C .

In liquefied gas carriers, low-temperature service requirements may be encountered in the cargo tanks, secondary barriers, and parts of the hull affected by the cargo. When the outer hull serves as the secondary barrier, such as in some liquefied petroleum gas carriers, it has the same toughness requirement as the tank material. With adoption of international conventions, such as the International Code for the Construction and Equipment of Ships Carrying Liquefied Gases in Bulk (IMO 1983), general requirements for liquid gas carriers have become applicable worldwide and have been adopted by many regulatory bodies. Related requirements in two categories—those for temperatures below 0°C and down to -55°C and those for temperatures below -55°C down to -165°C —are also specified in classification rules (for example, ABS Rules Part 5C 2008).

6.1.1.4.2 Corrosion-Resistant Steels. The major structural application of corrosion-resistant steels in merchant ships is to provide a surface that is resistant to chemical action from a liquid cargo. It is commonly used in the form of a layer of protective cladding on ordinary steel plates. It may also be used in solid form for relatively thin plates and for shapes where the clad product is not available. There are a wide variety of corrosion-resistant steels available, among which AISI types such as 304, 316, 304-L, and 316-L are some of the most commonly used corrosion-resistant steels.

6.1.1.4.3 Abrasion-Resistant Steels. The most common application for abrasion resistant materials is for components associated with the loading and unloading of bulk cargo. Two types of materials are available for abrasion resistance, namely, the non-weldable type and the weldable type. The non-weldable type abrasion-resistant steel with high carbon, manganese, or chromium is not generally used for structural applications. The weldable type is available in the standard structural condition or quenched and tempered to high hardness levels for superior abrasion resistance.

6.1.2 Aluminum Alloys. Aluminum alloys have been widely used where their special attributes such as low density and high strength-to-weight ratio, corrosion resistance in certain environments, or retention of toughness at low temperatures are of concern. Development of inert gas welding processes has facilitated the use of aluminum alloys for various ship structural applications. Aluminum alloys are frequently used in superstructures of large ships and for the entire hull structure of some ferries and small boats. The low density of aluminum alloys makes them particularly attractive for applications where high strength-to-weight ratios are of particular concern, such as in high-speed vessels. Aluminum alloys increase in strength and maintain toughness as temperature decreases, and therefore are particularly suitable for cryogenic services such as containment of LNG. Specifications of compositions, properties, and testing for aluminum alloys used in marine construction can be found in classification rules such as ABS (1975, 1997) and American National Standards Institute (ANSI/ASTM 1977).

6.1.2.1 Non-Heat Treatable Aluminum Alloys. Aluminum alloys such as 5083 (4.5% Mg), 5086 (4.0% Mg), and 5456 (5.0% Mg), which acquire increased strength from cold work and not from heat treatment, are most widely used for marine structures. The 5454 alloy is used for applications where service temperatures are above 65°C (149°F). These alloys, which have good weldability characteristics, are usually used in the mildly cold-worked (1/4 hard) temper to provide the desirable combination of strength and corrosion resistance. Higher-strength forms of these alloys obtained either by additional cold work up to fully hard or by magnesium contents over 5 percent are not generally used, as they tend to exhibit an undesirable increased susceptibility to

stress corrosion. For areas such as stagnant bilge areas where special corrosion problems are anticipated, alloys may be provided in special tempers, such as 5083-H116, 5086-H117, or 5454-H116, which are particularly resistant to exfoliation (a special form of intergranular corrosion that produces delamination). In general, in the vicinity of weld the base plate of the non-heat treatable alloy (such as the 5XXX series) is transformed to an annealed condition by the heat of welding. The effect is to reduce tensile properties in the vicinity of the weld to the annealed or non-work hardened values, which should be taken into account in design.

6.1.2.2 Heat Treatable Aluminum Alloys. Heat treatable aluminum alloys such 6061-T6 develop strength by heating to an annealing temperature, water quenching, and then reheating to a lower temperature to achieve a controlled precipitation of intermetallic compounds. The 6061-T6 alloy is occasionally used in marine service, particularly for extrusions, because it extrudes more readily than the 5083 or 5086 non-heat treatable alloys. The strength of the 6061-T6 alloy is greater than that of 5083 or 5086 alloys. However, the strength, ductility, and corrosion resistance of the 6061-T6 alloy base plate are severely degraded in the area in the vicinity of welds by the heat of welding. Such adverse effects limit the applicability of the 6061 alloy for welding applications.

The alloy grades cited here are of the U.S. ASTM/AA standards. For most of the industrial nations, equivalent standards are available, as shown in Table 13.

6.1.2.3 Corrosion of Aluminum Alloys. Aluminum alloys generally do not experience excessive corrosion under normal operating conditions. However, aluminum alloys when in contact with dissimilar materials may corrode at an accelerated rate. Such conditions can occur between faying surfaces of aluminum and other metals, between aluminum hulls and non-aluminum piping, or when non-aluminum piping passes through aluminum bulkheads and decks, for example. In such cases, aluminum should be isolated from the other metal by means of suitable non-water absorbing insulating tapes,

coatings, gaskets, or by use of special piping hangers of fittings.

Aluminum in contact with wood, insulating materials, or concrete should be protected against the corrosive effects of impurities in these materials by suitable coverings or coatings. Suitable precautions should be taken to avoid arrangements that could induce crevice corrosion in wet spaces. In certain stagnant water applications, such as bilge spaces or chain lockers where exfoliation corrosion may be of concern, use of the alloys specially heat-treated to resist this form of corrosion should be considered (see ABS 1975).

6.1.2.4 Fire Protection of Aluminum Alloys. In comparison with steel, aluminum alloys have relatively low softening and melting points (200°C and 650°C, respectively) and tend to lose strength rapidly upon exposure to elevated temperatures. In considering the use of aluminum, due consideration should be given to applications where retention of structural integrity would be required in cases of fire exposure. The use of appropriate insulation should be considered for such applications. However, attentions at the outset in the design process are required to the increased weight of insulation, as it can be significant for some vessels.

6.1.2.5 Aluminum Alloy Application in High-Speed Vessels. Aluminum alloys are the most commonly used light metals for high-speed craft. For vessels up to 50 m in length, the structural design is mainly based on local rather than global loads. For such vessels, aluminum alloy may be chosen as structural material unless they are built in a series of several units, where the fiber-reinforced plastics often provide the lightest and lowest cost solution. For vessels between 50 and 100 m in length, aluminum alloys are generally the best choice as structural material, taking into account that longitudinal strength behavior and hull deflection are more significant considerations than for smaller crafts. For vessels over 100 m, response to global loads is a major design consideration. Aluminum alloys can be used up to a point. Aluminum alloys have so far been used for catamarans up to

Table 13—Aluminum alloy equivalents (from ABS 1975)

U.S. ASTM AA ^a	Canada (CSA)	France (NF)	U.K (BS)	Italy (UNI)	Japan (JIS)	ISO
5052	GR20		2L.55, 2L.56, L80, L81	PAIMg2.5	A2.1	AlMg2.5Mn
5083	GM41 E54S ^b		N8		A2-7	AlMg4.5Mn
5086 5454	GM31N 55330 ^b	AG4MC				AlMg4 AlMg3Mn
5456 6061	GS11N		N61 H20		A2-4	AlMg1SiCu

^a AA = Aluminum Association

^b Commercial designations

124 m in length (Nordhammer 1998). For vessels over 120 m in length, higher-strength steel is likely to be preferred. However, the length at which the transition occurs varies according to the ship type and operating patterns.

A review of the state-of-the-art concerning aluminum alloy application to high-speed craft has been given by Bauger (1998), Sampath et al. (1998), and Ferraris (1999). In general, the 5XXX series alloys, which are generally supplied in wrought form as plates and strips, are used for high-speed hull applications below the water line because of their good corrosion properties. For areas not directly in contact with water, 6XXX series alloys are also used, particularly as extruded sections.

Recent advances of aluminum alloy applications have been achieved. A new 5383 aluminum alloy has been found (Ehrstrom et al. 1998) that has been shown to have better static strength, fatigue strength, and corrosion resistance than the conventional 5083 alloy. The 7108 alloy has also been adopted for extrusions on catamarans in Northern Europe, which is the first example of extensive use of 7XXX series in marine structures. However, when the 7XXX alloy is used improved corrosion protection systems are required, as corrosion problems of such alloys have arisen even in supposedly dry areas.

6.1.3 Composites. Modern-day composite materials were introduced with phenolic resins for marine structural applications at the turn of the last century. The start of using glass-reinforced plastics (GRP), which is a form of fiber-reinforced plastics (FRP), in boatbuilding began in the 1940s in the form of U.S. Navy personnel boats. Since that time, GRP has found widespread acceptance for yachts and small boats such as fishing trawlers due to its relative low cost and requiring virtually no maintenance.

One of the earlier published books of fiberglass design targeted directly at the boat building industry is the one by Gibbs and Cox (1960). In recent years, the source for design guidance of composite materials has been specialized conferences, such as those sponsored by the Society of the Plastic Industry (SPI) and the Society for Advancement of Materials Processing and Engineering (SAMPE). The Society of Naval Architects and Marine Engineers (SNAME), the Ship Structure Committee (SSC), and the American Society of Naval Engineers (ASNE) also address composite construction issues in their conferences and publications. SNAME has an active technical committee, HS-9, that is involved with composite materials. Relevant information can also be found among professional journals, such as those issued by SNAME, ASNE, the Composite Fabricators Association (CFA), SAMPE, and industry publications such as *Composite Technology*, *Composite Design & Application*, *Reinforced Plastics*, and *Professional Boatbuilder* magazines.

Composite material vessel constructions have relied on classification society rules such as ABS Rules (1978, 1994, 2000, 2001) to develop scantlings. Other classification society rules, such as DNV, Lloyd's, BV, GL, RINA, also similarly provide load and strength criteria of com-

posite crafts. Classification society rules are developed over a long period of time and have traditionally been based on "base" laminates and rules for developing required thickness. For example, ABS rules are based on a laminate consisting of general-purpose polyester resin and alternate plies of fiberglass mat and fiberglass woven roving, with specific average cured laminate thickness. Classification societies generally review FRP construction to 60.96 m (200 ft), although larger fast ferries being considered in Scandinavia would make use of advanced composite materials, as allowed by the International Code of Safety for High-Speed Craft (HSC Code) issued by the International Maritime Organization (IMO 2000).

In comparing steel and aluminum constructions, composite construction has a much larger number of new material choices and process variables. This gives the designer more design latitude and avenues for optimization, but without a full understanding of the material characteristics it may result in improper design, leading to premature failures. One major difference between composites and steel and aluminum is that the complex materials technology for aluminum and steel has essentially been completed when the material is delivered to the builders. However, with the complex materials technology of composites, the building process and quality control is applied during construction of the composites hull.

Extensive studies have been carried out to investigate the basic behavior of FRP and its utilization. Some are devoted to strength of structures made of FRP or structures with FRP components; others to fatigue assessments, design, and structural details of connections between FRP and metal structures. Relevant references are given in Ship Structure Committee report SSC-403 (Greene 1997). Other reference papers, particularly regarding the selection of structural materials for high-speed vessels, are given in proceedings of International Ship and Offshore Structures Congress (ISSC 2000). This section provides general information on material systems, analysis principles, available design tools, and failure mechanisms of the composite materials that are commonly used in marine structures. As the subject is truly multidisciplinary, this section considers only the concepts, principles, and methodologies of some selected topics, with emphasis on practical engineering application. The micromechanics and macromechanics of composites, composite test data, and the application of composite material in design and construction are included in references cited previously.

6.1.3.1 Composite Material Concepts. In general terms, *composite materials* are laminates consisting of filamentary reinforcements supported in a matrix of cured plastic resin that starts as a liquid and ends up a solid through a chemical reaction. The reinforcement is designed to resist the primary loads that act on the laminate, and the resin transmits loads between the fibers and the resin and between the plies of reinforcement

fibers, primarily through shear. When the laminate is subject to compression loading, the resin serves to “stabilize” the reinforcement fibers for in-plane loads and transmit loads via direct compression for out-of-plane loads. Thus, the bond between reinforcement fibers, which is influenced in its strength by resin formation, reinforcement sizing, processing techniques, and laminate void content, is critical to laminate performance, as this is the primary shear stress transfer mechanism.

The strain-to-failure value of the cured resin is very important, as it should correspond as much as possible with the strain-to-failure value of the fibers so that the resin does not fracture before the strength of the reinforcing fibers is adequately developed. This is one of the reasons why epoxy resins are used with carbon and aramid fibers.

6.1.3.1.1 Reinforcements. Reinforcements for marine composite structures are mostly glass fibers, aramid fibers, or carbon fibers. Glass fibers account for over 90 percent of the fibers used in reinforced plastics of marine use because they are inexpensive to produce, have relatively good strength-to-weight characteristics, and exhibit good chemical resistance and processability. The fiberglass reinforcements are in two general categories: E-glass or “electrical glass,” which was originally developed for the electrical industry due to its high resistivity, and S-glass with improved tensile strength, which was specifically developed for “structural” applications. Comparing with E-glass fiber, the S-glass fiber costs two to three times more, and for this reason E-glass is generally used in preference to S-glass in marine structures. Glass fiber also has the advantage of being fire resistant. Of the reinforcing fibers currently used in the marine industry, it is preferable to use glass fibers when fire resistance is a governing consideration.

The most common aramid fiber is Kevlar, developed by DuPont. This is the predominant organic reinforcing fiber whose use dates to the early 1970s as a replacement for steel belting in tires. The outstanding features of aramids are low weight, high tensile strength and modulus, impact and fatigue resistance, and weaveability. The compressive strength of aramid fiber-reinforced laminates does not match their tensile strength, and very often E-glass fiber or carbon fiber are used together with aramid fiber to improve the compressive strength of the laminate.

The carbon fibers offer the highest strength and stiffness of all the common reinforcement fibers. Carbon fibers are not subject to stress rupture or stress corrosion, as with glass and aramids. High-temperature performance is particularly outstanding. The major drawback to the PAN-based (polyacrylonitrile) carbon fibers is their relative cost, which is a function of high precursor costs and an energy-intensive manufacturing process. In general, carbon, aramid fibers, and other specialty reinforcements are used in the marine field where structures are highly engineered for optimum efficiency. Because of their greater adhesive and strain-to-failure

properties, epoxy resins are invariably used with carbon and aramid fibers.

Reinforcement materials are combined with resin systems in a variety of forms to create structural laminates. The woven composite reinforcements generally fall into the category of cloth or woven roving. The knitted reinforcements are constructed using a combination of unidirectional reinforcements that are stitched together with nonstructural synthetic, such as polyester. Woven and knitted fiber reinforcement can be bi-axial, tri-axial, or quadraxial. Off-axis or double-bias reinforcement is formed with fibers at $+45^\circ$ and -45° to the weft direction, and is very effective in resisting in-plane shear forces. The omnidirectional reinforcements are applied during hand lay-up as prefabricated mat or via the spray-up process as chopped strand mat. Chopped strand mat consists of randomly oriented glass fiber strands that are held together with soluble resinous binder. Continuous strand mat is similar to chopped strand mat, except that the fiber is continuous and laid down in a swirl pattern.

The unidirectional construction has about 90 percent of the fibers in the warp direction with only about 10 percent fiber reinforcement in the fill direction. Ultra high-strength/modulus material such as carbon fiber is sometimes used in this form due to its high cost and specificity of application. Typical applications for the unidirectional form include stem and centerline stiffening as well as the tops of stiffeners. Entire hulls are fabricated from unidirectional reinforcements when an ultra high-performance laminate is desired and load paths are well defined. The unidirectional plies are generally laminated in the longitudinal, transverse, and diagonal directions. Although allowing a most effective structure in that the plies can be arranged to correspond to the direction of the applied stresses, this form of laminating unidirectional plies is not so resistant to impact loading as woven or knitted tri-axial or quadraxial plies.

6.1.3.1.2 Resins. Commonly used *resins* in marine composite constructions are polyester, vinyl ester, epoxy, phenolic, and thermoplastics. Polyester, vinyl ester, and epoxy resins are the most frequently used resins for FRP hull structures. Polyester is by far the most frequently used. Vinyl ester resin has superior cured properties to polyester, and is used much less frequently than polyester but more often than epoxy. Epoxy resin has the best performance characteristics of these resins and is invariably used with advanced composite reinforcement of carbon and aramid fibers.

Polyester resins (unsaturated and saturated) are the simplest, most economical resin systems that are easiest to use and show good chemical resistance. The cured mechanical properties of isophthalic polyester resin are superior to those of cured orthophthalic polyester resin, particularly the very important greater value of strain-to-failure. Vinyl ester resins are unsaturated resins, which have the advantages of superior corrosion resistance, hydrolytic stability, and excellent physical properties such

as impact and fatigue resistance. They also have higher strain-to-failure values than all polyester resins.

Epoxy resins are a broad family of materials that contain a reactive functional group in their molecular structure. Epoxy resins show the best performance characteristics of all the resins used in the marine industry, and also exhibit the least shrinkage upon cure of all the thermosets. The high cost and more exacting application requirements limit the use of epoxy resins to large or high-performance marine structures. The applications of epoxy resins are also limited when high-temperature performance is critical.

Phenolic resins are in two general categories: novolacs and resoles. Phenolic resins perform much better than polyesters, vinyl esters, and epoxies in fires, showing reduced flame spread characteristics and increased time to ignition. However, their load-carrying mechanical properties are generally less than polyester, vinyl ester, and epoxy resins.

Thermoplastics generally come in the form of molding compounds that soften at high temperatures. Polyethylene, polystyrene, polypropylene, polyamides, and nylon are examples of thermoplastics. Their use in the marine industry has generally been limited to small boats and recreational items. Reinforced thermoplastic materials have recently been investigated for the large-scale production of structural components.

6.1.3.1.3 Core Materials. Commonly used core materials in sandwich constructions are the end-grain balsa, thermoset foams, syntactic foams, cross-linked polyvinyl chloride (PVC) foams, linear PVC foams, linear polymer foams, SAN foams, honeycomb, and polymethylacrylimide (PMI) foam. Thermoset foams are made of formed plastics such as cellular cellulose acetate (CCA), polystyrene, and polyurethane. Syntactic foams are made of hollow microspheres of glass, epoxy, and phenolic mixed into fluid resin. PVC foam cores are manufactured by combining a polyvinyl co-polymer with stabilizers, plasticizers, cross-linking compounds, and blowing agents. Honeycomb cores of various types are used extensively in the aerospace industry. Constituent materials of honeycomb include aluminum, phenolic resin-impregnated fiberglass, polypropylene, and aramid fiber phenolic treated paper. PMI foam is primarily for aerospace industry use.

PVC and SAN foam cores are the most frequently used cores in marine construction. End-grain balsa is used where weight is less important. Honeycomb cores are the lightest core materials, but they require a very high standard of quality control to ensure good performance when used in hulls subject to wave-slamming loads.

6.1.3.2 Composite Performance and Comparison with Metallic Structures. With the exception of chopped strand mat, reinforcements used in marine composite construction use bundles of fibers oriented in distinct directions. "Balanced" laminates have a proportion of fibers in 0° and 90° directions. Reinforcement products include $\pm 45^\circ$ fibers that are particularly effective in

resisting in-plane shear forces. Tri-axial knits have $\pm 45^\circ$ fibers, plus 0° or 90° fibers. Quadraxial knits have fibers in all four directions. Comparison of responses of panels made with various knit fabrics subject to out-of-plane loading can be found in such as the Knytex Fabric Handbook (1994). Whether the reinforcements are aligned in a single direction or a combination thereof, the strength of the laminate will vary depending on the direction of the applied force. When forces do not align directly with reinforcement fibers, it is necessary for the resin system to transmit a portion of the loads.

In comparing steel and aluminum used in shipbuilding, most composite materials have lower strength and stiffness values. However, because composite materials are much lighter than metals, thicker composite plating can be used, resulting in the panel stiffness of composite construction matching or exceeding that of metal hulls. In fact, frame spacing for composite vessels is often much larger. On the other hand, for a given strength composite panels may be quite more flexible, leading to in-service deflections that are larger than for metal structures.

The previous discussion addresses the behaviors of composite panels subject to hydrostatic and wave loads. For the global hull structural response, particularly of larger vessels, attention must be given to the overall hull girder bending stiffness. Because structural material cannot be located farther from the neutral axis (as is the case with thicker panels), the overall stiffness of large ships is limited when quasi-isotropic laminates (properties similar in all directions parallel to the skin) are used. This had led to concern about main propulsion machinery alignment when considering construction of FRP vessels over 91.44 m (300 ft) in length. With smaller, high-performance vessels such as racing sailboats, longitudinal stiffness is obtained through the use of longitudinal stringers, 0° unidirectional reinforcements, or high-modulus materials such as carbon fiber.

Damage and failure modes for composites also differ from metals. Whereas a metal grillage will transition from elastic to plastic behavior and collapse in its entirety, composite panels will fail one ply at a time, causing a change in strength and stiffness leading up to a catastrophic failure. In contrast to metals, crack propagation typically does not occur with composites; instead, interlaminar failure between successive plies often takes place. Because composite laminates do not exhibit the classic elastic to plastic stress-strain behavior that metals do, safety factors based on ultimate strength are greater, especially for compressive failure modes. In addition, there are more potential modes of failure for composite structures than for steel or aluminum, particularly for sandwich laminates. Lack of fully developed theories for some of the potential failure modes requires destructive or nondestructive production tests.

6.1.3.3 Design Aspects of Composite Marine Structures. The process for designing marine structures that are to be built with composite materials is first to define the loads, which consist of primary, secondary, and

tertiary. However, the load components do not necessarily follow the notational hierarchy as they do for large ocean-going ships. Instead, the terms could only be thought of as “global,” “regional,” and “local” for the composite crafts. With regard to hull structures, the design process for composite vessels is rather unique, interrelated, and does not always follow in a linear fashion because of the wide range of available materials and fabrication methods. In Fig. 167 (from SSC-403), a design flow chart consisting of two consecutive design cycles for primary hull laminate is shown to illustrate one of the available approaches that will produce safe structures. In general, composite marine vessels are constructed using one of the following design concepts:

- Monocoque single-skin construction
- Single-skin construction using bulkheads, transverse webs, and stringers
 - Monocoque sandwich construction
 - Sandwich construction using bulkheads, transverse webs, and stringers.

Monocoque single-skin construction creates panel structures that span across the turn in the bilge to the hull-to-deck joint and extend from bow to stern. Very thick skins are required to make this kind construction method feasible for anything but the smallest vessels such as canoes. Single-skin construction is more often combined with a system of bulkheads, transverse webs, and longitudinal stringers to limit the effective panel spans, and thus reduce the laminate strength and stiffness needed. Monocoque sandwich construction has thin, stiff skins on relatively thick cores. These sandwich laminates can resist loads over large spans, while at the same time possess sufficient overall longitudinal stiffness contribution to alleviate the need in smaller craft for added longitudinal stiffeners. A good example of monocoque sandwich construction is the America’s Cup yacht. Also, the Whitbread and Volvo Round-the-World Races have proven the strength of sandwich hull racing yachts designed and built to the ABS Guide for Building and Classing Offshore Racing Yachts.

Sandwich construction that makes use of bulkheads and stringers permits the use of softer skin and core materials. Panel spans are reduced as with single-skin construction, although stiffener spacing is typically much larger because the thick sandwich laminate have inherently greater moments of inertia.

There are a number of design tools available that can provide key “pieces” to the design spiral. After loads are defined, specific methodology for predicting the response of a composite material structural system must be chosen. Different design tools are usually used for modeling structures with varying degrees of details or complexity. Computer programs of laminate analysis based on laminate plate theory work well to define the behavior of composite material beams. Developed surfaces more complicated than panels with curvature are generally modeled with finite element analysis methods.

Classification society rules such as ABS (1978, 1994, 2000, 2001) serve well to specify minimum scantlings for major structural elements.

Composite materials afford the opportunity for optimization through combinations of reinforcements, resins, and cores. Engineering optimization always involves tradeoffs among performance variables. However, it should be noted that combinations of reinforcements, resins, and core systems might produce laminates that can either enhance or degrade constituent material properties.

6.1.3.4 Failure Modes of Composite Structures.

The failure modes of engineered composite structures are unique as compared with those of metal structures. The failures of composite laminates can be resin-dominated or fiber-dominated failures. The failures can result from either strength-limited failures, which occur when unit stress exceeds the load-carrying capacity of the laminate; stiffness failures, which take place when displacements exceed the strain limit (elongation to failure) of the laminate; failure of the fiber to resin bonds; or debonding of the outer skins from the cores of sandwich laminate.

Tensile failure on composite materials is fairly rare because filament reinforcements are strongest in tension along their primary axis. Stress- or strain-limited failure with off-axis loading scenarios must be studied case by case, as resin and fiber mechanical properties vary widely in tension. Compressive failures in composites can occur at a very small scale, such as the compression or buckling of individual fibers. With sandwich panels, skin faces can wrinkle or the panel itself may become unstable. With the out-of-plane loading scenarios such as when a sandwich panel is subject to hydrostatic and hydrodynamic loads, the loaded side of the panel is in compression, the other side is in tension, and the core will experience shear stresses distributed across its thickness. Core shear failure, core-to-skin debonds, and skin failures (tension, compression, and local failure) should be considered with the bending failure modes.

For FRP composite vessels operating with higher speed in rough seas, dynamic and slamming loads may be much more pronounced. Large wave impact on hull structure, particularly the bottom panels, may lead to large plastic deformation. Because composites—with the exception of thermoplastic materials—have limited ability of plastic deformation, impact energy levels associated with severe bottom slamming can exceed the capability of the structure, leading to catastrophic failure. An early study in investigating sandwich panels with different core materials, different fiber types, and different resins is given in Jones (1983). Some more recent studies associated with the local strength of high-speed vessels are cited in Section 6.2. Composite structures are not subject to corrosion, can sustain long-term damage from water, ultraviolet light, and elevated temperature exposure.

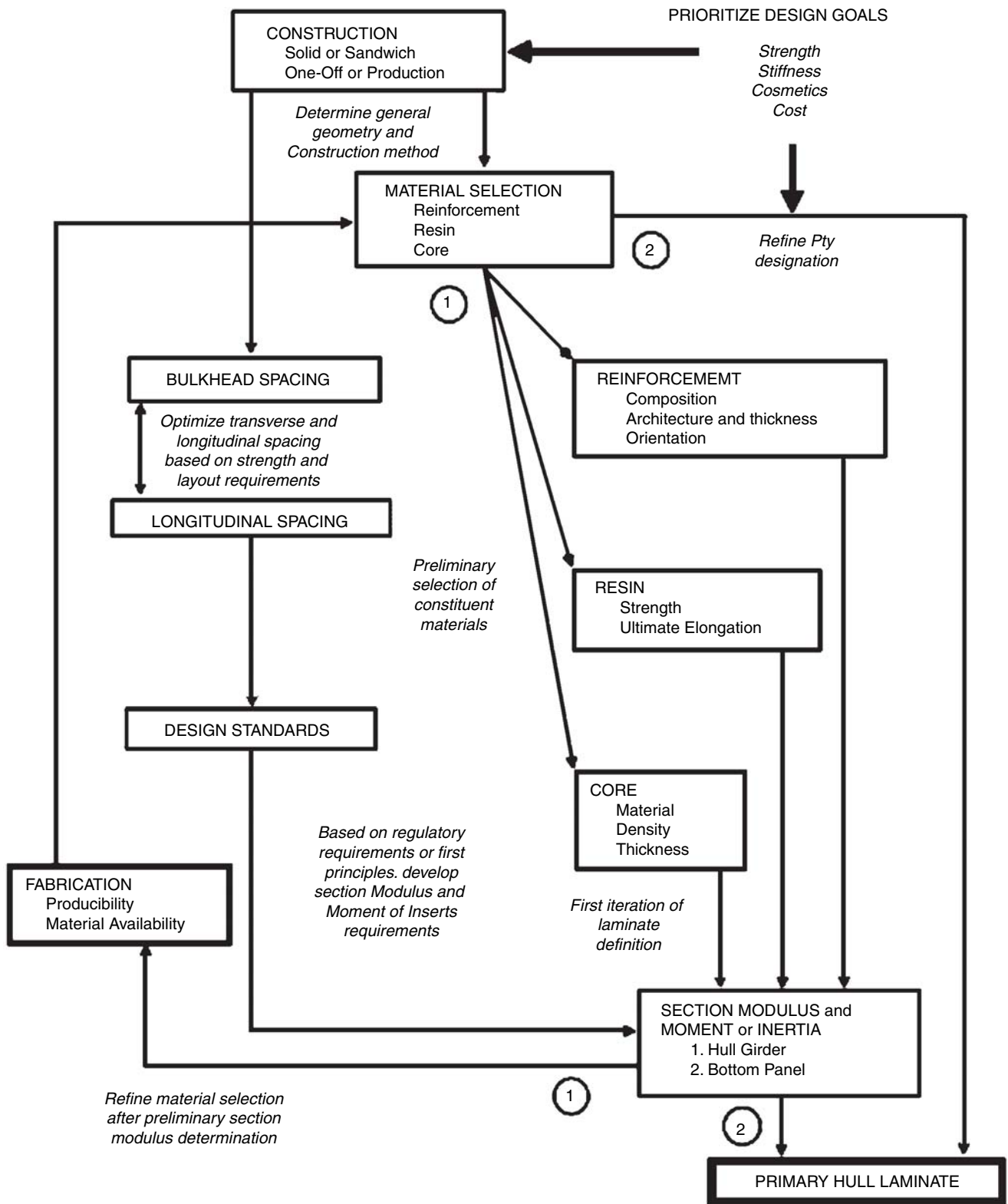


Fig. 167 Design flow chart for primary hull laminate. (SSC-403)

Another critical issue associated with the materials used in marine structures is the fire performance of the materials applied. Presently, steel is regarded by SOLAS as the reference structural material to be considered when assessing fire performance. Aluminum alloys can fulfill fire-safety requirements when suitably insulated. Composite materials based on organic matrices are flammable elements. In a fire, resins for general use will burn off, leaving only the reinforcement, which has no inherent structural strength. Glass-reinforced plastic laminates have high heat insulating properties, and when exposed to fire the resin burns, giving off noxious smoke. However, after burning off about 6 mm of resin the charred results form an insulating boundary.

The behavior of a given material system in a fire is dependent not only on the properties of the fuel but also on the fire environment to which the material system may be exposed. Extensive studies and test programs have been undertaken that are aimed at evaluating the fire properties to comply with published requirements such as the HSC Code for high-speed craft. Numerous papers concerning fire and FRP composites have also been published, but the vast majority concern aerospace applications whereas several address either offshore installations or naval ships. Materials and structures specifically for high-speed vessels in particular are still lacking. The composite structure must be insulated so that heat deflection temperature of the resin is not reached during the specified 30 or 60 min period under the test fire load. Fire tests on loaded GRP structures suggest that such a criteria may be conservative.

6.1.3.5 Tensile Failure. The tensile behavior of engineered composite materials is generally characterized by stress-strain curves. The key tensile failure terms including tensile strength, strain, yield point, elastic limit, modulus of elasticity, proportional limit, and so on are defined in ASTM specifications (1991). Tensile failures in plastics can be identified by some visible signs, including crazing (appearing as clean hairline fractures), cracks, and stress whitening. Large deflections of panels that are constrained laterally at the edges will produce tensile stresses on both sides of the panel due to membrane tension. Methodology for approximating deflections and stresses of isotropic plates when subjected to both bending and membrane stress can be found in the American Society of Civil Engineers (ASCE 1984).

6.1.3.6 Compressive Failures. The basic analytical methods for predicting compressive failures in solid and sandwich laminates can be found in U.S. Navy (1969) and U.S. Army Research Lab Composite Material Handbook. With sandwich panels of large unsupported span, buckling is likely to be the primary failure mode. If the core shear modulus is very low compared to the stiffness of the skins, crimping may be the first failure mode. For very thin skins and poor skin-to-core bonds, some type of skin wrinkling can result. Honeycomb cores with large cell size and thin skin can exhibit dimpling.

6.1.3.7 Bending Failures. The behavior of solid laminates and sandwich structures with stiff cores subjected to bending moments can be described by beam theory. Sandwich structures with relatively stiff cores efficiently transfer moments and shear forces between skins, and the total deflection of a beam is the sum of shear- and moment-induced displacement. In the case of sandwich laminates with soft cores, shear loads are not efficiently transmitted. As a result, the skins themselves carry a larger share of the load in bending about their own neutral axis. Shear and bending stress distribution for a simply supported beam is influenced by the shear flexibility, which is a function of panel span length and values of shear and bending stiffness (see ASCE 1984).

6.1.3.8 First Ply Failures. *First ply failure* is defined by the first ply or ply group that fails in a multidirectional laminate. The total number of plies, the relative stiffness of the plies, and the overall stress distribution determine the relationship between first ply failure and the last ply (ultimate) failure of the laminate. First ply failure can be strain-limited failure or stress-limited failure. Guidance of estimating strain-limited and stress-limited ply failures are provided in the ABS Rules (2001).

6.1.3.9 Creep. When composite materials are subjected to constant stress, strain in load path areas will increase over time. This is true particularly for the case of long-term loading. With long-term *creep*, the structural response is often characterized as viscoelastic, which is a combination of elastic and viscous behavior. The elastic behavior of material means that the material returns to its original shape after the release of load, and with viscous behavior there is no return to the original shape after the load is released. Composite material creep characteristics are presented by plotting strain versus time, usually using a log scale for time. Strain typically shows a steep slope at the initial time and gradually levels off to failure at some time. Loads, material composition, environment, and temperature all affect the degree of composite viscoelasticity, and therefore the system creep. Detailed information on composite creep is referred to ASCE (1984).

6.1.3.10 Fatigue Failures. A fundamental problem associated with engineering uses of FRP is the determination of the resistance to combined states of cyclic stress. Composite material exhibits very complex failure mechanisms under static and fatigue loading due to the anisotropic characteristics in strength and stiffness. In contrast to metals where the most common failure mechanism is a predominant single crack, there are four basic failure mechanisms in composite materials as a result of fatigue: matrix cracking, delamination, fiber breakage, and interfacial debonding. The different failure modes combined with the inherent anisotropies, complex stress distributions, and overall nonlinear response of composites lead to a situation that it is quite difficult to develop a general analytical theory to account for

all the possible failure processes in composite materials. Consequently, statistical methods using Weibull's distribution to describe fatigue life have been adopted (see Kim 1987; Talreja 1987). Another method used to describe fatigue behavior is to extend static strength theory to fatigue strength by replacing static strengths with fatigue functions (Sims & Brogdon 1977).

Fatigue failure of composite materials can be defined either as a loss of adequate stiffness or as a loss of adequate strength. Accordingly, there are two approaches to determine fatigue life, namely, constant stress cycling until loss of strength and constant amplitude cycling until loss of stiffness. The approach to use depends on the design requirements for the laminate. In general, stiffness reduction is an acceptable failure criterion for many components that incorporate composite materials. Stiffness change is a precise, easily measured, and easily interpreted indicator of damage that can be directly related to microscopic degradation of composite materials. Studies related to failure criteria of composites can be found in Hashin (1981), Chang et al. (1977), Highsmith and Reifsnider (1986), and Reifsnider et al. (1977). Sarkani et al. (1999) investigated the fatigue behavior of different composite joints and laminates under constant and random amplitude loading, and concluded that the well-known Palmgren-Miner fatigue damage hypothesis does not always accurately reflect the fatigue damage accumulation behavior in composite materials. A general review of fatigue behavior and fatigue damage prediction of FRP composite materials can be found in the ISSC (1997) Committee III.2 Report.

Although precise predictions of fatigue life expectancies for FRP laminates is currently beyond state-of-art analytical techniques, insight into relative performance of constituent materials can be obtained from test data. Burrall et al. (1986) presents a comparison of various polyester and vinyl ester resin formulations based on a series of fatigue tests on mat/woven roving laminates. With regard to reinforcement materials used in marine laminates, there is not a lot of comparative test data available to illustrate fatigue characteristics. Fatigue performance of reinforcement materials depends on its interface performance with resin. The construction and orientation of reinforcement also plays a critical role in determining fatigue performance. It is generally perceived that larger quantities of thinner plies perform better than a few layers of thick plies.

6.2 Design Approaches for Specialty Craft—High-Speed Mono-Hulls, Catamarans, Surface-Effect Ships, and Other Multi-Hull Craft. This section addresses some recent developments of classification requirements, loads, structural response, and strength evaluation that are related to the structural strength of high-speed vessels. High-speed craft are primarily the types of vessels that are covered by the International Code of Safety for High-Speed Craft (IMO 2000), also known as the HSC Code. These include high-speed mono-hulls, catamarans, surface-effect

ships, and other multi-hull crafts. Detail reviews of the structural design of such types of vessels can be found in the ISSC Specialist Committee V.2 Report (ISSC 2000).

As defined in the HSC Code, a high-speed light displacement craft is a craft that is capable of a maximum speed (in m/s) equal to or exceeding

$$V = 3.7(\nabla)^{0.1667} \quad (344)$$

where ∇ is the displacement corresponding to the design water line, in cubic meters. Equation (344) implies that for a vessel to be classed as high-speed, a 100-ton craft must have a maximum speed of at least 7.72 m/s (15 knots), whereas a 5,000-ton craft must have a maximum speed of at least 15.43 m/s (30 knots). Thus, the high-speed light displacement craft definition includes many fast-displacement ships as well as planing and semi-planing vessels. A more general definition of high-speed craft, unrelated to displacement, is

$$V = 2.36(L)^{0.5} \quad (345)$$

where V is the maximum speed in knots and L is the craft length in meters.

In contrast to conventional vessels, the operation of high-speed craft is restricted to specified environmental conditions, such that excessive wave loads can be avoided. The restriction of operation is the whole basis of the high-speed craft concept, which enables one to exclude the extreme load requirements that conventional vessels must consider. In essence, the philosophy of the HSC Code is based on management and reduction of risk rather than passive protection in case of an accident. Thus the HSC Code specifies requirements and guidance not only for the craft design but also for the operation of the craft, in contrast to the SOLAS framework applicable to conventional vessels. For that purpose, the HSC Code refers to well-defined specific conditions, namely, the normal operation conditions, the worst intended conditions, and the critical design conditions.

The *normal operation conditions* are those in which the craft will safely cruise at any heading while manually operated, auto-pilot assisted, or operated with any automatic control system in normal mode. The parameter defining these conditions is the horizontal acceleration in passenger spaces. The criteria given in the HSC Code for the normal operation conditions typically relates to comfort only. Thus, these conditions do not qualify the design of the vessel but only identify and formalize the operating conditions under which no specific operational care is required from the crew.

The *worst intended conditions* are the specific environmental conditions within which the intentional operation of the craft is provided for certification of the craft. These environmental conditions are restricted by the imposition of operational limits. In terms of performance, the craft in these conditions should to maintain a safe cruising operation without exceptional piloting skill.

The HSC Code explicitly describes requirements to be complied with and gives, among other things, criteria for horizontal acceleration level in passenger spaces and for the structural loads. These requirements relate to safety. The worst intended conditions describe the upper limit of the operational envelope under which the safe operation of the craft is proven and accepted for commercial use. These conditions include the ultimate weather conditions above which the craft is not authorized to sail. The worst intended conditions are not only linked with the operation of the craft but also address the craft design. In fact, these conditions are considered by the classification societies as the basis for structural design assessment (Thiberge 1999).

Using the significant wave height of the worst intended condition and referring to the sea state in which the craft can attain maximum service speed, a speed/significant wave height envelope can be developed. The average of the 1/100 greatest vertical accelerations at the LCG, corresponding to the speeds and significant wave heights of the envelope, is used to assess the strength of the bottom structure of the craft in accordance with classification society rules.

The *critical design conditions* are the limited specified conditions, chosen for design purposes, in which the craft should remain in the displacement mode. The HSC Code requires that the critical design conditions should be more severe than the worst intended conditions by a suitable margin to provide for adequate safety in survival conditions. The critical design conditions are considered to provide a safety margin for the uncertainties in the design process, such as design loads and structural responses.

6.2.1 Classification Societies Rules. The HSC Code deals with structures in a basic manner, providing only a generalized set of requirements without precise acceptance criteria. The structural requirements of high-speed vessels are covered in more detail by the scantling rules of the classification societies, which form the basis of the current design procedures. The requirements of classification rules were developed taking into account the unique characteristics associated with high-speed craft (i.e., higher speeds, small block coefficients, constructed with lightweight materials such as high strength steels, aluminum, and fiber reinforced polymer materials). Classification societies also accept the “direct calculations” or the “first principles approaches” in high-speed craft design to account for the recent trend of larger size of the crafts, for which the hull structures are more flexible with more pronounced dynamic behavior and experience higher stress levels.

Currently, there are four main sets of rules issued by the classification societies:

- American Bureau of Shipping (ABS) Guide for Building and Classing High-Speed Craft
- Det Norske Veritas (DNV) Rules for the Classification of High-Speed and Light Craft

- Lloyd’s Register (LR) Rules and Regulations for the Classification of Special Service Craft
- UNITAS (Germanischer Lloyd, Bureau Veritas, Registro Italiano Navale) Rules for Construction and Classification of High-Speed Craft.

The ABS Guide (ABS 2001) is applicable to high-speed craft of commercial or non-pleasure service with a speed in knots (m/s) not less than $2.36L^{1/2}$, where L is the craft length in meters. Applicable craft length depends on vessel type, for example, up to 130 m for mono-hulls, 100 m for multi-hulls, 90 m for surface effect ships, and 60 m for hydrofoils. When the length of craft constructed of steel or aluminum exceeds 61 m and when the length of craft constructed of FRP exceeds 50 m, or when the operation speed exceeds 25.72 m/s (50 knots), direct analysis is required for both hull girder strength and main supporting structure design. ABS direct calculation procedure is detailed in the “ABS Guide on Dynamic Load Approach (DLA) for High-Speed Crafts” (ABS 2002), which specifies the extreme wave load, equivalent wave, structural analysis, and acceptance criteria. In particular, emphases are made on whipping and vibration effects as well as the hydroelastic considerations for global and local structural responses. ABS requirements for high-speed crafts have recently been extended to cover the high-speed naval vessels, which was outlined in Curry and Novak (2001).

The DNV Rules (Det Norske Veritas 1999) apply to all types of craft for various materials of construction. The current version of DNV Rules is fully harmonized with the HSC Code, and covers naval surface craft. DNV has also issued a “Classification Note on the Strength Analysis of Hull Structures in High Speed and Light Craft” (DNV 1996), which specifies requirements for performing and documenting global and local finite element analyses, hydrodynamic analysis, and ultimate strength and fatigue strength analyses. Acceptance criteria for aluminum and steel structures are also given. Requirements of DNV direct calculation were reviewed in Pettersen and Wiklund (1999).

The LR Rules (Lloyd’s Register of Shipping 1998) covers all types of craft for various materials. The rules were officially introduced in 1996 and apply to craft greater than 24 m in length. Like other classification rules, LR Rules defines loads as well as strength criteria. Discussion on LR requirements can be found in Cheng and Turnbull (1995).

UNITAS, a collaboration between French, German, and Italian classification societies, has produced unified Rules for High Speed Craft (UNITAS 1997), which are formally issued by each respective society. The rules are arranged to augment the text of the IMO HSC Code with a necessarily large expansion to the chapter on hull structures. UNITAS Rules applies to all high-speed craft for various materials. Strength assessment procedures employed at the Bureau Veritas for global hull girder and local structures, such as bottom structure and

garage space structure, as well as acceptance criteria, including fatigue life prediction, can be found in Thiberge (1999).

Strength assessments carried out by the classification societies are based on the operational envelope but are differentiated dependent on operational restrictions imposed. Such restrictions are commonly expressed as limitations on significant wave height in which the vessel can operate, as in LR and UNITAS high-speed vessel rules, or on significant wave height and corresponding maximum speed, as in ABS high-speed craft rules, or on maximum distance from safe anchorage or refuge, as in DNV high-speed craft rules. Also, the design vertical acceleration is dependent on the operational restrictions and forms the basis of a formal operational envelope expressed as a relationship between speed and significant wave height. In addition, differences exist in the simplified load and structural response criteria among the class rules, and therefore different levels of structural weight. Fan and Mazonakis (1995) found that the different rules of ABS, DNV, and LR could lead to a weight range of 512 to 686 kg for a 1-m length of a midship section of an aluminum catamaran studied. Fan and Pinchin (1997) carried out a rudimentary weight comparison for structures designed according to LR, DNV, and Germanischer Lloyd (GL) rules and concluded that although the same conceptual approach is followed by each of the classification societies, there are differences in the derived scantlings.

Although there are some minor differences in the loads considered, the differences in scantlings are mainly due to the differences between the empirical formulas of load calculations contained in the rules. Fan and Pinchin (1997) further advocated the use of a “direct calculation” or “first principles” design methodology, which is in fact accepted by the classification societies. The direct calculation approach, such as ABS DLA for high-speed vessels, is meant to serve as an alternative to the explicitly stated local scantling requirements of classification rules, and is supplementary to the main class requirements. However, there remains a need for standardization of the direct calculation procedures employed by the classification societies. Besides, some of the differences in rule scantlings arise from the differing ways in which service restrictions, including the minimum plate thickness, corrosion margins, failure mode acceptance criteria, are handled by the respective societies. Because of this, some differences will remain even when direct calculation methods for loads and structural responses are unified. The recent advances of loading and structural response analyses for high-speed vessels are reviewed following, and further research needed for producing tools adequate for design purpose are also indicated.

6.2.2 Loads. This section is intended to highlight those aspects that are specific to loads related to structural strength analysis of high-speed vessels. A more comprehensive presentation of loads on ships in general is given in Beck et al. (2009) as well as in pre-

vious sections of this book. A thorough review of recent developments in load prediction methods, especially water impact problems, are presented in recent issues of the ISSC Technical Committee reports, proceedings of International Conference on Fast Sea Transportation (FAST), ITTC Loads and Responses Committee reports, and other reports. Detailed guidance for design loads and the specific load formulations of the HSC Code and classification rules can be found in respective documents.

6.2.2.1 Global Loads. High-speed craft require special consideration in their structural design, either because of the nature of the loads encountered, unusual configurations, or both. Because most of the high-speed vessels are intended for high-speed operation in rough seas, dynamic loads may be of much greater importance than for conventional ships.

In the case of high-speed mono-hulls, the global load types are basically the same as those of conventional vessels. The main differences are that in high-speed craft the impact or slamming loads can be more pronounced, and the global wave loads may contain higher-order load components that cannot be determined by linear methods (Karppinen et al. 1993; Leguen et al. 1997). In addition, due to greater speed and possibly a more flexible structure, the wave encounter frequency can be more likely closer to the lowest hull girder natural frequency, leading to springing with higher possibility. Some nonlinear hydrodynamic loads may also be associated with the springing vibration (see Friis-Hansen et al. 1995; Jensen & Wang 1998).

Procedures for computing hull girder load of high-speed vessels are available, such as the so-called high-speed strip theory (or $2\frac{1}{2}$ -dimensional theory) developed by Faltinsen and Zhao (1991a, 1991b), which has been extended to account for hull interaction (Hermundstad et al. 1999). Another computer code for high-speed vessels is the time domain three-dimensional nonlinear method by Kring et al. (1997). In the latter case, the SWAN computer code discussed in Section 2.5 was used to study motions and wave loads of fast mono-hull and multi-hull ships.

The linear, nonlinear frequency, and time-domain computer programs developed for sea-keeping analysis of conventional ships (Sections 2.3 and 2.5) were generally developed for low forward speed, and the range of its application to high-speed vessels must be validated. Zheng (1999) presented the study carried out by Lloyd's Register of Shipping and Kvaerner Masa Yards Technology to assess the global design loads of six designs of new generation of large, slender mono-hulls of lengths between perpendiculars of 155.80 to 175.80 m. The loads were calculated using three different sea-keeping programs and compared with the measured results from model tests.

The computer codes used for loading calculation are the program PRECAL, a linear three-dimensional sea-keeping program based on diffraction theory (Chen et al. 1988; CRS 1998); the program LR-Kryllo, a semi-empirical

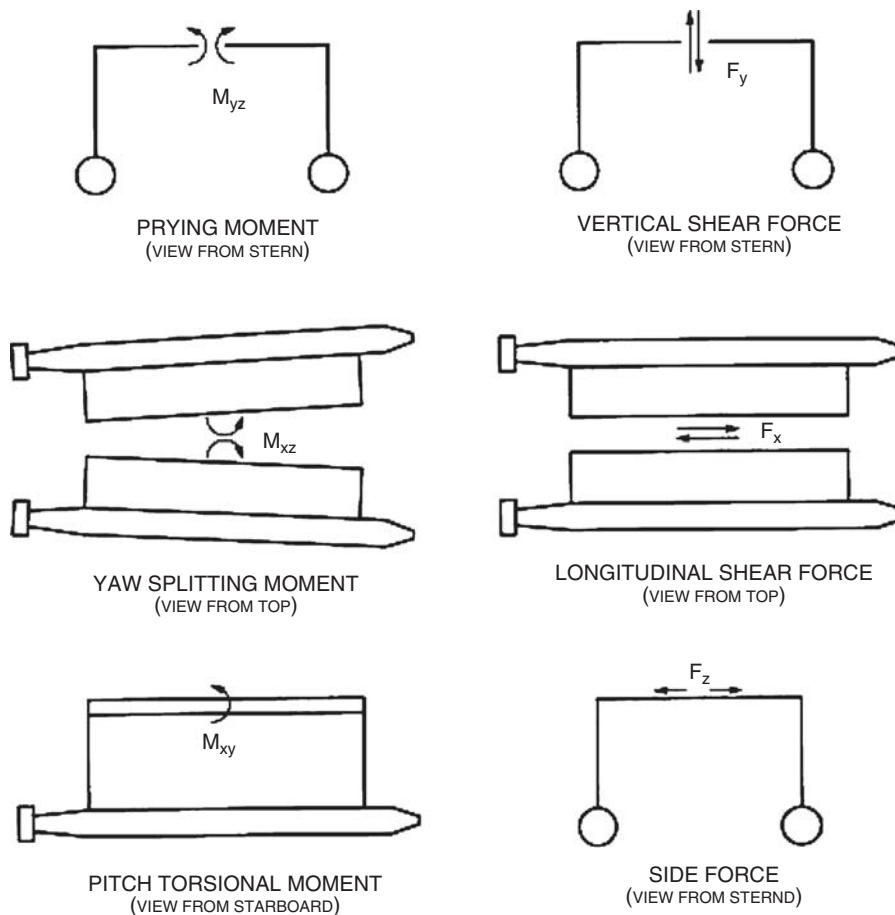


Fig. 168 New types of global loading of catamaran vessels.

prediction tool (Krylov 1995); and the quadratic strip theory (Dawkins 1985; Jensen & Pedersen 1979). The study indicates that for the case of low ship's speed of 1.03 m/s (2 knots), which corresponds to the survival speed in severe sea states, the numerical results compared well with tests for all three computer codes. For the case of 14.4 m/s (28 knots), which corresponds to a realistic operational speed for the vessels under consideration at the design sea-state of 5.0 m of significant wave height, the numerical results are substantially overpredicted at about 15 percent for hogging moments, and about 20 to 30 percent for sagging moments. Zheng (1999) further indicates that the LR Rules for Special Service Craft, as compared with the measurements, yields optimistic results for both hogging and sagging moments. The applicable speed range was also discussed in Werenskiold et al. (1999), where an approximate valid speed range for different theories, including two-dimensional, $2^{1/2}$ -dimensional, and three-dimensional linear, partly, or fully nonlinear, was suggested.

In addition to the valid speed range, the low-speed strip theory developed for conventional vessels cannot be used to predict wave-induced hull loads near zero

wave encounter frequency, which occurs most of the time in quartering and following seas. This is because terms inversely proportional to the encounter frequency will be infinite at zero encounter frequency. Even the high-speed strip theory has limitations when applied to high-speed vessels. The high-speed strip theory is valid only when there are no waves propagating from the stern to the bow, which is fulfilled when the Froude number is larger than 0.4 (Faltinsen & Zhao 1991a, 1991b). Furthermore, the applicability of high-speed theory in quartering and following seas still requires further verification (Heggelund et al. 2001).

In multi-hull vessels, there are several types of loads that are not encountered in mono-hulls. In twin-hull vessels (catamarans), the new types of loading are the vertical shear force, longitudinal shear force, side force, prying moment, yaw-splitting moment, and pitch torsional moment (pitching connecting moment), as shown in Fig. 168 (from ABS 1999). All are in the cross structure connecting the lower hulls (demi-hulls).

Early development of sea-keeping analysis methods for twin-hull vessels can be found in Lee and Curphey (1977), whereas early catamaran model tests for motion

and load measurements can be found in Wahab et al. (1975). Some of the sea-keeping computer programs originally developed for mono-hull analysis are extended to handle twin or multi-hull vessels, such as programs PRECAL, SWAN, and the high-speed strip theory, which is embodied in program VERES (Fathi 1998).

In twin-hull catamaran design, there is no general rule for determining whether primary transverse loads, longitudinal loads, or other load components are more decisive. The design consideration requires all to be studied case by case. For example, Hadler et al. (1974) found from their studies of the oceanographic research ship USNS *Hayes* that the most critical loadings on this structure were the prying moment and vertical shear. Patrakka et al. (1995) suggested that the splitting moment is the more dominant loading for large catamarans.

In computing the global loads of a twin-hull catamaran, the transverse global loads can be treated in a traditional way by analyzing a transverse strip of the catamaran structure. The antisymmetric loading, producing the pitch torsional (or pitch connecting) moment, is less straightforward. The pitch torsional moment calculated by direct integration of external wave loads is not a particularly useful quantity when calculating the structural stresses. The physical reason for this is that the vertical shear forces exerted on each other by the demi-hulls are distributed in a complex manner along the length of the cross structure. The catamaran hull girder behaves in this case like an open section beam, which under torsion is statically indeterminate, and exhibits warping torsion. This phenomenon is similar to the torsion problem encountered in open mono-hull ships, such as container ships.

As previously described, the high-speed vessels are more vulnerable to nonlinear loads, resulting from the nonlinear hydrodynamic loads and the effects of whipping and springing responses. The major contribution to nonlinearity in hydrodynamic loads is the nonlinear Froude-Krylov and restoring forces caused by nonvertical sides of the ship. The effects of whipping and springing result mainly from bow impact and bottom and wet-deck slamming. For nonlinear problems involved with high-speed vessels, mono-hulls, or multi-hulls, one cannot expect the independent maxima to be Rayleigh-distributed. In this case, the proper distribution of extreme values and the associated parameters must be found from a large number of nonlinear time domain simulations. To avoid these time-consuming analyses, the common practice is to use a design or equivalent wave system obtained from complete stochastic analyses based on linear ship motion theory. The effect of nonlinear hydrodynamic loading is accounted for through a correction factor, or a nonlinear time domain simulation in the design wave. The procedure of this type is generally used in the direct calculation methods of the classification societies, such as the ABS DLA (ABS 2002), DNV Classification Note 30.8 (DNV 1996), and LR Guidance Notes (LR 1996). The design wave approach

is also illustrated in Heggelund et al. (2001), where the high-speed strip linear theory (Faltinsen & Zhao 1991a, 1991b; Hermundstad et al. 1999) was applied to a 60-m catamaran.

In addition to the assessment of practical methods for determining design loads for non-planning high-speed catamarans, the study of Heggelund et al. (2001) also reviewed different models for transverse strength analysis of twin-hull vessels and relevant criteria for predicting operational limits. The study shows that at the operational speed, the calculated maximum sagging moment in regular waves is increased by 10 percent when controllable foils are used. In this case, the extreme vertical bending moment is at approximately the same level as the design moment given by classification rules. In even rougher conditions allowed at reduced speed, effects such as wet-deck slamming, bow diving, and so on give important contributions to the nonlinear wave loads, and the design loads for the wave-induced vertical bending moment given by the classification rules were not conservative. This conclusion seems to be in line with that obtained by Zheng (1999) for high-speed mono-hulls, implying the need of further investigation of proper calculation methods for high-speed hull girder loads.

6.2.2.2 Local Loads. The local loads of high-speed vessels are basically the same as those for conventional vessels. The main sources of local loads are:

- Static and dynamic loads due to the weight and acceleration of the mass of the structure itself
- Static and dynamic loads due to passengers, cargo, and vehicles carried by the vessel, including liquids in tanks
- Static and dynamic pressures on water-exposed parts due to contact with the sea, including those associated with bottom, bow flare and wet-deck slamming, green water on deck, and hydrodynamic wave pressures
- Pulsating pressures induced by high-power waterjets, which can cause vibration and fatigue in local structures near the propulsion device. This phenomenon can also involve flow-induced vibration with interaction between the structure and the fluid flow.
- Forces due to impact with objects floating or submerged in the water and due to berthing, objects dropping on decks, and so on, which can be a significant problem for high-speed craft. Such loads are rarely the subject of an explicit calculation but are treated indirectly either through minimum thickness requirements or, occasionally, by special testing of impact resistance.

Much research has concentrated on slamming and impact loads on hull and cross structures. These still represent the greatest uncertainty among local loads. Design procedures and classification rules for high-speed craft often use vertical acceleration at the LCG as a fundamental parameter in determining slamming pressures, as in the well-known approach developed by Heller and Jasper (1960), and Allen and Jones (1978). When slamming forces are the dominant forces on the vessel, the

magnitude of induced vertical acceleration gives a good indication of the slamming forces. This is the case particularly with smaller planing craft. For large high-speed craft, the slamming forces induce identifiable vertical acceleration peaks, but such forces and accelerations have short duration and are in many cases only a minor part of the total forces and accelerations experienced by the vessel. The slamming forces then have little effect on the vessel's motions, and slamming can be neglected when the motions are calculated. Thus, for large high-speed craft the vertical acceleration is not as relevant a parameter as for smaller craft—rather, the relative velocities and angle between the structural part and the water surface at the point of impact are more important parameters.

There have been a number of cases of slamming damage to yachts and high-speed crafts. It has become clear that some classification societies' rule indicate too low vertical accelerations and effective slamming pressures for craft exposed to severe conditions (Brown et al. 1996). Several studies on the acceleration were carried out based on measurements with patrol and experimental craft by Heller and Jasper (1960), Allen and Jones (1978), Merchant and Stevens (1990), and Haymen et al. (1991). These studies suggest that vertical accelerations of 5 to 7 g can be expected at the LCG of such vessels, whereas crews are either unwilling or unable to tolerate vertical accelerations over about 6 to 7 g. Such high accelerations are associated with severe slamming events and high slamming pressure, and are considerably greater than assumed in some classification rules. Generally, the duration of these high accelerations is so short that the hull structure does not have time to fully respond before the load is no longer present. Consequently, the loads corresponding to these greater accelerations are not experienced by the hull structure. The accelerations in some classification rules are considered of a duration that the associated wave impact forces are fully experienced by the structure.

6.2.3 Structural Response and Strength. High-speed vessels require the use of lightweight materials such as high tensile steels, aluminum, or FRP to reduce weight. The reduction in weight also leads to new structural concepts exploiting the whole strength potential of materials. The consequences of this are generally greater utilization in relation to the material strength and higher flexibility of structures, resulting often in fatigue problems and a more pronounced dynamic structural behavior. In addition, the trend to increased speed leads to higher wave encounter frequency, to higher-order load components, and to generally greater and more transient loads. As a result, fatigue, buckling, and ultimate strength in multi-axial stress states require special attention.

In the area of local strength of high-speed vessels, most recent studies are concentrated on the responses of lightweight materials. For example, Kaneko et al. (1993) performed analysis of craft with aluminum honeycomb panels by introducing an equivalent rigidity. Kristensen

and Moan (1999) investigated the collapse strength of rectangular aluminum plates under uni-axial and bi-axial compressive stresses. Studies on behaviors of composite sandwich panels and FRP plate panels were presented by Falk et al. (1995), Riber (1995), Vredeveltdt and Janssen (1998), Shenoj et al. (1995), McGeorge et al. (1998), and Hayman et al. (1998).

For the global strength of high-speed vessels, recent studies have been carried out in various areas, such as the ultimate bending moment of mono-hull fast ferries by Boote et al. (1999), and the effects of superstructures on global structural responses by Yamamoto et al. (1993). Heggelund et al. (1999) compared classification rules criteria of global loads and load effects in catamarans obtained from direct calculation procedures. The direct calculation was performed through the quasi-static finite element structural analyses based on loads calculated using the high-speed strip theory for sea-keeping analysis and the linear stochastic long-term prediction approach for the extreme value of loading.

As described previously, the use of lightweight structural materials for high-speed vessels tends to introduce a greater flexibility of the structure. Also, the increase of service speed will cause greater wave encounter frequency and larger dynamic amplification of the elastic structural responses. Consequently, fluid-structure interaction or hydroelastic effects are often observed in various dynamic responses of high-speed vessels.

Typical hydroelastic phenomena are divided into two categories. One is global structural dynamics, such as wave-induced springing or slamming-induced whipping, and the other is local dynamic behavior of panels to slamming pressure. Brief reviews for related topics are given in the following sections.

6.2.3.1 Global Structural Dynamic Responses. In contrast to quasi-static analysis, wherein structural responses can be statically determined and sectional forces (shear forces and bending moments) can be obtained by the use of equilibrium conditions combined with direct integration of wave and inertial loads, in hydroelastic analysis the structure is statically indeterminate. That is, the deflection of the structure must be first solved before stresses and sectional forces can be determined. In the statically indeterminate case, the direct integration of external loads to obtain sectional forces may be misleading, and some of the load quantities obtained in this manner may be irrelevant especially in high-speed multi-hull vessels.

In some cases, there is a true interaction of loads and responses, and one cannot treat them separately. These are the special cases of hydroelastic problems in wet-deck slamming, where the elastic deflections have a significant effect on the hydrodynamic loads and vice versa—which will be further considered. On the other hand, global loads on ships are not normally significantly affected by elastic deformations because the rigid body motions are dominant. In this case, the external loads such as slamming impacts can be first separately

determined and then applied to the elastic structure. The ensuing dynamic behavior of the ship is a hydroelastic phenomenon but basically similar to the linear problem of an elastic body vibrating in water. Examples considered in Section 3.14 are of this category.

Whipping-induced transient stresses are superimposed on the quasi-static stresses, and the resulting stress-time history cannot be directly treated in the frequency domain using a conventional statistical approach for fatigue life prediction. Instead, cycle-counting methods in the time domain (for example, the rainflow counting algorithm) must be applied. Recent studies in this respect can refer to Friis-Hansen et al. (1994, 1995), where the rainflow counting is applied for the response to a cluster of slamming impacts of high-speed vessels. Jensen and Wang (1998) describe a hydroelastic analysis of a fast mono-hull container ship including whipping and springing. Wu and Moan (1996) present generalized procedures for the linear and nonlinear hydroelastic analyses of high-speed vessels. The linear theory, which is developed based on the linear motion, is applicable to mono-hulls as well as catamarans, whereas the nonlinear theory, based on the nonlinear wave-induced loads resulting from large ship motions in heave and pitch, is applicable for mono-hulls in head or following seas.

6.2.3.2 Wet-Deck Slamming. The dynamic response of the wet-deck induced by slamming is representative of the local structure dynamic behaviors of high-speed vessels. The wet-deck is the lowest part of the cross structure that connects the two side hulls of a catamaran, or the two demi-hulls of a SWATH ship. The wave impact on the wet-deck may cause severe local loads, as well as whipping of the hull girder. Different physical effects may influence the slamming load. The compressibility of water will have small effects on the maximum slamming-induced stresses, and is therefore usually neglected in structural analysis. When the local angle between the water surface and the structure is small, an air pocket may be trapped between the structure and water surface. However, the effect of an air pocket has not thus far been taken into account in structural analysis, but its effects are identified in measured results of model tests.

The large hydrodynamic loads that occur during wave impacts may yield local time-dependent deformations of the structure, which again will influence the load. As previously mentioned, this effect is referred to as hydroelastic. Hydroelasticity is particularly important for wave impacts on flexible structures with small angles between the structure and the water surface, which is often the case of wet-decks. Both the maximum structural responses (stress levels) and the influence of hydroelastic effects depend on a combination of relative impact velocity and the angle between the structure and the water surface, as well as the structural (mostly the bending) stiffness. For impacts with zero or very small angles, the maximum stress levels are approximately proportional

to the relative impact velocity and almost independent of the radius of curvature of the incident waves, unless for very small values of radius of curvature. When the angle between the structure and the water surface increases, the maximum stress levels decrease and the response will finally become quasi-static, for which case the maximum stress levels are approximately proportional to the relative normal impact velocity squared and inversely proportional to the relative angle.

A number of studies on slamming against elastic bodies relevant to wet-deck slamming have recently been carried out. Examples are the theoretical works by Kvalsvold (1994), Faltinsen (1997), and Haugen (1999), and the experimental studies by Aarsnes (1994, 1996). In these studies, a part of the wet-deck was modeled theoretically as two-dimensional beams consisting of the bottom plate and longitudinal stiffeners between two or four transverse frames. The experiments were carried out as drop tests where horizontal or pitched flat plates of aluminum and steel, modeled with two or four transverse frames, were dropped on waves. To investigate slamming on wedge-shaped wet-decks, a three-dimensional model of both the structure as well as the hydrodynamic fluid flow was developed by Faltinsen (1999). A general review of recent advances in wet-deck slamming is given in Haugen and Faltinsen (1999).

Different from the global dynamic responses, where the slamming loads can be determined separately and then applied to the elastic structure, the wet-deck slamming is truly a hydroelastic problem where the loads cannot be determined in isolation. This is particularly true when the angle between the structure and the water surface is small and the impact is large. For this case, if the loads are specified the structural model used in determining these loads must also be specified, or the flexibility and dynamics of the structures must be incorporated in the load formulation. To illustrate this phenomenon, we consider a flat wet-deck of a catamaran in long crested waves, for which a beam model consisting of a longitudinal stiffener and the attached bottom plate of a width equal to the spacing between longitudinal stiffeners is introduced. The beam model is with a length between four transverse frames, and the axial and shear deformations and rotary inertia are neglected (i.e., the beam is considered as an Euler beam), and only a two-dimensional problem is addressed. The governing equation of motion for this case can be expressed as

$$M_B(\ddot{w}(x, t) + \dot{V}(t)) + EI \frac{\partial^4 w(x, t)}{\partial x^4} = p(x, w, t) \quad (346)$$

where M_B is the mass per unit length of the beam divided by the width of plate. The term EI is the bending stiffness, where E is the Young's modulus and I is the moment of inertia of sectional area of the beam divided by the width of plate. The term $V(t)$ in equation (346) is the global velocity due to ship motion,

t is the time, and the dots are the time derivatives. The term $p(x, w, t)$ is the hydrodynamic impact pressure, which is a function of both time, space, and the beam deflection. The governing beam equation of motion is solved by a modal analysis where the beam deflection is expressed by a linear combination of a complete set of functions, such as the dry eigenmodes of the beam model, which in turn can be expressed by trigonometric and hyperbolic functions. The solution of equation (346) will not be pursued here, but rather reference is made to Haugen and Faltinsen (1999), where one of the procedures of solving the beam equation of motion is outlined.

The previous example illustrates some basic background consideration in conjunction with the wet-deck slamming. However, to predict the wet-deck slamming on full-scale vessels accurately it is important to describe the wave elevation and relative normal impact velocities correctly. In this connection, the effects of hull interaction on wave elevation and fluid flow in the impact area between the side hulls, as well as the short crested incident waves, require further investigation for establishing a more refined three-dimensional slamming analysis procedure.

6.2.3.3 Fatigue Strength. General fatigue considerations and aspects regarding material characteristics and fatigue strength assessment as well as design procedures in conventional ships are valid in high-speed vessels. However, due to the lightweight materials used in construction, the hull structures of high-speed vessels are more flexible, for which dynamic phenomena such as springing and whipping are more pronounced. In addition, its greater speed leads to greater encounter wave frequencies and generally larger motions, causing greater and more transient loads as well as higher-order load components. Furthermore, high-speed vessels are quite often operated close to their design limits. As a result, fatigue is a more pronounced design factor in high-speed vessels than for conventional ships.

The previously mentioned factors also tend to increase the number of stress cycles as well as stress amplitudes due to dynamic amplification. Nonlinear loads and dynamic structural responses both result in a nonlinear relationship between wave amplitude and stresses. As such, spectral fatigue analysis based on linearity assumptions has limited applicability to high-speed vessels. Friis-Hansen et al. (1994, 1995) performed a long-term springing analysis for some mono-hull vessels of lightweight materials. In this study, it was shown that the nonlinearity in the hull girder is important for the fatigue damage estimate, and that the cumulative damage may be increased by an order of magnitude as compared to a linear, rigid body analysis.

Fatigue strength evaluation procedures can be found from the classification high-speed vessel rules, as well as in recently published studies such as Skjelby et al. (1999), where a procedure of fatigue life prediction

on high-speed craft based on direct load transfer from hydrodynamic analysis to finite element models was present. Hermundstad and Wu (1999) studied three different methods, namely, beam theory, pressure-application, and modal analysis for calculation of stresses in ship structures. All three methods were applied to a high-speed mono-hull and a catamaran for stress and fatigue damage calculation, where the nonlinearity due to springing or whipping was not considered. Berstad and Larsen (1997) established a procedure for calculating accumulated fatigue damage in hull structural details of high-speed vessels.

Some studies on fatigue strength of lightweight materials are reviewed and given in ISSC Specialist Committee V.2 Report (ISSC 2000). More recently, Polezhaeva and Malinowski (2001) described an experimental and numerical study on the fatigue strength of two common structural details found in aluminum ship designs, namely, the floor-to-frame connection and longitudinal stiffener-to-transverse web connection. Full-scale models of these connections were tested under static and dynamic loads to obtain stress distributions at critical locations and nominal S-N curves. Finite element structural analysis was performed for the hot-spot stress distributions, which were compared with the measured data.

REFERENCES

- Aarsnes, J. V. (1994). An experimental investigation of the effect of structural elasticity on slamming loads and structural response. Technical Report, Norwegian Marine Technology Research Institute.
- Aarsnes, J. V. (1996). Drop tests with elastic 3-beam model. Effect of forward speed. Technical Report, Norwegian Marine Technology Research Institute.
- Abramson, R. L., Bass, R. L., Faltinsen, O. M., and Olsen, H. A. (1974). Liquid sloshing in LNG carriers. Proceedings of the Tenth Symposium of Naval Hydrodynamics.
- Adamchak, J. C. (1982). ULTSTR: A program for estimating the collapse moment of a ship's hull under longitudinal bending. David W. Taylor NSRDC Report DTNSRDC-82/076, October.
- Adeegest, L., Braathen, A., and Vada, T. (1998). Evaluation of methods for estimation of extreme nonlinear ship responses based on numerical simulations and model tests. Proceedings of the 22nd Symposium of Naval Hydrodynamics, Washington, D.C.
- Admiralty Ship Committee (1953). *S.S. Ocean Vulcan* sea trials. Report No. R8.
- Aertssen, G. (1969). Service—Performance and trails at sea. 12th International Towing Tank Conference (ITTC).
- Akita, Y. (1967). Dynamic pressures of cargo oil due to pitching and effectiveness of swash bulkhead in long tanks. Report No. 62, *Japan Shipbuilding & Marine Engineering*, September.

t is the time, and the dots are the time derivatives. The term $p(x, w, t)$ is the hydrodynamic impact pressure, which is a function of both time, space, and the beam deflection. The governing beam equation of motion is solved by a modal analysis where the beam deflection is expressed by a linear combination of a complete set of functions, such as the dry eigenmodes of the beam model, which in turn can be expressed by trigonometric and hyperbolic functions. The solution of equation (346) will not be pursued here, but rather reference is made to Haugen and Faltinsen (1999), where one of the procedures of solving the beam equation of motion is outlined.

The previous example illustrates some basic background consideration in conjunction with the wet-deck slamming. However, to predict the wet-deck slamming on full-scale vessels accurately it is important to describe the wave elevation and relative normal impact velocities correctly. In this connection, the effects of hull interaction on wave elevation and fluid flow in the impact area between the side hulls, as well as the short crested incident waves, require further investigation for establishing a more refined three-dimensional slamming analysis procedure.

6.2.3.3 Fatigue Strength. General fatigue considerations and aspects regarding material characteristics and fatigue strength assessment as well as design procedures in conventional ships are valid in high-speed vessels. However, due to the lightweight materials used in construction, the hull structures of high-speed vessels are more flexible, for which dynamic phenomena such as springing and whipping are more pronounced. In addition, its greater speed leads to greater encounter wave frequencies and generally larger motions, causing greater and more transient loads as well as higher-order load components. Furthermore, high-speed vessels are quite often operated close to their design limits. As a result, fatigue is a more pronounced design factor in high-speed vessels than for conventional ships.

The previously mentioned factors also tend to increase the number of stress cycles as well as stress amplitudes due to dynamic amplification. Nonlinear loads and dynamic structural responses both result in a nonlinear relationship between wave amplitude and stresses. As such, spectral fatigue analysis based on linearity assumptions has limited applicability to high-speed vessels. Friis-Hansen et al. (1994, 1995) performed a long-term springing analysis for some mono-hull vessels of lightweight materials. In this study, it was shown that the nonlinearity in the hull girder is important for the fatigue damage estimate, and that the cumulative damage may be increased by an order of magnitude as compared to a linear, rigid body analysis.

Fatigue strength evaluation procedures can be found from the classification high-speed vessel rules, as well as in recently published studies such as Skjelby et al. (1999), where a procedure of fatigue life prediction

on high-speed craft based on direct load transfer from hydrodynamic analysis to finite element models was present. Hermundstad and Wu (1999) studied three different methods, namely, beam theory, pressure-application, and modal analysis for calculation of stresses in ship structures. All three methods were applied to a high-speed mono-hull and a catamaran for stress and fatigue damage calculation, where the nonlinearity due to springing or whipping was not considered. Berstad and Larsen (1997) established a procedure for calculating accumulated fatigue damage in hull structural details of high-speed vessels.

Some studies on fatigue strength of lightweight materials are reviewed and given in ISSC Specialist Committee V.2 Report (ISSC 2000). More recently, Polezhaeva and Malinowski (2001) described an experimental and numerical study on the fatigue strength of two common structural details found in aluminum ship designs, namely, the floor-to-frame connection and longitudinal stiffener-to-transverse web connection. Full-scale models of these connections were tested under static and dynamic loads to obtain stress distributions at critical locations and nominal S-N curves. Finite element structural analysis was performed for the hot-spot stress distributions, which were compared with the measured data.

REFERENCES

- Aarsnes, J. V. (1994). An experimental investigation of the effect of structural elasticity on slamming loads and structural response. Technical Report, Norwegian Marine Technology Research Institute.
- Aarsnes, J. V. (1996). Drop tests with elastic 3-beam model. Effect of forward speed. Technical Report, Norwegian Marine Technology Research Institute.
- Abramson, R. L., Bass, R. L., Faltinsen, O. M., and Olsen, H. A. (1974). Liquid sloshing in LNG carriers. Proceedings of the Tenth Symposium of Naval Hydrodynamics.
- Adamchak, J. C. (1982). ULTSTR: A program for estimating the collapse moment of a ship's hull under longitudinal bending. David W. Taylor NSRDC Report DTNSRDC-82/076, October.
- Adeegest, L., Braathen, A., and Vada, T. (1998). Evaluation of methods for estimation of extreme nonlinear ship responses based on numerical simulations and model tests. Proceedings of the 22nd Symposium of Naval Hydrodynamics, Washington, D.C.
- Admiralty Ship Committee (1953). *S.S. Ocean Vulcan* sea trials. Report No. R8.
- Aertssen, G. (1969). Service—Performance and trails at sea. 12th International Towing Tank Conference (ITTC).
- Akita, Y. (1967). Dynamic pressures of cargo oil due to pitching and effectiveness of swash bulkhead in long tanks. Report No. 62, *Japan Shipbuilding & Marine Engineering*, September.

- Allen, R. G., and Jones, R. R. (1978). A simplified method for determining structural design-limit pressures on high performance marine vehicles. Proceedings of the AIAA/SNAME Advance Marine Vehicle Conference, San Diego, California.
- Allen, R. G., and Jones, R. R. (1977). Consideration in the structural design of high performance marine vehicles. New York Metropolitan Section, SNAME, January.
- Alsos, H. S. and Amdahl, J. (2005). Intentional Grounding of Disabled Ships, Marine 2005 - Computational Methods in Marine Engineering, Oslo, Norway, June.
- Amdahl, J. (1983). Energy absorption in ship-platform impacts. Doctoral thesis, Norwegian Institute of Technology, Trondheim, Norway.
- Amdahl, J., Kavlie, D., and Johansen, A. (1995). Tanker grounding resistance. Sixth International Symposium on Practical Design of Ships and Mobile Units (PRADS'95), Seoul, South Korea, 2:1072–1083.
- American Bureau of Shipping (1975). Rules for building and classing aluminum vessels.
- American Bureau of Shipping (1978). Provisional rules for building and classing or certifying reinforced plastic vessels.
- American Bureau of Shipping (1978). Rules for building and classing reinforced plastic vessels.
- American Bureau of Shipping (1983). Rules for building and classing steel vessels under 61 meters (200 feet) in length.
- American Bureau of Shipping (1985). ABS/ShipMotion program—Theory.
- American Bureau of Shipping (1987a). Rules for building and classing steel vessels.
- American Bureau of Shipping (1987b). Rules for building and classing mobile offshore drilling units.
- American Bureau of Shipping (1993). Commentary documents of SafeHull criteria development.
- American Bureau of Shipping (1994). *Guide for Building and Classing Offshore Racing Yachts*.
- American Bureau of Shipping (1995). Guide for assessing hull girder residual strength for tankers.
- American Bureau of Shipping (1995). Guide for assessing hull girder residual strength for bulk carriers.
- American Bureau of Shipping (1997). Requirements for materials and welding—Aluminum and fiber reinforced plastics (FRP), Sections 4 and 5.
- American Bureau of Shipping (1997). *Rules for Building and Classing Offshore Installations*.
- American Bureau of Shipping (1999). Guide for building and classing small water plane area twin hull (SWATH).
- American Bureau of Shipping (2000). *Guide for Building and Classing Motor Pleasure Yachts*.
- American Bureau of Shipping (2001). Guide for building and classing high-speed craft.
- American Bureau of Shipping (2002). Guide on dynamic load approach for high speed craft.
- American Bureau of Shipping (2002). *Guide for Building and Classing Membrane Tank LNG Vessels*.
- American Bureau of Shipping (2006). Guide for SafeHull-dynamic loading approach vessels.
- American Bureau of Shipping (2008). Rules for building and classing steel vessels.
- American National Standards Institute (1977). Standard specification for aluminum alloy sheet and plate. ANSI/ASTM B-209-77.
- American Petroleum Institute (1987). Bulletin on design of flat plate structure. *API Bulletin*, 2V.
- American Society of Civil Engineers (1984). Structural plastics design manual. *ASCE Manual and Reports on Engineering Practice*, No. 63, New York.
- American Society of Testing and Materials (1991). Test methods for tensile properties of plastics. D 638-89, D 638M-89, ASTM, West Conshohocken, Pennsylvania.
- Anderson, T. L., et al. (1987). The benefits of new high-strength low-alloy (HSLA) steels. *Welding Journal*, September.
- Ang, A. H-S., and Tang, W. H. (1975). *Probability Concepts in Engineering Planning and Design*. New York: John Wiley & Sons.
- Arai, M., and Matsunaga, K. (1989). A numerical study of water entry of two-dimensional ship shaped bodies. PRADS '89, Varna, Bulgaria.
- Arai, M., Cheng, L. Y., and Inoue, Y. (1994). 3-D numerical simulation of impact load due to liquid cargo sloshing. *Journal of the Society of Naval Architects of Japan*.
- Bai, J. (2006). Time-variant ultimate strength reliability assessment of ship hulls considering corrosion and fatigue. Doctoral thesis, University of California, Berkeley.
- Band, E. G. U. (1966). Analysis of ship data to predict long-term trends of hull bending moments. *American Bureau of Shipping*, November.
- Bannerman, D. B., and Jan, H. Y. (1980). Analysis and design of principal hull structure. In: Taggart, R. (ed.), *Ship Design and Construction*, Chapter 6, Jersey City, NJ: published by SNAME.
- Bass, R. L., Hokanson, J. C., and Cox, P. A. (1976). Verification of LNG tank loading criteria. Ship Structure Committee Report SSC-258.
- Bauger, O. (1998). Alloy development. Third International Forum on Aluminum Ships, Haugesund, Norway.
- Beck, R. S., Dalzell, J., Faltinsen, O., and Reed A. M. (2009). Motions in waves. In: Paulling, J.R. (ed.), *Principles of Naval Architecture: The Series*, Jersey City, NJ:SNAME.
- Bennet, R., Ivarson, A., and Nordenström, N. (1962). Results from full-scale measurements and predictions of wave bending moments acting on ships. Report No. 32, Gothenburg, Sweden: Swedish Ship Research Foundation.
- Berstad, A. J., and Larsen, C. M. (1997). Fatigue crack growth in hull structure of high-speed vessels. Proceedings of the Fourth International Conference on Fast Sea Transportation (FAST '97), Sydney, Australia.

- Bertram, V., and Lamb, T. (2003). Hull materials and welding. In: Lamb, T. (ed.), *Ship Design and Construction*, Chapter 20, Jersey City, NJ: SNAME.
- Billingsley, D. W. (1980). Hull girder response to extreme bending moments. Spring Meeting/STAR-SNAME.
- Birmingham, J. T. (1971). Longitudinal bending moment predictions derived from results of seven ship trials. DTNSRDC Report 3718.
- Bishop, R. E. D., et al. (1978). A unified dynamic analysis of ship response to waves. *Transactions*, RINA, Vol. 120.
- Bitner-Gregersen, E. M., Guedes Soares, C., and Silvestre, A. (1998). On the average wave steepness. Wave '98, Houston, Texas.
- Bjoneboe, N., Simonsen, B. C., Hansen, P. F. (1999). Statistical and theoretical analysis of ship grounding accidents. 18th International Conference on Offshore Mechanics and Arctic Engineering (OMAE'99), St. Johns, Newfoundland, Canada.
- Bleich, F. (1952). *Buckling Strength of Metal Structures*. New York: McGraw Hill.
- Bleich, H. H. (1953). Nonlinear distribution of bending stresses due to distortion of the cross section. *Journal of Applied Mechanics*, March, 95–104.
- Blok, J. J. (1995). Model tests on green water loading—VLCC model. Final Report, MARIN, prepared for Netherlands Ship Model Basin Cooperative Research Ships (NSMB CRS).
- Bockenbauer, M. and Egge, E. D. (1995). Assessment of the collision resistance of ships for classification purposes. International Conference on Technologies for Marine Environment Preservation, Tokyo.
- Boentgen, R. R., et al. (1976). First season results from ship response instrumentation aboard the SL-7 class containership *SSSealand McLean* in North Atlantic service. Ship Structures Committee, Report SSC 264.
- Boon, B. (2003). Arrangement and structural component design. In: Lamb, T. (ed.), *Ship Design and Construction*, Chapter 17, Jersey City, NJ: SNAME.
- Boote, D., Figari, M., and Sculati, A. (1999). Ultimate strength assessment of fast mono-hull vessels. Proceedings of the Fifth International Conference on Fast Sea Transportation (FAST '99), Seattle, Washington.
- Boytssov, G. V., and Paley, O. M. (1979). *Strength and Structures of New Types of Ships* (in Russian). St. Petersburg: Publishing House Sudostroenie.
- British Maritime Technology (BMT). (1986). Global Wave Statistics. Primary contributors: Hogben, N., Da Cunha, L. F., and Oliver, H. N., London: Unwin Brothers Limited.
- Brock, J. (1957). DTMB Report 1149, November.
- Brook, A. K. (1989). Hull girder loads project—Summary report. BMT Report 289088.R01, prepared for Netherlands Ship Model Basin Cooperative Research Ships (NSMB CRS).
- Brown, A., Tikka, K., Daidola, J. C., Lutzen, M., and Choe, I. H. (2000). Structural design and response in collision and grounding. SNAME Annual Meeting, Vancouver, British Columbia, Canada.
- Brown, A. (2001). Collision scenarios and probabilistic collision damage. Second International Conference on Collision and Grounding of Ships (ICCGS), Copenhagen, Denmark, July 1–3, 2001.
- Brown, J. C. (1999). A wave induced fatigue strain recorder for surface ship. *Transactions*, SNAME.
- Brown, K. C., Joubert, P. N., and Yan, P. (1996). Tests on yacht hull plating. *Marine Technology*, 33:2.
- Bruzzone, D., Gualeni, P., and Sebastiani, L. (2001). Effects of different three-dimensional formulations on the seakeeping computations of high speed hulls. In: Wu, Y. S., Cui, W. C., and Zhou, G. J. (eds.), Eighth PRADS Symposium, Shanghai, China.
- Buchner, B. (1995). On the impact of green water loading on ship and offshore unit design. PRADS '95, Seoul, South Korea.
- Bullock, O. R., and Oldfield, B. (1976). Production PHM design-to-cost hull structure. SNAME/AIAA Advanced Marine Vehicles Conference, September.
- Burrall, P., et al. (1986). Cycle test evaluation of various polyester types and a mathematical model for projecting flexural fatigue endurance. 41st Annual Conference of Society of the Plastics Industry (SPI), Section Marine I, Session 7-D.
- Caldwell, J. B. (1965). Ultimate longitudinal strength. *Transactions*, RINA, Vol. 107, 411–430.
- Card, J. C. (1975). Effectiveness of double bottoms in preventing oil outflow from tanker bottom incidents. *Marine Technology*, 12.
- Cariou, A., and Casella, G. (1999). Liquid sloshing in ship tanks: A comparative study of numerical simulation. *Marine Structures*, 12:3.
- Cartwright, D. E., and Longuet-Higgins, M. S. (1956). The statistical distribution of the maxima of a random function. Proceedings of the Royal Society of London, Series A 237, 212–232.
- Chalmers, D. W. (1988). The properties and uses of marine structural materials. *Marine Structures*, 1.
- Chang, F. H., Gordon, D. E., and Gardner, A. H. (1977). A study of fatigue damage in composites by nondestructive testing techniques. In: Reifsnider, K. L., and Lauritis, K. N. (eds.), *Fatigue of Filamentary Composite Materials*, ASTM STP 636.
- Chang, P. Y., Seibold, F., and Thasanatorn, C. (1980). A rational methodology for the prediction of structural response due to collision of ships. *Transactions*, SNAME, Vol. 88.
- Chen, C., and Shen, J. (1990). Calculation of ship nonlinear bending moment in regular waves in the time domain. Selected papers of CSNAME.
- Chen, H. H., and Ng, R. C. (1982). Analytical study of bow flare impact—Phase IV. Technical Report OED-82011, American Bureau of Shipping.
- Chen, H. H., Tornig, J., and Shin, Y. S. (1988). Theoretical manual for three-dimensional hydrodynamic pressure calculation program, PRECAL. ABS Technical

- Report RD-88025, prepared for the Netherlands Ship Model Basin Cooperative Research Ships (NSMB CRS).
- Chen, H. H., Jan, H. Y., Conlon, J. F., and Liu, D. (1993). New approach for design and evaluation of double hull tanker structures. *Transactions*, SNAME.
- Chen, H. H., Akiyama, A., Yu, H., and Che, X. (1996). Recent progress toward design and evaluation of containership hull structures. Prepared for SAFESHIP Conference.
- Chen, H., Chen, H. H., and Hoffman, D. (1979). The implementation of the 20-year hindcast wave data in the design and operation of marine structure. Offshore Technology Conference, Houston.
- Chen, Y. K., Kutt, L. M., Piaszyk, C. M., and Bieniek, M. P. (1983). Ultimate strength of ship structures. *Transactions*, SNAME, Vol. 91.
- Chen, Y. N., and Mavrakis, S. A. (1988). Close-form spectral fatigue analysis for compliant offshore structures. *Journal of Ship Research*, December.
- Chen, Y. N., and Thayamballi, A. K. (1991). Considerations of global climatology and loading characteristics in fatigue damage assessment of ship structures. SNAME-SSC Symposium.
- Cheng, Y. F., and Turnbull, W. (1995). Some considerations on the structural requirement for the classification of high speed craft. Proceedings of the Third International Conference on Fast Sea Transportation (FAST '95), Lueback-Travemuende, Germany.
- Chiou, J., and Chen, Y. K. (1990). Fatigue prediction analysis validation from SL-7 hatch corner strain data. Ship Structure Committee Report SSC-338.
- Christein, J. P., and Warren, J. L. (1995). Implementation of HSLA-100 steel in aircraft carrier construction—CVN74. *Journal of Ship Construction*, 11:2.
- Christodoulides, J. C., and Oliveira, J. G. (1982). Plastic collapse of orthotropic plates. *Journal of Ship Research*, 26.
- Clarkson, J., Wilson, L. B., and McKeeman, J. L. (1959). Data sheets for the elastic design of flat grillages under uniform pressure. *European Shipbuilding*, Vol. 8, 174–198.
- Coker, E. G., Chakko, K. C., and Satake, Y. (1919-1920). Photo-elastic strain measurements. *Transactions*, IESS.
- Conlon, J. F. (1992). The role of ship design and evaluation criteria in improving hull structural safety. International Conference on Tankers and Bulk Carriers—The Way Ahead, London, UK, December.
- Conlon, J. F., and Spencer, J. S. (1991). Restatement of ABS hull structural criteria. SNAME West Coast Tankers Operations Symposium, October.
- Cowper, G. R., and Symonds, W. G. (1957). Strain-hardening and strain-rate effects in the impact loading of cantilever beams. Technical Report No. 28, Brown University, UK.
- Cox, P. A., Bowles, E. B., and Bass, R. L. (1980). Evaluation of liquid dynamic loads in slack LNG cargo tanks. Ship Structure Committee SSC-297.
- Crandall, S., and Mark, W. (1963). *Random Vibration in Mechanical Systems*. New York: Academic Press.
- Critchfield, M. (1973). Evaluation of hull vibratory (springing) response of Great Lakes ore carrier M/V *Stewart J. Cort*. DTMB Report 4225, November 1973.
- CRS (NSMB Cooperative Research for Ships) (1998). PRECAL User's Manual, Version 2.1.
- Cui, W., and Mansour, A. (1998). Effects of welding distortions and residual stresses on the ultimate strength of long rectangular plates under uniaxial compression. *Marine Structures*, Vol. 11, Issue 6.
- Curry, R., and Novak, D. (2001). Classification standards for small high-speed naval craft. Sixth International Conference on Fast Sea Transportation, FAST '2001, Southampton, UK.
- Curry, R. (1995). Merchant ship losses 1934–1993. RINA Spring Meeting, London, UK, April.
- Czyryca, E. J., et al. (1990). Development and certification of HSLA-100 steel for naval ship construction. *Naval Engineers Journal*, Vol. 102.
- D'Arcangelo, A. M. (1969). *A Guide to Sound Ship Structures*. Cambridge, MD: Cornell Maritime Press.
- Daidola, J. C. (1995). Tanker structure behavior during collision and grounding. *Marine Technology*, 32: 20–32.
- Dalzell, J. F. (1963). Summary of investigation of mid-ship bending moments experienced by models in extreme regular waves. SSC Report No. SSC-157.
- Dawkins, R. A. (1985). A method for determining the vertical non-linear wave induced bending moments in ships using a frequency domain technique. LR Hull Structures Report 85/39.
- Det Norske Veritas (1977). Rules for the design, construction and inspection of offshore structures. Det Norske Veritas, Hovik, Norway.
- Det Norske Veritas (1996). Strength analysis of hull structures in high speed and light craft. Classification Note No. 30.8.
- Det Norske Veritas (1999). Rules for classification of high speed, light craft and naval surface craft.
- DeWilde, G. (1967). Structural problems in ships with large hatch openings. *International Shipbuilding Progress*, Vol. 14.
- Dietz, J. S., Friis-Hansen, P., and Jensen, J. J. (2004). Design waves episodes for extreme value ship responses. Proceedings of PRADS'04, Travemünde, Germany, September, 286–293.
- Dow, R. S., Hugill, R. C., Clark, J. D., and Smith, C. S. (1981). Evaluation of ultimate ship hull strength, extreme loads response symposium. SNAME/SSC, Arlington, Virginia.
- Ehrstrom, J. C., Cottignies, L., Lequeu, P., and Raynaud, G. M. (1998). Fatigue resistance of high strength aluminum alloy weldments. Third International Forum on Aluminum Ships, Haugesund, Norway.
- Elbatouti, A. M. T., Jan, H. Y., and Stiansen, S. G. (1976). Structural analysis of a containership steel model and comparison with the test results. *Transactions*, SNAME, Vol. 84.
- Ellinas, C. P., and Valsgard, S. (1985). Collision and damage of offshore structure: A state-of-the-art. Fourth

International Symposium on Offshore Mechanics and Arctic Engineering, Dallas, Texas.

Endo, H. (2004). Rationalization in the Probabilistic Method Estimating the Mean Oil Outflow for Side Damage, Third International Conference on Collision and Grounding of Ships (ICCGS), Izu, Japan, Oct.

Engle, A., Lin, W. M., Salvesen, N., and Shin, Y. S. (1997). Application of 3-D nonlinear wave-loads and structural responses simulations in naval ship design. *Naval Engineers Journal*.

Fach, K., and Rothe, F. (1999). Leichtbaukonstruktionen im Schiffbau (in German). *Schiff & Hafen*, 8.

Falk, L., Baecklund, J., and Loenne, A. (1995). Membrane stresses in laterally loaded marine sandwich panels. Proceedings of the Third International Conference on Sandwich Construction, Southampton, UK.

Faltinsen, O., and Zhao, R. (1991a). Numerical prediction of ship motions at high forward speed. *Philosophical Transactions of the Royal Society*, London, A334.

Faltinsen, O., and Zhao, R. (1991b). Flow prediction around high-speed ships in waves. Proceedings of the Math. Appr. Hydrodyn. Soc. Ind. Appl. Math., Philadelphia, Pennsylvania.

Faltinsen, O. M. (1997). The effect of hydro-elasticity on ship slamming. *Philosophical Transactions of the Royal Society*, London, Vol. 355.

Faltinsen, O. M. (1999). Water entry of a wedge by hydro-elastic orthotropic plate theory. *Journal of Ship Research*.

Faltinsen, O. M., Rognebakke, O. F., Lukowsky, I. A., and Timokka, A. N. (2001). Multidimensional model analysis of nonlinear sloshing in rectangular tank with finite water depth. *Journal of Fluid Mechanics*, Vol. 5.

Fan, M., and Mazonzkis, C. (1995). Structural design philosophies and classification requirements for high speed craft. Third International Conference on Fast Sea Transportation, FAST '95, Luebeck-Travemuende, Germany.

Fan, M., and Pinchin, M. (1997). Structural design in high speed craft—A comparative study of classification requirements. Fourth International Conference on Fast Sea Transportation, FAST '97, Sydney, Australia.

Farinetti, V. (1998). General considerations on high tensile steel versus aluminum alloy and technical aspects related to the aluminum construction. Proceedings of the Third International Forum on Aluminum Ships, Hauge-sund, Norway.

Fathi, D. (1998). VERES Version 3.1—User's Manual. Technical report MT6098-014, MARINTEK, Trondheim, Norway.

Faulkner, D. (1975). A review of effective plating for use in the analysis of stiffened plating in bending and compression. *Journal of Ship Research*, Vol. 19, No. 1 (March), 1–17.

Faulkner, D., and Sadden, J. A. (1979). Toward a unified approach to ship safety. *Transactions*, RINA, Vol. 120.

Faulkner, D. (1981). Semi-probabilistic approach to the design of marine structures. Extreme Loads Response Symposium, SNAME/SSC, Arlington, Virginia.

Ferraris, S. (1999). Aluminum alloys and high-speed craft: Present and future applications. Proceedings of the Sixth International Conference on Materials and Material Processes for Transportation Industry, Turin, Italy.

FLOW3D (1999). User's Manual—Version 7.5. Los Alamos, New Mexico: Flow Science Inc.

Fonseca, N., and Guedes Soares, C. (1998). Time domain analysis of large amplitude vertical ship motions and wave loads. *Journal of Ship Research*, 42:2.

Frankland, J. M. (1942). Effects of impact on simple elastic structures. D. W. Taylor Model Basin Report, No. 481.

Freudenthal, A. M., and Gaither, W. S. (1969). Probabilistic approach to economic design of maritime structures. XXIIInd International Navigation Congress, Paris.

Friis-Hansen, P., Jensen, J. J., and Pedersen, P. T. (1994). Wave-induced springing and whipping of high-speed vessels. Proceedings of the Hydro-elasticity in Marine Technology, Trondheim, Norway.

Friis-Hansen, P., Jensen, J. J., and Pedersen, P. T. (1995). Long term springing and whipping stresses in high speed vessels. Proceedings of the Third International Conference on Fast Sea Transportation (FAST '95). Luebeck-Travemuende, Germany.

Friis-Hansen, P., Ravn, E. S., Hartmann, J. P. and Sorensen, A. (2004). FSA of the Navigational Safety in Baltic West, 3rd International Conference on Collision and Grounding of Ships, Izu, Japan, Oct.

Fujii, Y., Yamanouchi, H., and Mizuhi, N. (1974). i—Some factors affecting the frequency of accidents in marine traffic. ii—The probability of standing. iii—The effects of darkness on the probability of collision and stranding. *Journal of Navigation*, 27.

Fukuda, J. (1970). Long-term predictions of wave bending moment. Selected papers from the *Journal of SNA of Japan*.

Gallagher, R. H. (1975). *Finite Element Analysis: Fundamentals*. New York: Prentice Hall College Division.

Gerritsma, J., and Beukelman, W. (1964). The distribution of hydrodynamic forces on a heaving and pitching ship in still water. *International Shipbuilding Progress*, Vol. 11, 506–522.

Gibbs & Cox, Inc. (1960). *Marine Design Manual for Fiberglass Reinforced Plastics*. Sponsored by Owens-Corning Fiberglass Corporation. New York: McGraw-Hill.

Glasfeld, R. D. (1962). Design and construction of a 42-foot ship structural model testing facility. University of California, Institute of Engineering Research, Report Series 184, Issue 1.

Gluver, H., and Olsen, D. (eds.) (1998). Current practice in risk analysis of ship collision to bridges. In: *Ship Collision Analysis*. Rotterdam: Balkema.

- Glykas A., Das P. K., and Barltrop, N. (2001). Application of failure and fracture criteria during a tanker head-on collision. *Ocean Engineering*, 28: 375–395.
- Goodman, R. A. (1971). Wave excited main hull vibration in large tankers and bulk carriers. *Transactions*, RINA, Vol. 113.
- Goodman, R. A., and Mowatt, G. (1976). Allowance for imperfection in ship structural design. Conference on the Influence of Residual Stresses and Distortions on the Performance of Steel Structures, Institute of Mechanical Engineering.
- Goubalt, P., and Mayers, S. (1996). Comparative analysis of metal and composite materials for the primary structures of a patrol craft. *Naval Engineering Journal*, May.
- Greene, E. (1990). Investigation of fiberglass reinforced plastics in marine structures. Ship Structure Committee Report SSC-360.
- Greene, E. (1997). Design guide for marine applications of composites. Ship Structure Committee Report SSC-403.
- Guedes Soares, C. (1999). On the uncertainty in long-term prediction of wave induced loads on ships. *Marine Structures*, 12: 171–182.
- Gumble, E. J. (1958). *Statistics of Extremes*. New York: Columbia University Press.
- Hadler, J. B., Lee, C. M., Birmingham, J. T., and Jones, H. D. (1974). Ocean catamaran seakeeping design, based on the experience of USNS *Hayes*. *Transactions*, SNAME, Vol. 82.
- Hamlin, N. A., Lou, Y. K., Maclean, W. M., Seibold, F., and Chandras, L. M. (1986). Liquid sloshing in slack ship tanks—Theory, observations, and experiments. *Transactions*, SNAME.
- Hardler, J. B., Lee, C. M., Birmingham, J. T., and Jones, H. D. (1994). Ocean catamaran seakeeping design, based on the experience of USNS *Hayes*. *Transactions*, SNAME, Vol. 82.
- Hashin, Z. (1981). Fatigue failure criteria for unidirectional fiber composites. *Journal of Applied Mechanics*, Vol. 38.
- Haslum, K., and Tonnessen, A. (1972). An analysis of torsion in ship hulls. *European Shipbuilding*, No. 5/6, 67–89.
- Hasofer, A. M., and Lind, N. (1974). Exact and invariant second moment code format. *Journal of Engineering Mechanics Division*, ASCE, Vol. 100, 111–121.
- Haugen, E. M. (1999). Hydro-elastic analysis of slamming on stiffened plates with application to catamaran wet-decks. Dr. Ing. thesis, Department of Marine Hydrodynamics, Norwegian University of Science and Technology, NTNU, Trondheim, Norway.
- Haugen, E. M., and Faltinsen, O. M. (1999). Theoretical studies of wet-deck slamming and comparisons with full-scale measurements. Proceedings of the Fifth International Conference on Fast Sea Transportation (FAST '99), Seattle, Washington.
- Hayman, B., Huang, T., and Valsgard, S. (1991). Response of fast craft hull structures to slamming loads. Proceedings of the First International Conference on Fast Sea Transportation (FAST '91), Trondheim, Norway.
- Hayman, B., Wiese, M., Davies, P., Choqueuese, D., Hoyning, B., and Mitusch, P. (1998). Foam-cored sandwich panels under static pressure loading: Some new tests and analyses. Sandwich Construction 4. Proceedings of the Fourth International Conference on Sandwich Construction, Stockholm, Sweden.
- Heggelund, S. E., Moan, T., and Oma, S. (1999). Global structural analysis of large catamaran. Proceedings of the Fifth International Conference on Fast Sea Transportation (FAST '99), Seattle, Washington.
- Heggelund, S. E., Moan, T., Hoff, J. R., and Oma, S. (2001). Practical determination of global design loads for high speed large catamaran. Proceedings of the Sixth International Conference on Fast Sea Transportation (FAST '2001), Southampton, UK.
- Heller, S. R., and Jasper, H. H. (1960). On the structural design of planing craft. *Transactions*, RINA, Vol. 102.
- Heller, S. R., Brock, J. S., and Bart, R. (1959). DTMP Report No. 1290.
- Hermundstad, O. A., and Wu, M. K. (1999). Approaches in stress analysis of high-speed craft. Fifth International Conference on Fast Sea Transportation (FAST '99), Seattle, Washington.
- Hermundstad, O. A., Aarsnes, J. V., and Moan, T. (1999). Linear hydro-elastic analysis of high-speed catamaran and mono-hulls. *Journal of Ship Research*, 43(1).
- Highsmith, A. L., and Reifsnider, K. L. (1986). Internal load distribution effects during fatigue loading of composite laminates, composite materials: Fatigue and fracture. ASTM STP 907, Hahn, H. T. (ed.), Philadelphia: ASTM.
- Hirt, C. W., Nicholas, B. D., and Romero, N. C. (1975). *SOLA—A Numerical Solution Algorithm for Transient Fluid Flows*. Los Alamos, New Mexico: Los Alamos Scientific Laboratory.
- Hoffman, D., and Chen, H. H. (1978). The use of directional hindcast spectra as design wave data. Offshore Technology Conference, Houston, Texas.
- Hoffman, D., and Lewis, E. V. (1969). Analysis and interpretation of full-scale data on midship bending stresses of dry cargo ships. Ship Structure Committee Report SSC-198, June.
- Hoffman, D., and Lewis, E. V. (1969). Analysis and interpretation of full-scale data on bending stresses of dry cargo ships. Ship Structure Committee Report SSC-196.
- Hoffman, D., and van Hooff, R. W. (1973). Feasibility study of springing model tests of a Great Lakes bulk carrier. *International Shipbuilding Progress*, March.
- Hoffman, D., and van Hooff, R. W. (1976). Experimental and theoretical evaluation of springing of a Great Lakes bulk carrier. *International Shipbuilding Progress*, June.

Hogben, N., and Lumb, F. E. (1967). *Ocean Wave Statistics*. London: Her Majesty's Stationary Office.

Hong, S. Y., Lee, P. M., and Gong, D. S. (1990). Experimental study on the deck wetting of a containership in irregular head waves. *JSNACK*, 27.

Horn, G. (2005). The development of common structural rules for tankers. SNAME World Maritime Technology Conference, Houston, Texas.

Hughes, O. (1983). Design of laterally loaded plating—concentrated loads. *Journal of Ship Research*, Vol. 27, No. 4 (December), 252–265.

Inglis, R. B., and Price, W. G. (1982). A three-dimensional ship motion theory: Calculation of wave loading and response with forward speed. *Transactions*, RINA, 124.

International Association of Classification Societies (1989). Minimum longitudinal strength standards. UR S-7, Rev. 3.

International Association of Classification Societies (1997). Evaluation of scantlings of hatch covers of bulk carrier cargo holds. UR S-21.

International Association of Classification Societies (2000). Longitudinal strength of hull girder in flooded condition for single skin bulk carriers. UR S-17, Rev. 3.

International Association of Classification Societies (2000). Standard wave data for direct wave load analysis. Recommendation No. 34.

International Association of Classification Societies (2001). Requirements S11 on longitudinal strength standard. UR S-11, Rev. 2.

International Association of Classification Societies (2004). Longitudinal strength of hull girder in flooded condition for bulk carriers. UR S-17, Rev. 6.

International Association of Classification Societies (2004). Evaluation of scantlings of corrugated transverse watertight bulkheads in bulk carriers considering hold flooding. UR S-18, Rev. 6.

International Association of Classification Societies (2004). Evaluation of scantlings of the transverse watertight corrugated bulkhead between cargo holds nos. 1 and 2, with cargo hold no. 1 flooded, for existing bulk carriers. UR S-19, Rev. 5.

International Association of Classification Societies (2004). Harmonized notations and corresponding design loading conditions for bulk carriers. UR S-25, Rev. 2.

International Association of Classification Societies (2006). Common structural rules for double hull tankers.

International Association of Classification Societies (2006). Common structural rules for bulk carriers.

International Maritime Organization (IMO) (1983). *Code for the Construction and Equipment of Ships Carrying Liquefied Gases in Bulk (IGC Code)*, London.

International Maritime Organization (2000). International code of safety for high speed craft (HSC Code).

International Maritime Organization (2006). *International Convention for the Prevention of Pollution from Ships, 1973, as modified by the Protocol of 1978 (MARPOL 73/78)*, Consolidated Edition.

International Ship Structures Congress (1973). Report of Committee 10, Design procedure. Proceedings of the Fifth International Ship Structures Congress, Hamburg, Germany.

International Ship Structures Congress (1979). Report of Committee II.1, Linear structural response. Proceedings of the Seventh International Ship and Offshore Structures Congress, Paris, France.

International Ship Structures Congress (1997). Fatigue and fracture, Report of Committee III.2. Proceedings of the Thirteenth International Ship and Offshore Structures Congress, Trondheim, Norway.

International Ship Structures Congress (2000). Report of Specialist Committee VI.1, Extreme hull girder loading. Ohtsubo, H. and Sumi, Y. (eds.), Proceedings of the Fourteenth ISSC, Nagasaki, Japan.

International Ship Structures Congress (2000). Report of Specialist Committee V.6, Fabrication technologies. Proceedings of the Fourteenth International Ship and Offshore Structures Congress, Nagasaki, Japan.

International Ship Structures Congress (2000). Report of Committee II.1, Quasi-static response. Proceedings of the Fourteenth International Ship and Offshore Structures Congress, Nagasaki, Japan.

International Ship Structures Congress (2000). Report of Specialist Committee V.2, Structural design of high speed vessels. Proceedings of the Fourteenth International Ship and Offshore Structures Congress, Nagasaki, Japan.

International Ship Structures Congress (2000). Report of Committee I.2, Loads. Proceedings of the Fourteenth International Ship and Offshore Structures Congress, Nagasaki, Japan.

International Ship Structures Congress (2006). Report of Specialist Committee V.1, Collision and Grounding. Proceedings, 16th International Ship and Offshore Structures Congress, Southampton, UK.

Ishikawa, T., Imai, S., Inoue, T., Watanabe, K., Tada, M., and Hashimoto, K. (1997a). Practical assessment of structural integrity of ships attained by the use of SUF steel having crack-arrestability (SUF surface-layer with ultra-fine grain). Sixteenth OMEA, Vol. III.

Ishikawa, T., Yoshikawa, H., Inoue, T., Nomiyama, Y., and Imai, S. (1997b). Ultra-high crack-arresting steep plate (HIAREST) with super-refined grains in surface layers. Nippon Steel Technical Report 75.

Ishikawajima-Harima Heavy Industries Co. Ltd. (1986). A method for estimating the strength of ship hulls against sloshing load. *IHI Engineering Review*, April.

Ito, H., Kondo, K., Yoshimura, N., and Kawashima, N. (1992). A simplified method to analyze the strength of double hulled structures in collision. *Journal of Society of Naval Architects of Japan*, 160.

Jan, H. Y., Chang, K. T., and Wojnarowski, M. E. (1979). Comparison of stresses calculated using the DAISY system to those measured on the SL-7 containership program. Ship Structure Committee Report SSC-282.

- Jasper, N. H. (1956). Statistical distribution patterns of ocean waves and of wave-induced ship stresses and motions. *Transactions*, SNAME, Vol. 64.
- Jastrzebski, T. (1999). Titanium alloys in ship and offshore structures. Proceedings of the Sixth Symposium of Titanium and Its Alloys, Karpacz, Poland, May.
- Jensen, J. J., and Pedersen, P. T. (1979). Wave-induced bending moment in ships—A quadratic strip theory. RINA Supplementary Paper, Vol. 121.
- Jensen, J. J., and Wang, Z. (1998). Wave induced hydro-elastic response of fast mono-hull displacement ships. Hydroelasticity '98, Fukuoka, Japan.
- Jensen, J. J., and Dogliani, M. (1996). Wave-induced ship hull vibrations in stochastic seaways. *Marine Structures*, 9:3/4.
- Jensen, J., and Pedersen, T. (1981). Bending moments and shear forces in ships sailing in irregular waves. *Journal of Ship Research*, Vol. 25, No. 4 (December).
- Jiang, H. and Gu, Y. (2004). Study on Ship Collisions and Buffer Bow Structures, 3rd International Conference on Collision and Grounding of Ships, Izu, Japan, Oct.
- Jones, D. E. (1983). Dynamic loading analysis and advanced composites. SNAME Southeast Section.
- Jones, N., and Walters, R. M. (1971). Large deflections of rectangular plates. *Journal of Ship Research*, 15.
- Jones, N. (1989). *Structural Impact*. Cambridge, UK: Cambridge University Press.
- Jones, N. (1997). Dynamic plastic behavior of ship and ocean structures. *Transactions*, RINA, 139.
- Kajaste-Rudnitski, J., Varsta, P., and Matusiak, J. (2005). Some Finite Element Estimates of Ship Collision Event, International Congress of International Maritime Association of the Mediterranean, Lisbon, Portugal, September.
- Kaminishi, K., Taneda, M., and Shinji, T. (1992). Crack initiation and extension under penetration of thin metal plates. *International Journal of Japanese Society of Mechanical Science*, Vol. 34(4).
- Kaneko, Y., Takeuchi, K., and Aokage, K. (1993). Design and construction of a seawater survey ship built using aluminum honeycomb panels. Proceedings of the Second International Conference on Fast Sea Transportation (FAST '93), Yokohama, Japan.
- Kaplan, M., et al. (1984). Analysis and assessment of major uncertainties associated with ship hull ultimate failure. Report No. SSC-322, Ship Structure Committee, Washington, D.C.
- Kaplan, P., and Sargent, T. P. (1972). Further studies of computer simulation of slamming and other wave-induced vibratory structural loadings on ships in waves. Ship Structure Committee Report SSC-231.
- Kaplan, P., Sargent, T. P., and Cilmi, J. (1974). Theoretical estimates of wave loads on the SL-7 containerhips in regular and irregular seas. Ship Structures Committee Report SSC-246.
- Kaplan, P., Bentson, J., and Davis, S. (1981). Dynamics and hydrodynamics of surface-effect ships. *Transactions*, SNAME, Vol. 89.
- Karppinen, T., Rantanen, A., and Hellevaara, M. (1993). Wave-induced motions and loads on fast mono-hulls—Correlation of theoretical predictions with model and full scale measurements. Proceedings of the Second International Conference on Fast Sea Transportation (FAST '93), Yokohama, Japan.
- Karr, D., Li, Y., and Wang, G. (2007). Mesh Size Effects in Simulating Ductile Fracture of Metals, 10th International Symposium on Practical Design of Ships and Other Floating Structures, Houston, TX, Oct.
- Keane, R. G. (1978). Surface ships hydrodynamic design problems and R&D needs. NAVSEC Report No. 6136-78-37.
- Kim, C. H. (1975). Theoretical and experimental correlation of wave loads for SL-7 containership. Davidson Laboratory Report, SIT-DL-75-1829, June.
- Kim, C. H. (1982). Hydrodynamic loads on the hull surface of a seagoing vessel. SNAME Star Symposium, Paper No. 8.
- Kim, R. Y. (1987). Fatigue strength. In: *Engineered Materials Handbook*, Volume 1: Composites. Materials Park, Ohio: American Society of Materials International.
- Kim, Y. (2000). Numerical simulation of sloshing flows with impact load. *Applied Ocean Research*.
- Kitamura, O. (2001). FEM approach to the simulation of collision and grounding damage. Second International Conference on Collision and Grounding of ships, Copenhagen, Denmark, July 1–3.
- Kitamura, O. (1996). Comparative study on collision resistance of side structure. International Conference on Design and Methodologies for Collision and Grounding Protection of Ships, San Francisco, California.
- Kitamura, O. (1998). Research on the methodology for the prediction of accidental damage to tanker structure in case of collision or grounding and development of new hull design with improved crashworthiness. Conference on Prediction Methodology of Tanker Structural Failure and consequential Oil Spill, ASIS, Tokyo, Japan.
- Kitamura, O., Kuroiwa, T., Kawamoto, Y., and Kaneko, E. (1998). A study on the improvement tanker structure against collision and grounding damage. Seventh PRADS Symposium, The Hague, Netherlands, 173–179.
- Kite-Powell, H. L., Jin, D., Jebsen, J., Papakonstantinou, V., and Patrikalakis, N. (1999). Investigation of potential risk factors for groundings of commercial vessels in U.S. ports. *International Journal of Offshore and Polar Engineering*, 9:16–21
- Klanac, A., Ehlers, S., Tabri, K., Rudan, S., and Broekhuijsen, J. (2005). Qualitative Design Assessment of Crashworthy Structures, International Congress of International Maritime Association of the Mediterranean, Lisbon, Portugal, September.
- Knytex (1994). *Fabric Handbook*. New Braunfels, Texas.
- Krikke, E. M. (2001). Executive summary—Slamming loads on ships project, 1995–2000. Report prepared for Netherlands Ship Model Basin Cooperative Research Ships (NSMB CRS).

- Kring, D. C., Mantzaris, D. A., Tcheou, G. B., and Sclavounos, P. D. (1997). A time-domain sea-keeping simulation for fast ships. Proceedings of the Fourth International Conference on Fast Sea Transportation (FAST '97), Sydney, Australia.
- Kristensen, O. H. H., and Moan, T. (1999). Ultimate strength of aluminum plates under biaxial loading. Proceedings of the Fifth International Conference on Fast Sea Transportation (FAST '99), Seattle, Washington.
- Krivanec, C. E., and Bea, R. G. (1992). Analysis of static and dynamic pressures in the holds of bulk cargo carriers. Report submitted to American Bureau of Shipping, University of California at Berkeley, September.
- Krylov Shipbuilding Research Institute (1995). *Method for Computation of Global Loads for High Speed Crafts under Sea Service Conditions*.
- Kumai, T. (1974). On the exciting force and response of springing of ships. International Symposium on the Dynamics of Marine Vehicles and Structures in Waves, Institution of Mechanical Engineers, London, UK.
- Kuntsman, C. M., and Umberger, R. C. (1959). The stresses around reinforced square opening with rounded corners in a uniformly loaded plate. WINA Thesis, June (Fig. 59).
- Kuroiwa, T. (1995). Research on structural failure of tankers due to collision and grounding. Conference on Prediction Methodology of Tanker Structural Failure and consequential Oil Spill, ASIS, Tokyo, Japan.
- Kuroiwa, T. (1996). Numerical simulation of actual collision and grounding accidents. Proceedings of the International Conference on Designs and Methodologies for Collision and Grounding Protection of Ships, San Francisco, California, August.
- Kvaelsvold, J., Svensen, T., and Hovem, L. (1997). Bow impact loads on Ro-Ro vessels. *Transactions*, RINA.
- Kvaelsvold, J. (1994). Hydro-elastic modeling of wet-deck slamming on multi-hull vessels. Dr. Ing. thesis, Division of Marine Hydrodynamics, Norwegian Institute of Technology, Trondheim, Norway.
- Lamb, T. (ed.) (2003). *Ship Design and Construction*, Vols. I & II. Jersey City, New Jersey: SNAME.
- Lee, C. M., and Curphey, R. M. (1977). Prediction of motion, stability, and wave loads of small-waterplane-area, twin-hull ships. *Transactions*, SNAME, Vol. 85.
- Lee, S. H., Kim, J. Y., Lee, K. J., Kang, J. M., Yum, D. J., Seol, Y. S., Rashed, S., and Kawaha, A. (1995). Simulation of 3-D sloshing and structural response in ship's tanks taking account of fluid-structure interaction. *Transactions*, SNAME.
- Leguen, J. F., Babaud, G., and Thiberge, E. (1997). High speed mono-hulls, experimental determination of loads on structure by models and full scale tests. Proceedings of the Fourth International Conference on Fast Sea Transportation (FAST '97). Sydney, Australia.
- Lehmann, E., and Yu, X. (1995). Progressive folding of bulbous bows. Sixth International Symposium on Practical Design of Ships and Mobile Units. Kim, H., and Lee, J. W. (eds.), 2: 1048–1059.
- Lehmann, E., and Peschmann, J. (2001). Energy absorption by the steel structure of ships in the event of collisions. Second International Conference on Collision and Grounding of ships, Copenhagen, Denmark, July 1–3.
- Lehmann, E., and Biehl, F. (2004). Collision of Ships and Offshore Wind Turbines: Calculation and Risk Evaluation, 3rd International Conference on Collision and Grounding of Ships, Izu, Japan, Oct.
- Lemmen, P. M., Vredeveltdt, A. W., and Pinkster, J. A. (1996). Design analysis for grounding experiments. Proceedings of the International Conference on Designs and Methodologies for Collision and Grounding Protection of Ships, San Francisco, California, August.
- Lenselink, H., and Thung, K. G. (1992). Numerical simulations of the Dutch-Japanese full scale ship collision tests. Conference on Prediction Methodology of Tanker Structural Failure and Consequential Oil Spill, ASIS, Tokyo, Japan, July.
- Lepeix, R. (2001). Hydrodynamic trends in hull lines of podded driven large cruise vessels. Eighth PRADS Symposium, Wu, Y. S., Cui, W. C., and Zhou, G. J. (eds.), Shanghai, China.
- Lewis, E. V. (1954). Ship model tests to determine bending moments in waves. *Transactions*, SNAME, Vol. 62, 426–490.
- Lewis, E. V. (1967). Predicting long-term distribution of wave-induced bending moments in ships. SNAME Spring Meeting, Montreal, Quebec, Canada.
- Lewis, E. V., Hoffman, D., MacLean, W. M., vanHooff, R., and Zubaly, R. B. (1973). Load criteria for ship structural design. Ship Structure Committee Report SSC-240.
- Lewis, E. V., and Zubaly, R. B. (1981). Predicting hull bending moments for design. Extreme Loads Response Symposium, SNAME and SSC, Arlington, Virginia.
- Lewis, E. V. (ed.) (1988). *Principles of Naval Architecture*, 2nd rev. New York: SNAME.
- Lin, W. M., and Yue, D. K. P. (1993). Time-domain analysis for floating bodies in mid-slope waves of large amplitude. Proceedings of Eighth International Workshop on Water Wave and Floating Bodies, St. John's, Newfoundland, Canada.
- Lin, W. M., Neinholt, M. J., Salvesen, N., and Yue, D. K. P. (1994). Large amplitude motions and wave loads for ship design. Proceedings of the Twentieth Symposium on Naval Hydrodynamics, University of California, Santa Barbara, California.
- Little, P., Pippenger, D., and Simonsen, B. C. (1996). Development of a computational model for predicting damage of tankers. Proceedings of the International Conference on Designs and Methodologies for Collision and Grounding Protection of Ships, San Francisco, California, August.
- Little, R. S., and Lewis, E. V. (1971). A statistical study of wave-induced bending moments on large oceangoing tankers and bulk carriers. *Transactions*, SNAME, Vol. 79.
- Little, R. S., Lewis, E. V., and Bailey, F. C. (1971). A statistical study of wave-induced bending moments on large

- ocean-going tankers and bulk carriers. *Transactions, SNAME*, Vol. 79, 117–168.
- Liu, D., and Bakker, A. (1981a). Practical procedures for technical and economic analysis of ship structural details. *Marine Technology*, Vol. 18, No. 1 (January).
- Liu, D., Chen, H., and Lee, F. (1981b). Application of loading predictions to ship structure design: A comparative analysis of methods. Extreme Loads Response Symposium, SNAME/SSC, Arlington, Virginia.
- Liu, D., Spencer, J., Itoh, T., Kawachi, S., and Shigematsu, K. (1992). Dynamic load approach in tanker design. *Transactions, SNAME*, Vol. 100.
- Liu, D., Jan, H. Y., Chen, H. H., Scotto, F. J., and Akiyama, A. (1995). Recent development of design criteria for hull structures of bulk carriers. PRADS, Seoul, South Korea.
- Lloyd's Register of Shipping (1996). Shipright. Design, construction and lifetime ship care procedures; Structural design assessment; Direct calculations—Guidance notes.
- Lloyd's Register of Shipping (1998). Rules and regulations for the classification of special service craft.
- Lou, Y. K., Su, T. C., and Flipse, J. E. (1980). Nonlinear numerical analysis of liquid sloshing in rigid containers. Maritime Administration Contract No. MA-79 SAC-80018, August.
- Lu, G., and Calladine, C. R. (1990). On the cutting of a plate by a wedge. *International Journal of Mechanical Science*, Vol. 32.
- Macduff, J. (1974). The probability of vessel. *Ocean Industry*, September.
- MacLean, W. M., and Lewis, E. V. (1970). Analysis of slamming stresses on SS *Wolverine State*. Webb Institute of Naval Architecture Report No. 10-17 to ABS; also *Marine Technology*, January 1973.
- Mansour, A. E., and Faulkner, D. (1972). On applying the statistical approach to extreme sea loads and ship hull strength. *Transactions, RINA*, Vol. 114.
- Mansour, A. E. (1972). Probabilistic design concepts in ship structural safety and reliability. *Transactions, SNAME*, Vol. 80.
- Mansour, A. E., and D'Oliveira, J. M. (1975). Hull bending moment due to ship bottom slamming in regular waves. *Journal of Ship Research*, Vol. 19, No. 2, 80–92.
- Mansour, A. E. (1976). Charts for buckling and post-buckling analysis of stiffened plates under combined loading. *SNAME T&R Bulletin*, July 2–22.
- Mansour, A. E. (1977). Gross panel strength under combined loading. Ship Structures Committee Report SSC-270.
- Mansour, A. E., Jan, H. Y., Zigelman, C. I., Chen, Y. N., and Harding, S. J. (1984). Implementation of reliability methods to marine structures. *Transactions, SNAME*, Vol. 92.
- Mansour, A. E. (1987). Extreme value distributions of wave loads and their application to marine structures. Marine Structural Reliability Symposium, Arlington, Virginia, October.
- Mansour, A. (1989). An introduction to structural reliability theory. Defense Technical Information Center, SSC-351.
- Mansour, A. E., Yang, J. M., and Thayamballi, A. K. (1990). An experimental investigation of ship hull ultimate strength. *Transactions, SNAME*.
- Mansour, A. E., and Preston, D. B. (1995). Return periods and encounter probabilities. *Journal of Applied Ocean Research*, Vol. 236, November.
- Mansour, A. E. (1995). Extreme loads and load combinations. *Journal of Ship Research*, Vol. 39, No. 1, March, 53–61.
- Mansour, A. E., and Jensen, J. J. (1995). Slightly nonlinear extreme loads and load combinations. *Journal of Ship Research*, Vol. 39, No. 2, June.
- Mansour, A. E., Wirsching, P. H., Ayyub, B. M., and White, G. J. (1996) Probability-based design requirements with respect to failure in ship structures. Proceedings of the Seventh Specialty Conference, Probabilistic Mechanics and Structural Reliability, Worcester, Massachusetts, August (Also SSC-392).
- Mansour, A. E., Wirsching, P. H., Lucket, M. D., Plumptre, A. M., and Lin, Y. H. (1997). Structural safety of ships. *Transactions, SNAME*, November (also SSC-398).
- Mansour, A. E., et al., (1998). Reliability based optimum structural fabrication tolerances. Phase II final report. U.S. Navy Contract N00024-96-C-4123, SBIR Topic 93-067, August 19.
- Mantle, P. J. (1975). A technical summary of air cushion craft development. DTNSRDC Report No. 4727, October.
- Matthews, S. T. (1967). Main hull girder loads on a Great Lakes bulk carrier. Spring Meeting, SNAME.
- Masaoka, K., and Mansour, A. (2004). Ultimate strength of imperfect un-stiffened plates. *Journal of Ship Research*, Vol. 48, 191–201.
- McCallum, J. (1975). The strength of fast cargo ships. *Transactions, RINA*, Vol. 117.
- McGee, S. P., Troesch, A., and Vlahopoulos, N. (1999). Damage length predictor for high speed craft. *Marine Technology*, 36(4): 203–210.
- McGeorge, D., and Hayman, B. (1998). Shear strength of balsa-cored sandwich panels. Sandwich Construction 4. Proceedings of the Fourth International Conference on Sandwich Construction, Stockholm, Sweden.
- McKenny, T. L. (1991). Grounding resistance of unidirectionally stiffened double hulls. Joint MIT-Industry Program on Tanker Safety, Report No. 3.
- McTaggart, K., Datta, I., Stitling, A., Gibson, S., and Glen, I. (1997). Motions and loads of a hydroelastic frigate model in severe seas. *Transactions, SNAME*, Vol. 105.
- Mekilis, N. E. (1984). Sloshing in partially filled liquid tanks and its effect on ship motion: Numerical simulations and experimental verification. RINA Spring Meeting.
- Melitz, D., Robertson, A., and Davison, N. (1992). Structural performance management of VLCCs—An owner's approach. *Marine Technology*, October.

Merchant, A., and Stevens, K. T. (1990). The development of efficient composite (FRP) structures for high-speed vehicles by full scale testing. Proceedings of the Seventh International Conference on High-Speed Surface Craft, London, UK.

Meyers, W.G., Sheridan, D. J., and Salvesen, N. (1975). Manual NSRDC SHIPMOTION and SEALOAD computer program. NSRDC Report 3376, February.

Meyers, W. G., Applebee, T. R., and Baitis, A. E. (1981). User's manual for the standard ship motion program, SMP. DTNSRDC, Report SPD-0936-01.

Michelsen, F. C., and Nielsen, R. (1965). Grillage structure analysis through use of the Laplace integral transform. *Transactions*, SNAME, Vol. 73, 216–240.

Miner, M. A. (1945). Cumulative damage in fatigue. *Journal of Applied Mechanics*, September, A159–A164.

Minorsky, V. U. (1959). An analysis of ship collision with reference to protection of nuclear power ships. *Journal of Ship Research*, Vol. 3.

Moan, T. (1994). Reliability and risk analysis for design and operations planning of offshore structures in structural safety and reliability. Schuëller, G.I., Shinozuka, M., and Yao, J. T. P., (eds.), Proceedings of the Sixth ICOSSAR Conference. Rotterdam: Balkema, 21–43.

Morison, J. R., O'Brien, M. P., Johnson, J. W., and Schaaf, S. A. (1950). The forces exerted by surface waves on piles. *Transactions*, AIME, Vol. 189, 149–157.

Munse, W. H., Wilson, T. H., Tallalian, M. L., Nicoll, K., and Wilson, K. (1983). Fatigue characterization of fabricated ship details for design. Ship Structures Committee Report SSC-318.

Ng, R. (1992). Scantling requirements for bulkheads of partially filled tanks. Technical Notes, American Bureau of Shipping.

Ng, R. (1994). Commentary for impact load criteria development—Dynamic based design and evaluation of bulk carriers. SafeHull Report, American Bureau of Shipping.

Nieuwenhuijs, M. W., Segretain, J. F., and Baumans, P. (2005). IACS common structural rules for bulk carriers. RINA Proceedings of the Design and Operation of Bulk Carriers.

Nippon Kaiji Kyokai (1992). Study Report on Bulk Carrier Loss. Tokyo, Japan, January.

Nitta, A., Arai, H., and Magaino, A. (1992, 1992, 1995). Basis of IACS unified longitudinal strength standard. *Marine Structures*.

Nordenström, N. (1963). On estimation of long-term distributions of wave-induced midship bending moments in ships. Chalmers Tekniska Hogskola, Gothenberg, Sweden.

Nordenström, N. (1973). A method to predict long-term distributions of waves and wave-induced motions and loads. Det Norske Veritas Publication 81, April.

Nordhammer, H. (1998). Experience from construction and operation of the STENA HSS catamarans. Proceedings of the Third International Forum on Aluminum Ships, Haugesund, Norway.

Numata, E. (1960). Longitudinal bending and torsional moments acting on a ship model at oblique headings to waves. *Journal of Ship Research*, Vol. 4, No. 1 (June).

O'Dea, J. F., Powers, E. J., and Zselezky, J. (1992). Experimental determination of non-linearities in vertical plane ship motion. Nineteenth ONR Symposium.

Ochi, M. K. (1964). Prediction of occurrence and severity of ship slamming at sea. Proceedings of the Fifth Symposium on Naval Hydrodynamics, ONR ACR 112, 545–596.

Ochi, M. K., and Motter, L. E. (1969). Prediction of extreme value of impact pressure associated with ship slamming. *Journal of Ship Research*, June.

Ochi, M. K. (1973). On prediction of extreme values. *Journal of Ship Research*, Vol. 17, March, 29–37.

Ochi, M. K., and Motter, L. E. (1973). Prediction of slamming characteristics and hull response for ship design. *Transactions*, SNAME, Vol. 81, 144–176.

Ochi, M. K., and Bolton, W. E. (1973). Statistics for the prediction of ship performance in a seaway. *International Shipbuilding Progress*, Vol. 22, Nos. 222, 224, 229.

Ochi, M. K. (1978). Wave statistics for the design of ships and ocean structures. *Transactions*, SNAME, Vol. 86, 47–76.

O'Dea, J. F., and Walden, D. A. (1984). Effect of bow shape and non-linearity on the prediction of large amplitude motion and deck wetness. Proceedings of the Fifteenth ONR Symposium on Naval Hydrodynamics, Seoul, South Korea.

Ohtsubo, H., Astrup, O. C., Cazzulo, R., Kim, O. H., Luh, P. A., Spangerberg, S., Spencer, J. S., Sucharski, D. (1997). Structural design against collision and grounding. Thirteenth International Ship and Offshore Structures Congress (ISSC'97), Trondheim, Norway, 2: 83–116.

Ohtsubo, H., and Suzuki, K. (1994). The crushing mechanics of bow structures in head-on collision (first report) (in Japanese). *Journal of the Society of Naval Architects of Japan*, 176.

Ohtsubo, H., and Wang, G. (1995). An upper-bound solution to the problem of plate tearing. *Journal of Marine Science and Technology*, Vol. 1.

Ohtsubo, H., Suzuki, K., and Yonesato, N. (1995). Prediction of collision strength of side structures (in Japanese). *Journal of the Society of Naval Architects of Japan*, 178.

Okada, H., Oshima, K., and Fukumoto, Y. (1979). Compressive strength of long rectangular plates under hydrostatic pressure. *Journal of Society of Naval Architects of Japan*, Vol. 146 (December). English translation in *Naval Architecture and Ocean Engineering*, Vol. 18, 1980, SNA, Japan, 101–114.

Onat, E. T., and Haythornthwaite, R. M. (1956). The load-carrying capacity of circular plates at large deflection. *Journal of Applied Mechanics*, 23.

Otto, S., Pedersen, P. T., Samuelides, M., and Sames, P. C. (2001). Elements of risk analysis for collision and grounding of a Ro-Ro passenger ferry. Second International Conference on Collision and Grounding of Ships (ICCGS), Copenhagen, Denmark, July 1–3.

- Ozguç, O., Samuelides, M., and Das, P. K. (2005). A Comparative Study on the Collision Resistance of Single and Double Side Skin Bulk Carriers, International Congress of International Maritime Association of the Mediterranean, Lisbon, Portugal, September.
- Paik, J. K. (1993). ALPS/ISUM: A computer program for nonlinear analysis of large plated structures using the idealized structural unit method. Pusan National University, Pusan, South Korea.
- Paik, J. K. (1994). Cutting of a longitudinally stiffened plate by a wedge. *Journal of Ship Research*, Vol. 38 (4).
- Paik, J. K., and Mansour, A. (1995). A simple formulation for predicting the ultimate strength of ships. *Journal of Marine Science and Technology*, Vol. 1, No. 1 (December).
- Paik, J. K., and Pedersen, P. T. (1995). Ultimate and crushing strength of plated structures. *Journal of Ship Research*, 39(3).
- Paik, J. K., Yang, S. H., and Thayamballi, A. K. (1996). Residual strength assessment of ships after collision and grounding. Proceedings of the Internal Conference on Design and Methodologies for Collision and Grounding Protection of Ships, San Francisco, California, August.
- Paik, J. K., and Thayamballi, A. K. (1997). An empirical formulation for predicting ultimate compressive strength of stiffened panels. Proceedings of the Seventh International Offshore and Polar Engineering Conference, Honolulu, Hawaii, May 25–30, 328–338.
- Paik, J. K., Chung, J. Y., Choe, I. H., Thayamballi, A. K., Pedersen, P. T., and Wang, G. (1999). On the rational design of double hull tanker structures against collision. *Transactions, SNAME*.
- Paik, J. K. (2001). Photo gallery of ship structural mechanics laboratory. Pusan National University, Korea.
- Paik, J. K., Thayamballi, A. K., and Lee, J. M. (2004). Effect of initial deflection shape on the ultimate strength behavior of welded steel plates under biaxial compressive loads. *Journal of Ship Research*, Vol. 48, No. 1, 45–60.
- Paik, J. K., Kumar, Y. V. S., and Lee, J. M. (2005). Ultimate strength of cracked plate elements under axial compression or tension. *Thin-Walled Structures*, Vol. 43, 237–272.
- Patrakka, K., Arjave, J. P., Enlund, H., Kyyro, K., and Lausmaa, J. (1995). Influence of the distance between deihulls on the characteristics of a big, high speed catamaran. Proceedings of the Third International Conference on Fast Sea Transportation (FAST '95), Luebeck-Travenue, Germany.
- Paulling, J. R., and Payer, H. G. (1968). Hull-deckhouse interaction by finite-element calculations. *Transactions, SNAME*, Vol. 76.
- Paulling, J. R. (1974). Elastic response of stable platform structures to wave loading. International Symposium on the Dynamics of Marine Vehicles and Structures in Waves, IME, London, UK.
- Paulling, J. R. (1982). An equivalent linear representation of the forces exerted on the OTEC cold water pipe by combined effects of wave and current. *Ocean Engineering for OTEC*, Vol. 9, ASME.
- Pedersen, P. T. (1983). A beam model for the torsional-bending response of ship hulls. *Transactions*, Royal Institution of Naval Architects, Vol. 125, 171–182.
- Pedersen, P. T. (1985). Torsional response of containerships. *Journal of Ship Research*, Vol. 29, No. 3 (September), 194–205.
- Pedersen, P. T. (1994). Ship grounding and hull-girder strength. *Journal of Marine Structures*.
- Pedersen, P. T. (1995). Collision and grounding mechanics. WEMT'95, Danish Society of Naval Architecture and Marine Engineering, Copenhagen, Denmark.
- Pedersen, P. T., Valsgard, S., and Olsen, D. (1993). Ship impacts: Bow collision. *International Journal of Impact Engineering*, 13.
- Pedersen, P. T., and Zhang, S. (1998). On impact mechanics in ship collisions. *Marine Structures*, 11.
- Pedersen, P. T., and Zhang, S. (2000). Absorbed energy in ship collisions and grounding—Revising Minorsky's empirical method. *Journal of Ship Research*, Vol. 44, No. 2 (June).
- Peery, D. J. (1950). *Aircraft Structures*. New York: McGraw-Hill, 493.
- Petersen, M. J., and Pedersen, P. T. (1981). Collision between ships and offshore platforms. Offshore Technology Conference, Houston, Texas.
- Pettersen, O., and Wiklund, K. M. (1999). DNV requirements for direct calculation methods of high-speed and light craft. Fifth International Conference on Fast Sea Transportation, FAST '99, Seattle, Washington.
- Polezhaeva, H., and Malinowski, W. (2001). Fatigue strength of aluminum structural details of special service craft. Proceedings of the Sixth International Conference on Fast Sea Transportation (FAST 2001), Southampton, UK.
- Popov, E. P. (1968). *Introduction to Mechanics of Solids*. Englewood Cliffs, New Jersey: Prentice Hall.
- Primon, G., et al. (1989). Development of HSLA steels with high weldability and improved characteristics for offshore construction. Eighth International Conference OMAE, The Hague, Netherlands.
- Raff, A. (1972). Program SCORES—Ship structural response in waves. Ship Structure Committee Report SSC-230.
- Randrup-Thomsen, S., Christensen, C. F., and Rasmussen, F. M. (2001). Characteristics of the ship traffic distribution transverse to the navigation channel. Second International Conference on Collision and Grounding of Ships (ICCGS), Copenhagen, Denmark, July 1–3.
- Rawson, C., Crake, K., and Brown, A. J. (1998). Assessing the environmental performance of tankers in accidental groundings and collisions. *Transactions, SNAME*.
- Reardon, P. C., and Sprung, J. (1996). Validation of Minorsky's ship collision model and use of the model to estimate the probability of damaging a radioactive material transportation cask during a ship collision. Proceedings of the International Conference on Designs and

Methodologies for Collision and Grounding Protection of Ships, San Francisco, California, August.

Reid, S. R., and Reddy, T. Y. (1978). Effects of strain hardening on the large plastic deformation of a cantilever. *Journal of Applied Mechanics*, 45.

Reifsnider, K. L., Stinchcomb, W. W., and O'Brien, T. K. (1977). Frequency effects on a stiffness-based fatigue failure criterion in flawed composite specimens. Fatigue of filamentary composite materials. ASTM STP 636, Reifsnider, K. L. and Lauraitis, K. N. (eds.), ASTM.

Riber, H. J. (1995). Rational design of composite panels. Proceedings of the Third International Conference on Sandwich Construction, Southampton, UK.

Rice, S. O. (1944, 1954). Mathematical analysis of random noise. Bell System Technical Journal, Vol. 23, 1944; Vol. 24, 1945. Reprinted in Wax, N., *Selected Papers on Noise and Stochastic Processes*, New York: Dover.

Rigo, P., and Rizzuto, E. (2003). Analysis and design of ship structure. In: T. Lamb (ed.), *Ship Design and Construction*, Chapter 18, New York: SNAME.

Roberts, T. S., Watson, N. L., and Davis, M. R. (1997). Evaluation of sea loads in high speed catamaran. Proceedings of the Fourth International Conference on Fast Sea Transportation (FAST '97), Sydney, Australia.

Rodd, J. L. (1996). Observations on conventional and advanced double hull grounding experiments. Proceedings of the International conference on Design and Methodologies for Collision and Grounding Protection of Ships, San Francisco, California, August.

Roop, W. P. (1932). Elastic characteristics of a naval tank vessel. *Transactions*, SNAME, Vol. 40.

Ross, R. B. (1972). *Metallic Materials Specification Handbook*. New York: John Wiley & Sons.

Rutherford, S. E. and Caldwell, J. B. (1990). Ultimate strength of ships: a case study. *Transactions*, SNAME.

Salvesen, N., Tuck, E. O., and Faltinsen, O. (1970). Ship motions and sea loads. *Transactions*, SNAME, Vol. 78, 250–287.

Sampath, D., Moldenhauer, H. R., Schipper, H. R., and Schijvers, A. J. (1998). New semi-fabricated aluminum alloy products to marine applications. Proceedings of the Third International Forum on Aluminum Ships, Haugesund, Norway.

Sarkani, S., Michaelov, G., Kihl, D. P., and Beach, J. E. (1999). Stochastic fatigue damage accumulation of FRP laminates and joints. *Journal of Structural Engineering*.

Schade, H. A. (1938). Bending theory of ship bottom structure. *Transactions*, SNAME, Vol. 46, 176–205.

Schade, H. A. (1940). The orthogonally stiffened plate under uniform lateral load. *Journal of Applied Mechanics*, Vol. 7, No. 4 (December).

Schade, H. A. (1941). Design curves for cross-stiffened plating. *Transactions*, SNAME, Vol. 49, 154–182.

Schade, H. A. (1951). The effective breadth of stiffened plating under bending loads. *Transactions*, SNAME, Vol. 59.

Schade, H. A. (1953). The effective breadth concept in ship structure design. *Transactions*, SNAME, Vol. 61.

Schade, H. A. (1965). Two beam deckhouse theory with shear effects. University of California, Institute of Engineering, Research Report NA-65-3.

Slavounos, P. D. (1996). Computation of wave ship interaction. In: Ohkusu, M. (ed.), *Advances in Marine Hydrodynamics*, Boston: Computational Mechanics Publications.

Slavounos, P. D., Kring, D. C., Huang, Y., Mantzaris, D. A., Kim, S., and Kim, Y. (1997). A computational method as an advanced tool of ship hydrodynamic design. *Transactions*, SNAME, Vol. 105.

Scott, R. J. (1996). *Fiberglass Boat Design and Construction*, 2nd ed. New York: SNAME.

Shenoi, R. A., Allen, H. G., Moy, S. S. J., and Feng, Z. (1995). The behavior of single skin FRP plate structures under extreme lateral pressure loading. Proceedings of the Third International Conference on Fast Sea Transportation (FAST '95), Luebeck-Travemuende, Germany.

Shi, B., Liu, D., and Wiernicki, C. (2005). Dynamic loading approach for structural evaluation of ultra large container carriers. SNAME World Maritime Technology Conference, Houston, Texas.

Shin, Y. S. (2000). Official discussion on extreme hull girder loading. Special Task Committee VI.1 Report, Fourteenth ISSC.

Shin, Y. S., Chung, J. S., Lin, W. M., Zhang, S., and Engle, A. (1997). Dynamic loadings for structural analysis of fine form container ship based on a non-linear large amplitude motion and loads method. *Transactions*, SNAME.

Sikora, J. P., Dinsenbacher, A., and Beach, J. F. (1983). A method for estimating lifetime loads and fatigue lives for SWATH and conventional monohull ships. *Naval Engineers Journal*, May.

Silveria, W. A., and Brillinger, D. R. (1978). On maximum wave heights of severe seas. Proceeding of the Offshore Technology Conference, Paper #3232, Houston, Texas.

Silvia, P. A. (1978). Structural design of planing craft. *Chesapeake Section*, SNAME, March.

Simonsen, B. C. (1997). Mechanics of ship grounding. Doctoral thesis, Technical University of Denmark, Copenhagen.

Simonsen, B. C. (1999). Ship grounding on rock: I & II. *Marine Structures*, Vol. 10.

Simonsen, B. C., and Ocakli, H. C. (1999). Experiments and theory on deck and girder crushing. *Thin-Walled Structures*, Vol. 34.

Simonsen, B. C., and Lauridsen, L. P. (2000). Energy absorption and ductile failure in metal sheets under lateral indentation by a sphere. *International Journal of Impact Engineering*, Vol. 24.

Simonsen, B. C., and Törnqvist, R. (2004). Experimental and Numerical Modeling of Ductile Crack Propagation in Large-scale Shell Structures, *Journal of Marine Structures*, 17, 1–27.

Sims, D. F., and Brogdon, V. H. (1977). Fatigue behavior of composites under different loading modes.

- Fatigue of Filamentary Composite Materials, ASTM STP 636, Reifsnider, K. L. and Lauraitis, K. N. (eds.), ASTM.
- Skaar, K. T. (1974). On the finite element analysis of oil tanker structures. *Maritime Research*, Vol. 2, No. 2 (November), 2–11.
- Skjelby, T., Kindfren, M., and Kjeldaas, A. C. (1999). Fatigue evaluation for high-speed light craft based on direct load transfer procedures. Proceedings Fifth International Conference on Fast Sea Transportation (FAST '99), Seattle, Washington.
- Slaughter, S. B., Cheung, M. C., Sucharski, D., and Cowper, B. (1997). State of the art in hull response monitoring system. Ship Structure Committee Report SSC 401.
- Smith, C. S. (1975). Compressive strength of welded ship grillages. *Transactions*, RINA, Vol. 117, 325–359.
- Smith, C. S. (1977). Effect of local compressive failure on ultimate longitudinal strength of a ship's hull. PRADS Symposium, Tokyo, Japan.
- Smith, C. S. (1983). Structural redundancy and damage tolerance in relation to ultimate ship hull strength. Proceedings of the Symposium on Design, Inspection, Redundancy, Williamsburg, Virginia. Washington, D.C: National Academy Press.
- Soares, G., and T. Moan. (1985). Uncertainty analysis and code calibration of the primary load effects in ship structures. Fourth International Conference on Structural Safety and Reliability, Kobe, Japan, Vol. III, August, 501–512.
- Soeding, H. (1974). Calculation of long-term extreme loads and fatigue loads of marine structures. Symposium on the Dynamics of Marine Vehicles and Structures in Waves, IME, London, UK.
- Spencer, J. S., Wirsching, P. H., Wang, X., and Mansour, A. E. (2003). Development of reliability-based classification rules for tankers. *Transactions*, SNAME, Vol. 111.
- Spencer, J. S. (1975). Structural design of aluminum crew boats. *Marine Technology*, July.
- Spencer, J. S., Mansour, A., Chen, H. H., and Lockett, M. D. (1996). Reliability based comparative study of classification rules. OMEA, Florence, Italy, June.
- Spencer, J. S., Robinson, D. W., and Chen, H. H. (1995). Recent advances in classification rules for design and evaluation of ship hull structures. RINA New Building Conference, London, UK.
- Ship Structure Committee (1952). Considerations of welded hatch corner design. Report SSC-37, October 1.
- St. Denis, M., and Pierson, W. J. (1955). On the motion of ships in confused seas. *Transactions*, SNAME, 280
- St. Denis, M. (1970). A guide for the synthesis of ship structures, Part One: The midship hold of a transversely-framed dry cargo ship. Ship Structures Committee Report SSC-215.
- Stambaugh, K. A., and Wood, W. A. (1981). SL-7 research program summary, conclusions and recommendations. Ship Structure Committee Report AD-A120599.
- Stavovy, A. B., and Chuang, S. L. (1976). Analytical determination of slamming pressures for high-speed vehicles in waves. *Journal of Ship Research*, December; errata, December 1977.
- Sterndorff, M. J., and Pedersen, P. T. (1996). Grounding experiments on soft bottoms. *Journal of Marine Science and Technology*, 1(3): 174–181.
- Stiansen, S. G., and Mansour, A. E. (1975). Ship primary strength based on statistical data analysis. *Transactions*, SNAME.
- Stiansen, S. G., Mansour, A. E., and Chen, Y. N. (1977). Dynamic response of large Great Lakes bulk carriers to wave-excited loads. *Transactions*, SNAME, Vol. 85.
- Stiansen, S. G., Mansour, A. E., Jan, H. Y., and Thayamballi, A. (1980). Reliability methods in ship structures. *Transactions*, RINA, 381–406.
- Stiansen, S. G., and Chen, H. H. (1982). Application of probabilistic design methods to wave loads prediction for ship structures analysis. SNAME, *T&R Bulletin*, 2–27.
- Stiansen, S. G. (1984). Recent research on dynamic behavior of large Great Lakes bulk carriers. *Marine Technology*, Vol. 21, No. 4.
- Susuki, S., et al. (1989). Development of LBZ-free low Al-B-treated steel plates. Eighth International Conference OMAE, The Hague, Netherlands.
- Suzuki, K., Ohtsubo, H., and Sajit, K. S. (1999). Evaluation of absorbed energy in collision of ships—The effectiveness of Minorsky's formula in anti-collision structure. *Journal of the Society of Naval Architects of Japan*, 186.
- Suzuki, K., Ohtsubo, H., and Sajit, K. S. (2000). Evaluation method of absorbed energy in collision of ship with collision structure. Ship Structure Symposium on Ship Structures for the New Millennium: Supporting Quality in Shipbuilding, Arlington, Virginia.
- Swaan, W. A., and Vossers, G. (1961). The effect of forebody section shape on ship behavior in waves. *Transactions*, RINA, 103.
- Taggart, R. (ed.) (1980). *Ship Design and Construction*. New York: SNAME.
- Takagi, K., and Naito, S. (1993). Deck wetness and influence of the above water hull form at bow. *Journal of the Kansai Society of Naval Architects of Japan*, 220.
- Talreja, R. (1987). Estimation of Weibull parameters for composite material strength and fatigue life data. In: *Fatigue of Composite Material*. Lancaster, Pennsylvania: Technomic Publishing.
- Thayamballi, A. K. (1990). Fatigue screening for tankers. American Bureau of Shipping Technical Report RD-90005, May.
- Thiberge, E. (1999). Rational design assessment for classification purpose—Application to hull design of large mono-hulls. Fifth International Conference on Fast Sea Transportation (FAST '99), Seattle, Washington.
- Thoft-Christensen, P., and Baker, M. J. (1982). *Structural Reliability Theory and Its Applications*. New York: Springer-Verlag.
- Tikka, K. T., Fischbeck, P. S., Bergquist, J. R., and Tuckel, E. A. (2001). Analysis of hypothetical groundings in US waters. Second International Conference on

Collision and Grounding of Ships (ICCGS), Copenhagen, Denmark, July 1–3.

Timoshenko, S. (1956). *Strength of Materials*, Vol. I, 3rd ed.; Vol. II.

Timoshenko, S., and Goodier, J. N. (1970). *Theory of Elasticity*, 3rd ed. New York: McGraw-Hill.

Torhaug, R., Winterstein, S. R., and Braathen, A. (1998). Non-linear ship loads: Stochastic models for extreme response. *Journal of Ship Research*.

Törnqvist, R. (2003), Design of Crashworthy Ship Structures, PhD Thesis, Technical University of Denmark, Lyngby, Denmark.

Troesch, A. W. (1984a). Wave-induced hull vibrations: An experimental and theoretical study. *Journal of Ship Research*, Vol. 28, No. 2 (June).

Troesch, A. W. (1984b). Effects of nonlinearities on hull springing. *Marine Technology*, Vol. 21, No. 4 (October).

Ueda, Y., and Rashed, S. M. H. (1975). An ultimate transverse strength analysis of ship structures (in Japanese). *Journal of the Society of Naval Architects of Japan*, Vol. 136.

Ueda, Y., and Rashed, S. M. H. (1984). The idealized structural unit method and its application to deep girder structures. *Computers & Structures*, Vol. 18, No. 2.

UK Department of Energy (1990). *Offshore Installation: Guidance on Design, Construction and Certification*, 4th ed. London, UK: HMSO.

US Army Research Lab. Composite Material Handbook. MIL-HDBK-23, Watertown, Massachusetts.

US Navy (1969). Strength of glass reinforced plastic structural members. DDS-9110-9, August (document subject to export control).

Umamoto, K., Yoshikawa, T., Shimizu, H., and Murakami, A. (1997). A consideration on the structural response under sloshing loads. 16th OMAE Conference.

UNITAS (1997). Rules for construction and classification of high speed craft.

Urban, J., Pedersen, P. T., and Simonsen, B. C. (1999). Collision risk analysis for HSC. Fifth International Conference on Fast Ships (FAST'99), Seattle, Washington.

Vanmarcke, E. H. (1975). On the distribution of the first-passage time for normal stationary random process. *Journal of Applied Mechanics*, March, 215–220.

Vasilev, A. L., Glozman, M. K., Pavlinova, E. A., and Filippoe, M. V. (1964). *Corrugated Strength Bulkhead for Ships* (in Russian). St. Petersburg: Publishing House Sudostroenie.

Vasta, J. (1949). Structural tests on passenger ship S.S. *President Wilson*; Interaction between super-structure and main hull girder. *Transactions*, SNAME, Vol. 57.

Vasta, J. (1958). Lessons learned from full scale structural tests. *Transactions*, SNAME, Vol. 66, 165–243.

Vidic-Perunovic, J., and Jensen, J. J. (2005). Non-linear springing excitation due to a bi-directional wave field. *Marine Structures*, Vol. 18, No.4, 332–358.

Vredeveltdt, A. W., and Wevers, L. J. (1992). Full scale ship collision tests. Conference on Prediction Methodol-

ogy of Tanker Structural Failure and Consequential Oil Spill, ASIS. Tokyo, Japan, June.

Vredeveltdt, A. W., and Wevers, L. J. (1995). Full scale grounding experiments. Conference on Prediction Methodology of Tanker Structural Failure and Consequential Oil Spill, ASIS, Tokyo, Japan, June.

Vredeveltdt, A. W., and Janssen, G. T. M. (1998). X-joints in composite sandwich panels. Proceedings of the Seventh International Symposium on Practical Design of Ships and Mobile Units (PRAD '98), The Hague, Netherlands.

Wah, T. (1960). A guide for the analysis of ship structures. U.S. Dept. of Commerce, PB181168, Government Printing Office.

Wahab, R., Pritchett, C., and Ruth, L. C. (1975). On the behavior of the ASR catamaran in waves. *Marine Technology*, July.

Walden, H. (1966). Die Eigenschaften der Meereswellen in Nordatlantischen Ozean. Deutschen Wettendienst Seewetteramt, Publication No. 41, Humbert, Germany.

Wang, G. (1995). Structural analysis of ships' collision and grounding. Doctoral thesis, University of Tokyo, Tokyo, Japan.

Wang, G., Ohtsubo, H., and Liu, D. (1997). A simple method for predicting the grounding strength of ships. *Journal of Ship Research*, Vol. 41.

Wang, G., Ohtsubo, H., and Arita, K. (1998). Large deflection of a rigid-plastic circular plate pressed by a rigid sphere. *Journal of Applied Mechanics*, 65.

Wang, G., and Ohtsubo, H. (1999). Impact load of a supply vessel. Ninth International Offshore and Polar Engineering Conference & Exhibition (ISOPE), Brest, France, May 30–June 4, Vol. IV, 463–471.

Wang, G., Arita, K., and Liu, D. (2000). Behavior of a double hull in a variety of stranding or collision scenarios. *Marine Structures*, Vol. 13.

Wang, G., Spencer, J. S., and Chen, Y. (2001). Assessment of a ship's performance in accidents. *Marine Structures*.

Wang, G., Chen, Y., Zhang, H., and Peng, H. (2002). Longitudinal strength of ships with accidental damages. *Marine Structures*, 15.

Wang, G. (2002). Some recent studies on plastic behavior of plates subjected to large impact loads. Submitted to *Journal of Ocean Mechanics and Arctic Engineering* (ASME). January.

Wang G., and Pedersen P. T. (2007). A Literature Review of Risk Assessment of Ship-FPSO Collision, 26th Offshore Mechanics and Arctic Engineering Conference, San Diego, USA, June.

Wang, X., Jiao, G., and Moan, T. (1996). Analysis of oil production ships considering load combination, ultimate strength and structural reliability. *Transactions*, SNAME, 104, 3–30.

Wang, Z. H., Jensen, J. J., and Xia, J. (1998). On the effect of green water on deck in the wave bending moment. Seventh PRADS Symposium, The Hague, Netherlands.

- Watanabe, I., Udno, M., and Sawada, H. (1989). Effects of bow flare on the wave loads of a containership. *JSNAJ*.
- Werenskiold, P., Fathi, D. E., and Jullumstro, E. (1999). Documentation of HSC operational performance and limitations—The regulation regime and practical application. Fifth International Conference on Fast Sea Transportation (FAST '99), Seattle, Washington.
- Westin, H. (1981). Analysis of the torsional response of the SL-7 hull structure by use of the finite-beam technique and comparison with other techniques. *Journal of Ship Research*, Vol. 25, No. 1 (March), 62–75.
- White, G. J., and Ayyub, B. M. (1985). Reliability methods for ship structures. *Naval Engineers Journal*, ASNE, Vol. 97, No. 4, 86–96.
- Wierzbicki, T. (1983). *Crushing Behavior of Plate Intersections, Structural Crashworthiness*. Jones, N. and Wierzbicki, T. (eds.), London: Butterworths.
- Wierzbicki, T. (1995). Concertina tearing of metal plates. *International Journal of Solids Structures*, 19.
- Wierzbicki, T., and Abramowicz, W. (1983). On the crushing mechanics of thin-walled structures. *Journal of Applied Mechanics*, 50, 727–734.
- Wierzbicki, T., Peer, D. B., and Raddy, E. (1993). The anatomy of tanker grounding. *Marine Technology*, 30, 71–78.
- Wierzbicki, T., and Thomas, P. (1993). Closed-form solution for wedge cutting force through thin metal sheets. *International Journal of Mechanical Sciences*, Vol. 35.
- Wirsching, P., and Chen, Y. N. (1988) Considerations of probability-based fatigue design for marine structure. *Marine Structures*, 1, 23–45.
- Witmer, D. J., and Lewis, J. W. (1995). The BP oil tanker structural monitoring system. *Marine Technology*, October.
- Woisin, G. (1979). Design against collision. Proceedings of the International Symposium on Advances in Marine Technology, Trondheim, Norway, June.
- Wu, G. X., Ma, Q. W., and Taylor, R. E. (1998). Numerical simulation of sloshing waves in a 3D tank based on a finite element method. *Applied Ocean Research*.
- Wu, M. K., and Moan, T. (1996). Linear and non-linear hydro-elastic analysis of high-speed vessels. *Journal of Ship Research*, Vol. 40, No. 2.
- Wu, F., Spong, R., and Wang, G. (2004). Using Numerical Simulation to Analyze Ship Collision, 3rd International Conference on Collision and Grounding of Ships, Izu, Japan, October.
- Xia, J., Wang, Z., and Jensen, J. J. (1998). Non-linear wave loads and ship responses by a time domain strip theory. *Marine Structures*, 11.
- Xiang, D., Akiyama, A., and Lin, Y. H. (1999). Practical application of evolutionary algorithm to ship structure design. Thirteenth Asia Technical Exchange and Advisory Meeting on Marine Structures, Keelung, Taiwan, October.
- Yamada, Y., Endo, H., and Pedersen, P. T. (2005). Numerical Study on the Effect of Buffer Bow Structure in Ship-to-Ship Collisions, International Offshore and Polar Engineering Conference, Seoul, Korea, June.
- Yamada, Y. (2006). Bulbous Buffer Bows: A Measure to Reduce Oil Spill in Tanker Collisions, PhD Thesis, Technical University of Denmark, Lyngby, Denmark.
- Yamamoto, M., Sugimoto, H., Kada, K., and Higashi, K. (1993). Global strength analysis of wave piercing catamaran. Proceedings of the Second International Conference on Fast Sea Transportation (FAST '93), Yokohama, Japan.
- Yang, P. D. C., and Caldwell, J. B. (1988). Collision energy absorption of ships' bow structures. *International Journal of Impact Engineering*, 7, 181–196.
- Young, W. C. (1989). *Roark's Formulas for Stress and Strain*, 6th ed. New York: McGraw-Hill.
- Yu, X. (1996). Structural analysis with large deformations until fracture and with dynamic failure (in German). Doctoral thesis, Hamburg University, Hamburg, Germany.
- Yuille, I. M. (1963). Longitudinal strength of ships. *Transactions*, RINA, Vol. 105.
- Zaid, M. (1958). On the carrying capacity of plates of arbitrary shape and variable fixity under a concentrated load. *Journal of Applied Mechanics*, 25.
- Zhang, S. (2002). Plate tearing and bottom damage in ship grounding. *Marine Structures*, Vol. 15, 101–117.
- Zhao, R., and Faltinsen, O. (1993). Water entry of two dimensional bodies. *Journal of Fluid Mechanics*, Vol. 246.
- Zhao, R., Faltinsen, O. M., and Aarsnes, J. V. (1996). Water entry of arbitrary two-dimensional sections with and without flow separation. Proceedings of the 21st Symposium on Naval Hydrodynamics, Trondheim, Norway.
- Zheng, X. (1999). Global loads for structural design of large slender mono-hulls. Proceedings of the Fifth International Conference on Fast Sea Transportation (FAST '99), Seattle, Washington.
- Zheng, Z. M., and Wierzbicki, T. (1995). Steady-state wedge indentation. Joint MIT-Industry Project on Tanker Safety, Report No. 42.
- Zhou, Z. Q., De Kat, J. O., and Buchner, B. (1999). A non-linear 3-D approach to simulate green water dynamics on deck. Seventh International Conference on Numerical Ship Hydrodynamics, Nantes, France.
- Zienkiewicz, O. (1972). *Finite Element Method in Engineering Science*, 2nd ed. New York: McGraw-Hill.
- Zink, P. F., and Van Rynbach, E. (2003). Container ships. In: T. Lamb (ed.), *Ship Design and Construction*, Chapter 36. New York: SNAME.

INDEX

Index Terms

Links

A

Acceleration

forces	25	54	55
inertial loads	14	54	114
inertial reactions	4		

Airy stress function

69

Aluminum

elasticity of	60		
---------------	----	--	--

American Bureau of Shipping Rules

9 163 202

Areas

124 132

Arrestors, crack

3 134

Autocorrelation function

19 19*f* 24

B

Bending moment

diffusion of	86				
hull girder	9	13	40	50	56
	60	96	102	131	177
lateral	9	11	121	128	
on a section	10				
response to	11				
still water	9	40	101	107	168
	184				
vertical	9	11	28	40	96
	113	116	149	205	
in waves	9				

Bredt formula

66 75

Brittle fracture

3 134 135 150 189

192

Bryan formula

137

Index Terms

Links

Buckling failure					
in compression	137				
criteria of	137				
elastic	137				
of plating	137				
of stiffened panels	137				
C					
Cargo					
damping	97	101			
Center of gravity	7	25	61	114	127
<i>See also</i>					
Gravity, center of					
Classification Societies Rules	202				
Collision and grounding					
designing against	179 <i>f</i>				
residual strength after	183				
Computers					
applications	11				
Navy Ship Hull Characteristics Program	7				
Conditions of loading	41	43	90		
Conference, MARPOL					
(Marine Pollution)	184				
Containerships	98	117			
Convention SOLAS 1960					
(Safety of Life at Sea)	128				
Correlated wave loads	37 <i>f</i>	39 <i>f</i>			
Criteria	2	10	53	98	102
	135	202			
Crossing a threshold	21				
Cost optimization and economic value					
analysis	185				
Covariance	19	163			

Index Terms

Links

D

Deckhouses, superstructure					
forces on	77				
response of	77				
Definitions for regulations	iv	184			
Deflections					
deckhouse	77				
hull girder	59	73	75	77	78 <i>f</i>
	80	82			
mid-panel	142				
structural members	57				
Deterministic					
evaluation of wave-induced loading	14				
Discontinuities (structural)					
compensation for	92				
stress concentrations	92				
Dynamic loads					
non-linear	24	26	95	203	205
other dynamic loads	47				
quadratic theory	26	34			

E

End effect, erections	78				
Equilibrium					
Static	9	60	62	64	69
	182				
Euler critical load	134				
Extreme loads	99	155			
Extreme value	8	17	31	41	46
	60	96	98	106	112
	157	205			

Index Terms

Links

F

Fabrication imperfections					
influence on strength	188				
Factor of safety	18	89			
Failure					
brittle fracture	134				
fatigue	123	132	134	150	151
	153	200			
instability	134	137			
yielding	92	121	135	136	
Fatigue failure					
damage	98	128	133	150	
endurance limit	151	152 <i>f</i>			
high-cycle	134	152			
low-cycle	134	153			
strength	153				
Finite element analysis	92	104	109		
Flare	34	49	95		
Flooding	128	136	184		
Forces					
acceleration	25	54	55		
added mass	15	16	17	97	
damping	15				
wave-induced	15	17			
Foundations					
design considerations	46				
forces on	82				
modulus	77				
reaction loads	11	14	177		
Froude-Krylov force	14				
Full-scale tests					
bending moment in waves	10				

Index Terms

Links

G

Gravity, center of	7	25	61	114	127
Grounding	168	174	177		

H

Heaving forces	178	181			
Hooke's Law	60				
Hull girder					
beam theory	2	116			
bending moment lateral	9	11	111		
bending moment longitudinal	11	182			
deflection	59	73	77	147	194
shear flow	78				
shear lag	68				
torsion	56	95	128	131	
ultimate strength	106	146			
vertical	10	30	103	106	111
	131				
wrap	90	111			

I

Imperfect plates					
initial deflection	139				
cracks	145				
residual stresses	139				
International Maritime Organization (IMO)	99	168	184	193	195

L

Lateral bending moment	9	11	111		
Loads, structural					
carrying capability	9	137			
combination	35				
dynamic	4				
impact	5				

Index Terms

Links

Loads, structural (*Cont.*)

inertial	14	27	54
internal (sloshing)	5	53	
static	4		
wave induced	8		

Longitudinal bending moment

still water	11	40	102
in waves	11		

Long-term extreme values

12	41	112	114 <i>f</i>
----	----	-----	--------------

M

Materials

composite	189		
aluminum	189		
steel	189		
HSST	189		

Midship section (structural)

82

Model tests

bending moment in waves	11		
-------------------------	----	--	--

Modes of structural failure

brittle fracture	3	134	
elastic buckling	137		
excessive yield	3		
fatigue cracking	3		

Moment of inertia of midship section

59	61		
----	----	--	--

P

Pitching

forces due to	204		
---------------	-----	--	--

Plating, strength of

elastic buckling	141		
imperfect plates	140		
post buckling behavior	138		
ultimate strength	141	140	169

Index Terms

Links

Plating stress				
beam on elastic	82			
finite element	83			
grillage theory	83			
orthotropic theory	82	86	87 <i>f</i>	142
Post-buckling behavior	138			
Primary response	5	80		
Probabilistic analysis of wave-induced loads	17			
Probabilistic nature of ship's structural loads	2			
Probabilistic representation of random seas	17			
Probabilistic theory of reliability	155			
 R				
Racking				
transverse strength	89	90 <i>f</i>		
Radius of gyration	71	142	189	
Random Process				
stationary	19	21 <i>f</i>	23	24
non-stationary	32	38		37
Reaction loads	11	14	177	
Regulations	168	184	185	
Reliability of structure				
approximate methods	158			
basic concept	155			
bounds	165			
first order	159			
mean value first order second moment	158			
Monte Carlo simulation	160			
partial safety factors	163			
probabilistic design	155 <i>f</i>	156 <i>f</i>	185	
second order	160			
ship structural	161			
system reliability	164			
uncertainty associated with design				
variables	154			

Index Terms

Links

Response, structural

primary	5
secondary	6
tertiary	6

Rolling

forces due to	11	130	205
natural period	96		

S

Safety, factor of

2	3	18	135	154
189				

Safety of Life at Sea (SOLAS)

1960 Convention	128
-----------------	-----

Secondary response (structure)

6

Section modulus, calculation of

61

Shear flow

63 64 *f*

Shear lag

68 69 *f* 72 *f*

Shear stress (hull girder)

62

Slamming

loads	5	48
-------	---	----

stresses	207
----------	-----

Sloshing

52 52 *f*

Smearing

60

Snaking

75

Spectral density

of response	24
-------------	----

of waves	20
----------	----

Specific vessel types

bulk carriers	127
---------------	-----

containerships	130
----------------	-----

passengers	150
------------	-----

tankers	124
---------	-----

Specialty crafts

201

Spectrum

20 22 38

Springing

4 47 97

Stability

1 141 183 185

Index Terms

Links

Static loading in still water	5				
Stationary random process	19	21 <i>f</i>	24	32	37
Still-water bending moment	6	9			
Strength of ships					
classification society rules	59	88	195		
hull girder ultimate	106				
of material	59	61	190	193	
plating	89				
stiffened panels	1	57	81	103	123
transverse	89	91			
Stress components resultants					
dominant	62				
principal	89				
Stress concentration					
around circular openings	95				
around rectangular openings	92	93 <i>f</i>			
Stress distribution	69	71	91 <i>f</i>	124	136
	149				
Stresses					
primary direct	57	116			
secondary	6	39	57	58	80
	83	89			
tertiary	6				
Stress superposition	89				
Strip theory	11	12	14	17	47
	56	204			
Structures					
deterministic design	33	43			
probabilistic design	17				
reliability of	9				
secondary response	56				
tertiary response	56				
unconventional craft	9				
Structural Failure	2	134	178		
Superposition of stresses	89				

Index Terms

Links

Superstructure	76	80 <i>f</i>	92		
aluminum	79				
stresses in	78	78 <i>f</i>	79 <i>f</i>		
T					
Tankers	11	33	33 <i>f</i>	54	58 <i>f</i>
	89	90	99 <i>f</i>	106	117
	124	168	182		
Tertiary response (structure)	6	87			
Time domain simulation	14	27	27 <i>f</i>		
Thermal loads	4	5	35	41	
Torsion, hull girder	131				
Transverse strength	89	205			
Transverse distribution of wave loads	56				
U					
Ultimate strength					
of box girder	136	136 <i>f</i>			
of hull girder	146				
of imperfect plates	139				
of imperfect stiffened plates	145				
of plates	139				
of stiffened plates	142				
of stiffeners	145				
Uncertainty associated with ship's structural response	2				
U.S. Coast Guard	200				
U.S. Navy	7	9	28	195	200
V					
Vertical bending moment (VBM)	11	29	40	96	112
	205				

Index Terms

Links

W

Wave bending moment				
approximations	33			
long-term prediction	26			
in real seas	47			
transverse	107			
Wave induced loads				
deterministic evaluation	14			
extreme	12	17	30	
long-term	17			
on offshore platforms	35			
probabilistic estimate	17			
short-term	17			
Wave spectrum	22	25	27	30
Whipping	48	96	202	205
Wolverine State experiments	42			

Y

Yield criteria	135			
----------------	-----	--	--	--